MOLECULAR AND CELLULAR UNDERPINNINGS OF AGE-RELATED MEMORY LOSS

EDITED BY: Stylianos Kosmidis, Christine Ann Denny, Alex Dranovsky and Efthimios M. C. Skoulakis

PUBLISHED IN: Frontiers in Cell and Developmental Biology

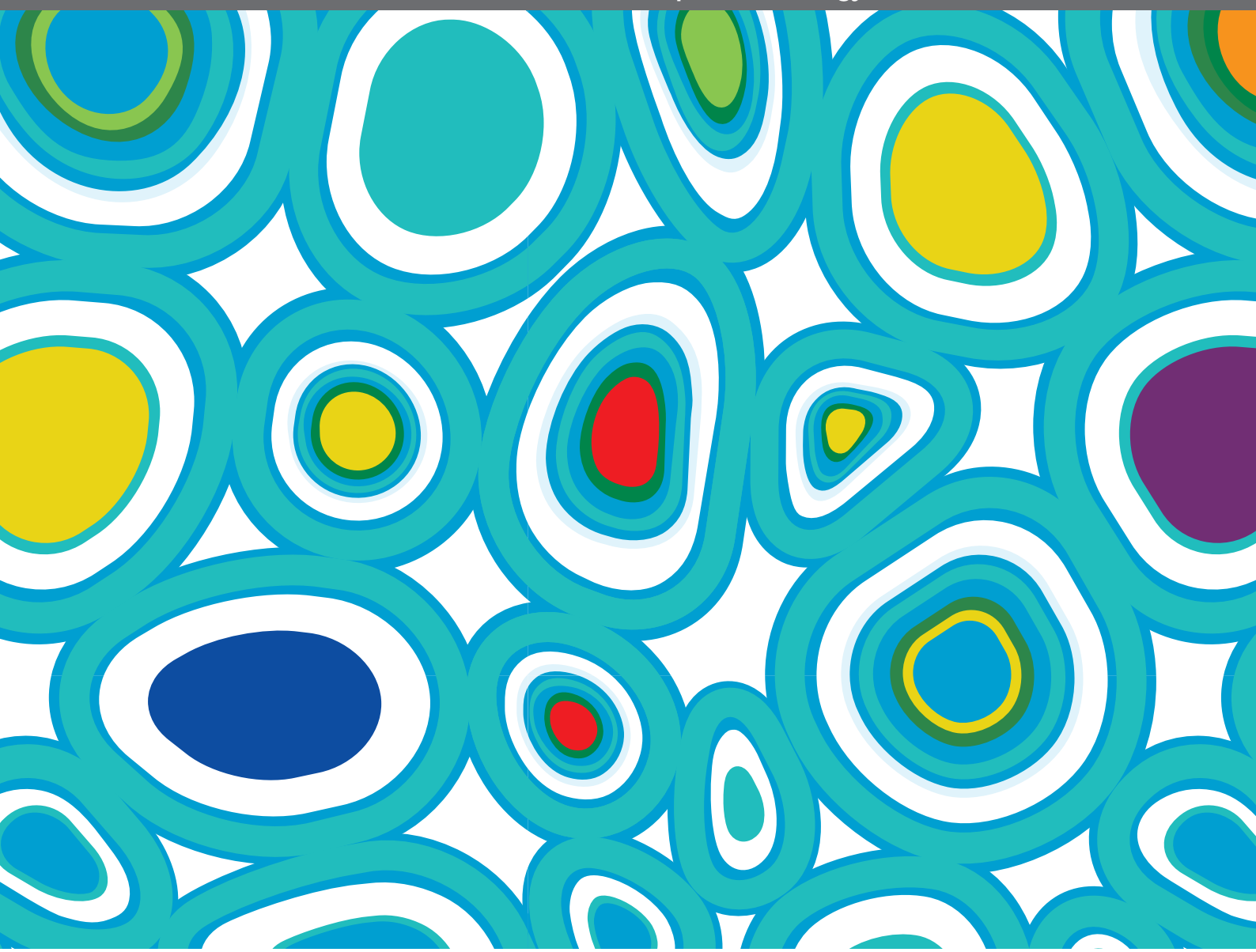

frontiers Research Topics

frontiers

ISSN 1664-8714
ISBN 978-2-88971-475-9
DOI 10.3389/978-2-88971-475-9

About Frontiers

Frontiers is more than just an open-access publisher of scholarly articles: it is a pioneering approach to the world of academia, radically improving the way scholarly research is managed. The grand vision of Frontiers is a world where all people have an equal opportunity to seek, share and generate knowledge. Frontiers provides immediate and permanent online open access to all its publications, but this alone is not enough to realize our grand goals.

Frontiers Journal Series

The Frontiers Journal Series is a multi-tier and interdisciplinary set of open-access, online journals, promising a paradigm shift from the current review, selection and dissemination processes in academic publishing. All Frontiers journals are driven by researchers for researchers; therefore, they constitute a service to the scholarly community. At the same time, the Frontiers Journal Series operates on a revolutionary invention, the tiered publishing system, initially addressing specific communities of scholars, and gradually climbing up to broader public understanding, thus serving the interests of the lay society, too.

Dedication to Quality

Each Frontiers article is a landmark of the highest quality, thanks to genuinely collaborative interactions between authors and review editors, who include some of the world's best academicians. Research must be certified by peers before entering a stream of knowledge that may eventually reach the public - and shape society; therefore, Frontiers only applies the most rigorous and unbiased reviews.
Frontiers revolutionizes research publishing by freely delivering the most outstanding research, evaluated with no bias from both the academic and social point of view. By applying the most advanced information technologies, Frontiers is catapulting scholarly publishing into a new generation.

What are Frontiers Research Topics?

Frontiers Research Topics are very popular trademarks of the Frontiers Journals Series: they are collections of at least ten articles, all centered on a particular subject. With their unique mix of varied contributions from Original Research to Review Articles, Frontiers Research Topics unify the most influential researchers, the latest key findings and historical advances in a hot research area! Find out more on how to host your own Frontiers Research Topic or contribute to one as an author by contacting the Frontiers Editorial Office: frontiersin.org/about/contact

MOLECULAR AND CELLULAR UNDERPINNINGS OF AGE-RELATED MEMORY LOSS

Topic Editors:
Stylianos Kosmidis, Columbia University, United States
Christine Ann Denny, Columbia University Irving Medical Center, United States
Alex Dranovsky, Columbia University, United States
Efthimios M. C. Skoulakis, Alexander Fleming Biomedical Sciences Research Center, Greece

Citation: Kosmidis, S., Denny, C. A., Dranovsky, A., Skoulakis, E. M. C., eds. (2021). Molecular and Cellular Underpinnings of Age-Related Memory Loss. Lausanne: Frontiers Media SA. doi: 10.3389/978-2-88971-475-9

Table of Contents

frontiers in Cell and Developmental Biology

EDITORIAL
published: 20 August 2021
doi: 10.3389/fcell.2021.743187

Editorial: Molecular and Cellular Underpinnings of Age-Related Memory Loss

Stylianos Kosmidis[1]*, *Christine A. Denny*[2,3], *Alex Dranovsky*[2] and *Efthimios M. C. Skoulakis*[4]

[1] Zuckerman Institute, Howard Hughes Medical Institute, Columbia University, New York, NY, United States, [2] Department of Psychiatry, Columbia University Irving Medical Center (CUIMC), New York, NY, United States, [3] Division of Systems Neuroscience, Research Foundation for Mental Hygiene, Inc. (RFMH)/New York State Psychiatric Institute (NYSPI), New York, NY, United States, [4] Alexander Fleming Biomedical Sciences Research Center, Vari, Greece

Keywords: aging, cognitive decline, model organism, neurogenesis, therapeutic intervention

Editorial on the Research Topic

Molecular and Cellular Underpinnings of Age-Related Memory Loss

Our memories define who we are. Normal aging is often accompanied by a decline in memory functions leading to a condition known as age-related memory loss (ARML). With the aged population predicted to double in the next 30 years according to UN population dynamics (https://www.un.org/en/global-issues/ageing), ARML is expected to be a significant attenuator of life quality and elevate the financial burden of elderly care for families and society at large. Understanding the mechanisms underlying age-related memory decline is imperative for developing pharmaceutical interventions, which will ameliorate loss or restore cognitive functions in older individuals. Improving memory in the affected population will pave the road for restoring quality of life and alleviating dire socioeconomic consequences.

The collection of research articles herein provides novel contributions in the field of aging research, with specific focus on the molecular constituents of memory loss.

In the first article of this topic, Hahn et al. propose that the DNA methyltransferase DNMT1 function is implicated in age-related loss of cortical inhibitory interneurons. Interestingly, DNMT1-deficient mice exhibited improved sensory-motor performance and reduced aging-associated transcriptional changes, leading the authors to posit that the DNMT1 protein may act indirectly on interneuron survival in aged mice, potentially by modulating the proteostasis network.

To provide a link between aging and glucose metabolism, Ripoli et al. used a mouse model of type 1 diabetes and discovered that memory impairment related to aging appears associated with inhibition of the transcription factor cAMP-response element-binding protein (CREB). The authors show that experimentally induced hyperglycemia, can downregulate CREB phosphorylation and CREB-mediated mRNA expression of synaptic proteins in hippocampal primary neurons. Their findings highlighted interesting mechanisms underlying hyperglycemia-related memory loss and the necessity of further studying the role of glucose-driven CREB transcriptional activity in the process, as well as its potential impact on personalized medicine approaches.

Scott et al. studied the impact of the gut microbiome on hippocampal neurogenesis, contextual fear memory, and aging, providing a novel functional connection. Their results show that disruption of the gut microbiome can affect hippocampal neurogenesis in an age- and

Edited and reviewed by:
Gong-Ping Liu,
Huazhong University of Science and Technology, China

***Correspondence:**
Stylianos Kosmidis
sk3440@columbia.edu

Specialty section:
This article was submitted to Molecular and Cellular Pathology, a section of the journal Frontiers in Cell and Developmental Biology

Received: *17 July 2021*
Accepted: *27 July 2021*
Published: *20 August 2021*

Citation:
Kosmidis S, Denny CA, Dranovsky A and Skoulakis EMC (2021) Editorial: Molecular and Cellular Underpinnings of Age-Related Memory Loss. Front. Cell Dev. Biol. 9:743187. doi: 10.3389/fcell.2021.743187

sex-dependent manner, suggesting that these changes can in principle alter the dentate gyrus functional network and, subsequently, memory-related processes in an age-dependent manner.

Moreover, Arredondo et al. summarize current knowledge on the roles of Wnt signaling and review data suggesting distinct roles for the canonical and non-canonical Wnt signaling cascades in the regulation of different stages of neurogenesis. Wnt signaling in fact, may be a highly conserved molecular pathway underlying aging in many species.

In accord, Inestrosa et al. used the Andean rodent *Octodon degus* (*O. degus*, common degu), often kept as a pet, to explore the age-related changes in the expression of key Wnt components. Their findings are in congruence with those from other species and suggest that the brain of *O. degus* can be used as model to study brain aging and its consequences.

In an effort to further delineate the molecular signatures of aging, Dunn et al. used a genetically diverse mouse population to characterize individual differences in cognitive abilities in adulthood, and to search for evidence of cognitive reserve and/or resilience in middle-aged mice. Using RNA-Sequencing, they present evidence nominating the Rho guanine nucleotide exchange factor-encoding gene Trio as a modulator of working memory ability, implicating the actin cytoskeleton in the process. More importantly, they propose that the usage of B6-BXD recombinant inbred lines, are a promising tool to study the molecular mechanisms of ARML before onset and translate these findings to humans.

This special issue also focused on diagnostic and therapeutic interventions for ARML. To this end, Cocco et al. propose that plasma levels of brain-derived neurotrophic factor (BDNF) can serve as a simple and low-cost diagnostic tool with several clinical applications. Using transcranial direct current stimulation (tDCS) in 3 × Tg-Alzheimer's disease (AD) mice, the authors showed that tDCS induced a significant increase of plasma BDNF levels in wild type mice, but not in 3 × Tg-AD mice. They also discuss the potential of identifying memory-related disorders in a pre-clinical stage, allowing more effective disease-modifying interventions.

In a similar fashion, Sun et al. propose that pro-BDNF protein is implicated in memory. Using a variety of molecular and behavioral assays the authors showed that blocking hippocampal pro-BDNF early in development plays a role in spatial cognition in adults. These findings are consistent with the hypothesis that postnatal pro-BDNF plays an essential role in synaptic and cognitive functions and can be used for therapeutic interventions to alleviate memory impairments and consequently ARML.

Lastly, Mhillaj et al. explored the possibility that celecoxib (CXB), a selective inhibitor of the pro-inflammatory cyclooxygenase-2 can have neuroprotective properties in subjects with early AD or mild cognitive impairment (MCI). Importantly, using *in vitro* methods, they showed that celecoxib modulates the heme oxygenase/biliverdin reductase (HO/BVR) system, counteracting the β-amyloid peptide (Aβ)-induced reactive oxygen species (ROS) production, lipid peroxidation, and the growth rate of Aβ oligomers with a mechanism dependent on Heme oxygenase −1.

In conclusion, we are confident that this Special Research Topic Issue contributes a significant amount of information regarding the molecular underpinnings of Age-Related Memory Loss. It is timely and of paramount importance to continue pushing the boundaries of aging research to promote ameliorative strategies that combat cognitive decline and improve the quality of life of the elderly.

AUTHOR CONTRIBUTIONS

SK, CD, AD, and ES wrote the manuscript. All authors contributed to the article and approved the submitted version.

FUNDING

CD was supported by an NICHD R01 HD101402, an NIA R56 AG058661, an NIA R21 AG064774, an NINDS R21 NS114870, an NIH DP5 OD017908, and a Whitehall Foundation Grant.

Conflict of Interest: The authors declare that the research was conducted in the absence of any commercial or financial relationships that could be construed as a potential conflict of interest.

Publisher's Note: All claims expressed in this article are solely those of the authors and do not necessarily represent those of their affiliated organizations, or those of the publisher, the editors and the reviewers. Any product that may be evaluated in this article, or claim that may be made by its manufacturer, is not guaranteed or endorsed by the publisher.

frontiers in Cell and Developmental Biology

BRIEF RESEARCH REPORT
published: 29 May 2020
doi: 10.3389/fcell.2020.00407

Disrupted Neurogenesis in Germ-Free Mice: Effects of Age and Sex

*Gavin A. Scott†, Dylan J. Terstege†, Alex P. Vu†, Sampson Law, Alexandria Evans and Jonathan R. Epp**

Cumming School of Medicine, Hotchkiss Brain Institute, Department of Cell Biology and Anatomy, University of Calgary, Calgary, AB, Canada

The gut microbiome has profound effects on development and function of the nervous system. Recent evidence indicates that disruption of the gut microbiome leads to altered hippocampal neurogenesis. Here, we examined whether the effects of gut microbiome disruption on neurogenesis are age-dependent, given that both neurogenesis and the microbiome show age-related changes. Additionally, we examined memory induced functional connectivity of hippocampal networks. Control and germ-free mice at three different ages (4, 8, and 12 weeks) were trained in contextual fear-conditioning, then subsequently tested the following day. Hippocampal neurogenesis, quantified via BrdU and doublecortin, exhibited age-dependent changes relative to controls, with the established age-dependent decrease in neurogenesis being delayed in germ-free mice. Moreover, we found sex-dependent effects of germ-free status on neurogenesis, with 4 week old male germ-free mice having decreased neurogenesis and 8 week old female germ-free mice having increased neurogenesis. To assess systems-level consequences of disrupted neurogenesis, we assessed functional connectivity of hippocampal networks by inducing c-Fos expression with contextual memory retrieval and applying a previously described network analysis. Our results indicate impaired connectivity of the dentate gyrus in germ-free mice in a pattern highly correlated with adult neurogenesis. In control but not germ-free mice, functional connectivity became more refined with age, indicating that age dependent network refinement is disrupted in germ-free mice. Overall, the results show that disruption of the gut microbiome affects hippocampal neurogenesis in an age- and sex-dependent manner and that these changes are also related to changes in the dentate gyrus functional network.

Keywords: neurogenesis, hippocampus, microbiome, germ-free, proliferation

OPEN ACCESS

Edited by:
Alex Dranovsky,
Columbia University, United States

Reviewed by:
Victor Luna,
Columbia University Irving Medical Center, United States
Paul J. Lucassen,
University of Amsterdam, Netherlands

***Correspondence:**
Jonathan R. Epp
jonathan.epp1@ucalgary.ca

† These authors have contributed equally to this work

Specialty section:
This article was submitted to Molecular Medicine, a section of the journal Frontiers in Cell and Developmental Biology

Received: *11 March 2020*
Accepted: *04 May 2020*
Published: *29 May 2020*

Citation:
Scott GA, Terstege DJ, Vu AP, Law S, Evans A and Epp JR (2020) Disrupted Neurogenesis in Germ-Free Mice: Effects of Age and Sex. Front. Cell Dev. Biol. 8:407. doi: 10.3389/fcell.2020.00407

INTRODUCTION

Emerging evidence indicates that the gut microbiome plays a substantial role in cognition due to direct and indirect communication with the brain via the gut-brain axis (Dinan and Cryan, 2017; Sarkar et al., 2018). In humans, gut microbiome diversity is correlated with cognitive performance (Arnoriaga-Rodríguez and Fernández-Real, 2019) and supplementation with probiotics has been shown to improve cognition (Allen et al., 2016). Additionally, numerous rodent studies now

report impaired cognition when the microbiome is disrupted (Gareau et al., 2011; Wang et al., 2015; Fröhlich et al., 2016; Möhle et al., 2016) and improved cognition resulting from probiotic supplementation (Savignac et al., 2015; Wang et al., 2015; Gronier et al., 2018).

Notably, evidence indicates that the gut microbiome is also linked with depression and anxiety (Foster and McVey Neufeld, 2013). In humans, supplementation with probiotics has been shown to alleviate low mood (Benton et al., 2007). Disruptions of the gut microbiome via infection or inflammation have also been shown to increase anxiety-like behavior (Lyte et al., 2006; Goehler et al., 2008). Fecal transplants from subjects with a depressed or anxious phenotype to normal subjects can also transfer these mood impairments (Bercik et al., 2011; Kelly et al., 2016). Germ-free mice, which are devoid of gut microbiota, show a reduction in basal anxiety behaviors (Neufeld et al., 2011), but germ-free status leads to heightened HPA responses to acute stress in both rats (Crumeyrolle-Arias et al., 2014) and mice (Clarke et al., 2013).

Recent studies have established that adult hippocampal neurogenesis and behavior can change with perturbations in the gut microbiome (Ogbonnaya et al., 2015; Möhle et al., 2016). Neurogenesis has been heavily implicated in multiple cognitive processes relating to learning, memory, and cognitive flexibility (Winocur et al., 2006; Sahay et al., 2011; Epp et al., 2016). Furthermore, it is also implicated in anxiety- and depression-related behavior (Duman, 2004). Reduced neurogenesis is observed in rodents subjected to chronic stress (Lucassen et al., 2015). Additionally, antidepressant drugs increase neurogenesis, which appears to be necessary for mediating the improvement in depression-related behaviors in mice (Santarelli et al., 2003). Thus, the relationship between the gut microbiome and anxiety/depression may be mediated in part by changes in neurogenesis.

Importantly, both neurogenesis and the gut microbiome undergo age-dependent changes. Rates of neurogenesis decrease sharply with age (Kuhn et al., 1996; Amrein et al., 2004). The composition and the diversity of gut microbiota increase during postnatal development (Eckburg et al., 2005; Claesson et al., 2011). Hence, the relationship between neurogenesis, the gut microbiome, and anxiety- and depression-like behavior may be further modulated by the age of the animal.

In the present study, we compared rates of neurogenesis in the dentate gyrus between germ-free and control mice at different ages to determine whether the relationship between neurogenesis and gut microbiota changed with age. We also trained animals in contextual fear conditioning at these ages in order to assess age-modulated differences between control and germ-free mice in the expression of fear memory, which is related to anxiety and depression. Furthermore, we applied a graph theoretical approach to examine task-specific networks of neuronal activation during the expression of this fear memory to determine how changes in neurogenesis and fear memory expression might coincide with altered functional connectivity between the DG and other brain areas. This approach allows us to determine the impact of altered neurogenesis on brain connectivity. Relatively little previous research has examined the link between the microbiome and neurogenesis (Ogbonnaya et al., 2015; Möhle et al., 2016) and no previous study, to our knowledge, has examined age as an independent variable in this context.

METHODS

Animals

A total of 45 control C57BL/6J and 45 germ-free C57BL/6J mice were purchased from Charles River (Wilmington, MA, United States) and the International Microbiome Facility (IMC) (University of Calgary, Canada). To produce the germ-free line, C57BL/6J mice were re-derived to germ-free status via two-cell embryo transfer. Axenic mice were bred and maintained long-term in flexible-film isolators at the IMC. Germ-free status was routinely monitored by culture-dependent and -independent methods and all germ-free colonies were independently confirmed to be pathogen-free. Germ-free status was maintained until the first behavioral experiments. Specifically, behavioral procedures began on the same day that germ-free animals were brought into the laboratory from the suppliers. Male and female mice from three age groups (4 weeks old, 8 weeks old, and 12 weeks old) were housed in groups of 5 and provided food and water *ad libitum*. All mice were housed under a 12-h light/12-h dark cycle. Mice were used in accordance with protocols approved by the University of Calgary, Health Sciences Animal Care Committee, following guidelines of the Canadian Council for Animal Care.

Contextual Fear Conditioning

Mice were trained in contextual fear conditioning. Training was conducted in a sound-attenuated chamber (Ugo Basile, Gemonio, Italy) with a grated floor from which shocks (0.5 mA; 2 s) were delivered. Behavior was monitored via an overhead camera and automated tracking software (ANY-Maze, Stoelting, Wood Dale, IL, United States). During the training phase, mice were allowed to explore the chamber for 2 min before a series of 3 shocks were delivered with a 1 min interval between each shock. The addition of ∼500 μL of bleach into the test chamber provided an additional olfactory cue. Mice were returned to the chamber 24 h after training for a 5-min retention test in which no shocks were delivered. The chamber was cleaned using 70% ethanol and allowed to dry after each animal.

Perfusions and Histology

Ninety minutes after retention testing in contextual fear conditioning, animals were perfused with 0.1 M phosphate buffered saline (PBS) followed by 4% formaldehyde. Brains were extracted and postfixed in 4% formaldehyde for 24 h. Fixed brains were then stored at 4°C in 30% W/V sucrose until they were no longer buoyant. Serial sections were collected on a cryostat (Leica Biosystems, Concord, ON, Canada) at a thickness of 40 μm and stored in 10 series at −20°C in antifreeze solution.

Immunohistochemistry

Doublecortin Labeling

Tissue sections were washed 3 times in 0.1 M PBS before being placed in a primary antibody solution containing 1:200 rabbit anti-DCX (4604S, Cell Signaling Technology, Danvers, MA, United States), 0.03% Triton-X, and 3% normal donkey serum and incubated for 48 h. Tissue sections then underwent 3 10-min PBS washes before being placed in a secondary antibody solution containing 1:500 donkey anti-goat Alexa Fluor 488 antibody (CLAS10-1116, Cedarlane Labs, Burlington, ON, Canada) and incubated for 24 h. The subsequent day, tissue sections were incubated in a 1:2000 dilution of 4,6-diamidino-2-phenylindole (DAPI) for at least 10 min before being mounted to slides and coverslipped using PVA-DABCO mounting medium.

BrdU Labeling

Two hours before perfusion, mice were weighed and given a single intraperitoneal injection of 200 mg kg^{-1} BrdU (B-5002, Sigma Aldrich, Oakville, ON, Canada) dissolved in 20 mg/ml sterile saline. Following perfusion and tissue sectioning, brain sections were washed 3 times in 0.1 M PBS, then incubated in a 45°C oven in 2N HCl for 30 min to denature DNA. The HCl was then neutralized by rinsing sections using 1 M sodium borate buffer (pH 8.5) for 10 min followed by 3 × 10 min washes in 0.1 M PBS. BrdU was labeled by incubating sections for 48 h at 4°C with 1:250 mouse monoclonal anti-BrdU primary antibody (Bu20a, BioLegend, San Diego, CA, United States) in blocking solution (3% normal donkey serum, 0.03% Triton-X in 0.1 M PBS). Sections were rinsed 3 times in 0.1 M PBS then incubated at 4°C with a donkey anti-mouse secondary antibody conjugated to Alexa Fluor 488 (715-545-150, Jackson ImmunoResearch Laboratories Inc., West Grove, PA, United States) diluted 1:500 in 0.1 M PBS. Tissue was then transferred to a 1:3000 solution of propidium iodide for 10 min. Tissue was rinsed with PBS before mounting in PVA-DABCO.

C-Fos Labeling

Tissue sections were washed 3 times in 0.1 M PBS before being transferred to a primary antibody solution containing 1:2000 rabbit anti-cfos antibody (226 003, Synaptic Systems, Göttingen, Germany), 3% normal donkey serum, and 0.03% Triton-X and were incubated at room temperature for 48 h. Tissue sections were then washed 3 times in PBS and transferred to a secondary antibody solution containing 1:500 donkey anti-rabbit Alexa Fluor 488 (111-545-003, Cedarlane Labs, Burlington, ON, Canada) secondary antibody and incubated for 24 h. Sections were then transferred to 1:2000 DAPI and incubated for 15 min before being mounted to slides and coverslipped with PVA-DABCO mounting medium.

Quantification of Neurogenesis and Pyknosis

Neurogenesis was quantified by counting the number of doublecortin and BrdU positive cells in the subgranular zone (SGZ) and granule cell layer of the DG. Labeled cells were identified using a 60× oil immersion objective on an Olympus FLUOVIEW FV3000 confocal microscope (Richmond Hill, ON, Canada) by an experimenter blind to the subject age, sex, and germ-free status. Approximately 7–10 sections per brain were sampled and exhaustive counts of every positive cell were obtained for each section. For DCX, brains were quantified unilaterally. The number of positive cells was standardized to the area of the DG, which in the case of DCX quantification was captured using a 2× objective lens with 2× zoom and, in the case of BrdU quantification, was captured with a 10× objective. The area of the DG was quantified via manual tracing in *ImageJ* software (United States NIH). Pyknotic cells were imaged by staining a separate series of tissue sections with cresyl violet and were counted exhaustively in the same manner. We operationally defined pyknotic cells as those exhibiting darker staining and condensed chromatin in the nucleus (Falconer and Galea, 2003; Pawluski et al., 2010). In order to avoid counting cell caps, we also counted only the cells that were surrounded by translucent cytoplasm and were not situated at the extreme upper or lower focal planes of the section. The area of the DG for cresyl violet-stained sections was quantified by capturing images on an Olympus VS120-L100-W slide scanner (Richmond Hill, ON, Canada) and the DG in these images was manually traced in *ImageJ*.

Functional Connectivity of Hippocampal Networks

Analysis of functional connectivity was performed via an automated process that we developed, which builds upon analyses of correlated regional cFos expression density (Wheeler et al., 2013). In brief, tissue sections stained for cFos expression were imaged using an Olympus VS120-L100-W slide scanner (Richmond Hill, ON, Canada). Regional cFos expression density was measured using a semi-automated image processing pipeline. Fluorescent cFos labels were segmented using the machine learning-based pixel and object classification program *Ilastik* (Berg et al., 2019). Images were then registered to a selection of regions from the Allen Mouse Brain Atlas (Region list and abbreviations are provided in **Supplementary Table 1**) using a custom and user input-driven *ImageJ* plug-in. The regional c-Fos densities were then correlated within each group to construct pairwise correlation matrices. To generate a binary adjacency matrix, correlations were filtered by an alpha value of 0.95 and only statistically significant correlations with a Pearson's r of at least 0.8 were considered. In such a matrix, all comparisons in which the filter criteria were met are denoted with a one while all other comparisons are denoted with a zero. Binary adjacency matrices can then be analyzed as network graphs by plotting all regions being analyzed and connecting all pairs of regions which were marked with a one in the adjacency matrix. A graph theoretical approach guided by the use of the Brain Connectivity Toolbox (Rubinov and Sporns, 2010) was used to analyze measures of network connectivity and generate graphs of each network in an automated manner.

Among these measures, node degree and global network density were highlighted. In the case of our neuroanatomical networks, each region is defined as a node and correlated activity between a pair of regions is represented by a vertex

between nodes (Bullmore et al., 2009). Node degree signifies the connectedness of a node and is calculated by counting the number of vertices connected to that node. Network density extends upon this and is expressed as a proportion of the total number of possible vertices in a graph with an equivalent number of nodes (Achard and Bullmore, 2007).

Statistical Analysis

All statistical tests for neurogenesis, pyknosis, and behavior in the fear conditioning test were performed using Statistica (version 13 TIBCO software). To analyze the differences between the groups, a two-way ANOVA followed by a Newman-Keuls multiple comparisons *post hoc* test was utilized. To detect statistically significant differences between the groups a p-value of 0.05 was set as the threshold for significance. The analysis of functional networks was performed as per the described procedure above. Brains were excluded from tissue analyses if the quality of the tissue was insufficient (e.g., poor perfusion or damaged sections) or lacked adequate expression of BrdU. In all cases, exclusion occured blind to condition and prior to quantification to avoid bias.

RESULTS

Germ-Free Mice Show Altered Adult Neurogenesis

To examine how the gut microbiome might impact adult hippocampal neurogenesis we quantified DCX, a marker of immature neurons, within the DG of the hippocampus in germ-free and control mice. Representative photomicrographs of DCX-positive cells are shown in **Figures 1E–J**. Because adult neurogenesis is not a static process we performed this analysis at three different ages, 4, 8 or 12 weeks of age. As expected, our results demonstrated a statistically significant decline in doublecortin-labeled cells in control mice with increasing age. This effect was evident in both male (**Figure 1A**; $F(2,51) = 44.97$, $p < 0.0001$) and female mice (**Figure 1B**; $F(2,22) = 68.84$, $p < 0.0001$). However, in germ-free mice, the same relationship between age and doublecortin was not observed and the result was sexually dimorphic. In males, there was a significant decrease in doublecortin at 4 weeks in germ-free mice compared to control mice ($p = 0.006$) but no difference at 8 or 12 weeks (p's > 0.498). In female mice we observed a significant increase in doublecortin in 8 week old germ-free mice compared to control mice ($p = 0.014$) and no significant differences at 4 or 12 weeks of age (p's > 0.307). To compare the rate of change of doublecortin-labeling across male and female germ-free and control mice, we examined the percent change in labeling from the respective 4 week old mice. In doing so we observed that in both male and female germ-free mice, the decline in neurogenesis that occurs between 4 and 8 week old control mice was absent in germ-free mice [Male (**Figure 1C**): significant main effect of group $F(1,51) = 4.43$, $p = 0.04$, Female (**Figure 1D**): Significant group $\times$ age interaction ($F(2,22) = 6.79$, $p < 0.0050$)]. In the case of females, there was even a small but significant increase in doublecortin labeling between 4 and 8 weeks ($p = 0.028$).

Germ-Free Mice Show Altered Cell Proliferation

In addition to the number of immature neurons, we also measured cell proliferation by quantifying BrdU in the dentate gyrus. Representative photomicrographs of BrdU-positive cells are shown in **Figures 2E–G**. Again, as expected we identified a significant decrease in proliferation with age in control mice for both males (**Figure 2A**; significant interaction of Age*Group: $F(2,39) = 3.53$, $p = 0.038$) and females (**Figure 2B**; significant interaction of Age*Group: $F(2,15) = 5.09$, $p = 0.021$). However, in germ-free mice the age dependent decrease in neurogenesis was disrupted, following the same pattern as observed for DCX labeling. That is, a decrease in proliferation at 4 weeks in male mice ($p = 0.018$) and an increase in proliferation at 8 weeks in female mice ($p = 0.017$). As a function of percent change from 4 weeks of age, male (**Figure 2C**) and female (**Figure 2D**) germ-free mice showed a flat or slight increase in proliferation between 4 and 8 weeks of age, respectively, compared to control mice that show a decrease in both sexes over this time [Male: significant main effect of group ($F(1,39) = 4.45$, $p = 0.041$), Female: Significant group $\times$ age interaction ($F(2,15) = 5.96$, $p < 0.012$)].

Germ-Free Mice Have Increased Cell Death in the Dentate Gyrus at 4 Weeks of Age

As a measure of cell death, we quantified the number of pyknotic cells in the dentate gyrus. Representative images of cresyl violet-stained pyknotic cells are shown in **Figure 3A**. We observed a pattern of cell death across ages in both male (**Figure 3B**) and female (**Figure 3C**) control mice that replicated the previously described pattern of reduced cell death across age (Sun et al., 2004) and was slightly reminiscent of the previously described inverted U pattern of cell death across age (Ben Abdallah et al., 2010), although the rate of pyknosis was very similar between 4 and 8 weeks with only slight increases in males and females that did not reach statistical significance. Mainly, the results show a sharp reduction in the rate of pyknosis at 12 weeks compared to 4 or 8 weeks (p's ≤ 0.000165). In male germ-free mice, there was a significant group by age interaction ($F(2,51) = 4.07$, $p = 0.023$) in the density of pyknotic cells. *Post hoc* tests showed a significant difference between control and germ-free mice at 4 weeks of age ($p = 0.025$). There was no significant main effect of group ($p = 0.91$) or group by age interaction ($p = 0.90$) in female mice but there was a significant main effect of age ($F(2,18) = 14.87$, $p = 0.00015$). 12 week old mice had significantly fewer pyknotic cells than 4 week ($p = 0.0012$) and 8 week old mice ($p = 0.00028$).

Germ-Free Mice Show Reduced Functional Connectivity of the Dentate Gyrus

We next sought to determine the impact that altered rates of hippocampal neurogenesis have on correlated activity with other brain regions. To do so, we used a c-fos-based approach to determine functional connectivity. This technique, which

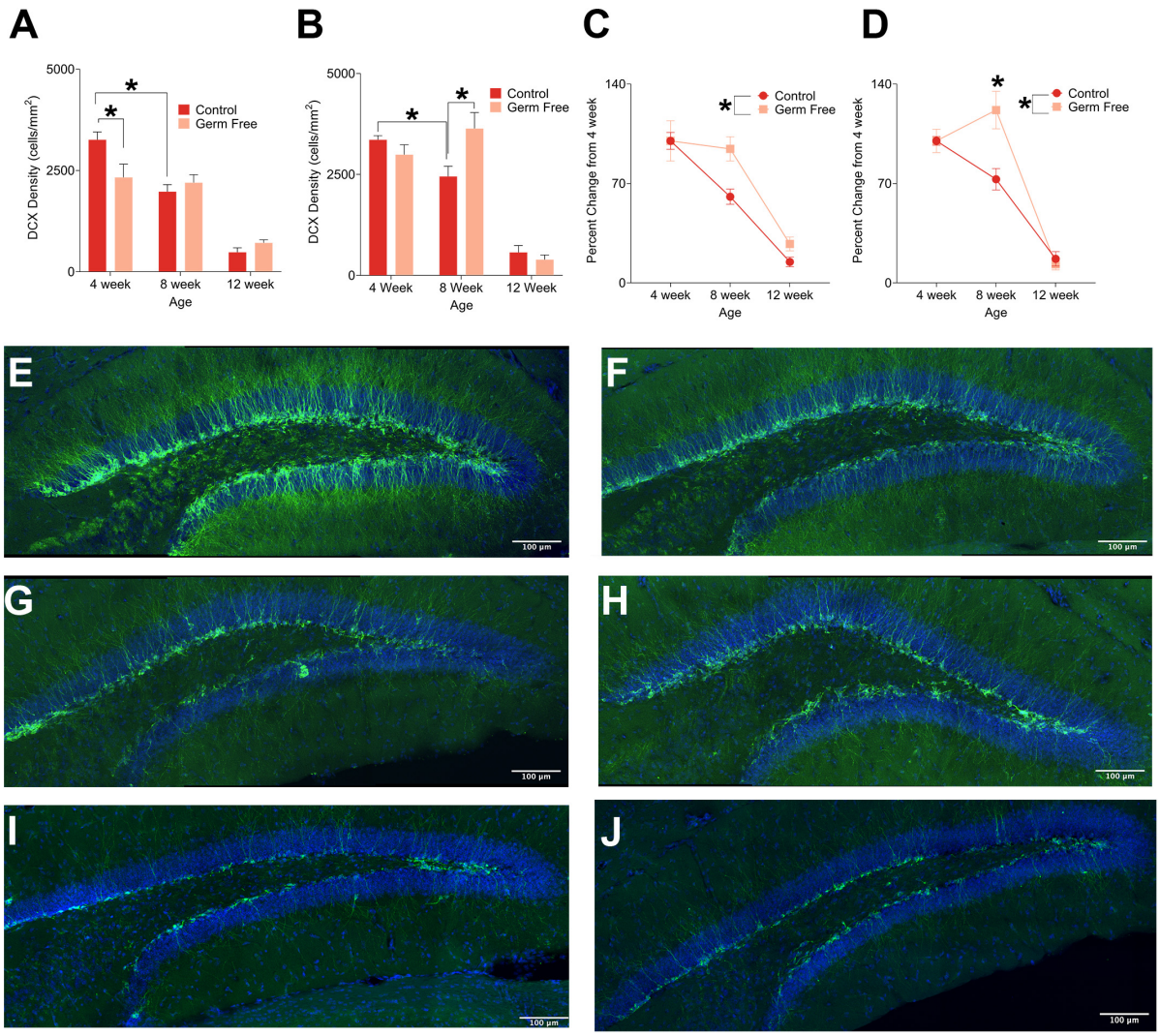

FIGURE 1 | (A) Mean (± SEM) DCX-positive cells in the DG of male germ-free and control mice. Control mice show a clear age-dependent decrease in neurogenesis, but this pattern is altered in germ-free mice. At 4 weeks old, male germ-free mice had reduced neurogenesis relative to controls and exhibited no reduction in neurogenesis between 4 and 8 weeks of age. **(B)** Mean (± SEM) DCX-positive cells in the DG of female germ-free and control mice. Similarly to males, female control mice showed a clear age-related decrease in neurogenesis with this effect being absent in female germ-free mice. In contrast to male germ-free mice, female germ-free mice showed no difference relative to controls at 4 weeks old, but had significantly elevated neurogenesis at 8 weeks old. **(C)** Mean (± SEM) neurogenesis in males depicted as percent-change from the baseline (4 week old) number of DCX-positive DG cells. Neurogenesis remains abnormally elevated in germ-free mice as they age relative to controls **(D)**. Mean (± SEM) neurogenesis in females depicted as percent-change from the baseline (4 week old) number of DCX-positive DG cells. As with male germ-free mice, neurogenesis in female germ-free mice remains abnormally elevated relative to controls particularly at 8 weeks of age. **(E–J)** Representative photomicrographs of DCX-positive cells (green) and DAPI (blue) in the DG of 4 week old controls **(E)** and germ-free mice **(F)**, 8 week old controls **(G)** and germ-free mice **(H)**, and 12 week old controls **(I)** and germ-free mice **(J)**. Control male 4 week $n = 11$, 8 week $n = 11$, 12 week $n = 8$. Control female 4 week $n = 5$, 8 week, $n = 5$, 12 week $n = 4$. Germ-free male 4 week $n = 11$, 8 week $n = 11$, 12 week $n = 6$. Germ-free female 4 week $n = 5$, 8 week, $n = 5$, 12 week $n = 4$. $^*p < 0.05$.

has been used previously, is based on detection of correlated activity between regions within a group of mice. In order to induce c-fos activity we perfused mice 90 min following fear memory recall. For this analysis, we used male mice only because we observed highly variable behavior in female mice due to typical periodic bouts of darting behavior which interfere with the functional connectivity interpretations. Interestingly, germ-free mice spent significantly more time freezing during the contextual memory test in all age groups (**Figure 4A**, main effect of treatment, $F(1,55) = 10.49$, $p = 0.0002$). The difference appeared most pronounced in 4-week-old mice but, there was no significant effect of age ($F(2,55) = 0.98$, $p = 0.38$) or Age by Group interaction ($F(2,55) = 0.59$, $p = 0.56$). There was no difference in the absolute number of c-fos-positive cells in the DG (cells/mm^2) between controls and germ-free mice although c-fos expression was greater in older mice than younger

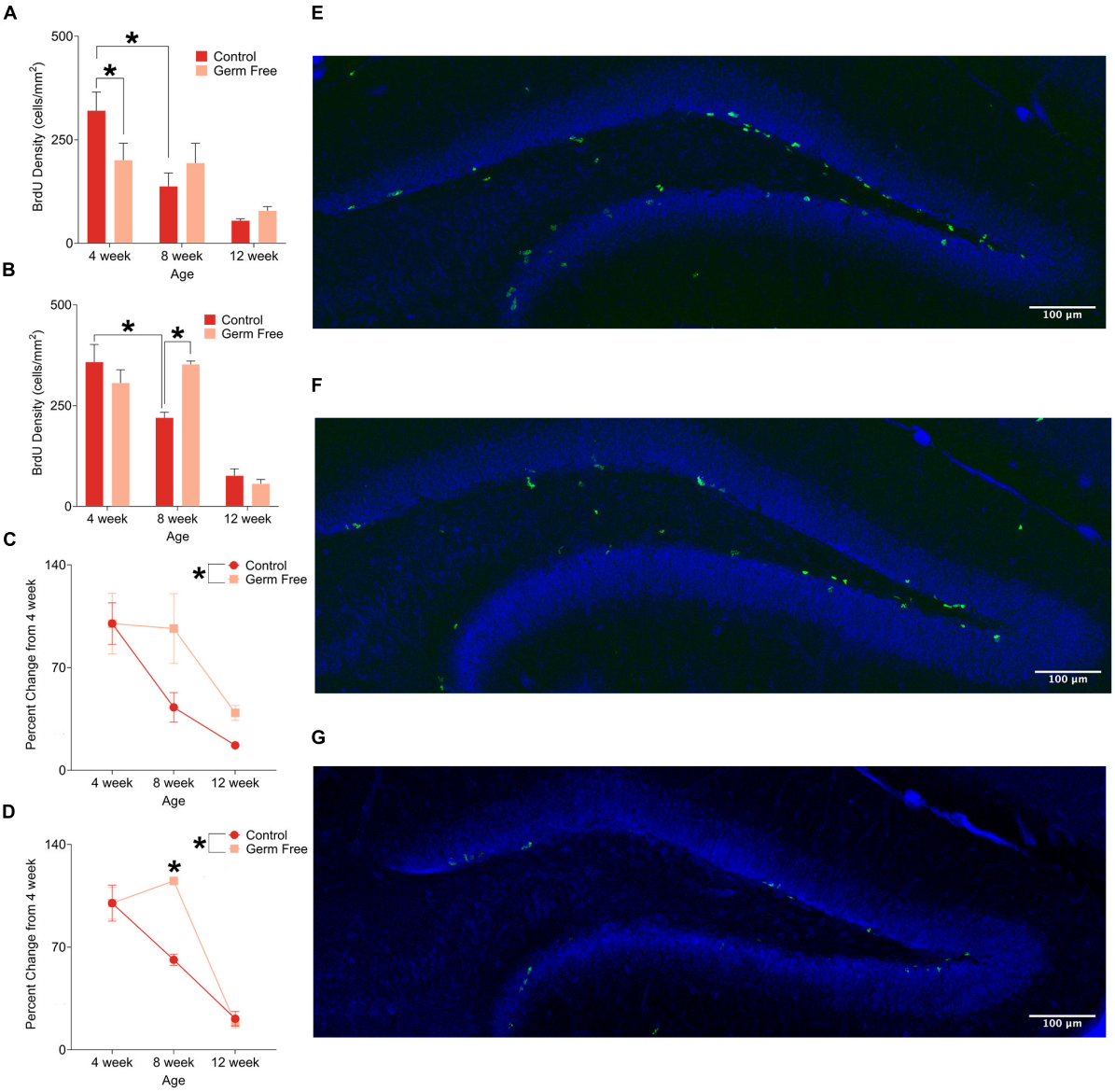

FIGURE 2 | (A) Mean (± SEM) BrdU-positive cells in the DG of male germ-free and control mice. Control mice show a clear pattern of age-related decline in cell proliferation, whereas germ-free mice show no such reduction between 4 and 8 weeks of age. Germ-free mice also show reduced cell proliferation relative to controls at 4 weeks of age. **(B)** Mean (± SEM) BrdU-positive cells in the DG of female germ-free and control mice. As with males, female control mice show an age-related decline in cell proliferation with this effect being absent in germ-free mice between 4 and 8 weeks of age. Moreover, female germ-free mice have increased cell proliferation relative to controls at 8 weeks of age. **(C)** Mean (± SEM) cell proliferation in males depicted as percent-change from the baseline (4 week old) number of BrdU-positive DG cells. Cell proliferation remains abnormally elevated in germ-free mice as they age relative to controls **(D)**. Mean (± SEM) cell proliferation in females depicted as percent-change from the baseline (4 week old) number of BrdU-positive DG cells. As with male germ-free mice, cell proliferation in female germ-free mice remains abnormally elevated relative to controls particularly at 8 weeks of age. **(E–G)** Representative photomicrographs of BrdU-positive cells (green) and propidium iodide (blue) in the DG of 4 week old **(E)**, 8 week old **(F)**, and 12 week old **(G)** control mice illustrating the age-related decrease in cell proliferation. Control male 4 week n = 10, 8 week n = 7, 12 week n = 8. Control female 4 week n = 4, 8 week, n = 5, 12 week n = 4. Germ-free male 4 week n = 5, 8 week n = 7, 12 week n = 8. Germ-free female 4 week n = 4, 8 week, n = 3, 12 week n = 3. *$p < 0.05$.

mice (**Figure 4B** and **Supplementary Figure 1**; significant main effect of Age: $F(2,28) = 11.50$, $p = 0.0002$). Based on pairwise correlations of c-fos activity (**Figure 4C**) across mice we next examined alterations in functional connectivity. Control mice exhibited a decrease in network density with increasing age (i.e., total number of functional connections in the network). The decrease in network density across age was non-linear, with the greatest change occurring between 4 and 8 weeks of age (**Figure 4C**). This indicated a refinement in the network in older mice. In germ-free mice, on the other hand, the network

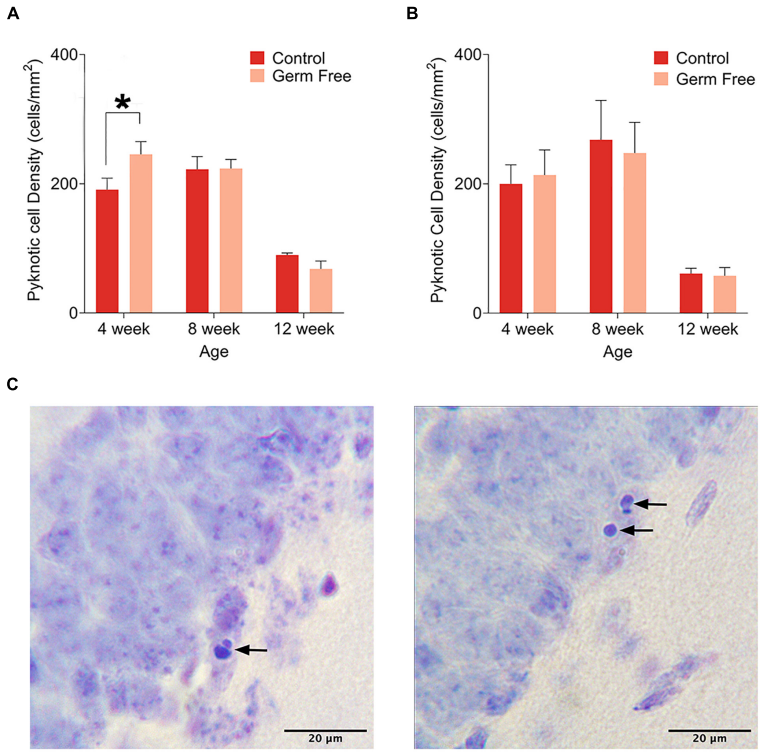

FIGURE 3 | (A) Mean (± SEM) pyknotic cells in the DG of male germ-free and control mice. The number of pyknotic cells is highest in 4 week old animals and lowest in 12 week old animals. Additionally, germ-free mice show an increased rate of cell death at 4 weeks of age. **(B)** Mean (± SEM) pyknotic cells in the DG of female germ-free and control mice. As is the case in male mice, the rate of cell death is highest in 4 week old animals and lowest in 12 week old animals. There is also a slight trend toward elevated cell death at 8 weeks of age. In contrast to male mice, female germ-free mice showed no change in the rate of cell death relative to controls. Control male 4 week $n = 10$, 8 week $n = 10$, 12 week $n = 9$. Control female 4 week $n = 4$, 8 week, $n = 4$, 12 week $n = 4$. Germ-free male 4 week $n = 9$, 8 week $n = 9$, 12 week $n = 10$. Germ-free female 4 week $n = 4$, 8 week, $n = 4$, 12 week $n = 4$. **(C)** Representative photomicrographs of DG cells with pyknotic morphology. $^*p < 0.05$.

density remained stable across ages suggesting an impairment in maturation of the hippocampal networks (**Figure 4D**). In addition, we looked specifically at the connectivity of the dentate gyrus and observed, in control mice, an age-dependent decrease in the number of regions exhibiting significantly correlated activity with the dentate gyrus (**Figures 4F–H**). However, in germ-free mice, there was a reduced number of functionally connected regions in the youngest age group and this level of connectivity was relatively constant with age (**Figures 4I–K**). Because the network properties are determined per group rather than per mouse we correlated the node degree of the DG for each group (i.e., number of functionally connected regions) with the group mean doublecortin densities to determine the relationship between neurogenesis and DG functional connectivity. We found a significant correlation between DG node degree and the number of doublecortin labeled neurons (**Figure 4E**, $r(4) = 0.83$, $p = 0.043$).

DISCUSSION

In the present experiment, we examined whether alteration of the gut microbiome exerts age-dependent changes on neurogenesis, HPC-dependent memory, and the functional connectivity of hippocampal networks. We found that the established (Kuhn et al., 1996; Amrein et al., 2004) pattern of age-related changes in neurogenesis was altered in germ-free mice, with the classic sharp decline in postnatal neurogenesis being delayed in germ-free mice relative to controls. These results are partially consistent with previous research showing that disruptions of the gut microbiome can alter neurogenesis (Ogbonnaya et al., 2015; Möhle et al., 2016). We extend these previous findings by showing that microbiome-related alteration in neurogenesis is age-dependent, with differences in neurogenesis between germ-free and controls appearing to normalize as animals age. The effects of disrupted gut microbiota on neurogenesis may therefore be most critical in younger animals.

Our results partially replicate an aspect of a previous report examining neurogenesis in germ-free mice (Ogbonnaya et al., 2015) found that neurogenesis in germ-free mice was elevated at 10 weeks of age. We found elevation of both BrdU- and DCX-positive cells specifically in female germ-free mice at 8 weeks of age. Conversely, we found decreased neurogenesis in male germ-free mice at 4 weeks of age. Overall, our findings indicate that neurogenesis is not uniformly elevated in germ-free mice and that this effect is both age-

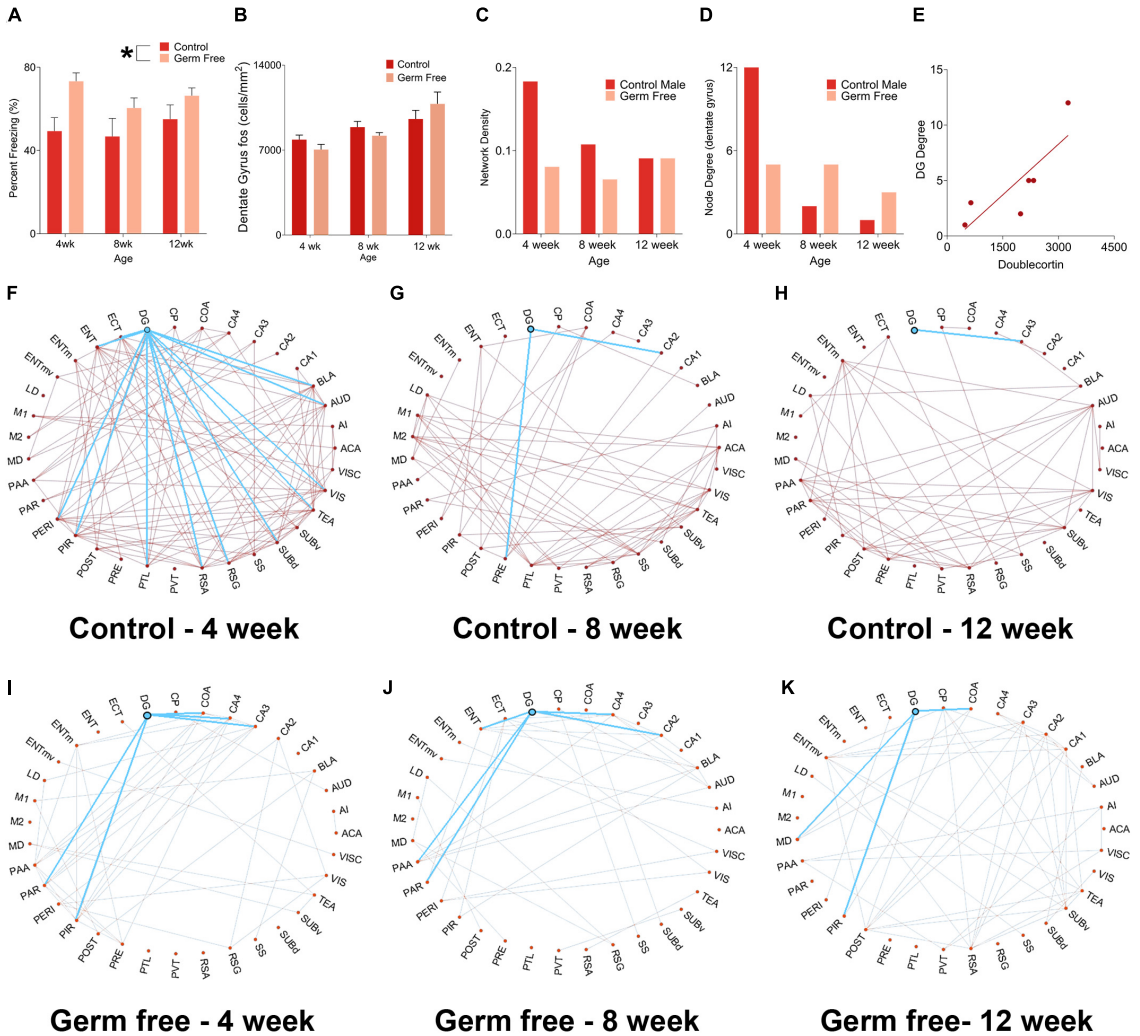

FIGURE 4 | (A) Mean (± SEM) percent freezing in contextual fear conditioning in male mice. Germ-free mice froze significantly more than control mice, indicating enhanced expression of fear memory. The effect was most pronounced in 4-week-old mice. **(B)** Mean (± SEM) c-fos-positive cells per mm^2 in the DG of germ-free and control mice. There was no difference in absolute c-fos expression between groups. However, c-fos expression increased significantly with age. **(C)** Network density, expressed as the ratio of number of connections:total possible connections, in control and germ-free mice. Control mice exhibited an age-related decrease in network density, whereas germ-free mice had an initially reduced network density which did not decrease with age. **(D)** Node degree of the DG in germ-free and control mice. Controls show a large decrease in node degree as they age, indicating a refinement of the DG network as it exhibits a progressive reduction in the number of regions it has correlated activity with. The DG of germ-free mice has an initial reduction in node degree relative to controls and, in contrast to controls, does not undergo a reduction in its node degree as a function of age, indicating that the DG of germ-free mice maintains correlated activity with a greater number of regions across age than in controls. **(E)** A scatterplot showing the correlation between DG node degree and DCX expression. The node degree of the DG is positively correlated with DCX expression, suggesting the possibility that increased neurogenesis may drive an increase in the number of regions with which the DG has correlated activity. **(F–H)** Network graphs for control mice at 4 weeks old **(F)**, 8 weeks old **(G)**, and 12 weeks old **(H)** with the functional connectivity of the DG shown in blue. Control mice show a decrease in both network density and DG node degree across ages. **(I–K)**. Network graphs for germ-free mice at 4 weeks old **(F)**, 8 weeks old **(G)**, and 12 weeks old **(H)** with the functional connectivity of the DG highlighted. Germ-free mice show no change across ages in network density or DG node degree. Control male 4 week $n = 6$, 8 week $n = 5$, 12 week $n = 7$. Germ-free male 4 week $n = 5$, 8 week $n = 7$, 12 week $n = 5$. *$p < 0.05$.

and sex-dependent. However, when we analyzed rates of neurogenesis as a percent change from baseline, germ-free status in both sexes leads to the same basic pattern of a delayed age-related reduction in neurogenesis as a result of germ-free status.

The causes of the complex pattern of results across age and sex cannot be determined from the present experiment, but the pattern of neurogenesis is similar to that of Gobinath et al. (2017). These authors treated nursing rat dams with either corticosterone (CORT) or vehicle and found that neurogenesis in the dorsal HPC of the offspring declined more slowly in both males and females and that neurogenesis was initially lower in males compared to the offspring of vehicle-treated dams. Previous research has shown that serum levels of CORT are elevated in germ-free rats (Crumeyrolle-Arias et al., 2014). Thus, the present results could potentially be explained in part by differences in

serum CORT concentration which shows similar age- and sex-dependent effects on neurogenesis (Gobinath et al., 2017).

The absence of gut microbiota causes a range of effects in addition to increasing CORT such as alterations in serotonin biosynthesis (Yano et al., 2015) and hippocampal serotonergic signaling (Clarke et al., 2013) which has been shown to play a role in regulating neurogenesis (Alenina and Klempin, 2015). Additionally, disruption of the gut microbiome has been shown to impair neurogenesis through a mechanism involving Ly6Chi monocytes (Möhle et al., 2016). The gut microbiome's role in the maturation of microglia (Thion et al., 2018), another cell type with influence on hippocampal neurogenesis (Stefani et al., 2018), could act as an additional pathway between the gut and the brain. Hence, there are multiple mechanisms that could be driving the effects we presently observe of germ-free status on neurogenesis.

To determine whether altered neurogenesis was accompanied by altered rates of cell death, we also quantified the number of pyknotic cells in the DG. Across both sexes, the rate of DG cell death was higher in younger animals than in older animals, consistent with previous findings (Sun et al., 2004; Ben Abdallah et al., 2010). Interestingly, male germ-free mice had increased cell death at 4 weeks of age whereas this effect was absent in females. Although the mechanisms underlying this sex difference are unclear, this effect could potentially be related to the decrease in neurogenesis in our 4 week old male germ-free mice, a decrease that was not present in female germ-free mice at this age. However, the pattern of cell death was largely similar between germ-free and control mice, indicating that germ-free status had much less influence on cell death than it did on neurogenesis.

We also examined the behavior of germ-free mice in contextual fear conditioning and found that germ-free mice had an increased freezing response during retention testing, indicating an enhancement of fear memory expression. The difference was greatest at 4 weeks of age with smaller increases in the freezing of 8-week-old and 12-week-old mice. Previous research in rodents has shown that, generally, learning and memory is impaired following disruption of the gut microbiome (Gareau et al., 2011; Wang et al., 2015; Fröhlich et al., 2016; Möhle et al., 2016). The results may be explained by an increase in anxiety-like behavior. Although some previous research has found that germ-free mice exhibit decreased basal anxiety (Neufeld et al., 2011), germ-free status causes heightened HPA responses to induced stress (Clarke et al., 2013; Crumeyrolle-Arias et al., 2014). Our present behavioral findings may thus be explained by an increased neuroendocrine response to footshock stress.

We also examined functional connectivity of hippocampal networks in male mice. As control animals aged, they exhibited a decrease in the density of network connections. In contrast, germ-free mice exhibited relatively stable network density at all ages examined, although network density in germ-free was lower than controls at the younger ages. When we examined the functional connectivity of the dentate gyrus specifically, we identified an age related decrease in connectivity in control mice but this trend was altered in germ-free mice. In germ-free mice, the connectivity was initially reduced in 4 week old mice but remained relatively stable between 4 and 8 weeks of age. Activity in the DG is very sparse with most cells being unresponsive to any spatial context (Jung and McNaughton, 1993; Alme et al., 2010). This limited size of the "functional" pool of DG cells may lead to a reduced opportunity for correlated activity with other brain regions and a more sparse functional network. It has been proposed that neurogenesis replenishes the functional pool of DG cells (Lisman, 2011) and, indeed, newly born DG neurons are more active than older DG neurons in response to environmental enrichment (for example Tashiro et al., 2007). Thus, the lack of a decrease in the degree of DG functional connectivity in germ-free mice may be explained by the delay in the age-related decrease of neurogenesis. In fact, we found a strong correlation between doublecortin labeling and dentate gyrus node degree which accounts for 68% of the variability in dentate connectivity. These results indicate that under control conditions, the functional network involving the DG becomes more sparse over the course of development consistent with increasing refinement and path efficiency (Bullmore et al., 2009; Rubinov and Sporns, 2010). In germ-free mice, and very possibly as a result of disrupted neurogenesis, this "refinement" of functional networks is impaired and this may form part of the mechanism of impaired cognition in germ-free animals. Importantly, the present findings are correlational, and further experiments involving ablation or enhancement of neurogenesis would be required to establish that these functional connectivity changes in germ-free mice are causally related to neurogenesis.

A secondary but noteworthy finding from our functional connectivity analysis was the lack of functional connectivity between the DG and the entorhinal cortex. Given the dense anatomical connections between these two regions and that functional connectivity is often strongly predicted by anatomical connectivity (Goñi et al., 2014), this finding is rather surprising. However, anatomical connectivity does not always predict functional connectivity (Honey et al., 2009). We are also not the first to observe little or no functional connectivity between the DG and entorhinal cortex after a 24 h retention interval in contextual fear conditioning, whereas a 4 week retention interval does evoke functional connectivity between the DG and entorhinal cortex (Wheeler et al., 2013; Vetere et al., 2017). Thus, different task parameters may result in stronger functional connectivity between the two regions.

The pattern of functional connectivity that we observed may also have been influenced by the fact that animals were tested post-BrdU injection and injection stress may have affected the pattern of neuronal activation. We used BrdU as a method for measuring cell proliferation in order to align with the methods of Ogbonnaya et al. (2015). However, all mice received BrdU injections and therefore effects of BrdU administration should be consistent across groups.

We examined the age- and sex-dependent effects of germ-free status on hippocampal neurogenesis, and functional connectivity of hippocampal networks. We show that germ-free status delays the normal age-related decline in neurogenesis and that this effect was also sex-dependent. The results show that there is an important age component to the effects of the gut microbiome on hippocampal neurogenesis. Specifically, alterations in neurogenesis as a result of microbiome dysfunction

may be most apparent in younger animals. Moreover, this effect is sexually dimorphic, with male germ-free mice initially having reduced rates of neurogenesis at 4 weeks and female germ-free mice having elevated neurogenesis at 8 weeks. We also show that the development and maturation of the DG functional network is disrupted with germ-free status, an effect that seems reflected in the lack of age-dependent changes seen in the neurogenesis of germ-free animals and represents a major, systems-level alteration in functional connectivity as a consequence of germ-free status. Given the strong correlation between neurogenesis and node degree, these results indicate that disruption of the gut microbiome may be driven to a major extent by disrupted neurogenesis. Thus, disrupted neurogenesis may be a major mechanism through which gut dysbiosis causes cognitive impairments particularly early in neurodevelopment.

DATA AVAILABILITY STATEMENT

The raw data supporting the conclusions of this article will be made available by the authors, without undue reservation, to any qualified researcher.

ETHICS STATEMENT

Experiments were conducted in accordance with the Canadian Council on Animal Care guidelines were approved by the University of Calgary Health Sciences Animal Care Committee.

AUTHOR CONTRIBUTIONS

AV, GS, and SL conducted the behavioral experiments. AV, GS, DT, SL, and AE performed the histology and image analysis. DT performed the network analysis. AV, DT, and JE performed the data analysis. AV, GS, DT, and JE conceived the experiments and wrote the manuscript.

FUNDING

Funding for this study was provided by an NSERC Discovery Grant (RGPIN-2018-05135) and Brain Canada/The Azrieli Foundation Early Career Capacity Building Grant (4709) to JE. GS received funding from the Hotchkiss Brain Institute and the Cumming School of Medicine.

ACKNOWLEDGMENTS

The authors wish to acknowledge the support of the Hotchkiss Brain Institute Advanced Microscopy Platform Core Facility.

SUPPLEMENTARY MATERIAL

The Supplementary Material for this article can be found online at: https://www.frontiersin.org/articles/10.3389/fcell.2020.00407/full#supplementary-material

REFERENCES

Achard, S., and Bullmore, E. (2007). Efficiency and cost of economical brain functional networks. *PLoS Comput. Biol.* 3:e17. doi: 10.1371/journal.pcbi.0030017

Alenina, N., and Klempin, F. (2015). The role of serotonin in adult hippocampal neurogenesis. *Behav. Brain Res.* 277, 49–57. doi: 10.1016/j.bbr.2014.07.038

Allen, A. P., Hutch, W., Borre, Y. E., Kennedy, P. J., Temko, A., Boylan, G., et al. (2016). Bifidobacterium longum 1714 as a translational psychobiotic: modulation of stress, electrophysiology and neurocognition in healthy volunteers. *Transl. Psychiatry* 6:e939. doi: 10.1038/tp.2016.191

Alme, C. B., Buzzetti, R. A., Marrone, D. F., Leutgeb, J. K., Chawla, M. K., Schaner, M. J., et al. (2010). Hippocampal granule cells opt for early retirement. *Hippocampus* 20, 1109–1123. doi: 10.1002/hipo.20810

Amrein, I., Slomianka, L., Poletaeva, I. I., Bologova, N. V., and Lipp, H. P. (2004). Marked species and age-dependent differences in cell proliferation and neurogenesis in the hippocampus of wild-living rodents. *Hippocampus* 14, 1000–1010. doi: 10.1002/hipo.20018

Arnoriaga-Rodríguez, M., and Fernández-Real, J. M. (2019). Microbiota impacts on chronic inflammation and metabolic syndrome - related cognitive dysfunction. *Rev. Endocr. Metab. Disord.* 20, 473–480. doi: 10.1007/s11154-019-09537-5

Ben Abdallah, N. M.-B., Slomianka, L., Vyssotski, A. L., and Lipp, H.-P. (2010). Early age-related changes in adult hippocampal neurogenesis in C57 mice. *Neurobiol. Aging* 31, 151–161. doi: 10.1016/j.neurobiolaging.2008.03.002

Benton, D., Williams, C., and Brown, A. (2007). Impact of consuming a milk drink containing a probiotic on mood and cognition. *Eur. J. Clin. Nutr.* 61, 355–361. doi: 10.1038/sj.ejcn.1602546

Bercik, P., Denou, E., Collins, J., Jackson, W., Lu, J., Jury, J., et al. (2011). The intestinal microbiota affect central levels of brain-derived neurotropic factor and behavior in mice. *Gastroenterology* 141, 599–609.

Berg, S., Kutra, D., Kroeger, T., Straehle, C. N., Kausler, B. X., Haubold, C., et al. (2019). ilastik: interactive machine learning for (bio)image analysis. *Nat. Methods* 16, 1226–1232. doi: 10.1038/s41592-019-0582-9

Bullmore, E., Sporns, O., Bullmore, E., Sporns, O., and Sporns, O. (2009). Complex brain networks: graph theoretical analysis of structural and functional systems. *Nat. Rev. Neurosci.* 10, 186–198. doi: 10.1038/nrn2575

Claesson, M. J., Cusack, S., O'Sullivan, O., Greene-Diniz, R., De Weerd, H., Flannery, E., et al. (2011). Composition, variability, and temporal stability of the intestinal microbiota of the elderly. *Proc. Natl. Acad. Sci. U.S.A.* 108, 4586–4591.

Clarke, G., Grenham, S., Scully, P., Fitzgerald, P., Moloney, R. D., Shanahan, F., et al. (2013). The microbiome-gut-brain axis during early life regulates the hippocampal serotonergic system in a sex-dependent manner. *Mol. Psychiatry* 18, 666–673. doi: 10.1038/mp.2012.77

Crumeyrolle-Arias, M., Jaglin, M., Bruneau, A., Vancassel, S., Cardona, A., Daugé, V., et al. (2014). Absence of the gut microbiota enhances anxiety-like behavior and neuroendocrine response to acute stress in rats. *Psychoneuroendocrinology* 42, 207–217. doi: 10.1016/j.psyneuen.2014.01.014

Dinan, T. G., and Cryan, J. F. (2017). The microbiome-gut-brain axis in health and disease. *Gastroenterol. Clin. North Am.* 46, 77–89.

Duman, R. S. (2004). Depression: a case of neuronal life and death? *Biol. Psychiatry* 56, 140–145. doi: 10.1016/j.biopsych.2004.02.033

Eckburg, P. B., Bik, E. M., Bernstein, C. N., Purdom, E., Dethlefsen, L., Sargent, M., et al. (2005). Diversity of the human intestinal microbial flora. *Science* 308, 1635–1638. doi: 10.1126/science.1110591

Epp, J. R., Silva Mera, R., Kohler, S., Josselyn, S. A., and Frankland, P. W. (2016). Neurogenesis-mediated forgetting minimizes proactive interference. *Nat. Commun.* 7, 5–12.

Falconer, E. M., and Galea, L. A. M. (2003). Sex differences in cell proliferation, cell death and defensive behavior following acute predator odor stress in adult rats. *Brain Res.* 975, 22–36. doi: 10.1016/s0006-8993(03)02542-3

Foster, J. A., and McVey Neufeld, K. A. (2013). Gut-brain axis: how the microbiome influences anxiety and depression. *Trends Neurosci.* 36, 305–312. doi: 10.1016/j.tins.2013.01.005

Fröhlich, E. E., Farzi, A., Mayerhofer, R., Reichmann, F., Jačan, A., Wagner, B., et al. (2016). Cognitive impairment by antibiotic-induced gut dysbiosis: analysis of gut microbiota-brain communication. *Brain Behav. Immun.* 56, 140–155. doi: 10.1016/j.bbi.2016.02.020

Gareau, M. G., Wine, E., Rodrigues, D. M., Cho, J. H., Whary, M. T., Philpott, D. J., et al. (2011). Bacterial infection causes stress-induced memory dysfunction in mice. *Gut* 60, 307–317. doi: 10.1136/gut.2009.202515

Gobinath, A. R., Workman, J. L., Chow, C., Lieblich, S. E., and Galea, L. A. M. (2017). Sex-dependent effects of maternal corticosterone and SSRI treatment on hippocampal neurogenesis across development. *Biol. Sex Differ.* 8, 1–13.

Goehler, L. E., Park, S. M., Opitz, N., Lyte, M., and Gaykema, R. P. A. (2008). Campylobacter jejuni infection increases anxiety-like behavior in the holeboard: possible anatomical substrates for viscerosensory modulation of exploratory behavior. *Brain Behav. Immun.* 22, 354–366. doi: 10.1016/j.bbi.2007.08.009

Goñi, J., van den Heuvel, M. P., Avena-Koenigsberger, A., Velez de Mendizabal, N., Betzel, R. F., Griffa, A., et al. (2014). Resting-brain functional connectivity predicted by analytic measures of network communication. *Proc. Natl. Acad. Sci. U.S.A.* 111, 833–838. doi: 10.1073/pnas.1315529111

Gronier, B., Savignac, H. M., Di Miceli, M., Idriss, S. M., Tzortzis, G., Anthony, D., et al. (2018). Increased cortical neuronal responses to NMDA and improved attentional set-shifting performance in rats following prebiotic (B-GOS®) ingestion. *Eur. Neuropsychopharmacol.* 28, 211–224. doi: 10.1016/j.euroneuro.2017.11.001

Honey, C. J., Sporns, O., Cammoun, L., Gigandet, X., Thiran, J. P., Meuli, R., et al. (2009). Predicting human resting-state functional connectivity from structural connectivity. *Proc. Natl. Acad. Sci. U.S.A.* 106, 2035–2040. doi: 10.1073/pnas.0811168106

Jung, M. W., and McNaughton, B. L. (1993). Spatial selectivity of unit activity in the hippocampal granular layer. *Hippocampus* 3, 165–182. doi: 10.1002/hipo.450030209

Kelly, J. R., Borre, Y., O' Brien, C., Patterson, E., El Aidy, S., Deane, J., et al. (2016). Transferring the blues: depression-associated gut microbiota induces neurobehavioural changes in the rat. *J. Psychiatr. Res.* 82, 109–118. doi: 10.1016/j.jpsychires.2016.07.019

Kuhn, H.-G., Dickinson-Anson, H., and Gage, F. H. (1996). Neurogenesis in the dentate gyrus of the adult rat: age-related decrease of neuronal progenitor proliferation. *J. Neurosci.* 16, 2027–2033. doi: 10.1523/jneurosci.16-06-02027.1996

Lisman, J. (2011). Formation of the non-functional and functional pools of granule cells in the dentate gyrus: role of neurogenesis, LTP and LTD. *J. Physiol.* 589, 1905–1909. doi: 10.1113/jphysiol.2010.201137

Lucassen, P. J., Oomen, C. A., Naninck, E. F. G., Fitzsimons, C. P., van Dam, A.-M., Czeh, B., et al. (2015). Regulation of adult neurogenesis and plasticity by (early) stress, glucocorticoids, and inflammation. *Cold Spring Harb. Perspect. Biol.* 7:a021303. doi: 10.1101/cshperspect.a021303

Lyte, M., Li, W., Opitz, N., Gaykema, R. P. A., and Goehler, L. E. (2006). Induction of anxiety-like behavior in mice during the initial stages of infection with the agent of murine colonic hyperplasia Citrobacter rodentium. *Physiol. Behav.* 89, 350–357. doi: 10.1016/j.physbeh.2006.06.019

Möhle, L., Mattei, D., Heimesaat, M. M., Bereswill, S., Fischer, A., Alutis, M., et al. (2016). Ly6Chi monocytes provide a link between antibiotic-induced changes in gut microbiota and adult hippocampal neurogenesis. *Cell Rep.* 15, 1945–1956. doi: 10.1016/j.celrep.2016.04.074

Neufeld, K. M., Kang, N., Bienenstock, J., and Foster, J. A. (2011). Reduced anxiety-like behavior and central neurochemical change in germ-free mice. *Neurogastroenterol. Motil.* 23, 255–264. doi: 10.1111/j.1365-2982.2010.01620.x

Ogbonnaya, E. S., Clarke, G., Shanahan, F., Dinan, T. G., Cryan, J. F., and O'Leary, O. F. (2015). Adult hippocampal neurogenesis is regulated by the microbiome. *Biol. Psychiatry* 78, e7–e9. doi: 10.1016/j.biopsych.2014.12.023

Pawluski, J. L., Barakauskas, V. E., and Galea, L. A. M. (2010). Pregnancy decreases oestrogen receptor alpha expression and pyknosis, but not cell proliferation or survival, in the hippocampus. *J. Neuroendocrinol.* 22, 248–257. doi: 10.1111/j.1365-2826.2010.01960.x

Rubinov, M., and Sporns, O. (2010). Complex network measures of brain connectivity: uses and interpretations. *Neuroimage* 52, 1059–1069. doi: 10.1016/j.neuroimage.2009.10.003

Sahay, A., Scobie, K. N., Hill, A. S., O'Carroll, C. M., Kheirbek, M. A., Burghardt, N. S., et al. (2011). Increasing adult hippocampal neurogenesis is sufficient to improve pattern separation. *Nature* 472, 466–470. doi: 10.1038/nature09817

Santarelli, L., Saxe, M., Gross, C., Surget, A., Battaglia, F., Dulawa, S., et al. (2003). Requirement of hippocampal neurogenesis for the behavioral effects of antidepressants. *Science* 301, 805–809. doi: 10.1126/science.1083328

Sarkar, A., Harty, S., Lehto, S. M., Moeller, A. H., Dinan, T. G., Dunbar, R. I. M., et al. (2018). The microbiome in psychology and cognitive neuroscience. *Trends Cogn. Sci.* 22, 611–636.

Savignac, H. M., Tramullas, M., Kiely, B., Dinan, T. G., and Cryan, J. F. (2015). Bifidobacteria modulate cognitive processes in an anxious mouse strain. *Behav. Brain Res.* 287, 59–72. doi: 10.1016/j.bbr.2015.02.044

Stefani, J., Tschesnokowa, O., Parrilla, M., Robaye, B., Boeynaems, J.-M., Acker-Palmer, A., et al. (2018). Disruption of the MICROGLIAL ADP receptor p2y13 enhances adult hippocampal neurogenesis. *Front. Cell. Neurosci.* 12:134. doi: 10.3389/fncel.2018.00134

Sun, W., Winseck, A., Vinsant, S., Park, O. H., Kim, H., and Oppenheim, R. W. (2004). Programmed cell death of adult-generated hippocampal neurons is mediated by the proapoptotic gene bax. *J. Neurosci.* 24, 11205–11213. doi: 10.1523/jneurosci.1436-04.2004

Tashiro, A., Makino, H., and Gage, F. H. (2007). Experience-specific functional modification of the dentate gyrus through adult neurogenesis: a critical period during an immature stage. *J. Neurosci.* 27, 3252–3259. doi: 10.1523/jneurosci.4941-06.2007

Thion, M. S., Low, D., Silvin, A., Chen, J., Grisel, P., Schulte-Schrepping, J., et al. (2018). Microbiome influences prenatal and adult microglia in a sex-specific manner. *Cell* 172, 500.e16–516.e16.

Vetere, G., Kenney, J. W., Tran, L. M., Xia, F., Steadman, P. E., Parkinson, J., et al. (2017). Chemogenetic interrogation of a brain-wide fear memory network in mice. *Neuron* 94, 363.e4–374.e4.

Wang, T., Hu, X., Liang, S., Li, W., Wu, X., Wang, L., et al. (2015). Lactobacillus fermentum NS9 restores the antibiotic induced physiological and psychological abnormalities in rats. *Benef. Microbes* 6, 707–717. doi: 10.3920/bm2014.0177

Wheeler, A. L., Teixeira, C. M., Wang, A. H., Xiong, X., Kovacevic, N., Lerch, J. P., et al. (2013). Identification of a functional connectome for long-term fear memory in mice. *PLoS Comput. Biol.* 9:e1002853. doi: 10.1371/journal.pcbi.1002853

Winocur, G., Wojtowicz, J. M., Sekeres, M. J., Snyder, J. S., and Wang, S. (2006). Inhibition of neurogenesis interferes with hippocampus-dependent memory function. *Hippocampus* 16, 296–304. doi: 10.1002/hipo.20163

Yano, J. M., Yu, K., Donaldson, G. P., Shastri, G. G., Ann, P., Ma, L., et al. (2015). Indigenous bacteria from the gut microbiota regulate host serotonin biosynthesis. *Cell* 161, 264–276. doi: 10.1016/j.cell.2015.02.047

Conflict of Interest: The authors declare that the research was conducted in the absence of any commercial or financial relationships that could be construed as a potential conflict of interest.

frontiers in Cell and Developmental Biology

ORIGINAL RESEARCH
published: 03 July 2020
doi: 10.3389/fcell.2020.00541

Plasma BDNF Levels Following Transcranial Direct Current Stimulation Allow Prediction of Synaptic Plasticity and Memory Deficits in 3×Tg-AD Mice

Sara Cocco[1], Marco Rinaudo[1], Salvatore Fusco[1,2], Valentina Longo[1], Katia Gironi[1], Pietro Renna[1], Giuseppe Aceto[1], Alessia Mastrodonato[1], Domenica Donatella Li Puma[1,2], Maria Vittoria Podda[1,2] and Claudio Grassi[1,2]**

[1] Department of Neuroscience, Università Cattolica del Sacro Cuore, Rome, Italy, [2] Fondazione Policlinico Universitario A. Gemelli IRCCS, Rome, Italy

Early diagnosis of Alzheimer's disease (AD) supposedly increases the effectiveness of therapeutic interventions. However, presently available diagnostic procedures are either invasive or require complex and expensive technologies, which cannot be applied at a larger scale to screen populations at risk of AD. We were looking for a biomarker allowing to unveil a dysfunction of molecular mechanisms, which underly synaptic plasticity and memory, before the AD phenotype is manifested and investigated the effects of transcranial direct current stimulation (tDCS) in 3×Tg-AD mice, an experimental model of AD which does not exhibit any long-term potentiation (LTP) and memory deficits at the age of 3 months (3×Tg-AD-3M). Our results demonstrated that tDCS differentially affected 3×Tg-AD-3M and age-matched wild-type (WT) mice. While tDCS increased LTP at CA3-CA1 synapses and memory in WT mice, it failed to elicit these effects in 3×Tg-AD-3M mice. Remarkably, 3×Tg-AD-3M mice did not show the tDCS-dependent increases in pCREB^{Ser133} and pCaMKII^{Thr286}, which were found in WT mice. Of relevance, tDCS induced a significant increase of plasma BDNF levels in WT mice, which was not found in 3×Tg-AD-3M mice. Collectively, our results showed that plasticity mechanisms are resistant to tDCS effects in the pre-AD stage. In particular, the lack of BDNF responsiveness to tDCS in 3×Tg-AD-3M mice suggests that combining tDCS with dosages of plasma BDNF levels may provide an easy-to-detect and low-cost biomarker of covert impairment of synaptic plasticity mechanisms underlying memory, which could be clinically applicable. Testing proposed here might be useful to identify AD in its preclinical stage, allowing timely and, hopefully, more effective disease-modifying interventions.

Keywords: Alzheimer's disease, blood biomarkers, BDNF, neuroplasticity, personalized medicine, tDCS

OPEN ACCESS

Edited by:
Stylianos Kosmidis, Columbia University, United States

Reviewed by:
Tangui Maurice, INSERM U1198 Mécanismes Moléculaires dans les Démences Neurodégénératives, France
Kei Cho, King's College London, United Kingdom
Victor Luna, Columbia University Irving Medical Center, United States

***Correspondence:**
Maria Vittoria Podda
mariavittoria.podda@unicatt.it
Claudio Grassi
claudio.grassi@unicatt.it

Specialty section:
This article was submitted to Molecular Medicine, a section of the journal Frontiers in Cell and Developmental Biology

Received: *09 April 2020*
Accepted: *09 June 2020*
Published: *03 July 2020*

Citation:
Cocco S, Rinaudo M, Fusco S, Longo V, Gironi K, Renna P, Aceto G, Mastrodonato A, Li Puma DD, Podda MV and Grassi C (2020) Plasma BDNF Levels Following Transcranial Direct Current Stimulation Allow Prediction of Synaptic Plasticity and Memory Deficits in 3×Tg-AD Mice. Front. Cell Dev. Biol. 8:541. doi: 10.3389/fcell.2020.00541

INTRODUCTION

Alzheimer's disease (AD) is a progressive neurodegenerative disorder responsible for the most common form of dementia. To date, therapeutic interventions against AD failed most likely because of late treatment initiation, i.e., when brain function and structure are already irreversibly damaged. Several lines of evidence suggest that pathogenic mechanisms of AD may affect the brain in the dark for many years owing to the brain's ability to cope with failures exploiting the so-called "cognitive reserve." Compensatory mechanisms can stave off neurodegeneration symptoms maintaining memory encoding for long time, and exhaustion of such brain ability may mark AD onset (Merlo et al., 2019). Thus, one primary goal is to detect preclinical AD, inasmuch as therapeutic interventions may have a higher success probability. Furthermore, some signs and symptoms, which manifested at early AD stages (e.g., depressive and cognitive symptoms in the measure of semantic memory and conceptual formation), are sometimes not recognized and/or mistaken for symptoms of other pathologies (Bature et al., 2017). This further stresses the need of reliable disease biomarkers, which may help early AD diagnosis.

Cognitive decline in AD is linked to pathological accumulation of amyloid-beta (Aβ) and Tau proteins and their aggregation in brain regions which are essential for memory encoding and storage, such as the medial temporal lobe and related cortical areas (Serrano-Pozo et al., 2011; Bloom, 2014). Striking evidence from preclinical studies indicates that both Aβ and Tau have detrimental effects on molecular machinery of synapses, ultimately leading to decreased hippocampal long-term potentiation (LTP), a cellular correlate of memory (Irvine et al., 2008; Kopeikina et al., 2012; Ripoli et al., 2014; Fá et al., 2016; Puzzo et al., 2017; Gulisano et al., 2018a,b). However, decreased synaptic plasticity, similarly, to memory impairment, is manifested when the pathology has already developed. Molecular pathways, underlying synaptic plasticity, potentially deregulated or vulnerable in the pre-symptomatic stage, might provide early biomarkers to predict the onset and/or progression of the disease.

Recent studies, including ours, have shown that molecular determinants of synaptic plasticity, including brain-derived neurotrophic factor (BDNF), phosphorylation of CREB at Ser133 (pCREB^{Ser133}), calcium-calmodulin kinase II (CaMKII) at Thr286 (pCaMKII^{Thr286}) and AMPA receptor GluA1 subunit at Ser831 (pGluA1^{Ser831}), are engaged and boosted by transcranial direct current stimulation (tDCS) – a non-invasive neuromodulatory technique – resulting in increased LTP and enhanced cognitive or motor functions, depending on the stimulated brain area (Ranieri et al., 2012; Rohan et al., 2015; Podda et al., 2016; Kim et al., 2017; Paciello et al., 2018; Stafford et al., 2018; Barbati et al., 2019; Yu et al., 2019; Kronberg et al., 2020).

We hypothesized that tDCS might differentially impact LTP and memory in 3×Tg-AD mice, a common model of AD, at a stage when the AD phenotype is not manifested yet (i.e., at 3 months of age, hereinafter referred to as 3×Tg-AD-3M mice) (Oddo et al., 2003; Stover et al., 2015; Belfiore et al., 2019), thus unveiling early dysfunction of synaptic plasticity mechanisms.

We found that tDCS failed to enhance LTP at CA3-CA1 synapses and memory in 3×Tg-AD-3M mice whereas it increased these parameters in age-matched wild-type (WT) mice. Of note, 3×Tg-AD-3M mice did not show increased pCREB^{Ser133}, pCaMKII^{Thr286}, and BDNF following tDCS, suggesting that these molecular changes could serve as novel early biomarkers for AD. Remarkably, BDNF responsiveness to tDCS was assessed in blood samples, providing an easy-to-detect and low-cost biomarker.

MATERIALS AND METHODS

Animals

Data of male triple transgenic AD (3×Tg-AD) mice, harboring the Swedish human APP, presenilin M146V and tauP301L mutations (Oddo et al., 2003) were compared to C57BL/6 wild-type (WT) mice (Li et al., 2018; Chakroborty et al., 2019; Joseph et al., 2019). The colonies were established in-house at the Animal Facility of the Università Cattolica from breeding pairs purchased from the Jackson Laboratory. The study was performed on 3-month-old (3M) 3×Tg-AD and WT mice (n = 78 and n = 88, respectively). Seven-month-old (7M) 3×Tg-AD mice and aged-matched WT mice (n = 21 each group) were also tested to validate the time course of AD phenotype in terms of synaptic plasticity and memory impairment in our experimental conditions. The animals were housed under a 12 h light-dark cycle at a controlled temperature (22–23°C) and constant humidity (60–75%).

Ethics Statement

All animal procedures were approved by the Ethics Committee of the Catholic University and were fully compliant with guidelines of the Italian Ministry of Health (Legislative Decree No. 26/2014) and European Union (Directive No. 2010/63/UE) legislations on animal research. All efforts were made to minimize the number of animals used and their suffering.

Electrode Implantation and tDCS Protocol

TDCS over the hippocampus was delivered using a unilateral epicranial electrode arrangement as previously described (Podda et al., 2016; Barbati et al., 2019). The active electrode consisted of a tubular plastic cannula (internal diameter 3.0 mm) filled with saline solution (0.9% NaCl) just prior to stimulation; the counter electrode was a conventional rubber-plate electrode surrounded by a wet sponge (5.2 cm^2) positioned over the ventral thorax. The center of the active electrode was positioned on the skull over the left hippocampal formation 1 mm posterior and 1 mm lateral to the bregma (Franklin and Paxinos, 1997). A unilateral arrangement was chosen, as in our previous study, to reduce the electrode contact area and to prevent currents bypassing the two juxtaposed epicranial electrodes, which might occur using a bipolar configuration. Stimulation of the left side was preferred since experimental evidence suggests that long-term

memory processing are strictly dependent on this hemisphere (Shipton et al., 2014). This electrode montage was previously shown to target the hippocampus causing neurophysiological, behavioral and molecular changes all related to this brain structure. Furthermore, no changes in BDNF levels were detected in non-stimulated areas such as the cerebellum, and tDCS of the motor cortex caused no changes in the hippocampus (see details in Podda et al., 2016). For electrode implant, animals were anesthetized by an intraperitoneal injection of a cocktail with ketamine (87.5 mg/Kg) and xylazine (12.5 mg/Kg) and temperature during surgery was maintained at 37°C. The scalp and underlying tissues were removed and the electrode was implanted using a carboxylate cement (3M ESPE, Durelon, 3M Deutschland GmbH, Germany). All animals were allowed to recover for 3–5 days before tDCS. During this period, as well as during the electrical stimulations, mice were placed in individual cages.

TDCS was applied to awake mice using a battery-driven, constant current stimulator (BrainSTIM, EMS, Italy). The current intensity was ramped for 10 s instead of switching it on and off to avoid a stimulation break effect.

A repeated tDCS protocol was used consisting in 3 single stimulation sessions (at a current intensity of 250 μA for 20 min, current density of 35.4 A/m^2) once per day, on 3 consecutive days. According to clinical and brain slice conventions (Jackson et al., 2016; Rahman et al., 2017), we applied "anodal" tDCS corresponding to a positive electric field (positive electrode over the hippocampus). Electrode montage and current density were similar to those recently adopted for rodent models and close to the recommended safety limits in rodents (Rohan et al., 2015; Podda et al., 2016; Jackson et al., 2017; Paciello et al., 2018).

On the 3 consecutive days, tDCS was performed approximately at the same time (around 10 a.m.). No abnormal behaviors were observed related to the stimulation and no morphological alterations were found in brain tissues of mice subjected to tDCS.

Three-month-old WT and 3×Tg-AD mice were randomly assigned to the following experimental groups: (i) sham mice (sham-WT-3M, sham-3×Tg-AD-3M), which underwent the same manipulations as in the "real" stimulation condition, but no current was delivered; (ii) tDCS mice (tDCS-WT-3M, tDCS-3×Tg-AD-3M), which were subjected to repeated anodal tDCS. Different groups of mice were used for each experimental test.

Electrophysiology

Field recordings were performed on hippocampal coronal slices (400 μm-thick) as previously described (Podda et al., 2008, 2016). Briefly mice were anesthetized by isoflurane inhalation (Esteve) and decapitated. The brain was rapidly removed and placed in ice-cold cutting solution (in mM: 124 NaCl, 3.2 KCl, 1 NaH_2PO_4, 26 $NaHCO_3$, 2 $MgCl_2$, 1 $CaCl_2$, 10 glucose, 2 sodium pyruvate, and 0.6 ascorbic acid, bubbled with 95% O_2-5% CO_2; pH 7.4). Slices were cut with a vibratome (VT1200S) and incubated in artificial cerebrospinal fluid (aCSF; in mM: 124 NaCl; 3.2 KCl; 1 NaH_2PO_4, 26 $NaHCO_3$, 1 $MgCl_2$, 2 $CaCl_2$, 10 glucose; 95% O_2-5% CO_2; pH 7.4) at 32°C for 60 min and then at RT until use. Slices were prepared ∼30 min after tDCS or sham stimulation protocol. Slices containing the stimulated hippocampus were used for subsequent analyses.

Slices were transferred to a submerged recording chamber and continuously perfused with aCSF (flow rate: 1.5 ml/min). The bath temperature was maintained at 30–32°C with an in-line solution heater and temperature controller (TC-344B, Warner Instruments). Identification of slice subfields and electrode positioning were performed with 4× and 40× water immersion objectives on an upright microscope (BX5IWI, Olympus) and video observation (C3077-71 CCD camera, Hamamatsu Photonics).

All recordings were made using MultiClamp 700B amplifier (Molecular Devices). Data acquisition and stimulation protocols were performed with the Digidata 1440A Series interface and pClamp 10 software (Molecular Devices). Data were filtered at 1 kHz, digitized at 10 kHz, and analyzed both online and offline.

Field recordings were made using glass pipettes filled with aCSF (tip resistance 2–5 MΩ) and placed in the stratum radiatum of the CA1 region. Field excitatory post-synaptic potentials (fEPSPs) were evoked by stimulation of the Schaffer collateral using a concentric bipolar tungsten electrode (FHC) connected to a constant current isolated stimulator (Digitimer Ltd.). The stimulation intensity that produced one-third of the maximal response was used for the test pulses and LTP induction. The fEPSP amplitude was measured from baseline to peak. The slope of the rising phase of the fEPSP was also calculated.

For LTP recordings, stable baseline responses were recorded to test stimulations (0.05 Hz for 10 min) and then a high-frequency stimulation (HFS) protocol was delivered (4 trains of 50 stimuli at 100 Hz, 500 ms each, repeated every 20 s). Responses to test pulses were recorded every 20 s for 60 min to assess LTP. LTP was expressed as the percentage of change in the mean fEPSP slope or peak amplitude normalized to baseline values (i.e., mean values for the last 5 min of recording before HFS, taken as 100%). HFS-elicited fEPSP changes in both amplitude and slope higher than 15% of baseline values were subjected to data analysis.

Memory Test

Object recognition test, also known as novel object recognition (NOR) test and Morris water maze (MWM) test were used to assess non-spatial (i.e., recognition) and spatial memory, respectively. These tests were chosen since they are the most widely used and standardized tests of hippocampal-dependent forms of learning and memory (Vorhees and Williams, 2014; Cohen and Stackman, 2015).

Behavioral tests were carried out from 9 a.m. to 4 p.m. and data were blindly analyzed using an automated video tracking system (Any-Maze).

The NOR protocol lasted 3 consecutive days including a familiarization session, a training session and a test session. On the first day, animals were familiarized for 10 min to the test arena (45 cm×45 cm). On the second day (training session), they were allowed to explore two identical objects placed symmetrically in the arena for 10 min. On the third day (test session), a new object replaced one of the old objects. Animals were allowed to explore for 10 min and a preference index, calculated as the ratio between time spent exploring the novel object and time spent

exploring both objects, was used to measure recognition memory (Fusco et al., 2019).

MWM was performed as previously described (Podda et al., 2014, 2016). A circular plastic pool (127 cm in diameter) filled with water colored with nontoxic white paint, to obscure the location of an hidden platform, was used as experimental apparatus. The pool was ideally separated into four equal quadrants (NE, corresponding to the target quadrant, SE, NW, and SW) and the platform (10 cm×10 cm) was placed at the center of the target quadrant. Visual cues were placed on the walls around the pool to orient the mice. Animals were trained for 4 days, six times a day and the probe test was administered 24 h after the last training day. Starting positions were varied daily and latencies to reach the platform were recorded. In the probe test, the platform was removed and time spent in the target quadrant was measured (60 s of test duration).

According to published protocols, the following exclusion criteria were applied: total exploration time < 5 s in the NOR test and floating behavior during training (i.e., not actively searching for the platform) in the MWM test. No animal met exclusion criteria and all results of behavioral studies were included in data analysis.

Western Immunoblot

Total proteins were extracted from the stimulated hippocampus of control and tDCS-mice sacrificed 2 h after stimulation, using ice cold RIPA buffer [Pierce; 50 mM Tris, 150 mM NaCl, 1 mM EDTA, 1% DOC, 1% Triton X-100, 1% SDS, and 1× protease, phosphatase-1, and phosphatase-2 inhibitor cocktails (Sigma)]. Tissues were incubated for 15 min on ice with occasional vortexing and the lysate was spun down at 22,000×g for 15 min, 4°C, and 2 μl aliquot of the supernatant was assayed to determine the protein concentration (microBCA kit, Pierce). SDS-PAGE reducing sample buffer was added to the supernatant, and samples were heated to 95°C for 5 min. Protein lysates (40 μg) were loaded onto 10% or 8% Tris-glycine polyacrylamide gels for electrophoretic separation. Precision Plus Protein Dual Color Standards (Bio-Rad) were used as molecular mass standards. Proteins were then transferred onto nitrocellulose membranes at 330 mA for 2 h at 4°C in transfer buffer containing 25 mM Tris, 192 mM glycine and 20% methanol. Membranes were incubated for 1 h with blocking buffer (5% skim milk in TBST), and then incubated overnight at 4°C with primary antibodies directed against one of the following proteins: pCREB^{Ser133}, CREB, pCaMKII^{Thr286}, CaMKII, and GAPDH (**Supplementary Table 1**). After three 10 min rinses in TBST, membranes were incubated for 2 h at RT with HRP-conjugated secondary antibodies (**Supplementary Table 1**). The membranes were then washed, and the bands were visualized with an enhanced chemiluminescence detection kit (GE Healthcare, United Kingdom). Protein expression was evaluated and documented using UVItec Cambridge Alliance. Experiments were performed in triplicate.

ELISA Measurements

Blood samples were collected from the retro-orbital plexus with sterile glass Pasteur pipettes. Samples were taken before and 1 week after tDCS. After centrifugation, plasma was separated and stored at −80°C until further use. Plasma levels of BDNF were determined using commercially available ELISA kits (Immunological Sciences). The assay was performed according to the manufacturer's instructions on samples collected from 4 animals per group, and each sample was analyzed in duplicate.

Statistical Analysis

Sample sizes were chosen with adequate statistical power (0.8) according to results of prior pilot data sets or studies, including our own using similar methods or paradigms. Sample estimation and statistical analysis were performed using the SigmaPlot 14.0 software. Data were first tested for equal variance and normality (Shapiro-Wilk test) and then the appropriate statistical tests were chosen. The statistical tests used [i.e., one-way ANOVA, one-way ANOVA for repeated measures (RM), Friedman RM ANOVA on Ranks, two-way ANOVA, two-way RM ANOVA] are indicated in the main text and in the corresponding figure legends for each experiment. *Post hoc* multiple comparisons were performed with Bonferroni correction. The level of significance was set at 0.05. Results are presented as mean ± SEM. Analyses were performed blinded.

RESULTS

Characterization of Memory and Synaptic Plasticity Impairments in 3×Tg-AD Mice

The objective of the study was to test whether anodal tDCS can be exploited to unmask covert impairment of brain plasticity mechanisms in 3×Tg-AD mice before synaptic plasticity and memory deficits are clearly manifested in this AD mouse model, with the ultimate goal to identify early neurophysiological and molecular biomarkers allowing to predict disease onset.

Our first step was to characterize the time course of the 3×Tg-AD mouse phenotype in our experimental conditions, given that some variability has been reported in literature (Belfiore et al., 2019). Specifically, memory and LTP were assessed in 3 and 7 months old AD mice, chosen as putative pre-symptomatic and AD models, respectively. Different cohorts of mice were used for 3 and 7 months.

Results were compared to those obtained in age-matched WT animals. We found that, at 3 months of age, 3×Tg-AD mice did not exhibit any impairment in recognition and spatial memory, as assessed by NOR and MWM tests, respectively (**Figures 1A–C**). In particular, in the NOR test the preference index was comparable in 3×Tg-AD and age-matched WT mice (63.8 ± 1.7% and 65.7 ± 1.7%, respectively, $n = 9$ for each group; $P = 0.40$, one-way ANOVA; **Figure 1A**; exploration time: WT-3M mice, novel object (NO) 11.3 ± 1 s, familiar object (FO) 5.9 ± 0.5 s; 3×Tg-AD-3M mice, NO 11.5 ± 2.6 s, FO 6.4 ± 1.3 s). Similarly, in the acquisition session of the MWM, all mice successfully acquired the task with latency to reach the platform decreasing progressively across training days [main effect of days: $F_{(3,48)} = 34.13$, $P < 0.001$, two-way RM ANOVA] and no

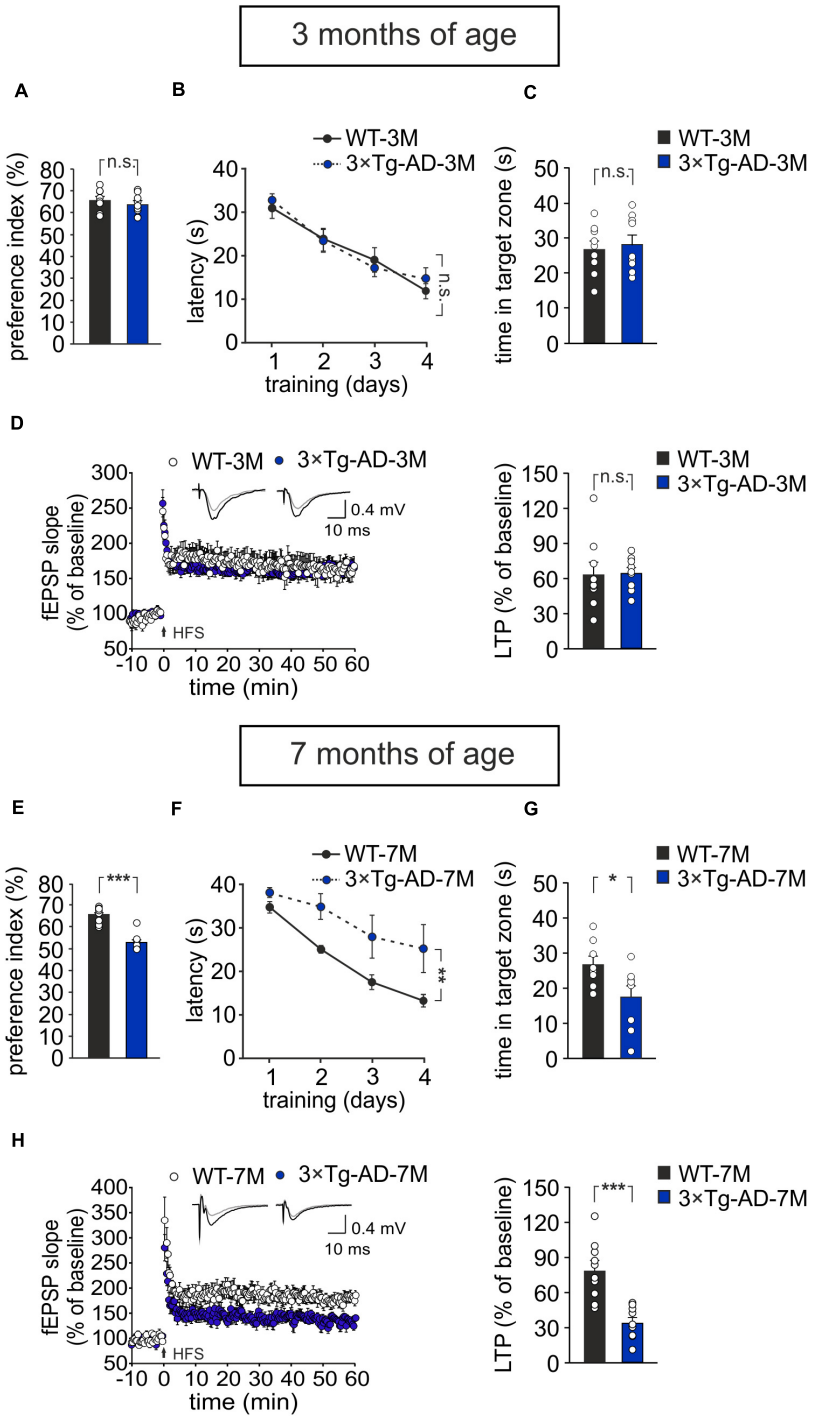

FIGURE 1 | Age-dependent pathological memory and synaptic plasticity changes in 3×Tg-AD mice. **(A–D)** 3-month-old 3×Tg-AD mice did not differ from age-matched WT mice in: **(A)** the preference toward the novel object in the NOR test (n = 9 mice for each group; P = 0.40, one-way ANOVA); **(B)** the latency to platform in the training phase of the MWM test (n = 9 mice for each group; P = 0.73, two-way RM ANOVA) and **(C)** the time spent in the target quadrant during the probe test performed on day 5 of MWM (P = 0.66, one-way ANOVA); **(D)** the magnitude of LTP at hippocampal CA3-CA1 synapses (n = 9 slices from 5 3×Tg-AD-3M mice; n = 9 slices from 6 WT-3M mice; P = 0.89, one-way ANOVA). Time course shows LTP at CA3-CA1 synapses induced by HFS (4 trains of 50 stimuli at 100 Hz for 500 ms repeated every 20 s) delivered at time 0 (arrow). Results are expressed as percentages of baseline fEPSP slope (= 100%). Insets show representative fEPSPs at baseline (gray line) and during the last 5 min of LTP recording (black line). Bar graphs compare LTP observed during the last 5 min of recording. **(E–H)** Compared to aged-matched WT mice, 7-month-old 3×Tg-AD mice showed significant decreases in: **(E)** preference index in the NOR test ($P < 0.001$); **(F)** latency to platform in the training phase of the MWM test (n = 8 mice for each group; P = 0.009, two-way RM ANOVA) and **(G)** time spent in the target quadrant during the probe test of MWM (P = 0.032, one-way ANOVA); **(H)** LTP (n = 10 slices from 5 3×Tg-AD-7M mice; n = 10 slices from 5 WT-7M mice, P = 0.0001, one-way ANOVA). Data are expressed as mean ± SEM. *$P < 0.05$; **$P < 0.01$; ***$P < 0.001$; n.s., not significant.

significant differences between WT-3M and 3×Tg-AD-3M mice in all trials ($n = 9$ for each group; $P = 0.73$, two-way RM ANOVA; **Figure 1B**) were noted. In the probe test, the time spent in the target quadrant was similar in 3×Tg-AD-3M and WT-3M mice (28.6 ± 2.8 s vs. 27.0 ± 2.5 s, respectively, $P = 0.66$, one-way ANOVA; **Figure 1C**). Both groups spent significantly more time in the target quadrant compared to random quadrant occupancy [i.e., 15 s; WT-3M mice, $F_{(1,19)} = 16.38$, $P = 0.0006$; 3×Tg-AD-3M mice, $F_{(1,19)} = 18.50$, $P = 0.0003$, one-way ANOVA]. Memory deficits were, instead, manifested in 7-month-old 3×Tg-AD mice (3×Tg-AD-7M). In the NOR test, they showed a lower preference index than age-matched WT mice (53.2 ± 1.5% vs. 65.6 ± 1.4% in WT-7M mice; $n = 8$ for each group; $P < 0.001$, one-way ANOVA; **Figure 1E**; exploration time: WT-7M mice, NO 9.2 ± 1.2 s, FO 4.9 ± 0.7 s; 3×Tg-AD-7M, NO 6.2 ± 1.5 s, FO 5.5 ± 1.3 s). In the acquisition session of the MWM, all mice displayed decreased latency to reach the hidden platform over training days [main effect of days: $F_{(3,42)} = 14.72$, $P < 0.001$, two-way RM ANOVA, but 3×Tg-AD-7M mice took longer time to find the platform than WT-7M mice ($n = 8$ for each group; $P = 0.009$, two-way RM ANOVA; **Figure 1F**). In the probe test, 3×Tg-AD-7M mice explored the target quadrant less than controls (17.4 ± 3.5 s vs. 27.0 ± 2.5 s in WT-7M mice; $P = 0.032$, one-way ANOVA; **Figure 1G**). Finally, WT-7M mice spent significantly more time in the target quadrant compared to random quadrant occupancy while 3×Tg-AD-7M mice failed to do so [WT-7M mice, $F_{(1,18)} = 16.17$, $P = 0.0008$; 3×Tg-AD-7M mice, $F_{(1,18)} = 0.85$, $P = 0.36$, one-way ANOVA].

As expected, behavioral data were paralleled by electrophysiological data showing a significant reduction of LTP at CA3–CA1 hippocampal synapses in brain slices from 3×Tg-AD-7M mice [34.37 ± 4.36% ($n = 10$ slices from 5 mice) vs. 78.85 ± 8.09% ($n = 10$ slices obtained from 5 WT-7M mice); $P = 0.0001$, one-way ANOVA; **Figure 1H**], whereas LTP was not significantly different in transgenic and WT mice at 3 months of age [65.11 ± 4.86% ($n = 9$ slices from 5 3×Tg-AD-3M mice) vs. 63.68 ± 10.74% ($n = 9$ slices from 6 WT-3M mice); $P = 0.89$, one-way ANOVA; **Figure 1D**]. Data reported above refer to analysis of fEPSP slope. A similar picture emerged when LTP was assessed by analyzing fEPSP amplitude (**Supplementary Figures 1A,B**). In agreement with our previous result (Leone et al., 2019). Western immunoblot experiments, performed with the 6E10 antibody recognizing human Aβ, revealed Aβ oligomers in hippocampal lysates of 3×Tg-AD-7M mice (**Supplementary Figure 1C**). A faint band was observed at the same molecular weight in tissues from 3×Tg-AD-3M.

Altogether these data indicate that, at 3 months of age, 3×Tg-AD mice do not show synaptic plasticity and memory deficits and, therefore, they are a suitable model of a pre-symptomatic AD stage to test our hypothesis.

Anodal tDCS Fails to Enhance Recognition and Spatial Memory in 3×Tg-AD-3M Mice

We then compared memory performances of 3×Tg-AD-3M and age-matched WT mice subjected to a protocol of triple tDCS or sham stimulation. Consistently with our previous findings (Podda et al., 2016), WT mice subjected to tDCS showed a greater preference toward the novel object than sham-stimulated mice [preference index: 70.7 ± 1.1% ($n = 10$) and 63.5 ± 1.8% ($n = 9$), respectively, $P = 0.001$, one-way ANOVA; **Figure 2A**]. As expected from data reported above, sham-3×Tg-AD-3M mice showed intact recognition memory [preference index: 61.0 ± 2.1% ($n = 9$), $P = 0.36$ vs. sham-WT-3M mice, one-way ANOVA; **Figure 2A**]. Of note, preference for the novel object was not increased by tDCS in 3×Tg-AD-3M mice [preference index: 64.6 ± 4.3% ($n = 8$), $P = 0.42$ vs. sham-3×Tg-AD-3M mice ($n = 9$) one-way ANOVA; **Figure 2A**]. Similar results were obtained with MWM, as shown in **Figures 2B,C**. In the acquisition session of the MWM, all mice successfully acquired the task with latency to reach the platform decreasing progressively across training days

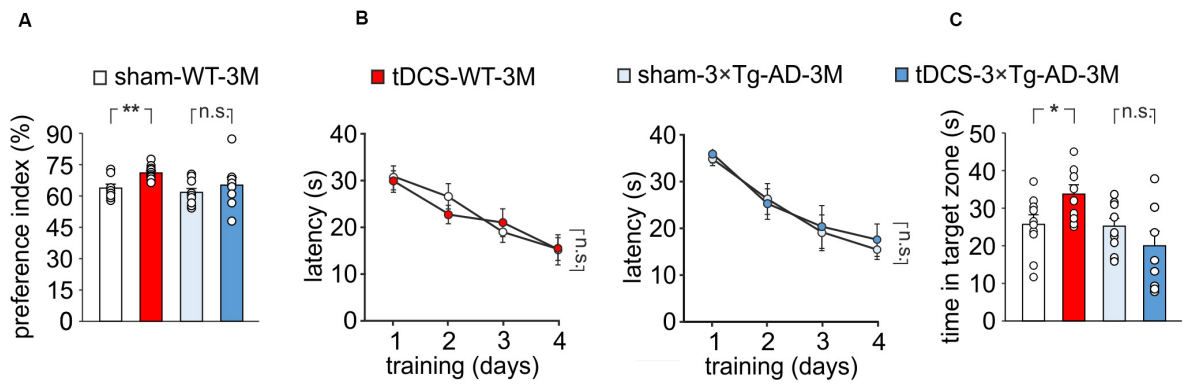

FIGURE 2 | Effect of tDCS on memory in 3×Tg-AD-3M and WT-3M mice. **(A–C)** Memory was enhanced by tDCS in 3-month-old WT but not in 3×Tg-AD-3M mice, as shown by: **(A)** preference toward the novel object in NOR test ($n = 9$ sham-WT-3M mice vs. $n = 10$ tDCS-WT-3M mice, $P = 0.001$; $n = 9$ sham-3×Tg-AD-3M mice vs. $n = 8$ tDCS-3×Tg-AD-3M mice, $P = 0.42$, one-way ANOVA); **(B)** latency to reach the platform in the training phase of the MWM test ($n = 10$ sham-WT-3M mice and $n = 9$ tDCS-WT-3M mice, $P < 0.001$; $n = 9$ sham-3×Tg-AD-3M mice and $n = 9$ tDCS-3×Tg-AD-3M mice, $P < 0.001$, two-way RM ANOVA across training days) and **(C)** time spent in the target quadrant during probe test (sham-WT-3M mice vs. tDCS-WT-3M mice, $P = 0.029$; sham-3×Tg-AD-3M mice vs. tDCS-3×Tg-AD-3M mice; $P = 0.24$, one-way ANOVA). Data are expressed as mean ± SEM. $^*P < 0.05$; $^{**}P < 0.01$; n.s., not significant.

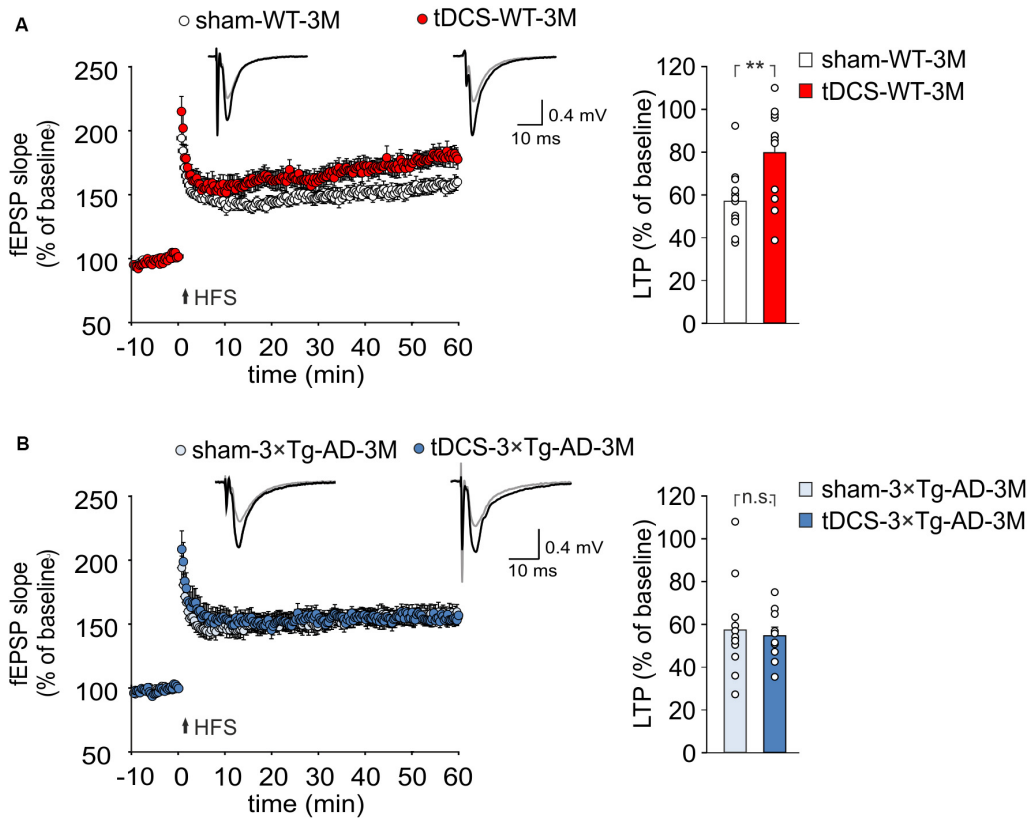

FIGURE 3 | tDCS differentially impacts hippocampal LTP in 3×Tg-AD-3M and WT mice. **(A,B)** Time course of LTP at CA3-CA1 synapses induced by HFS delivered at time 0 (arrow). Results are expressed as percentages of baseline fEPSP slope (= 100%). Insets show representative fEPSPs at baseline (gray line) and during the last 5 min of LTP recording (black line). Bar graphs compare LTP observed during the last 5 min of recording. **(A)** Slices obtained from tDCS-WT-3M mice (n = 12 slices from 7 mice) showed enhanced LTP compared to sham-WT-3M mice (n = 12 slices from 9 mice, P = 0.007, one-way ANOVA). **(B)** tDCS failed to enhance LTP in 3×Tg-AD-3M mice (n = 10 slices from 5 tDCS mice; n = 12 slices from 5 sham mice, P = 0.71; one-way ANOVA). Data are expressed as mean ± SEM; $^{**}P < 0.01$; n.s., not significant.

[WT-3M mice: main effect of days: $F_{(3,51)} = 23.85$, $P < 0.001$, two-way RM ANOVA; 3×Tg-AD-3M mice: main effect of days: $F_{(3,48)} = 21.33$, $P < 0.001$, two-way RM ANOVA; **Figure 2B**], with no significant differences between sham and tDCS in both groups (WT-3M mice: $P = 0.81$; 3×Tg-AD-3M: $P = 0.71$, two-way RM ANOVA). In the probe test, WT mice, but not 3×Tg-AD-3M mice, showed improvement following tDCS [tDCS-WT-3M, 33.5 ± 2.5 s (n = 9) vs. 25.5 ± 2.5 s (n = 10) sham-WT-3M; P = 0.029, one-way ANOVA; tDCS-3×Tg-AD-3M, 19.8 ± 3.9 s (n = 9) vs. 24.9 ± 2.2 s (n = 9) sham-3×Tg-AD-3M; P = 0.24, one-way ANOVA; **Figure 2C**).

Anodal tDCS Fails to Enhance LTP in 3×Tg-AD-3M Mice

TDCS effects on memory have been reportedly associated to increased hippocampal LTP (Podda et al., 2016; Yu et al., 2019). We therefore asked whether the behavioral unresponsiveness to tDCS of 3×Tg-AD-3M mice was associated to the lack of tDCS effects on synaptic plasticity. FEPSP slope was measured in the CA1 area after standard HFS of Schaffer collaterals and LTP was studied in slices from WT and 3×Tg-AD-3M mice subjected to tDCS or sham stimulation. Sixty min after HFS, slices from tDCS-WT mice showed significantly greater LTP than slices from sham-WT mice [79.65 ± 6.58% (n = 12 slices from 7 tDCS mice) vs. 57.0 ± 4.4% (n = 12 slices from 9 sham mice); P = 0.007, one-way ANOVA; **Figure 3A** and **Supplementary Figure 2A**]. Conversely, LTP was not increased by tDCS in 3×Tg-AD-3M mice [54.71 ± 3.89% (n = 10 slices from 5 tDCS mice) vs. 57.49 ± 6.23% (n = 12 slices from 5 sham mice); P = 0.71, one-way ANOVA; **Figure 3B** and **Supplementary Figure 2B**], demonstrating that in these mice the cellular correlate of memory is also resistant to the boosting action of tDCS.

Molecular Determinants of Plasticity Are Resistant to tDCS Boosting Effects in 3×Tg-AD-3M Mice

The above reported results demonstrate that, before the AD-like phenotype is manifested, 3×Tg-AD mice – despite normal memory and hippocampal LTP – exhibit decreased responsiveness to the boosting action of tDCS. The reduced response to tDCS might result from initial dysfunction

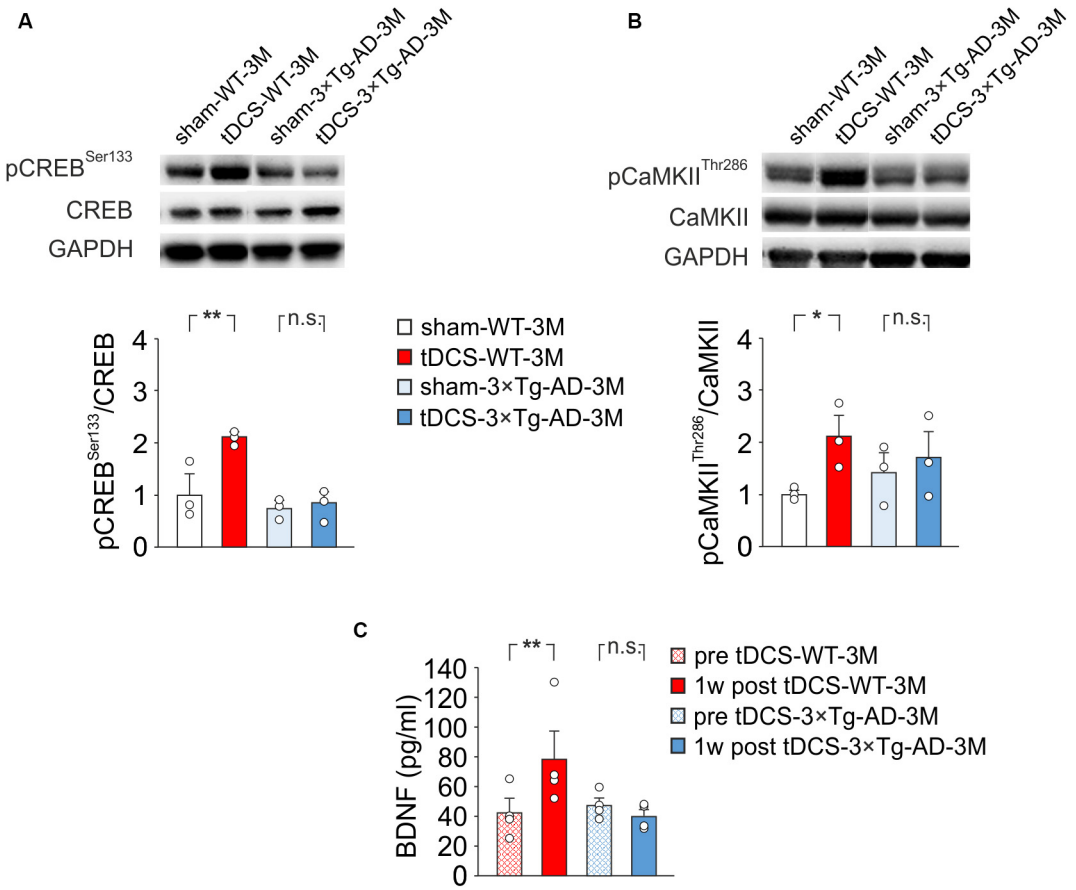

FIGURE 4 | Molecular changes in 3×Tg-AD-3M and WT-3M mice following tDCS. Representative immunoblots revealed increased pCREB^{Ser133} **(A)** and pCaMKII^{Thr286} **(B)** following tDCS in WT-3M mice but not in 3×Tg-AD-3M mice. Bar graphs in the lower panel show results of densitometric analyses on all samples (n = 3 mice for each group; pCREB^{Ser133}, P = 0.003 tDCS-WT-3M vs. sham-WT-3M; P = 0.77 tDCS-3×Tg-AD-3M vs. sham-3×Tg-AD-3M; pCaMKII^{Thr286}, P = 0.045 tDCS-WT-3M vs. sham-WT-3M; P = 0.58 tDCS-3×Tg-AD-3M vs. sham-3×Tg-AD-3M two-way ANOVA, Bonferroni *post hoc*) normalized to both the corresponding total protein levels and GAPDH. **(C)** Plasma BDNF levels were measured before (pre) and 1 week after (1 w post) tDCS. BDNF was increased by tDCS in WT mice (P = 0.031, one-way RM ANOVA) but not in 3×Tg-AD-3M mice (P = 0.12, Friedman RM ANOVA on Ranks) (n = 4 mice for each group). Data are expressed as mean ± SEM. *P < 0.05; **P < 0.01; n.s., not significant.

of the molecular pathways underlying plasticity that are challenged by tDCS.

To test this hypothesis, we performed molecular analyses on hippocampi and blood samples from WT and 3×Tg-AD-3M mice subjected to tDCS or sham stimulation. Our analyses were focused on known upstream mechanisms of tDCS action, such as Ca^{2+}-dependent phosphorylation of CREB at Ser133 and of CaMKII at Thr286, and a pivotal downstream effector, i.e., the neurotrophin BDNF (Podda et al., 2016; Kim et al., 2017; Paciello et al., 2018; Stafford et al., 2018; Barbati et al., 2019).

Our previous observations indicated that tDCS induced CREB activation in the hippocampus 2 h after stimulation (Podda et al., 2016). Accordingly, immunoblot analyses revealed that, 2 h after the end of the last tDCS session, hippocampi of WT mice (n = 3) showed increased levels of pCREB^{Ser133} [+110% vs. sham-WT-3M mice (n = 3), P = 0.003; two-way ANOVA, Bonferroni *post hoc*; **Figure 4A**] and pCaMKII^{Thr286} (+109% vs. sham-WT-3M mice, P = 0.045 two-way ANOVA, Bonferroni *post hoc*; **Figure 4B**]. Intriguingly, these post-translational modifications were not observed in 3×Tg-AD-3M mice following tDCS (pCREB^{Ser133}: +11% vs. sham-3×Tg-AD-3M mice; P = 0.77; pCaMKII^{Thr286}: +19% vs. sham-3×Tg-AD-3M mice; P = 0.58; two-way ANOVA, Bonferroni *post hoc*; n = 3 mice each group; **Figures 4A,B**).

We previously reported that enhanced pCREB^{Ser133} following tDCS increases BNDF expression in the hippocampus by epigenetic regulation of *Bdnf* promoter I (Podda et al., 2016), and similar results were observed in auditory and motor cortices exposed to tDCS (Paciello et al., 2018; Barbati et al., 2019). We, therefore, hypothesized that tDCS could differentially impact BNDF expression in WT-3M and 3×Tg-AD-3M mice. Given that changes of brain BDNF expression are reflected in blood (Laske et al., 2006; Brunoni et al., 2015), we asked whether assessment of changes in plasma BDNF following tDCS could be a reliable biomarker of altered brain plasticity in AD. Blood samples used for BDNF testing were collected from each studied

mice before starting the tDCS and 1 week after the completion of the tDCS protocol. This time point was chosen based on the results of a meta-analysis showing that increased plasma BDNF levels are more frequently observed some days after different protocols of non-invasive brain stimulation (NIBS) than soon after (Brunoni et al., 2015), and our previous studies demonstrated enhanced BDNF expression in the hippocampus 1 week after tDCS (Podda et al., 2016).

Remarkably, we found that plasma BNDF levels were significantly increased after tDCS in WT-3M (78.5 ± 20.2 vs. 42.3 ± 9.9 pg/ml pre-stimulation, $n = 4$ mice; $P = 0.031$, one-way RM ANOVA) but not in 3×Tg-AD-3M mice (40.1 ± 4.9 vs. 47.8 ± 5.0 pg/ml pre-stimulation, $n = 4$ mice; $P = 0.12$, Friedman RM ANOVA on Ranks; **Figure 4C**).

Our findings indicate that in 3×Tg-AD-3M mice molecular determinants of plasticity such as CREB, CaMKII and BDNF are resistant to the boosting effects of tDCS. More importantly, the early impairment of molecular machinery underlying synaptic plasticity and memory in 3×Tg-AD-3M mice can be detected by BDNF blood testing following tDCS.

DISCUSSION

AD is the most common form of dementia in elderly, characterized by a severe and progressive cognitive decline. So far, no effective treatments have been identified, but accumulating evidence suggests that therapeutics might work best if started at an early disease stage. The preclinical and prodromal phases of AD are considered promising time-windows for disease-modifying interventions (Galluzzi et al., 2016; Joe and Ringman, 2019). Therefore, early diagnosis is critical to successfully implement effective treatments.

The diagnosis of preclinical and prodromal AD is presently performed using cerebrospinal fluid analysis, neuroimaging investigations and neuropsychological testing (Lashley et al., 2018). Recently, graph theory analysis of brain connectivity from EEG signals combined with apolipoprotein E genotyping has been proposed to distinguish prodromal to AD from non-prodromal mild cognitive impairment (MCI) subjects (Vecchio et al., 2018). While these diagnostic approaches are valid and reliable, they cannot be employed for a wide ranging screening of persons at risk of AD, because they are invasive, expensive and require equipment and expertise usually only available in specialized hospitals.

Looking for an easy, non-invasive, low-cost and affordable method to screen populations at risk of AD, we investigated brain plasticity responses to tDCS in an AD mouse model before phenotype manifestation. This approach unveiled early electrophysiological and molecular dysfunction leading to the unresponsiveness of 3×Tg-AD-3M mice to tDCS boosting effects on memory, LTP and molecular determinants of synaptic plasticity.

Our data suggest that the assessment of plasticity-related molecular biomarkers before and after tDCS could represent a novel approach to predict AD onset and progression. Of particular relevance for a translational point of view, are the differential effects of tDCS on plasma BDNF levels.

In this study 3-month-old 3×Tg-AD mice were used as a model of preclinical AD. These mice showed normal memory, as their performance in the NOR and MWM tests was similar to that of age-matched WT mice. At 3 months of age LTP values were also comparable in WT and transgenic mice. Impaired memory and LTP were, instead, observed in AD mice at 7 months of age. Although a certain degree of 3×Tg-AD mouse model heterogeneity has been reported regarding the onset and progression of cognitive deficits, the timeline of the AD phenotype, in our experimental conditions, is in agreement with literature (Chakroborty et al., 2019; Joseph et al., 2019).

The NIBS techniques have recently gained considerable attention as promising approaches to slow the progression of AD (Rajji, 2019a). Despite encouraging data, conflicting results have been reported so far, likely due to different study designs, patient selection criteria, populations, or sample sizes, therefore, the efficacy of NIBS in AD is still uncertain (Rajji, 2019b). As far as animal models are concerned, tDCS failed to rescue learning and memory deficits in 3×Tg-AD mice when the phenotype is manifested (i.e., >6 months of age) (Gondard et al., 2019).

We propose to use tDCS in AD differently, namely, as a tool to probe and challenge plasticity pathways in the pre-symptomatic phase of the disease in order to unveil their earliest alterations.

Indeed, several studies, including our own, indicated that molecular determinants of plasticity and, particularly, the neurotrophin BDNF, are engaged and boosted by anodal tDCS, leading to enhanced plasticity and memory (Rohan et al., 2015; Podda et al., 2016; Kim et al., 2017; Cocco et al., 2018; Paciello et al., 2018; Stafford et al., 2018; Barbati et al., 2019; Kronberg et al., 2020).

Consistently, we found that 3-month-old WT mice, subjected to a daily session of anodal tDCS for three consecutive days, showed enhanced hippocampus-dependent recognition and spatial memory as assessed by NOR and MWM tests as well as enhanced LTP – the cellular underpinning of memory (Bliss and Collingridge, 1993). Interestingly enough, none of these effects was seen in 3×Tg-AD-3M mice.

We, therefore reasoned that the lack of tDCS effects on LTP and memory in 3×Tg-AD-3M mice might be due to the unsuccessful recruitment of plasticity-related pathways. We previously identified the signaling cascade engaged by tDCS in the hippocampus, including increased CREB phosphorylation at Ser133 that triggers epigenetic modifications relying on CREB binding to the *Bdnf* promoter I and recruitment of the histone acetyltranferase CREB-binding protein leading to enhanced acetylation at lysine 9 on *Bdnf* promoter I and increased BDNF expression. Blockade of H3 acetylation as well as of BDNF-specific TrkB receptors hindered tDCS effects on LTP and memory. Collectively, data summarized above suggested a causal link among the tDCS-induced increases in: (i) CREB phosphorylation; (ii) BDNF expression; (iii) synaptic plasticity; and (iv) memory (Podda et al., 2016). It has also been hypothesized that molecular events underlying tDCS effects are initiated by increased Ca^{2+} signaling via

NMDAR and voltage-gated calcium channel activation (Pelletier and Cicchetti, 2014; Rohan et al., 2015). Indeed, Ca^{2+}-dependent intracellular responses observed following tDCS include increased phosphorylation of CREB and CaMKII along with nitric oxide synthase activation (Kim et al., 2017; Cocco et al., 2018; Barbati et al., 2019). In keeping with these data, our Western immunoblot analyses showed enhanced $pCREB^{Ser133}$ and $pCaMKII^{Thr286}$ in tDCS-WT-3M mice. Of relevance, the lack of tDCS effects on LTP and memory in 3×Tg-AD-3M mice was paralleled by its inability to enhance $pCREB^{Ser133}$ and $pCaMKII^{Thr286}$, indicating that these differential response could serve as novel AD biomarker. Investigating the role of Ca^{2+} signal dysregulation in the tDCS ineffectiveness on LTP and memory in 3×Tg-AD-3M mice was beyond the scope of this research. However, it is worth mentioning that enhanced Ca^{2+} signaling has been reported in the earliest stages of the disease in mouse AD models (Del Prete et al., 2014; Chakroborty et al., 2019) and it has also been observed in cells from familial AD patients (Nelson et al., 2010). Furthermore, convergent evidence indicates Ca^{2+} dyshomeostasis within synaptic compartments as an early and critical factor in driving synaptic pathophysiology, leading to cognitive impairment in AD (Whitcomb et al., 2015).

The main purpose of our study was to identify an early and easy-to-detect AD biomarker potentially translatable to clinical application. Of course, molecular changes only occurring in the brain would not meet these requirements; therefore, we looked for biomarkers available in the circulating blood. Changes in pCREB and pCaMKII levels in the brain might be paralleled by similar changes in neuron-derived exosomes isolated from circulating blood, which is a promising though still experimental approach (Shi et al., 2016; Badhwar and Haqqani, 2020) we are planning to implement in future studies. Instead, we focused on a much simpler and cheaper approach, based on plasma BDNF level assessment by ELISA (Naegelin et al., 2018), which could be employed in any laboratory performing blood sample testing and therefore, widely accessible to any population. As already mentioned, enhanced BDNF expression in hippocampal lysates was demonstrated in our previous study following tDCS. Although different organs may contribute to determine plasma BDNF levels, several evidences suggest that changes in blood BDNF levels may reflect changes occurring in the brain. Indeed, changes in blood BDNF levels have been associated with a number of neurological diseases including AD (Laske et al., 2006), and they have also been more frequently reported days or weeks after stimulation following tDCS in different clinical conditions or experimental models (Brunoni et al., 2015). We, therefore, compared plasma BDNF levels before and 1 week after tDCS and found that they were significantly increased in WT but not in 3×Tg-AD-3M mice. Investigating the specific contribution of hippocampus vs. other cortical and subcortical areas underneath the stimulating electrode to plasma BDNF levels as well as its different forms (i.e., mature vs. pro-BDNF) was beyond the scope of this paper. Similarly, our study did not address the role of BDNF in AD pathophysiology.

Instead, our novel finding provides a peripheral biomarker of covert neuroplasticity impairment that could be detected in blood samples and easily translated to clinical use. The non-invasiveness and lack of adverse effects of tDCS (Antal et al., 2017) support future longitudinal studies in patient cohorts at risk of AD including elderly people diagnosed for amnestic MCI or those with genetic risk factors. In summary, our study unravels the unresponsiveness of neuroplasticity mechanisms in the hippocampus to boosting stimuli in a pre-AD stage. The combined use of a non-invasive method such as tDCS and plasma BDNF level assessment before and after treatment appears a novel promising approach to detect synaptic dysfunction far earlier than the appearance of any clinical signs. Although our findings still need to be validated in humans, they indicate a very promising perspective for large population analyses of subjects at risk to develop AD, with far reaching implications for both a personalized approach to AD patients and public health.

DATA AVAILABILITY STATEMENT

The raw data supporting the conclusions of this article will be made available by the authors, without undue reservation, to any qualified researcher.

ETHICS STATEMENT

The animal study was reviewed and approved by the Ethics Committee of the Catholic University and Italian Ministry of Health.

AUTHOR CONTRIBUTIONS

CG and MP conceived the study and supervised the work. SC, VL, PR, and GA performed the electrophysiological experiments. MR and AM performed the behavioral experiments. SF performed the ELISA experiments. KG and SF performed the WB experiments. DL performed the analysis of Aβ oligomers. MP and CG wrote the manuscript. All authors contributed to the article and approved the submitted version.

FUNDING

This work was supported by the Italian Ministry of Health – Ricerca Finalizzata # RF-2013-02356444.

SUPPLEMENTARY MATERIAL

The Supplementary Material for this article can be found online at: https://www.frontiersin.org/articles/10.3389/fcell.2020.00541/full#supplementary-material

REFERENCES

Antal, A., Alekseichuk, I., Bikson, M., Brockmöller, J., Brunoni, A. R., and Chen, R. (2017). Low intensity transcranial electric stimulation: safety, ethical, legal regulatory and application guidelines. *Clin. Neurophysiol.* 128, 1774–1809. doi: 10.1016/j.clinph.2017.06.001

Badhwar, A., and Haqqani, A. S. (2020). Biomarker potential of brain-secreted extracellular vesicles in blood in Alzheimer's disease. *Alzheimers Dement.* 12:e12001. doi: 10.1002/dad2.12001

Barbati, S. A., Cocco, S., Longo, V., Spinelli, M., Gironi, K., Mattera, A., et al. (2019). Enhancing plasticity mechanisms in the mouse motor cortex by anodal transcranial direct-current stimulation: the contribution of nitric oxide signaling. *Cereb. Cortex* 30, 2972–2985. doi: 10.1093/cercor/bhz288

Bature, F., Guinn, B. A., Pang, D., and Pappas, Y. (2017). Signs and symptoms preceding the diagnosis of Alzheimer's disease: a systematic scoping review of literature from 1937 to 2016. *BMJ Open* 7:e015746. doi: 10.1136/bmjopen-2016-015746

Belfiore, R., Rodin, A., Ferreira, E., Velazquez, R., Branca, C., Caccamo, A., et al. (2019). Temporal and regional progression of Alzheimer's disease-like pathology in 3xTg-AD mice. *Aging Cell* 18:e12873. doi: 10.1111/acel.12873

Bliss, T. V., and Collingridge, G. L. (1993). A synaptic model of memory: long-term potentiation in the hippocampus. *Nature* 361, 31–39. doi: 10.1038/361031a0

Bloom, G. S. (2014). Amyloid-β and tau: the trigger and bullet in Alzheimer disease pathogenesis. *JAMA Neurol.* 71, 505–508. doi: 10.1001/jamaneurol.2013.5847

Brunoni, A. R., Baeken, C., Machado-Vieira, R., Gattaz, W. F., and Vanderhasselt, M. A. (2015). BDNF blood levels after non-invasive brain stimulation interventions in major depressive disorder: a systematic review and meta-analysis. *World J. Biol. Psychiatry* 16, 114–122. doi: 10.3109/15622975.2014.958101

Chakroborty, S., Hill, E. S., Christian, D. T., Helfrich, R., Riley, S., Schneider, C., et al. (2019). Reduced presynaptic vesicle stores mediate cellular and network plasticity defects in an early-stage mouse model of Alzheimer's disease. *Mol. Neurodegener.* 14:7. doi: 10.1186/s13024-019-0307-7

Cocco, S., Podda, M. V., and Grassi, C. (2018). Role of BDNF signaling in memory enhancement induced by transcranial direct current stimulation. *Front. Neurosci.* 12:427. doi: 10.3389/fnins.2018.00427

Cohen, S. J., and Stackman, R. W. Jr. (2015). Assessing rodent hippocampal involvement in the novel object recognition task: a review. *Behav. Brain Res.* 285, 105–117. doi: 10.1016/j.bbr.2014.08.002

Del Prete, D., Checler, F., and Chami, M. (2014). Ryanodine receptors: physiological function and deregulation in Alzheimer disease. *Mol. Neurodegener.* 9:21. doi: 10.1186/1750-1326-9-21

Fá, M., Puzzo, D., Piacentini, R., Staniszewski, A., Zhang, H., Baltrons, M. A., et al. (2016). Extracellular tau oligomers produce an immediate impairment of LTP and memory. *Sci. Rep.* 6:19393. doi: 10.1038/srep19393

Franklin, K. B. J., and Paxinos, G. T. (1997). *The Mouse Brain in Stereotaxic Coordinates*. New York, NY: Academic Press.

Fusco, S., Spinelli, M., Cocco, S., Ripoli, C., Mastrodonato, A., Natale, F., et al. (2019). Maternal insulin resistance multigenerationally impairs synaptic plasticity and memory via gametic mechanisms. *Nat. Commun.* 10:4799. doi: 10.1038/s41467-019-12793-3

Galluzzi, S., Marizzoni, M., Babiloni, C., Albani, D., Antelmi, L., Bagnoli, C., et al. (2016). Clinical and biomarker profiling of prodromal Alzheimer's disease in workpackage 5 of the Innovative Medicines Initiative PharmaCog project: a 'European ADNI study'. *J. Intern. Med.* 279, 576–591. doi: 10.1111/joim.12482

Gondard, E., Soto-Montenegro, M. L., Cassol, A., Lozano, A. M., and Hamani, C. (2019). Transcranial direct current stimulation does not improve memory deficits or alter pathological hallmarks in a rodent model of Alzheimer's disease. *J. Psychiatr. Res.* 114, 93–98. doi: 10.1016/j.jpsychires.2019.04.016

Gulisano, W., Maugeri, D., Baltrons, M. A., Fà, M., Amato, A., Palmeri, A., et al. (2018a). Role of amyloid-β and tau proteins in Alzheimer's disease: confuting the amyloid cascade. *J. Alzheimers Dis.* 64, S611–S631. doi: 10.3233/JAD-179935

Gulisano, W., Melone, M., Li Puma, D. D., Tropea, M. R., Palmeri, A., Arancio, O., et al. (2018b). The effect of amyloid-β peptide on synaptic plasticity and memory is influenced by different isoforms, concentrations and aggregation status. *Neurobiol. Aging* 71, 51–60. doi: 10.1016/j.neurobiolaging.2018.06.025

Irvine, G. B., El-Agnaf, O. M., Shankar, G. M., and Walsh, D. M. (2008). Protein aggregation in the brain: the molecular basis for Alzheimer's and Parkinson's diseases. *Mol. Med.* 14, 451–464. doi: 10.2119/2007-00100

Jackson, M. P., Rahman, A., Lafon, B., Kronberg, G., Ling, D., Parra, L. C., et al. (2016). Animal models of transcranial direct current stimulation: methods and mechanisms. *Clin. Neurophysiol.* 127, 3425–3454. doi: 10.1016/j.clinph.2016.08.016

Jackson, M. P., Truong, D., Brownlow, M. L., Wagner, J. A., McKinley, R. A., Bikson, M., et al. (2017). Safety parameter considerations of anodal transcranial direct current stimulation in rats. *Brain Behav. Immun.* 64, 152–161. doi: 10.1016/j.bbi.2017.04.008

Joe, E., and Ringman, J. M. (2019). Cognitive symptoms of Alzheimer's disease: clinical management and prevention. *BMJ* 367:l6217. doi: 10.1136/bmj.l6217

Joseph, D. J., Liu, C., Peng, J., Liang, G., and Wei, H. (2019). Isoflurane mediated neuropathological and cognitive impairments in the triple transgenic Alzheimer's mouse model are associated with hippocampal synaptic deficits in an age-dependent manner. *PLoS One* 14:e0223509. doi: 10.1371/journal.pone.0223509

Kim, M. S., Koo, H., Han, S. W., Paulus, W., Nitsche, M. A., Kim, Y. H., et al. (2017). Repeated anodal transcranial direct current stimulation induces neural plasticity-associated gene expression in the rat cortex and hippocampus. *Restor. Neurol. Neurosci.* 35, 137–146. doi: 10.3233/RNN-160689

Kopeikina, K. J., Hyman, B. T., and Spires-Jones, T. L. (2012). Soluble forms of tau are toxic in Alzheimer's disease. *Transl Neurosci.* 3, 223–233. doi: 10.2478/s13380-012-0032-y

Kronberg, G., Rahman, A., Sharma, M., Bikson, M., and Parra, L. C. (2020). Direct current stimulation boosts hebbian plasticity in vitro. *Brain Stimul.* 13, 287–301. doi: 10.1016/j.brs.2019.10.014

Lashley, T., Schott, J. M., Weston, P., Murray, C. E., Wellington, H., Keshavan, A., et al. (2018). Molecular biomarkers of Alzheimer's disease: progress and prospects. *Dis. Model. Mech.* 11:dmm031781. doi: 10.1242/dmm.031781

Laske, C., Stransky, E., Leyhe, T., Eschweiler, G. W., Wittorf, A., Richartz, E., et al. (2006). Stage-dependent BDNF serum concentrations in Alzheimer's disease. *J. Neural Transm.* 113, 1217–1224. doi: 10.1007/s00702-005-0397-y

Leone, L., Colussi, C., Gironi, K., Longo, V., Fusco, S., Li Puma, D. D., et al. (2019). Altered Nup153 expression impairs the function of cultured hippocampal neural stem cells isolated from a mouse model of Alzheimer's disease. *Mol. Neurobiol.* 56, 5934—5949. doi: 10.1007/s12035-018-1466-1

Li, T., Jiao, J. J., Hölscher, C., Wu, M. N., Zhang, J., Tong, J. Q., et al. (2018). A novel GLP-1/GIP/Gcg triagonist reduces cognitive deficits and pathology in the 3xTg mouse model of Alzheimer's disease. *Hippocampus* 28, 358–372. doi: 10.1002/hipo.22837

Merlo, S., Spampinato, S. F., and Sortino, M. A. (2019). Early compensatory responses against neuronal injury: a new therapeutic window of opportunity for Alzheimer's disease? *CNS Neurosci. Ther.* 25, 5–13. doi: 10.1111/cns.13050

Naegelin, Y., Dingsdale, H., Säuberli, K., Schädelin, S., Kappos, L., and Barde, Y. A. (2018). Measuring and validating the levels of brain-derived neurotrophic factor in human serum. *eNeuro* 5:ENEURO.0419-17.2018. doi: 10.1523/ENEURO.0419-17.2018

Nelson, O., Supnet, C., Liu, H., and Bezprozvanny, I. (2010). Familial Alzheimer's disease mutations in presenilins: effects on endoplasmic reticulum calcium homeostasis and correlation with clinical phenotypes. *J. Alzheimers Dis.* 21, 781–793. doi: 10.3233/JAD-2010-100159

Oddo, S., Caccamo, A., Shepherd, J. D., Murphy, M. P., Golde, T. E., Kayed, R., et al. (2003). Triple-transgenic model of Alzheimer's disease with plaques and tangles: intracellular Aβ and synaptic dysfunction. *Neuron* 39, 409–421. doi: 10.1016/S0896-6273(03)00434-3

Paciello, F., Podda, M. V., Rolesi, R., Cocco, S., Petrosini, L., Troiani, D., et al. (2018). Anodal transcranial direct current stimulation affects auditory cortex plasticity in normal-hearing and noise-exposed rats. *Brain Stimul.* 11, 1008–1023. doi: 10.1016/j.brs.2018.05.017

Pelletier, S. J., and Cicchetti, F. (2014). Cellular and molecular mechanisms of action of transcranial direct current stimulation: evidence from in vitro and in vivo models. *Int. J. Neuropsychopharmacol.* 18:yu047. doi: 10.1093/ijnp/pyu047

Podda, M. V., Cocco, S., Mastrodonato, A., Fusco, S., Leone, L., Barbati, S. A., et al. (2016). Anodal transcranial direct current stimulation boosts synaptic plasticity

and memory in mice via epigenetic regulation of Bdnf expression. *Sci. Rep.* 6:22180. doi: 10.1038/srep22180

Podda, M. V., D'Ascenzo, M., Leone, L., Piacentini, R., Azzena, G. B., and Grassi, C. (2008). Functional role of cyclic nucleotide-gated channels in rat medial vestibular nucleus neurons. *J. Physiol.* 586, 803–815. doi: 10.1113/jphysiol.2007.146019

Podda, M. V., Leone, L., Barbati, S. A., Mastrodonato, A., Li Puma, D. D., and Piacentini, R. (2014). Extremely low-frequency electromagnetic fields enhance the survival of newborn neurons in the mouse hippocampus. *Eur. J. Neurosci.* 39, 893–903. doi: 10.1111/ejn.12465

Puzzo, D., Piacentini, R., Fà, M., Gulisano, W., Li Puma, D. D., Staniszewski, A., et al. (2017). LTP and memory impairment caused by extracellular Aβ and Tau oligomers is APP-dependent. *eLife* 6:e26991. doi: 10.7554/eLife.26991

Rahman, A., Lafon, B., Parra, L. C., and Bikson, M. (2017). Direct current stimulation boosts synaptic gain and cooperativity in vitro. *J. Physiol.* 595, 3535–3547. doi: 10.1113/JP273005

Rajji, T. K. (2019a). Impaired brain plasticity as a potential therapeutic target for treatment and prevention of dementia. *Expert. Opin. Ther. Targets* 23, 21–28. doi: 10.1080/14728222.2019.1550074

Rajji, T. K. (2019b). Transcranial magnetic and electrical stimulation in alzheimer's disease and mild cognitive impairment: a review of randomized controlled trials. *Clin. Pharmacol. Ther.* 106, 776–780. doi: 10.1002/cpt.1574

Ranieri, F., Podda, M. V., Riccardi, E., Frisullo, G., Dileone, M., and Profice, P. (2012). Modulation of LTP at rat hippocampal CA3-CA1 synapses by direct current stimulation. *J. Neurophysiol.* 107, 1868–1880. doi: 10.1152/jn.00319.2011

Ripoli, C., Cocco, S., Li Puma, D. D., Piacentini, R., Mastrodonato, A., Scala, F., et al. (2014). Intracellular accumulation of amyloid-β (Aβ) protein plays a major role in Aβ-induced alterations of glutamatergic synaptic transmission and plasticity. *J. Neurosci.* 34, 12893–12903. doi: 10.1523/jneurosci.1201-14.2014

Rohan, J. G., Carhuatanta, K. A., McInturf, S. M., Miklasevich, M. K., and Jankord, R. (2015). Modulating hippocampal plasticity with in vivo brain stimulation. *J. Neurosci.* 35, 12824–12832. doi: 10.1523/JNEUROSCI.2376-15.2015

Serrano-Pozo, A., Frosch, M. P., Masliah, E., and Hyman, B. T. (2011). Neuropathological alterations in Alzheimer disease. *Cold Spring Harb. Perspect. Med.* 1:a006189. doi: 10.1101/cshperspect.a006189

Shi, M., Kovac, A., Korff, A., Cook, T. J., Ginghina, C., Bullock, K. M., et al. (2016). CNS tau efflux via exosomes is likely increased in Parkinson's disease but not in Alzheimer's disease. *Alzheimers Dement.* 12, 1125–1131. doi: 10.1016/j.jalz.2016.04.003

Shipton, O. A., El-Gaby, M., Apergis-Schoute, J., Deisseroth, K., Bannerman, D. M., Paulsen, O., et al. (2014). Left-right dissociation of hippocampal memory processes in mice. *Proc. Natl. Acad. Sci. U.S.A.* 111, 15238–15243. doi: 10.1073/pnas.1405648111

Stafford, J., Brownlow, M. L., Qualley, A., and Jankord, R. (2018). AMPA receptor translocation and phosphorylation are induced by transcranial direct current stimulation in rats. *Neurobiol. Learn. Mem.* 150, 36–41. doi: 10.1016/j.nlm.2017.11.002

Stover, K. R., Campbell, M. A., Van Winssen, C. M., and Brown, R. E. (2015). Early detection of cognitive deficits in the 3xTg-AD mouse model of Alzheimer's disease. *Behav. Brain Res.* 289, 29–38. doi: 10.1016/j.bbr.2015.04.012

Vecchio, F., Miraglia, F., Iberite, F., Lacidogna, G., Guglielmi, V., Marra, C., et al. (2018). Sustainable method for Alzheimer dementia prediction in mild cognitive impairment: electroencephalographic connectivity and graph theory combined with apolipoprotein E. *Ann. Neurol.* 84, 302–314. doi: 10.1002/ana.25289

Vorhees, C. V., and Williams, M. T. (2014). Assessing spatial learning and memory in rodents. *ILAR J.* 55, 310–332. doi: 10.1093/ilar/ilu013

Whitcomb, D. J., Hogg, E. L., Regan, P., Piers, T., Narayan, P., Whitehead, G., et al. (2015). Intracellular oligomeric amyloid-beta rapidly regulates GluA1 subunit of AMPA receptor in the hippocampus. *Sci. Rep.* 9:10934. doi: 10.1038/srep10934

Yu, T. H., Wu, Y. J., Chien, M. E., and Hsu, K. S. (2019). Transcranial direct current stimulation induces hippocampal metaplasticity mediated by brain-derived neurotrophic factor. *Neuropharmacology* 144, 358–367. doi: 10.1016/j.neuropharm.2018.11.012

Conflict of Interest: The authors declare that the research was conducted in the absence of any commercial or financial relationships that could be construed as a potential conflict of interest.

frontiers in Cell and Developmental Biology

ORIGINAL RESEARCH
published: 22 July 2020
doi: 10.3389/fcell.2020.00639

DNA Methyltransferase 1 (DNMT1) Function Is Implicated in the Age-Related Loss of Cortical Interneurons

*Anne Hahn[1†], Daniel Pensold[1,2†], Cathrin Bayer[1,2], Jessica Tittelmeier[1], Lourdes González-Bermúdez[1], Lisa Marx-Blümel[1], Jenice Linde[2,3], Jonas Groß[1], Gabriela Salinas-Riester[4], Thomas Lingner[4], Julia von Maltzahn[5], Marc Spehr[3,6], Tomas Pieler[7], Anja Urbach[8] and Geraldine Zimmer-Bensch[1,2,3]**

[1] Department of Functional Epigenetics, Institute of Human Genetics, University Hospital Jena, Jena, Germany, [2] Department of Functional Epigenetics in the Animal Model, Institute of Biology II, RWTH Aachen University, Aachen, Germany, [3] Research Training Group 2416 MultiSenses – MultiScales, RWTH Aachen University, Aachen, Germany, [4] Transcriptome and Genome Analysis Laboratory (TAL), Department of Developmental Biochemistry, University of Göttingen, Göttingen, Germany, [5] Leibniz Institute on Aging – Fritz Lipmann Institute (FLI), Jena, Germany, [6] Department of Chemosensation, Institute of Biology II, RWTH Aachen University, Aachen, Germany, [7] Centre for Nanoscale Microscopy and Molecular Physiology of the Brain (CNMPB), Department of Developmental Biochemistry, University of Göttingen, Göttingen, Germany, [8] Institute of Neurology, University Hospital Jena, Jena, Germany

OPEN ACCESS

Edited by:
Alex Dranovsky, Columbia University, United States

Reviewed by:
Sriharsa Pradhan, New England Biolabs, United States
Sarah Canetta, Columbia University Irving Medical Center, United States

***Correspondence:**
Geraldine Zimmer-Bensch
zimmer@bio2.rwth-aachen.de;
zimmer_geraldine@yahoo.de

† These authors have contributed equally to this work

Specialty section:
This article was submitted to Molecular Medicine, a section of the journal Frontiers in Cell and Developmental Biology

Received: *06 March 2020*
Accepted: *25 June 2020*
Published: *22 July 2020*

Citation:
Hahn A, Pensold D, Bayer C, Tittelmeier J, González-Bermúdez L, Marx-Blümel L, Linde J, Groß J, Salinas-Riester G, Lingner T, von Maltzahn J, Spehr M, Pieler T, Urbach A and Zimmer-Bensch G (2020) DNA Methyltransferase 1 (DNMT1) Function Is Implicated in the Age-Related Loss of Cortical Interneurons. Front. Cell Dev. Biol. 8:639. doi: 10.3389/fcell.2020.00639

Increased life expectancy in modern society comes at the cost of age-associated disabilities and diseases. Aged brains not only show reduced excitability and plasticity, but also a decline in inhibition. Age-associated defects in inhibitory circuits likely contribute to cognitive decline and age-related disorders. Molecular mechanisms that exert epigenetic control of gene expression contribute to age-associated neuronal impairments. Both DNA methylation, mediated by DNA methyltransferases (DNMTs), and histone modifications maintain neuronal function throughout lifespan. Here we provide evidence that DNMT1 function is implicated in the age-related loss of cortical inhibitory interneurons. *Dnmt1* deletion in parvalbumin-positive interneurons attenuates their age-related decline in the cerebral cortex. Moreover, conditional *Dnmt1*-deficient mice show improved somatomotor performance and reduced aging-associated transcriptional changes. A decline in the proteostasis network, responsible for the proper degradation and removal of defective proteins, is implicated in age- and disease-related neurodegeneration. Our data suggest that DNMT1 acts indirectly on interneuron survival in aged mice by modulating the proteostasis network during life-time.

Keywords: aging, inhibitory interneurons, GABA, cerebral cortex, synapse, proteostasis, DNA methylation, transcriptional control

INTRODUCTION

Aging mediates structural, neurochemical, and physiological alterations in the brain that are associated with behavioral changes, memory decline, and cognitive impairments (Rozycka and Liguz-Lecznar, 2017). Cognitive aging results in metabolic, hormonal and immunological dysregulation, increased oxidative stress and inflammation, altered neurotransmission and

synaptic plasticity as well as reduced neurotrophic support of neurons (Rozycka and Liguz-Lecznar, 2017). Notably, in the aging brain, distinct cell types and circuits are affected differently (reviewed in Zimmer-Bensch, 2019a).

Inhibitory interneurons of the cerebral cortex are key players in cortical information processing (Kann et al., 2014) and particularly affected by aging. Reduced interneuron numbers were reported across diverse species and cortical regions (reviewed in Zimmer-Bensch, 2019a). Additionally, morphological abnormalities and dysfunction of GABAergic synapses emerge as major factors in aging-related impairments of nervous system function (Morrison and Baxter, 2012). These findings confirm previous reports of declined inhibition (Shetty and Turner, 1998; Stanley and Shetty, 2004; Cheng and Lin, 2013). In line with reduced neurotransmitter release, major changes in the expression of genes related to neurotransmission and transcriptional repression of GABA-related transcripts have been described for the human prefrontal cortex (Loerch et al., 2008), but also in brains across different mammalian species (reviewed in Zimmer-Bensch, 2019a). Diminished expression of genes involved in synaptic function indeed appears to be a conserved feature of mammalian brain aging (Jiang et al., 2001; Loerch et al., 2008; Ianov et al., 2016).

Given the importance of GABAergic inhibitory interneurons in cortical information processing, age-associated defects in inhibitory circuits contribute to cognitive decline and age-related disorders (Rozycka and Liguz-Lecznar, 2017). Such defects include the loss of synaptic contacts, decreased GABA release, and reduced postsynaptic responsiveness, thus disturbing the excitation/inhibition balance in the aging brain. Fast-spiking parvalbumin (PV) positive interneurons represent the most abundant subset of cortical inhibitory interneurons (Druga, 2009). They execute both feedforward and feedback inhibition, and are responsible for generating gamma-frequency oscillations (Sohal et al., 2009; Buzsáki and Wang, 2012; Kann et al., 2014; Willems et al., 2018). In schizophrenia patients, a reduction in PV interneurons and their dysfunction have been associated with the loss of gamma oscillations, manifesting in working memory and executive function deficits (Torrey et al., 2005; Sohal et al., 2009). Upon aging, PV interneurons are diminished in cell numbers in the somatosensory, auditory, and motor cortices of rats as well as in the hippocampus (Miettinen et al., 1993; Ouda et al., 2008). Moreover, altered PV interneuron function is implicated in age-related diseases like Alzheimer's disease (AD; Rossignol, 2011; Verret et al., 2012). Together, these studies emphasize the role of PV interneurons in cortical function. Hence, detailed analysis of age-related changes in this interneuron subpopulation might help to understand the processes underlying cognitive aging and age-related memory impairments.

Apart from synaptic defects, aging is accompanied by a declining proteostasis network that causes ineffective protein degradation, which can lead to neuronal death (Douglas and Dillin, 2010). Lysosomal degradation is critical for removing defective proteins or protein aggregates delivered by autophagy- or endocytosis-triggered endosomal pathways (Nixon and Cataldo, 1995; Nixon et al., 2000; Winckler et al., 2018). Moreover, lysosomal dysfunction is associated with age-related neurodegenerative pathologies like Parkinson's and Alzheimer's disease (Zhang et al., 2009; Carmona-Gutierrez et al., 2016). Another protein removal pathway is built upon inclusion into multivesicular bodies (MVBs) and exosome release (Riva et al., 2019). The latter has recently been implicated in contributing to neurodegenerative disease and mental disorders (Bellingham et al., 2012; Delpech et al., 2019; Saeedi et al., 2019).

At the molecular level, epigenetic mechanisms emerge as crucial players in the physiology of healthy aging and the pathophysiology of age-related neurological disorders. Epigenetic mechanisms involve inheritable as well as reversible chromatin modifications, including DNA methylation and histone modifications, which influence gene transcription and post-transcriptional events (Fuks, 2005). Further epigenetic key players are represented by non-coding RNAs, which can act on transcriptional, post-transcriptional, and translational level (Geisler and Coller, 2013; Cech and Steitz, 2014; Zimmer-Bensch, 2019b).

DNA methylation executed by DNA methyltransferases (DNMTs) affects gene expression through diverse mechanisms (Maunakea et al., 2010; Gelfman et al., 2013; Lyko, 2018) and is implicated in the pathogenesis of brain aging (Cui and Xu, 2018). We have recently found that DNMT1-dependent DNA methylation modulates synaptic function of cortical PV interneurons by acting on endocytosis-mediated vesicle recycling (Pensold et al., 2020). Since regulation of both synaptic function and DNA methylation are involved in brain aging, we here investigate whether DNMT1-dependent transcriptional control in PV interneurons contributes to their age-related defects.

MATERIALS AND METHODS

Animals

The following mouse strains were used: C57BL/6 wild-type mice and transgenic mice on the C57BL/6 background including *Pvalb-Cre*/*tdTomato*/*Dnmt1* control as well as *Pvalb-Cre*/*tdTomato*/*Dnmt1 loxP*^{2} mice. The transgenic mice were established by crossing the *Pvalb-Cre* line (obtained from Christian Huebner, University Hospital Jena, Germany and described in Hippenmeyer et al., 2005) with the *tdTomato* transgenic reporter mice (obtained from Christian Huebner, University Hospital Jena, Germany and described in Madisen et al., 2010) and the *Dnmt1 loxP*^{2} mice (B6;129Sv-Dnmt1^{TM4Jae}/J, Jaenisch laboratory, Whitehead Institute; United States). The *Dnmt1 loxP*^{2} mice have LoxP-sites flanking exons 4 and 5 of the *Dnmt1* gene. To avoid germline recombination due to instable Cre expression in sperm, as already described for this *Pvalb-Cre* line (Kobayashi and Hensch, 2013), only maternal Cre inheritance was permitted. For this, males from the *tdTomato* line or *tdTomato*/*Dnmt1 loxP*^{2} line were cross-bred with Cre-positive females of the *Pvalb-Cre*/*tdTomato* or *Pvalb-Cre*/*tdTomato*/*Dnmt1 loxP*^{2} lines to achieve the *Pvalb-Cre*/*tdTomato*/*Dnmt1* control and *Pvalb-Cre*/*tdTomato*/*Dnmt1 loxP*^{2} mice, respectively. Cre-positive males were used for

experiments but not for further breeding. Transgenic *Pvalb-Cre/tdTomato/Dnmt1* control and *Pvalb-Cre/tdTomato/Dnmt1 loxP*^{2} mice are abbreviated as *Dnmt1* WT (*wild-type*) and *Dnmt1* KO (*knockout*) in the figures, respectively. Both lines were parallel back-crossed over more than 8 generations. CRE-mediated deletion leads to out-of-frame splicing from exon 3 to exon 6, resulting in a null *Dnmt1* allele (Jackson-Grusby et al., 2001). The floxed *Dnmt1* allele was genotyped with forward GGGCCAGTTGTGTGACTTGG and reverse CCTGGGCCTGGATCTTGGGGA primer pairs resulting in a 334 bp WT and 368 bp mutant band. The *tdTomato* allele was genotyped using the following set of four primers: WT forward AAGGGAGCTGCAGTGGAGTA, WT reverse CCGA AAATCTGTGGGAAGTC, mutant forward CTGTTCCTGTAC GGCATGG, mutant reverse CTGTTCCTGTACGGCATGG giving WT (297 bp) and mutant (196 bp) bands. The *Pvalb-Cre* genotyping was performed by applying AAACGTT GATGCCGGTGAACGTGC forward and TAACATTCTCCC ACCGTCAGTACG reverse primer resulting in a 214 bp fragment. All animal procedures were performed in strict compliance with the EU directives 86/609/EWG and 2007/526/EG guidelines for animal experiments and were approved by the local government (Thüringer Landesamt, Bad Langensalza, Germany). Animals were housed under 12 h light/dark conditions with *ad libitum* access to food and water.

Ladder Rung Test

Cohorts of *Pvalb-Cre/tdTomato/Dnmt1* control as well as *Pvalb-Cre/tdTomato/Dnmt1 loxP*^{2} mice were consecutively tested over different ages starting from 3 to 21 months. Mice were placed onto a ladder beam (transparent) with rungs in a regular pattern (every 10 mm) at a slight incline (∼30°) with the home box at the end. Time to cross the ladder was measured, not including the time spent in a stop or walking back toward the starting point. The scoring system according to Metz and Whishaw (2009) was used for foot placement accuracy. In each test session the animals had to cross the ladder consecutively for three times.

Isolation and Primary Cultivation of Dissociated Embryonic Single Cells

Pregnant dams were anesthetized by an intraperitoneal injection of 50% chloral hydrate in phosphate buffered saline (PBS; pH 7.4; 2.5 µg chloral hydrate per g body weight). After death of the dam, all embryos were dissected out of both uterine horns and instantly decapitated. The brain was dissected in ice-cold and sterile filtered Gey's Balanced Salt Solution (GBSS; 1.53 mM $CaCl_2$, 3.66 mM KCl, 0.22 mM KH_2PO_4, 1.03 mM $MgCl_2$*$6H_2O$, 0.28 mM $MgSO_4$*$7H_2O$, 137.93 mM NaCl, 2.702 mM $NaHCO_3$, 0.84 mM Na_2HPO_4, and 5.56 mM D(+)-Glucose).

Dissociated embryonic medial ganglionic eminence (MGE)-derived single cells for primary culture were prepared from MGE explants dissected from coronal brain sections according to Zimmer et al. (2011). Briefly, embryonic brains were prepared in Krebs buffer (126 mM NaCl, 2.5 mM KCl, 1.2 mM NaH_2PO_4, 1.2 mM $MgCl_2$, 2.1 mM $CaCl_2$, 10 mM D(+)-Glucose, and 12.5 mM $NaHCO_3$), embedded in 4% low-melt agarose (Carl Roth, Germany) at 37°C for coronal sectioning with a vibratome at 4°C. MGE explants were collected in ice-cold Hank's Balanced Salt Solution (HBSS; Invitrogen, United States) supplemented with 0.65% D(+)-Glucose. After incubation with 0.04% trypsin (Invitrogen) in HBSS for 17 min at 37°C, cells were dissociated by trituration and filtering through nylon gauze (pore size 140 µm; Millipore).

Dissociated neurons were plated on coverslips coated with 19 µg/mL laminin (Sigma-Aldrich, Germany) and 5 µg/mL poly-L-lysine (Sigma-Aldrich) at a density of 225 cells/mm^2 in Neurobasal Medium (Thermo Fisher Scientific) supplemented with 1xB27 (Thermo Fisher Scientific), 100 U/mL penicillin, 100 µg/mL streptomycin, and 0.5 mM GlutaMax (Thermo Fisher Scientific). After incubation at 37°C, 5% CO_2 in a humid atmosphere with 95% relative humidity for 7 days *in vitro* (DIV), cells were fixed in 4% paraformaldehyde (PFA) in PBS (pH 7.4) for 10 min at room temperature (RT).

Cell Culture

Cerebellar granule (CB) cells were cultured in Dulbecco's Modified Eagle's Medium with high glucose (DMEM; Invitrogen) supplemented with 10% fetal bovine serum (FBS; Biowest), 1% GlutaMAX, 24 mM of KCl, 100 U/mL penicillin, 100 µg/mL streptomycin incubated at 33°C, 95% relative humidity, 5% CO_2.

Transfection With siRNA Oligos and CD63-pEGFP

For siRNA transfections of dissociated embryonic MGE cells of C57BL/6 WT mice and CB cells, reverse lipofection with Lipofectamin© 2000 (Thermo Fisher Scientific, United States) was applied according to the manufacturer's protocol and as described in Zimmer et al. (2011) using 15 nM control siRNA (BLOCK-iT Alexa Fluor red or green fluorescent oligo, Invitrogen, United States) and 30 nM *Dnmt1* siRNA, *Rab7* siRNA (Santa Cruz Biotechnology) for 5 h in Opti-MEM I Reduced Serum Medium without antibiotics (Thermo Fisher Scientific). MGE-derived neurons were transfected after six DIV, whereas CB cells were plated on coverslips 1 day prior to transfection. Cells were cultured overnight at 37 or 33°C, 5% CO_2 and 95% relative humidity using the aforementioned cell line specific culture medium prior to fixation.

Transfection for the CD63 overexpression construct was done as described above for siRNA transfection using 2 µg/mL of CD63-pEGFP (Addgene, United States) added for 5 h in Opti-MEM I Reduced Serum Medium (Thermo Fisher Scientific). Cells were cultured overnight at 33°C, 95% relative humidity and 5% CO_2 using the aforementioned cell line specific culture medium applied to live cell imaging in a petri dish inserted in a chamber heated to 33°C using imaging media of HBSS (Thermo Fisher Scientific) supplemented with 0.65% D(+)-Glucose, 10% FBS, 1% GlutaMAX (Thermo Fisher Scientific), 100 U/mL penicillin, 100 µg/mL streptomycin, and 25 µM HEPES (Thermo Fisher Scientific).

EGF Endocytosis

Epidermal growth factor (EGF) coupled to Alexa-488 (Molecular Probes, Invitrogen, United States) was used as an endocytic probe. siRNA-transfected CB cells were incubated in serum-free DMEM supplemented with 1% BSA for 1 h at 33°C followed by incubation in uptake media (DMEM, 1% BSA, 50 mM HEPES) containing 0.5 μg/mL EGF coupled to Alexa-488 on ice for 1 h. Cells were then washed 3× with ice-cold PBS (pH 7.4) to remove unbound ligands and then incubated for the indicated time points in serum-free DMEM, 1% BSA 1 h at 33°C. Cells were then put on ice, washed 3× with ice-cold PBS (pH 7.4), then placed in an acid wash [0.2 M acetic acid, 0.5 M NaCl (pH 2.8)] to remove any non-internalized ligands. After fixation in 4% PFA in PBS (pH 7.4) for 10 min, cells were stained against LAMP1.

Brain Tissue Preparation

Mice were deeply anesthetized by intraperitoneal injection of 50% chloral hydrate in PBS (pH 7.4; 2.5 μg chloral hydrate per g body weight). For *in situ* hybridization experiments, freshly prepared brains were immediately frozen in liquid nitrogen and stored at −80°C. For immunohistochemistry, mice were perfused with PBS (pH 7.4) followed by 4% PFA in PBS (pH 7.4) and brains were dissected. Post-fixation occurred over night at 4°C. Cryoprotection with 10 and 30% sucrose in PBS overnight was applied before freezing in liquid nitrogen and storage at −80°C.

In situ Hybridization, Immunohistochemistry and Immunocytochemistry

For *in situ* hybridizations, adult brains were cryo-sectioned coronally at −20°C (20 μm). *In situ* hybridizations were performed as described by Zimmer et al. (2011) using digoxigenin-labeled riboprobes. The following primers were used to generate the riboprobe: forward GAGAGCTCTGTCGATGACAGACGTGCTC and reverse GA GGTACCTTCTTCAACCCCAATCTTGC for *Pvalb* (NM_01 3645.3). The riboprobe was obtained by *in vitro* transcription using DIG-11-UTP (Roche, Germany) from cDNA fragments cloned in pBluescript II SK (Stratagene, United States). For Nissl staining, adult brains were cryo-sectioned at −20°C (20 μm) and fixed on slides for 30 min in fixation solution [95% (v/v) ethanol and 5% (v/v) acetic acid]. After washing in water, sections were incubated in 0.5% (w/v) cresyl violet for 25 min, and washed in water. Then an ethanol-series (50, 70, and 99%) was applied for 2.5 min each. Subsequently, sections were incubated in xylol for 5 min and mounted in Depex mounting media (Serva, Germany).

For immunocytochemistry on dissociated MGE cells, permeabilization and washing between different incubation steps was performed with 0.1% (v/v) Triton X-100 in PBS (pH 7.4) for 10 min. Blocking with 5% (v/v) normal goat serum in PBS (pH 7.4) was performed for 30 min and primary antibodies were applied overnight at 4°C, secondary antibodies were applied for 1 h. Cells were washed prior to nuclei staining with DAPI (Molecular Probes, United States) for 5 min. CB cells were permeabilized with 0.2% (v/v) Triton X-100 in PBS (pH 7.4) for 10 min prior to blocking with 5% (v/v) normal goat serum in PBS (pH 7.4) for 1 h. Primary antibodies were applied overnight at 4°C, secondary antibodies for 1 h at RT. After nuclei staining with DAPI (Molecular Probes, United States) for 5 min, coverslips were embedded in Mowiol (Carl Roth, Germany). Unless noted differently, all steps were performed at RT.

The following primary antibodies were used: mouse anti-RFP (1:500, Thermo Fisher Scientific), mouse anti-Parvalbumin (1:2,000, Swant Switzerland), rabbit anti-CD63 (1:500, gift from Markus Damme, Biochemisches Institut Christian-Albrechts-Universitaet Kiel), rat anti-LAMP1 (1:200, Thermo Fisher Scientific).

The following secondary antibodies were applied: goat Alexa-488 anti-mouse (1:1,000, Vector), goat Alexa-488 anti-rat (1:1,000, Thermo Fisher Scientific), goat Cy3 anti-mouse (1:1,000, Jackson Immunoresearch), goat Cy5 anti-mouse (1:1,000, Thermo Fisher Scientific), and goat Cy5 anti-rabbit (1:1,000, Thermo Fisher Scientific).

Isolation of Adult and Aged Cortical Interneurons for FACS

The optimized protocol used to collect the material for DNA and RNA-sequencing was modified based on different protocols (Brewer, 1997; Eide and McMurray, 2005; Brewer and Torricelli, 2007; Saxena et al., 2012). Adult and aged brains were dissected in GBSS (1.53 mM $CaCl_2$, 3.66 mM KCl, 0.22 mM KH_2PO_4, 1.03 mM $MgCl_2{*}6H_2O$, 0.28 mM $MgSO_4{*}7H_2O$, 137.93 mM NaCl, 2.7 mM $NaHCO_3$, 0.84 mM Na_2HPO_4, 5.56 mM D(+)-Glucose, pH 7.4). Cortical hemispheres were dissected and subsequently handled separately. All following volumes are calculated per cortical hemisphere, which were cut into small pieces and transferred to 5 mL HBSS w/o Ca^{2+} and Mg^{2+} supplemented with 7 mM HEPES, 100 U/mL penicillin, 100 μg/mL streptomycin and 0.65% D(+)-Glucose and washed twice. The tissue was then transferred to 5 mL pre-warmed (20 min at 37°C) Trypsin/EDTA (Life Technologies, United States) supplemented with 132 mM trehalose (Sigma-Aldrich, Germany), 100 U/mL penicillin, 100 μg/mL streptomycin, 10 mM HEPES, and 600 U DNase (Applichem, Germany) and incubated for 30 min at 37°C, rotating the samples every 5 min. Samples were washed with 2.1 mL pre-warmed DMEM/F12 supplemented with 10% FBS, 100 U/mL penicillin, 100 μg/mL streptomycin, and 132 mM trehalose. After adding 0.9 mL pre-warmed HBSS containing 10 mg/mL Collagenase Type 2 (Worthington, United Kingdom) samples were incubated for 25 min at 37°C rotating every 5 min and then washed with 2 mL pre-warmed DMEM/F12 supplemented with 10% FBS, 100 U/mL penicillin, 100 μg/mL streptomycin, 3.3 mM EDTA, and 132 mM trehalose prior to cool down on ice for 2 min. Dissolving of samples occurred in 1.5 mL DMEM/F12 supplemented with 10% FBS, 100 U/mL penicillin, 100 μg/mL streptomycin, and 132 mM trehalose. Trituration was performed using fire-polished and heat-treated (180°C for 8 h) glass capillaries of three different diameters (about 500, 250 μm, and 100 μm), which were coated with DMEM/F12 supplemented with 10% FBS, 100 U/mL penicillin, and 100 μg/mL streptomycin prior to use. Mechanical

dissociation was performed by pipetting up and down gently 3–5 times for each diameter starting with the largest, avoiding air bubbles. After each step, the supernatant was collected in 1 mL DMEM/F12 supplemented with 10% FBS, 100 U/mL penicillin, 100 µg/mL streptomycin, and 132 mM trehalose was added to the original sample. After trituration with the smallest glass capillary, the suspension was filtered through nylon gauze (80–100 µm) and centrifuged for 5 min at 160 g, 4°C. After supernatant removal, the pellet was dissolved in 4 mL HBSS w/o Ca^{2+} and Mg^{2+} supplemented with 7 mM HEPES, 100 U/mL penicillin, 100 µg/mL streptomycin, 0.65% D(+)-Glucose and 132 mM trehalose. After centrifugation (5 min, 160 g, 4°C), the pellet was dissolved in PBS (pH 7.4) with 30% Percoll (Sigma-Aldrich, United States) and 132 mM trehalose to perform a density gradient centrifugation for 10 min at 500 g and 4°C. The supernatant was removed and the pellet was dissolved in 250 µL HBSS w/o Ca^{2+} and Mg^{2+} supplemented with 7 mM HEPES, 100 U/mL penicillin, 100 µg/mL streptomycin, 0.65% D(+)-Glucose, and 132 mM trehalose for fluorescence activated cell sorting (FACS).

FACS Enrichment of tdTomato Cells

Cell suspensions subjected to FACS were prepared from the cortical hemispheres of adult 6 and 18 months old *Pvalb-Cre/tdTomato/Dnmt1* control as well as *Pvalb-Cre/tdTomato/Dnmt1 loxP*^{2} mice. Following addition of DAPI, cells were sorted using an ARIA III FACS sorter (BD Biosciences, United States) with a maximal flow rate of six. The tdTomato reporter was excited by a 561 nm yellow/green solid-state laser and emission signal was detected in a range of 579 to 593 nm. According to their forward scatter/side scatter criteria (FSC/SSC) followed by cell doublet exclusion via an FSC-H vs FSC-W criterium, DAPI-negative living cells were sorted based on a distinctive tdTomato signal. Cells of interest were collected in HBSS w/o Ca^{2+} and Mg^{2+} supplemented with 7 mM HEPES, 100 U/mL penicillin, 100 µg/mL streptomycin, 0.65% D(+)-Glucose, and 132 mM trehalose at 4°C and pelleted by centrifugation. Enriched tdTomato cells of one hemisphere were prepared for RNA-sequencing, while cells of the contralateral hemisphere were subjected to DNA-isolation for MeDIP-sequencing for each brain used. For RNA isolation, pellets were dissolved in 500 µL Trizol® Reagent (Life Technologies, United States) and subsequently frozen on dry ice. For MeDIP-Seq analysis, cell pellets were frozen at −80°C until further use. Only male mice were used for RNA and MeDIP sequencing.

RNA/DNA Isolation of Tissue and FAC-Sorted Cells

Adult cortical hemispheres were dissected from whole brain and frozen in liquid nitrogen as described above. For RNA-sequencing, samples were subjected to standard RNA isolation procedure using Trizol® Reagent (Life Technologies, United States). The FACS-enriched tdTomato cells were processed accordingly, with additional application of GlycoBlue (Thermo Fisher Scientific, United States) to a final concentration of 0.2% during RNA precipitation for better visualization of the pellet.

DNA isolation of FACS-enriched tdTomato cells was performed using QIAamp DNA Micro Kit (Qiagen, Germany) according to manufacturer's instruction and checked for integrity by capillary gel electrophoresis (Bioanalyzer, Agilent Technologies, Inc., United States).

RNA Sequencing of Adult Cortical Tissue

To reveal potentially relevant genes for age related processes in the brain, we performed RNA sequencing of 6 and 16 months old cortical hemispheres of C57BL/6 mice. The TruSeq RNA Sample Preparation Kit (Illumina, Cat. N°RS-122-2002, United States) was used for library preparation (1 µg total RNA), the QuantiFluor™ dsDNA System (Promega, United States) for quantitation and the DNA 1000 chip on the Bioanalyzer 2100 (Agilent Technologies) to determine the size range of final cDNA libraries prior to amplification and sequencing (cBot and HiSeq2000 from Illumina; PE; 2 × 100 bp; ca. 30 million reads per sample). Sequences were trimmed for adaptor sequences and phred scores <30 via fastq-mcf (ea-utils v1.1.2-484). This data was uploaded to the Galaxy web platform; 2.11.40.6, and we used the public server at *usegalaxy.eu* for further analysis (Afgan et al., 2018). If not stated differently, default settings were applied. Quality check was done via fastqc; v. 0.11.8 (Andrews, 2010) before alignment to the UCSC mouse reference genome mm10 was performed using STAR; v2.7.2b (Dobin et al., 2013) with 2-pass mapping. Reads were aligned to the reference genome using gapped alignment as RNA transcripts are subject to splicing and reads might therefore span distant exons. Data was converted and sorted by samtools; v1.9 (Li et al., 2009). Counting the reads to each gene was done via HTSeq; v0.9.1 (Anders et al., 2015) to the Ensembl gene annotation. Data analysis was performed using R/Bioconductor 3.0.2/2.12 (Luo and Brouwer, 2013); loading DESeq2; v1.22.1 (Love et al., 2014).

Sequence data will be deposited in NCBI's Gene Expression Omnibus and are accessible through GEO Series upon acceptance of the manuscript.

RNA Sequencing of FACS-Enriched tdTomato Cells

RNA was isolated using the Trizol® Reagent protocol according to manufacturer's instructions. RNA quality was assessed by measuring the RIN (RNA Integrity Number) using the fragment analyzer from Advanced Analytical (United States). Library preparation for RNA-Seq was performed using the TruSeq™ RNA Sample Prep Kit v2 (Illumina, Cat. N°RS-122-2002, United States) starting from 50 ng of total RNA. Accurate quantitation of cDNA libraries was performed by using the QuantiFluor™ dsDNA System (Promega, United States). The size range of final cDNA libraries was determined applying the DNA chip on the fragment analyzer (average 350 bp; Advanced Analytical). cDNA libraries were amplified and

sequenced by using the cBot and HiSeq2000 from Illumina (SR; 1 × 50 bp; ∼30–40 million reads per sample). Sequence images were transformed with Illumina software BaseCaller to bcl files, which were demultiplexed to fastq files with CASAVA v1.8.2. Quality check was done via fastqc; v0.10.0 (Andrews, 2010). Read alignment was performed using STAR; v2.3.0 (Dobin et al., 2013) to the mm10 reference genome with 2-pass mapping. Data was converted and sorted by samtools; v0.1.19 (Li et al., 2009) and reads per gene were counted via HTSeq; v0.5.4.p3 (Anders et al., 2015). Data analysis was performed using R/Bioconductor 3.0.2/2.12 (Luo and Brouwer, 2013); loading DESeq2 (Love et al., 2014). Sequence data will be deposited in NCBI's Gene Expression Omnibus and are accessible through GEO Series upon acceptance of the manuscript.

MeDIP Sequencing of FACS-Enriched tdTomato Cells

For genome-wide methylation analysis we applied immunoprecipitation methods for the enrichment of 5-methylcytosines. Specifically, 100 ng of genomic DNA were used as starting material. The Methylated-DNA IP Kit from Zymo (Cat. N° D5101) was applied according to manufacturer's instructions. The product of the IP and control reaction were then used for preparation of Illumina compatible libraries according to the TruSeq Nano DNA Library Prep Kit (Cat. N° FC-121-4001). Libraries were sequenced on a HiSeq 2000 yielding 50 bp single end reads. The sequencing reads were demultiplexed using the Illumina CASAVA tool and sequence quality was checked using fastqc; v0.10.0 (Andrews, 2010). The reads were then aligned to the genome of *Mus musculus* (mm10) using Bowtie 2; v2.0.2 (Langmead and Salzberg, 2012). Briefly, reads were aligned using default parameters allowing for two mismatches using seed alignment. Differentially methylated regions (DMRs) were identified using the MEDIPS package for R; v1.16.0 (Lienhard et al., 2014) with a window size of 700 bp and a minimum coverage of 5% of the window length. Differential methylation analysis from low number of replicates was done using edgeR (Robinson et al., 2010) to estimate the biological variability and model the count data using negative binomial distribution. DMRs were considered gene-associated DMRs, or differentially methylated genes (DMGs), if they were inside a gene, in the promoter region [−1000, 0] of the transcription start site (TSS) or in the terminator region [0, +300] from the transcript termination site (TTS). DMRs were those with adjusted *P*-value <0.05. A detailed description of the analysis pipeline can be found in Halder et al. (2015). Sequence data will be deposited in NCBI's Gene Expression Omnibus and are accessible through GEO Series upon acceptance of the manuscript.

Integrative Analysis of FACS-Sorted Sequencing Data

Genes in the FACS RNA sequencing data were considered differentially expressed with a Benjamini-Hochberg adjusted *P* value $P < 0.05$ and a $|\text{logfc}| > 1$. Gene list overlaps between differentially expressed and methylated genes were quantified using the Jaccard coefficient. Absolute numbers of DMGs were determined without regard to multiple sites of differential methylation in a single gene. Significance of enrichment of methylated genes was calculated using Fisher's exact test.

Gene lists including the genes showing both, differential methylation and expression, were submitted to the *Database for Annotation, Visualization and Integrated Discovery*[1] (DAVID) for Gene Ontology (GO) or KEGG Pathway term enrichment analysis. Results of GO enrichment analysis were visualized in a bar diagram including the respective *Benjamini-Hochberg* corrected *P*-value, the number of genes and the enrichment fold change included in a certain term.

Heat maps were generated using R package pheatmap[2]. For heat maps showing comparison between two datasets, data was normalized to 6 months WT. In case of heat maps illustrating more than two samples, data was scaled. Significance levels: $^{*}P < 0.05$; $^{**}P < 0.01$; and $^{***}P < 0.001$.

Microscopy and Image Data Analysis

Images of immunohistochemistry staining of adult tissue sections or immunocytochemistry of stained cell culture was recorded either with an inverted confocal laser scanning microscope TCS SP5 (Leica Microsystems, Germany) or with an inverted transmitted light microscope Axio CellObserver Z1 equipped with MosaiX module for tile scanning and apotome for confocal like imaging (Carl Zeiss Microscopy, Germany). Photographs were analyzed using the free FIJI software (Schindelin et al., 2012).

For life cell imaging of CB cells transfected with the CD63-pEGFP and either control or *Dnmt1* siRNA, images were taken with Axio CellObserver Z1, ×40 optical magnification using apotome. Z-stack was applied over the whole cell and acquisition was performed every 5 min for 1 h. *.zvi-files were opened with FIJI; maximum intense projection was performed and data were exported as *.avi with five frames per second. The movement of CD63-pEGFP positive vesicles was measured direction specific from one timepoint to the next and speed was calculated based on the time interval. Analysis of cell number in adult sections was performed with ImageJ cell counter plugin. Counted cell numbers in section analysis were normalized to the area of the counted region.

For fluorescence intensity measurements, each experimental design was imaged at one particular microscope with consistent settings regarding exposure time and light intensity at the CellObserver Z1 or laser power, gain and spectral settings at the SP5 LSM. Fluorescence intensity measurement for the CD63 staining and LAMP1 staining was performed in the processes of the cells. For each picture, background correction

[1] https://david.ncifcrf.gov

[2] https://CRAN.R-project.org/package=pheatmap

was performed by subtracting the mean fluorescent intensity from three background areas. Mean fluorescent intensity of the *Dnmt1* siRNA treated cells was normalized to control siRNA. Photoshop CC was applied for image composition. Boxplots were plotted using R.

Significance was analyzed with two-tailed Student's *t*-test or two-way ANOVA. Significance levels: $^{*}P < 0.05$; $^{**}P < 0.01$; and $^{***}P < 0.001$.

RESULTS

Vulnerability of PV-Expressing Neocortical GABAergic Interneurons Toward Aging

Aging-dependent functional defects in the cortical inhibitory GABAergic system were reported for humans (Cheng and Lin, 2013) as well as for different animal models (Miettinen et al., 1993; Ouda et al., 2008) including mice (Jessen et al., 2017). Since mice serve as key models to study the neurobiology of aging and age-associated neurodegenerative diseases (Jucker and Ingram, 1997; Bilkei-Gorzo, 2014), we tested whether the neocortical GABAergic system is compromised in aged mice. As an initial approach we performed differential gene expression analysis of the whole neocortex from young (6 months) and aged (16 months) C57BL/6 mice. In general, RNA sequencing revealed comparatively low numbers of age-dependent differentially expressed genes (DEG = 470 genes, **Figure 1A**), which additionally displayed small fold changes (ranging from $-0.78 < \log2fc < 1.14$). This was also observed by others when using whole cortical tissue containing a mixed population of cells (e.g., glia versus neurons), which likely show different responses toward aging (Kimmel et al., 2019). In accordance with elevated inter-individual variability of gene expression observed in aged human brains (Kedlian et al., 2019), we also detected a similar variability in the cortical samples of aged mice (**Figure 1B**). These inter-individual differences heavily impact fold changes and differential gene expression analysis. Another hallmark of the aging brain is mRNA–protein decoupling (Wei et al., 2015), with numerous changes occurring mainly on the protein level (Liguz-Lecznar et al., 2015). However, as one of the most prominently differentially expressed genes *Pvalb* was identified, showing significantly diminished transcript levels in 16 months old cortex samples (adjusted P = 2.73E-50, log2fc = 1.04, **Figures 1A,C**), the time point when aging begins in mice (Xu et al., 2007). This finding was confirmed by *in situ* hybridization experiments, indicating an age-related reduction of *Pvalb*-expressing cells in motor, somatosensory and visual neocortical areas (**Figures 1D,E**). Consistently, we found less PV-immunoreactive cells (**Figures 1F,G**) in the same cortical regions in aged mice. Together, our data suggest a loss of PV-positive cortical interneurons in aged mice, being in line with the decrease of PV interneurons in somatosensory, auditory, and motor cortical areas of aged rats (Miettinen et al., 1993; Ouda et al., 2008).

In contrast to this depletion of inhibitory PV interneurons in the cerebral cortex, excitatory neurons, which account for >80% of cortical neurons (DeFelipe and Fariñas, 1992), appear less affected. Pan-neuronal density analysis of NeuN-positive cells did not reveal significant age-related changes (**Supplementary Figure S1**). In summary, we identified a vulnerability of PV-positive cortical inhibitory interneurons upon aging in mice.

DNMT1 Affects the Long-Term Survival of Neocortical Interneurons

Changes of the epigenetic landscape by genomic methylation and histone modifications contribute to transcriptional control in aging and lifespan regulation (Zampieri et al., 2015). DNA methylation, executed by DNMTs, is a major epigenetic mechanism regulating gene expression in mammals during different stages of life (Johnson et al., 2012; Zampieri et al., 2015). DNMT1 is one of the main DNMTs expressed in the developing and adult brain. DNMT1 modulates neuronal survival (Hutnick et al., 2009; Feng et al., 2010; Pensold et al., 2017; Symmank and Zimmer, 2017) and synaptic function of both excitatory neurons (Meadows et al., 2015, 2016) as well as inhibitory interneurons (Pensold et al., 2020). Hence, we asked whether DNMT1 is involved in the regulation of cortical interneuron survival during aging. To this end, we exploited a mouse model described previously (Pensold et al., 2020), in which *Dnmt1* deletion is restricted to PV-cells (*Pvalb-Cre*/*tdTomato*/*Dnmt1 loxP*^{2}). As controls, we used *Pvalb-Cre*/*tdTomato* mice. *Pvalb* promoter-dependent CRE recombinase-mediated *loxP* recombination drives persistent tdTomato protein expression, reported to start at the 5th week of life (Madisen et al., 2010). The analysis of the *Pvalb-Cre*/*tdTomato* interneuron density in adult versus aged mice confirmed the findings we obtained by RNA sequencing of whole cortical tissue, *in situ* hybridization, and immunostainings in C57BL/6 wildtype mice (**Figure 1**). We found a significant age-related reduction of tdTomato positive cells in motor and visual cortical areas of *Pvalb-Cre*/*tdTomato* mice (**Figures 2A,C**). Both superficial and deep cortical layers were affected by the reduction in interneurons (**Figure 2D**). Although less prominent, we also observed a significant decline of tdTomato cells in the somatosensory cortex (**Figures 2A,C**). This reduction was mainly restricted to the deep cortical layers (**Figure 2D**). At an intermediate stage (12 months old mice) we found a trend for reduced cell density, indicating that interneuron degeneration starts about one year of life (**Figures 2A,C**).

Next, we comparatively analyzed tdTomato cells in 6, 12, and 16 months old *Pvalb-Cre*/*tdTomato*/*Dnmt1 loxP*^{2} mice in the motor, somatosensory and visual cortical areas. While in young mice no differences in interneuron numbers were observed compared to controls (**Figures 2B,C**), 16 months old *Dnmt1* KO mice maintained a significantly higher density of tdTomato positive interneurons in

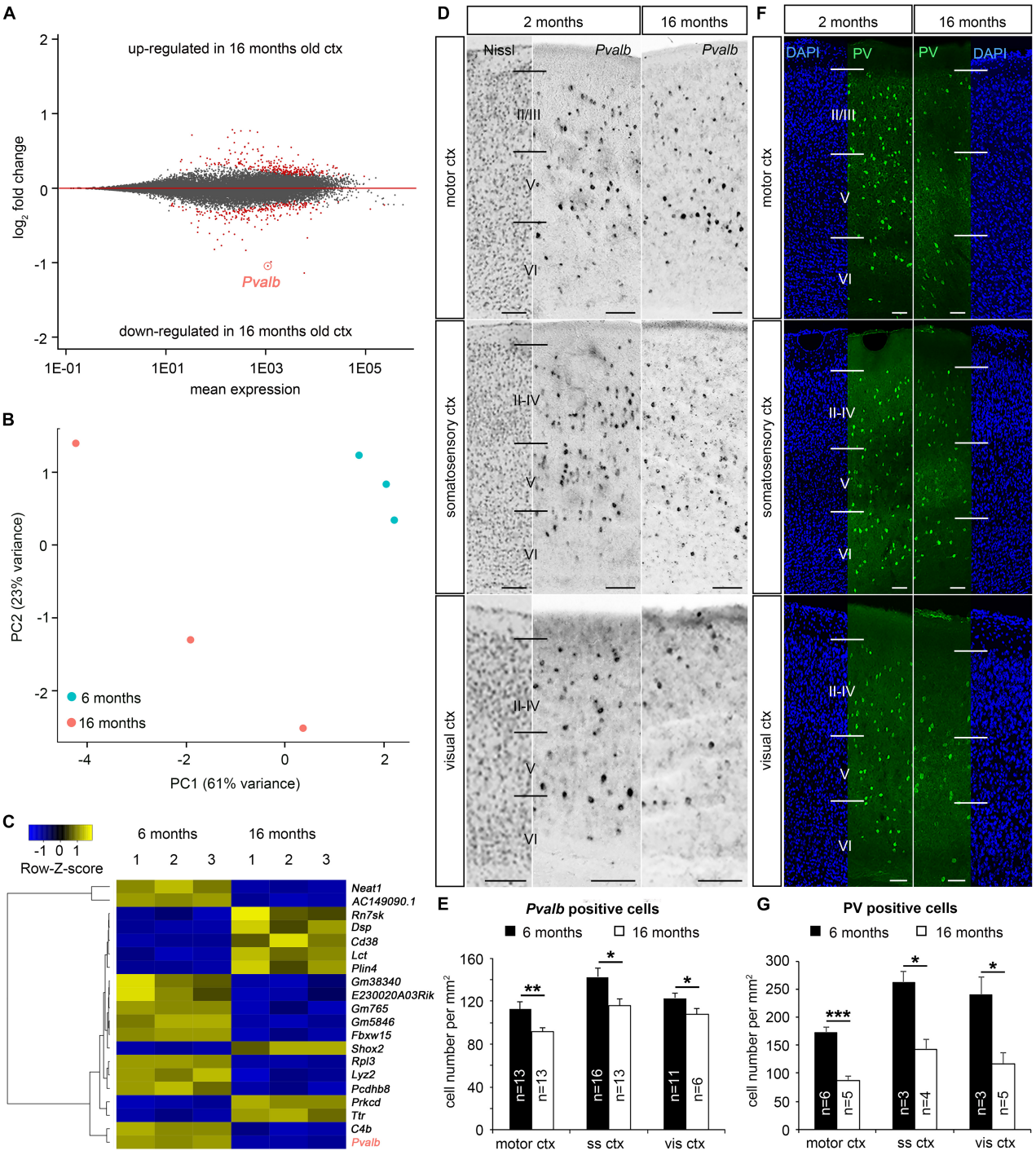

FIGURE 1 | Age-dependent reduction of parvalbumin expression in the mouse cortex. **(A)** MA-plot illustrating differential gene expression between whole cortical tissue of 6 months (n = 3 brains) and 16 months old (n = 3 brains) C57BL/6 mice. RNA sequencing was performed to reveal age-dependent differential gene expression (red dots, $P < 0.05$, Benjamini adjusted). **(B)** Principal component analysis (PCA) illustrates the segregation of the different samples, whereby the first and second PC account for 61 and 23% of the variance, respectively. **(C)** Heat-map illustrating the 20 genes with highest absolute foldchanges among the differentially expressed genes between cortical tissue samples of 6 and 16 months old C57BL/6 WT mice including *Pvalb*, which is significantly reduced in aged samples. **(D–G)** *In situ* hybridization and immunohistochemistry against *Pvalb* mRNA **(D)** and PV protein **(F)** in the motor cortex, somatosensory cortex and visual cortex in 6 months and 16 months old C57BL/6 mice (N = 3 different brains per age), quantified in **(E)** and **(G)**, respectively (*$P < 0.05$; **$P < 0.01$; ***$P < 0.001$, *Student's t-test*). Scale bars: 100 μm in **(D)** and **(F)**.

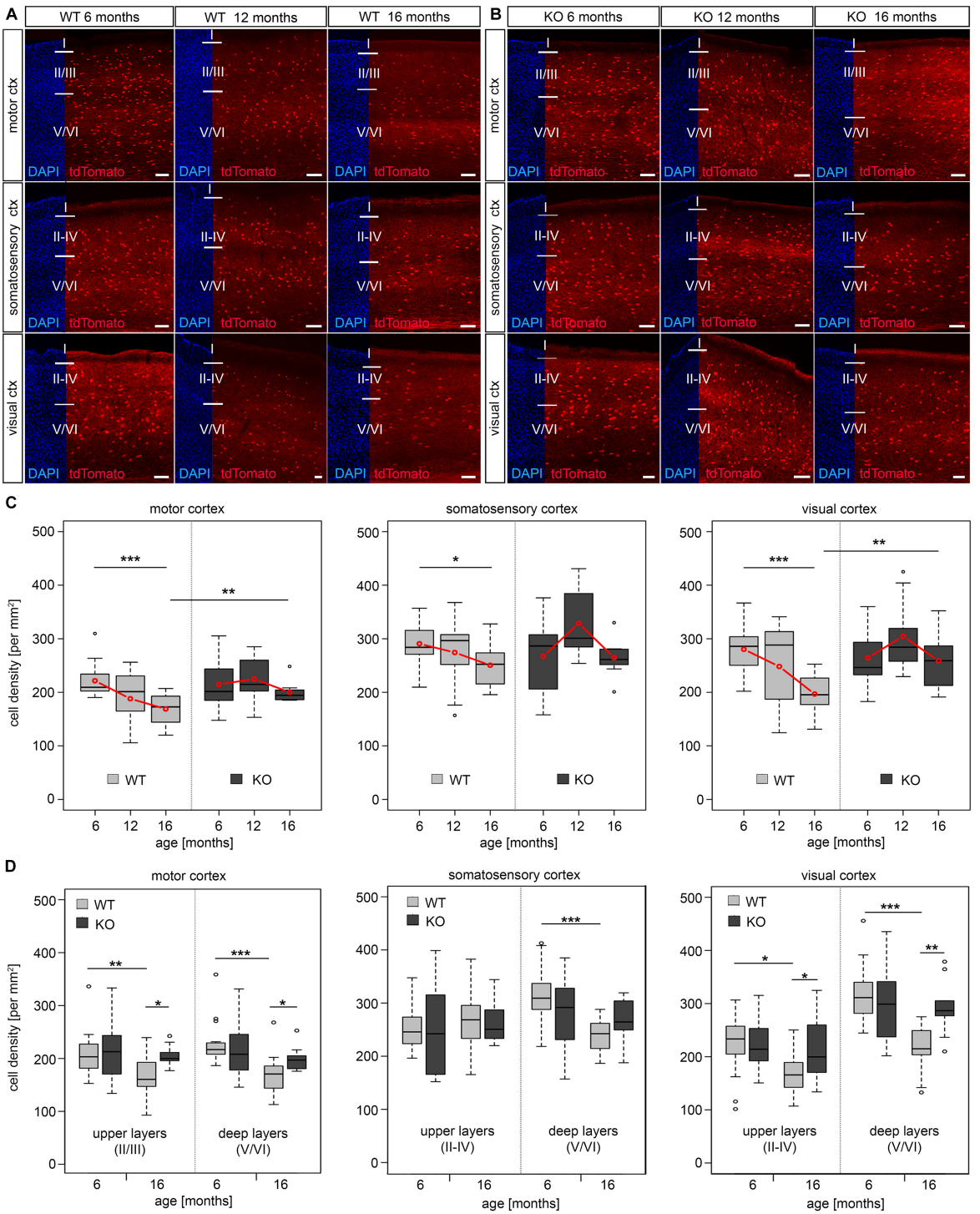

FIGURE 2 | *Dnmt1* knockout enhanced long-term survival of cortical interneurons. **(A,B)** Microphotographs of sagittal sections (Bregma 1.44) illustrating the motor, somatosensory, and visual cortex of 6, 12 and 16 months old *Pvalb-Cre/tdTomato* (WT, **A**) and *Pvalb-Cre/tdTomato/Dnmt1 loxP*^{2} (KO, **B**) mice showing tdTomato (red) and DAPI positive cells (blue). The cell density per area is quantified in **(C)**, which revealed a significant loss of interneurons upon aging in *Dnmt1* WT (*$P < 0.05$, ***$P < 0.001$) for the motor, somatosensory and visual cortex, respectively (two-way ANOVA, Bonferroni corrected), but no significant age-dependent differences in *Dnmt1* KO mice. Comparison of aged genotypes revealed significant differences in the motor and visual cortex (**$P < 0.01$; *Student's t-test*) **(D)** Layer-specific analysis of cell density in 6 and 16 months old *Dnmt1* WT and KO mice in the motor, somatosensory, and visual cortex (*$P < 0.05$, **$P < 0.01$; ***$P < 0.001$, *Student's t-test*). The numbers of analyzed sections are listed as follows: 6 months old WT: $n = 16$, $n = 15$, and $n = 13$ for motor, somatosensory and visual cortex, respectively; 6 months old KO: $n = 19$ for motor cortex and $n = 16$ for somatosensory and visual cortex; 12 months old WT and KO: $n = 9$ sections for each cortical area; 16 months old WT: $n = 14$ for motor and visual cortex and $n = 12$ for somatosensory cortex; 16 months old KO: $n = 9$ for each cortical region (from $N = 3$ different brains per genotype and age). WT, wild-type; KO, knockout. Scale bars: 100 μm.

motor and visual cortical areas (**Figures 2A–C**). In the somatosensory cortex, we again observed a trend toward increased densities of *Dnmt1*-deficient interneurons compared to age-matched controls (**Figures 2A,C**). Hence *Dnmt1* deficiency substantially improves long-term survival of PV-expressing cortical interneurons, indicating that DNMT1 function either directly or indirectly impairs cortical PV-interneuron survival in aged mice. This is in striking contrast to DNMT1 function during brain development, where it promotes POA-derived interneuron survival through non-canonical actions (Pensold et al., 2017; Symmank et al., 2018, 2020).

The Ameliorated Interneuron Survival in Aged *Dnmt1*-Deficient Mice Correlates With Improved Somatomotor Performances

Given their important role in cortical information processing, cortical interneuron decline was proposed to contribute to the cognitive and motoric impairments observed in the elderly (Bordner et al., 2011). To test whether attenuated interneuron loss correlates with improved skills in aged *Dnmt1*-deficient mice, we applied the ladder rung test to analyze motor performance that depends on somatomotor cortical activity (Metz and Whishaw, 2009). We continuously tested *Pvalb-Cre*/*tdTomato*/*Dnmt1 loxP*^{2} and *Pvalb-Cre*/*tdTomato* mice at distinct stages of life ranging from 3 to 21 months. Consistent with observations of others (Hebert and Gerhardt, 1998) and the age-dependent changes in interneuron numbers, the motor performances of control mice deteriorated with age as determined by measuring the foot placement accuracy and crossing time (**Figures 3A–C**). In stark contrast, *Dnmt1*-deficient mice did not show corresponding age-related impairments for the parameters and the time course analyzed, hence performing significantly better than controls at 16 to 21 months of age (**Figures 3A–C**). When plotting the percentage of perfect steps against crossing time for KO and control mice at 6, 12, and 18 months (**Figures 3D–F**), cohort segregation increased with age.

In addition to cortical information processing, locomotion depends on cerebellar Purkinje cells and skeletal muscle function, tissues that also display *Pvalb* and *Dnmt1* expression (**Supplementary Figures S2a,b**; Racay et al., 2006). In skeletal muscle, DNMT1 indeed plays a role during differentiation and regeneration (Aguirre-Arteta et al., 2000; Wang et al., 2015). However, neither in skeletal muscle nor in the cerebellum, obvious abnormalities were observed upon *Dnmt1* deletion. Purkinje cell numbers in the cerebellum were not affected by PV-CRE mediated *Dnmt1* deletion, neither in the young nor in the aged mice (**Supplementary Figures S2c–e**). Moreover, muscle integrity, structure, and innervation were not altered by *Dnmt1*-deletion at the stages investigated, as determined by hematoxylin/eosin, laminin and neuromuscular junction staining, respectively (**Supplementary Figures S2f–k**). These data strongly suggest that the motor impairments in aged controls are caused by the loss of cortical interneurons, which can be attenuated by *Dnmt1* deletion.

PV Interneurons Show an Increase in Degradation- and a Decline in Synapse-Related Gene Expression Upon Aging

Highlighting age-mediated transcriptional changes might help to approach the underlying mechanisms of the DNMT1-dependent PV-interneuron loss. This requires enrichment of PV-positive cortical interneurons from adult versus aged brains, as these interneurons represent a minority of the neocortical neuronal population (Druga, 2009). To this end, we applied an optimized protocol for adult cortical neuron isolation applicable for FACS. We combined mechanical and trypsin/collagenase-based enzymatic dissociation with trehalose treatment and *Percoll* density gradient centrifugation, as described and validated recently (Pensold et al., 2020).

Previously, Xu et al. (2007) investigated murine brain tissue at 6, 16 and 24 months of age, and found that most age-dependent genes are not differentially expressed at the age of 16 months. Hence, we chose to analyze interneurons of 18 months old control versus conditional *Dnmt1* knockout mice to monitor an advanced stage of aging, and compare interneuron transcriptional profiles with 6 months old mice for each genotype. Consistent with the PV interneuron loss in aged controls, we revealed significantly reduced FACS-events per hemisphere for aged *Pvalb-Cre*/*tdTomato* mice compared to the 6 months old mice (**Supplementary Figure S3a**). Transcriptome comparison between FAC-sorted young and old control interneurons illustrated that aging is associated with prominent changes in gene expression (**Figure 4A** and **Supplementary Figures S3b–d**). A total of 3,384 genes were differentially regulated (adjusted $P < 0.05$, $|\text{logfc}| > 1$), of which 65% were down-regulated and 35% up-regulated with age (**Figure 4A**). This high number of age-dependent transcriptional changes exceeds the transcriptional alterations revealed for the whole cortex (**Figures 1A,B**), which captures different aging signatures of diverse cell types collected in the cortical samples (Stegeman and Weake, 2017; Kimmel et al., 2019).

Among the genes we found to be up-regulated upon aging, GO-enrichment analysis revealed significantly enriched transcripts related to *membrane*, *endoplasmatic reticulum*, *endosome*, and *exosome* (**Supplementary Table S1**). The up-regulation of endosome and exosome-related genes in cortical interneurons might reflect an elevation of degradative actions and mechanisms upon aging in response to the accumulation of defective proteins, to maintain neuronal functionality over life time.

Of note, functional impairment of exosomes in transferring proteins, mRNAs, and miRNAs has been related to synaptopathies (Pitt et al., 2017), and synaptic dysfunction is considered a hallmark in neuronal aging (Deak and Sonntag, 2012; Azpurua and Eaton, 2015) and neurodegenerative disorders (Freeman and Mallucci, 2016; Ghiglieri et al., 2018). Altered or impaired synaptic function of aged PV-expressing interneurons

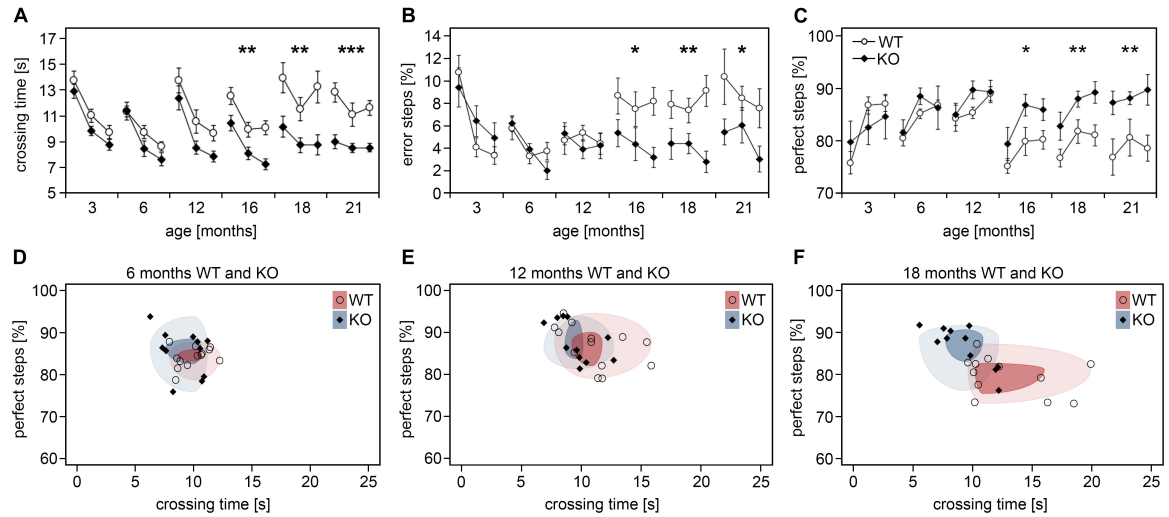

FIGURE 3 | Aged *Pvalb-Cre/tdTomato/Dnmt1* KO mice show improved somatomotor performances. **(A–C)** Performance of *Pvalb-Cre/tdTomato/Dnmt1* KO ($N = 10$) and WT ($N = 8$) mice were tested in the inclined ladder rung test at distinct stages of life ranging from 3 to 21 months (three consecutive trials per stage). Crossing time **(A)**, error steps **(B)**, and perfect steps **(C)** were quantified (two-way ANOVA; data are shown as mean ± SEM; $^{*}P < 0.05$, $^{**}P < 0.01$, $^{***}P < 0.001$). **(D–F)** The scatter plots of perfect steps against crossing time for the distinct *Pvalb-Cre/tdTomato/Dnmt1* KO and WT mice at 6 months **(D)**, 12 months **(E)**, and 18 months **(F)** illustrate the stronger segregation of the cohorts with age shown by the decreasing overlap of the circles upon aging representing the 1st (dark colored) and 3rd quartile (light colored) of the data range per group.

is strongly supported by the profile of genes that were down-regulated upon aging. By GO analysis, synapse-related genes were detected as most significantly overrepresented, displaying by far the highest enrichment scores (Benjamini-adjusted P = 1.91E-61; FDR = 4.6E-61; **Supplementary Table S1**). Moreover, genes collected in the GO-terms *membrane*, *cell junction*, *plasma membrane*, *dendrite* and diverse ion transport and ion channel-related genes were strongly enriched among the genes determined as transcriptionally down-regulated in aged wild-type interneurons (**Supplementary Table S1**). Of note, we have not identified a significant enrichment of cell death or survival associated genes among the genes changed in expression between young and old interneurons (**Supplementary Table S1**). In sum, the transcriptional alterations that we detected in aged neocortical PV-positive interneurons suggest an age-related impairment of synaptic functionality. Moreover, alterations in the degradation machinery can be assumed from the transcriptional alterations, which can influence neuronal survival (Kim and Seo, 2014).

Dnmt1 Deficient PV Interneurons Display Diminished Age-Associated Transcriptional Alterations

In addition to ameliorated locomotion, the attenuated decline in interneuron density in aged *Dnmt1* knockout mice coincides with diminished age-associated quantitative transcriptional changes in *Pvalb-Cre/tdTomato/Dnmt1 loxP*^{2} interneurons (**Figure 4B**; **Supplementary Table S2**). Compared to control interneurons, aging in *Pvalb-Cre/tdTomato/Dnmt1 loxP*^{2} cortical interneurons was characterized by both fewer differentially expressed genes and decreased fold changes. Only 383 genes were differentially expressed (adjusted $P < 0.05$, $|\text{logfc}| > 1$, **Figures 4A,B**). For better illustration of the discrete changes in expression between all samples, we re-scaled the expression levels of genes relative to the expression range of all groups (young and old control as well as knockout samples; **Figure 4D**). The heatmap shown in **Figure 4D** depicts prominent age-related transcriptional alterations in controls, but rather mild alterations in *Dnmt1*-deficient interneurons. These data are consistent with the attenuated age-associated decline observed for conditional *Dnmt1*-knockout mice at cellular and behavioral level.

A common denominator of age-mediated transcriptional remodeling in both genotypes is that age-related down-regulation dominates over up-regulation for the significantly altered genes with $|\text{logfc}| > 1$ (**Figures 4A,B**). For age-associated gene expression changes in *Pvalb-Cre/tdTomato/Dnmt1 loxP*^{2} interneurons, about 96% of differentially expressed genes were down-regulated (**Figure 4B**). Consistently, a "shutdown" of transcription in the aged cortex has been described before (Xu et al., 2007). Another similarity between aging control and *Dnmt1*-knockout interneurons was a significant enrichment of down-regulated synapse-related genes (**Supplementary Tables S1**, **S2**).

Potential Implication of DNA Methylation in Age-Mediated Transcriptional Remodeling

DNA methylation was frequently proposed to contribute to the aging-associated transcriptional changes (Issa, 2002; Jones et al., 2015). To this end, we conducted differential methylation analysis by MeDIP-sequencing of FAC-sorted interneurons from young (6 months) and aged (18 months) control mice to

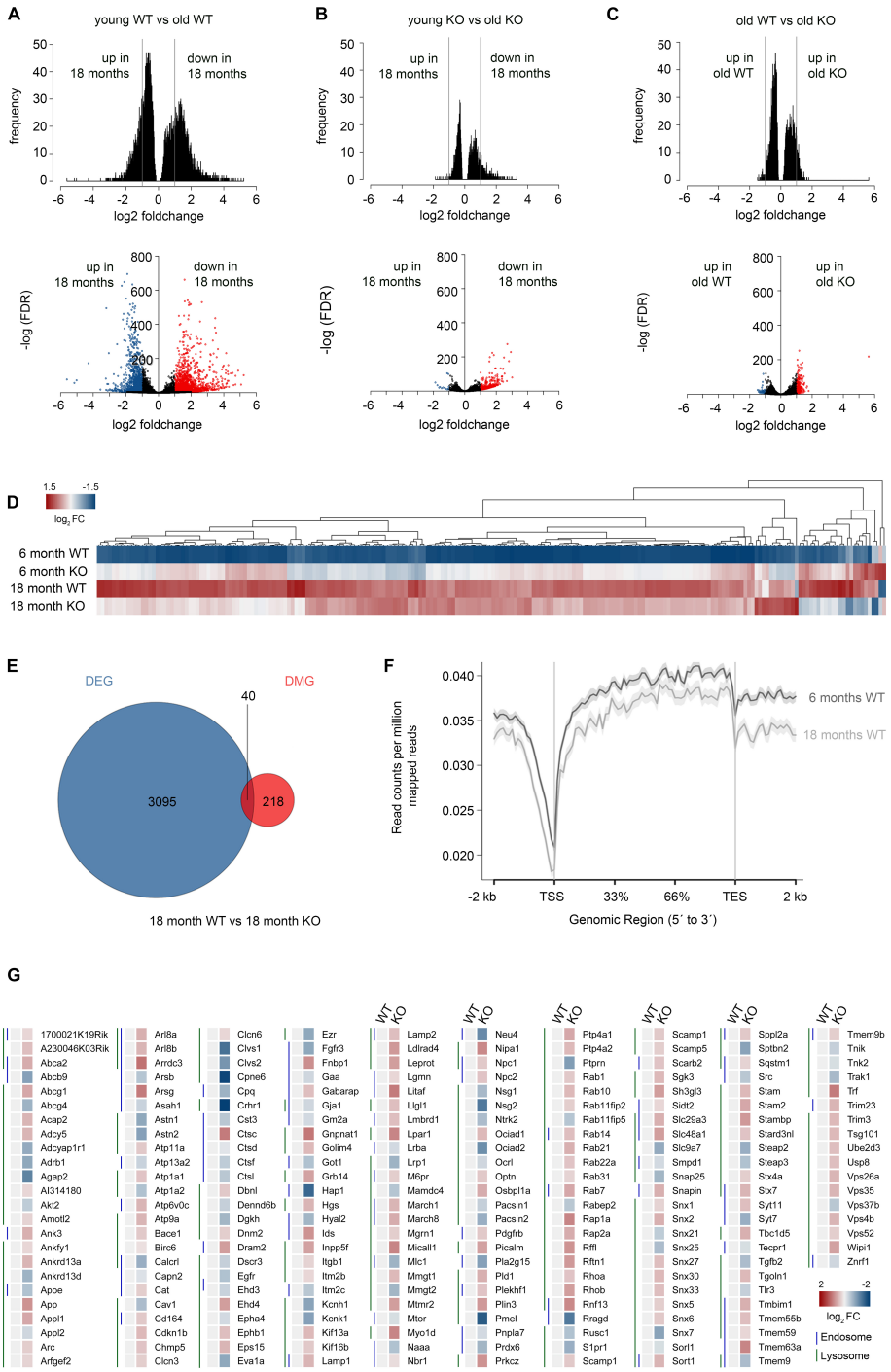

FIGURE 4 | Correlative transcriptome and methylation analysis of adult and aged *Dnmt1*-deficient and wild-type *Pvalb*-expressing cortical interneurons. **(A–C)** Density plots (upper panel) and volcano plots (lower panel) illustrating significant changes in gene expression determined between FACS-enriched young and old *Dnmt1* WT interneurons **(A)**, young and old *Dnmt1* knockout (KO) cortical interneurons **(B)**, as well as between old WT and KO interneuron samples (**C**; $P < 0.05$, Benjamini adjusted; pooled samples from $N = 6$ WT and KO mice at 6 months; and $N = 9$ WT and $N = 12$ KO mice at 18 months analyzed in technical duplicates). Blue and red-colored dots in the volcano plots represent genes with |logfc| > 1. **(D)** Heat-map illustrating the re-scaled expression of genes in all samples, which were found differentially expressed between young (6 months) KO and young WT interneurons. **(E)** Venn diagram illustrating the overlap ($P = 3.388E\text{-}5$, *Fisher's Exact test*) of differentially expressed genes (DEG) and differentially methylated genes (DMG) between aged FACS-enriched *Pvalb-Cre/tdTomato/Dnmt1* WT and KO cortical interneurons as determined by RNA-sequencing ($P < 0.05$, Benjamini-adjusted) and MeDIP-sequencing ($n = 9$ WT and $n = 12$ KO mice; $P < 0.05$, Benjamini-adjusted). **(F)** Methylation plot illustrating the average DNA methylation levels of a random sample of 10% of the genes from the *mm10* reference genome in young (6 months) and old (18 months) cortical interneurons from *Dnmt1* WT mice. **(G)** Heat-map of differentially expressed genes associated to the GO terms *endosome* and *lysosome*, normalized to 6 months old WT.

monitor age-related alterations in DNA methylation levels. Further, we determined genes whose age-related transcriptional changes (adjusted $P < 0.05$) correlated with alterations in the DNA methylation level (adjusted $P < 0.05$). Among the 201 genes which demonstrated changes in expression and DNA methylation upon aging, *synapse*, *cytoskeleton*, *dendrite*, *postsynaptic density*, and *membrane*-related genes were significantly overrepresented (**Supplementary Table S3**), indicating that DNA methylation is implicated in the age-related transcriptional changes of these genes.

To determine which genes are differentially expressed and methylated in aged interneurons in a DNMT1-dependent manner, we first compared transcriptional profiles and DNA methylation signatures of old control and *Dnmt1*-deficient interneuron samples. We obtained only 258 differentially expressed genes (adjusted $P < 0.05$) displaying a $|\log fc| > 1$ (**Figure 4C**). A similar number of 218 genes showed differential methylation (adjusted $P < 0.05$). However only two of these DMGs were overlapping with the pool of differentially expressed genes. Hence, we included all significantly differentially expressed genes independent of their fold change (3,095 genes) for correlation analysis between changes in methylation and transcription. Only 40 genes were significantly changed in both expression and methylation between the aged genotypes (**Figure 4E**). This indicates that DNMT1-dependent DNA methylation might play a rather minor role for the transcriptional changes, once the interneurons reach the age of 18 months. Indeed, the efficiency of the catalytic activity of DNMT1 is described to be reduced in an age-dependent manner (Casillas et al., 2003). This is in line with the global reduction of DNA methylation levels observed upon aging in control interneurons with MeDIP sequencing (**Figure 4F**), a finding that corroborates the age-related global hypomethylation reported by others (Shimoda et al., 2014; Lardenoije et al., 2015).

For those 40 genes (**Figure 4E**) which simultaneously changed in both expression and DNA methylation between aged genotypes, GO analysis revealed a significant enrichment of *actin cytoskeleton* and *postsynaptic density*-related genes, which are putatively regulated by DNMT1-dependent DNA methylation even in interneurons of advanced age (**Supplementary Table S4**). This fits to our finding that synapse and cytoskeleton-related genes are DNA methylation-dependently changed in expression upon aging in control cells (**Supplementary Table S3**). Albeit MeDIP sequencing covers only 15–16% of total 5-mC content (Stirzaker et al., 2014), for which the data provide only limited information, having a closer look on DNMT1 target genes identified in younger mice might provide further insights in the causes of impaired long-term interneuron survival.

DNMT1-Dependent DNA Methylation in Adult Interneurons Affects Degradative Pathways

In stark contrast to the comparison of the 18 months old genotypes, we determined a highly significant overlap ($P = 2.2E\text{-}16$, *Fisher's Exact test* for gene set enrichment analysis; odds ratio = 0.434) of 645 genes between young control and *Dnmt1* knockout interneurons, which display significant differences in both DNA methylation and gene expression (Pensold et al., 2020).

In general, far more genes were differentially expressed (3,868 genes) and/or methylated (3,135 genes) between young genotypes (Pensold et al., 2020). However, among neither the differentially expressed genes, nor among those genes both differentially expressed and methylated, we found a significant enrichment of apoptosis or cell death-related genes (data not shown). Hence, in contrast to developing interneurons, in which DNMT1 regulates expression of apoptosis genes (Pensold et al., 2017), survival regulation of interneurons in the aged cortex seems to result from different actions and targets of DNMT1.

Among the genes which we identified as repressed by DNMT1-dependent DNA methylation in young controls, we found an overrepresentation of *endocytosis* and *endosome*-related genes (Pensold et al., 2020). Furthermore, during analysis of all genes differentially expressed upon *Dnmt1* deletion, irrespective of altered DNA methylation, *lysosome* and *ubiquitination*-related genes were also found repressed by DNMT1 (Pensold et al., 2020; **Figure 4G**). Together these results demonstrate that endocytosis and degradative pathways are controlled by DNMT1. In a previous study we confirmed that dynamic DNMT1-dependent DNA methylation regulates synaptic transmission through the modulation of endocytosis-mediated vesicle recycling, which was improved upon *Dnmt1* deletion (Pensold et al., 2020). Hence, elevated GABAergic transmission and synaptic activity could indirectly promote interneuron survival of *Dnmt1*-deficient interneurons upon aging. However, endocytosis and endosomal function are crucial not only for synaptic activity regulation, but also affect degradative pathways (Ehlers, 2000; Gruenberg, 2001). Consistent with the transcriptional changes in 6 months old *Dnmt1*-deficient cortical interneurons (**Figure 4G**), siRNA-mediated *Dnmt1* depletion (knockdown efficiency of *Dnmt1* siRNA is illustrated in **Supplementary Figure S4a**) caused augmented CD63 and LAMP1 immunoreactivity, labeling endosomal, and lysosomal structures, respectively. This was determined in neurites of interneurons prepared from the embryonic MGE (**Figures 5A–C**) that give rise to PV interneurons, as well as in neurite-like processes of CB cells and neuroblastoma N2a cells 24 hours after transfection (**Supplementary Figures S4b–d**).

Endosomal-based degradation involves ubiquitination, retrograde transport to the cell soma, and fusion with lysosomes (McMahon and Boucrot, 2011; Haglund and Dikic, 2012). To quantify whether retrograde shuttling of endosomal compartments is influenced by DNMT1, we transfected CB cells with a CD63-GFP construct and analyzed transport velocity in the neurite-like processes upon *Dnmt1* knockdown and control siRNA transfections. While anterograde transportation was not changed in speed, we determined significantly faster velocities for retrograde transport of CD63-GFP particles after *Dnmt1* depletion (**Figures 5D,E**; **Supplementary Movies 1**, **2**).

As the binding of EGF to epidermal growth factor receptors (EGFR) induces their internalization and degradation via the endo-lysosomal pathway (Haglund and Dikic, 2012), we next applied Alexa488-coupled EGF to CB cells and monitored

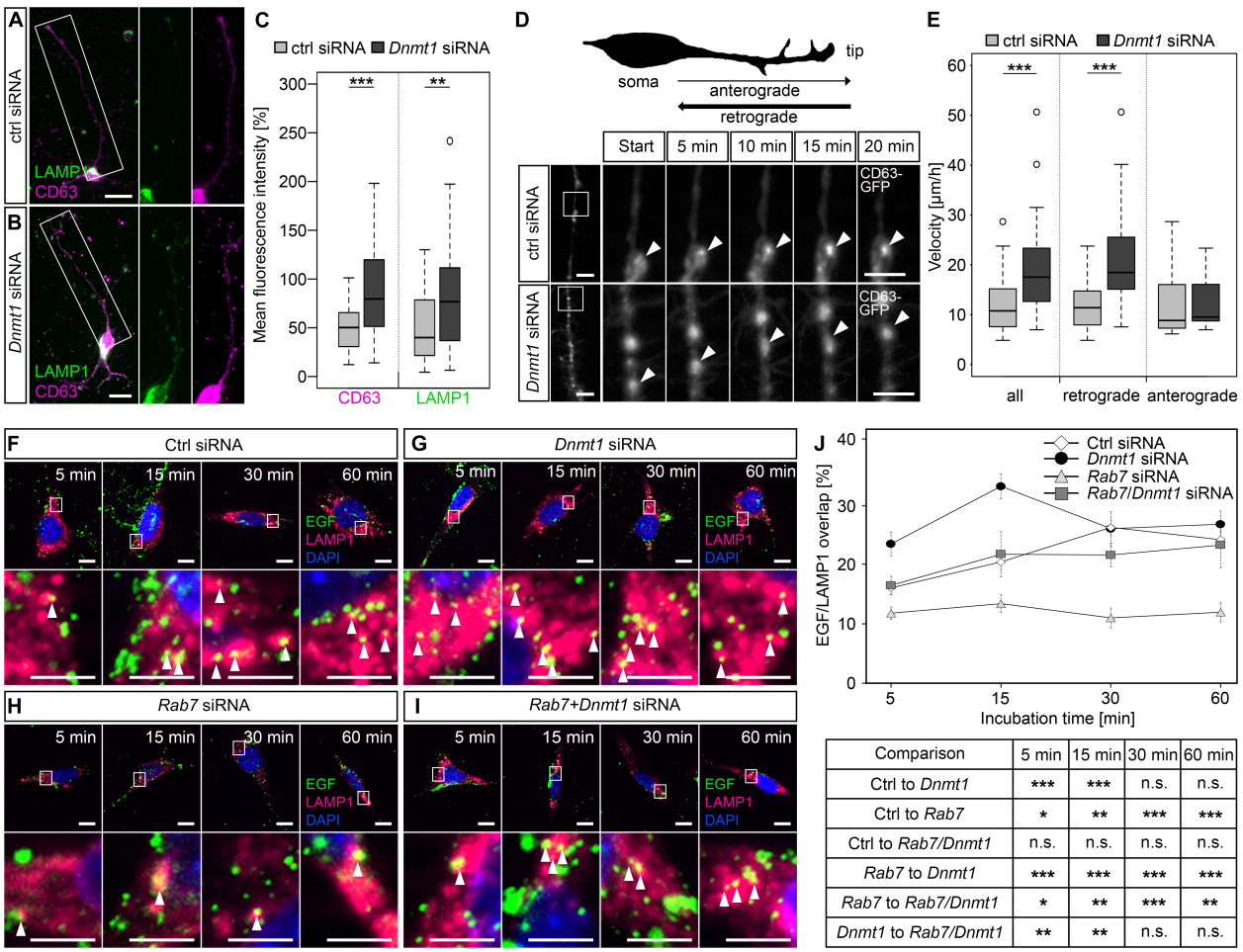

Comparison	5 min	15 min	30 min	60 min
Ctrl to *Dnmt1*	***	***	n.s.	n.s.
Ctrl to *Rab7*	*	**	***	***
Ctrl to *Rab7/Dnmt1*	n.s.	n.s.	n.s.	n.s.
Rab7 to *Dnmt1*	***	***	***	***
Rab7 to *Rab7/Dnmt1*	*	**	***	**
Dnmt1 to *Rab7/Dnmt1*	**	**	n.s.	n.s.

FIGURE 5 | DNMT1 regulates retrograde transport of endosomes and endocytic-based degradation. **(A,B)** CD63 (magenta) and LAMP1 (green) antibody staining in MGE cells (E15 + 7 div) 24 h after control and *Dnmt1* siRNA treatment. The white rectangles in **(A,B)** illustrate the locations of the magnified parts of the processes. Quantification of fluorescence intensities is shown in **(C)**. **(D,E)** Cerebellar granule (CB) cells were co-transfected either with control or *Dnmt1* siRNA and a CD63-GFP expression plasmid, and the movement of CD63-GFP positive structures was imaged for 20 min. The location of the highly magnified sections along the neurite-like processes are illustrated by white squares in the low magnifications. **(D)** Schematic illustration of the morphology of a cultured cerebellar granule (CB) cell. The quantification is depicted in **(E)**. **(F–J)** The EGF-degradation assay with CB cells either transfected with **(F)** control siRNA, **(G)** *Dnmt1* siRNA, **(H)** *Rab7* siRNA, or **(I)** *Dnmt1* and *Rab7* siRNA. The co-localization of Alexa488-labeled EGF (green) and LAMP1 positive lysosomal structures (red) was quantified after 5, 15, 30, and 60 min, as quantified in **(J)**. CB cells, cerebellar granule cells; N2a cells, neuroblastoma cells. *Student's t-test* in **(C,E,J)** with $^{*}P < 0.05$, $^{**}P < 0.01$, and $^{***}P < 0.001$. Scale bars: 20 µm in **(A,B)**; 10 µm in **(D, F–I)**; 5 µm in magnified sections in **(D,F–I)**.

the co-localization of EGF with LAMP1-positive lysosomal compartments at different time points. Indeed, siRNA-mediated *Dnmt1* depletion caused increased co-localization of EGF with LAMP1-positive lysosomes, both 5 and 15 min after EGF application (**Figures 5F,G,J**), indicating transport to lysosomal compartments. With longer incubation times, no differences to control siRNA-treated cells were observed (**Figures 5F,G,J**).

Lysosomal trafficking of the EGF-EGFR complex depends on RAB7, which mediates the fusion of late endosomes with lysosomes (Bucci et al., 2000). Consistently, we revealed a reduced EGF/LAMP1 co-localization after *Rab7* siRNA transfection of CB cells at all-time points tested (**Figures 5H,J**). *Rab7* expression was significantly up-regulated in *Dnmt1*-deficient PV-positive cortical interneurons (**Figure 4G**), and shown to be regulated by DNMT1-dependent DNA methylation (Pensold et al., 2020). Thus, we additionally analyzed the EGF/LAMP1 co-localization in *Dnmt1* siRNA-treated CB cells that were co-transfected with *Rab7* siRNA (knockdown efficiency of *Rab7* siRNA is depicted in **Supplementary Figure S4a**) to counteract the gain in *Rab7* expression in *Dnmt1*-siRNA transfected cells. This reversed the *Dnmt1* siRNA-triggered increase in EGF/LAMP1 co-localization (**Figures 5I,J**), suggesting that DNMT1 restricts endocytic-based degradation partly through repression of *Rab7* expression.

Ubiquitination is a common denominator in the targeting of substrates to the main protein degradation pathways (Clague and Urbé, 2010), including lysosomal degradation (reviewed in Clague and Urbé, 2006). Interestingly, we determined elevated proportions of ubiquitin-positive cortical interneurons evident

in *Dnmt1*-deficient mice (50 ± 0.8%) compared to wild-type controls (39.5 ± 2%; $^{**}P < 0.01$, *Student*'s *t*-test; $n = 3$ mice per genotype; **Supplementary Figures S4e,f**). Together, our data indicate that DNMT1 acts repressive on intracellular degradative pathways, which could affect long-term neuronal survival.

DISCUSSION

We here provided evidence that DNMT1 is implicated in the compromised long-term survival of inhibitory PV interneurons in the murine cerebral cortex. Aging is characterized by reduced PV interneuron numbers accompanied by declined somatomotor performance and prominent transcriptional remodeling. All effects were attenuated by *Dnmt1* deletion in PV interneurons. While DNMT1 promotes neuronal survival in the developing nervous system, it seems to compromise the long-term survival of PV-interneurons in the aged cortex. However, global transcriptome analyses did not point to a DNMT1-dependent transcriptional regulation of survival or cell death related genes causing the age-related interneuron loss. As repressive DNMT1-dependent DNA methylation restricts synaptic transmission as well as degradative pathways in adult PV interneurons, we hypothesize that impaired long-term survival is an indirect consequence of DNMT1-mediated modulation of synaptic activity and degradation over life-time.

Besides reduced excitability and plasticity (Clark and Taylor, 2011) and declined inhibitory function (Shetty and Turner, 1998; Stanley and Shetty, 2004; Cheng and Lin, 2013), a selective vulnerability of particular neuronal subtypes, like inhibitory interneurons, and GABAergic synapses (Rozycka and Liguz-Lecznar, 2017) was reported in the context of brain aging. Indeed, given the crucial role GABAergic inhibitory interneurons have in cortical information processing, age-dependent defects in inhibitory circuits provide an attractive hypothesis for cognitive decline and age-associated disorders (Rozycka and Liguz-Lecznar, 2017).

Our finding of reduced PV interneuron numbers in old cortices confirms previous studies, that reported a decline in SOM-, CB-, VIP-, and NPY-positive interneurons across species and brain regions (reviewed in Zimmer-Bensch, 2019a). Surprisingly, DNMT1 is implicated in the age-related PV interneuron loss.

Physiological aging involves a decline in synaptic density and functionality (Tanaka et al., 1996; Burke and Barnes, 2006; Polydoro et al., 2009; Berchtold et al., 2013), which includes inhibitory cortical synapses in the cerebral cortex (Rozycka and Liguz-Lecznar, 2017; Calì et al., 2018). Accordingly, aged control mice revealed synapse-related gene downregulation in PV interneurons (**Supplementary Table S1**), which correlated with altered DNA methylation (**Supplementary Table S3**). Similarly, others reported major changes in neurotransmission-related gene expression and repression of GABA-related transcripts in the human prefrontal cortex (Loerch et al., 2008) and across different species (reviewed in Rozycka and Liguz-Lecznar, 2017; Zimmer-Bensch, 2019a).

Some age-regulated synapse-related genes appear to be subject to DNMT1-dependent DNA methylation (**Supplementary Table S4**). Thus, we propose an age- and DNMT1-dependent shutdown of synapse-associated gene expression, which impairs synaptic function. As activity-dependent signaling is described to boost neuronal health through diverse mechanisms, decreased synaptic functionality could affect neuronal survival. Besides transcriptional control of pro- and anti-apoptotic genes, availability of neurotrophic factors and elevation of antioxidant defenses are modulated by neuronal activity (reviewed in Bell and Hardingham, 2011).

We have recently shown that DNMT1 acts on synaptic function of cortical PV interneurons in young mice, modulating GABAergic transmission (Pensold et al., 2020). Alterations in transmitter release affect synaptic strength and both are decreased upon aging (Kumar et al., 2007). Hence, it is conceivable that increased synaptic transmission rates in young *Dnmt1*-deficient interneurons exert protective effects on age-associated synaptic impairments, thereby indirectly promoting survival in aged *Dnmt1*-deficient mice.

Indeed, despite reports of DNMT-dependent developmental regulation of neuronal survival (Hutnick et al., 2009; Rhee et al., 2012; Pensold et al., 2017), direct evidence in the aging brain is still lacking. Comparing gene expression among PV interneuron populations, we found no evidence – in contrast to developing interneurons – that DNMT1 does affect long-term survival in aging brains by transcriptional control of survival- and/or cell death-related genes. Albeit, profiled at high resolution, we did not detect significant expression changes of cell survival or death-associated genes, neither among young and aged controls, nor when comparing *Dnmt1*-deficient and control interneurons. The same is true for genes which were both changed in methylation and transcription upon aging in controls, or between the genotypes, indicating that DNMT1-dependent DNA methylation modulates other processes, which then indirectly affect interneuron survival. Yet, MeDIP sequencing was reported to provide only a limited picture and resolution, e.g., compared to whole genome bisulfide sequencing (Stirzaker et al., 2014). For this our methylation analysis should be interpreted with caution and does not claim to provide an exhaustive picture. What we can state is that our analytical pipeline revealed DNMT1- and age-dependent changes in expression and methylation of proteostasis associated genes, which is supported by functionally validation studies.

Of note, long-term neuronal health ultimately depends on the proteostasis network. Age-related decline in protein homeostasis can cause diverse cellular dysfunctions, contributing to numerous neurodegenerative disorders (Douglas and Dillin, 2010). Endosome-based degradative pathways are crucial for processing and removing defective proteins or protein aggregates by proteolytic degradation in lysosomes (McMahon and Boucrot, 2011). Lysosomes digest both intra- and extracellular material after autophagy or endocytosis, respectively (Stoka et al., 2016). Lysosomal degradation is

compromised in aged neurons (reviewed in Loeffler, 2019), and lysosomal dysfunction is associated with aging and numerous neurodegenerative disorders (Jiang et al., 2001), including Parkinson's and Alzheimer's disease (Büttner et al., 2013; McBrayer and Nixon, 2013; Wolfe et al., 2013; Menezes et al., 2015).

Lysosome-dependent lifespan regulation relies on their fundamental role in autophagy, which reportedly influences longevity. Mice lacking *Atg7* (autophagy related 7), encoding for the E1-like activating enzyme, that is essential for autophagy (Komatsu et al., 2005), develop neuronal loss and die within 28 weeks (Komatsu et al., 2006). In addition, suppression or loss of autophagy in the central nervous system causes neurodegenerative disease in mice (Hara et al., 2006; Komatsu et al., 2006), illustrating the relevance of the proteostasis network for neuronal survival.

A declining proteostasis network accompanies aging and triggers ineffective protein degradation. Aggregation of defective proteins, in turn, eventually leads to cell death (Douglas and Dillin, 2010). Hence, up-regulation of proteostasis-related genes in control interneurons indicates a compensatory response of aging neurons to counteract the remittent proteostasis network (Douglas and Dillin, 2010). This corroborates a previous report of age-related increases in LAMP-2a and HSPA8/Hsc70 concentrations in the mouse retina (Rodríguez-Muela et al., 2013), suggested to compensate for an age-related decrease in macroautophagy. Age-dependent HSPA8/hsc70 elevation was also seen in hippocampus, cortex, cerebellum, septum, and striatum (Calabrese et al., 2004).

Interestingly, such increase in proteostasis-associated gene expression was not detected upon aging in *Dnmt1*-deficient interneurons. This can be explained by the finding that *Dnmt1* deletion itself acts on proteostasis-associated gene expression in young interneurons. Compared to equal-aged controls, *endocytosis*-, *endosome*-, and *lysosome*-related gene expression was augmented in *Dnmt1*-deficient samples (Pensold et al., 2020, **Figure 4G**). While we previously verified that endocytosis-mediated elevated vesicle recycling increases GABAergic transmission of *Dnmt1*-deficient interneurons (Pensold et al., 2020), DNMT1-dependent regulation of degradative pathways so far remained unattended. Here, we validate that *Dnmt1* depletion elevates retrograde endosomal transport and lysosomal targeting, pointing to an improved degradative machinery upon *Dnmt1* depletion. Such boosted degradative actions could be neuroprotective or beneficial for neuronal survival in the long run, preventing age-related interneuron loss as seen in *Dnmt1*-deficient mice.

Together, our data suggest that dysregulation of cell death and/or survival related genes by DNMT1-dependent actions appears to play, if at all, a rather minor role as a potential mechanism underlying the age-related interneuron loss. We anticipate that DNMT1-dependent changes in aged interneurons result from cumulative effects of DNMT1 function during life-time, as the enzyme modulates two crucial aspects of neuronal function: synaptic activity and proteostasis. Hence, we propose a scenario, in which *Dnmt1* deficiency-induced enhancement of synaptic and/or proteostasis function in PV interneurons prevents or delays the age-related degeneration of these cells.

DATA AVAILABILITY STATEMENT

The datasets generated for this study can be found in the GEO database [Series GSE145026].

ETHICS STATEMENT

The animal study was reviewed and approved by Thüringer Landesamt, Bad Langensalza, Germany.

AUTHOR CONTRIBUTIONS

AH performed experiments, data analysis, design of data analysis, figure illustration, and assisted in writing the manuscript. DP, JT, and JG designed and performed experiments, data analysis, and figure illustration. CB performed experiments, data analysis, figure illustration, and assisted in writing the manuscript. LG-B performed experiments, data analysis, and figure illustration. JL performed experiments, figure illustration, and manuscript correction. TP provided help with conceptual design and discussion of results. TL data analysis and design of data analysis. GS-R performed experiments. LM-B performed experiments and data analysis. JM and AU designed and performed experiments, data analysis, and manuscript correction. MS conceptual design and assisted in writing the manuscript. GZ-B conceptual design of the study, designed and performed experiments, data analysis, figure illustration, and wrote the manuscript. All authors contributed to the article and approved the submitted version.

FUNDING

This work was funded by the Deutsche Forschungsgemeinschaft (DFG, German Research Foundation) – 368482240/GRK2416 associated to GZ-B and MS, as well as by the DFG (ZI 1224/8-1) and the IZKF Jena, both associated to GZ-B; in addition to the DFG (MA-3975/2-1) associated to JM.

ACKNOWLEDGMENTS

We thank Susanne Luthin and Fabian Ludewig from the transcriptome analysis laboratory Göttingen for excellent technical assistance. Moreover, we thank Katrin Schubert from the FACS-core facility of the FLI Jena.

SUPPLEMENTARY MATERIAL

The Supplementary Material for this article can be found online at: https://www.frontiersin.org/articles/10.3389/fcell.2020.00639/full#supplementary-material

REFERENCES

Afgan, E., Baker, D., Batut, B., van den Beek, M., Bouvier, D., Cech, M., et al. (2018). Galaxy platform for accessible, reproducible and collaborative biomedical analyses: 2018 update. *Nucleic Acids Res.* 46, W537–W544.

Aguirre-Arteta, A. M., Grunewald, I., Cardoso, M. C., and Leonhardt, H. (2000). Expression of an alternative Dnmt1 isoform during muscle differentiation. *Cell Growth Differ.* 11, 551–559.

Anders, S., Pyl, P. T., and Huber, W. (2015). HTSeq-a Python framework to work with high-throughput sequencing data. *Bioinformatics* 31, 166–169. doi: 10.1093/bioinformatics/btu638

Andrews, S. (2010). *FastQC: A Quality Control Tool for High Throughput Sequence Data*. Available online at: http://www.bioinformatics.babraham.ac.uk?/projects/fastqc/ (accessed October 6, 2011).

Azpurua, J., and Eaton, B. A. (2015). Neuronal epigenetics and the aging synapse. *Front. Cell. Neurosci.* 9:208. doi: 10.3389/fncel.2015.00208

Bell, K. F. S., and Hardingham, G. E. (2011). The influence of synaptic activity on neuronal health. *Curr. Opin. Neurobiol.* 21, 299–305. doi: 10.1016/j.conb.2011.01.002

Bellingham, S. A., Guo, B. B., Coleman, B. M., and Hill, A. F. (2012). Exosomes: Vehicles for the transfer of toxic proteins associated with neurodegenerative diseases? *Front. Physiol.* 3:124. doi: 10.3389/fphys.2012.00124

Berchtold, N. C., Coleman, P. D., Cribbs, D. H., Rogers, J., Gillen, D. L., and Cotman, C. W. (2013). Synaptic genes are extensively downregulated across multiple brain regions in normal human aging and Alzheimer's disease. *Neurobiol. Aging* 34, 1653–1661. doi: 10.1016/j.neurobiolaging.2012.11.024

Bilkei-Gorzo, A. (2014). Genetic mouse models of brain ageing and Alzheimer's disease. *Pharmacol. Ther.* 142, 244–257. doi: 10.1016/j.pharmthera.2013.12.009

Bordner, K. A., Kitchen, R. R., Carlyle, B., George, E. D., Mahajan, M. C., Mane, S. M., et al. (2011). Parallel declines in cognition, motivation, and locomotion in aging mice: association with immune gene upregulation in the medial prefrontal cortex. *Exp. Gerontol.* 46, 643–659. doi: 10.1016/j.exger.2011.03.003

Brewer, G. J. (1997). Isolation and culture of adult rat hippocampal neurons. *J. Neurosci. Methods* 71, 143–155. doi: 10.1016/S0165-0270(96)00136-7

Brewer, G. J., and Torricelli, J. R. (2007). Isolation and culture of adult neurons and neurospheres. *Nat. Protoc.* 2, 1490–1498. doi: 10.1038/nprot.2007.207

Bucci, C., Thomsen, P., Nicoziani, P., McCarthy, J., and Van Deurs, B. (2000). Rab7: a key to lysosome biogenesis. *Mol. Biol. Cell* 11, 467–480. doi: 10.1091/mbc.11.2.467

Burke, S. N., and Barnes, C. A. (2006). Neural plasticity in the ageing brain. *Nat. Rev. Neurosci.* 7, 30–40. doi: 10.1038/nrn1809

Büttner, S., Faes, L., Reichelt, W. N., Broeskamp, F., Habernig, L., Benke, S., et al. (2013). The Ca^{2+} /Mn^{2+} ion-pump PMR1 links elevation of cytosolic Ca^{2+} levels to -synuclein toxicity in Parkinson's disease models. *Cell Death Differ.* 20, 465–477. doi: 10.1038/cdd.2012.142

Buzsáki, G., and Wang, X.-J. (2012). Mechanisms of Gamma Oscillations. *Annu. Rev. Neurosci.* 35, 203–225. doi: 10.1146/annurev-neuro-062111-150444

Calabrese, V., Scapagnini, G., Ravagna, A., Colombrita, C., Spadaro, F., Butterfield, D. A., et al. (2004). Increased expression of heat shock proteins in rat brain during aging: relationship with mitochondrial function and glutathione redox state. *Mech. Ageing Dev.* 125, 325–335. doi: 10.1016/j.mad.2004.01.003

Calì, C., Wawrzyniak, M., Becker, C., Maco, B., Cantoni, M., Jorstad, A., et al. (2018). The effects of aging on neuropil structure in mouse somatosensory cortex—A 3D electron microscopy analysis of layer 1. *PLoS One* 13:e0198131. doi: 10.1371/journal.pone.0198131

Carmona-Gutierrez, D., Hughes, A. L., Madeo, F., and Ruckenstuhl, C. (2016). The crucial impact of lysosomes in aging and longevity. *Ageing Res. Rev.* 32, 2–12. doi: 10.1016/j.arr.2016.04.009

Casillas, M. A., Lopatina, N., Andrews, L. G., and Tollefsbol, T. O. (2003). Transcriptional control of the DNA methyltransferases is altered in aging and neoplastically-transformed human fibroblasts. *Mol. cell. biochem.* 252, 33–43. doi: 10.1023/a:1025548623524

Cech, T. R., and Steitz, J. A. (2014). The noncoding RNA revolution - Trashing old rules to forge new ones. *Cell* 157, 77–94. doi: 10.1016/j.cell.2014.03.008

Cheng, C.-H., and Lin, Y.-Y. (2013). Aging-related decline in somatosensory inhibition of the human cerebral cortex. *Exp. Brain Res.* 226, 145–152. doi: 10.1007/s00221-013-3420-9

Clague, M. J., and Urbé, S. (2006). Endocytosis: the DUB version. *Trends Cell Biol.* 16, 551–559. doi: 10.1016/j.tcb.2006.09.002

Clague, M. J., and Urbé, S. (2010). Ubiquitin: same molecule, different degradation pathways. *Cell* 143, 682–685. doi: 10.1016/j.cell.2010.11.012

Clark, B. C., and Taylor, J. L. (2011). Age-related changes in motor cortical properties and voluntary activation of skeletal muscle. *Curr. Aging Sci.* 4, 192–199. doi: 10.2174/1874609811104030192

Cui, D., and Xu, X. (2018). DNA methyltransferases, DNA methylation, and age-associated cognitive function. *Int. J. Mol. Sci.* 19:1315. doi: 10.3390/ijms19051315

Deak, F., and Sonntag, W. E. (2012). Aging, synaptic dysfunction, and insulin-like growth factor (IGF)-1. *J. Gerontol.* 67, 611–625.

DeFelipe, J., and Fariñas, I. (1992). The pyramidal neuron of the cerebral cortex: morphological and chemical characteristics of the synaptic inputs. *Prog. Neurobiol.* 39, 563–607. doi: 10.1016/0301-0082(92)90015-7

Delpech, J.-C., Herron, S., Botros, M. B., and Ikezu, T. (2019). Neuroimmune crosstalk through extracellular vesicles in health and disease. *Trends Neurosci.* 42, 361–372. doi: 10.1016/j.tins.2019.02.007

Dobin, A., Davis, C. A., Schlesinger, F., Drenkow, J., Zaleski, C., Jha, S., et al. (2013). STAR: ultrafast universal RNA-seq aligner. *Bioinformatics* 29, 15–21.

Douglas, P. M., and Dillin, A. (2010). Protein homeostasis and aging in neurodegeneration. *J. Cell Biol.* 190, 719–729. doi: 10.1083/jcb.201005144

Druga, R. (2009). Neocortical inhibitory system. *Folia Biol.* 55, 201–217.

Ehlers, M. D. (2000). Reinsertion or degradation of AMPA receptors determined by activity-dependent endocytic sorting. *Neuron* 28, 511–525. doi: 10.1016/S0896-6273(00)00129-X

Eide, L., and McMurray, C. T. (2005). Culture of adult mouse neurons. *BioTechniques* 38, 99–104. doi: 10.2144/05381RR02

Feng, J., Zhou, Y., Campbell, S. L., Le, T., Li, E., Sweatt, J. D., et al. (2010). Dnmt1 and Dnmt3a maintain DNA methylation and regulate synaptic function in adult forebrain neurons. *Nat. Neurosci.* 13, 423–430. doi: 10.1038/nn.2514

Freeman, O. J., and Mallucci, G. R. (2016). The UPR and synaptic dysfunction in neurodegeneration. *Brain Res.* 1648, 530–537. doi: 10.1016/j.brainres.2016.03.029

Fuks, F. (2005). DNA methylation and histone modifications: teaming up to silence genes. *Curr. Opin. Genet. Dev.* 15, 490–495. doi: 10.1016/j.gde.2005.08.002

Geisler, S., and Coller, J. (2013). RNA in unexpected places: long non-coding RNA functions in diverse cellular contexts. *Nat. Rev. Mol. Cell Biol.* 14, 699–712. doi: 10.1038/nrm3679

Gelfman, S., Cohen, N., Yearim, A., and Ast, G. (2013). DNA-methylation effect on cotranscriptional splicing is dependent on GC architecture of the exon-intron structure. *Genome Res.* 23, 789–799. doi: 10.1101/gr.143503.112

Ghiglieri, V., Calabrese, V., and Calabresi, P. (2018). Alpha-synuclein: from early synaptic dysfunction to neurodegeneration. *Front. Neurol.* 9:295. doi: 10.3389/fneur.2018.00295

Gruenberg, J. (2001). The endocytic pathway: a mosaic of domains. *Nat. Rev. Mol. Cell Biol.* 2, 721–730. doi: 10.1038/35096054

Haglund, K., and Dikic, I. (2012). The role of ubiquitylation in receptor endocytosis and endosomal sorting. *J. Cell Sci.* 125, 265–275. doi: 10.1242/jcs.091280

Halder, R., Hennion, M., Vidal, R. O., Shomroni, O., Rahman, R. U., Rajput, A., et al. (2015). DNA methylation changes in plasticity genes accompany the formation and maintenance of memory. *Nat. Neurosci.* 19, 102–110. doi: 10.1038/nn.4194

Hara, T., Nakamura, K., Matsui, M., Yamamoto, A., Nakahara, Y., Suzuki-Migishima, R., et al. (2006). Suppression of basal autophagy in neural cells causes neurodegenerative disease in mice. *Nature* 441, 885–889. doi: 10.1038/nature04724

Hebert, M. A., and Gerhardt, G. A. (1998). Normal and drug-induced locomotor behavior in aging: comparison to evoked DA release and tissue content in Fischer 344 rats. *Brain Res.* 797, 42–54. doi: 10.1016/S0006-8993(98)00370-9

Hippenmeyer, S., Vrieseling, E., Sigrist, M., Portmann, T., Laengle, C., Ladle, D. R., et al. (2005). A developmental switch in the response of DRG Neurons to ETS transcription factor signaling. *PLoS Biol.* 3:e159. doi: 10.1371/journal.pbio.0030159

Hutnick, L. K., Golshani, P., Namihira, M., Xue, Z., Matynia, A., Yang, X. W., et al. (2009). DNA hypomethylation restricted to the murine forebrain induces

cortical degeneration and impairs postnatal neuronal maturation. *Hum. Mol. Genet.* 18, 2875–2888. doi: 10.1093/hmg/ddp222

Ianov, L., Rani, A., Beas, B. S., Kumar, A., and Foster, T. C. (2016). Transcription profile of aging and cognition-related genes in the medial prefrontal cortex. *Front. Aging Neurosci.* 8:113. doi: 10.3389/fnagi.2016.00113

Issa, J.-P. (2002). Epigenetic variation and human disease. *J. Nutr.* 132, 2388S–2392S. doi: 10.1093/jn/132.8.2388s

Jackson-Grusby, L., Beard, C., Possemato, R., Tudor, M., Fambrough, D., Csankovszki, G., et al. (2001). Loss of genomic methylation causes p53-dependent apoptosis and epigenetic deregulation. *Nat. Genet.* 27, 31–39. doi: 10.1038/83730

Jessen, S. B., Mathiesen, C., Lind, B. L., and Lauritzen, M. (2017). Interneuron deficit associates attenuated network synchronization to mismatch of energy supply and demand in aging mouse brains. *Cereb. Cortex* 27, 646–659. doi: 10.1093/cercor/bhv261

Jiang, C. H., Tsien, J. Z., Schultz, P. G., and Hu, Y. (2001). The effects of aging on gene expression in the hypothalamus and cortex of mice. *Proc. Natl. Acad. Sci. U.S.A.* 98, 1930–1934. doi: 10.1073/pnas.98.4.1930

Johnson, A. A., Akman, K., Calimport, S. R. G., Wuttke, D., Stolzing, A., and De Magalhães, J. P. (2012). The role of DNA methylation in aging, rejuvenation, and age-related disease. *Rejuvenation Res.* 15, 483–494. doi: 10.1089/rej.2012.1324

Jones, M. J., Goodman, S. J., and Kobor, M. S. (2015). DNA methylation and healthy human aging. *Aging Cell* 14, 924–932. doi: 10.1111/acel.12349

Jucker, M., and Ingram, D. K. (1997). Murine models of brain aging and age-related neurodegenerative diseases. *Behav. Brain Res.* 85, 1–25. doi: 10.1016/S0166-4328(96)02243-7

Kann, O., Papageorgiou, I. E., and Draguhn, A. (2014). Highly energized inhibitory interneurons are a central element for information processing in cortical networks. *J. Cereb. Blood Flow Metab.* 34, 1270–1282. doi: 10.1038/jcbfm.2014.104

Kedlian, V. R., Donertas, H. M., and Thornton, J. M. (2019). The widespread increase in inter-individual variability of gene expression in the human brain with age. *Aging* 11, 2253–2280. doi: 10.18632/aging.101912

Kim, W., and Seo, H. (2014). Baclofen, a GABAB receptor agonist, enhances ubiquitin-proteasome system functioning and neuronal survival in Huntington's disease model mice. *Biochem. Biophys. Res. Commun.* 443, 706–711. doi: 10.1016/j.bbrc.2013.12.034

Kimmel, J. C., Penland, L., Rubinstein, N. D., Hendrickson, D. G., Kelley, D. R., and Rosenthal, A. Z. (2019). Murine single-cell RNA-seq reveals cell-identity- and tissue-specific trajectories of aging. *Genome Res.* 29, 2088–2103. doi: 10.1101/gr.253880.119

Kobayashi, Y., and Hensch, T. K. (2013). Germline recombination by conditional gene targeting with Parvalbumin-Cre lines. *Front. Neural Circuits* 7:168. doi: 10.3389/fncir.2013.00168

Komatsu, M., Waguri, S., Chiba, T., Murata, S., Iwata, J.-I., Tanida, I., et al. (2006). Loss of autophagy in the central nervous system causes neurodegeneration in mice. *Nature* 441, 880–884. doi: 10.1038/nature04723

Komatsu, M., Waguri, S., Ueno, T., Iwata, J., Murata, S., Tanida, I., et al. (2005). Impairment of starvation-induced and constitutive autophagy in Atg7-deficient mice. *J. Cell Biol.* 169, 425–434. doi: 10.1083/jcb.200412022

Kumar, A., Thinschmidt, J. S., Foster, T. C., and King, M. A. (2007). Aging effects on the limits and stability of long-term synaptic potentiation and depression in rat hippocampal area CA1. *J. Neurophysiol.* 98, 594–601. doi: 10.1152/jn.00249.2007

Langmead, B., and Salzberg, S. L. (2012). Fast gapped-read alignment with Bowtie 2. *Nat. Methods* 9, 357–359. doi: 10.1038/nmeth.1923

Lardenoije, R., Iatrou, A., Kenis, G., Kompotis, K., Steinbusch, H. W. M., Mastroeni, D., et al. (2015). The epigenetics of aging and neurodegeneration. *Prog. Neurobiol.* 131, 21–64. doi: 10.1016/j.pneurobio.2015.05.002

Li, H., Handsaker, B., Wysoker, A., Fennell, T., Ruan, J., Homer, N., et al. (2009). The Sequence Alignment/Map format and SAMtools. *Bioinformatics* 25, 2078–2079. doi: 10.1093/bioinformatics/btp352

Lienhard, M., Grimm, C., Morkel, M., Herwig, R., and Chavez, L. (2014). MEDIPS: genome-wide differential coverage analysis of sequencing data derived from DNA enrichment experiments. *Bioinformatics* 30, 284–286. doi: 10.1093/bioinformatics/btt650

Liguz-Lecznar, M., Lehner, M., Kaliszewska, A., Zakrzewska, R., Sobolewska, A., and Kossut, M. (2015). Altered glutamate/GABA equilibrium in aged mice cortex influences cortical plasticity. *Brain Struct. Funct.* 220, 1681–1693. doi: 10.1007/s00429-014-0752-6

Loeffler, D. A. (2019). Influence of normal aging on brain autophagy: a complex scenario. *Front. Aging Neurosci.* 11:49. doi: 10.3389/fnagi.2019.00049

Loerch, P. M., Lu, T., Dakin, K. A., Vann, J. M., Isaacs, A., Geula, C., et al. (2008). Evolution of the aging brain transcriptome and synaptic regulation. *PLoS One* 3:e3329. doi: 10.1371/journal.pone.0003329

Love, M. I., Huber, W., and Anders, S. (2014). Moderated estimation of fold change and dispersion for RNA-seq data with DESeq2. *Genome Biol.* 15:550. doi: 10.1186/s13059-014-0550-8

Luo, W., and Brouwer, C. (2013). Pathview: an R/Bioconductor package for pathway-based data integration and visualization. *Bioinformatics* 29, 1830–1831. doi: 10.1093/BIOINFORMATICS

Lyko, F. (2018). The DNA methyltransferase family: a versatile toolkit for epigenetic regulation. *Nat. Rev. Genet.* 19, 81–92. doi: 10.1038/nrg.2017.80

Madisen, L., Zwingman, T. A., Sunkin, S. M., Oh, S. W., Zariwala, H. A., Gu, H., et al. (2010). A robust and high-throughput Cre reporting and characterization system for the whole mouse brain. *Nat. Neurosci.*13, 133–140. doi: 10.1038/nn.2467

Maunakea, A. K., Nagarajan, R. P., Bilenky, M., Ballinger, T. J., Dsouza, C., Fouse, S. D., et al. (2010). Conserved role of intragenic DNA methylation in regulating alternative promoters. *Nature* 466, 253–257. doi: 10.1038/nature09165

McBrayer, M., and Nixon, R. A. (2013). Lysosome and calcium dysregulation in Alzheimer's disease: partners in crime. *Biochem. Soc. Trans.* 41, 1495–1502. doi: 10.1042/BST20130201

McMahon, H. T., and Boucrot, E. (2011). Molecular mechanism and physiological functions of clathrin-mediated endocytosis. *Nat. Rev. Mol. Cell Biol.* 12, 517–533. doi: 10.1038/nrm3151

Meadows, J. P., Guzman-Karlsson, M. C., Phillips, S., Brown, J. A., Strange, S. K., Sweatt, J. D., et al. (2016). Dynamic DNA methylation regulates neuronal intrinsic membrane excitability. *Sci. Signal.* 9:ra83. doi: 10.1126/scisignal.aaf5642

Meadows, J. P., Guzman-Karlsson, M. C., Phillips, S., Holleman, C., Posey, J. L., Day, J. J., et al. (2015). DNA methylation regulates neuronal glutamatergic synaptic scaling. *Sci. Signal.* 8:ra61. doi: 10.1126/scisignal.aab0715

Menezes, R., Tenreiro, S., Macedo, D., Santos, C. N., and Outeiro, T. F. (2015). From the baker to the bedside: yeast models of parkinson's disease. *Microb. Cell* 2, 262–279. doi: 10.15698/mic2015.08.219

Metz, G. A., and Whishaw, I. Q. (2009). The ladder rung walking task: a scoring system and its practical application. *J. Vis. Exp.* 28:e1204. doi: 10.3791/1204

Miettinen, R., Sirviö, J., Riekkinen, P., Laakso, M. P., Riekkinen, M., and Riekkinen, P. (1993). Neocortical, hippocampal and septal parvalbumin- and somatostatin-containing neurons in young and aged rats: correlation with passive avoidance and water maze performance. *Neuroscience* 53, 367–378. doi: 10.1016/0306-4522(93)90201-P

Morrison, J. H., and Baxter, M. G. (2012). The ageing cortical synapse: hallmarks and implications for cognitive decline. *Nat. Rev.* 13, 240–250. doi: 10.1038/nrn3200

Nixon, R. A., and Cataldo, A. M. (1995). The endosomal-lysosomal system of neurons: new roles. *Trends Neurosci.* 18, 489–496. doi: 10.1016/0166-2236(95)92772-I

Nixon, R. A., Cataldo, A. M., and Mathews, P. M. (2000). The endosomal-lysosomal system of neurons in Alzheimer's disease pathogenesis: a review. *Neurochem. Res.* 25, 1161–1172. doi: 10.1023/A:1007675508413

Ouda, L., Druga, R., and Syka, J. (2008). Changes in parvalbumin immunoreactivity with aging in the central auditory system of the rat. *Exp. Gerontol.* 43, 782–789. doi: 10.1016/j.exger.2008.04.001

Pensold, D., Reichard, J., Van Loo, K. M. J., Ciganok, N., Hahn, A., Bayer, C., et al. (2020). DNA methylation-mediated modulation of endocytosis as potential mechanism for synaptic function regulation in murine inhibitory cortical interneurons. *Cereb. Cortex* 30, 3921–3937. doi: 10.1093/cercor/bhaa009

Pensold, D., Symmank, J., Hahn, A., Lingner, T., Salinas-Riester, G., Downie, B. R., et al. (2017). The DNA methyltransferase 1 (DNMT1) controls the shape and dynamics of migrating POA-derived interneurons fated for the murine cerebral cortex. *Cereb. Cortex* 27, 5696–5714. doi: 10.1093/cercor/bhw341

Pitt, J., Wilcox, K. C., Tortelli, V., Diniz, L. P., Oliveira, M. S., Dobbins, C., et al. (2017). Neuroprotective astrocyte-derived insulin/insulin-like growth factor 1 stimulates endocytic processing and extracellular release of neuron-bound Aβ oligomers. *Mol. Biol. Cell* 28, 2623–2636. doi: 10.1091/mbc.E17-06-0416

Polydoro, M., Acker, C. M., Duff, K., Castillo, P. E., and Davies, P. (2009). Age-dependent impairment of cognitive and synaptic function in the htau mouse model of Tau pathology. *J. Neurosci.* 29, 10741–10749. doi: 10.1523/JNEUROSCI.1065-09.2009

Racay, P., Gregory, P., and Schwaller, B. (2006). Parvalbumin deficiency in fast-twitch muscles leads to increased "slow-twitch type" mitochondria, but does not affect the expression of fiber specific proteins. *FEBS J.* 273, 96–108. doi: 10.1111/j.1742-4658.2005.05046.x

Rhee, K.-D., Yu, J., Zhao, C. Y., Fan, G., and Yang, X.-J. (2012). Dnmt1-dependent DNA methylation is essential for photoreceptor terminal differentiation and retinal neuron survival. *Cell Death Dis.* 3:e427. doi: 10.1038/cddis.2012.165

Riva, P., Battaglia, C., and Venturin, M. (2019). Emerging role of genetic alterations affecting exosome biology in neurodegenerative diseases. *Int. J. Mol. Sci.* 20:4113. doi: 10.3390/ijms20174113

Robinson, M. D., McCarthy, D. J., and Smyth, G. K. (2010). edgeR: a Bioconductor package for differential expression analysis of digital gene expression data. *Bioinformatics* 26, 139–140. doi: 10.1093/BIOINFORMATICS

Rodríguez-Muela, N., Koga, H., García-Ledo, L., de la Villa, P., de la Rosa, E. J., Cuervo, A. M., et al. (2013). Balance between autophagic pathways preserves retinal homeostasis. *Aging Cell* 12, 478–488. doi: 10.1111/acel.12072

Rossignol, E. (2011). Genetics and function of neocortical GABAergic interneurons in neurodevelopmental disorders. *Neural Plast.* 2011:649325. doi: 10.1155/2011/649325

Rozycka, A., and Liguz-Lecznar, M. (2017). The space where aging acts: focus on the GABAergic synapse. *Aging Cell* 16, 634–643. doi: 10.1111/acel.12605

Saeedi, S., Israel, S., Nagy, C., and Turecki, G. (2019). The emerging role of exosomes in mental disorders. *Transl. Psychiatry* 9:122. doi: 10.1038/s41398-019-0459-9

Saxena, A., Wagatsuma, A., Noro, Y., Kuji, T., Asaka-Oba, A., Watahiki, A., et al. (2012). Trehalose-enhanced isolation of neuronal sub-types from adult mouse brain. *BioTechniques* 52, 381–385. doi: 10.2144/0000113878

Schindelin, J., Arganda-Carreras, I., Frise, E., Kaynig, V., Longair, M., Pietzsch, T., et al. (2012). Fiji: an open-source platform for biological-image analysis. *Nat. Methods* 9, 676–682. doi: 10.1038/nmeth.2019

Shetty, A. K., and Turner, D. A. (1998). Hippocampal interneurons expressing glutamic acid decarboxylase and calcium-binding proteins decrease with aging in Fischer 344 rats. *J. Comp. Neurol.* 394, 252–269. doi: 10.1002/(sici)1096-9861(19980504)394:2<252::aid-cne9>3.0.co;2-1

Shimoda, N., Izawa, T., Yoshizawa, A., Yokoi, H., Kikuchi, Y., and Hashimoto, N. (2014). Decrease in cytosine methylation at CpG island shores and increase in DNA fragmentation during zebrafish aging. *Age* 36, 103–115. doi: 10.1007/s11357-013-9548-5

Sohal, V. S., Zhang, F., Yizhar, O., and Deisseroth, K. (2009). Parvalbumin neurons and gamma rhythms enhance cortical circuit performance. *Nature* 459, 698–702. doi: 10.1038/nature07991

Stanley, D. P., and Shetty, A. K. (2004). Aging in the rat hippocampus is associated with widespread reductions in the number of glutamate decarboxylase-67 positive interneurons but not interneuron degeneration. *J. Neurochem.* 89, 204–216. doi: 10.1111/j.1471-4159.2004.02318.x

Stegeman, R., and Weake, V. M. (2017). Transcriptional signatures of aging. *J. Mol. Biol.* 429, 2427–2437. doi: 10.1016/j.jmb.2017.06.019

Stirzaker, C., Taberlay, P. C., Statham, A. L., and Clark, S. J. (2014). Mining cancer methylomes: prospects and challenges. *Trends Genet.* 30, 75–84. doi: 10.1016/j.tig.2013.11.004

Stoka, V., Turk, V., and Turk, B. (2016). Lysosomal cathepsins and their regulation in aging and neurodegeneration. *Ageing Res. Rev.* 32, 22–37. doi: 10.1016/j.arr.2016.04.010

Symmank, J., and Zimmer, G. (2017). Regulation of neuronal survival by DNA methyltransferases. *Neural Regen. Res.* 12, 1768–1775. doi: 10.4103/1673-5374.219027

Symmank, J., Bayer, C., Reichard, j., Pensold, D., and Zimmer-Bensch, G. (2020). Neuronal *Lhx1* expression is regulated by DNMT1-dependent modulation of histone marks. *Epigenetics* doi: 10.1080/15592294.2020.1767372

Symmank, J., Bayer, C., Schmidt, C., Hahn, A., Pensold, D., and Zimmer-Bensch, G. (2018). DNMT1 modulates interneuron morphology by regulating Pak6 expression through crosstalk with histone modifications. *Epigenetics* 13, 536–556. doi: 10.1080/15592294.2018.1475980

Tanaka, Y., Hasegawa, A., and Ando, S. (1996). Impaired synaptic functions with aging as characterized by decreased calcium influx and acetylcholine release. *J. Neurosci. Res.* 43, 63–70. doi: 10.1002/jnr.490430108

Torrey, E. F., Barci, B. M., Webster, M. J., Bartko, J. J., Meador-Woodruff, J. H., and Knable, M. B. (2005). Neurochemical markers for schizophrenia, bipolar disorder, and major depression in postmortem brains. *Biol. Psychiatry* 57, 252–260. doi: 10.1016/j.biopsych.2004.10.019

Verret, L., Mann, E. O., Hang, G. B., Barth, A. M. I., Cobos, I., Ho, K., et al. (2012). Inhibitory interneuron deficit links altered network activity and cognitive dysfunction in Alzheimer model. *Cell* 149, 708–721. doi: 10.1016/j.cell.2012.02.046

Wang, L., Zhao, Y., Bao, X., Zhu, X., Kwok, Y. K. Y., Sun, K., et al. (2015). LncRNA Dum interacts with Dnmts to regulate Dppa2 expression during myogenic differentiation and muscle regeneration. *Cell Res.* 25, 335–350. doi: 10.1038/cr.2015.21

Wei, Y. N., Hu, H. Y., Xie, G. C., Fu, N., Ning, Z. B., Zeng, R., et al. (2015). Transcript and protein expression decoupling reveals RNA binding proteins and miRNAs as potential modulators of human aging. *Genome Biol.* 16:41. doi: 10.1186/s13059-015-0608-2

Willems, J. G. P., Wadman, W. J., and Cappaert, N. L. M. (2018). Parvalbumin interneuron mediated feedforward inhibition controls signal output in the deep layers of the perirhinal-entorhinal cortex. *Hippocampus* 28, 281–296. doi: 10.1002/hipo.22830

Winckler, B., Faundez, X. V., Maday, S., Cai, Q., Cláudia, X., Almeida, G., et al. (2018). The Endolysosomal system and proteostasis: from development to degeneration. *J. Neurosci.* 38, 9364–9374. doi: 10.1523/JNEUROSCI.1665-18.2018

Wolfe, D. M., Lee, J. H., Kumar, A., Lee, S., Orenstein, S. J., et al. (2013). Autophagy failure in Alzheimer's disease and the role of defective lysosomal acidification. *Eur. J. Neurosci.* 37, 1949–1961. doi: 10.1111/ejn.12169

Xu, X., Zhan, M., Duan, W., Prabhu, V., Brenneman, R., Wood, W., et al. (2007). Gene expression atlas of the mouse central nervous system: impact and interactions of age, energy intake and gender. *Genome Biol.* 8:R234. doi: 10.1186/gb-2007-8-11-r234

Zampieri, M., Ciccarone, F., Calabrese, R., Franceschi, C., Bürkle, A., and Caiafa, P. (2015). Reconfiguration of DNA methylation in aging. *Mech. Ageing Dev.* 151, 60–70. doi: 10.1016/j.mad.2015.02.002

Zhang, L., Sheng, R., and Qin, Z. (2009). The lysosome and neurodegenerative diseases. *Acta Biochim. Biophys. Sin.* 41, 437–445. doi: 10.1093/ABBS/GMP031

Zimmer, G., Rudolph, J., Landmann, J., Gerstmann, K., Steinecke, A., Gampe, C., et al. (2011). Bidirectional EphrinB3/EphA4 signaling mediates the segregation of medial ganglionic eminence-and preoptic area-derived interneurons in the deep and superficial migratory stream. *J. Neurosci.* 31, 18364–18380. doi: 10.1523/JNEUROSCI.4690-11.2011

Zimmer-Bensch, G. (2019a). "Functional implications of dynamic DNA methylation for the developing, aging and diseased brain," in *The DNA, RNA, and Histone Methylomes*, eds S. Jurga, and J. Barciszewski (Cham: Springer), 141–163. doi: 10.1007/978-3-030-14792-1_6

Zimmer-Bensch, G. (2019b). Emerging Roles of Long Non-Coding RNAs as Drivers of Brain Evolution. *Cells* 8:1399. doi: 10.3390/cells8111399

Conflict of Interest: The authors declare that the research was conducted in the absence of any commercial or financial relationships that could be construed as a potential conflict of interest.

frontiers in Cell and Developmental Biology

ORIGINAL RESEARCH
published: 05 August 2020
doi: 10.3389/fcell.2020.00734

Wnt Signaling Pathway Dysregulation in the Aging Brain: Lessons From the *Octodon degus*

Nibaldo C. Inestrosa[1,2], Cheril Tapia-Rojas[2], Carolina B. Lindsay[2] and Juan Manuel Zolezzi[1]*

[1] Centro de Envejecimiento y Regeneración (CARE), Departamento de Biología Celular y Molecular, Facultad de Ciencias Biológicas, Pontificia Universidad Católica de Chile, Santiago, Chile, [2] Centro de Excelencia en Biomedicina de Magallanes (CEBIMA), Universidad de Magallanes, Punta Arenas, Chile

Wnt signaling constitutes a fundamental cellular and molecular pathway, necessary from proper embryogenesis to function-maintenance of fully developed complex organisms. In this regard, Wnt pathway plays a crucial role in both the development of the central nervous system and in maintaining the structure and function of the neuronal circuits, and it has been suggested that its dysregulation is critical in the onset of several pathologies including cancer and neurodegenerative disorders, such as Alzheimer's disease (AD). Due to its relevance in the maintenance of the neuronal activity and its involvement in the outbreak of devastating diseases, we explored the age-related changes in the expression of Wnt key components in the cortex and hippocampus of 7 to 72-months-old *Octodon degus* (*O. degus*), a Chilean long-living endemic rodent that has been proposed and used as a natural model for AD. We found a down-regulation in the expression of different Wnt ligands (Wnt3a, Wnt7a, and Wnt5a), as well as in the Wnt co-receptor LRP6. We also observed an increase in the activity of GSK-3β related to the down-regulation of Wnt activity, a fact that was confirmed by a decreased expression of Wnt target genes. Relevantly, an important increase was found in secreted endogenous Wnt inhibitors, including the secreted-frizzled-related protein 1 and 2 (SFRP-1 and SFRP-2) and Dickkopf-1 (Dkk-1), all them antagonists at the cell surface. Furthermore, treatment with Andrographolide, a labdane diterpene obtained from *Andrographis paniculata*, prevents Wnt signaling loss in aging *degus*. Taken together, these results suggest that during the aging process Wnt signaling activity decreases in the brain of *O. degus*.

Keywords: Wnt signaling, aging, *O. degus*, neurodegeneration, Alzheimers' disease

OPEN ACCESS

Edited by:
Stylianos Kosmidis, Columbia University, United States

Reviewed by:
Nady Braidy, University of New South Wales, Australia
Paola Bovolenta, Consejo Superior de Investigaciones Científicas (CSIC), Spain
Clorinda Arias, National Autonomous University of Mexico, Mexico

****Correspondence:***
Nibaldo C. Inestrosa
ninestrosa@bio.puc.cl

Specialty section:
This article was submitted to Molecular Medicine, a section of the journal Frontiers in Cell and Developmental Biology

Received: *22 April 2020*
Accepted: *15 July 2020*
Published: *05 August 2020*

Citation:
Inestrosa NC, Tapia-Rojas C, Lindsay CB and Zolezzi JM (2020) Wnt Signaling Pathway Dysregulation in the Aging Brain: Lessons From the Octodon degus. Front. Cell Dev. Biol. 8:734. doi: 10.3389/fcell.2020.00734

HIGHLIGHTS

- The aging process involves the dysregulation of the Wnt signaling pathway, including ligands, downstream effectors and Wnt target genes in both hippocampus and cortex of *O. degus*.
- Soluble endogenous inhibitors of Wnt signaling pathway increase in an age-dependent manner in both hippocampus and cortex of *O. degus*.
- Age-related Wnt signaling impairments in *O. degus* were recovered by Andrographolide (ANDRO) treatment.

INTRODUCTION

Increased aging of the world population has become a worldwide concern mainly because the close relationship between age and the appearance of different pathologies. Indeed, aging is considered the main risk factor for several pathologies, including cancer, and neurodegenerative disorders, such as Alzheimer's disease (AD) and Parkinson's disease, among others (Inestrosa and Toledo, 2008; Nusse and Clevers, 2017; Oliva et al., 2018; Steinhart and Angers, 2018; Palomer et al., 2019).

Behind the aged phenotype, a relevant feature of the aging process is the gradual loss of activity or alteration of several molecular components necessary for cell physiology. Molecular pathways, which usually encompass an amply range of biological molecules, drive the different cellular processes and, ultimately, determine the cellular fate. In this regard, the signaling pathways mediated by the Wnt ligands are involved in diverse aspects of cell-cell communication, including the regulation of cell proliferation, the occurrence of fibrosis, and cellular morphogenesis (Cisternas et al., 2014; Fuenzalida et al., 2016; Gammons and Bienz, 2018). Currently, 19 Wnt ligands have been described in vertebrates, which may initiate either of two signaling pathways called the canonical and the non-canonical pathways (Nusse and Clevers, 2017; Oliva et al., 2018). Relevantly, although Wnt pathway has been recognized as critical for the central nervous system development, several Wnt components retain their expression in the adult brain, including the hippocampus, and have proven to be fundamental in both the development and function of synapses (Inestrosa and Arenas, 2010; Inestrosa and Varela-Nallar, 2015). Indeed, different studies have indicated a strong correlation between Wnt signaling alteration and the appearance of neurodegenerative disorders, such as AD (Caricasole et al., 2004; Inestrosa and Toledo, 2008; Garcia-Velazquez and Arias, 2017). In this particular case, it is clear that the expression of some Wnt components change during the progression of AD, such as β-catenin which was reduced in patients carrying presenilin-1-inherited mutations (Zhang et al., 1998). Moreover, Wnt signaling activation can inhibit the formation of the amyloid-β peptide (Aβ) aggregates; and Apolipoprotein E ε4, the main risk factor for AD, can inhibits Wnt signaling (Roses, 1994; Liu M. et al., 2014). Altogether, these findings strongly suggest that Wnt signaling might be down-regulated during aging, leading to increased vulnerability of the neural network and increasing the risk for the onset and progression of age-related pathologies, such as AD. Considering that Wnt signaling activation attenuates the cognitive decline observed in the rodent adult brain (Toledo and Inestrosa, 2010; Vargas et al., 2014), it is likely that the modulation of endogenous Wnt signaling components might represent a promising strategy to achieve healthy aging (Gammons and Bienz, 2018; Palomer et al., 2019).

Interestingly, during the last decade several studies have identified the *Octodon degus,* a South American rodent endemic to Central Chile, as a model that naturally develops several molecular and physiological hallmarks attributable to neuropathological changes, including neuronal plasticity decrease, cognitive decline, and neuroinflammation (Inestrosa et al., 2005; Rivera et al., 2016; Cisternas et al., 2018; Lindsay et al., 2020). Remarkably, these events resemble the molecular features observed during AD development, suggesting that *O. degus* may constitute a more reliable model of this pathology (Inestrosa et al., 2005; Cisternas et al., 2018).

Thus, in the present work we studied the brain expression and activity of several Wnt signaling components, critical for the proper functioning of this pathway, during the aging of *O. degus.* We observed in both, cortex and hippocampus, a significant decrease in the expression of several Wnt ligands and Wnt components in an age-dependent manner. These results were correlated with a decrease in the expression of Wnt target genes. Together, our results are consistent with the idea that the loss of function of the Wnt signaling pathway is a feature of the aged brain and it might be responsible, at least in part, for the cognitive deficits observed in aged rodents (Oliva et al., 2018).

MATERIALS AND METHODS

Animals

Octodon degus were obtained from a breeding colony at the animal facility of the Universidad de Valparaiso, Chile, and were maintained in a controlled temperature room (23 ± 1°C) under a 12:12 light/dark cycle with water and food *ad libitum*. *O. degus* of either sex were grouped by age: 7 to 72 months old, where no differences were observed between males and females animals. *O. degus* live on average 7 years in captivity, making it a useful model for longitudinal studies (Lee, 2004). As well as in our study, former researchers in the laboratory have classified the *O. degus* age-groups in young (1–2 years), adult (3–5 years old), and old (6 years old or more; Inestrosa et al., 2015). This classification was made based on previous studies performed in *O. degus*. van Groen et al. (2011) classified them in young (1 year old), adult (3 years old), and aged (6 years old; van Groen et al., 2011), and Du et al. (2015) divide them in young (average 1 year old), adult (average 2 years), and old (average 6 years; Du et al., 2015).

Another group of adult female *O. degus* (56 months old) and young female *O. degus* (12 months old) obtained from our colony at Faculty of Biological Sciences, Pontificia Universidad Católica de Chile were also used. These animals were all derived from laboratory-bred lines. *O. degus* were randomly divided into three groups (n = 8 per group) with bedding of hardwood chips and with water and food *ad libitum*. For the appropriated group, intraperitoneal (IP) injections were administered as previously described by our laboratory. Briefly, 2.0 or 4.0 mg/kg Andrographolide (ANDRO) from Sigma Aldrich was injected in saline vehicle, administered 3 times per week during 3 months. Control animals were injected with only vehicle (saline solution). Each week, we measured body mass, and the doses for IP injections were recalculated. All experiments followed the guidelines of the National Institutes of Health (NIH, Baltimore, MD, United States). All procedures

were approved by the Bioethical and Biosafety Committee of the Faculty of Biological Sciences of the Pontificia Universidad Católica de Chile (CBB-121-2013). All efforts were made to minimize animal suffering and to reduce the number of animals used.

Perfusion

All animals (young and aged) were anesthetized with Equitesin (2.5 ml/kg, i.p.) and injected with heparin (4 USP/kg, i.p.) before perfusion. Afterward, they were perfused through the heart with perfusion buffer containing 0.1% sodium nitrite, followed by fixation with 4% *p*-formaldehyde in 0.l M phosphate buffer (PB) for 30 min. Brains were surgically removed and post-fixed in the same fixative for 3 h at room temperature, followed by storage in 10% sucrose in phosphate-buffered saline (PBS) at 4°C overnight. After fixation, brains were cooled to ensure unbiased processing and analysis. The brains were subdivided into three coronal parts (approximately 3 mm in size): frontal, medial, and caudal areas. Each area was sectioned into 36 coronal sections 50 μm thick with a cryostat at −20°C.

Immunofluorescence

Immunofluorescence (IF) of brain sections was performed as described previously (Lindsay et al., 2020). After PBS and PBS-T washes, brain sections were incubated in 0.15 M glycine, and 10 mg/ml $NaBH_4$ to diminish background auto-fluorescence. Sections were washed with PBS and PBS-T and blocked with 3% bovine serum albumin (BSA) at room temperature for 1.5 h to avoid non-specific binding. Detection of the target protein was performed using a corresponding primary antibody, incubated overnight at 4°C in PBS-T containing 0.5% BSA. After washing with PBS-T, sections were incubated for 2 h at room temperature with a secondary antibody in PBS-T containing 3% BSA. Then, they were washed with PBS-T, PBS, and water and mounted on gelatin-coated slides. Coverslips with fluorescence mounting medium were added. The following primary antibodies were used: rabbit anti-phospho-S9 GSK-3β (9336) from Cell Signaling, United States (1:50), mouse anti-phospho-Y216-GSK-3β (13A) from BD Bioscience, United States (1:50), rabbit anti-Dkk-1 (sc-25516) from Santa Cruz Biotechnology, United States (1:200), rabbit anti-SFRP-1 (ab4193) from Abcam, United Kingdom (1:200), and rabbit anti-SFRP-2 (ab111874) from Abcam, United Kingdom (1:200).

Westernblotting

The brains of animals were dissected on ice and were processed or frozen at –150°C. Briefly, hippocampal tissue was homogenized in RIPA buffer (50 mM, Tris–Cl, pH 7.5, 150 mM NaCl, 1% NP-40, 0.5% sodium deoxycholate, and 1% SDS) supplemented with a protease inhibitor cocktail (Sigma-Aldrich P8340) and phosphatase inhibitors (50 mM NaF, 1 mM Na_3VO_4, and 30 μM $Na_4P_20_7$) using a Potter homogenizer. The homogenate was then passed through different caliber syringes. Protein samples were centrifuged at 14000 rpm at 4°C twice for 15 min (Tapia-Rojas et al., 2016; Tapia-Rojas and Inestrosa, 2018). Protein concentration was determined using a BCA Protein Assay Kit (Pierce Biotechnology, Rockford, IL, United States). A total of 20 μg of whole hippocampal or cortex samples was resolved by 10% SDS-PAGE and transferred to a PVDF membrane. The reactions were followed by incubation with a primary antibody, incubation with a secondary peroxidase-conjugated antibody (Pierce), and development of the membranes using an enhanced chemiluminescence (ECL) kit (Western Lightning Plus ECL, PerkinElmer). The rabbit anti-Wnt3a (ab28472; 1:1000), rabbit anti-phospho-Ser235 *tau* (ab30664; 1:1000), rabbit anti- phospho-Thr-231 *tau* (ab30665), rabbit anti-SFRP-1 (ab4193; 1:500), rabbit anti-SFRP-2 (ab111874; 1:500), and rabbit anti-CAMKIV (ab3557; 1:1000) primary antibodies were purchased from Abcam, United Kingdom. Goat anti-Wnt7a (sc-26361), mouse anti-Dvl3 (sc-8027; 1:200), mouse anti-GSK-3β (sc-9166; 1:1000), rabbit anti-Dkk-1 (sc-25516), rabbit anti-c-jun (sc-1694), mouse anti-CyclinD1 (sc-450; 1:1000), mouse anti-TAU (sc-5587), and mouse anti-β-catenin (sc-7963; 1:500) were purchased from Santa Cruz Biotechnology, United States. Rabbit anti-phospho-S9 GSK-3β (9336; 1:1000), and rabbit anti-phospho-Ser33/37/Thr41β-catenin (9561) were purchased from Cell Signaling, United States. Goat anti-Wnt-5a (AF645; 1:1000) was purchased from R&D Systems United States. Mouse anti-Actin (11978) was purchased from Sigma-Aldrich, United States (1:10000) and mouse anti-phospho-Y216-GSK-3β (13A) was purchased from BD Bioscience, United States (1:1000).

Image Analysis

Stained brain sections were photographed using an Olympus BX51 microscope coupled to a Micro-publisher 3.3 RTV camera (QImaging). The luminescence of the incident light and the time of exposure were calibrated to assign pixel values ranging from 0 to 255 in RGB images (no-light to full-light transmission) and was used in all preparations. The images were loaded into ImageJ v.1.40 *g* software (NIH) for analysis. The selection of areas for measurement was performed by manual threshold adjustment or by direct manual selection of regions of interest (ROIs) in heterogeneous stains. IF images of neurons were captured with a Zeiss LSM 5 Pascal confocal microscope. We typically examined a series of 15–20 confocal layers representing fluorescence data from the region of interest.

The quantification of the images was performed using the average signal intensity per area. Additionally, statistical analyses include the normalization of the data, where the value (average signal intensity per area) obtained for each slice (from old and young animals) is then divided by the average value of the young slices. By using this method, young value reaches always the normalized value 1, and able us to perform analyses based on the fold-of-change between young and old animals.

Preparation of Images

Digital images were obtained using Adobe Photoshop 7.0. General adjustments in color, contrast and brightness were performed, and images were converted into figures.

Statistical Analysis

Results are expressed as the mean ± standard error of the mean. Data were analyzed by one-way ANOVA, followed by Bonferroni's *post hoc* test. Statistical significance was set at $p \leq 0.05$. Statistical analysis was performed using Prism software (GraphPad Software Inc).

RESULTS

Wnt Ligands Decline With Age in the Brain of *O. degus*

Wnt ligand activates the canonical Wnt pathway by binding to LRP6 and Frizzled receptors, leading to the stabilization of β-catenin. In turn, the stabilized β-catenin translocates to the nucleus where it binds to the TCF/LEF transcription factor inducing the expression of Wnt target genes (Nusse and Varmus, 2012; **Figure 1A**). To address whether Wnt signaling is deregulated during aging in the brain of *O. degus,* through immunoblotting we evaluated the protein levels of the Wnt ligand in the whole cortex and the hippocampus at different ages. We studied the canonical ligands Wnt3a and Wnt7a and the non-canonical Wnt5a ligand, which are highly expressed in the brain. Our results indicate that adult *O. degus* exhibited decreased protein levels of the three ligands in the hippocampus. Indeed, old *O. degus* displayed a greater decrease in the expression of the ligands compared to adult animals (**Figure 1B**). However, at the cortex, although a significant decrease in the levels of Wnt3a and Wnt7a ligands in adult and old *O. degus* was observed, the Wnt5a expression remaining unchanged (**Figure 1C**). Taken together, these results indicate that Wnt ligands protein levels decrease in the brain *O. degus* during aging. Similarly, when we evaluated the protein abundance of the Wnt ligand co-receptor, LRP6, in young, adult and old *O. degus*, a significant decrease was observed in the hippocampus of the adult and old animals (**Figure 2A**). In the cortex, however, the levels of LRP6 diminished only in old *O. degus* (**Figure 2B**).

GSK-3β Activity Increased in the Brain of Aged *O. degus*

The activation of the canonical Wnt signaling triggers downstream the inactivation of the Glycogen Synthase Kinase-3β (GSK-3β; Nusse and Varmus, 2012). In the *O. degus* brain, two phosphorylated forms of GSK-3β are present. Phosphorylation of GSK-3β at serine 9 (Ⓟ Ser9) leads to the inactive form of the enzyme, while GSK-3β phosphorylated at tyrosine 216 (Ⓟ-Tyr216) corresponds to the active form of the enzyme (Giese, 2009). Our IF results show that the levels of the inactive form of GSK-3β (Ⓟ Ser9), slightly decreased in the dentate gyrus and the CA1 hippocampal region, and did not change in the cortex and CA3 regions of the hippocampus with advanced aging (**Figures 3A,B**, *upper panels*). By contrast, the levels of active GSK-3β (Ⓟ Tyr 216) were clearly increased in all the hippocampal regions studied (**Figure 3A**, *lower panels*). Additionally, we measured the protein levels of inactive GSK-3β (Ⓟ Ser9) using western blotting in total cortical and hippocampal extracts (**Figures 3C,D**). The levels of the inactive form of GSK-3β gradually decreased in adult and old *O. degus* in both brain areas. Conversely, the expression of the active form of GSK-3β (Ⓟ Tyr216) increased similarly in adult and old animals compared to younger animals in both cortex and hippocampus (**Figures 3C,D**). These results indicate that during aging *O. degus* increase the activity of GSK3β in both hippocampus and cortex.

Wnt Signaling Effector Changes in the Aging Brain of *O. degus*

We measured the levels of β-catenin phosphorylated at the Ser33/Ser37/Thr41 sites, which are associated with GSK-3β regulation to promote the proteasome degradation of β-catenin. Consistent with previous works (Ghanevati and Miller, 2005) we found that phospho-β-catenin protein levels were increased in old *O. degus* compared with young and adult animals in the hippocampus (**Figure 4A**). However, we did not observe a significant change in the levels of phospho-β-catenin in the cortex of adult and old *O. degus* (**Figure 4B**). Considering that phospho-β-catenin is degraded via the proteasome and is not available for the activation of Wnt target genes, we measured the levels of c-jun protein, a target gene of the canonical Wnt signaling (Oliva et al., 2018). We observed that c-jun levels were significantly reduced in adult and old *O. degus* in the hippocampus and the cortex (**Figures 4A,B**), in agreement with the decreased LRP6 in both cortex and hippocampus and increased phospho-β-catenin levels observed in the hippocampus.

The Protein Levels of the Wnt Antagonist Dkk-1 and SFRP Increase in the Brain of Aged *O. degus*

Dickkopf -1 (Dkk-1) is a secreted glycoprotein that inhibit the canonical Wnt signaling pathway by binding to the LRP6 co-receptor, thereby preventing the formation of the Wnt-Fz-LRP6 complex required for the activation of Wnt signaling (Ahn et al., 2011). In this context, we evaluated whether Dkk-1 protein levels change during aging in *O. degus*. Our results indicated that Dkk-1 is up-regulated in an age-dependent manner in both cortex and hippocampus. Through IF assays, we observed that the levels of this protein were significantly elevated in the cortex, dentate gyrus and CA3 region of old *O. degus* compared to young animals (**Figures 5A,B**). Western blot analysis further indicated that Dkk-1 protein was increased only in the adult hippocampus, and in both the adult and old cortex (**Figures 5C,D**). Increased Dkk-1 protein levels are likely to result in the inhibition of the canonical Wnt pathway (Niehrs, 2006; Purro et al., 2012). Therefore, the increase in Dkk-1 observed in the present work provides additional supporting evidence to suggest that the activity of the Wnt signaling pathway decreases in the brain of aged *O. degus.*

On the other hand, secreted scavenger-antagonists also regulated Wnt signaling activity by direct interaction with Wnt

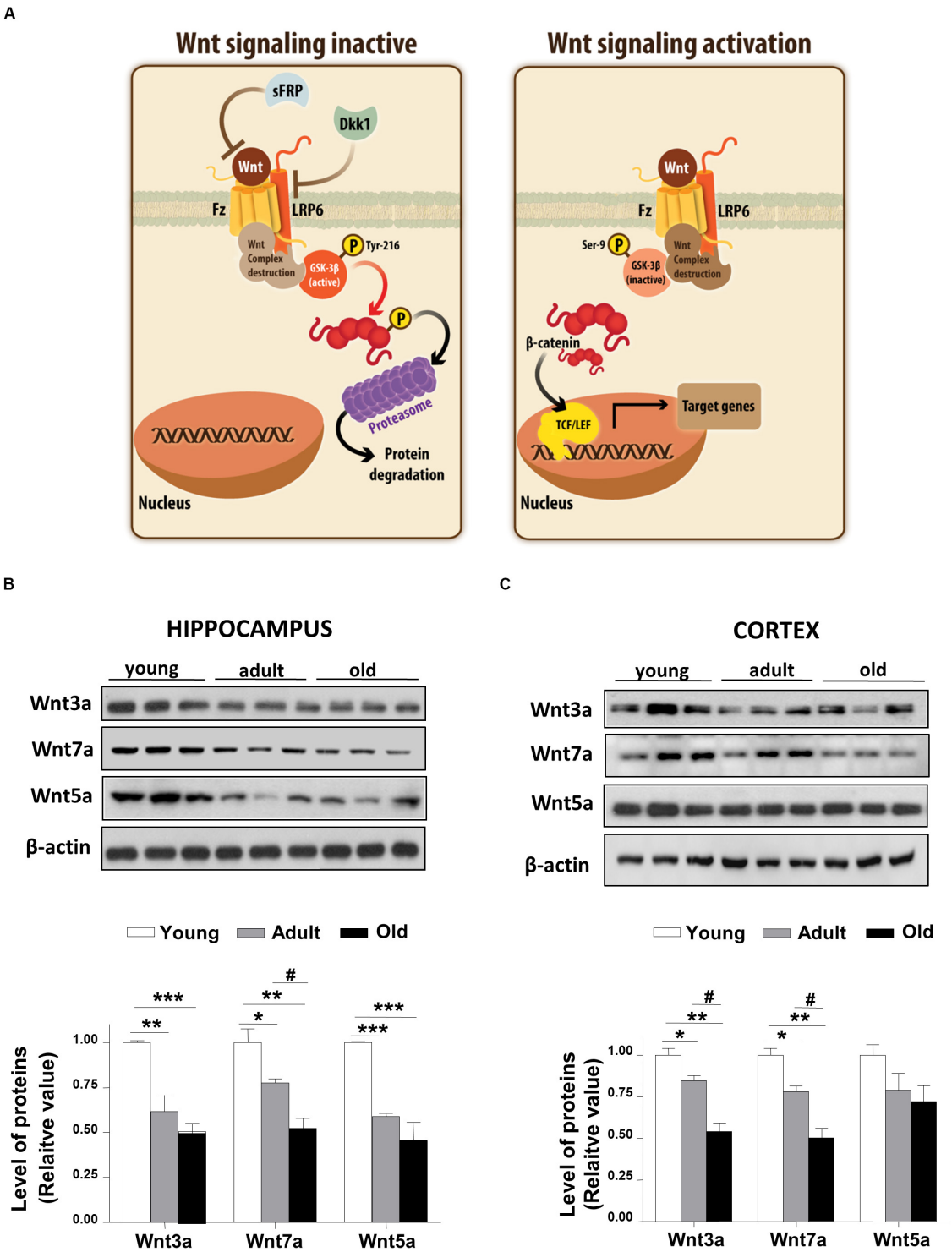

FIGURE 1 | Wnt ligand levels decline in the brains of *O. degus* at different ages. **(A)** *Scheme of the Wnt signaling inactive*, we observed that GSK-3β phosphorylate β-catenin, which is eventually labeled for destruction in the proteasome. *Scheme of Wnt signaling activation,* here the Wnt ligand interacted with the Frizzled receptor and the co-receptor LRP6, which activates the intracellular signaling, GSK-3β is inhibited and the destruction complex is separated, then β-catenin translocates to the nuclei where activate the transcription of Wnt target genes. The levels of the Wnt ligands Wnt3a, Wnt7a, and Wnt5a were detected in **(B)** the hippocampus and **(C)** the cortex of *O. degus* at different ages (young: between 7 and 12 months old, adult: between 24 and 48 months old, and old: between 60 and 72 months old) by western blot analysis. Densitometric analysis of the western blots is shown below each one. Data are presented as the mean ± S.E.M. of measurements from three animals. Differences were evaluated by ANOVA, followed by Bonferronit's *post hoc* test. Asterisks indicate significance of the observed differences ($^{\#\#\#/***}p < 0.001$; $^{\#\#/**}p < 0.01$; and $^{\#/*}p < 0.05$).

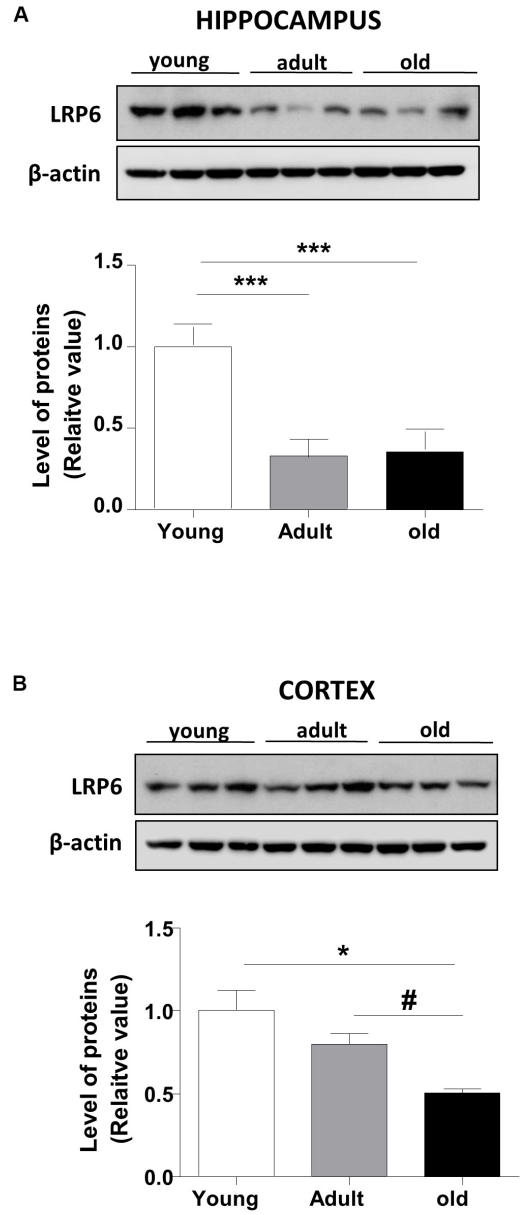

FIGURE 2 | LRP6 levels changes in the brains of *O. degus* at different ages. The level of the co-receptor LRP6 as detected in **(A)** the hippocampus and **(B)** the cortex of *O. degus* at different ages (young: between 7 and 12 months old, adult: between 24 and 48 months old, and old: between 60 and 72 months old) by western blot analysis using a specific antibody. Densitometric analysis of the western blots is shown below each one. Data are presented as the mean ± S.E.M. of measurements from three animals. Differences were evaluated by ANOVA, followed by Bonferroni's *post hoc* test. Asterisks indicate significance of the observed differences ($^{###/***}p < 0.001$; $^{##/**}p < 0.01$; and $^{#/*}p < 0.05$).

ligands. These inhibitors encode secreted frizzled-related proteins (SFRPs), which have an N-terminal cysteine-rich domain (CRD) with a sequence similarity with the Frizzled receptors (Bafico et al., 1999; Cruciat and Niehrs, 2013). We determined the protein levels of SFRP-1 and SFRP-2 in the brain of young and aged *O. degus* by IF. Our data show that SFRP-1 is increased in different regions of the hippocampus of aged animals compared to young animals (**Figures 6A,B**, *upper panels*). Also, a significant increase in SFRP-2 protein was detected in aged *O. degus* in both the cortex and the three hippocampal regions analyzed (**Figures 6A,B**, *lower panels*). Consistently, we found that SFRP-1 and SFRP-2 are both gradually up-regulated in the cortex and the hippocampus of *O. degus* with the age, according to western blot analysis (**Figures 6C,D**).

ANDRO Recovers the Wnt Signaling Loss in Adult *O. degus* Brain

At present, our results described an age-dependent downregulation of components and function of Wnt signaling, mainly in the canonical pathway, of *O. degus*. In this context, we decided to study whether an activator of the Wnt canonical signaling could reestablish the protein levels and activity of Wnt components in adult animals, where the first alterations begin. In this regard, ANDRO, a bioactive molecule extracted from a medicinal plant used as pain-killer in China called *Andrographis paniculata*, is able to cross the blood brain barrier and therefore has been highly studied previously in our laboratory (Lu et al., 2019). Our results indicate that ANDRO activates Wnt signaling pathway through direct inactivation of the enzyme GSK3β (Tapia-Rojas et al., 2015). Thus, we treated the adult *O. degus* with IP injections of ANDRO and we observed recovery of various canonical Wnt signaling components. First, the β-catenin levels, a key Wnt signaling component that decreased in the aged brain, were clearly recovered after ANDRO application (**Figure 7**). Moreover, a significant decrease in GSK-3β activity, expressed as an increase in the Ser9 phosphorylation levels, was also observed in adult animals treated with ANDRO compared to the non-treated aged animals. Previously, we observed that a Wnt target gene, c-jun was significantly reduced with the age *O. degus* in the hippocampus and the cortex (**Figure 4**). Here we measured the protein levels of other two Wnt target genes, Cyclin D1 and CAMK-IV. Both proteins are decreased in the adult brain, however, after ANDRO treatment a clear recovery in Cyclin D1 and CAMK-IV protein levels were observed in *O. degus* compared with the non-treated *O. degus* (**Figure 8**). Altogether, these results indicate that ANDRO treatment reestablishes the protein levels of keys component of canonical Wnt signaling, strongly suggesting that the recovery of the activity of the Wnt pathway could be involved in memory improvement previously observed in O. degus treated with ANDRO (Rivera et al., 2016).

DISCUSSION

Wnt signaling is recognized as fundamental for both the development and function of the central nervous system (Inestrosa and Varela-Nallar, 2015). It has been demonstrated that the Wnt signaling pathway is involved in several processes necessary for the maintenance and performance of the neuronal network, including adult hippocampal neurogenesis, the establishment of the synapses, neuronal firing activity,

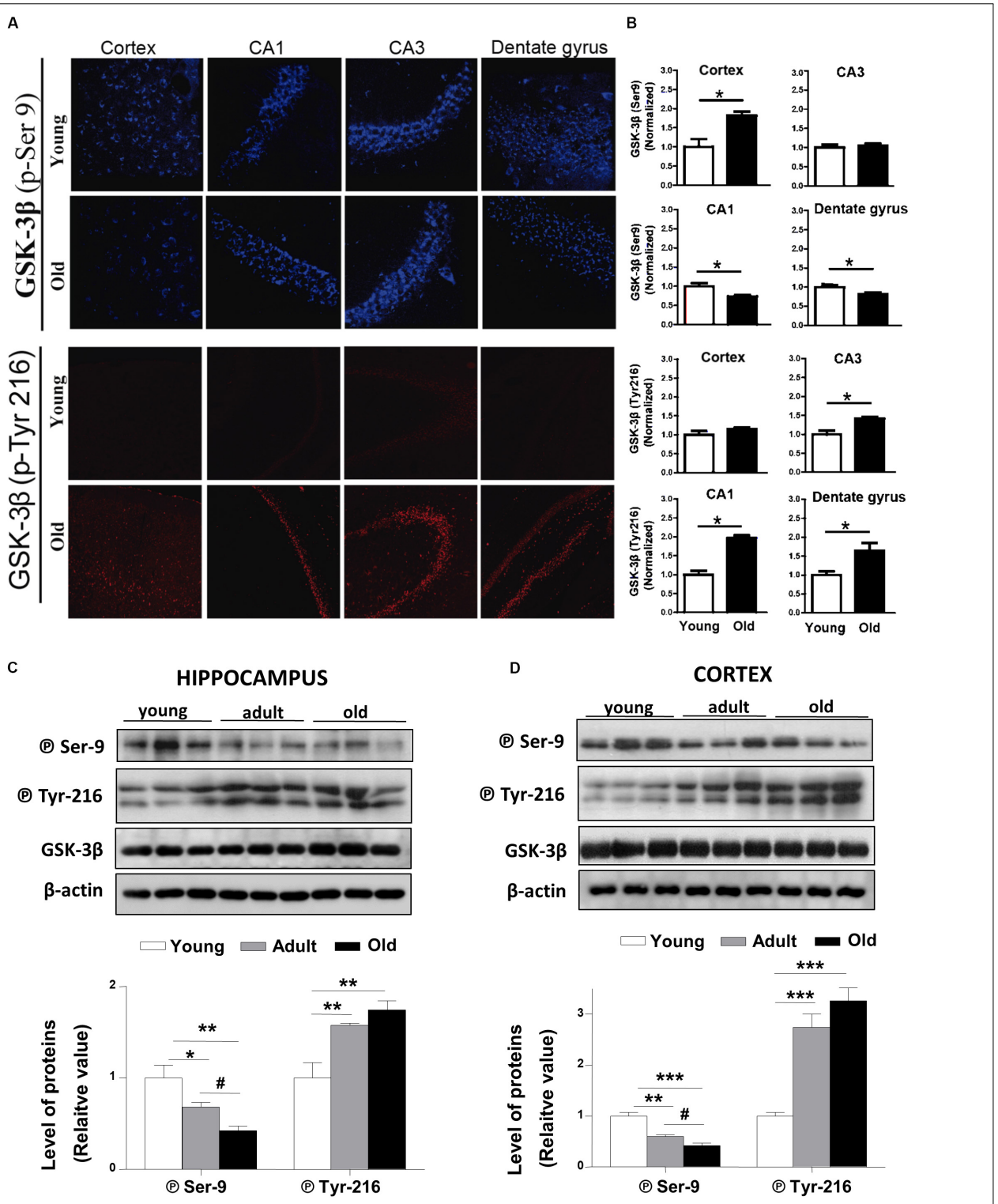

FIGURE 3 | GSK-3β phosphorylation states are altered in the brains of *O. degus* at different ages. **(A)** Representative cytochemical micrographs of GSK-3β phosphorylated at Ser9 (blue, *upper panel*) and Tyr216 (red, *lower panel*) in brain slices of *O. degus*; the cortex and hippocampus (CA1, CA3, and dentate gyrus regions) are shown. **(B)** Quantification of the images in **(A)**. Western blot analysis using antibodies directed against phosphorylated GSK-3β (phospho-Ser9 and –Tyr216) and total GSK-3β in **(C)** the hippocampus and **(D)** the cortex of *O. degus* at different ages (young: between 7 and 12 months old, adult: between 24 and 48 months old, and old: between 60 and 72 months old). Quantification of the western blots is shown below. Data are presented as the mean ± S.E.M. of measurements from three animals. Differences were evaluated by ANOVA, followed by Bonferronit's *post hoc* test. Asterisks indicate significance of the observed differences ($^{\#\#\#/***}p < 0.001$; $^{\#\#/**}p < 0.01$; and $^{\#/*}p < 0.05$).

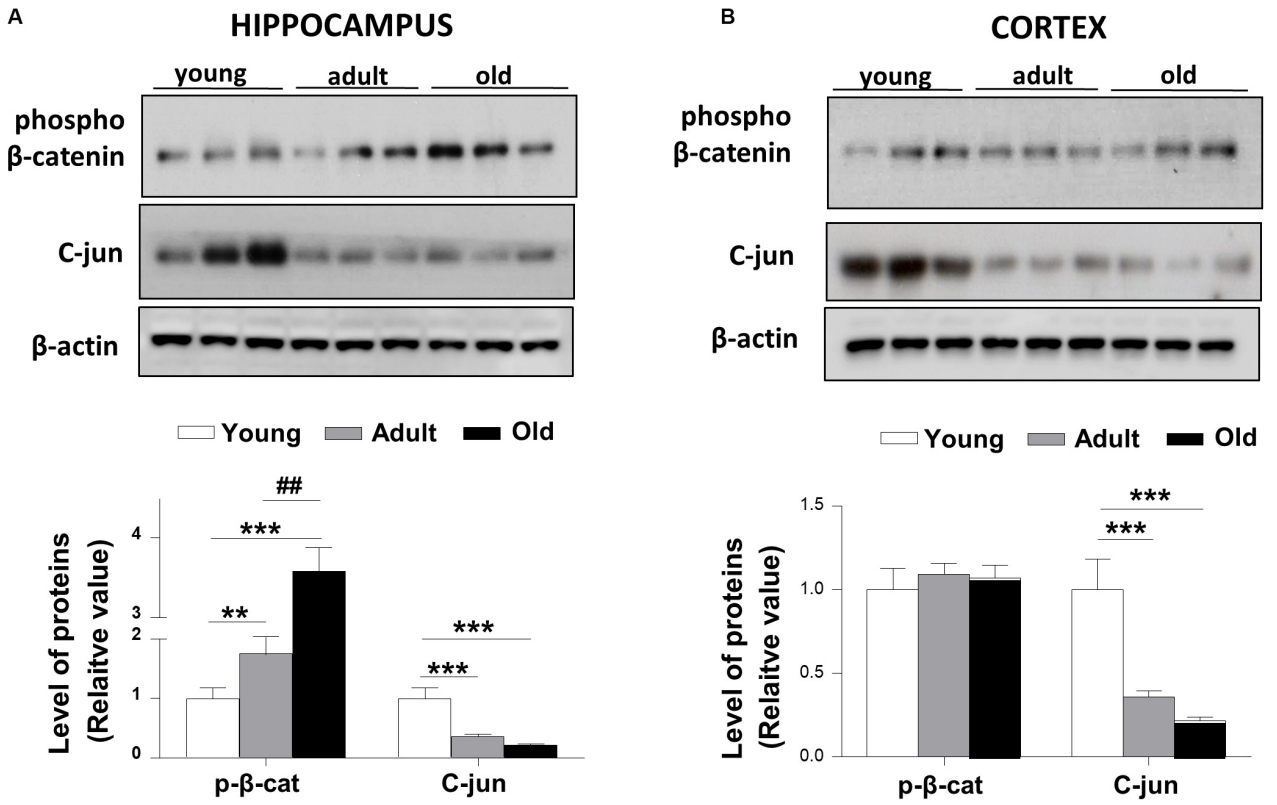

FIGURE 4 | Phospho-β-catenin levels are increased and c-Jun target gene protein levels decreased in the brains of *O. degus* at different ages. Western blot analysis in **(A)** the hippocampus and **(B)** the cortex of *O. degus* (young, adult and old) using antibodies directed against phosphorylated β-catenin and c-jun (a Wnt target gene). Densitometric analysis of the western blots is shown below. Data are presented as the mean ± S.E.M. of measurements from three animals. Differences were evaluated by ANOVA, followed by Bonferronit's *post hoc* test. Asterisks indicate significance of the observed differences ($^{###/***}p < 0.001$; $^{##/**}p < 0.01$; and $^{#/*}p < 0.05$).

neuronal plasticity, nerve transmission, and mitochondrial dynamics (Varela-Nallar et al., 2016; Oliva et al., 2018; Steinhart and Angers, 2018). Moreover, different canonical Wnt ligands have been demonstrated to have a direct effect on the architecture and function of the presynaptic region. The present study identified specific age-related changes in the canonical Wnt ligands (Wnt3a and Wnt7a) in both hippocampus and cortex and, to a lesser extent, in the non-canonical Wnt5a ligand (only in the hippocampus; Cerpa et al., 2008; Farias et al., 2009; Oliva et al., 2018). Wnt7a, for example, increases the formation of clusters of synaptophysin and acetylcholine receptors in hippocampal neurons (Farias et al., 2007). Wnt3a stimulates the exocytosis and recycling of synaptic vesicles in hippocampal neurons (Cerpa et al., 2008), and Wnt5a, a non-canonical ligand stimulates the postsynaptic region and PSD-95 (Farias et al., 2009; Ramos-Fernandez et al., 2019). Our results indicate an overall decrease of Wnt ligands, suggesting that Wnt-dependent synaptic stability declines with age.

Wnt ligands bind to Frizzled receptor leading to the LRP6 co-receptor recruitment, triggering the intracellular cascade that mediates synaptic stability (Liu C.C. et al., 2014). Our results also indicate a decrease in LRP6 protein levels. Considering that recent studies propose a role for LRP6 in Wnt signaling, particularly in dendritic synapse structure and long-term potentiation (LTP) in AD (Liu C.C. et al., 2014), is possible to suggest that a dysregulation of the more upstream Wnt signaling components might be related with both aging and age-related pathological conditions of the CNS in *O. degus*. Indeed, early work showed a close link between late-onset AD and the disruption of the Wnt signaling pathway in human AD patients by polymorphisms in the LRP6 gene (De Ferrari et al., 2007).

Similarly, we also observed an increase in GSK-3β activity in the brains of *O. degus* with advanced age. It is important to mention that GSK-3β activation of the rat hippocampus inhibits LTP, leading to significant synaptic impairments reminiscent of age-related neuropathology (Kremer et al., 2011). Moreover, the age-related changes observed in GSK-3β activity in *O. degus* are similar to those described during neurodegeneration in AD models (Giese, 2009; Kremer et al., 2011). Interestingly, ANDRO treatments were able to restore the Wnt signaling loss observed in the adult *O. degus* by the inhibition of GSK-3β, leading to the accumulation of β-catenin and increased expression of Wnt target genes. In regards to ANDRO treatments, we compared young and adult animals because we aimed to observe changes in the early stages of the appearance of Wnt signaling downregulation,

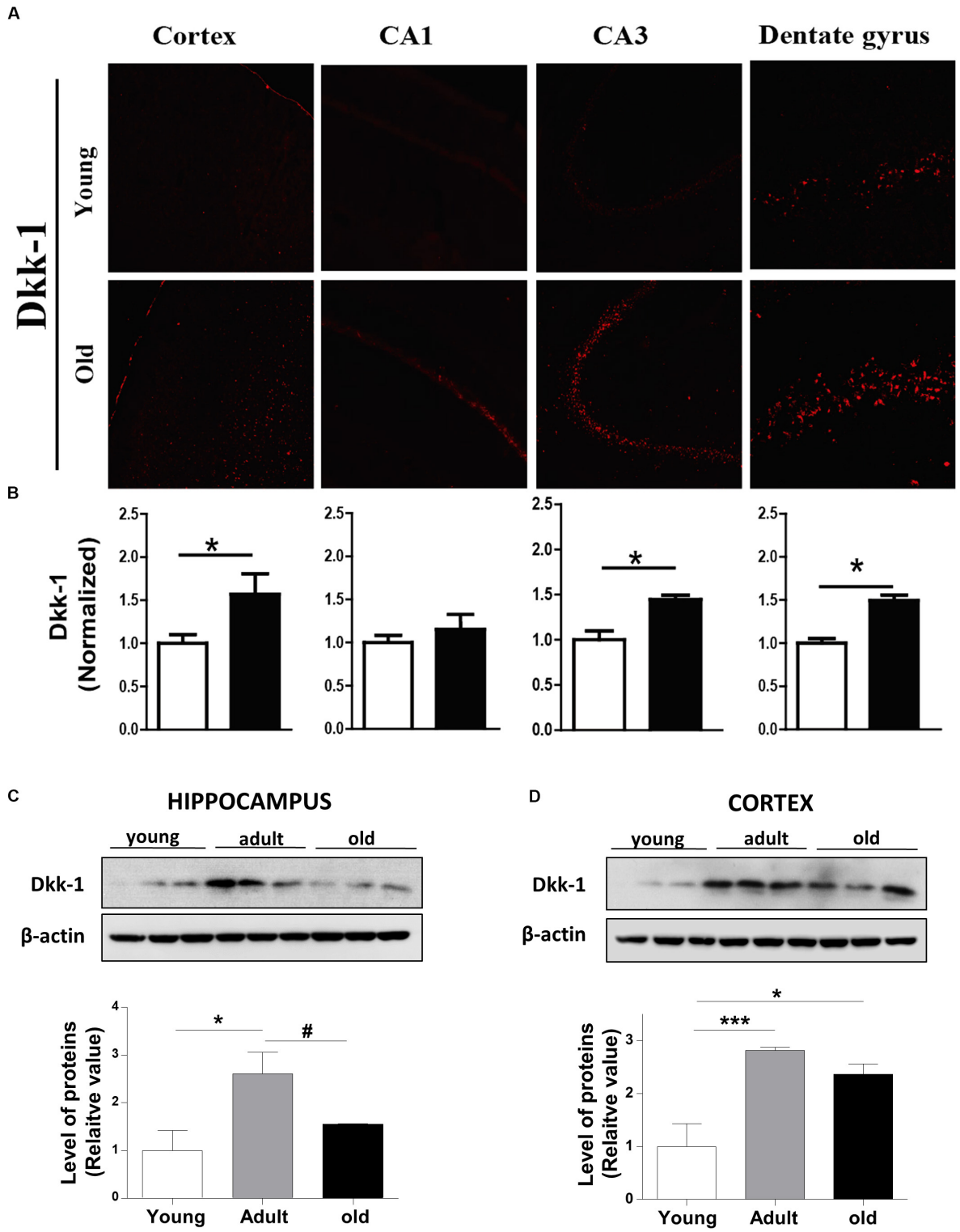

FIGURE 5 | The protein levels of Dkk-*1,* a negative modulator of Wnt signaling, are increased with the age in the brains of *O. degus*. **(A)** Representative cytochemical micrographs of Dkk-1 expression (red) in brain slices of *O. degus*; the cortex and the hippocampus (CA1, CA3, and dentate gyrus regions) are shown. **(B)** Quantification of the images in **(A)**. Western blot analysis of Dkk-1 levels in **(C)** the hippocampus and **(D)** the cortex of *O. degus* at different ages (young: between 7 and 12 months old, adult: between 24 and 48 months old, and old: between 60 and 72 months old). Quantification of the western blots is shown below. Data are presented as the mean ± S.E.M. of measurements from three animals. Differences were evaluated by ANOVA, followed by Bonferronit's *post hoc* test. Asterisks indicate significance of the observed differences ($^{###/***}p < 0.001$; $^{##/**}p < 0.01$; and $^{#/*}p < 0.05$).

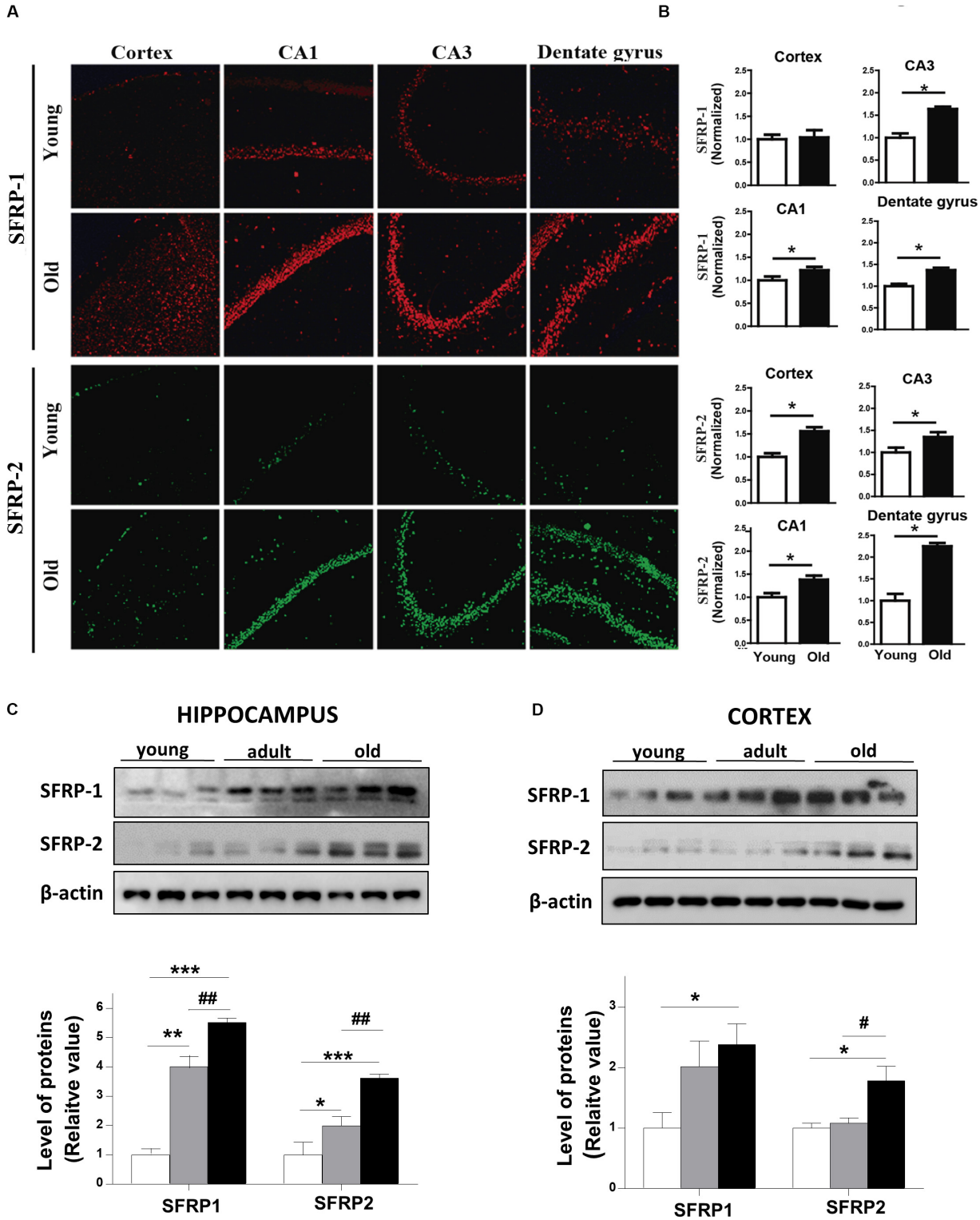

FIGURE 6 | Protein levels of SFRPs, antagonists of Wnt signaling, are increased in brains of aged *O. degus*. **(A)** Representative micrographs of SFRP-1 (red, *upper panel*), and SFRP-2 (green, lower panel) protein expression in brain slices of *O. degus*; the cortex and the hippocampus (CA1, CA3, and dentate gyrus regions) are shown. **(B)** Quantification of the images in **(A)**. Western blot analysis of both SFRP-1 and SFRP-2 protein levels in **(C)** the hippocampus and **(D)** the cortex of *O. degus* at different ages (young: between 7 and 12 months old, adult: between 24 and 48 months old, and old: between 60 and 72 months old). Quantification of the western blots is shown below. Data are presented as the mean ± S.E.M. of measurements from three animals. Differences were evaluated by ANOVA, followed by Bonferronit's *post hoc* test. Asterisks indicate significance of the observed differences ($^{###/***}p < 0.001$; $^{##/**}p < 0.01$; and $^{#/*}p < 0.05$).

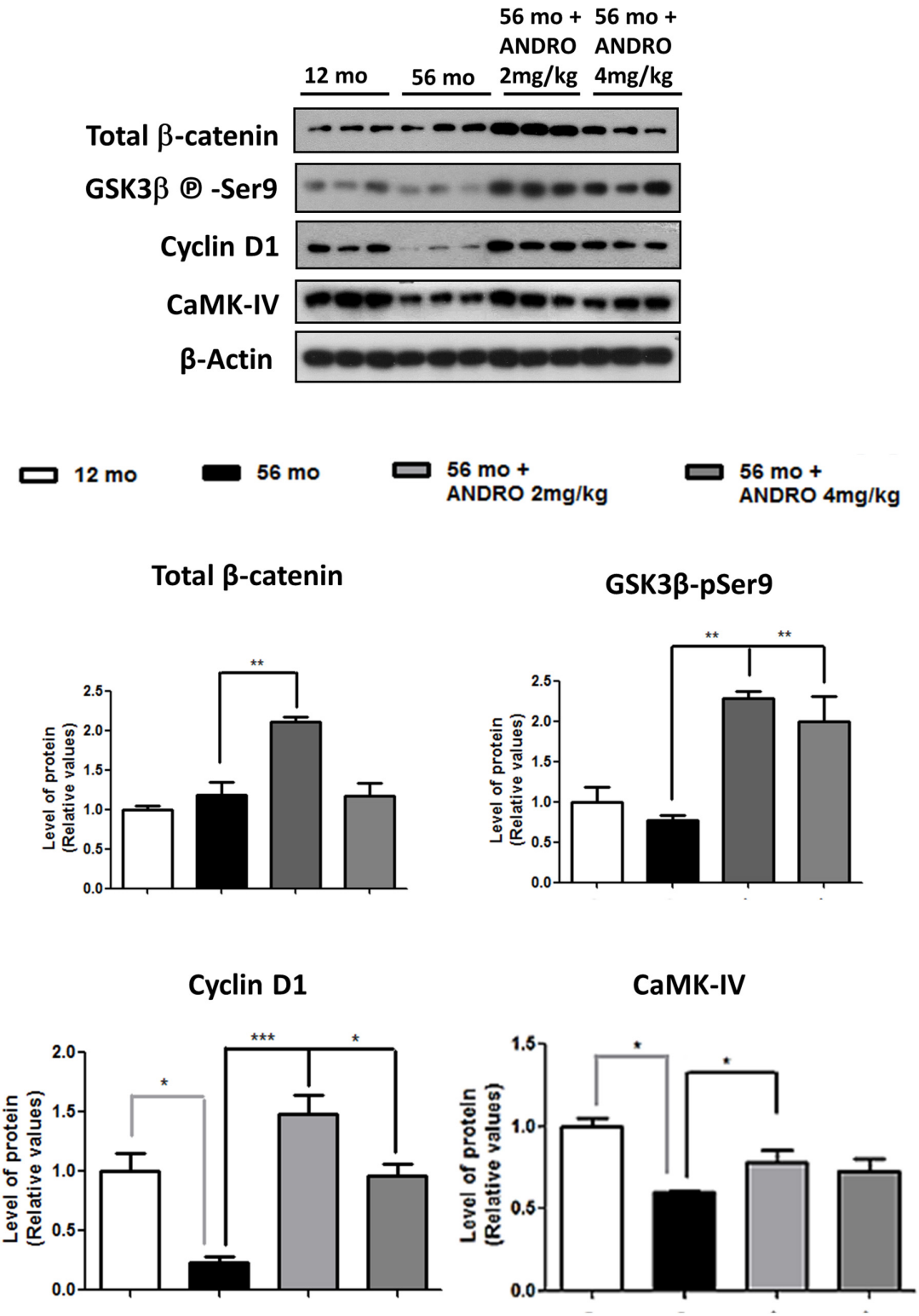

FIGURE 7 | ANDRO treatment recovers the Wnt signaling loss presented in adult *O. degus*. Western blot analysis in the hippocampus of *O. degus* (young-12 months old, adult-56 months old, adult-56 months old treated with ANDRO 2 and 4 mg/kg) using antibodies directed against β-catenin, GSK3β-phospho Ser9, Cyclin D, CAMK IV, and β-actin. Densitometric analysis of the western blots is shown below. Data are presented as the mean ± S.E.M. of measurements from three animals. Differences were evaluated by ANOVA, followed by Bonferronit's *post hoc* test. Asterisks indicate significance of the observed differences ($^{###/***}p < 0.001$; $^{##/**}p < 0.01$; and $^{#/*}p < 0.05$).

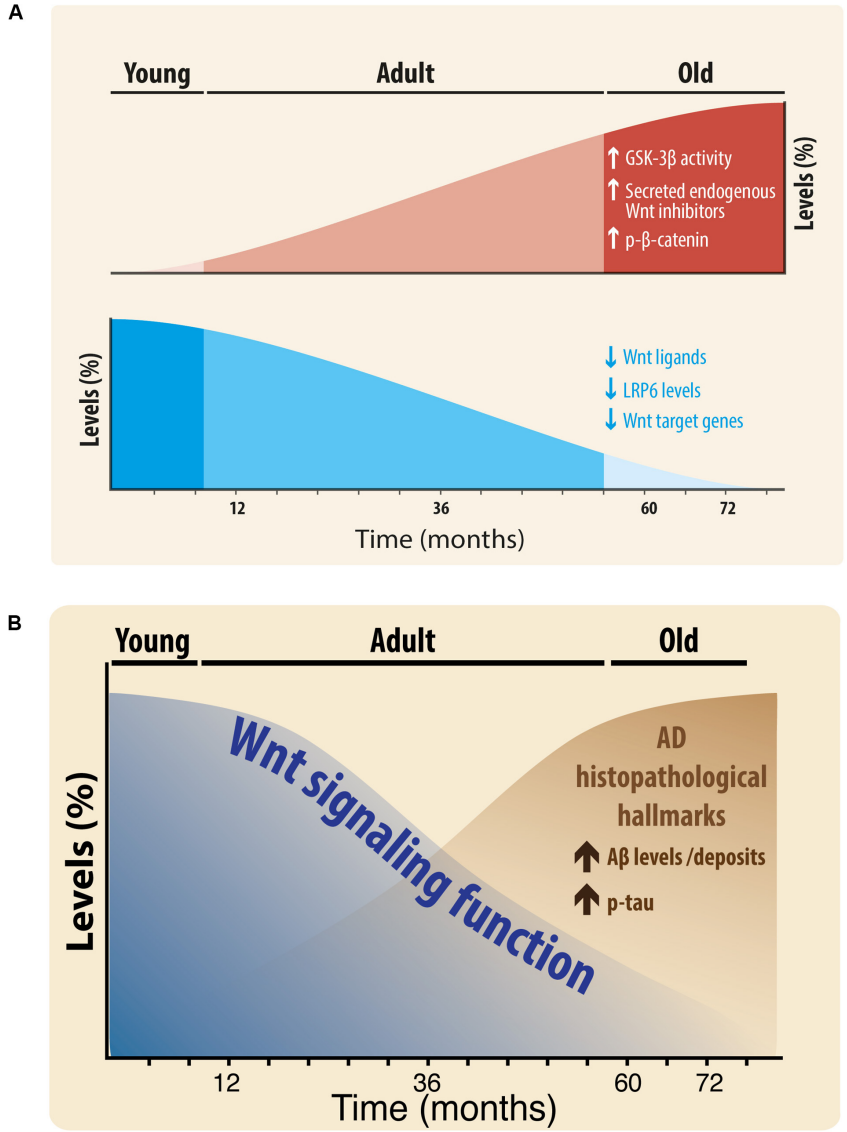

FIGURE 8 | (A) Scheme of the Changes in Wnt signaling Components during aging of the brain of *O. degus*. Wnt components that increase during aging: GSK-3β activity, secreted endogenous Wnt antagonists, and phospho-β-catenin (red color, up). Wnt components that decrease during aging: Wnt ligands Wnt3a, Wnt7a, and Wnt5a, LRP6, and Wnt target genes (blue color, down). **(B)** Relationship of Wnt signaling function with Alzheimer's histopathological hallmarks. Wnt signaling function decreases during aging, at the same time that key AD lesions are increased.

which were observed primarily in the adult brains. In addition, we previously demonstrated that ANDRO promotes behavioral changes in the ANDRO-treated group compared to control, enhancing recognition and long-term working memory, along with improved learning performance in adult *O. degus* (Barnes Maze and NOR experiments; Rivera et al., 2016). However, the significance of our analysis relies on how Wnt signaling is affected along with the aging of this longitudinal animal model that has been proposed as an important model of AD-like neurodegeneration.

On the other hand, previous studies have also indicated that alterations in the levels of the soluble Wnt inhibitors might modulate the Wnt signaling activation (Ehrlund et al., 2013). In this regard, we observed an age-related increase in the protein levels of the Wnt antagonist SFRP-1 and SFRP-2, further suggesting that the aging-related decrease of Wnt activity is caused not only by structural component reduction or lack of activation signals, but also due to the increase of inhibitory signals. In this regard, an increase in the levels of SFRP1 has been related to cellular senescence on other cell types, including in Human Cardiac Stem Cells (Nakamura et al., 2017), and fibroblasts (Elzi et al., 2012). Recent studies also demonstrate that SFRP-1 is increased in the brain of patients with AD, binds to amyloid-β and accumulates in amyloid plaques. SFRP-1 overexpression in an Alzheimer-like mouse model anticipates the appearance

of senile plaque and dystrophic neurites, whereas its genetic inactivation or the infusion of α-SFRP-1-neutralizing antibodies favors non-amyloidogenic amyloid precursor protein (APP) processing. Decreased SFRP-1 function lowers senile plaque accumulation, preventing LTP loss and cognitive deficits (Esteve et al., 2019). This study of Esteve and coworkers unveils SFRP-1 as a crucial player in AD pathogenesis through the inhibition of ADAM10, but other studies indicate that SFRP act as Wnt antagonist sequestering Wnt ligands in the extracellular space (Folke et al., 2018), therefore, these effects also could be due, almost in part, to the inhibition of Wnt signaling. More studies are necessary to validate this possibility.

Concomitantly, early evidence indicates that Dkk-1 is barely present in the healthy brain, but its protein levels are increased under pathological conditions, such as in AD (Caricasole et al., 2004). Evidence suggests that Dkk-1 is required for amyloid-β -mediated synapse loss in hippocampal neurons (Scali et al., 2006; Purro et al., 2012; Palomer et al., 2019), and its expression induces *tau* phosphorylation. Moreover, local infusion of Dkk-1 in rats caused neuronal cell death and astrogliosis in the CA1 region of the hippocampus and the death of cholinergic neurons in the nucleus basalis (Scali et al., 2006). Increased expression of Dkk-1 is causally related to neurodegeneration processes in several central nervous system disorders other than AD, such as brain ischemia and temporal lobe epilepsy (Seib et al., 2013). Moreover, dysfunctional Wnt signaling caused by increased levels of Dkk-1 has been implicated also in the age-related decline in hippocampal neurogenesis (Seib et al., 2013). As a result, mice deficient in Dkk-1 exhibit enhanced spatial working memory and memory consolidation and also show improvements in affective behavior (Caricasole et al., 2003, 2004). Accordingly, our Westernblotting (WB) data indicate that Dkk-1 is increased in the hippocampus and cortex of adult *O. degus,* possibly inhibiting Wnt signaling, this fact is consistent with previously published results obtained in different systems. However, comparing young with old animals, the differences in the cortical expression of Dkk-1 persist over time, a result contrary to our observation by IF assay. We could explain these distinct results between IF and WB based on technical differences; IF experiments allow us to sub-divide the hippocampal analyses in CA1, CA3, and DG, whereas WB were performed using the complete hippocampal tissue.

Our work shows that in agreement with previous studies, the Wnt signaling pathway is active in young *O. degus* and becomes attenuated in aged rodents. We found that the levels of certain Wnt components increase, i.e., GSK-3β activity, Dkk-1, SFRP-1, SFRP-2, and phospho-β-catenin, however, other Wnt components decrease during aging: Wnt ligands (Wnt3a, Wnt7a, and Wnt5a), LRP6, and Wnt target genes (**Figure 8A**). Also, is important to highlight that although the first alterations were observed in the adulthood, significant differences were also observed between adult and old brains in hippocampal Wnt7a, GSK3β-Ser9, phospho-β-catenin, Dkk-1, SFRP1, and SFRP2 proteins, in addition to significant changes in Wnt7a, Wnt3a, GSK3β-Ser9, LRP6, and SFRP2 in the cortex. Furthermore, we interpret the difference between hippocampus and cortex as a temporal-dependent difference. Previous studies indicated that AD hallmarks occur first in the hippocampus and then spread to cortex (Braak and Braak, 1997). Therefore, adult brains might show higher levels of AD-like hallmarks in the hippocampus, whereas old brains should show them in the hippocampus and cortex as we observe in our study.

Moreover, recent studies from our laboratory indicate that the inhibition of the canonical Wnt signaling induces an increase in the amyloidogenic processing of the APP, leading to an increased Aβ secretion and formation of Aβ oligomers (Tapia-Rojas et al., 2016), a critical hallmark in AD. Similarly, the Wnt signaling loss accelerates the appearance of the neuropathological hallmarks of AD in the J20-APP transgenic and wild-type mice (Tapia-Rojas and Inestrosa, 2018). Also, our results are consistent with Bai et al. (2020) in which characterizing AD stage-associated protein networks, by multi-omics, they corroborate that the Wnt pathway is associated with AD (Bai et al., 2020).

Furthermore, the treatment of aged *O. degus* with ANDRO has shown protection from several aspects of AD-pathogenesis: i.e., decreased Aβ accumulation and lower *tau* phosphorylation, recovery of synaptic protein loss and cognitive impairment (Serrano et al., 2014; Rivera et al., 2016). Moreover, several studies using ANDRO treatments had reported other effects such as adult neurogenesis (Varela-Nallar et al., 2016), neurite out-growth (Xu et al., 2019), and neuroprotection (Lindsay et al., 2020), along with decreased neuroinflammation, oxidative stress, and synaptic dysfunction in aged animals (Serrano et al., 2014; Lu et al., 2019; Zolezzi and Inestrosa, 2019; Lindsay et al., 2020). Specifically, ANDRO activates Wnt signaling pathway by inhibiting directly GSK-3β (Tapia-Rojas et al., 2015), but also it has been described as a modulator of other cellular signaling including the BACE1-dependent amyloid processing, the Nrf2-mediated p62, the Keap1/Nrf2/ARE/HO-1, the PI3K-Akt, and the NF-kB pathways (Seo et al., 2017; Gu et al., 2018, 2019; Panche et al., 2019). All these signaling pathways, complimentarily to the Wnt signaling, could be increasing the beneficial effects related to Wnt signaling modulation (Zolezzi and Inestrosa, 2019), and should be assessed in the future to better understand the mechanisms underlying ANDRO's effects.

Taken together, our results suggest that during the aging process the Wnt signaling function decreases in the brain of the *O. degus*. Moreover, considering our previous work, we suggest that this decrease is inverse to what observed under neuropathological conditions, such as in AD, where the expression of key AD lesions increases (**Figure 8B**). Additionally, considering that ANDRO, is able to rescue Wnt signaling impairment, at the levels of β-catenin, GSK-3β and target genes, we can hypothesize that Wnt signaling might play a pivotal role not only in the aging process itself, but influencing the outcome of such process in terms of an improved healthy aging.

DATA AVAILABILITY STATEMENT

The raw data supporting the conclusions of this article will be made available by the authors, without undue reservation.

ETHICS STATEMENT

The animal study was reviewed and approved by Bioethical and Biosafety Committee of the Faculty of Biological Sciences of the Pontificia Universidad Católica de Chile (CBB-121-2013).

AUTHOR CONTRIBUTIONS

NI conceived the research, projected the experimental approach, and wrote the manuscript. CT-R and CL conducted the experiments and process the data. NI and JZ discussed and elaborated the final version of the manuscript. All authors contributed to the article and approved the submitted version.

FUNDING

This work was supported by the Basal Center of Excellence of Aging and Regeneration (AFB 170005) and a special grant "Lithium in Health and Disease" from the Sociedad Quìmica y Minera de Chile (SQM).

REFERENCES

Ahn, V. E., Chu, M. L., Choi, H. J., Tran, D., Abo, A., and Weis, W. I. (2011). Structural basis of Wnt signaling inhibition by Dickkopf binding to LRP5/6. *Dev. Cell* 21, 862–873. doi: 10.1016/j.devcel.2011.09.003

Bafico, A., Gazit, A., Pramila, T., Finch, P. W., Yaniv, A., and Aaronson, S. A. (1999). Interaction of frizzled related protein (FRP) with Wnt ligands and the frizzled receptor suggests alternative mechanisms for FRP inhibition of Wnt signaling. *J. Biol. Chem.* 274, 16180–16187. doi: 10.1074/jbc.274.23.16180

Bai, B., Wang, X., Li, Y., Chen, P. C., Yu, K., Dey, K. K., et al. (2020). Deep multilayer brain proteomics identifies molecular networks in Alzheimer's disease progression. *Neuron* 105:e977.

Braak, H., and Braak, E. (1997). Frequency of stages of Alzheimer-related lesions in different age categories. *Neurobiol. Aging* 18, 351–357. doi: 10.1016/s0197-4580(97)00056-0

Caricasole, A., Copani, A., Caraci, F., Aronica, E., Rozemuller, A. J., Caruso, A., et al. (2004). Induction of Dickkopf-1, a negative modulator of the Wnt pathway, is associated with neuronal degeneration in Alzheimer's brain. *J. Neurosci.* 24, 6021–6027. doi: 10.1523/jneurosci.1381-04.2004

Caricasole, A., Ferraro, T., Iacovelli, L., Barletta, E., Caruso, A., Melchiorri, D., et al. (2003). Functional characterization of WNT7A signaling in PC12 cells: interaction with A FZD5 x LRP6 receptor complex and modulation by Dickkopf proteins. *J. Biol. Chem.* 278, 37024–37031. doi: 10.1074/jbc.m300191200

Cerpa, W., Godoy, J. A., Alfaro, I., Farias, G. G., Metcalfe, M. J., Fuentealba, R., et al. (2008). Wnt-7a modulates the synaptic vesicle cycle and synaptic transmission in hippocampal neurons. *J. Biol. Chem.* 283, 5918–5927. doi: 10.1074/jbc.m705943200

Cisternas, P., Vio, C. P., and Inestrosa, N. C. (2014). Role of Wnt signaling in tissue fibrosis, lessons from skeletal muscle and kidney. *Curr. Mol. Med.* 14, 510–522. doi: 10.2174/1566524014666140414210346

Cisternas, P., Zolezzi, J. M., Lindsay, C., Rivera, D. S., Martinez, A., Bozinovic, F., et al. (2018). New insights into the spontaneous Human Alzheimer's disease-like model *Octodon degus*: unraveling amyloid-beta peptide aggregation and age-related amyloid pathology. *J. Alzheimers Dis.* 66, 1145–1163. doi: 10.3233/jad-180729

Cruciat, C. M., and Niehrs, C. (2013). Secreted and transmembrane wnt inhibitors and activators. *Cold Spring Harb. Perspect. Biol.* 5:a015081. doi: 10.1101/cshperspect.a015081

De Ferrari, G. V., Papassotiropoulos, A., Biechele, T., Wavrant De-Vrieze, F., Avila, M. E., Major, M. B., et al. (2007). Common genetic variation within the low-density lipoprotein receptor-related protein 6 and late-onset Alzheimer's disease. *Proc. Natl. Acad. Sci. U.S.A.* 104, 9434–9439.

Du, L. Y., Chang, L. Y., Ardiles, A. O., Tapia-Rojas, C., Araya, J., Inestrosa, N. C., et al. (2015). Alzheimer's disease-related protein expression in the retina of *Octodon degus*. *PLoS One* 10:e0135499. doi: 10.1371/journal.pone.0135499

Ehrlund, A., Mejhert, N., Lorente-Cebrian, S., Astrom, G., Dahlman, I., Laurencikiene, J., et al. (2013). Characterization of the Wnt inhibitors secreted frizzled-related proteins (SFRPs) in human adipose tissue. *J. Clin. Endocrinol. Metab.* 98, E503–E508.

Elzi, D. J., Song, M., Hakala, K., Weintraub, S. T., and Shiio, Y. (2012). Wnt antagonist SFRP1 functions as a secreted mediator of senescence. *Mol. Cell. Biol.* 32, 4388–4399. doi: 10.1128/mcb.06023-11

Esteve, P., Rueda-Carrasco, J., Ines Mateo, M., Martin-Bermejo, M. J., Draffin, J., Pereyra, G., et al. (2019). Elevated levels of secreted-frizzled-related-protein 1 contribute to Alzheimer's disease pathogenesis. *Nat. Neurosci.* 22, 1258–1268. doi: 10.1038/s41593-019-0432-1

Farias, G. G., Alfaro, I. E., Cerpa, W., Grabowski, C. P., Godoy, J. A., Bonansco, C., et al. (2009). Wnt-5a/JNK signaling promotes the clustering of PSD-95 in hippocampal neurons. *J. Biol. Chem.* 284, 15857–15866. doi: 10.1074/jbc.m808986200

Farias, G. G., Valles, A. S., Colombres, M., Godoy, J. A., Toledo, E. M., Lukas, R. J., et al. (2007). Wnt-7a induces presynaptic colocalization of alpha 7-nicotinic acetylcholine receptors and adenomatous polyposis coli in hippocampal neurons. *J. Neurosci.* 27, 5313–5325. doi: 10.1523/jneurosci.3934-06.2007

Folke, J., Pakkenberg, B., and Brudek, T. (2018). Impaired Wnt signaling in the prefrontal cortex of Alzheimer's disease. *Mol. Neurobiol.* 56, 873–891. doi: 10.1007/s12035-018-1103-z

Fuenzalida, M., Espinoza, C., Perez, M. A., Tapia-Rojas, C., Cuitino, L., Brandan, E., et al. (2016). Wnt signaling pathway improves central inhibitory synaptic transmission in a mouse model of Duchenne muscular dystrophy. *Neurobiol. Dis.* 86, 109–120. doi: 10.1016/j.nbd.2015.11.018

Gammons, M., and Bienz, M. (2018). Multiprotein complexes governing Wnt signal transduction. *Curr. Opin. Cell Biol.* 51, 42–49. doi: 10.1016/j.ceb.2017.10.008

Garcia-Velazquez, L., and Arias, C. (2017). The emerging role of Wnt signaling dysregulation in the understanding and modification of age-associated diseases. *Ageing Res. Rev.* 37, 135–145. doi: 10.1016/j.arr.2017.06.001

Ghanevati, M., and Miller, C. A. (2005). Phospho-beta-catenin accumulation in Alzheimer's disease and in aggresomes attributable to proteasome dysfunction. *J. Mol. Neurosci.* 25, 79–94.

Giese, K. P. (2009). GSK-3: a key player in neurodegeneration and memory. *IUBMB Life* 61, 516–521. doi: 10.1002/iub.187

Gu, L., Lu, J., Li, Q., Wu, N., Zhang, L., Li, H., et al. (2019). A network-based analysis of key pharmacological pathways of *Andrographis paniculata* acting on Alzheimer's disease and experimental validation. *J. Ethnopharmacol.* 251:112488. doi: 10.1016/j.jep.2019.112488

Gu, L., Yu, Q., Li, Q., Zhang, L., Lu, H., and Zhang, X. (2018). Andrographolide protects PC12 cells against beta-amyloid-induced autophagy-associated cell death through activation of the Nrf2-mediated p62 signaling pathway. *Int. J. Mol. Sci.* 19:2844. doi: 10.3390/ijms19092844

Inestrosa, N. C., and Arenas, E. (2010). Emerging roles of Wnts in the adult nervous system. *Nat. Rev. Neurosci.* 11, 77–86. doi: 10.1038/nrn2755

Inestrosa, N. C., Reyes, A. E., Chacon, M. A., Cerpa, W., Villalon, A., Montiel, J., et al. (2005). Human-like rodent amyloid-beta-peptide determines Alzheimer pathology in aged wild-type *Octodon degu*. *Neurobiol. Aging* 26, 1023–1028. doi: 10.1016/j.neurobiolaging.2004.09.016

Inestrosa, N. C., Rios, J. A., Cisternas, P., Tapia-Rojas, C., Rivera, D. S., Braidy, N., et al. (2015). Age progression of neuropathological markers in the brain of the chilean rodent *Octodon degus*, a natural model of Alzheimer's disease. *Brain Pathol.* 25, 679–691. doi: 10.1111/bpa.12226

Inestrosa, N. C., and Toledo, E. M. (2008). The role of Wnt signaling in neuronal dysfunction in Alzheimer's disease. *Mol. Neurodegener.* 3:9. doi: 10.1186/1750-1326-3-9

Inestrosa, N. C., and Varela-Nallar, L. (2015). Wnt signalling in neuronal differentiation and development. *Cell Tissue Res.* 359, 215–223. doi: 10.1007/s00441-014-1996-4

Kremer, A., Louis, J. V., Jaworski, T., and Van Leuven, F. (2011). GSK3 and Alzheimer's disease: facts and fiction. *Front. Mol. Neurosci.* 4:17. doi: 10.3389/fnmol.2011.00017

Lee, T. M. (2004). *Octodon degus*: a diurnal, social, and long-lived rodent. *ILAR J.* 45, 14–24. doi: 10.1093/ilar.45.1.14

Lindsay, C. B., Zolezzi, J. M., Rivera, D. S., Cisternas, P., Bozinovic, F., and Inestrosa, N. C. (2020). Andrographolide reduces neuroinflammation and oxidative stress in aged *Octodon degus*. *Mol. Neurobiol.* 57, 1131–1145. doi: 10.1007/s12035-019-01784-6

Liu, C. C., Tsai, C. W., Deak, F., Rogers, J., Penuliar, M., Sung, Y. M., et al. (2014). Deficiency in LRP6-mediated Wnt signaling contributes to synaptic abnormalities and amyloid pathology in Alzheimer's disease. *Neuron* 84, 63–77. doi: 10.1016/j.neuron.2014.08.048

Liu, M., Zhang, Y., Huo, Y. R., Liu, S., Liu, S., Wang, J., et al. (2014). Influence of the rs1080985 single nucleotide polymorphism of the CYP2D6 Gene and APOE polymorphism on the response to donepezil treatment in patients with Alzheimer's disease in China. *Dement. Geriatr. Cogn. Dis. Extra* 4, 450–456. doi: 10.1159/000367596

Lu, J., Ma, Y., Wu, J., Huang, H., Wang, X., Chen, Z., et al. (2019). A review for the neuroprotective effects of andrographolide in the central nervous system. *Biomed. Pharmacother.* 117:109078. doi: 10.1016/j.biopha.2019.109078

Nakamura, T., Hosoyama, T., Murakami, J., Samura, M., Ueno, K., Kurazumi, H., et al. (2017). Age-related increase in Wnt inhibitor causes a senescence-like phenotype in human cardiac stem cells. *Biochem. Biophys. Res. Commun.* 487, 653–659. doi: 10.1016/j.bbrc.2017.04.110

Niehrs, C. (2006). Function and biological roles of the Dickkopf family of Wnt modulators. *Oncogene* 25, 7469–7481. doi: 10.1038/sj.onc.1210054

Nusse, R., and Clevers, H. (2017). Wnt/beta-catenin signaling, disease, and emerging therapeutic modalities. *Cell* 169, 985–999. doi: 10.1016/j.cell.2017.05.016

Nusse, R., and Varmus, H. (2012). Three decades of Wnts: a personal perspective on how a scientific field developed. *EMBO J.* 31, 2670–2684. doi: 10.1038/emboj.2012.146

Oliva, C. A., Montecinos-Oliva, C., and Inestrosa, N. C. (2018). Wnt signaling in the central nervous system: new insights in health and disease. *Prog. Mol. Biol. Transl. Sci.* 153, 81–130. doi: 10.1016/bs.pmbts.2017.11.018

Palomer, E., Buechler, J., and Salinas, P. C. (2019). Wnt signaling deregulation in the aging and Alzheimer's brain. *Front. Cell. Neurosci.* 13:227. doi: 10.3389/fncel.2019.00227

Panche, A. N., Chandra, S., and Diwan, A. D. (2019). Multi-target beta-protease inhibitors from *Andrographis paniculata*: in silico and in vitro studies. *Plants (Basel)* 8:231. doi: 10.3390/plants8070231

Purro, S. A., Dickins, E. M., and Salinas, P. C. (2012). The secreted Wnt antagonist Dickkopf-1 is required for amyloid beta-mediated synaptic loss. *J. Neurosci.* 32, 3492–3498. doi: 10.1523/jneurosci.4562-11.2012

Ramos-Fernandez, E., Tapia-Rojas, C., Ramirez, V. T., and Inestrosa, N. C. (2019). Wnt-7a stimulates dendritic spine morphogenesis and PSD-95 expression through canonical signaling. *Mol. Neurobiol.* 56, 1870–1882. doi: 10.1007/s12035-018-1162-1

Rivera, D. S., Lindsay, C., Codocedo, J. F., Morel, I., Pinto, C., Cisternas, P., et al. (2016). Andrographolide recovers cognitive impairment in a natural model of Alzheimer's disease (*Octodon degus*). *Neurobiol. Aging* 46, 204–220. doi: 10.1016/j.neurobiolaging.2016.06.021

Roses, A. D. (1994). Apolipoprotein E affects the rate of Alzheimer disease expression: beta-amyloid burden is a secondary consequence dependent on APOE genotype and duration of disease. *J. Neuropathol. Exp. Neurol.* 53, 429–437. doi: 10.1097/00005072-199409000-00002

Scali, C., Caraci, F., Gianfriddo, M., Diodato, E., Roncarati, R., Pollio, G., et al. (2006). Inhibition of Wnt signaling, modulation of Tau phosphorylation and induction of neuronal cell death by DKK1. *Neurobiol. Dis.* 24, 254–265. doi: 10.1016/j.nbd.2006.06.016

Seib, D. R., Corsini, N. S., Ellwanger, K., Plaas, C., Mateos, A., Pitzer, C., et al. (2013). Loss of Dickkopf-1 restores neurogenesis in old age and counteracts cognitive decline. *Cell Stem Cell* 12, 204–214. doi: 10.1016/j.stem.2012.11.010

Seo, J. Y., Pyo, E., An, J. P., Kim, J., Sung, S. H., and Oh, W. K. (2017). Andrographolide activates Keap1/Nrf2/ARE/HO-1 Pathway in HT22 Cells and suppresses microglial activation by Abeta42 through Nrf2-related inflammatory response. *Mediators Inflamm.* 2017:5906189.

Serrano, F. G., Tapia-Rojas, C., Carvajal, F. J., Hancke, J., Cerpa, W., and Inestrosa, N. C. (2014). Andrographolide reduces cognitive impairment in young and mature AbetaPPswe/PS-1 mice. *Mol. Neurodegener.* 9:61. doi: 10.1186/1750-1326-9-61

Steinhart, Z., and Angers, S. (2018). Wnt signaling in development and tissue homeostasis. *Development* 145:dev146589. doi: 10.1242/dev.146589

Tapia-Rojas, C., Burgos, P. V., and Inestrosa, N. C. (2016). Inhibition of Wnt signaling induces amyloidogenic processing of amyloid precursor protein and the production and aggregation of Amyloid-beta (Abeta)42 peptides. *J. Neurochem.* 139, 1175–1191. doi: 10.1111/jnc.13873

Tapia-Rojas, C., and Inestrosa, N. C. (2018). Wnt signaling loss accelerates the appearance of neuropathological hallmarks of Alzheimer's disease in J20-APP transgenic and wild-type mice. *J. Neurochem.* 144, 443–465. doi: 10.1111/jnc.14278

Tapia-Rojas, C., Schuller, A., Lindsay, C. B., Ureta, R. C., Mejias-Reyes, C., Hancke, J., et al. (2015). Andrographolide activates the canonical Wnt signalling pathway by a mechanism that implicates the non-ATP competitive inhibition of GSK-3beta: autoregulation of GSK-3beta in vivo. *Biochem. J.* 466, 415–430. doi: 10.1042/bj20140207

Toledo, E. M., and Inestrosa, N. C. (2010). Activation of Wnt signaling by lithium and rosiglitazone reduced spatial memory impairment and neurodegeneration in brains of an APPswe/PSEN1DeltaE9 mouse model of Alzheimer's disease. *Mol. Psychiatry* 15:228.

van Groen, T., Kadish, I., Popovic, N., Popovic, M., Caballero-Bleda, M., Bano-Otalora, B., et al. (2011). Age-related brain pathology in *Octodon degu*: blood vessel, white matter and Alzheimer-like pathology. *Neurobiol. Aging* 32, 1651–1661. doi: 10.1016/j.neurobiolaging.2009.10.008

Varela-Nallar, L., Arredondo, S. B., Tapia-Rojas, C., Hancke, J., and Inestrosa, N. C. (2016). Andrographolide stimulates neurogenesis in the adult hippocampus. *Neural. Plast.* 2015:935403.

Vargas, J. Y., Fuenzalida, M., and Inestrosa, N. C. (2014). In vivo activation of Wnt signaling pathway enhances cognitive function of adult mice and reverses cognitive deficits in an Alzheimer's disease model. *J. Neurosci.* 34, 2191–2202. doi: 10.1523/jneurosci.0862-13.2014

Xu, Y., Wei, H., Wang, J., Wang, W., and Gao, J. (2019). Synthesis of andrographolide analogues and their neuroprotection and neurite outgrowth-promoting activities. *Bioorg. Med. Chem.* 27, 2209–2219. doi: 10.1016/j.bmc.2019.04.025

Zhang, Z., Hartmann, H., Do, V. M., Abramowski, D., Sturchler-Pierrat, C., Staufenbiel, M., et al. (1998). Destabilization of beta-catenin by mutations in presenilin-1 potentiates neuronal apoptosis. *Nature* 395, 698–702. doi: 10.1038/27208

Zolezzi, J. M., and Inestrosa, N. C. (2019). Diterpenes and the crosstalk with the arachidonic acid pathways, relevance in neurodegeneration. *Neural. Regen. Res.* 14, 1705–1706.

Conflict of Interest: The authors declare that the research was conducted in the absence of any commercial or financial relationships that could be construed as a potential conflict of interest.

frontiers in Cell and Developmental Biology

ORIGINAL RESEARCH
published: 19 August 2020
doi: 10.3389/fcell.2020.00810

Glucose Overload Inhibits Glutamatergic Synaptic Transmission: A Novel Role for CREB-Mediated Regulation of Synaptotagmins 2 and 4

Cristian Ripoli[1,2†], Matteo Spinelli[1†], Francesca Natale[1], Salvatore Fusco[1,2] and Claudio Grassi[1,2]*

[1] Department of Neuroscience, Università Cattolica del Sacro Cuore, Rome, Italy, [2] Fondazione Policlinico Universitario A. Gemelli IRCCS, Rome, Italy

OPEN ACCESS

Edited by:
Christine Ann Denny,
Columbia University Irving Medical Center, United States

Reviewed by:
Hélène Marie,
Centre National de la Recherche Scientifique (CNRS), France
Xiao-Bing Gao,
School of Medicine, Yale University, United States

***Correspondence:**
Salvatore Fusco
salvatore.fusco@unicatt.it

[†] These authors have contributed equally to this work

Specialty section:
This article was submitted to Molecular Medicine, a section of the journal Frontiers in Cell and Developmental Biology

Received: 09 April 2020
Accepted: 31 July 2020
Published: 19 August 2020

Citation:
Ripoli C, Spinelli M, Natale F, Fusco S and Grassi C (2020) Glucose Overload Inhibits Glutamatergic Synaptic Transmission: A Novel Role for CREB-Mediated Regulation of Synaptotagmins 2 and 4. Front. Cell Dev. Biol. 8:810. doi: 10.3389/fcell.2020.00810

Glucose metabolism derangement is critically involved in the age-related memory loss but the underlying molecular mechanisms are still poorly understood. In a mouse model of type 1 diabetes we found memory impairment associated with inhibition of the transcription factor CREB and alteration of pre- and post-synaptic protein expression in the hippocampus. Accordingly, glucose excess negatively affected activity-dependent CREB phosphorylation and CREB-mediated mRNA expression of synaptic proteins in hippocampal primary neurons. Specifically, glucose excess inhibited the activity-dependent recruitment of CREB on the regulatory sequences of synaptotagmin (SYT) 2 and 4 promoters and the expression of SYT4 protein. As a result, high glucose affected both the frequency of miniature excitatory postsynaptic currents and NMDA receptor-mediated currents in autaptic hippocampal neuronal cultures. Collectively, our findings highlight novel mechanisms underlying hyperglycaemia-related memory loss, including CREB-dependent downregulation of synaptotagmin expression.

Keywords: synaptic vesicle release, hippocampus, type 1 diabetes, hyperglycaemia, synaptic proteins, memory loss, metabolism

INTRODUCTION

In response to physiological stimuli and environmental conditions, the central nervous system undergoes functional and structural changes (Pascual-Leone et al., 2005). Molecular mechanisms underlying synaptic transmission and plasticity play a pivotal role in the regulation of learning and memory. A plethora of synaptic proteins, including synaptophysin, synapsin family and the SNAP receptor (SNARE) complex regulates the fusion of neurotransmitter vesicles to the synaptic membrane and their release (Brose et al., 2019). Moreover, Ca^{2+} sensor proteins such as synaptotagmins are crucial for Ca^{2+}-dependent exocytosis (Fernández-Chacón et al., 2001; Südhof and Rothman, 2009). In glutamatergic synapses, activity-dependent rapid changes in the composition of α-amino-3-hydroxy-5-methyl-4-isoxazolepropionic acid (AMPA) and N-methyl-D-aspartate (NMDA) glutamate receptors at the postsynaptic compartment enhance the amplitude of postsynaptic responses and strengthen the synaptic functions (Zito and Svoboda, 2002).

Importantly, glucose metabolism derangement and type 2 diabetes negatively impact on synaptic plasticity and cognitive functions through multiple mechanisms including oxidative stress,

endothelial dysfunctions, microglia activation and neurotrophin depletion (Kullmann et al., 2016; Duffy et al., 2019; Spinelli et al., 2019). However, how glucose excess affects synaptic transmission and neuron-to-neuron communication is still poorly understood. The transcription factor cAMP response element-binding protein (CREB) has been widely investigated as a metabolic sensor and regulator of glucose homeostasis in liver and fat tissue (Altarejos and Montminy, 2011), and as a master switch of Ca^{2+} and neurotrophin-triggered transcriptional programs regulating neuronal differentiation, survival, and plasticity in central and peripheral nervous systems (Riccio et al., 1999; Finkbeiner, 2000, Mantamadiotis et al., 2002). Furthermore, brain plasticity and high-order cognitive functions are as well influenced by nutrient cues and energy metabolism through CREB-dependent expression of genes involved in adult neurogenesis, chromatin silencing and neuronal metabolism (Fusco et al., 2012, 2016). Here we demonstrated that glucose overload inhibits CREB activity in hippocampal neurons and alters the expression of genes encoding pre- and post-synaptic proteins. High glucose concentration also impairs the spontaneous vesicle release and both the amplitude and the kinetics of NMDA receptor-mediated currents at the post-synaptic level. Finally, we identified synaptotagmin 2 and 4 (SYT2 and SYT4, respectively) as novel glucose-responsive CREB target genes involved in hyperglicaemia-dependent impairment of synaptic function.

MATERIALS AND METHODS

Ethics Statement

The animal study was reviewed and approved by the Ethics Committee of Università Cattolica del Sacro Cuore and were fully compliant with Italian (Ministry of Health guidelines, Legislative Decree No. 116/1992) and European Union (Directive No. 86/609/EEC) legislations on animal research.

Animals

Male C57BL/6 mice (30 days-old), derived from the Animal Facility of Università Cattolica del Sacro Cuore, were used and randomly assigned to two treatments: (i) intraperitoneal injection of saline (CTR, control) and (ii) intraperitoneal injection of streptozotocin (STZ). Mice were housed in groups (3–5 animals per cage) and they were daily monitored. To induce hyperglycaemia, mice were intraperitoneally injected with 50 mg/Kg of streptozotocin (Sigma-Aldrich) for five consecutive days. The drug was freshly prepared in Na^{+} citrate solution buffered to 4.5 pH. Before each streptozotocin injection, animals were fasted for 6 h. After each injection, mice were supplied with 10% sucrose water to avoid sudden hypoglycaemia post injection. Mice were tested for sufficient levels of hyperglycaemia at 2 weeks after last injection (defined as time 0) and only mice with plasma glucose levels higher than 300 mg/dL were used for experiments. Blood sugar dosages and behavioral analyses were performed at both 1 and 3 weeks from time 0. Molecular analyses were performed on whole hippocampi collected 3 weeks from time 0 on different cohorts of mice. The animals were housed under a 12-h light-dark cycle at room temperature (RT: 19–22 °C) and received both food and water *ad libitum*.

Culture of Primary Neurons

Primary cultures of hippocampal neurons were obtained from E18 C57BL/6 mice embryos according to standard procedures. Briefly, hippocampi were dissected and incubated for 10 min at 37 °C in PBS containing 0.025% trypsin/0.01% EDTA (Biochrom AG). The tissue was then mechanically dissociated at room temperature (23–25 °C) using a fire-polished Pasteur pipette and the cell suspension was harvested and centrifuged at 100 × *g* for 8 min. The pellet was suspended in 88.8% (vol/vol) minimum essential medium (Biochrom), 5% FBS, 5% (vol/vol) horse serum, 1% glutamine (2 mM), 0.2% gentamicin (0.1 mg/mL) and glucose (25 mM). At 24 h after plating (1st day in vitro, DIV1), the culture medium was replaced with a medium containing 97.3% (vol/vol) neurobasal medium (Invitrogen), 2% (vol/vol) B-27 (Invitrogen), 0.5% glutamine (2 mM), and 0.2% gentamicin (0.1 mg/mL). After 72 h (DIV4), the culture medium was replaced with a similar medium lacking glutamine and supplemented with 2 μM cytosineβ-D-arabinofuranoside to inhibit glial cell proliferation. Autaptic hippocampal neurons were prepared as previously described (Attar et al., 2012; Ripoli et al., 2013). In brief, cortical astrocytes from P0–P2 brains of C57BL/6 mice were plated onto agarose-coated glass coverslips on which microislands where astrocytes could be grown were created by spraying a mixture of poly-D-lysine and collagen (both from Sigma). After 4 days, the medium (consisting of DMEM supplemented with 10% fetal bovine serum and antibiotics) was conditioned replacing half the medium volume with neuronal medium (Neurobasal medium, 2% B-27, 0.5% glutamine, and 1% penicillin-streptomycin-neomycin antibiotic mixture). Hippocampal neurons from P0 to P2 C57BL/6 were plated onto glial microislands at low density (25,000/cm^2) to obtain a ratio of one neuron per island. Both cultures (hippocampal neurons and autaptic hippocampal neurons) were maintained at 37°C in a humidified atmosphere of 5% CO_2 until experimental procedures. Every 3 days glucose levels in neuronal media were analyzed with glucometer. At DIV7 and DIV11 half the medium volume was replaced with fresh medium containing 25 mM (HG) or 0–5.5 mM (NG) in order to gradually decrease the level of glucose in NG samples and to obtain the experimental glucose concentration at DIV11. Molecular and electrophysiological experiments were performed at DIV14, after 3 days of HG (25 mM) and NG (5.5 mM). For molecular analyses, hippocampal neurons were stimulated with either 20 mM potassium chloride (Sigma Aldrich) or 10 μM forskolin (Sigma Aldrich). These compounds were applied for 30 min to investigate CREB phosphorylation and for 6 h to study gene expression modifications.

Behavioral Experiments

Behavioral tests were carried out from 9 a.m. to 4 p.m. and data were analyzed in blind using an automated video tracking system (Any-Maze^{TM}). Recognition memory was evaluated by novel object recognition (NOR) test. On first day, animals were familiarized for 10 min to the test arena (45 cm × 45 cm). On second day (training session), they were allowed to explore two

identical objects placed symmetrically in the arena for 10 min. Mice exhibiting a total exploration time lower than 30 s or exploring one of two identical objects for more than 60% of the total exploration time during training session were excluded from the test. On third day (test session), a new object replaced one of the old objects. Animals were allowed to explore for 10 min and preference index, calculated as the ratio between time spent exploring the novel object and time spent exploring both objects, was used to measure recognition memory. To exclude place preference in the test session, the position of novel object was alternated when testing the different animals. All objects and the box were cleaned with 70% ethanol at the end of each test.

Western Blotting

Tissues (hippocampi) or cells (hippocampal neurons) were lysed in ice-cold lysis buffer (NaCl 150 mM, Tris–HCl 50 mM pH 7.4, EDTA 2 mM) containing 1% Triton X-100, 0.1% SDS, 1 × protease inhibitor cocktail (Sigma-Aldrich), 1 mM sodium orthovanadate (Sigma-Aldrich) and 1 mM sodium fluoride (Sigma-Aldrich). Cells were incubated for 10 min on ice with occasional vortexing and spun down at 22,000 × g, 4°C. Supernatant was quantified for protein content (DC Protein Assay; Bio-Rad). Equal amounts of protein were diluted in Laemmli buffer, boiled and resolved by SDS-PAGE. The primary antibodies (available in **Supplementary Table S1**) were incubated overnight and revealed with HRP-conjugated secondary antibodies (Cell Signaling Technology Inc., Danvers, MA) and chemiluminescent substrates (Cyanagen). Band density was assessed by using UVItec Cambridge Alliance (Cambridge, United Kingdom). Protein expression levels were quantified by calculating the band intensity ratio of the target protein and actin (loading control) in each lane. Phosphorylation level of target proteins was quantified by calculating the band intensity ratio of phospho-target protein, target protein and actin (loading control) in each lane. In each bar graph, the mean value of controls was set to 1 and the expression or phosphorylation levels of target protein were shown as fold changes compared to the control (relative units). Images shown were cropped for presentation with no manipulations.

Real-Time PCR

Quantitative Real-Time PCR (qRT-PCR) amplifications were performed using SYBR GREEN qPCR Master Mix (Fisher Molecular Biology) on AB7500 instrument (Life Technologies) according to the manufacturer's instructions. The thermal cycling profile featured a pre-incubation step of 94°C for 10 min, followed by 40 cycles of denaturation (94°C, 15 s), annealing (55°C, 30 s), and elongation (72°C, 20 s). Melting curves were subsequently generated (94°C for 15 s, 50°C for 30 s, slow heating to 94°C in increments of 0.5°C).

Melting-curve analyses confirmed that only single products had been amplified. The primer sequences are shown in **Supplementary Table S2**. All data were normalized by reference to the amplification levels of the Gapdh gene; a reference dye was included in the SYBR master mix. RNA of all samples was analyzed in triplicate. The thresholds calculated by the software were used to determine specific mRNA expression levels using the cycle-at-threshold (Ct) method, and all results are expressed as fold changes (compared to control) for each transcript, employing the $2-\Delta\Delta Ct$ approach.

Immunocytochemistry

Hippocampal neurons were fixed in PBS solution (4% PFA, pH 7.4; Sigma-Aldrich) for 15 min at RT. Neurons were then permeabilized with 0.2% Triton X-100 (Sigma-Aldrich) for 15 min, blocked for 60 min in 5% NGS, and then incubated overnight at 4°C with anti-MAP2 (HM-2 clone, 1:400, Sigma-Aldrich). Cells were subsequently incubated for 90 min at RT with secondary antibody (Alexa-Fluor Donkey Anti-Mouse 1:1000). Finally, nuclei were counterstained with 4′, 6- diamidino-2-phenylindole (DAPI, 0.5 μg per mL for 10 min; Thermo Fisher), and cells were coverslipped with ProLong Gold anti-fade reagent (Thermo Fisher). Images of 1024 × 1024 pixels were obtained with an A1 MP, Nikon confocal microscope (Tokyo, Japan) equipped with 20× and 40× magnification objectives (numerical aperture 1.4), plus additional magnification.

Electrophysiology in Autaptic Microcultures

All electrophysiological recordings were performed using whole-cell patch clamp. Recordings were obtained with an Axopatch 200B amplifier (Molecular Devices), and stimulation and data acquisition were performed with the Digidata 1200 series interface and pCLAMP 11 software (Molecular Devices). Basal synaptic transmission was studied from 14 to 21 DIV using the patch-clamp technique in the whole-cell configuration as previously described (Ripoli et al., 2014). Cells were approached under DIC with 3–5 MΩ pipettes pulled from borosilicate glass (Warner Instruments, Inc) using a vertical Narishige PC-10 puller (Japan) and filled with an internal solution containing (in mM): 146 K-gluconate, 18 HEPES, 1 EGTA, 4.6 $MgCl_2$, 4 NaATP, 0.3 Na_2GTP, 15 creatine phosphate, and 5 U/ml phosphocreatine kinase. External Tyrode's solution containing the following (in mM): 140 NaCl, 2 KCl, 10 HEPES, 10 glucose, 4 $MgCl_2$, and 4 $CaCl_2$, pH 7.4, 312 mOsm. NMDA receptor-mediated currents were evoked using Mg-free Tyrode's solution containing 10 mM of the AMPA receptor blocker NBQX (Tocris Bioscience). Neurons were maintained at −70 mV holding potentials, and EPSCs were elicited with stimuli mimicking action potentials (2 ms at 0 mV) delivered every 10 s or 20 s. The paired-pulse ratio consisted of the ratio of the amplitude of the second EPSC to that of the first recorded at 50 ms intervals (Fattorini et al., 2019). To obtain the AMPA/NMDA ratio, evoked responses were recorded successively from the same cell. The amplitude and frequency of miniature excitatory postsynaptic currents (mEPSCs) were evaluated in 60 s recordings. The decay time was estimated by fitting a single exponential to the 10–90% decay-phase. We monitored the access resistance and membrane capacity before and at the end of the experiments to ensure recording stability and the health of studied cells. Whole-cell recordings were performed 5–15 min after the culture medium replacement with external Tyrode's solution. The culture plates were changed every half-hour. All experiments were performed at RT.

Chromatin Immunoprecipitation

Chromatin immunoprecipitation (ChIP) assays were performed as previously described (Fusco et al., 2019). Neurons were resuspended in 200 μl lysis buffer containing 1% SDS, 50 mM Tris–HCl pH 8.0, and 10 mM EDTA and sonicated on ice with six 10-s pulses with a 20-s interpulse interval. Sample debris was removed by centrifugation and supernatants were precleared with protein-G Sepharose 4B beads (Sigma-Aldrich) for 1 h at 4°C. 2 μg of anti-CREB or control IgG were added overnight at 4°C. Immune complexes were collected by incubation with protein-G Sepharose 4B beads for 2 h at 4°C. After seven sequential washes, immune complexes were eluted from beads by vortexing in elution buffer (1% SDS and $NaHCO_3$ 0.1 M; pH 8.0). NaCl was added (final concentration 0.33 M), and cross-linking was reversed by incubation overnight at 65 °C. DNA fragments were purified by using the PCR DNA fragments purification kit (Geneaid). The primer sequences are shown in **Supplementary Table S2**.

PCR conditions and cycle numbers were determined empirically and each PCR reaction was performed in triplicate. Data are expressed as percentage of input calculated by the "Adjusted input value" method according to the manufacturer's instructions (ThermoFisher Scientific ChIP Analysis). To determine the Adjusted input the Ct value of input was subtracted by 6.644 (i.e., log2 of 100). Next, the percent input of samples was estimated using the formula: 100*2^(Adjusted input – Ct(ChIP). The percent input of IgG samples was calculated using the formula 100*2^(Adjusted input – Ct(IgG).

Statistical Analysis

Sample sizes were chosen with adequate power (0.8) according to results of prior pilot data sets or studies, including our own, which used similar methods or paradigms. Sample estimation and statistical analyses were performed using SigmaPlot 12 software. Data were first tested for equal variance and normality (Shapiro-Wilk test) and the appropriate statistical tests were chosen. The statistical tests used (i.e., Student's *t*-test, two-way ANOVA) are indicated in the main text and in the corresponding figure legends for each experiment. N numbers are reported in the figure legends. Degrees of freedom are n–1 for each condition in both unpaired *t*-test and ANOVA tests. *Post-hoc* multiple comparisons were performed with Bonferroni correction. All statistical tests were two-tailed and the level of significance was set at 0.05. Results are shown as mean ± SEM.

RESULTS

Hyperglicemia Reduces the Expression of Pre- and Post-synaptic Proteins in the Hippocampus

Glucose metabolism dysregulation has been reported to affect synaptic function (Zhong et al., 2019). Previous studies demonstrated alterations of hippocampus-dependent-learning and memory in experimental models of hyperglycaemia (Gispen and Biessels, 2000) but the underlying molecular mechanisms remain still poorly understood. To investigate the effects of glucose excess on the expression of pre- and post-synaptic proteins in the hippocampus, we set up an *in vivo* model of streptozotocin (STZ)-induced hyperglycaemia. First, we evaluated glucose plasma levels and hippocampus-dependent cognitive function one and 3 weeks after the onset of hyperglicaemia. As expected, multiple STZ injections induced elevated values of fasting glycaemia and this alteration persisted after 3 weeks (400.44 ± 8.29 mg dL^{-1} vs 102.77 ± 6.06 mg dL^{-1}, $p = 1.11 \times 10^{-15}$ after 1 week; 406.22 ± 9.38 mg dL^{-1} vs 107.00 ± 3.28 mg dL^{-1}, $p = 6.09 \times 10^{-16}$ after 3 weeks; **Figure 1A**). More importantly, STZ mice already showed lower preference index than controls after the first week of high glucose levels, and their performances in novel object recognition (NOR) task even got worse after 3 weeks of hyperglicaemia (after 1 week: preference index 59.0 ± 0.9% vs 68.5 ± 0.5%, $p = 7.05 \times 10^{-8}$, exploration time toward novel object/old object 40.7 ± 6.7 s / 29.5 ± 8.2 s vs 42.2 ± 6.5 s / 19.4 ± 4.2 s; after 3 weeks: preference index 56.0 ± 0.7% vs 69.0 ± 1.1%, $p = 1.23 \times 10^{-8}$, exploration time toward novel object/old object 41.1 ± 4.4 s / 32.3 ± 4.6 s vs 47.1 ± 4.9 s / 21.1 ± 3.2 s; **Figure 1B**).

We also investigated the expression of glutamate receptor subunits and the activity-dependent phosphorylation of neuroplasticity proteins CaMKIIα and CREB in the hippocampus of hyperglicaemic mice. The immunoblot analysis of hippocampal lysates from STZ mice revealed lower expression of NMDA receptor subunits GluN1 and GluN2a and AMPA receptor subunit GluA2 compared to controls (−41 ± 5, −67 ± 8, and −47 ± 4%, respectively, $p < 0.001$ for all proteins; **Figure 1C**). In addition, STZ treatment reduced the activatory phosphorylation of transcription factor CREB on serine 133 ($CREB^{Ser133}$) (−75 ± 7%, $p = 0.0004$; **Figure 1C**). Instead, no significant changes were observed for the expression of GluN2b and GluA1 and the activatory phosphorylation of CaMKIIα on threonine 286 (**Figure 1C**). CREB-mediated transcription of presynaptic proteins has been demonstrated to promote synaptic enhancement and memory (Wagatsuma et al., 2006). Therefore, we analyzed the mRNA expression of several synaptic transmission-associated proteins in the hippocampus of STZ mice. We found lower expression of synaptotagmin 2 and 4 (SYT2 and SYT4, respectively) in hyperglycaemic mice (−49 ± 5%, $p = 3.34 \times 10^{-5}$ and −56 ± 6%, $p = 3.96 \times 10^{-5}$, respectively; **Figure 1D**), whereas we did not detect any significant changes of synaptotagmin 1 (SYT1), synaptophysin (SYP) and synapsin 1 (SYN1). We also found a significant decrease of Bdnf expression in the hippocampus of STZ mice compared to controls (−59 ± 5%, $p = 7.12 \times 10^{-5}$; **Figure 1D**). Collectively, *in vivo* data demonstrated that STZ-induced hyperglycaemia reduced CREB activation and the expression of hippocampal pre- and post-synaptic proteins involved in synaptic function and memory.

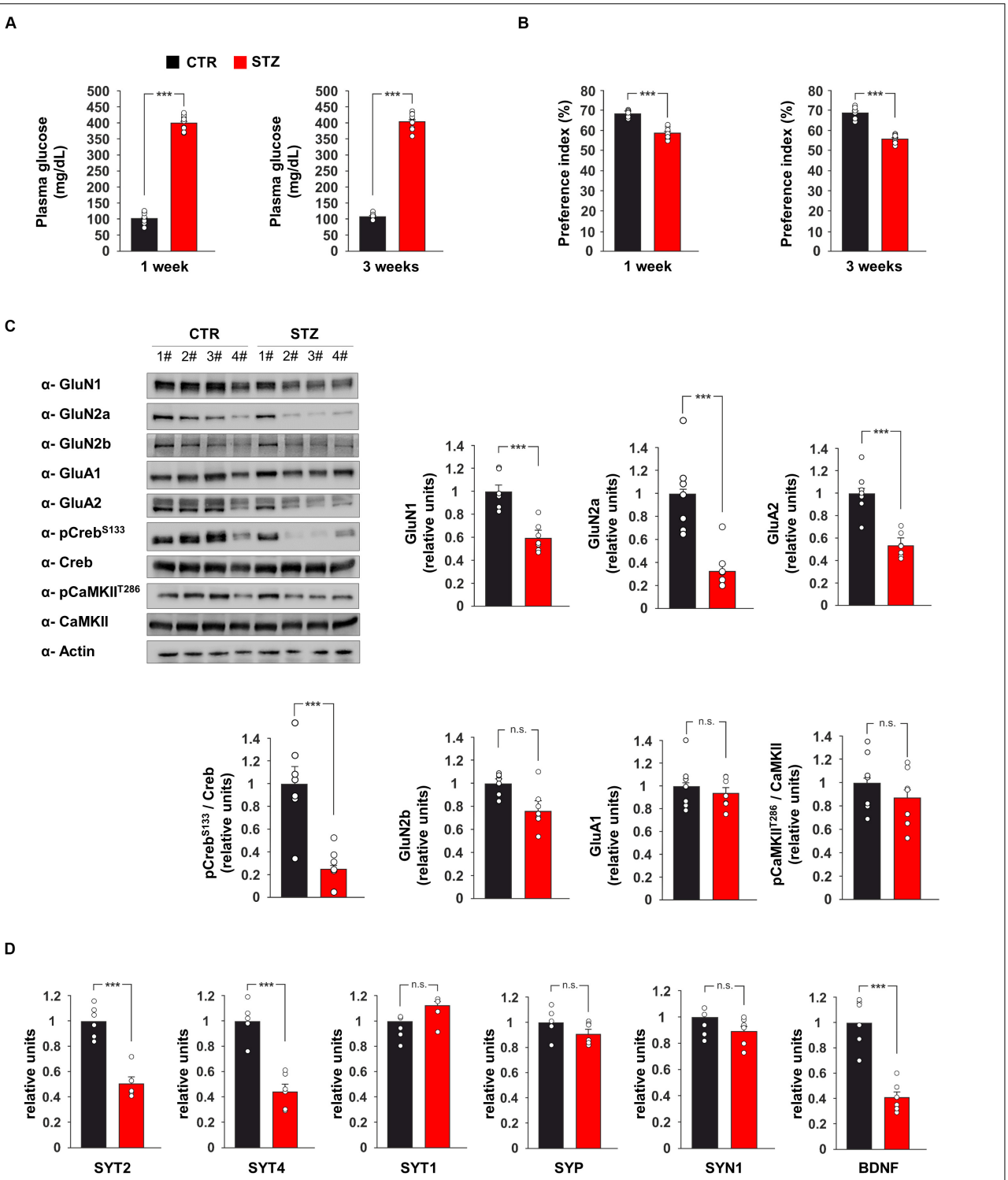

FIGURE 1 | Hyperglicaemia affects the expression of pre- and post-synaptic proteins in the hippocampus. **(A)** Plasma levels of glucose in C57BL/6 mice i.p. injected with saline (CTR) or streptozotocin (STZ, 50 mg/Kg/day for 5 days). Glycaemia levels were detected after 1 or 3 weeks from the onset of hyperglycaemia in STZ mice (n = 9 mice per group; statistics by unpaired Student's t-test). **(B)** Preference for the novel object in the NOR paradigm after 1 or 3 weeks from the onset of hyperglycaemia in CTR and STZ mice (n = 9 mice; statistics by unpaired Student's t-test). **(C)** Immunoblot analysis and bar graphs showing the expression of GluN1, GluN2a, GluN2b, GluA1, GluA2 and the phosphorylation of both Creb on serine 133 ($Creb^{S133}$) and CaMKII on threonine 286 ($CaMKII^{T286}$) in the hippocampus of CTR and STZ mice (n = 7 mice; statistics by unpaired Student's t-test). **(D)** mRNA expression of synaptotagmin 1, 2 and 4 (SYT1, SYT2, and SYT4, respectively), synaptophysin (SYP), synapsin 1 (SYN1) and BDNF in the hippocampus of CTR and STZ mice (n = 6 mice; statistics by unpaired Student's t-test). Real Time analysis was performed in triplicate. Gene expression was normalized to Gapdh. Data are expressed as mean ± SEM. $^*p < 0.05$; $^{***}p < 0.001$; n.s. not significant.

Glucose Excess Inhibits CREB-Dependent Gene Expression

To deeply investigate the effect of hyperglycaemia on CREB transcriptional activity, we set up an *in vitro* model of hippocampal primary neurons cultivated in media containing either normal (NG) or high glucose (HG) concentrations (1 g/L or 4.5 g/L, respectively; **Figure 2A**). In neurons, synaptic activity enhances the intracellular concentration of Ca^{2+} and cyclic adenosine monophosphate (cAMP), both leading to phosphorylation and activation of CREB (Deisseroth et al., 1996). Accordingly, compounds inducing intracellular increase of either Ca^{2+} (20 mM KCl) or cAMP (10 μM forskolin [Fsk]) induced $CREB^{Ser133}$ phosphorylation in neurons exposed to normal glucose levels ($F_{2,71}$ = 16.82, +49 ± 12% NG_{KCl} vs NG_{NT}, p = 0.011; +99 ± 18% NG_{Fsk} vs NG_{NT}, p = 0.004, **Figure 2B**). Conversely, HG significantly reduced the basal phosphorylation levels of CREB and inhibited its activation upon KCl stimulation (−34 ± 6% HG_{NT} vs NG_{NT}, p = 0.009; +33 ± 9% HG_{KCl} vs HG_{NT}, p = 0.088, **Figure 2B**). We also analyzed the mRNA expression of both CREB target genes and synaptic proteins that we found downregulated in the hippocampus of STZ mice. In standard conditions, both KCl

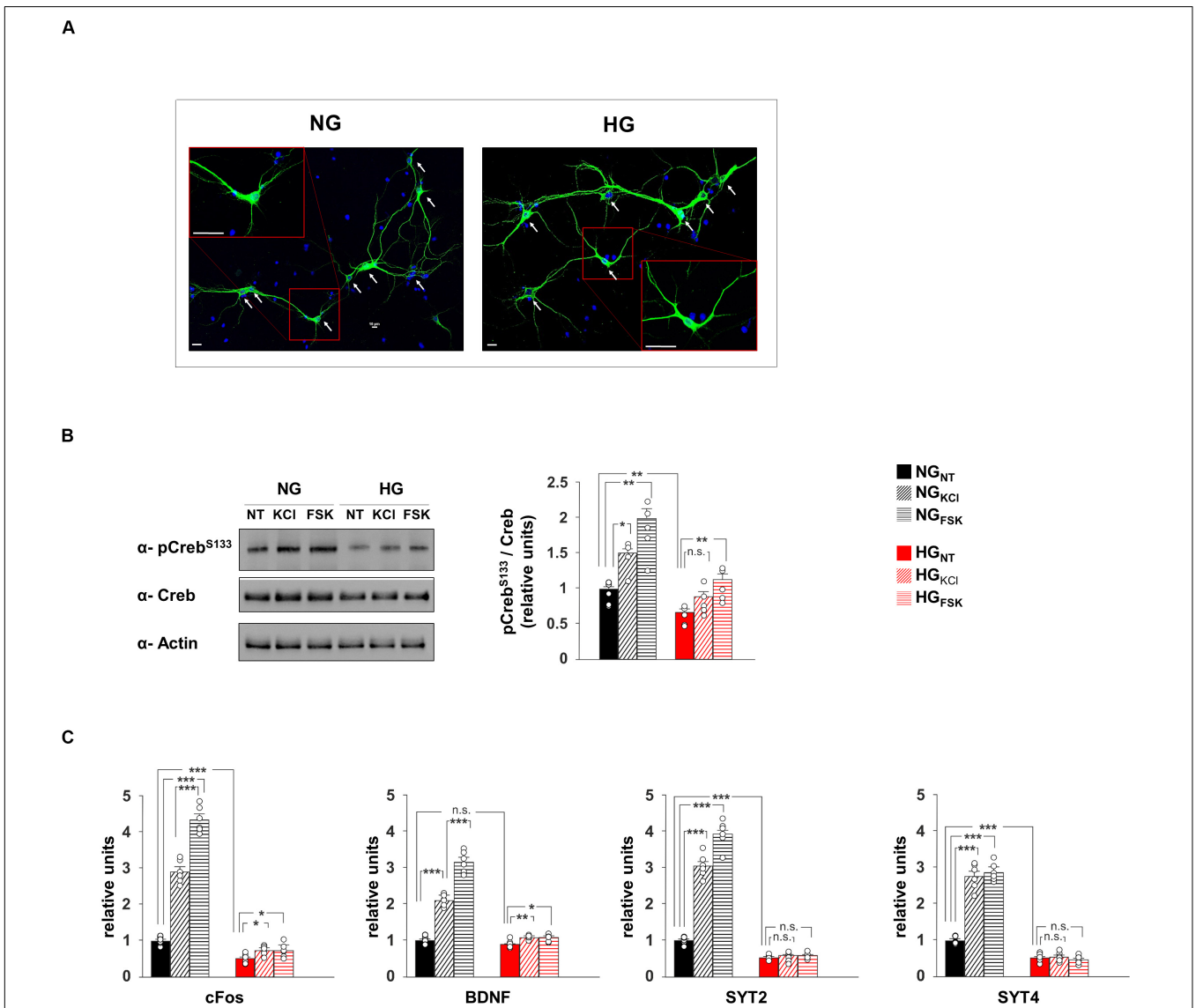

FIGURE 2 | Glucose excess impairs both CREB phosphorylation and expression of plasticity-related genes in neurons. **(A)** Representative images of hippocampal neurons cultivated in media containing normal (NG, 1.0 g/L) or high glucose (HG, 4.5 g/L) levels. Scale bar: 50 μM. **(B)** Immunoblot analyses and bar graphs showing CrebS133 phosphorylation in NG or HG neurons treated with vehicle (NT), 20 mM potassium chloride (KCl) or 10 μM forskolin (Fsk). The experiment was repeated five times (statistics by two-way ANOVA and Bonferroni *post hoc*). **(C)** mRNA expression of cFos, BDNF, SYT2, and SYT4 in NH and HG neurons. Real Time analysis was performed in triplicate. Gene expression was normalized to Gapdh. The experiment was repeated six times using independent RNA samples (statistics by two-way ANOVA and Bonferroni post hoc). Data are expressed as mean ± SEM. *p < 0.05; **p < 0.01; ***p < 0.001; n.s. not significant.

and Fsk largely enhanced the transcription of CREB targets c-Fos and Bdnf, whereas this enhancement was cut down by HG treatment ($F_{2.60}$ = 270.15 for cFos, +189 ± 14% NG_{KCl} vs NG_{NT}, $p = 8.39 \times 10^{-6}$; +334 ± 16% NG_{Fsk} vs NG_{NT}, $p = 5.86 \times 10^{-7}$; +48 ± 5% HG_{KCl} vs HG_{NT}, p = 0.012; +48 ± 8% HG_{Fsk} vs HG_{NT}, p = 0.038; $F_{2.60}$ = 191.32 for Bdnf, +109 ± 7% NG_{KCl} vs NG_{NT}, $p = 1.06 \times 10^{-7}$; +215 ± 13% NG_{Fsk} vs NG_{NT}, $p = 6.85 \times 10^{-7}$; +20 ± 2% HG_{KCl} vs HG_{NT}, p = 0.006; +19 ± 4% HG_{Fsk} vs HG_{NT}, p = 0.015; **Figure 2C**). Moreover, molecules activating CREB enhanced the expression of both SYT2 and SYT4 genes. More importantly, glucose excess lowered the transcription of synaptotagmins and abolished their CREB activity-related upregulation reproducing *in vitro* the molecular changes observed *in vivo* ($F_{2.60}$ = 286.79 for SYT2, +203 ± 14% NG_{KCl} vs NG_{NT}, $p = 5.36 \times 10^{-6}$; +292 ± 16% NG_{Fsk} vs NG_{NT}, $p = 1.57 \times 10^{-6}$; −49 ± 3% HG_{NT} vs NG_{NT}, $p = 6.82 \times 10^{-6}$; HG_{KCl} vs HG_{NT}, p = 0.955; HG_{Fsk} vs HG_{NT}, p = 0.254; $F_{2.60}$ = 188.26 for SYT4, +176 ± 16% NG_{KCl} vs NG_{NT}, $p = 2.24 \times 10^{-5}$; +187 ± 11% NG_{Fsk} vs NG_{NT}, $p = 5.37 \times 10^{-7}$; −49 ± 5% HG_{NT} vs NG_{NT}, $p = 1.72 \times 10^{-5}$; HG_{KCl} vs HG_{NT}, p = 0.711; HG_{Fsk} vs HG_{NT}, p = 0.511; **Figure 2C**). Our data indicate that HG negatively impacts on CREB phosphorylation and its transcriptional activity in hippocampal neurons, correlating with the impairment of synaptic protein expression.

HG Inhibited the Recruitment of CREB on Both SYT2 and SYT4 Promoters

The transcription factor CREB modulates synaptic activity by modifying its binding on the promoters of neuronal genes and regulating their expression (West and Greenberg, 2011). Our data suggested that SYT2 and SYT4 might represent novel molecular targets of CREB and be involved in the HG-related alteration of synaptic function. To verify whether the HG-dependent inhibition of CREB activity was implicated in the changes of SYT2 and SYT4 expression, we first analyzed the regulatory sequences of these genes. The bioinformatics analysis revealed the presence of several putative cAMP Responsive Elements (CRE) on the regulatory sequences of both SYT2 and SYT4 (**Figure 3A**). Chromatin immunoprecipitation experiments from hippocampal neurons showed that CREB binds the same genomic region in a fashion inducible by KCl and Fsk ($F_{2.60}$ = 102.19 for SYT2, +256 ± 31% NG_{KCl} vs NG_{NT}, $p = 2.87 \times 10^{-4}$; +308 ± 25% NG_{Fsk} vs NG_{NT}, $p = 4.63 \times 10^{-5}$; $F_{2.60}$ = 99.53 for SYT4, +229 ± 23% NG_{KCl} vs NG_{NT}, $p = 4.5 \times 10^{-5}$; +257 ± 25% NG_{Fsk} vs NG_{NT}, $p = 3.47 \times 10^{-5}$; **Figure 3B**). Moreover, glucose excess affected the recruitment of transcription factor on the promoters of SYT2 and SYT4 in both basal and inducible conditions ($F_{2.60}$ = 102.19 for SYT2, −51 ± 8% HG_{NT} vs NG_{NT}, $p = 3.28 \times 10^{-4}$; HG_{KCl} vs HG_{NT}, p = 0.422; HG_{Fsk} vs HG_{NT}, p = 0.732; $F_{2.60}$ = 99.53 for SYT4, −40 ± 8% HG_{NT} vs NG_{NT}, $p = 3.61 \times 10^{-3}$; HG_{KCl} vs HG_{NT}, p = 0.740; HG_{Fsk} vs HG_{NT}, p = 0.620; **Figure 3B**). Accordingly, CREB-activating stimuli induced SYT4 expression in NG-treated hippocampal neurons, whereas HG decreased SYT4 at protein level and inhibited its Fsk-dependent upregulation ($F_{2.71}$ = 49.66, +43 ± 4% NG_{KCl} vs NG_{NT}, p = 0.0019; +136 ± 15% NG_{Fsk} vs NG_{NT}, $p = 2.29 \times 10^{-5}$; −22 ± 2% HG_{NT} vs NG_{NT}, p = 0.018; +21 ± 11% HG_{Fsk} vs HG_{NT}, p = 0.089; **Figure 3C**). Moreover, SYT4 expression was significantly reduced in the hippocampi of hyperglycaemic mice (−32 ± 9%, p = 0.0102; **Figure 3D**). Collectively, our findings identify SYT2 and SYT4 as novel activity-dependent targets of CREB and indicate the CREB-dependent downregulation of vesicle release as a potential mechanism leading HG-dependent impairment of glutamatergic synaptic transmission.

HG Alters the Basal Glutamatergic Synaptic Transmission in Autaptic Hippocampal Neurons

Our molecular data demonstrate that glucose excess can alter the expression of pre- and post-synaptic proteins in hippocampal neurons. To evaluate the functional role of glucose dyshomeostasis on glutamatergic synaptic transmission, we performed patch-clamp experiments in autaptic hippocampal neuronal cultures grown in NG or HG conditions. First, we measured the membrane capacitance of autaptic hippocampal neurons that was unchanged by HG treatment (90.5 ± 2.9 pF in NG condition *vs* 94.8 ± 3.0 pF in HG condition, p = 0.3994; **Figure 4A**).

Glucose overload did not affect evoked basal synaptic transmission, measured as the amplitude of excitatory postsynaptic currents (EPSCs) elicited by stimuli mimicking action potentials (5.0 ± 0.4 nA in NG condition *vs* 5.6 ± 0.5 nA in HG condition, p = 0.4155; **Figures 4B,C**). Analysis of mEPSCs in autapses exposed to HG revealed a significant decrease in the mEPSC frequency (5.9 ± 0.6 Hz in NG condition vs 3.2 ± 0.4 Hz in HG condition, p = 0.0011; **Figures 4D–F**) whereas the mean amplitude and the kinetics of mEPSCs (i.e., rise and decay time constants) were unaffected (mEPSC amplitude: 21.5 ± 1.7 pA in NG condition vs 22.0 ± 2.0 pA in HG condition, p = 0.8928, **Figures 4D,E,G**; mEPSC rise time: 1.1 ± 0.1 ms in NG condition vs 1.0 ± 0.1 ms in HG condition, p = 0.5279; mEPSC decay time 3.5 ± 0.2 ms in NG condition vs 3.7 ± 0.2 in HG condition, p = 0.2995). To test whether the decrease in mEPSC frequency reflected a change in presynaptic vesicle release, we studied the paired-pulse ratio in response to two depolarizing stimuli delivered at 50 ms interval. The paired pulse ratio was not significantly different in NG and HG conditions (67.3 ± 4.9% [n = 10] and 61.7 ± 6.4% [n = 11], respectively, p = 0.5952), indicating that the HG-related depression of mEPSCs frequency was not due to changes in the initial release probability of presynaptic vesicles.

To extend our analysis to the postsynaptic side, we recorded the responses to glutamate-receptor activation by applying 100 μM glutamate through the extracellular solution perfusing the recorded neuron. In line with results on evoked EPSCs, the amplitude of the glutamatergic receptor-mediated current was not significantly different in autaptic neurons cultivated in NG or HG conditions (4.1 ± 0.4 nA vs 4.0 ± 0.5 nA, respectively, n = 14 each condition, p = 0.9910). Of note,

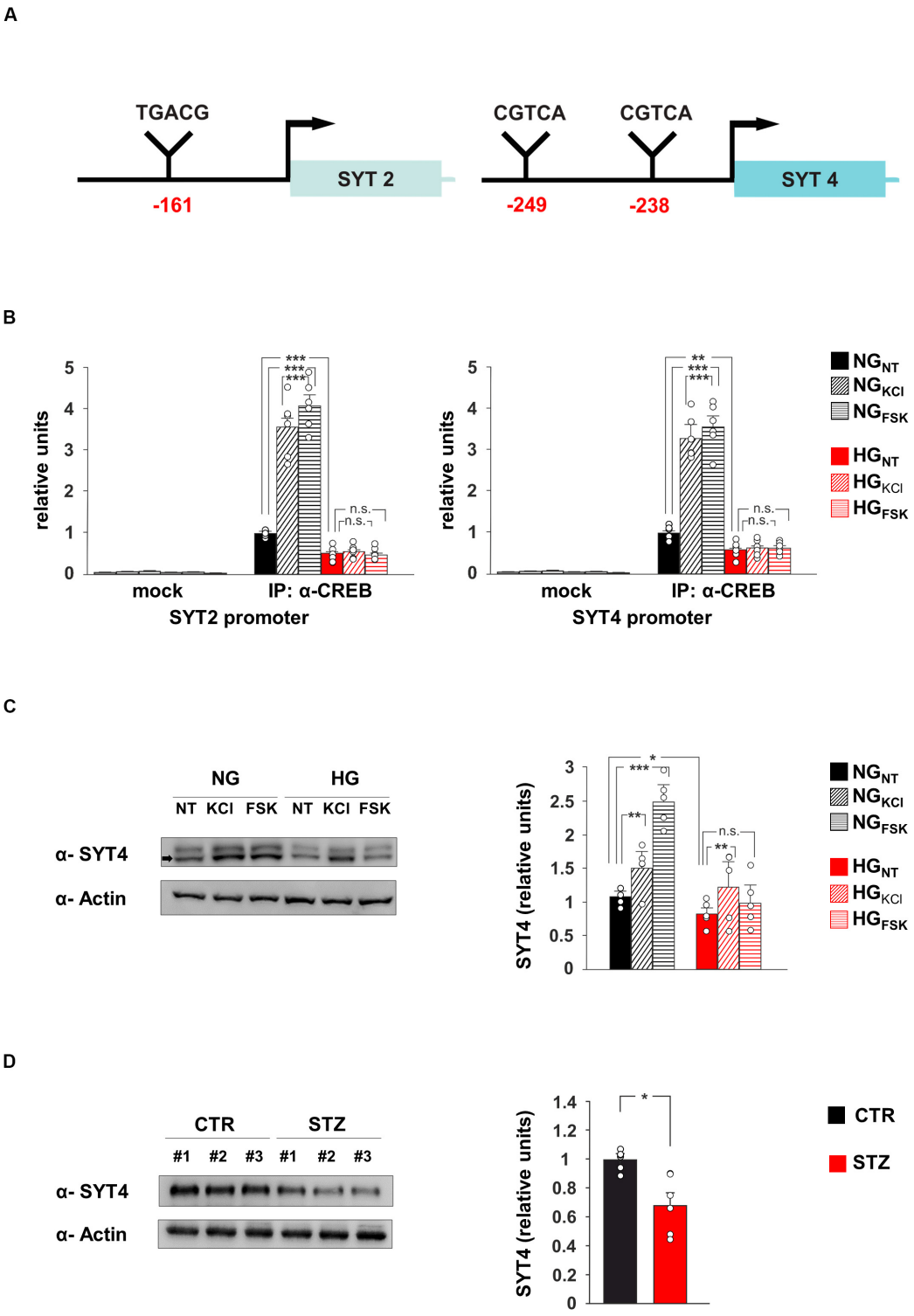

FIGURE 3 | CREB regulates SYT4 in a glucose-dependent fashion. **(A)** Schematic representation of putative CRE regions identified on the promoters of SYT2 (–161 bp from transcription start site) and SYT4 (–249 and –238 bp upstream the starting codon) genes. **(B)** ChIP analysis of both non-specific IgG (mock) and CREB binding to the SYT2 and SYT4 promoters in NG and HG neurons stimulated with vehicle (NT), 20 mM potassium chloride (KCl) or 10 μM forskolin (Fsk). Real Time analysis was performed in triplicate. Experiments were repeated six times using independent DNA samples (statistics by two-way ANOVA and Bonferroni post hoc). **(C)** Immunoblot analysis and bar graphs showing the expression of SYT4 in NG or HG neurons treated with vehicle, KCl or Fsk. The experiment was repeated five times (statistics by two-way ANOVA and Bonferroni post hoc). **(D)** Immunoblot analysis and bar graphs showing the expression of SYT4 in the hippocampus of CTR and STZ mice (n = 6 mice; statistics by unpaired Student's t-test). Data are expressed as mean ± SEM. $^{*}p < 0.05$; $^{**}p < 0.01$; $^{***}p < 0.001$; n.s. not significant.

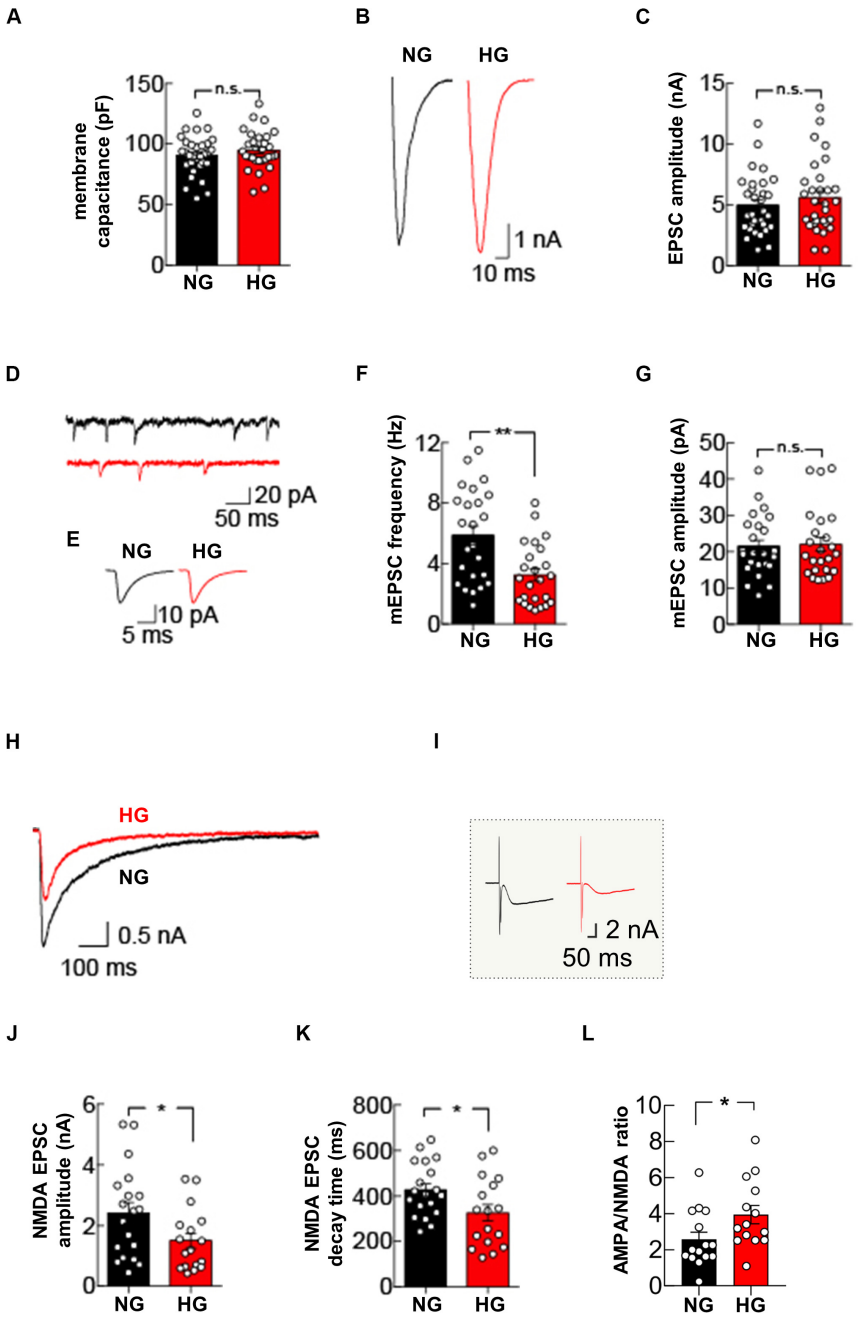

FIGURE 4 | High glucose treatment impairs mEPSC frequency and NMDA receptor-mediated currents. **(A)** Quantification of membrane capacitance recorded in autaptic microcultures grown in NG (n = 31) or HG conditions (n = 30). **(B)** Representative traces of EPSC evoked by stimuli mimicking single action potentials recorded in NG- and HG-treated autaptic neurons. **(C)** Summary graphs of EPSC amplitudes recorded from autaptic neurons grown in either NG (n = 31) or HG (n = 31). **(D)** Example traces showing spontaneous mEPSCs from NG- and HG-treated autaptic neurons. **(E)** Representative mEPSC averaged traces. Summary graphs of mEPSC frequency (n = 24 per group) **(F)** and mEPSC amplitudes (n = 24 per group) **(G)**. **(H)** Representative traces of NMDA receptor-mediated currents evoked by stimuli mimicking single action potentials and recorded in NG- and HG-treated autaptic neurons. (**I**) Inset: raw traces of H. Summary graphs of NMDA receptor-mediated currents amplitude **(J)** and decay time **(K)** from autaptic neurons grown in NG (n = 19) and in HG (n = 17). **(L)** Summary graphs of the AMPA:NMDA ratio recorded from autaptic neurons grown in either NG (n = 15) or HG (n = 14). Data are expressed as mean ± SEM. *$p < 0.05$; **$p < 0.001$; n.s. not significant. Statistic by Mann–Whitney U-test, mEPSC amplitudes were analyzed with the Kolmogorov-Smirnov test.

with bath application of glutamate we stimulated the entire AMPA receptors pool expressed on cell membrane, instead of the synaptic pool only, without significantly affecting the NMDA receptors that, at resting membrane potential, are mostly blocked by extracellular Mg^{2+}. To test whether glucose dyshomeostasis affected NMDA receptors, we measured evoked

NMDA receptor-mediated currents by using a Mg^{2+}-free external solution and suppressing the AMPA receptor-mediated component of the EPSC with 10 μM 2,3-dihydroxy-6-nitro-7-sulfamoyl-benzo(F)quinoxaline-2,3-dione (NBQX).

Under NG conditions, hippocampal autapses depolarized with stimuli mimicking action potentials evoked robust NMDA receptor-mediated currents (2.4 ± 0.4 nA). Conversely, HG significantly reduced the NMDA receptor-mediated currents (1.5 ± 0.3 nA, $p = 0.03$; **Figures 4H–J**). Interestingly, HG also significantly changed the decay time of NMDA receptor-mediated currents (426.8 ± 28.1 ms, in NG condition and 326.2 ± 38.0 ms, in HG condition, $p = 0.04$; **Figures 4H,K**). Finally, we measured the ratio between AMPA receptor-mediated and NMDA receptor-mediated EPSCs, which is a standard test to detect changes in synaptic strength (Kauer and Malenka, 2007). Autaptic hippocampal neurons grown in HG condition displayed a significant increase in the AMPA/NMDA ratio (3.9 ± 0.5, compared with 2.6 ± 0.4 seen in the NG autaptic hippocampal neurons; $p = 0.0292$, **Figure 4L**). Collectively, our data demonstrate that glucose overload impairs glutamatergic synaptic transmission at both pre- and post-synaptic levels.

DISCUSSION

Epidemiological evidence indicated that diabetic patients are significantly more susceptible to develop cognitive impairment, and elevated blood glucose levels increase the risk of dementia in both diabetic and non-diabetic individuals (Cukierman-Yaffee, 2009; Crane et al., 2013). Several molecular mechanisms have been proposed to underlie the hyperglycaemia-related alterations of brain plasticity, including the depletion of stem cell niche, the development of brain insulin resistance, microvascular complications and neuroinflammation (Hsu and Kanoski, 2014; Fusco et al., 2016; Spinelli et al., 2019). However, how glucose overload affects synaptic transmission and plasticity remains still poorly understood. Here, we found that a well-established animal model of hyperglycaemia, i.e., the STZ-injected mice, exhibited memory deficits (**Figure 1B**) associated with molecular changes in the hippocampus including lower amounts of NMDA receptor subunits GluN1 and GluN2a (**Figure 1C**), reduced phosphorylation levels of memory-related transcription factor CREB (**Figure 1C**) and decreased expression of genes encoding for synaptic proteins regulating synaptic transmission and plasticity such as SYT2, SYT4 and BDNF (**Figure 1D**). CREB is a pivotal hub in the activity-driven neuronal gene expression (Benito et al., 2011) and its activity has been reported to be critically reduced in the context of aging and age-associated brain diseases (Zuccato et al., 2001; Cui et al., 2006; Caccamo et al., 2010). In the last years, we identified CREB as novel metabolic sensor in the brain, whose transcriptional activity was finely regulated by the nutrient availability (Fusco et al., 2012; Fusco and Pani, 2013). To deeply investigate the CREB-related molecular and functional changes due to the glucose overload on hippocampal neurons, we studied the effect of medium containing HG levels on both hippocampal primary neurons and autaptic hippocampal neurons. Exposure of neurons to HG simulated the molecular changes observed in the hippocampus of STZ mice, including the inhibition of CREB activity (**Figure 2B**). More importantly, HG impaired the CREB phosphorylation induced by drugs mimicking neuronal activity and abolished the upregulation of synaptotagmins 2 and 4 (**Figure 2B,C**). This sort of "negative priming" of activity-dependent CREB response might be mediated by the inhibition of CREB activators AMP-activated protein kinase and Sirtuin 1 in high glucose condition (Fusco et al., 2012; Peng et al., 2016). Interestingly, it has been demonstrated that SYTs, in addition to control the neurotransmitter release on presynaptic side, can also play a critical role in regulating the exocytosis of postsynaptic receptors at postsynaptic level (Wu et al., 2017). Accordingly, SYT4 mutant mice showed deficits of hippocampus-dependent learning and memory (Ferguson et al., 2000).

Our electrophysiological experiments performed in autaptic hippocampal neurons indicated that glucose excess impaired the spontaneous release of glutamate from presynaptic terminals whereas the evoked release and paired-pulse ratio were not affected (**Figure 4**). The decreased mEPSCs frequency we observed could be attributed to the downregulated expression of key proteins involved in synaptic vesicles fusion (**Figure 2**). However, other mechanisms might be also involved. First, glycaemia homeostasis imbalance has been reported to decrease intracellular Ca^{2+} levels (Chan and Greenberg, 1991). Another possible explanation of mEPSCs frequency alteration observed in HG-treated neurons is that the number of vesicles in presynaptic terminals and in the readily releasable pool of synaptic vesicles were different in NG- and HG-treated neurons. Furthermore, prolonged exposure to high levels of extracellular glucose may induce insulin resistance desensitizing insulin receptors. Specifically, it has been demonstrated that downregulation of insulin receptors signaling resulted in a significant reduction in the frequency of mEPSCs without affecting either the distribution of their amplitudes or the presynaptic release probability (Chiu et al., 2008; Lee et al., 2011).

To answer the fundamental question on how HG adversely impacts synapse function, we extended our analysis to the postsynaptic site by recording the NMDA receptor-mediated currents. We observed that HG differentially affected the evoked AMPA and NMDA receptor-mediated currents. Specifically, AMPA receptor-mediated currents were unaffected by HG treatment (**Figures 4B,C**). Conversely, we observed a significant reduction of NMDA receptor-mediated currents together with a reduction of the decay time in HG-treated neurons (**Figure 4H–K**). These data, including the increased AMPA/NMDA ratio observed in HG neurons, suggest that glucose dyshomeostasis preferentially targets NMDA receptors, although our Western blotting analysis performed in the hippocampus of STZ mice revealed a significant reduction of GluA2 subunits (**Figure 1C**). Of note, the streptozotocin-induced type 1 diabetes model is characterized by more complex metabolic changes, including drastic decrease of insulin levels and alteration of leptin signalling, which may explain the differences between our *in vivo* and *in vitro* models (MacDougald et al., 1995).

NMDA is a tetrameric receptor with two obligatory GluN1 subunits and two regulatory subunits, GluN2A and GluN2B (Yashiro and Philpot, 2008). The kinetics of NMDA receptor mediated currents reflect a different subunit composition of NMDA receptors which influences their Ca^{2+} permeability. Faster kinetics indicates lower Ca^{2+} influx through NMDA receptors (Yashiro and Philpot, 2008; Lee et al., 2010). In HG neurons, we found faster NMDA decay times suggesting lower Ca^{2+} influx (**Figures 4H,J**). Thus, we are proposing that glucose excess would influence the threshold for synaptic plasticity by affecting synaptic metaplasticity. Intriguingly, spontaneous glutamate release, instead of evoked release, adjusts functional and structural plasticity threshold at single synapses by local regulation of NMDA receptors (Lee et al., 2010). Our data support the idea that dietary regimen may influence brain plasticity, at least in part, by modifying CREB activity via altered glucose metabolism homeostasis (Mainardi et al., 2012). Of note, the beneficial effects of calorie restriction on synaptic plasticity and memory were abolished in mice lacking CREB in the forebrain (Fusco et al., 2012). However, glucose excess could also negatively impact on synaptic function by changing the intracytoplasmatic Ca^{2+} clearance (Nakashima et al., 1996), enhancing oxidative stress (Treviño et al., 2015) and impairing astrocyte energy metabolism (Li et al., 2018).

Here, we identified novel CRE regions on the regulatory sequences of SYT 2 and SYT4 genes, which may trigger the HG-dependent changes of synaptic function (**Figure 3A**). A fundamental question is whether SYTs also contribute to postsynaptic responses during neurotransmission. SYT4 deficiency has been demonstrated to modify the release of neurotrophic factor BDNF at postsynaptic level (Dean et al., 2009). BDNF has been recognized as strong modulator of multiple neuronal functions including synaptic plasticity, learning and memory (Minichiello, 2009; Fusco et al., 2019). Collectively, our data provide new insights into the glucose-responsive CREB modulation of synaptic proteins regulating synaptic vesicle release. An intriguing hypothesis is that glucose availability influences the activity-dependent recruitment of CREB to the synaptotagmin promoters (**Figure 3B**) and the level of synaptic proteins controlling the vesicle release. The inhibition of spontaneous glutamate release together with the decrease of neurotrophin levels could contribute to synaptic function deficit observed in experimental models of diabetes. Specifically, the observed defects in mEPSC frequency may adversely affect the activity of NMDA receptors, which in turn regulate synaptic plasticity, learning and memory. Moreover, lower expression of synaptic proteins may elicit the decrease of both dendritic branching and spine density observed in experimental models of hyperglycaemia (Malone et al., 2008).

As mentioned above, hyperglicaemia and alteration of glucose homeostasis have been implicated in age-dependent cognitive decline and memory loss, although the molecular mechanisms are still elusive. Our findings reveal a novel molecular circuit that regulates synaptic transmission at pre- and post-synaptic levels involving CREB-dependent-downregulation of SYTs. A different model of insulin resistance-dependent hyperglycaemia, i.e., high fat diet (HFD)-fed mice, showed similar memory deficits and impairment of synaptic functions compared to STZ mice that were primarily attributed to aberrant protein palmitoylation (Yan et al., 2016; Spinelli et al., 2017). HFD also inhibits CREB phosphorylation in the hippocampus (Wu et al., 2018), as well as the expression of genes encoding SYT2 and SYT4 in mouse cerebral cortex (Yoon et al., 2019). However, despite sharing several functional and behavioral alterations, HFD and STZ models also differ for a number of intracellular molecular cascades relying on insulin resistance primarily occurring in the former. Future studies are needed to better understand the role of glucose-driven CREB transcriptional activity in age-dependent memory loss and its potential impact on personalized medicine approaches.

DATA AVAILABILITY STATEMENT

The raw data supporting the conclusions of this article will be made available by the authors, without undue reservation.

ETHICS STATEMENT

The animal study was reviewed and approved by the Ethics Committee of Università Cattolica del Sacro Cuore and were fully compliant with Italian (Ministry of Health guidelines, Legislative Decree No. 116/1992) and European Union (Directive No. 86/609/EEC) legislations on animal research.

AUTHOR CONTRIBUTIONS

CR, SF, and CG conceived the study, supervised the work, and wrote the manuscript. CR performed the electrophysiological experiments. MS performed the metabolic analyses and western blotting experiments. FN performed the gene expression analysis. SF designed and performed the behavioral and ChIP experiments. All authors commented on the manuscript and approved its final version.

FUNDING

This work was supported by the Italian Ministry of Health (GR-2018-12366381 to SF) and intramural grants from the Catholic University (Linea D.3.2 2017 to CG).

SUPPLEMENTARY MATERIAL

The Supplementary Material for this article can be found online at: https://www.frontiersin.org/articles/10.3389/fcell.2020.00810/full#supplementary-material

REFERENCES

Altarejos, J. Y., and Montminy, M. (2011). CREB and the CRTC co-activators: sensors for hormonal and metabolic signals. *Nat. Rev. Mol. Cell Biol.* 12, 141–151. doi: 10.1038/nrm3072

Attar, A., Ripoli, C., Riccardi, E., Maiti, P., Puma, D. D. L., Liu, T., et al. (2012). Protection of primary neurons and mouse brain from Alzheimer's pathology by molecular tweezers. *Brain* 135(Pt 12), 3735–3748. doi: 10.1093/brain/aws289

Benito, E., Valor, L. M., Jimenez-Minchan, M., Huber, W., and Barco, A. (2011). cAMP response element-binding protein is a primary hub of activity-driven neuronal gene expression. *J. Neurosci.* 31, 18237–18250. doi: 10.1523/jneurosci.4554-11.2011

Brose, N., Brunger, A., Cafiso, D., Chapman, E. R., Diao, J., Hughson, F. M., et al. (2019). Synaptic vesicle fusion: today and beyond. *Nat. Struct. Mol. Biol.* 26, 663–668.

Caccamo, A., Maldonado, M. A., Bokov, A. F., Majumder, S., and Oddo, S. (2010). CBP gene transfer increases BDNF levels and ameliorates learning and memory deficits in a mouse model of Alzheimer's disease. *Proc. Natl. Acad. Sci. U.S.A.* 107, 22687–22692. doi: 10.1073/pnas.1012851108

Chan, J., and Greenberg, D. A. (1991). Effects of glucose on calcium channels in neural cells. *Neurosci. Lett.* 121, 34–36. doi: 10.1016/0304-3940(91)90642-7

Chiu, S. L., Chen, C. M., and Cline, H. T. (2008). Insulin receptor signaling regulates synapse number, dendritic plasticity, and circuit function in vivo. *Neuron* 58, 708–719. doi: 10.1016/j.neuron.2008.04.014

Crane, P. K., Walker, R., and Larson, E. B. (2013). Glucose levels and risk of dementia. *N. Engl. J. Med.* 369, 1863–1864. doi: 10.1056/nejmc1311765

Cui, L., Jeong, H., Borovecki, F., Parkhurst, C. N., Tanese, N., and Krainc, D. (2006). Transcriptional repression of PGC-1alpha by mutant huntingtin leads to mitochondrial dysfunction and neurodegeneration. *Cell* 127, 59–69. doi: 10.1016/j.cell.2006.09.015

Cukierman-Yaffee, T. (2009). The relationship between dysglycemia and cognitive dysfunction. *Curr. Opin. Invest. Drugs* 10, 70–74.

Dean, C., Liu, H., Dunning, F. M., Chang, P. Y., Jackson, M. B., and Chapman, E. R. (2009). Synaptotagmin-IV modulates synaptic function and LTP by regulating BDNF release. *Nat. Neurosci.* 12, 767–776. doi: 10.1038/nn.2315

Deisseroth, K., Bito, H., and Tsien, R. W. (1996). Signaling from synapse to nucleus: postsynaptic CREB phosphorylation during multiple forms of hippocampal synaptic plasticity. *Neuron* 16, 89–101. doi: 10.1016/s0896-6273(00)80026-4

Duffy, C. M., Hofmeister, J. J., Nixon, J. P., and Butterick, T. A. (2019). High fat diet increases cognitive decline and neuroinflammation in a model of orexin loss. *Neurobiol. Learn. Mem.* 157, 41–47. doi: 10.1016/j.nlm.2018.11.008

Fattorini, G., Ripoli, C., Cocco, S., Spinelli, M., Mattera, A., Grassi, C., et al. (2019). Glutamate/GABA co-release selectively influences postsynaptic glutamate receptors in mouse cortical neurons. *Neuropharmacology* 161:107737. doi: 10.1016/j.neuropharm.2019.107737

Ferguson, G. D., Anagnostaras, S. G., Silva, A. J., and Herschman, H. R. (2000). Deficits in memory and motor performance in synaptotagmin IV mutant mice. *Proc. Natl. Acad. Sci. U.S.A.* 97, 5598–5603. doi: 10.1073/pnas.100104597

Fernández-Chacón, R., Königstorfer, A., Gerber, S. H., García, J., Matos, M. F., Stevens, C. F., et al. (2001). Synaptotagmin I functions as a calcium regulator of release probability. *Nature* 410, 41–49. doi: 10.1038/35065004

Finkbeiner, S. (2000). CREB couples neurotrophin signals to survival messages. *Neuron* 25, 11–14. doi: 10.1016/s0896-6273(00)80866-1

Fusco, S., Leone, L., Barbati, S. A., Samengo, D., Piacentini, R., Maulucci, G., et al. (2016). A CREB-Sirt1-Hes1 circuitry mediates neural stem cell response to glucose availability. *Cell Rep.* 14, 1195–1205. doi: 10.1016/j.celrep.2015.12.092

Fusco, S., Maulucci, G., and Pani, G. (2012). Sirt1: def-eating senescence? *Cell Cycle* 11, 4135–4146. doi: 10.4161/cc.22074

Fusco, S., and Pani, G. (2013). Brain response to calorie restriction. *Cell Mol. Life Sci.* 70, 3157–3170. doi: 10.1007/s00018-012-1223-y

Fusco, S., Ripoli, C., Podda, M. V., Ranieri, S. C., Leone, L., Toietta, G., et al. (2012). A role for neuronal cAMP responsive-element binding (CREB)-1 in brain responses to calorie restriction. *Proc. Natl. Acad. Sci. U.S.A.* 109, 621–626. doi: 10.1073/pnas.1109237109

Fusco, S., Spinelli, M., Cocco, S., Ripoli, C., Mastrodonato, A., Natale, F., et al. (2019). Maternal insulin resistance multigenerationally impairs synaptic plasticity and memory via gametic mechanisms. *Nat. Commun.* 10:4799. doi: 10.1038/s41467-019-12793-3

Gispen, W. H., and Biessels, G. J. (2000). Cognition and synaptic plasticity in diabetes mellitus. *Trends Neurosci.* 23, 542–549. doi: 10.1016/s0166-2236(00)01656-8

Hsu, T. M., and Kanoski, S. E. (2014). Blood-brain barrier disruption: mechanistic links between Western diet consumption and dementia. *Front. Aging Neurosci.* 6:88. doi: 10.3389/fnagi.2014.00088

Kauer, J. A., and Malenka, R. C. (2007). Synaptic plasticity and addiction. *Nat. Rev. Neurosci.* 8, 844–858. doi: 10.1038/nrn2234

Kullmann, S., Heni, M., Hallschmid, M., Fritsche, A., Preissl, H., and Haring, H. U. (2016). 'Brain insulin resistance at the crossroads of metabolic and cognitive disorders in humans. *Physiol. Rev.* 96, 1169–1209. doi: 10.1152/physrev.00032

Lee, C. C., Huang, C. C., and Hsu, K. S. (2011). Insulin promotes dendritic spine and synapse formation by the PI3K/Akt/mTOR and Rac1 signaling pathways. *Neuropharmacology* 61, 867–879. doi: 10.1016/j.neuropharm.2011.06.003

Lee, M. C., Yasuda, R., and Ehlers, M. D. (2010). Metaplasticity at single glutamatergic synapses. *Neuron* 66, 859–870. doi: 10.1016/j.neuron.2010.05.015

Li, W., Roy Choudhury, G., Winters, A., Prah, J., Lin, W., Liu, R., et al. (2018). Hyperglycemia alters astrocyte metabolism and inhibits astrocyte proliferation. *Aging Dis.* 9, 674–684.

MacDougald, O. A., Hwang, C. S., Fan, H., and Lane, M. D. (1995). Regulated expression of the obese gene product (leptin) in white adipose tissue and 3T3-L1 adipocytes. *Proc. Natl. Acad. Sci. U.S.A.* 92, 9034–9037. doi: 10.1073/pnas.92.20.9034

Mainardi, M., Fusco, S., and Grassi, C. (2012). Modulation of hippocampal neural plasticity by glucose-related signaling. *Neural Plast.* 2015:657928. doi: 10.1155/2015/657928

Malone, J. I., Hanna, S., Saporta, S., Mervis, R. F., Park, C. R., Chong, L., et al. (2008). Hyperglycemia not hypoglycemia alters neuronal dendrites and impairs spatial memory. *Pediatr. Diabetes* 9, 531–539. doi: 10.1111/j.1399-5448.2008.00431.x

Mantamadiotis, T., Lemberger, T., Bleckmann, S. C., Kern, H., Kretz, O., Martin Villalba, A., et al. (2002). Disruption of CREB function in brain leads to neurodegeneration. *Nat. Genet.* 31, 47–54. doi: 10.1038/ng882

Minichiello, L. (2009). TrkB signalling pathways in LTP and learning. *Nat. Rev. Neurosci.* 10, 850–860. doi: 10.1038/nrn2738

Nakashima, Y., Ishibashi, H., Harata, N., and Akaike, N. (1996). Effects of glucose deprivation on NMDA-induced current and intracellular Ca2+ in rat substantia nigra neurons. *J. Neurophysiol.* 75, 740–749. doi: 10.1152/jn.1996.75.2.740

Pascual-Leone, A., Amedi, A., Fregni, F., and Merabet, L. B. (2005). The plastic human brain cortex. *Annu. Rev. Neurosci.* 28, 377–401.

Peng, Y., Liu, J., Shi, L., Tang, Y., Gao, D., Long, J., et al. (2016). Mitochondrial dysfunction precedes depression of AMPK/AKT signaling in insulin resistance induced by high glucose in primary cortical neurons. *J. Neurochem.* 137, 701–713. doi: 10.1111/jnc.13563

Riccio, A., Ahn, S., Davenport, C. M., Blendy, J. A., and Ginty, D. D. (1999). Mediation by a CREB family transcription factor of NGF-dependent survival of sympathetic neurons. *Science* 286, 2358–2361. doi: 10.1126/science.286.5448.2358

Ripoli, C., Cocco, S., Li Puma, D. D., Piacentini, R., Mastrodonato, A., Scala, F., et al. (2014). Intracellular accumulation of amyloid-β (Aβ) protein plays a major role in Aβ-induced alterations of glutamatergic synaptic transmission and plasticity. *J. Neurosci.* 34, 12893–12903. doi: 10.1523/JNEUROSCI.1201-14.2014

Ripoli, C., Piacentini, R., Riccardi, E., Leone, L., Li Puma, D. D., Bitan, G., et al. (2013). Effects of different amyloid β-protein analogues on synaptic function. *Neurobiol. Aging* 34, 1032–1044. doi: 10.1016/j.neurobiolaging.2012.06.027

Spinelli, M., Fusco, S., and Grassi, C. (2019). Brain insulin resistance and hippocampal plasticity: mechanisms and biomarkers of cognitive decline. *Front. Neurosci.* 13:788. doi: 10.3389/fnins.2019.00788

Spinelli, M., Fusco, S., Mainardi, M., Scala, F., Natale, F., Lapenta, R., et al. (2017). Brain insulin resistance impairs hippocampal synaptic plasticity and memory by increasing GluA1 palmitoylation through FoxO3a. *Nat. Commun.* 8:2009. doi: 10.1038/s41467-017-02221-9

Südhof, T. C., and Rothman, J. E. (2009). Membrane fusion: grappling with SNARE and SM proteins. *Science* 323, 474–477. doi: 10.1126/science.1161748

Treviño, S., Aguilar-Alonso, P., Flores Hernandez, J. A., Brambila, E., Guevara, J., Flores, G., et al. (2015). A high calorie diet causes memory loss, metabolic

syndrome and oxidative stress into hippocampus and temporal cortex of rats. *Synapse* 69, 421–433. doi: 10.1002/syn.21832

Wagatsuma, A., Azami, S., Sakura, M., Hatakeyama, D., Aonuma, H., and Ito, E. (2006). De novo synthesis of CREB in a presynaptic neuron is required for synaptic enhancement involved in memory consolidation. *J. Neurosci. Res.* 84, 954–960. doi: 10.1002/jnr.21012

West, A. E., and Greenberg, M. E. (2011). Neuronal activity-regulated gene transcription in synapse development and cognitive function. *Cold Spring Harb. Perspect. Biol.* 3:a005744. doi: 10.1101/cshperspect.a005744

Wu, D., Bacaj, T., Morishita, W., Goswami, D., Arendt, K. L., Xu, W., et al. (2017). Postsynaptic synaptotagmins mediate AMPA receptor exocytosis during LTP. *Nature* 544, 316–321. doi: 10.1038/nature21720

Wu, H., Liu, Q., Kalavagunta, P. K., Huang, Q., Lv, W., An, X., et al. (2018). Normal diet Vs High fat diet – a comparative study: behavioral and neuroimmunological changes in adolescent male mice. *Metab. Brain Dis.* 33, 177–190. doi: 10.1007/s11011-017-0140-z

Yan, S., Du, F., Wu, L., Zhang, Z., Zhong, C., Yu, Q., et al. (2016). F1F0 ATP synthase-Cyclophilin D interaction contributes to diabetes-induced synaptic dysfunction and cognitive decline. *Diabetes* 65, 3482–3494. doi: 10.2337/db16-0556

Yashiro, K., and Philpot, B. D. (2008). Regulation of NMDA receptor subunit expression and its implications for LTD, LTP, and metaplasticity. *Neuropharmacology* 55, 1081–1094. doi: 10.1016/j.neuropharm.2008.07.046

Yoon, G., Cho, K. A., Song, J., and Kim, Y.-K. (2019). Transcriptomic analysis of high fat diet fed mouse brain cortex. *Front. Genet.* 10:83. doi: 10.3389/fgene.2019.00083

Zhong, Y., Zhu, Y., He, T., Li, W., Li, Q., and Miao, Y. (2019). Brain-derived neurotrophic factor inhibits hyperglycemia-induced apoptosis and downregulation of synaptic plasticity-related proteins in hippocampal neurons via the PI3K/Akt pathway. *Int. J. Mol. Med.* 43, 294–304. doi: 10.3892/ijmm.2018.3933

Zito, K., and Svoboda, K. (2002). Activity-dependent synaptogenesis in the adult Mammalian cortex. *Neuron.* 35, 1015–1017. doi: 10.1016/s0896-6273(02)00903-0

Zuccato, C., Ciammola, A., Rigamonti, D., Leavitt, B. R., Goffredo, D., Conti, L., et al. (2001). Loss of huntingtin-mediated BDNF gene transcription in Huntington's disease. *Science* 293, 493–498. doi: 10.1126/science.1059581

Conflict of Interest: The authors declare that the research was conducted in the absence of any commercial or financial relationships that could be construed as a potential conflict of interest.

frontiers in Cell and Developmental Biology

ORIGINAL RESEARCH
published: 11 September 2020
doi: 10.3389/fcell.2020.562662

Identifying Mechanisms of Normal Cognitive Aging Using a Novel Mouse Genetic Reference Panel

*Amy R. Dunn[1], Niran Hadad[1], Sarah M. Neuner[1,2], Ji-Gang Zhang[1], Vivek M. Philip[1], Logan Dumitrescu[3], Timothy J. Hohman[3], Jeremy H. Herskowitz[4], Kristen M. S. O'Connell[1] and Catherine C. Kaczorowski[1]**

[1] The Jackson Laboratory, Bar Harbor, ME, United States, [2] Department of Anatomy and Neurobiology, The University of Tennessee Health Science Center, Memphis, TN, United States, [3] Vanderbilt Memory and Alzheimer's Center and Vanderbilt Genetics Institute, Vanderbilt University Medical Center, Nashville, TN, United States, [4] Center for Neurodegeneration and Experimental Therapeutics and Department of Neurology, The University of Alabama at Birmingham, Birmingham, AL, United States

OPEN ACCESS

Edited by:
Alex Dranovsky, Columbia University, United States

Reviewed by:
Shannon J. Moore, University of Michigan, United States
Jiaxing Wang, Emory University, United States
Felix L. Struebing, Ludwig Maximilian University of Munich, Germany

***Correspondence:**
Catherine C. Kaczorowski
Catherine.Kaczorowski@jax.org

Specialty section:
This article was submitted to Molecular Medicine, a section of the journal Frontiers in Cell and Developmental Biology

Received: *15 May 2020*
Accepted: *17 August 2020*
Published: *11 September 2020*

Citation:
Dunn AR, Hadad N, Neuner SM, Zhang JG, Philip VM, Dumitrescu L, Hohman TJ, Herskowitz JH, O'Connell KMS and Kaczorowski CC (2020) Identifying Mechanisms of Normal Cognitive Aging Using a Novel Mouse Genetic Reference Panel. Front. Cell Dev. Biol. 8:562662. doi: 10.3389/fcell.2020.562662

Developing strategies to maintain cognitive health is critical to quality of life during aging. The basis of healthy cognitive aging is poorly understood; thus, it is difficult to predict who will have normal cognition later in life. Individuals may have higher baseline functioning (cognitive reserve) and others may maintain or even improve with age (cognitive resilience). Understanding the mechanisms underlying cognitive reserve and resilience may hold the key to new therapeutic strategies for maintaining cognitive health. However, reserve and resilience have been inconsistently defined in human studies. Additionally, our understanding of the molecular and cellular bases of these phenomena is poor, compounded by a lack of longitudinal molecular and cognitive data that fully capture the dynamic trajectories of cognitive aging. Here, we used a genetically diverse mouse population (B6-BXDs) to characterize individual differences in cognitive abilities in adulthood and investigate evidence of cognitive reserve and/or resilience in middle-aged mice. We tested cognitive function at two ages (6 months and 14 months) using y-maze and contextual fear conditioning. We observed heritable variation in performance on these traits ($h^2_{RI\bar{x}}$ = 0.51–0.74), suggesting moderate to strong genetic control depending on the cognitive domain. Due to the polygenetic nature of cognitive function, we did not find QTLs significantly associated with y-maze, contextual fear acquisition (CFA) or memory, or decline in cognitive function at the genome-wide level. To more precisely interrogate the molecular regulation of variation in these traits, we employed RNA-seq and identified gene networks related to transcription/translation, cellular metabolism, and neuronal function that were associated with working memory, contextual fear memory, and cognitive decline. Using this method, we nominate the *Trio* gene as a modulator of working memory ability. Finally, we propose a conceptual framework for identifying strains exhibiting cognitive reserve and/or resilience to assess whether these traits can be observed in middle-aged B6-BXDs. Though we found that earlier cognitive reserve evident early in life protects against cognitive impairment later

in life, cognitive performance and age-related decline fell along a continuum, with no clear genotypes emerging as exemplars of exceptional reserve or resilience – leading to recommendations for future use of aging mouse populations to understand the nature of cognitive reserve and resilience.

Keywords: cognitive aging, cognitive reserve, cognitive resilience, Weighted Gene Co-expression Network Analysis, quantitative trait locus mapping, Y-maze, contextual fear conditioning

INTRODUCTION

Cognitive decline with age, even in the absence of overt dementia, is common and highly heritable (Dutta et al., 2014; Reynolds and Finkel, 2015). Cognitive function in old age is an important predictor of quality of life (Pan et al., 2011, 2015), and developing strategies to improve cognitive longevity (i.e., ability to maintain high level of cognitive function into old age) will be critical as life expectancy continues to increase through modern medicine. To understand cognitive stability in aging, it is important to first consider baseline cognitive function: namely, knowing individuals' baseline function in early adulthood is necessary to fully capture cognitive aging trajectories, and understanding how baseline cognitive function is regulated may help to inform strategies to maintain those cognitive abilities in aging. Recent studies have identified over 300 loci associated with general cognitive function and related traits in adulthood (Davies et al., 2011, 2015, 2018; Hill et al., 2014; Hibar et al., 2015, 2017; Trampush et al., 2015; Clarke et al., 2016; Krapohl and Plomin, 2016; Okbay et al., 2016; Sniekers et al., 2017; Savage et al., 2018; Zabaneh et al., 2018). Given the lack of longitudinal molecular data, and to a lesser extent, longitudinal cognitive data from human populations, it remains unclear if the mechanisms underlying baseline cognitive function also mediate normal cognitive aging. These factors are highly complex and poorly understood, despite extensive study (Harris and Deary, 2011; Bis et al., 2012; De Jager et al., 2012; Davies et al., 2014; Mukherjee et al., 2014; Zhang and Pierce, 2014; Debette et al., 2015; Lu et al., 2017; Raj et al., 2017; Tasaki et al., 2018; Yen et al., 2018; Kamboh et al., 2019; Wingo et al., 2019). Discovering high-impact targets for bolstering baseline cognitive function and enhancing cognitive longevity will facilitate the development of pharmacotherapeutics to enhance cognitive health in middle-age and beyond.

Identifying molecular networks that promote the maintenance of cognitive function in aging requires understanding of cognitive reserve and resilience. Cognitive reserve is often defined as higher baseline function (Montine et al., 2019), whereas cognitive resilience is characterized by slower cognitive decline. Reserve and resilience have often been attributed to environmental factors; for example, socioeconomic status, education level, and physical activity are all associated with greater cognitive reserve and better cognitive status in late adulthood (Arenaza-Urquijo et al., 2015; Walhovd et al., 2019; Zahodne et al., 2019). However, given the heritability of cognitive decline [∼30–60% genetic control based on twin and community studies (Swan et al., 1990; McGue and Christensen, 2001; Harris and Deary, 2011)], there is also a significant genetic component. Perhaps unsurprisingly, molecular pathways that have been implicated in mediating human cognitive aging and reserve include synaptic function (Honer et al., 2012; Arenaza-Urquijo et al., 2015; Lesuis et al., 2018; Kamboh et al., 2019; Wingo et al., 2019), mitochondrial function (Wingo et al., 2019), and inflammation (Stacey et al., 2017).

In order to fully understand molecular contributors to cognitive aging, it will be necessary to study transcriptomic, proteomic and epigenetic changes across the lifespan and how they relate to and predict changes in cognitive function. Human studies of aging often recruit participants in middle age and necessarily collect brain tissue postmortem, at which point molecular signatures of those processes underlying the onset and progression of cognitive aging may have been ongoing for decades. Even studies that begin sampling cognitive function earlier in life are unable to capture molecular changes within the brain until after death, which precludes the possibility of understanding early molecular regulators of cognitive reserve and resilience.

Given the challenges in studying the genetics of cognitive decline in humans, animal models of aging provide a unique and critical opportunity to study molecular mechanisms of cognitive aging, as well as cognitive reserve and resilience, across the lifespan. In this study, we utilized a novel genetic reference population, an F1 population of C57BL/6J (B6) mice crossed with 27 strains of the BXD genetic reference panel of mice (B6-BXD), to interrogate molecular mediators of baseline cognitive function and age-related cognitive decline. The advantage of working with this population of mice is: (1) a well characterized, diverse and replicable genome, (2) the ability to sample a range of cognitive domains in both longitudinal and cross-sectional manners, (3) the availability of postmortem brain tissue at multiple ages for assessing gene and protein expression, and (4) the enhanced ability to identify genetic factors in the B6 genome that may confer protection against age-related decline. With this panel, we are able to take advantage of testing reproducible genotypes in controlled environments to study how age interacts with genetic background to influence cognitive decline. As in humans, we found that individual differences in cognitive function and changes across the lifespan are highly heritable and polygenetic in nature. To reveal the underlying molecular mechanisms, we performed RNA sequencing and identified gene co-expression networks involving intracellular, organelle and neuronal function whose expression profiles were strongly associated with cognitive function and cognitive aging. Finally, we evaluated operational definitions for cognitive reserve, resilience and reserve/resilience that we pre-registered to assess whether any B6-BXD strains exemplify cognitive reserve and resilience. From this work, we

provide recommendations for incorporating genetically diverse, recombinant inbred mouse populations for aging studies and developing definitions of reserve and resilience for animal studies, as these are needed to advance our understanding of the mechanisms of reserve and resilience.

MATERIALS AND METHODS

Animals

Animals were kept on a 12 h light/dark cycle and provided food and water *ad libitum*. Mice were group-housed (2–5 per cage). All routine procedures were approved by the Institutional Animal Care and Use Committee (IACUC) at The University of Tennessee Health Science Center, and in accordance with the standards of the Association for the Assessment and Accreditation of Laboratory Animal Care (AAALAC) and the National Institutes of Health Guide of the Care and Use of Laboratory Animals.

Generation of Ntg B6-BXD F1 Panel

Non-transgenic littermates of the AD-BXD panel were generated as described in Neuner et al. (2019). Briefly, hemizygous 5XFAD female mice on a congenic C57BL/6J background were crossed to male BXD mice (27 BXD strains). One-half of the resultant F1 offspring harbored the 5XFAD transgene to represent a familial Alzheimer's disease population (AD-BXDs). The remaining half of the resultant F1 offspring did not inherit the 5XFAD transgene and were thus "normal aging" controls. Data collected from non-transgenic F1 population (B6-BXD) were comprehensively analyzed and interpreted here, though some behavioral and molecular data from these non-transgenic littermates was made available to the research community as controls for the AD-BXD panel first reported in Neuner et al., 2019. Because we had more thorough representation of female animals, we focused our behavioral and transcriptomic analyses on females only for this manuscript.

Behavioral Analysis, Phenotype Derivation

Behavioral tasks (**Figure 1A**) were described in Neuner et al., 2019; a subset of these animals (i.e., all female non-transgenic animals) are described here. A total of 192 animals were included in the present analyses, and these animals numbers per strain, age, and assay may be found in **Supplementary Table S1**. Y-maze was conducted at both 6 months (n = 171) and 14 months (n = 100), with animals in the 14 months cohort having been previously tested at 6 months. The same cohort underwent contextual fear conditioning as a terminal assay at either 6 months (n = 83) or 14 months (n = 106). Brief descriptions of each phenotyping task are described below.

Y-Maze

To assess working memory function, mice were placed in a clear acrylic Y-maze for 8 min. External visual spatial cues were placed approximately one foot outside of the maze. Mouse movement was recorded with a video camera and spontaneous alternations were tracked by Any-Maze software. Spontaneous alternations were defined as successive entries into each arm before re-entering any arm. Chance performance was defined as less than 50% correct spontaneous alternations. Animal order was randomized, and experimenters were blind to mouse strain, age, and genotype.

Contextual Fear Conditioning

To assess contextual fear acquisition (CFA) and long-term contextual memory (CFM), animals underwent a standard contextual fear conditioning paradigm (Neuner et al., 2015). Training consisted of a 150 s baseline period followed by four footshocks (1 s, 0.9 mA) separated by 140 ± 5 s. A 40 s period following each shock was considered the postshock (PS) interval. Total freezing during the fourth PS interval (PS4) was defined as CFA. To measure CFM, animals were placed in the same chamber 24 h later for 10 min with no footshocks. Percent time spent freezing during training and testing was determined using FreezeFrame software.

Decline Scores

Age-related decline on memory function was determined by subtracting performance at 6 months from performance at 14 months to achieve a strain average "decline score" in each memory assay.

Heritability Calculations

Heritability of behavioral phenotypes was calculated as a ratio of genetic variance to total variance (genetic + environmental variance), normalized to the number of biological replicates per strain (i.e., $h^2_{RI\bar{x}}$; **Figure 1A**). Heritability scores can range from 0 to 1.0, with an $h^2_{RI\bar{x}}$ = 1.0 indicating that 100% of the variance in that trait is controlled by genetics (Belknap, 1998).

Trait and Module QTL Mapping

Genotypes for BXD strains were obtained from GeneNetwork.org. Quantitative trait locus (QTL) mapping was performed using the R package qtl2 (Broman et al., 2019) using the LOCO method for kinship correction (**Figure 1A**). Permutation tests (1,000) were used to determine statistical significance. Power calculations and percent variance explained were calculated using the R package qtlDesign and reported in **Table 1**.

RNA Sequencing

RNA sequencing data from the present cohort has been previously reported in part in Neuner et al. (2019). The previous publication focused primarily on RNA expression in the 5XFAD-positive transgenic littermates (AD-BXDs) of the non-transgenic mice included herein, with expression data presented for certain genes of interest in transgenic mice in relation to non-transgenic mice. Here, we focus on the female non-transgenic B6-BXD mice only and the gene networks relevant to normal cognition and cognitive aging (**Figure 1B**). Sequencing methods were also described in Neuner et al. (2019). Briefly, hippocampi were snap-frozen at 6 m and 14 m (n = 39 for 6 months, n = 45 for 14 months) immediately following contextual fear conditioning,

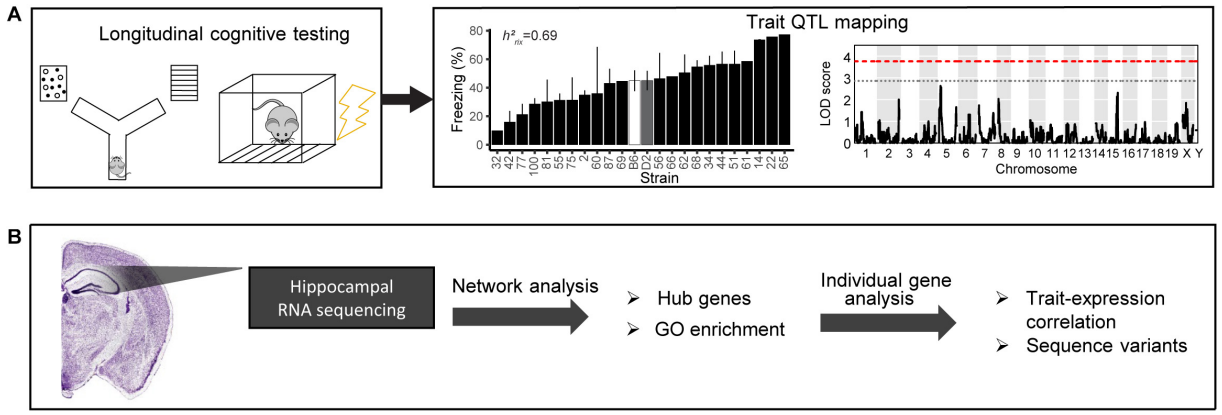

FIGURE 1 | Schematic of our pipeline to identify mechanisms underlying cognitive function and aging. **(A)** We cognitively tested a large cohort of B6-BXD mice using y-maze (working memory) and contextual fear conditioning (short- and long-term memory). We performed quantitative trait locus (QTL) mapping on all traits. **(B)** We also performed bulk RNA sequencing of the hippocampus to identify molecular candidates mediating age-related cognitive decline. We analyzed transcriptomic data on a network level to identify gene networks underlying cognitive traits and age-related decline, as well as gene ontology (GO) terms summarizing the function of those networks. We also performed individual gene analysis, including identifying network hub genes and genes with high-impact sequence variants to prioritize genes within networks that underlying variation in cognitive decline.

and RNA was isolated using a Qiacube and RNeasy Mini kit (Qiagen). Libraries were prepared using Truseq Stranded mRNA Sample Preparation Kit and sequenced by 75 bp paired-end sequencing on an Illumina HiSeq2500. We aligned reads from the non-transgenic female cohort to a diploid B6/D2 transcriptome using the EMASE pipeline (Raghupathy et al., 2018). Genes were filtered to require an average of at least 1 transcript per million in 50% of the samples and averaged across age and strain for downstream analyses. 15,327 genes survived this filter and were included in our final analyses.

Gene Co-expression Network Analysis

Co-expressed gene modules were generated from 6-months, 14 months, and population-wide female non-transgenic B6-BXD RNA-seq data by Weighted Gene Co-expression Network Analysis (WGCNA) (Langfelder and Horvath, 2008). A minimum module size of 30 was implemented, and the modules were assembled by block-wise network construction. In this study, the power β with scale-free $R^2 > 0.80$ was adopted as a soft-thresholding index to construct a scale-free co-expression network. Module eigengene expression values from each module were used for downstream analyses.

TABLE 1 | Heritability and QTL power calculation results for each cognitive trait.

Trait	$h^2_{RI\bar{x}}$	Peak marker SNP	Power	Minimum percent variance explained by peak marker
Y-maze (6 months)	0.51	rs29776171	0.82	44.2%
Y-maze (14 months)	0.62	rs29525970	0.84	47.1%
CFA (6 months)	0.69	rs31878001	0.007	6.3%
CFA (14 months)	0.68	rs215717346	0.95	56.4%
CFM (6 months)	0.64	Affy_PC2_15	0.94	53.9%
CFM (14 months)	0.74	Affy_17539964	0.87	51.4%

Hub Gene Analysis

Module hub genes were defined as the gene with the highest connectivity in each module and identified using the function "*chooseTopHubInEachModule*" in the WGCNA R package.

Trait-Expression Correlations (Figure 1B)

To identify modules that were significantly associated with each given trait, we calculated the Pearson's correlation coefficient of the module eigengene with each cognitive trait. Co-expression modules were identified as showing significant associations with a trait with an FDR < 0.05.

Co-expression Module Characterization (Figure 1B)

To characterize genes within our WGCNA modules, we performed functional enrichment analysis using the R package anRichment. Results were filtered to include only "Biological process" and "Molecular function" GO terms. FDR < 0.05 was used as the threshold to identify GO terms/pathways significantly enriched within each of the modules.

Identification of Sequence Variants

For genes of interest, we used the Sanger Mouse Genomes Project SNP Query tool[1] to identify sequence variants (SNPs, Indels, and structural variants) between the C56BL/6J and DBA/2J mouse strains, the parental strains of the BXD panel. Variant consequences are predicted using the Ensembl Variant Effect Predictor.

Statistics

Statistics were completed in R and figures were generated using the R packages ggplot2 (cognitive performance, reserve/resilience plots), corrplot (correlation matrices), and qtl2 (QTL plots), or Microsoft Excel (module enrichment plots). Significance

[1]https://www.sanger.ac.uk/sanger/Mouse_SnpViewer/rel-1505

thresholds were set to alpha = 0.05 and adjusted for multiple corrections as specified.

RESULTS

Working Memory Is Heritable, Polygenetic, and Regulated by Cellular Metabolism Transcriptomic Pathways

We assessed hippocampus-dependent working memory by measuring spontaneous alternations in y-maze at both 6 months and 14 months of age (**Figure 2A**). A majority of strains had a mean performance above chance (i.e., 50% spontaneous alternations) at 6 months, demonstrating that these mice were generally able to perform this task at baseline. We also performed one-sample *t*-tests within each strain (with $n > 2$) to identify which strains performed statistically significantly above chance. Several strains did not perform significantly above chance levels (CI = 99%; see **Supplementary Table S2** for a summary of these one-sample *t*-tests), though this is likely due to reduced power given the relatively low number of biological replicates per strain required for such a study using a genetic reference panel. By 14 months, two of the 25 strains tested (B6-BXD62 and B6-BXD14) had a mean (±standard error) performance below chance, indicating vulnerability to cognitive impairment by middle age, and all but three strains (B6-BXD56, B6-BXD77, B6-BXD81; see **Supplementary Table S3** for a summary of these *t*-tests) were performing statistically equal to chance by one-sample *t*-tests. We then calculated heritability, $h^2_{RI\bar{x}}$, to determine the proportion of trait variation that is genetically controlled. Heritability of working memory improved with age ($h^2_{RI\bar{x}}$ = 0.51 at 6 months vs. 0.62 at 14 months – or 51% and 62% of the variance at 6 and 14 months, respectively, may be attributed to genetic factors) (**Figure 2B** and **Table 1**). Such high heritability of working memory implies genetic control; to identify potential genetic drivers of these traits, we performed QTL mapping. QTL mapping revealed no single locus controlling a significant proportion of the variance on performance on y-maze at either 6 months or 14 months of age (**Figure 2C**), or combined with age as a covariate (data not shown). We then employed RNA sequencing to identify mechanisms underlying the variation in working memory.

We performed weighted gene co-expression network analysis (WGCNA) from 6 to 14 months RNA-seq data to identify clusters of genes (i.e., modules) that have highly correlated expression across our population. We calculated Pearson's correlations for expression of each module (i.e., expression of the module eigengene) with cognitive function at concurrent time points (i.e., 6 months RNA expression to 6 months phenotypes and 14 months RNA expression to 14 months phenotypes) to determine which modules were most likely underlying working memory. To characterize each module, we identified the hub gene most highly connected within the module, and performed gene ontology (GO) enrichment to describe biological pathways and molecular functions associated with each module. Four WGCNA modules were significantly positively associated with strain differences in working memory performance at 6 months (**Figure 2D**). These modules were associated with functions encompassing cellular metabolism (lightyellow; R = 0.62, nominal p-value = 0.004; 23 significant GO terms by FDR < 0.05), RNA and protein localization (saddlebrown; R = 0.56, p-value = 0.02; 9 significant GO terms by FDR < 0.05), DNA stability (darkred; R = 0.47, p = 0.049; 36 significant GO terms by FDR < 0.05), and receptor recycling (darkolivegreen, p-value = 0.02; 9 significant GO terms by FDR < 0.05) (see **Table 2** for hub genes and top GO significant terms by enrichment ratio for these modules). The most strongly correlated module, lightyellow, was regulated by its hub gene, *Trio*, a guanine nucleotide exchange factor. *Trio* is important in neuronal development and synapse function and has been previously associated with cognitive ability: mutations in *TRIO* lead to intellectual disability in humans (Ba et al., 2016; Pengelly et al., 2016), and hippocampal and cortical knockout of *Trio* leads to impaired learning in memory in mice (Zong et al., 2015). There is one missense variant in *Trio* in the DBA/2J genome compared to the C57BL/6J genome. This variant (Chr 15:27752684, a/c) is within the coding region of *Trio* and results in a change from a valine to glycine and has a SIFT (Sorting Intolerant From Tolerant) score of 0, indicating a deleterious effect on protein expression. This indicates that there is likely differential function of *Trio* across our B6-BXD cohort that may disrupt the larger lightyellow network, associated cellular metabolism pathways, and ultimately working memory ability (**Figure 2E**).

At 14 months, working memory was correlated with the two modules, only one of which (greenyellow) was significantly enriched for GO terms ($R = -0.48$, p-value = 0.008; 31 significant GO terms by FDR < 0.05; **Figure 2F** and **Table 3**). This module was enriched for genes associated with DNA binding and metabolism pathways, and is regulated by its hub gene, *Ptpn6*– a protein tyrosine phosphatase. *Ptpn6* has not previously been associated with learning and memory, though protein stability and specifically protein phosphatases are important for learning, memory, and synaptic functions (Graff et al., 2010). These data suggest that disrupted nucleic acid metabolism may be associated with poorer cognitive function in aging.

Contextual Fear Acquisition and Memory Are Not Significantly Regulated by Specific Genomic Loci

To assess hippocampus-dependent acquisition of contextual fear memory in young adulthood, animals underwent contextual fear conditioning (**Figure 3A**). Acquisition of contextual fear conditioning (CFA) was highly heritable, as measured by comparing within strain versus across strain variability using percent freezing during the interval following the fourth shock (postshock 4 interval; $h^2_{RI\bar{x}}$ = 0.69 at 6 months) (**Figure 3B**). The high degree of heritability indicates strong genetic control, therefore we performed QTL mapping for CFA (using mean freezing in the final postshock interval) and did not identify any locus significantly associated with this trait. Similarly, although contextual fear memory was also highly heritable (CFM; $h^2_{RI\bar{x}}$ = 0.64 at 6 months), we did not identify any loci

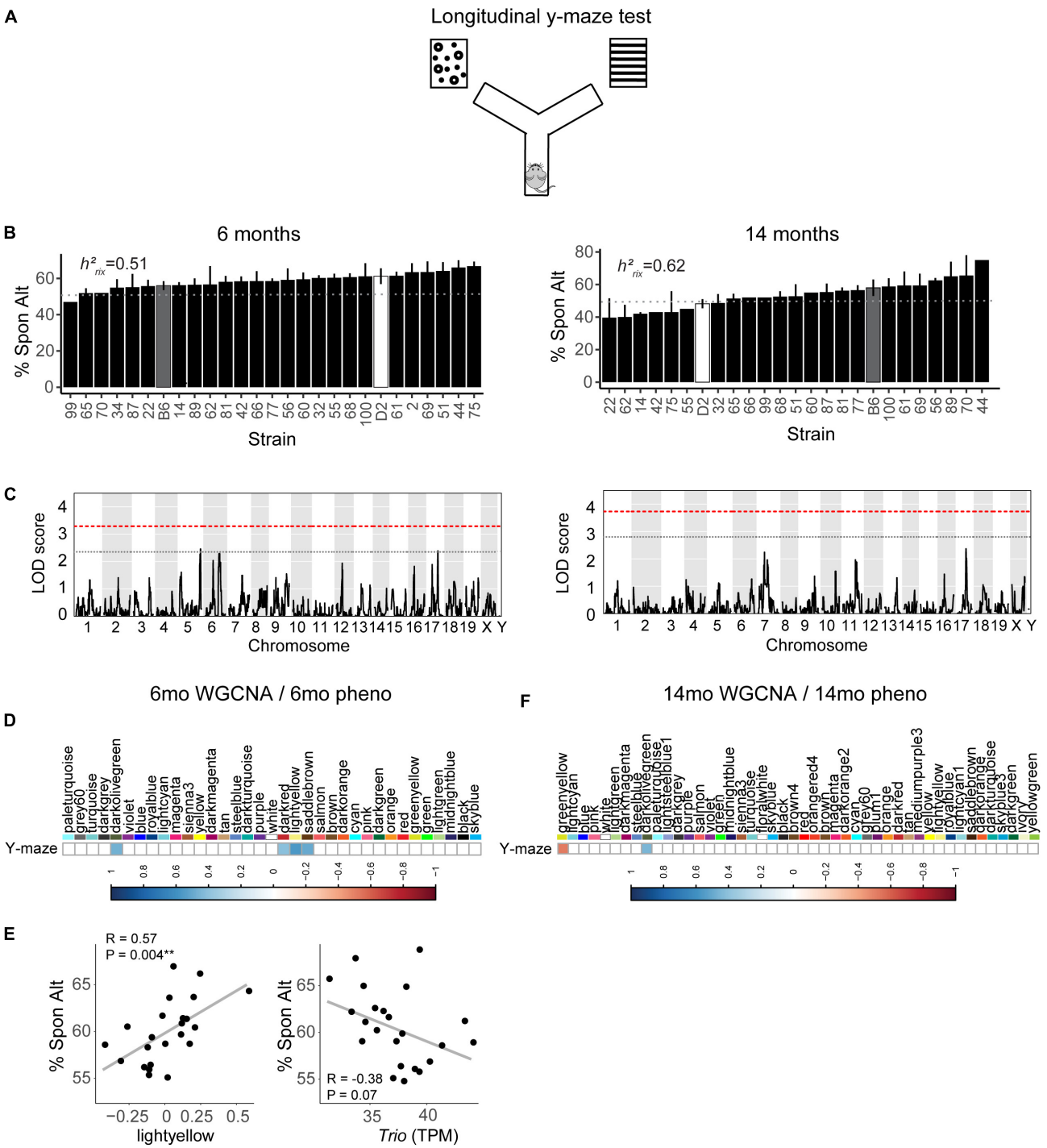

FIGURE 2 | Variation in working memory is heritable in early adulthood (6 months) and middle age (14 months) but is not significantly controlled by a single genetic locus. **(A)** We used the y-maze as a test of working memory in B6-BXD mice at both 6 months and 14 months. In this version of the y-maze test, we used visual cues placed outside of the maze and allowed the mouse to freely explore each arm. Entering each of the three arms in succession was considered a successful spontaneous alternation ("Spon Alt"). **(B)** Performance on the y-maze test is heritable ($h^2_{RI\bar{x}}$ = 0.51 at 6 months and 0.62 at 14 months). **(C)** Quantitative trait locus mapping indicated that no single genetic locus contributed significantly to performance on the y-maze at either age, suggesting that working memory is a polygenetic trait. **(D)** The relationship between each WGCNA module eigengene expression and cognitive function at 6 months was assessed using Pearson correlations. Significant correlations are represented by blue (positive correlation) or red (negative correlation) shading, with color intensity corresponding with correlation strength. Four WGCNA modules were associated with y-maze at 6 months: darkolivegreen, darkred, lightyellow, and saddlebrown. **(E)** Expression of the lightyellow module was significantly positively associated with working memory at 6 months ($R = 0.57$, $p = 0.004$); however, expression of the hub gene of this module *Trio*, was not significantly associated with working memory ($R = -0.38$, $p = 0.07$). **(F)** Two modules at 14 months were significantly correlated to performance on y-maze at 14 months: greenyellow and darkolivegreen. *QTL significance thresholds: red line, alpha = 0.05; black line, alpha = 0.33.*

significantly associated with contextual fear memory, suggesting polygenetic control of long-term contextual fear memory at 6 months (**Figure 3C**).

Contextual Fear Acquisition and Memory in Young Adulthood (6 Months) Are Associated With Gene Networks Involved in Cell Metabolism and Gene Transcription

Here, we turned to WGCNA to identify gene co-expression networks underlying performance on CFA and CFM (**Figure 3D**). CFA at 6 months was significantly associated with two WGCNA modules (**Figure 3D**). The module with the strongest positive association with CFA, lightgreen (R = 0.34, p-value = 0.01), was significantly enriched for 39 GO terms encompassing cellular metabolism and gene transcription (FDR < 0.05). Similarly, the red module was significantly positively associated with CFM (R = 0.43, p-value = 0.04) and was also significantly enriched for 50 GO terms encompassing gene transcription and protein synthesis pathways (FDR < 0.05; See **Table 2** for top GO terms and hub genes for these modules). These data highlight the requirement of synapse remodeling and protein expression changes in learning and memory consolidation in a task such as fear conditioning (Alberini and Kandel, 2015).

Wide Variation in Cognitive Performance of 14 Months (Middle-Aged) Mice Is Regulated by Networks Involved in Gene Transcription

We then looked at performance on contextual fear conditioning in middle age (14 months). Although performance on both CFA and CFM was highly heritable at 14 months (CFA: $h^2_{RI\bar{x}}$ = 0.68 at 14 months; CFM: $h^2_{RI\bar{x}}$ = 0.74 at 14 months; **Table 3**), QTL mapping revealed no genome-wide loci associated with either CFA or CFM at 14 months (**Figure 4A**), again hinting at the highly polygenetic nature of these traits. To interrogate the molecular underpinnings of phenotypic variation of contextual fear conditioning in middle age, we again turned to WGCNA. Here, two modules were significantly positively correlated with CFA (tan: R = 0.41, p-value = 0.049, 37 significant GO terms by FDR < 0.05; plum1: R = 0.40, p-value = 0.03, 1 significant GO term by FDR < 0.05), and no modules correlated with CFM in middle age (**Figure 4B**). Similar to modules underlying CFA and CFM at 6 months, networks important in gene transcription and biosynthesis (tan module), and protein transport (plum1 module) were important in regulating CFA at 14 months (see **Table 4** for top GO terms and hub genes for these modules).

TABLE 2 | Top GO terms and hub genes for 6 months gene modules significantly associated with 6 months cognitive function.

WGCNA Module	Associated phenotype	Top GO term (top enrichment score with FDR < 0.05)	Hub gene
darkolivegreen	Y-maze	positive regulation of receptor recycling	*Krt2*
darkred	Y-maze	DNA topoisomerase type I activity	*Cfap20*
lightyellow	Y-maze	heterocyclic compound binding	*Trio*
saddlebrown	Y-maze	establishment of protein localization to Golgi	*Smim10l2a*
black	CFA	regulation of cell differentiation	*Qars*
lightgreen	CFA	positive regulation of protein targeting to mitochondrion	*Mccc1*
paleturquoise	CFM	ubiquitin-ubiquitin ligase activity	*Herc3*
red	CFM	cellular response to stress	*Szt2*

TABLE 3 | Top GO terms and hub genes for 14 months gene modules significantly associated with 14 months cognitive function.

WGCNA Module	Associated phenotype	Top GO term (top enrichment score with p < 0.05)	Hub gene
darkolivegreen	Y-maze	None	*Usp2*
greenyellow	Y-maze	DNA recombination	*Ptpn6*
plum1	CFA	retrograde vesicle-mediated transport, Golgi to ER	*Fam160b2*
tan	CFA	regulation of transcription, DNA-templated	*Nkrf*

TABLE 4 | Top GO terms and hub genes for 6 months gene modules significantly associated with later (14 months) cognitive function and/or decline.

6 months WGCNA Module	Associated phenotype	Top GO term (top enrichment score with p < 0.05)	Hub gene
blue	14 months CFA	receptor localization to synapse	*Glg1*
darkgreen	14 months CFA	central nervous system myelination	*Cnp*
darkgray	CFA decline	n/a	*Klhl23*
darkmagenta	14 months CFM, CFM decline	binding	*Eda*
darkorange	14 months CFA, CFA decline	GPI-anchor transamidase activity	*Ngb*
darkturquoise	CFM decline, CFA decline	response to cold	*Cnrip1*
greenyellow	14 months CFA	regulation of transcription involved in meiotic cell cycle	*Kat2b*
orange	CFM decline	U1 snRNP binding	*Otub2*
pink	14 months CFA	structural constituent of ribosome	*Eml5*
tan	14 months CFA, CFM decline, CFA decline	cellular localization	*Nkrf*
turquoise	14 months CFA, CFA decline	syntaxin binding	*Mdfic*
white	CFA decline	protein binding	*Gm22291*
yellow	14 months CFA	rRNA processing	*Gria1*

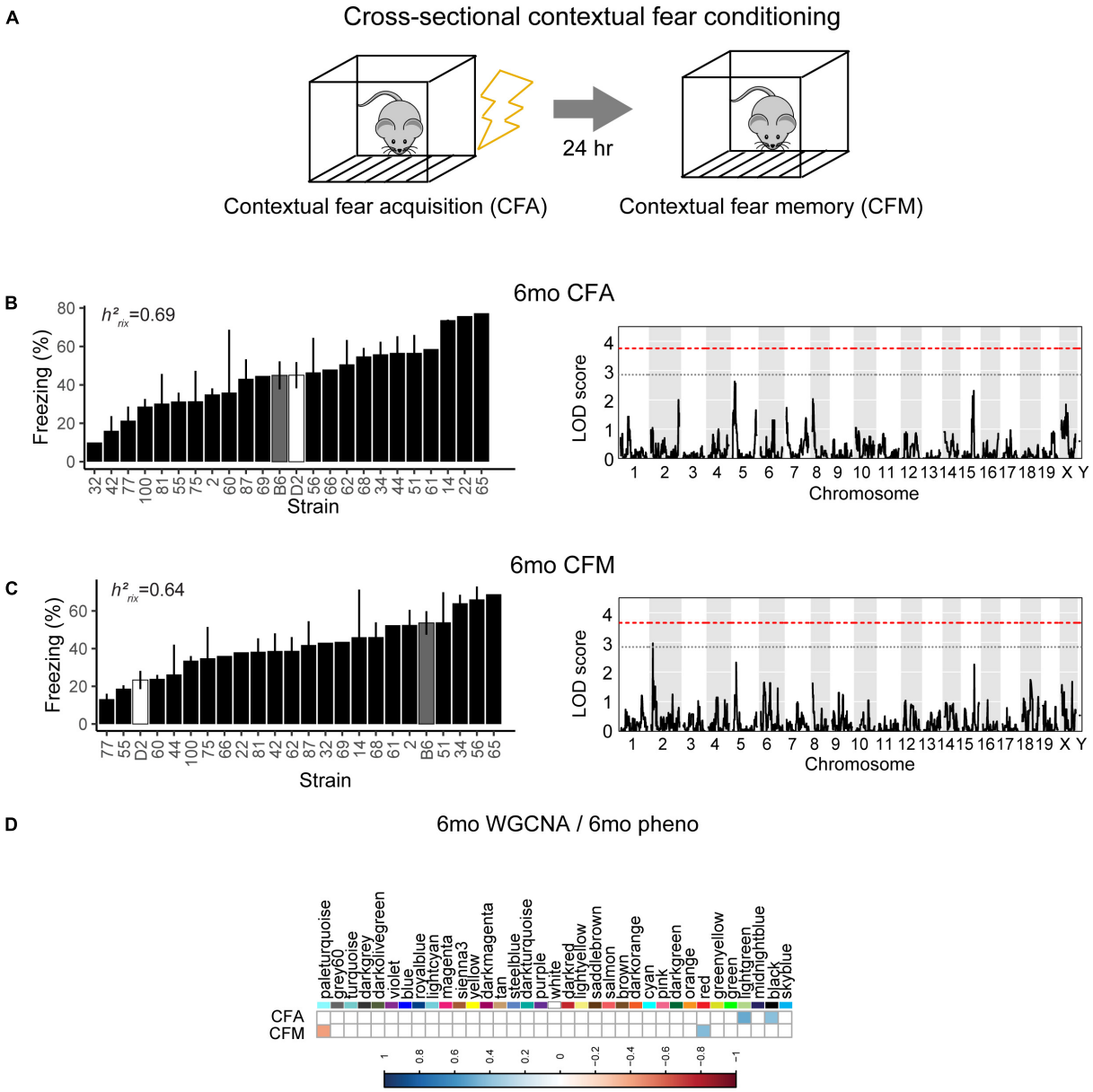

FIGURE 3 | Variation in short- and long-term memory is heritable and not controlled by a single genetic mechanism at 6 months of age. **(A)** B6-BXD mice underwent contextual fear conditioning to assess short- and long-term memory. Mice received four mild footshocks and were tested for contextual memory by measuring freezing 24 h later. **(B)** Contextual fear acquisition, or freezing during the postshock 4 (PS4) interval, was heritable ($h^2_{RI\bar{x}}$ = 0.69) at 6 months. QTL mapping revealed that no locus was significantly associated with performance on contextual fear acquisition. **(C)** Contextual fear memory performance is also highly heritable ($h^2_{RI\bar{x}}$ = 0.64); however, QTL mapping failed to identify significant loci controlling contextual fear memory. **(D)** Four WGCNA modules were associated with contextual fear conditioning traits at 6 months: CFA was significantly associated with the lightgreen and black modules' expression. CFM was significantly associated with the paleturquoise and red modules' expression. *QTL significance thresholds: red line, alpha = 0.05; black line, alpha = 0.33.*

Age-Related Cognitive Decline Is Polygenetic and Predicted by 6 Months Neuronal Gene Networks

One strength of our B6-BXD model of cognitive aging is that each strain has a stable, reproducible genome and as such may be resampled to assess individual strain differences age-related cognitive decline. In general, in our B6-BXD population, cognitive performance declined with age. We found a significant main effect of age on y-maze by ANOVA ($F = 18.54$, $p < 0.001$), though there was no significant effect of age by ANOVA at the population level on contextual fear memory traits (CFA: $F = 0.422$, $p = 0.52$; CFM: $F = 2.48$, $p = 0.11$). We then calculated a "decline score" for each strain on each trait: this was done by subtracting strain average performance at baseline (6 months, adult) from performance at 14 months (middle-aged).

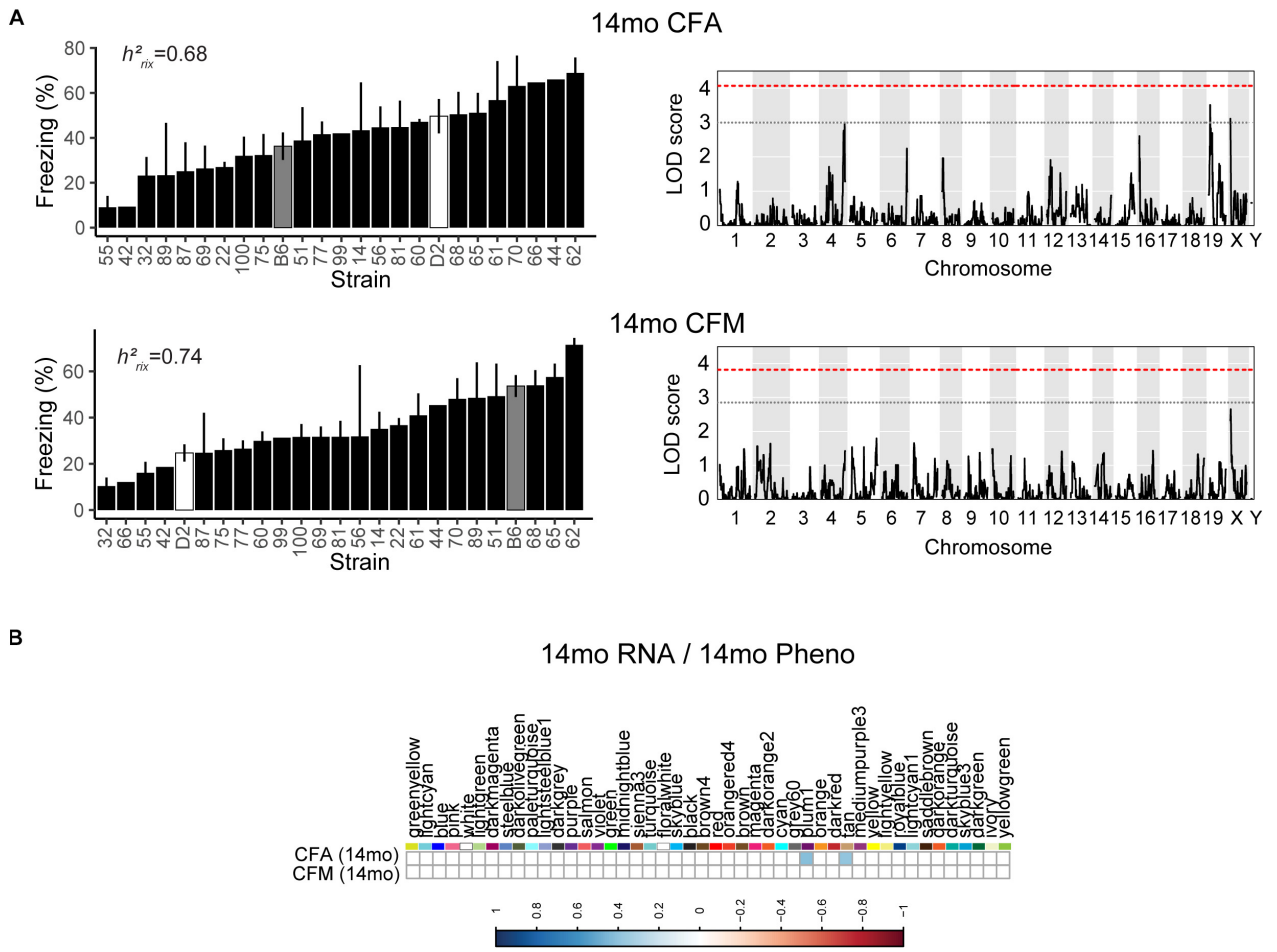

FIGURE 4 | Contextual fear conditioning performance in middle age is also highly heritable and polygenetic, and is associated with neuronal function. **(A)** Contextual fear acquisition and contextual fear memory were both highly heritable at 14 months (CFA: h^2_{RIX} = 0.68, CFM: h^2_{RIX} = 0.74), though we did not identify any significant locus associated with CFA or CFM in middle age. **(B)** We identified two WGCNA modules that were associated with CFA, but not CFM, at 14 months.

The majority of strains (17/24) showed poorer working memory at 14 months compared to 6 months (**Figure 5A**). However, only about half of the strains exhibited declined on CFA and memory, 12/22 and 14/22, respectively with age, and some performed better at mid-life (**Figures 5B,C**). These data indicate strong individual differences in cognitive decline that may be genetically controlled and resolved through genetic mapping. We thus performed QTL mapping on cognitive decline scores generated for working memory, CFA and CFM, and did not identify any loci significantly associated with cognitive decline on any of the traits measured. These data suggest that, like in the human population, complex polygenetic interactions determine the rate of cognitive decline in our mice, where no single locus had a sufficiently large effect size for us to detect given our sample size (**Figures 5A–C**). This finding is another indication of the translational relevance of our model; an additional advantage this model has over human populations is that we were then able to turn to longitudinal hippocampal brain transcriptomic co-expression networks to interrogate the molecular networks underlying decline. We observed several strong associations between gene expression in earlier adulthood (6 months) and later performance and decline on contextual fear conditioning (14 months), with 13 modules' expression at 6 months significantly correlated with performance and/or decline on one or more of the measured cognitive domains (**Figure 5D**). These modules were enriched largely for neuronal pathways and gene transcription. In particular, myelination and synaptic function at 6 months were strongly associated with later cognitive function and decline (see **Table 4** for top GO terms and hub genes for each module). This suggests that maintenance of cognitive function through middle age may be particularly regulated by both neuronal function and gene transcription/protein stability. More broadly, the strong relationships between hippocampal gene expression in earlier adulthood and mid-life cognitive performance suggests that age-related cognitive decline is sensitive to early life molecular processes, and that interventions to prevent age-related cognitive decline should target these early perturbations in relevant gene networks.

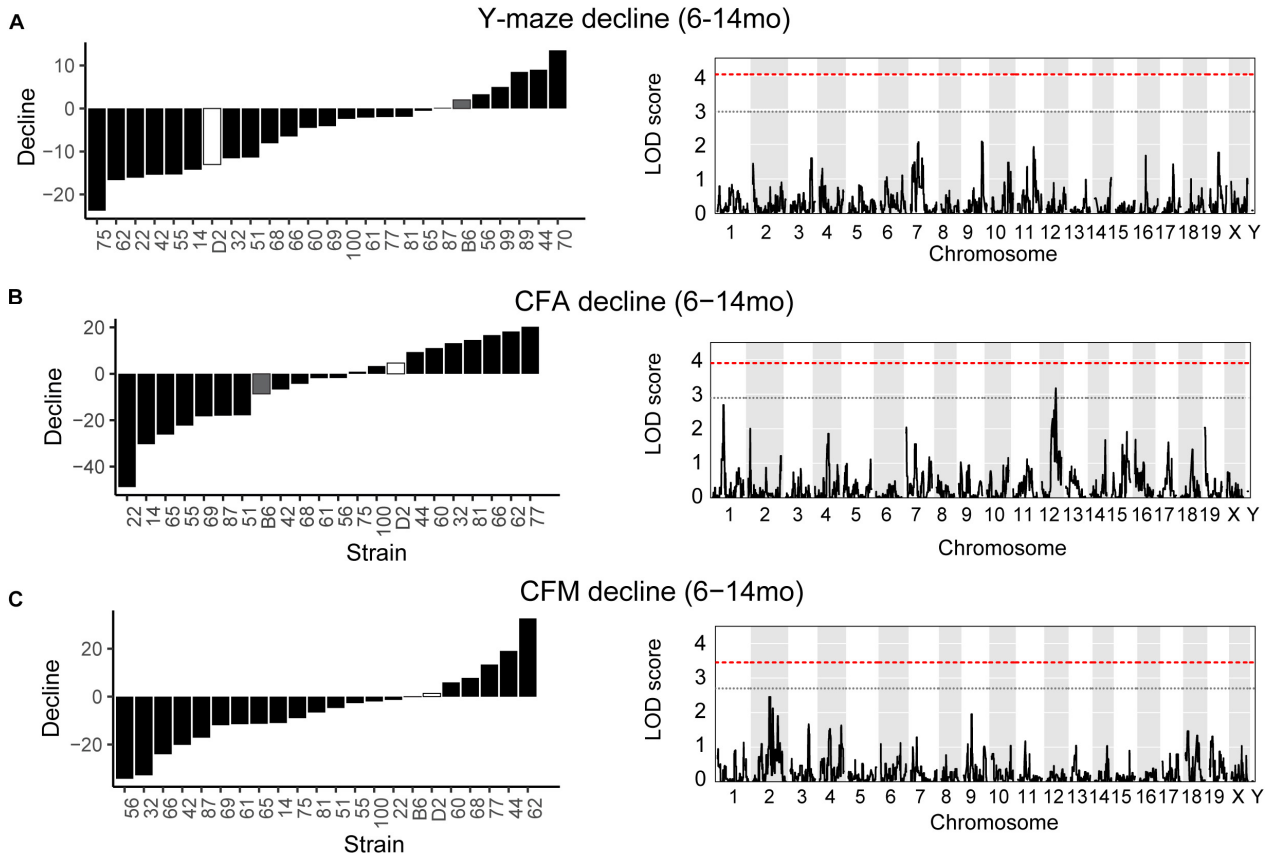

FIGURE 5 | Cognitive decline is polygenetic and may be predicted by early life gene co-expression networks. **(A)** B6-BXD strains generally declined on working memory between 6 and 14 months of age, though there was wide variation in degree of change. QTL mapping revealed no significant locus regulating this decline. **(B,C)** B6-BXD strains showed a wide range in change in performance on contextual fear conditioning between 6 and 14 months. Again, no single locus was associated with decline on either contextual fear acquisition or memory. **(D)** We identified several WGCNA modules whose expression at 6 months were significantly associated with later performance and/or decline on contextual fear acquisition and memory.

Characterization of Cognitive Reserve and Resilience in the B6-BXDs

To assess whether higher baseline cognitive function results in better cognitive function in aging (i.e., early cognitive reserve conferring protection against later decline) (Cook and Fletcher, 2015; Lesuis et al., 2018; Bettcher et al., 2019; Walhovd et al., 2019; Zahodne et al., 2019), we compared baseline cognitive function at 6 months to later cognitive performance at 14 months. To do this, we plotted later (14 months) performance as a function of earlier (6 months) performance and calculated the Pearson's R to assess whether there was a correlation between early life and midlife cognitive function. We saw no association between early y-maze performance and later y-maze performance (**Figure 6A**; $R = 0.11$, $p = 0.61$), suggesting that better performance at young ages on this task does not confer protection against decline in working memory. However, better performance on contextual fear CFA and CFM in adulthood predicted superior memory performance on CFM in middle-aged mice (**Figures 6B,C**; CFA: $R = 0.46$,

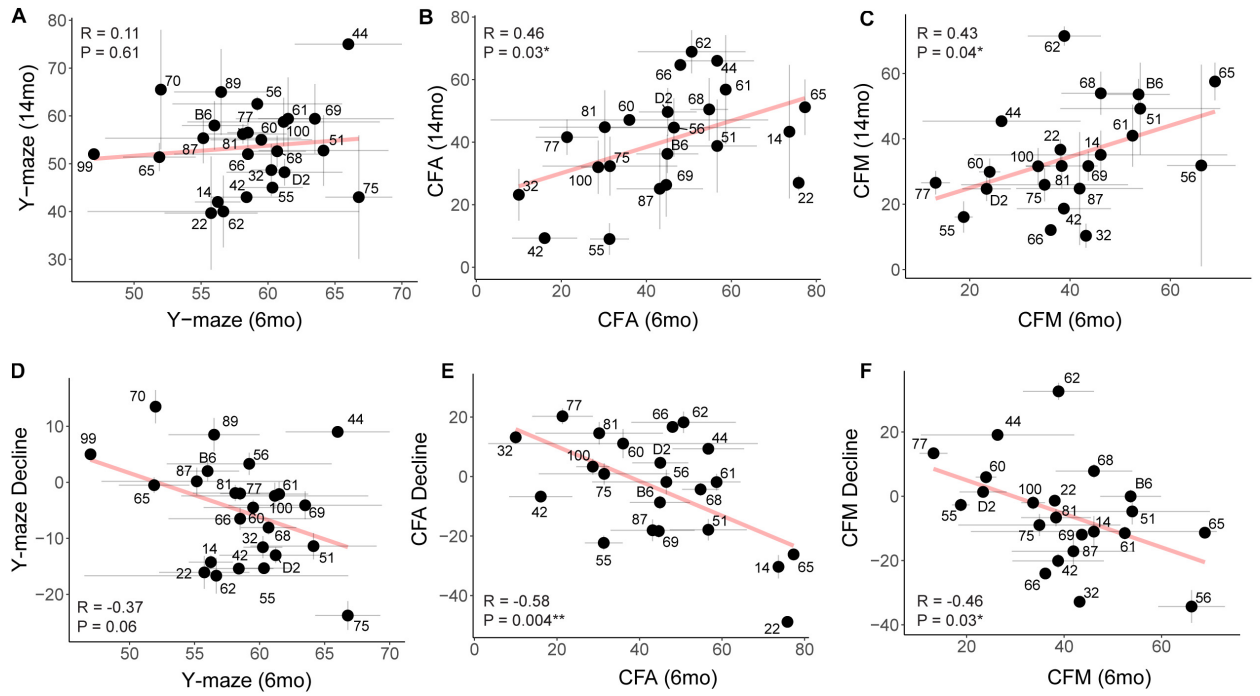

FIGURE 6 | Early performance on contextual fear memory, but not y-maze, predicts later performance. **(A)** Pearson's correlation indicates no significant relationship between early (6 months) and later (14 months) performance on the y-maze test ($R = 0.11$, $p = 0.61$). Gray dashed lines in the y-maze plot indicate 50% spontaneous alternations, or chance performance. Performance below 50% indicates cognitive impairment on this test. Error bars represent standard error. **(B,C)** Pearson's correlation indicates that early (6 months) performance on contextual fear conditioning predicts later (14 months) performance by both CFA and CFM. Better performance at 6 months predicts better relative performance at 14 months ($R = 0.46$, $p = 0.03$ for CFA; $R = 0.43$, $p = 0.04$ for CFM). **(D–F)** Pearson's correlations indicate that higher performance in early adulthood (6 months) is associated with greater decline by midlife (14 months), particularly in short- and long-term memory ($R = -0.37$, $p = 0.06$ for y-maze; $R = -0.58$, $p = 0.004$ for CFA; $R = -0.46$, $p = 0.03$ for CFM). *$p < 0.05$; **$p < 0.01$.

$p = 0.03$; CFM: $R = 0.43$, $p = 0.04$). These data suggest short-term and long-term memory performance later in life is protected to some degree by either having greater cognitive reserve evident in early adulthood or cognitive resilience protecting against decline in midlife. To further clarify this, we next asked whether higher baseline (6 months) function protected against cognitive *decline*. In fact, higher performance at 6 months generally resulted in greater decline by 14 months (**Figures 6D–F**), which may simply reflect the mathematically greater potential for decline in baseline high-performers, or it may reflect the ability of greater cognitive reserve to protect against cognitive *impairment* even when an individual experiences cognitive decline from their own baseline.

Working Definition of Cognitive Reserve and Resilience

Because our population-level data hinted at a role for cognitive reserve or resilience protecting against midlife cognitive decline, we sought to objectively operationally define cognitive reserve and resilience using our B6-BXD population and identify individual strains which may represent these cognitive aging strategies. In **Figure 7A**, we demonstrate hypothetical cognitive trajectories for normal aging (black line), dementia (red), and cognitive aging in populations with cognitive reserve (pink) and/or resilience (blue, green). In these latter cases, cognitive decline is buffered by cognitive reserve and slowed by cognitive resilience. We expected that a small number of B6-BXD strains might exemplify either cognitive reserve or resilience by middle-age given the variation in cognitive decline we observed, so we first objectively defined reserve and resilience, preregistered these definitions, and then tested whether any strains in our population met these criteria. This definition and identification of potential "strains of interest" will be particularly useful for future studies – both using the BXD panel to more deeply characterize resilience and reserve within these strains, and also to inform human studies toward a more mechanistic definition of "reserve" and "resilience" based in the biological processes underlying these characteristics.

Cognitive reserve is commonly defined as higher cognitive function at baseline (Montine et al., 2019; **Figure 7A, pink** and **green** lines), which allows for more cognitive flexibility and buffering against cognitive decline. For our definition, we considered strains in the top quartile to display cognitive reserve. Higher cognitive function at baseline allows for "reserve capacity" to buffer against any cognitive decline, but does not necessarily stem cognitive decline. However, because cognitive reserve necessarily should protect against later cognitive *impairment* (regardless of decline from baseline), and because our terminal time point (14 months) is in middle age for mice, we also required strains with cognitive reserve to still function above the median population performance at 14 months. Ideally, cognitive

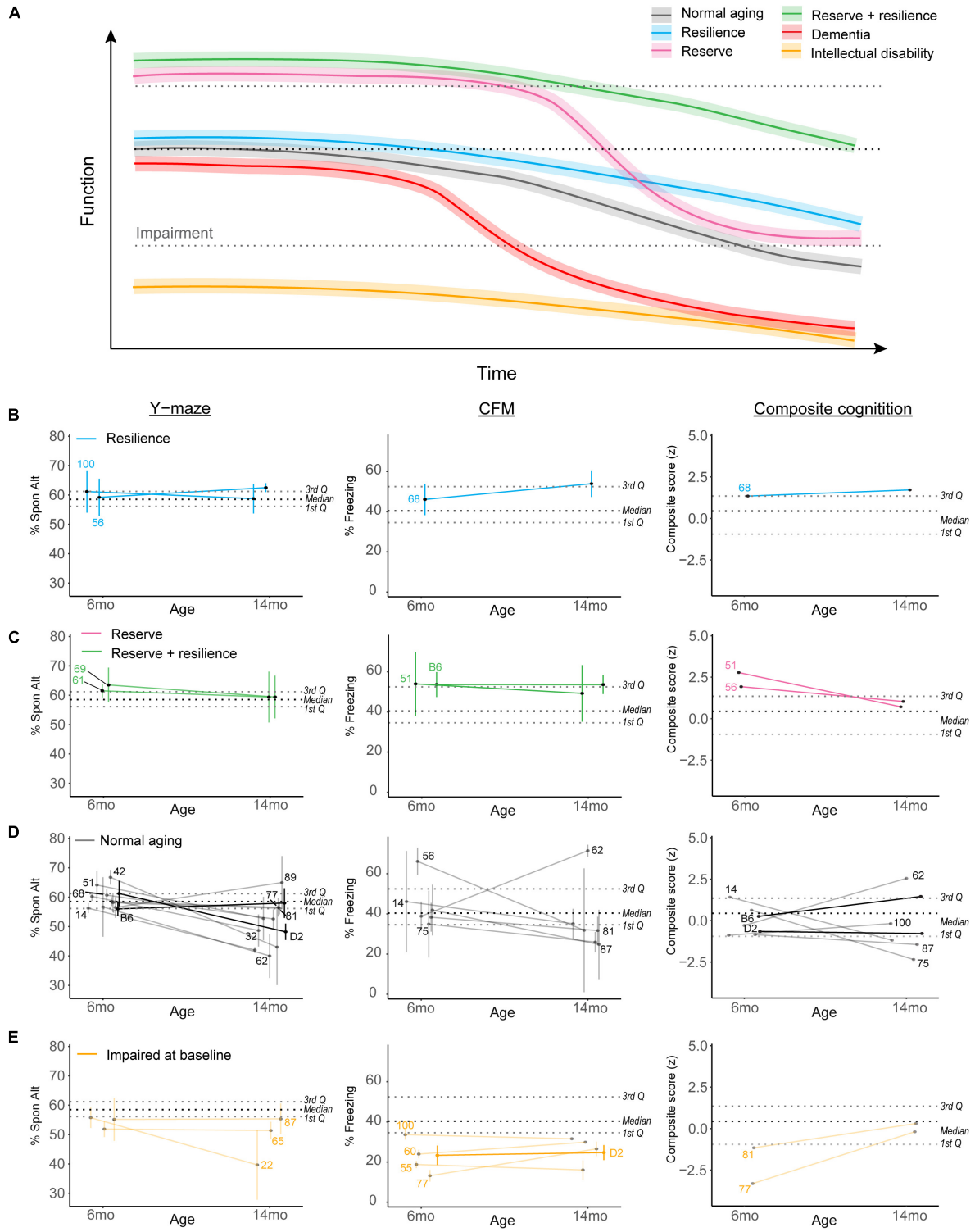

FIGURE 7 | Complex cognitive trajectories in aging may be modeled in the B6-BXD mice. **(A)** Visualization of idealized data exemplifying cognitive functional decline in normal aging (gradual decline after midlife; black line), dementia (rapid decline to impairment in midlife; red line), cognitive reserve (higher baseline; pink line), cognitive resilience (slower decline; blue line), or both cognitive reserve and resilience (green line). Individuals with intellectual disability or impaired performance at baseline (orange line) are typically excluded from human studies in cognitive aging. **(B,C)** We identified strains displaying suggestive reserve and/or resilience on individual cognitive measures; these strains remain only suggestively in their categories because, though strain averages fall within the limits of our definitions, within-strain variability exceeded our margins of error in every case. For individual traits, B6-BXD100 and B6-BXD56 were suggestive resilient strains, and B6-BXD69

(Continued)

FIGURE 7 | Continued
and B6-BXD61 were suggestive reserve + resilient strains in y-maze. B6-BXD68 was a suggestive resilient strain, and B6-BXD51 and B6 homozygotes were suggestive reserve + resilient strains in CFM. Right panels: We also calculated a composite score for cognitive performance across three traits (y-maze, CFA, and CFM) by summing the z-score for each trait within each strain. B6-BXD68 was a suggestive resilient strain, and B6-BXD51 and B6-BXD56 were suggestive reserve strains. **(D)** Strains that had baseline (6 months) performance below the 3rd Quartile (i.e., no cognitive reserve), midlife (14 months) performance below the median (i.e., insufficient cognitive reserve), or a greater than average rate of decline (i.e., no cognitive resilience) were considered "normal agers". For **(B–E)**, color scheme is as in **(A)**. Black dashed line is median, gray dashed lines are 1st and 3rd quartile. For ease of visualization, each category of aging trajectory was visualized separately. Strains with $n < 2$ at either time point were excluded from categorization and visualization. **(E)** Strains with baseline performance below the 1st quartile were considered impaired.

reserve and resilience would manifest globally, or protect against impairment across cognitive domains (i.e., working, short-term, and long-term memory in our dataset), so in addition to individual cognitive traits, we also calculated a composite score for cognitive function by calculating z-scores for each strain for each cognitive trait and timepoint, and summing these scores to achieve a composite score.

Resiliency to cognitive decline is commonly defined as a relatively slow rate of decline over time (e.g., the annual rate of change in humans; **Figure 7A** green and blue lines) (Montine et al., 2019). Though performance across the spectrum (from "good" performers to "poor" performers at baseline) may be stable across time and thus display a type of resilience to decline, we required that strains that displayed "true" resilience to be relatively good performers at baseline (i.e., performing above the median as indicated by the black dashed line in **Figures 7B–E**) and to decline more slowly than average. Initially, we defined slow decline as "no significant difference from 6 to 14 months performance." However, this criterion proved too permissive, as few individual strains exhibited significant decline after adjusting for multiple comparisons (see previous sections). Our final definition of cognitive resilience required strains start above median population performance (indicated in **Figures 7B–E** as the middle black dashed lines) and have an "annual rate of decline" (or decline slope) slower than average.

Finally, in identifying strains that met these definitions, we required that strain average ± strain standard error fit within these criteria. Ultimately, these strains fell along a continuum of cognitive performance and decline, and due to the within-strain variance, no single strain exemplified true reserve or resilience based on our working definition. We identified strains that may potentially fit these definitions given more thorough characterization and a higher sample size; these "suggestive" strains may be promising strains to investigate with a higher sample size to identify molecular signatures of reserve and/or resilience and are delineated in **Figures 7B–E**. For ease of visualization, we have plotted resilience, reserve and reserve/resilience, normal aging, and impaired strains in separate plots. Strains with an $n < 2$ at any given timepoint were excluded from these visualizations, as we were unable to assess within-strain variance. Strains meeting suggestive criteria for reserve and resilience included: for resilience, B6-BXD100 and B6-BXD56 for working memory and B6-BXD68 for long-term memory and in our composite cognitive score (**Figure 7B**, blue lines); for reserve, B6-BXD51 and B6-BXD56 with composite cognitive score (**Figure 7C**, pink lines); for reserve + resilience, B6-BXD61 and B6-BXD69 for working memory, and B6 and B6-BXD51 in contextual fear memory (**Figure 7C**, green lines). Most strains fell within "normal aging" parameters (that is, starting within the middle quartile ranges at baseline and/or not meeting our reserve/resilience criteria). In **Figure 7E**, we identified several strains (orange lines) whose baseline performance fell below the first quartile (lower gray dashed lines in **Figures 7B–E**), suggesting baseline impairment.

Further characterization of these strains to specifically test for and more deeply characterize cognitive reserve and resilience will be necessary, including aging mice much longer (e.g., to 22 months or older), though we demonstrate here that the B6-BXD population is a powerful tool to begin understanding the nature of reserve and resilience and to identify the molecular networks underlying these traits.

DISCUSSION

Genetics of cognition, cognitive decline, and cognitive reserve are highly complex and difficult to study in humans. However, as we make strides in improving lifespan, increasing cognitive longevity should become a priority in order to maximize quality of life in old age. Understanding the molecular mediators of baseline cognitive function, cognitive reserve, resiliency and susceptibility with regards to age-related cognitive decline and identification of novel pharmacological targets/pathways regulating cognitive health may allow cognitive health span to catch up to lifespan improvements afforded by modern medicine. To achieve these goals, we first need to identify models that can best address these questions. Here, we have utilized a novel model of age-related cognitive decline to extract genetic mediators of normal cognitive function and age-related decline. Because our B6-BXD population is a recombinant inbred backcross rather than a homozygous BXD population, the result is enrichment for identifying B6 effects on phenotypes by genetic mapping, and a loss of detecting recessive D2 effects. However, given the great interest in identifying genetic factors harbored by the B6 strain that confer documented resilience against cognitive impairment compared to D2 (Neuner et al., 2019), we hypothesized we would identify genetic resilience mechanisms within our population.

We Observed Heritable Variation in Cognitive Tasks and Age-Related Cognitive Decline

The heritability estimates ($h^2_{RI\bar{x}}$) of working, short- and long-term memory ranged from 0.51 to 0.74, indicating that these traits are strongly genetically controlled. However, QTL mapping

identified no single significant peak associated with any trait, meaning that no individual genetic locus accounted for a substantial proportion of the variance on these traits as could be detected by our sample size. These data indicate that cognitive function is polygenetic and controlled by many variants with small effect sizes, as we did not identify additional loci associated with later cognitive function or cognitive decline. This is not surprising, given recent GWAS in humans have found hundreds of SNPs associated with cognitive function and other highly complex traits (Davies et al., 2018). Given the importance of understanding the molecular contributors to cognitive function and reserve against decline with age, though, we sought to develop alternative approaches to identifying genes and pathways that mediate cognitive function and promoting cognitive reserve and resilience.

Prioritization of Molecular/Genetic Candidates of Cognitive Function and Decline in Adulthood

To complement our QTL mapping and to identify gene networks underlying complex cognitive traits, we conducted molecular experiments to identify target genes associated with cognition. We performed RNA sequencing followed by weighted gene co-expression analysis (WGCNA), and measured the association of WGCNA modules and individual genes with level of cognitive performance and decline. We identified pathways and highly interconnected "hub" genes from our WGCNA modules, which are functionally important within gene networks and may represent candidate genes and mechanisms underlying "normal" cognitive aging. Given that cognitive function and decline are incredibly complex and are affected by a wide range of factors, we hypothesized that associated gene networks would be more biologically relevant than single candidate genes, and provide more insight to the mechanisms underlying cognitive function and decline. These gene networks, in turn, may be manipulated therapeutically by targeting their hub genes with the goal of enhancing cognitive function in aging. Perhaps unsurprisingly, the modules that were most significantly associated with cognitive function in adulthood were enriched for GO terms associated with cellular metabolism and transcription/translation, highlighting the importance of physical remodeling of synapses in learning and memory through regulation of gene transcription and protein expression/localization (Alberini and Kandel, 2015). Notably, evidence from postmortem human brain studies suggest that synapse or dendritic spine remodeling is a primary neurobiological mechanism of cognitive resilience to aging and Alzheimer's disease pathology (Boros et al., 2017, 2019).

As with baseline cognitive function, we also identified gene networks that primarily included neuronal, transcription/translation, and cellular metabolism functions as underlying cognitive decline. This was in contrast to our previous analyses of our genetically diverse population of mice with familial Alzheimer's disease mutations (AD-BXDs; Neuner et al., 2019), where we observed largely neuroinflammatory pathways as underlying AD-related cognitive decline. Our AD-BXD and B6-BXD populations did have pathways enriched in neuronal function in common. These findings suggest that an individual's risk for disease-related cognitive decline versus "normal" aging mechanisms may have some common elements (e.g., neuronal function); though we also observe an interesting divergence in pathways, where disease may be regulated by neuroinflammatory processes, and normal aging may be regulated by cell metabolism and maintenance of proper gene expression and nucleic acid stability.

Intriguingly, we identified the strongest and most numerous gene co-expression network-trait associations between 6 months gene expression and later cognitive function and decline. This indicates that variation in gene expression in early adulthood may likely determine cognitive decline, rather than later gene expression perturbations being most significant to underlying in cognitive decline. In addition to implying that interventions must happen early in order to curb age-related cognitive decline, this also highlights the value in collecting behavioral data and brain molecular information at early time points, a process which is impossible in human studies. Thus, to understand the molecular mechanisms of cognitive aging, we need to focus on animal models such as our B6-BXD population where we are able to sample timepoints across the lifespan.

Identifying Strains Characterized by Cognitive Reserve and Resilience in the B6-BXD Population

Finally, we assessed whether we observe cognitive reserve and resilience in our population of mice. In human literature, cognitive reserve and resilience are inconsistently defined, which has contributed to a general lack of focus in understanding of the mechanisms underlying these processes. For example, many studies use "years of education"–or related measures such as being multilingual or having a cognitively engaging occupation–as a proxy for cognitive reserve. Defining cognitive reserve in this way is problematic for multiple reasons: namely, though the two are often correlated, we do not believe that socioeconomic opportunity is intrinsically required for cognitive reserve. Additionally, to study cognitive reserve in animals–and the genetic basis thereof–we also cannot rely on external factors such as education that are inapplicable to animals. Cognitive reserve is likely plastic and may be enhanced by environmental enrichment in both humans and animals – an additional goal of our laboratory will be to evaluate individual differences in how environmental enrichment may enhance cognitive reserve.

Cognitive resilience has also been inconsistently defined in the literature and often implies resilience to disease-related processes, such as atrophy or neurodegenerative disease pathologies. We sought to define cognitive resilience behaviorally, and in the future will extend this definition to identify anatomical, cellular, molecular signatures of cognitive resilience to maximize translatability to human studies (Bettcher et al., 2019). Namely, we required that cognitive resilience was characterized by slow (or non-existent) cognitive decline over time. Our late-life timepoint for measuring cognitive function was 14 months,

which approximates middle age. Although 14 months is not considered "aged" for these strains of mice, this does raise an important point in the context of translatability of these measures: in human studies, participants are typically enrolled in mid-life when some degree of cognitive decline may have already occurred, even if "control" participants are still performing cognitive tasks well. A strength of our mouse model is the ability to sample both cognitive and molecular data at early time points to relate early changes with mid- and late-life cognitive function. Our observation that gene perturbations in early adulthood (i.e., 6 months) may be more important in regulating cognitive decline than later transcriptomic changes indicates that human studies may be starting too late to fully characterize reserve and resilience trajectories and mechanisms. On the other hand, our study likely ended too early (middle age) and thus we were unable to observe robust effects of cognitive resilience. It is likely that to truly identify cognitive resilience to age-related decline, we will need to observe cognitive function through late life, or to at least a 22–24 months timepoint.

Ultimately, we established a stringent set of criteria to operationally define cognitive reserve and resilience in the B6-BXD population that may be extended to other animal models as well as human studies. First, we required that animals with cognitive reserve have baseline functioning in the upper quartile. We expected that cognitive reserve would vary based on cognitive domain – that is, strains could display cognitive reserve as measured by one or a subset of tasks. We also expect that cognitive reserve functions to protect against cognitive impairment with age, so we also required that strains would still be performing at or above median performance by 14 months.

We expected the effects of cognitive resilience to be global and exhibit protection against decline across cognitive domains. In this case, we required strains with cognitive resilience to start at or above the median population performance. We also required that there be no significant decline in cognitive function between 6 and 14 months. To fit within these criteria, strains would have to perform on average, ±standard error, within their category. In our population, we did not observe sufficient evidence to identify true exemplars of cognitive reserve or resilience, though we were able to identify multiple strains that *may* represent either cognitive reserve, resilience or both. Thus, with our criteria, we will need additional biological replicates per strain, and likely additional strains, to fully capture cognitive reserve and resilience. This highlights the main advantage of our mouse model of normal aging: because each strain has a replicable genome, we are able to add biological replicates to more deeply characterize any strain or trait of interest. In the future, we will expand our studies to include more strains, more animals per strain, and extended timepoints in order to capture the a more precise picture of within-strain performance and a full range of cognitive performance and decline. This will allow us to identify molecular signatures of cognitive reserve and resilience in our B6-BXD population, and – most importantly – assess the translational potential of these findings to human studies. By establishing objective definitions of cognitive reserve and resilience, and by identifying mouse models of these traits, we will be able to inform human studies of candidate molecular mechanisms for successful cognitive aging that may, in turn, be used to develop therapeutics to prevent age-related cognitive impairment.

CONCLUSION

Harnessing the underlying mechanisms of cognitive reserve and resilience will be a promising strategy to maintaining cognitive health until late life. Our understanding of the molecular underpinnings of reserve and resilience have been limited, but the development and usage of animal models of these processes, such as the B6-BXD recombinant inbred lines described herein, will provide an unprecedented opportunity to interrogate the early molecular mechanisms thereof and translate these findings to humans.

DATA AVAILABILITY STATEMENT

The raw RNA-seq data is also associated with earlier publications and, as such, has been previously uploaded to GEO (Accession Numbers GSE101144, GSE119215, and GSE119408).

ETHICS STATEMENT

The animal study was reviewed and approved by the Institutional Animal Care and Use Committee (IACUC) at The University of Tennessee Health Science Center.

AUTHOR CONTRIBUTIONS

SN, KO'C, and CK conceived of and designed the experiments. SN conducted the behavioral experiments. AD, NH, SN, JGZ, VP, LD, TH, JH, KO'C, and CK conceived of and designed subsequent analyses, and assisted in data analysis and interpretation of results. AD, NH, SN, and JGZ performed the data analyses. AD and CK wrote the manuscript. All authors read and reviewed the final manuscript.

FUNDING

This study is part of the National Institute on Aging Resilience-AD program and is supported through the NIA grant award R01AG057914 to CK. This work was also supported by the National Institute on Aging (R01 AG054180 to CK and F31AG050357 to SN), BrightFocus Foundation (A2016397S to CK), and the Alzheimer's Association Research Fellowship (AARF-18-565506 to AD).

SUPPLEMENTARY MATERIAL

The Supplementary Material for this article can be found online at: https://www.frontiersin.org/articles/10.3389/fcell.2020.562662/full#supplementary-material

REFERENCES

Alberini, C. M., and Kandel, E. R. (2015). The regulation of transcription in memory consolidation. *Cold Spring Harbor Perspect. Biol.* 7:a021741. doi: 10.1101/cshperspect.a021741

Arenaza-Urquijo, E. M., Wirth, M., and Chetelat, G. (2015). Cognitive reserve and lifestyle: moving towards preclinical Alzheimers disease. *Front. Aging Neurosci.* 7:134. doi: 10.3389/fnagi.2015.00134

Ba, W., Yan, Y., Reijnders, M. R., Schuurs-Hoeijmakers, J. H., Feenstra, I., Bongers, E. M., et al. (2016). TRIO loss of function is associated with mild intellectual disability and affects dendritic branching and synapse function. *Hum. Mol. Genet.* 25, 892–902. doi: 10.1093/hmg/ddv618

Belknap, J. K. (1998). Effect of within-strain sample size on QTL detection and mapping using recombinant inbred mouse strains. *Behav. Genet.* 28, 29–38.

Bettcher, B. M., Gross, A. L., Gavett, B. E., Widaman, K. F., Fletcher, E., Dowling, N. M., et al. (2019). Dynamic change of cognitive reserve: associations with changes in brain, cognition, and diagnosis. *Neurobiol. Aging* 83, 95–104. doi: 10.1016/j.neurobiolaging.2019.08.016

Bis, J. C., DeCarli, C., Smith, A. V., van der Lijn, F., Crivello, F., Fornage, M., et al. (2012). Common variants at 12q14 and 12q24 are associated with hippocampal volume. *Nat. Genet.* 44, 545–551. doi: 10.1038/ng.2237

Boros, B. D., Greathouse, K. M., Gearing, M., and Herskowitz, J. H. (2019). Dendritic spine remodeling accompanies Alzheimers disease pathology and genetic susceptibility in cognitively normal aging. *Neurobiol. Aging* 73, 92–103. doi: 10.1016/j.neurobiolaging.2018.09.003

Boros, B. D., Greathouse, K. M., Gentry, E. G., Curtis, K. A., Birchall, E. L., Gearing, M., et al. (2017). Dendritic spines provide cognitive resilience against Alzheimers disease. *Ann. Neurol.* 82, 602–614. doi: 10.1002/ana.25049

Broman, K. W., Gatti, D. M., Simecek, P., Furlotte, N. A., Prins, P., Sen, S., et al. (2019). R/qtl2: software for mapping quantitative trait loci with high-dimensional data and multiparent populations. *Genetics* 211:genetics.301595.2018. doi: 10.1534/genetics.118.301595

Clarke, T. K., Lupton, M. K., Fernandez-Pujals, A. M., Starr, J., Davies, G., Cox, S., et al. (2016). Common polygenic risk for autism spectrum disorder (ASD) is associated with cognitive ability in the general population. *Mol. Psychiatry* 21, 419–4425. doi: 10.1038/mp.2015.12

Cook, C. J., and Fletcher, J. M. (2015). Can education rescue genetic liability for cognitive decline? *Soc. Sci. Med.* 127, 159–170. doi: 10.1016/j.socscimed.2014.06.049

Davies, G., Armstrong, N., Bis, J. C., Bressler, J., Chouraki, V., Giddaluru, S., et al. (2015). Genetic contributions to variation in general cognitive function: a meta-analysis of genome-wide association studies in the CHARGE consortium (N=53949). *Mol. Psychiatry* 20, 183–192.

Davies, G., Harris, S. E., Reynolds, C. A., Payton, A., Knight, H. M., Liewald, D. C., et al. (2014). A genome-wide association study implicates the APOE locus in nonpathological cognitive ageing. *Mol. Psychiatry* 19, 76–87. doi: 10.1038/mp.2012.159

Davies, G., Lam, M., Harris, S. E., Trampush, J. W., Luciano, M., Hill, W. D., et al. (2018). Study of 300,486 individuals identifies 148 independent genetic loci influencing general cognitive function. *Nat. Commun.* 9:2098.

Davies, G., Tenesa, A., Payton, A., Yang, J., Harris, S. E., and Liewald, D. (2011). Genome-wide association studies establish that human intelligence is highly heritable and polygenic. *Mol. Psychiatry* 16, 996–1005. doi: 10.1038/mp.2011.85

De Jager, P. L., Shulman, J. M., Chibnik, L. B., Keenan, B. T., Raj, T., Wilson, R. S., et al. (2012). A genome-wide scan for common variants affecting the rate of age-related cognitive decline. *Neurobiol. Aging* 33, 1017.e1–1017.e15.

Debette, S., Ibrahim Verbaas, C. A., Bressler, J., Schuur, M., Smith, A., Bis, J. C., et al. (2015). Genome-wide studies of verbal declarative memory in nondemented older people: the cohorts for heart and aging research in genomic epidemiology consortium. *Biol. Psychiatry* 77, 749–763.

Dutta, A., Henley, W., Robine, J. M., Llewellyn, D., Langa, K. M., Wallace, R. B., et al. (2014). Aging children of long-lived parents experience slower cognitive decline. *Alzheimers Dement.* 10, S315–S322.

Graff, J., Koshibu, K., Jouvenceau, A., Dutar, P., and Mansuy, I. M. (2010). Protein phosphatase 1-dependent transcriptional programs for long-term memory and plasticity. *Learn. Mem.* 17, 355–363. doi: 10.1101/lm.1766510

Harris, S. E., and Deary, I. J. (2011). The genetics of cognitive ability and cognitive ageing in healthy older people. *Trends Cogn. Sci.* 15, 388–394.

Hibar, D. P., Adams, H. H. H., Jahanshad, N., Chauhan, G., Stein, J. L., Hofer, E., et al. (2017). Novel genetic loci associated with hippocampal volume. *Nat. Commun.* 8:13624.

Hibar, D. P., Stein, J. L., Renteria, M. E., Arias-Vasquez, A., Desrivieres, S., Jahanshad, N., et al. (2015). Common genetic variants influence human subcortical brain structures. *Nature* 520, 224–229.

Hill, W. D., Davies, G., van de Lagemaat, L. N., Christoforou, A., Marioni, R. E., Fernandes, C. P., et al. (2014). Human cognitive ability is influenced by genetic variation in components of postsynaptic signalling complexes assembled by NMDA receptors and MAGUK proteins. *Transl. Psychiatry* 4:e341. doi: 10.1038/tp.2013.114

Honer, W. G., Barr, A. M., Sawada, K., Thornton, A. E., Morris, M. C., Leurgans, S. E., et al. (2012). Cognitive reserve, presynaptic proteins and dementia in the elderly. *Transl. Psychiatry* 2:e114. doi: 10.1038/tp.2012.38

Kamboh, M. I, Fan, K. H., Yan, Q., Beer, J. C., Snitz, B. E., Wang, X., et al. (2019). Population-based genome-wide association study of cognitive decline in older adults free of dementia: identification of a novel locus for the attention domain. *Neurobiol. Aging* 84, 239.e15–239.e24.

Krapohl, E., and Plomin, R. (2016). Genetic link between family socioeconomic status and childrens educational achievement estimated from genome-wide SNPs. *Mol. Psychiatry* 21, 437–443. doi: 10.1038/mp.2015.2

Langfelder, P., and Horvath, S. (2008). WGCNA: an R package for weighted correlation network analysis. *BMC Bioinformatics* 9:559. doi: 10.1186/1471-2105-9-559

Lesuis, S. L., Hoeijmakers, L., Korosi, A., de Rooij, S. R., Swaab, D. F., Kessels, H. W., et al. (2018). Vulnerability and resilience to Alzheimers disease: early life conditions modulate neuropathology and determine cognitive reserve. *Alzheimers Res. Ther.* 10:95.

Lu, A. T., Hannon, E., Levine, M. E., Crimmins, E. M., Lunnon, K., Mill, J., et al. (2017). Genetic architecture of epigenetic and neuronal ageing rates in human brain regions. *Nat. Commun.* 8:15353.

McGue, M., and Christensen, A. (2001). The heritability of cognitive functioning in very old adults: evidence from Danish twins aged 75 years and older. *Psychol. Aging* 16, 272–280. doi: 10.1037/0882-7974.16.2.272

Montine, T. J., Cholerton, B. A., Corrada, M. M., Edland, S. D., Flanagan, M. E., Hemmy, L. S., et al. (2019). Concepts for brain aging: resistance, resilience, reserve, and compensation. *Alzheimer Res. Ther.* 11:22.

Mukherjee, S., Kim, S., Ramanan, V. K., Gibbons, L. E., Nho, K., Glymour, M. M., et al. (2014). Gene-based GWAS and biological pathway analysis of the resilience of executive functioning. *Brain Imaging Behav.* 8, 110–118. doi: 10.1007/s11682-013-9259-7

Neuner, S. M., Heuer, S. E., Huentelman, M. J., OConnell, K. M. S., and Kaczorowski, C. C. (2019). Harnessing genetic complexity to enhance translatability of Alzheimers Disease mouse models: a path toward precision medicine. *Neuron* 101, 399.e5–411.e5.

Neuner, S. M., Wilmott, L. A., Hope, K. A., Hoffmann, B., Chong, J. A., Abramowitz, J., et al. (2015). TRPC3 channels critically regulate hippocampal excitability and contextual fear memory. *Behav. Brain Res.* 281, 69–77. doi: 10.1016/j.bbr.2014.12.018

Okbay, A., Beauchamp, J. P., Fontana, M. A., Lee, J. J., Pers, T. H., Rietveld, C. A., et al. (2016). Genome-wide association study identifies 74 loci associated with educational attainment. *Nature* 533, 539–542.

Pan, C. W., Wang, X., Ma, Q., Sun, H. P., Xu, Y., and Wang, P. (2015). Cognitive dysfunction and health-related quality of life among older Chinese. *Sci. Rep.* 5:17301.

Pan, Y., Wang, K. S., and Aragam, N. (2011). NTM and NR3C2 polymorphisms influencing intelligence: family-based association studies. *Prog. Neuropsychopharmacol. Biol. Psychiatry* 35, 154–160. doi: 10.1016/j.pnpbp.2010.10.016

Pengelly, R. J., Greville-Heygate, S., Schmidt, S., Seaby, E. G., Jabalameli, M. R., Mehta, S. G., et al. (2016). Mutations specific to the Rac-GEF domain of TRIO cause intellectual disability and microcephaly. *J. Med. Genet.* 53, 735–742. doi: 10.1136/jmedgenet-2016-103942

Raghupathy, N., Choi, K., Vincent, M. J., Beane, G. L., Keith Sheppard, S., Munger, S. C., et al. (2018). Heirarchical analysis of RNA-seq reads improves

the accuracy of allele-specific expression. *Bioinformatics* 34, 2177–2184. doi: 10.1093/bioinformatics/bty078

Raj, T., Chibnik, L. B., McCabe, C., Wong, A., Replogle, J. M., Yu, L., et al. (2017). Genetic architecture of age-related cognitive decline in African Americans. *Neurol. Genet.* 3:e125. doi: 10.1212/nxg.0000000000000125

Reynolds, C. A., and Finkel, D. (2015). A meta-analysis of heritability of cognitive aging: minding the "missing heritability" gap. *Neuropsychol. Rev.* 25, 97–112. doi: 10.1007/s11065-015-9280-2

Savage, J. E., Jansen, P. R., Stringer, S., Watanabe, K., Bryois, J., de Leeuw, C. A., et al. (2018). Genome-wide association meta-analysis in 269,867 individuals identifies new genetic and functional links to intelligence. *Nat. Genet.* 50, 912–919.

Sniekers, S., Stringer, S., Watanabe, K., Jansen, P. R., Coleman, J. R. I., Krapohl, E., et al. (2017). Genome-wide association meta-analysis of 78,308 individuals identifies new loci and genes influencing human intelligence. *Nat. Genet.* 49, 1107–1112.

Stacey, D., Ciobanu, L. G., and Baune, B. T. (2017). A systematic review on the association between inflammatory genes and cognitive decline in non-demented elderly individuals. *Eur. Neuropsychopharmacol.* 27, 568–588. doi: 10.1016/j.euroneuro.2015.12.017

Swan, G. E., Carmelli, D., Reed, T., Harshfield, A., Fabsitz, R., and Eslinger, P. J. (1990). Heritability of cognitive performance in aging twins. The nationalal heart, lung, and blood institute Twin study. *Arch. Neurol.* 47, 259–262. doi: 10.1001/archneur.1990.00530030025010

Tasaki, S., Gaiteri, C., Mostafavi, S., Yu, L., Wang, Y., De Jager, P. L., et al. (2018). Multi-omic directed networks describe features of gene regulation in aged brains and expand the set of genes driving cognitive decline. *Front. Genet.* 9:294. doi: 10.3389/fgene.2018.00294

Trampush, J. W., Lencz, T., Knowles, E., Davies, G., Guha, S., Peer, I., et al. (2015). Independent evidence for an association between general cognitive ability and a genetic locus for educational attainment. *Am. J. Med. Genet. B Neuropsychiatr. Genet.* 168, 363–373.

Walhovd, K. B., Howell, G. R., Ritchie, S. J., Staff, R. T., and Cotman, C. W. (2019). What are the earlier life contributions to reserve and resilience? *Neurobiol. Aging* 83, 135–139. doi: 10.1016/j.neurobiolaging.2019.04.014

Wingo, A. P., Dammer, E. B., Breen, M. S., Logsdon, B. A., Duong, D. M., Troncosco, J. C., et al. (2019). Large-scale proteomic analysis of human brain identifies proteins associated with cognitive trajectory in advanced age. *Nat. Commun.* 10:1619.

Yen, K., Wan, J., Mehta, H. H., Miller, B., Christensen, A., Levine, M. E., et al. (2018). Humanin prevents age-related cognitive decline in mice and is associated with improved cognitive age in humans. *Sci. Rep.* 8:14212.

Zabaneh, D., Krapohl, E., Gaspar, H. A., Curtis, C., Lee, S. H., Patel, H., et al. (2018). A genome-wide association study for extremely high intelligence. *Mol. Psychiatry* 23, 1226–1232. doi: 10.1038/mp.2017.121

Zahodne, L. B., Mayeda, E. R., Hohman, T. J., Fletcher, E., Racine, A. M., Gavett, B., et al. (2019). The role of education in a vascular pathway to episodic memory: brain maintenance or cognitive reserve. *Neurobiol. Aging* 84, 109–118. doi: 10.1016/j.neurobiolaging.2019.08.009

Zhang, C., and Pierce, B. L. (2014). Genetic susceptibility to accelerated cognitive decline in the US Health and Retirement Study. *Neurobiol. Aging* 35:1512.e11–e18.

Zong, W., Liu, S., Wang, X., Zhang, J., Zhang, T., Liu, Z., et al. (2015). Trio gene is required for mouse learning ability. *Brain Res.* 1608, 82–90. doi: 10.1016/j.brainres.2015.02.040

Conflict of Interest: The authors declare that the research was conducted in the absence of any commercial or financial relationships that could be construed as a potential conflict of interest.

frontiers in Cell and Developmental Biology

REVIEW
published: 16 September 2020
doi: 10.3389/fcell.2020.00860

Role of Wnt Signaling in Adult Hippocampal Neurogenesis in Health and Disease

*Sebastian B. Arredondo, Daniela Valenzuela-Bezanilla, Muriel D. Mardones and Lorena Varela-Nallar**

Institute of Biomedical Sciences, Faculty of Medicine and Faculty of Life Sciences, Universidad Andres Bello, Santiago, Chile

OPEN ACCESS

Edited by:
Alex Dranovsky, Columbia University, United States

Reviewed by:
Andrea Erika Münsterberg, University of East Anglia, United Kingdom
Rahul N. Kanadia, University of Connecticut, United States

***Correspondence:**
Lorena Varela-Nallar
lorena.varela@unab.cl

Specialty section:
This article was submitted to Molecular Medicine, a section of the journal Frontiers in Cell and Developmental Biology

Received: *23 May 2020*
Accepted: *10 August 2020*
Published: *16 September 2020*

Citation:
Arredondo SB, Valenzuela-Bezanilla D, Mardones MD and Varela-Nallar L (2020) Role of Wnt Signaling in Adult Hippocampal Neurogenesis in Health and Disease. Front. Cell Dev. Biol. 8:860. doi: 10.3389/fcell.2020.00860

Neurogenesis persists during adulthood in the dentate gyrus of the hippocampus. Signals provided by the local hippocampal microenvironment support neural stem cell proliferation, differentiation, and maturation of newborn neurons into functional dentate granule cells, that integrate into the neural circuit and contribute to hippocampal function. Increasing evidence indicates that Wnt signaling regulates multiple aspects of adult hippocampal neurogenesis. Wnt ligands bind to Frizzled receptors and co-receptors to activate the canonical Wnt/β-catenin signaling pathway, or the non-canonical β-catenin-independent signaling cascades Wnt/Ca^{2+} and Wnt/planar cell polarity. Here, we summarize current knowledge on the roles of Wnt signaling components including ligands, receptors/co-receptors and soluble modulators in adult hippocampal neurogenesis. Also, we review the data suggesting distinctive roles for canonical and non-canonical Wnt signaling cascades in regulating different stages of neurogenesis. Finally, we discuss the evidence linking the dysfunction of Wnt signaling to the decline of neurogenesis observed in aging and Alzheimer's disease.

Keywords: adult neurogenesis, hippocampus, Wnt, aging, Alzheimer's disease

INTRODUCTION

The subgranular zone (SGZ) of the hippocampal dentate gyrus is one of the neurogenic niches of the adult brain where the generation of new neurons persist during adulthood. Compelling evidence indicate that this process is conserved in mammals including humans (Eriksson et al., 1998; Roy et al., 2000; Coras et al., 2010; Knoth et al., 2010; Spalding et al., 2013; Dennis et al., 2016; Mathews et al., 2017; Boldrini et al., 2018; Moreno-Jimenez et al., 2019; Tobin et al., 2019). New neurons are generated from radial glia-like neural stem cells (NSCs) located in the SGZ, that express nestin, glial fibrillary acidic protein (GFAP) and Sox2 (Kempermann et al., 2004; Bonaguidi et al., 2011). These NSCs, also referred as type 1 cells, are slowly dividing or quiescent, and after activation proliferate asymmetrically and give rise to highly proliferate intermediate progenitor

cells or type 2 cells, that transition between type 2a cells and neuronal committed type 2b cells (Kronenberg et al., 2003). Type 2b cells differentiate into neuroblasts or type 3 cells that develop into immature neurons and subsequently to mature granule cells, that become integrated into the hippocampal circuitry (van Praag et al., 2002; Ge et al., 2006; Zhao et al., 2006; Toni and Schinder, 2015). In rodents, these stages are well characterized by morphological features, and the expression of specific markers (Kempermann et al., 2004; Encinas et al., 2011). Among these, doublecortin (DCX) is transiently expressed, from neuronal committed progenitor cells until newborn cells begin to express mature neuronal markers (Brown et al., 2003). Thus, DCX has been a crucial marker used for the identification of newborn neurons in the adult human dentate gyrus (Knoth et al., 2010; Dennis et al., 2016; Boldrini et al., 2018; Moreno-Jimenez et al., 2019; Tobin et al., 2019).

Although the role of adult hippocampal neurogenesis has been challenging to determine in humans, increasing evidence in rodents and non-human primates indicate that adult-born neurons contribute to the structural and functional plasticity of the hippocampus (Snyder et al., 2001; Lacefield et al., 2012; Marin-Burgin et al., 2012; Toni and Schinder, 2015; Drew et al., 2016), and to spatial learning and memory, cognitive flexibility, mood regulation and pattern separation (Deng et al., 2010; Aimone et al., 2011; Denny et al., 2012; Gu et al., 2012; Danielson et al., 2016; Lazarov and Hollands, 2016; Anacker and Hen, 2017), the latter known to be associated to the function of the dentate gyrus in humans (Bakker et al., 2008). Accumulating evidence suggests that dysregulation of adult hippocampal neurogenesis may contribute to cognitive decline in aging and neurological disorders [reviewed in Artegiani and Calegari (2012); Seib and Martin-Villalba (2015); Hollands et al. (2016); Choi and Tanzi (2019)]. Therefore, there has been an evolving interest in the therapeutic potential of strategies aimed to enhance endogenous neurogenesis in conditions affecting cognitive abilities.

Neurogenesis in the adult hippocampus is highly regulated by local environmental cues. The SGZ provides an essential environmental niche for NSCs that allows their proliferation and maintenance, and supports the neurogenesis process (Suh et al., 2009; Schwarz et al., 2012; Faigle and Song, 2013; Toda and Gage, 2018). The neurogenic niche comprises cells, signaling molecules and neurotransmitter components. Growing evidence indicate that Wnt signals are key modulators of different stages of neurogenesis. The first member of the Wnt family was discovered more than 30 years ago (Nusse and Varmus, 1982), and thereafter the interest in Wnts has grown exponentially, since these ligands are involved in diverse developmental and adult processes in health and disease (Logan and Nusse, 2004; Clevers and Nusse, 2012; Jackstadt et al., 2020; Serafino et al., 2020). Wnts are secreted glycoproteins that signal through seven-pass transmembrane Frizzled (FZD) receptors. To date, 19 members of the Wnt family have been identified in mammals, along with 10 members of the FZD family of receptors. Wnt ligands bind to the extracellular cysteine rich domain (CRD) of FZDs to trigger the canonical Wnt/β-catenin signaling pathway (Gordon and Nusse, 2006), or the non-canonical or β-catenin-independent pathways Wnt/planar cell polarity (PCP) (Yang and Mlodzik, 2015; Butler and Wallingford, 2017), and Wnt/Ca^{2+} (Kuhl et al., 2000b; Kohn and Moon, 2005).

Although some Wnts mainly activate one specific Wnt cascade, it also occurs that one Wnt ligand can activate different signaling cascades depending on the receptor and co-receptor context (Mikels and Nusse, 2006; van Amerongen et al., 2008; Grumolato et al., 2010), increasing the possibilities of interaction and the complexity of the Wnt signaling activation. Wnt co-receptors include the single transmembrane low-density lipoprotein receptor-related protein 5 and 6 (LRP5/6) that trigger Wnt/β-catenin signaling activation, the single-pass transmembrane receptor tyrosine kinase-like orphan receptors 1 and 2 (Ror1/2), and Ryk that activate non-canonical Wnt signaling (Bovolenta et al., 2006; Grumolato et al., 2010; Gao et al., 2011; Green et al., 2014). In addition, Wnt signaling is modulated by a number of evolutionary conserved inhibitors and activators [for review see Logan and Nusse (2004); Cruciat and Niehrs (2013)]. Endogenous activators include the family of four secreted glycoproteins R-spondin (RSPO1-4) and Norrin, described as agonists of the canonical Wnt signaling (Cruciat and Niehrs, 2013). Endogenous inhibitors include secreted frizzled-related proteins (sFRPs) composed by five members sFRP1-5, and Wnt inhibitory factor-1 (WIF-1), which directly bind to Wnt proteins preventing their interaction with FZD receptors (Rattner et al., 1997; Hsieh et al., 1999); Dickkopf 1, 2, and 3 (Dkk1-3), which bind LRP5/6 and the transmembrane proteins Kremen to disrupt the interaction of Wnt/FZD (Bafico et al., 2001); and Wise/SOST that bind to LRP5/6 to block Wnt-induced FZD-LRP5/6 interaction (Semenov et al., 2005).

Activation of canonical Wnt/β-catenin signaling involves the formation of Wnt/LRP/FZD ternary complex, which induces the recruitment of the scaffolding protein Disheveled (Dvl), and the multiprotein complex composed of the scaffolding protein Axin, APC, and the enzymes casein kinase 1 (CK1) and glycogen synthase kinase 3β (GSK3-β) (Cong et al., 2004; Zeng et al., 2005; Bilic et al., 2007). In consequence, β-catenin phosphorylation is inhibited, thus preventing its ubiquitination and degradation (Aberle et al., 1997). β-catenin accumulates in the cytoplasm and translocate into the nucleus where it interacts with members of the T cell factor/lymphoid enhancer binding factor (TCF/LEF) family of transcription factors displacing the transcriptional repressor Groucho, and regulating the expression of target genes (Logan and Nusse, 2004; MacDonald et al., 2009). In the Wnt/PCP pathway the binding of the Wnt ligand causes the activation of the small GTPases Rho and Rac, and downstream c-Jun N-terminal kinase (JNK) which regulates cytoskeleton dynamics and activation of activator protein-1 (AP-1) family transcription factors (Jones and Chen, 2007; Yang and Mlodzik, 2015). Other PCP components include the transmembrane proteins Van Gogh-like (Vangl) and Celsr1-3, and the cytoplasmic factors Prickle and Diversin (Jones and Chen, 2007; Yang and Mlodzik, 2015). The Wnt/PCP pathway regulates the coordinated polarization of cells or structures in the plane of a tissue, and orientation of subcellular structures and cellular processes [reviewed in Devenport

(2014); Butler and Wallingford (2017)]. The Wnt/Ca^{2+} signaling cascade is a G protein-dependent signaling pathway that triggers the activation of phospholipase C and phosphodiesterase (Kohn and Moon, 2005), increasing the levels of intracellular inositol 1,4,5-triphosphate (IP3) and 1,2 diacylglycerol (DAG) (Koval and Katanaev, 2011). IP3 and DAG lead to the release of calcium from the endoplasmic reticulum and the consequent activation of calcium sensitive proteins such as calcium calmodulin dependent protein kinase II (CamKII) (Kuhl et al., 2000a), protein kinase C (PKC) (Sheldahl et al., 1999) or the phosphatase calcineurin that activates the Nuclear factor of activated T-cells (NFAT) (Saneyoshi et al., 2002; De, 2011).

In the central nervous system, Wnt signaling pathways play pivotal roles during development, controlling cell division, differentiation, polarity, migration, and synaptogenesis (Freese et al., 2010; Bielen and Houart, 2014; Bengoa-Vergniory and Kypta, 2015; Inestrosa and Varela-Nallar, 2015). In the adult brain, Wnt signaling regulates synaptic plasticity, adult neurogenesis and behavior [reviewed in Varela-Nallar and Inestrosa (2013); Oliva et al. (2018)]. Here we summarize evidence supporting that the Wnt signaling is a key regulator of adult hippocampal neurogenesis in health and disease.

Wnt SIGNALING IN THE REGULATION OF ADULT HIPPOCAMPAL NEUROGENESIS

Compelling evidence indicate that components of the Wnt signaling pathway play multiple roles during adult neurogenesis. As will be discussed, the data also suggest that canonical and non-canonical Wnt signaling cascades regulate different stages of neurogenesis: Wnt/β-catenin signaling regulates proliferation and fate commitment, while non-canonical Wnt signaling controls the differentiation and development of newborn neurons. In this section, we summarize current knowledge on the role of Wnt signaling components and pathways in controlling different stages of adult hippocampal neurogenesis (**Figure 1**).

Wnt Ligands

Wnts are secreted lipid-modified glycoproteins that act as autocrine and paracrine signaling molecules (Rios-Esteves and Resh, 2013; Rios-Esteves et al., 2014). Wnts are expressed in neural progenitor cells (NPCs) isolated from the adult hippocampus (Wexler et al., 2009), and in dentate gyrus astrocytes (Lie et al., 2005; Okamoto et al., 2011). In co-culturing experiments, it was demonstrated that Wnts secreted by astrocytes promote neuronal differentiation of NPCs (Lie et al., 2005; Okamoto et al., 2011). In addition, sequestering Wnts secreted by cultured adult hippocampal progenitors (AHPs) reduced proliferation and the expression of genes involved in the maintenance of progenitors cells, while inducing an upregulation of genes involved in neuronal differentiation (Wexler et al., 2009). This indicates that autocrine Wnt signaling controls maintenance and proliferation of NPCs.

The first study directly linking Wnt proteins and adult hippocampal neurogenesis *in vivo* showed that general blockade of Wnt signaling with a dominant negative of Wnt1 ligand, which non-autonomously blocks Wnt signaling, almost completely eliminated the generation of new neurons in adult rat hippocampus (Lie et al., 2005). On the other hand, lentivirus-mediated overexpression of Wnt3, which is normally expressed in the SGZ and mostly by niche astrocytes (Okamoto et al., 2011), induced neurogenesis in the adult rat dentate gyrus (Lie et al., 2005). In cultured AHPs, overexpression of Wnt3 and Wnt3a, which activate the Wnt/β-catenin pathway (Lie et al., 2005; Kuwabara et al., 2009), increased neuronal fate commitment and enhanced the proliferation of neuroblasts, suggesting that canonical Wnt signaling regulates these processes. In agreement, expression of dominant-negative Lef1 (dnLef1) reduced neuronal differentiation induced by co-culture with hippocampal astrocytes (Lie et al., 2005). Wnt7a was also described as an endogenous modulator of hippocampal neurogenesis that regulates proliferation and neuronal differentiation. Wnt7a knockout mice showed fewer NPCs, which exhibited lengthened cell cycles and a reduced cell cycle reentry, and also showed impaired neuronal differentiation (Qu et al., 2013). On the contrary, chronic infusion of Wnt7a directly into the rat hippocampus increased the number of immature neurons (Ortiz-Matamoros and Arias, 2019). Wnt7a knockdown in NSCs reduced the expression of Cyclin D1, while when NSCs were induced to differentiate into neurons Wnt7a knockdown reduced mRNA levels of neurogenin 2 (Ngn2). In cultured progenitors β-catenin binds to TCF/LEF binding sites in the promoter region of Cyclin D1, while in neurons β-catenin binds to TCF/LEF binding site in the promoter region of Ngn2. These findings indicate that Wnt7a regulates proliferation and differentiation through the canonical Wnt/β-catenin signaling pathway (Qu et al., 2013). In addition, immature neurons in Wnt7a knockout mice exhibited reduced dendritic arborization (Qu et al., 2013). These data indicate that Wnt7a has multiple roles during adult hippocampal neurogenesis controlling proliferation, differentiation and development of newborn neurons.

More recently, Wnt5a was also identified as an endogenous niche factor that regulates hippocampal neurogenesis. We determined that reducing the levels of Wnt5a in the dentate gyrus of adult mice decreased the generation of new neurons (Arredondo et al., 2020). Lentivirus-mediated knockdown of Wnt5a reduced the differentiation of neuronal committed progenitor cells, which remained as non-proliferative intermediate Sox2-expressing progenitors that failed to continue with the neuronal differentiation program. In addition, impaired dendritic arborization of newborn neurons was observed when knocking down Wnt5a. A similar effect was observed when Wnt5a was reduced in cultured AHPs, in which neuronal differentiation and morphological development of the derived neurons were reduced, while treatment with Wnt5a had the opposite effect (Arredondo et al., 2020). In agreement, chronic infusion of Wnt5a ligand into the adult rat hippocampus increased the number of immature neurons and altered their pattern of neurite outgrowth (Ortiz-Matamoros and Arias, 2019). In cultured AHPs, Wnt5a activated CamKII, PKC and JNK (Arredondo et al., 2020), and activated AP1 and c-jun in

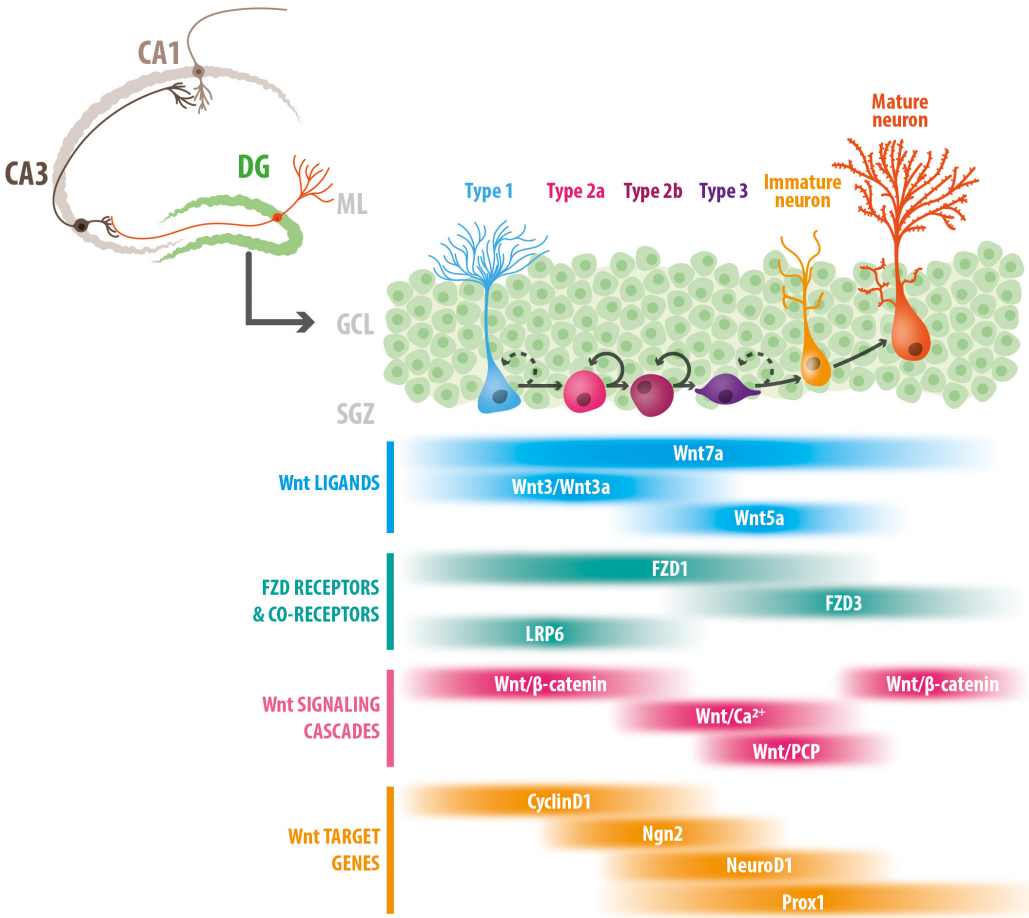

FIGURE 1 | Stage-specific roles of Wnt signaling components in adult hippocampal neurogenesis. Schematic representation of the adult mouse hippocampus, and the stages of neurogenesis in the dentate gyrus. Type 1 NSCs proliferate asymmetrically to give rise to type 2 cells (types 2a and 2b), that differentiate into type 3 cells or neuroblast that develop into immature neurons, and ultimately into mature granule cells. The bottom panel indicates the temporal windows in which Wnt ligands, FZD receptors and co-receptors, Wnt signaling cascades and Wnt target genes have been involved (see text for details). DG, dentate gyrus; ML, molecular layer; GCL, granule cell layer; SGZ, subgranular zone.

differentiated but not proliferative AHPs (Schafer et al., 2015), indicating that Wnt5a triggers activation of non-canonical Wnt signaling cascades. Moreover, we found that the effect of Wnt5a on neuronal differentiation was mediated Wnt/Ca^{2+}/CamKII signaling, while the effect on morphological development involved Wnt/Ca^{2+} and Wnt/JNK cascades (Arredondo et al., 2020), indicating that Wnt5a is an endogenous factor regulating neurogenesis through non-canonical Wnt signaling.

Wnt Receptors and Co-receptors

Frizzleds are the primary receptors for Wnt signals. All FZD isoforms present conserved structural characteristics, including a N-terminus extracellular region containing the highly conserved CRD, seven transmembrane regions, and an intracellular C-terminus that mediate the interaction between FZD and Dvl [reviewed in Huang and Klein (2004); Schulte (2010)]. Several FZD receptors are expressed in cultured AHPs, and some of them show specific expression patterns during differentiation (Wexler et al., 2009; Cui et al., 2011; Schafer et al., 2015; Mardones et al., 2016). In the adult dentate gyrus, FZD3 is expressed in immature and mature neurons, but not in NSCs or NPCs, suggesting FZD3 is required for later stages of adult neurogenesis (Schafer et al., 2015). In agreement, FZD3 expression increased upon differentiation in cultured AHPs (Schafer et al., 2015). Retrovirus-mediated knockdown of FZD3 did not affect neuronal differentiation of newborn cells, however, the dendritic arborization of FZD3-deficient newborn neurons was reduced. In addition, the orientation and positioning of these neurons within the granule cell layer (GCL) was affected (Schafer et al., 2015). FZD3 knockdown reduced the Wnt5a-dependent activation of c-Jun and JNK in differentiated AHPs, indicating FZD3 activates Wnt/PCP signaling in these cells. The same study demonstrated that *in vivo* knockdown of Celsr 1-3 impaired the development and maturation of adult-born neurons without affecting neuronal differentiation (Schafer et al., 2015). Celsr1-3, the mammalian homologs of Drosophila Flamingo, are a family of atypical cadherins that contain seven transmembrane segments, and are part of the so-called Wnt/PCP core proteins

in vertebrates (Yang and Mlodzik, 2015). Newborn neurons deficient in Celsr 2/3 showed impaired dendritic arborization and altered positioning within the GCL, while Celsr 1-deficient neurons displayed abnormal orientation (Schafer et al., 2015). Celsr 3 knockdown also altered dendritic pruning of adult-born neurons (Goncalves et al., 2016). Altogether, these data suggest that Wnt/PCP signaling is involved in polarization and dendritic development of adult-born neurons, but not in fate commitment.

FZD1 receptor is also expressed in the adult dentate gyrus, where it was found in NSC, NPCs and immature neurons, and its expression is reduced in mature neurons (Mardones et al., 2016), suggesting the role of this receptor is restricted to early stages of adult neurogenesis. We determined that retrovirus-mediated knockdown of FZD1 in the dentate gyrus of adult mice reduced neuronal differentiation of newborn cells, while increasing the differentiation into astrocytes (Mardones et al., 2016). Additionally, FZD1-deficient immature neurons showed altered migration within the GCL, but exhibit normal dendritic arborization (Mardones et al., 2016). FZD1 has been largely described as a receptor for the canonical Wnt signaling, and in agreement, FZD1 knockdown reduced β-catenin levels and the expression of proneural Wnt target genes in AHPs (Mardones et al., 2016). These results suggest that FZD1 regulates neuronal fate commitment through the canonical Wnt/β-catenin signaling pathway. In accordance, knockdown of the co-receptor for the canonical Wnt pathway LRP6, lead to a reduction in neuronal differentiation of newborn cells (Schafer et al., 2015). Interestingly, as observed by FZD1 knockdown, no effect on morphological development was observed in LRP6-deficient newborn neurons. In agreement with its role in early stages of neurogenesis LRP6 is expressed in proliferating AHPs and its expression was reduced upon differentiation (Schafer et al., 2015). Altogether, these evidences suggest that specific receptors and co-receptors activate canonical Wnt/β-catenin to control neuronal fate commitment. Interestingly, β-catenin reporter mouse lines showed a peak of Wnt/β-catenin activity during early stages of adult hippocampal neurogenesis. Different transgenic reporter mouse lines have been used to evaluate the activity of Wnt/β-catenin signaling in the dentate gyrus: the BATGAL mice (Lie et al., 2005; Garbe and Ring, 2012; Heppt et al., 2020), the ins-topGal mice (Garbe and Ring, 2012), and the $Axin2^{LacZ/+}$ mice (Heppt et al., 2020). Although the expression pattern of the reporter activity is not exactly the same in the different mouse lines likely for the molecular construct of the transgenes, the use of BrdU birth-dating strategies and specific molecular markers together with the reporter activity showed that Wnt/β-catenin signaling is active during early stages of adult hippocampus neurogenesis (including NPCs and proliferating neuroblasts), and is attenuated in immature neurons (Lie et al., 2005; Garbe and Ring, 2012; Heppt et al., 2020). Considering that activation of a specific Wnt signaling pathway may antagonize the activation of other Wnt signaling cascades (Ishitani et al., 2003; Topol et al., 2003; Mikels and Nusse, 2006; Grumolato et al., 2010; Sato et al., 2010; Mentink et al., 2018), it is feasible to suggest that the Wnt/β-catenin pathway might be inhibited after fate commitment by the activation of non-canonical Wnt signaling cascades, which as discussed, regulate the development of newborn neurons (Schafer et al., 2015; Arredondo et al., 2020). Interestingly, Wnt/β-catenin activity is reactivated in mature newborn neurons (Garbe and Ring, 2012; Heppt et al., 2020), suggesting that the canonical Wnt pathway might also control later stages of neurogenesis such as maturation or synaptic integration. Notably, it was recently shown that the attenuation of Wnt/β-catenin signaling in early stages of newborn neurons is required for correct dendrite development, and Wnt/β-catenin reactivation in maturing neurons modulates the tempo of dendritic growth and spine formation (Heppt et al., 2020), indicating that a precise control of Wnt signaling activity is required for the generation of new granule cells in the adult hippocampus.

Interestingly, a dual role in adult hippocampal neurogenesis was determined for ATP6AP2 (Schafer et al., 2015), an adaptor protein between Wnt/β-catenin and Wnt/PCP signaling that possess a dual function forming a signalosome to initiate canonical Wnt signaling, and acting as a Wnt/PCP core protein (Buechling et al., 2010; Hermle et al., 2013). ATP6AP2 knockdown in proliferating progenitors reduced the activity of the TCF/LEF in response to Wnt3a, while in differentiated progenitors ATP6AP2 knockdown reduced AP-1 signaling in response to Wnt5a (Schafer et al., 2015). This evidence indicates that ATP6AP2 modulates the activation of canonical Wnt/β-catenin and non-canonical Wnt/PCP signaling in NPCs at different stages of the neurogenic process. *In vivo*, ATP6AP2 knockdown had a dual effect reducing the number of immature neurons and inducing defects in several aspects of the morphological development, migration and orientation of new neurons in the adult hippocampus (Schafer et al., 2015).

Altogether, the discussed evidence suggests that Wnt signaling components mediate the activation of specific signaling cascades, which coordinately control the progression of neurogenesis in the adult hippocampus.

Soluble Modulators of the Wnt Signaling Pathway

The endogenous Wnt antagonists sFRP3 and Dkk1 have shown to regulate neurogenesis in the adult hippocampus (Jang et al., 2013; Seib et al., 2013). sFRP3 is highly expressed in the dentate gyrus by mature granule cells in the GCL and regulates different stages of neurogenesis (Jang et al., 2013). sFRP3 knockout mice exhibited increased proliferation of NSC, together with increased dendritic development, spine density and accelerated maturation of newborn neurons. Interestingly, in the adult hippocampus there is a septo-temporal gradient of expression of this Wnt inhibitor that is inversely related to NSCs proliferation, suggesting that sFRP3 levels, and therefore Wnt signaling activity, contribute to the graded distribution of neurogenesis in the adult dentate gyrus (Sun et al., 2015). sFRP3 is also involved in the physiological modulation of neurogenesis by electroconvulsive stimulation (ECS) and wheel running, which concomitantly with the increase in neuronal activity, lead to a reduction in the levels of sFRP3 in the dentate gyrus and to the activation of the Wnt/β-catenin signaling pathway (Jang et al., 2013). Besides, Dkk1 regulates self-renewal of NPCs and morphological

maturation of newborn neurons (Seib et al., 2013). In NPCs loss of Dkk1 increased Wnt/β-catenin signaling reporter activity, indicating that Dkk1 negatively regulates the canonical Wnt pathway in the adult hippocampus (Seib et al., 2013). Dkk1 was involved in the age-dependent decrease in neurogenesis, which will be discussed later.

Wnt/β-Catenin Target Genes

Wnt/β-catenin target genes have been involved in multiple stages of adult hippocampal neurogenesis. Cyclin D1 is involved in the Wnt-mediated induction of proliferation in neural progenitors (Shtutman et al., 1999; Tetsu and McCormick, 1999). In proliferative NPCs, β-catenin is bound to the TCF/LEF motif in the Cyclin D1 promoter, associated with the active chromatin markers acetylated histone H3 (AcH3) and trimethylated histone H3 at lysine 4 (H3K4me3). But when NPCs are induced to differentiate, β-catenin dissociate from the Cyclin D1 promoter (Qu et al., 2013). On the contrary, upon differentiation β-catenin binds a TCF/LEF binding site in the Ngn2 gene promoter in association with active chromatin markers AcH3 and H3K4me3 (Qu et al., 2013). Ngn2 is a proneural basic helix-loop-helix (bHLH) transcription factor that promotes neuronal differentiation (Israsena et al., 2004). Prior to differentiation, no β-catenin was detected in the TCF/LEF binding site of the Ngn2 promoter in NPCs.

NeuroD1 is also a bHLH proneural transcription factor involved in the Wnt-mediated induction of neuronal differentiation (Kuwabara et al., 2009). NeuroD1 is expressed in neuronal committed progenitors and immature neurons, but not in NSCs (Gao et al., 2009). Overexpression of NeuroD1 in cultured adult NSC increased their neuronal differentiation, while reducing their differentiation into oligodendrocytes and astrocytes (Hsieh et al., 2004), indicating NeuroD1 promotes neuronal fate-commitment. In the adult dentate gyrus, β-catenin knockdown in Sox2 cells induced the loss of NeuroD1 progenitors, as well as a decrease in newborn granule neurons, with no effect on the NSC pool (Kuwabara et al., 2009). *Neurod1* gene promoter contains a TCF/LEF binding site that is overlapped with a binding site for Sox2 (Sox/LEF site). In undifferentiated NSCs, Sox2 and the histone deacetylase HDAC1 repressor protein are associated with the Sox/LEF site in the *Neurod1* promoter. In differentiated neurons β-catenin, along with acetylated histone H3 and methylated histone H3 at lysine 4, which are related with transcriptional activation, are present in the *Neurod1* promoter (Kuwabara et al., 2009). The data indicate that the *Neurod1* promoter is repressed by Sox2 in NSCs, and in response to Wnt stimulation it is transcriptionally activated by β-catenin leading to NeuroD1 expression and neurogenesis (Kuwabara et al., 2009). The gene encoding prospero-related homeodomain transcription factor 1 (Prox1) also contains TCF/LEF sites overlapped with Sox2 binding sites in promoter/enhancer regions (Karalay et al., 2011). Prox1 is expressed in type 2 cells, neuroblasts, immature neurons and mature granule neurons restricted to the dentate gyrus (Kempermann et al., 2004; Lavado et al., 2010; Karalay et al., 2011). Prox1 is required for the maintenance of intermediate progenitor cells (Lavado et al., 2010), and for neuronal differentiation of granule cells (Karalay et al., 2011). Altogether, these data suggest that in adult hippocampal neurogenesis Wnt/β-catenin signaling regulates proliferation through the expression of Cyclin D1 and promotes neuronal differentiation through the expression of proneural transcription factors including Ngn2, NeuroD1 and Prox1.

Wnt SIGNALING IN THE DECLINE OF NEUROGENESIS IN THE AGING HIPPOCAMPUS

An age-related decline in adult hippocampal neurogenesis has been evidenced in rodents, non-human primates and humans (Kuhn et al., 1996; Gould et al., 1999; Leuner et al., 2007; Olariu et al., 2007; Ben Abdallah et al., 2010; Knoth et al., 2010; Kohler et al., 2011; Dennis et al., 2016; Mathews et al., 2017; Boldrini et al., 2018; Sorrells et al., 2018), suggesting that conserved mechanisms may underlie the reduced capacity of the aged hippocampus to generate new neurons. Recently, a correlation between the loss of immature neurons and an early cognitive decline was determined in aged humans (Tobin et al., 2019), suggesting that efforts to promote neurogenesis may foster new therapeutic possibilities for the aging brain.

The reduced neurogenesis is likely a consequence of a deteriorated neurogenic niche unable to sustain neurogenesis (Hattiangady and Shetty, 2008; Kalamakis et al., 2019). Growing evidence suggest that the Wnt signaling pathway is part of the signaling mechanisms affected, that might contribute to the decline in neurogenesis (**Figure 2**). In support of this idea, β-catenin reporter mice exhibit a strong decrease in β-catenin signaling activity in the GCL with age, and increasing β-catenin activity counteracts the age-associated maturation defects of adult-born dentate granule neurons (Heppt et al., 2020). In addition, the expression of Wnt3 and Wnt3a in the dentate gyrus decreases with age, concomitantly with the decrease in newborn neurons positive for NeuroD1 (Okamoto et al., 2011). In aged rats (22-month-old) almost no expression of Wnt3 was observed in astrocytes of the SGZ compared to young rats (4-week-old), although the number of astrocytes remained unaffected (Okamoto et al., 2011). This was also determined in cultured primary astrocytes from the hippocampus of aged mice (9-month-old), which showed reduced levels of Wnt3 and Wnt3a compared to astrocytes cultured from young animals (4-week-old). Interestingly, the same study determined that NSCs isolated from the hippocampus of young and aged mice exhibited a more effective neuronal differentiation when cultured on young versus aged primary astrocyte layer. This effect was not observed when Wnt3 was knocked down in young astrocytes (Okamoto et al., 2011), suggesting that loss of Wnt signals might contribute to the impaired neurogenesis in the aged hippocampus. Of note, the expression of FZD receptors and co-receptors were almost unchanged between young and aged NSC (Okamoto et al., 2011). Another study determined that conditioned media from young astrocytes induced promoter activity of the anti-apoptotic protein Survivin in aged and young NPCs, while conditioned medium from aged astrocytes

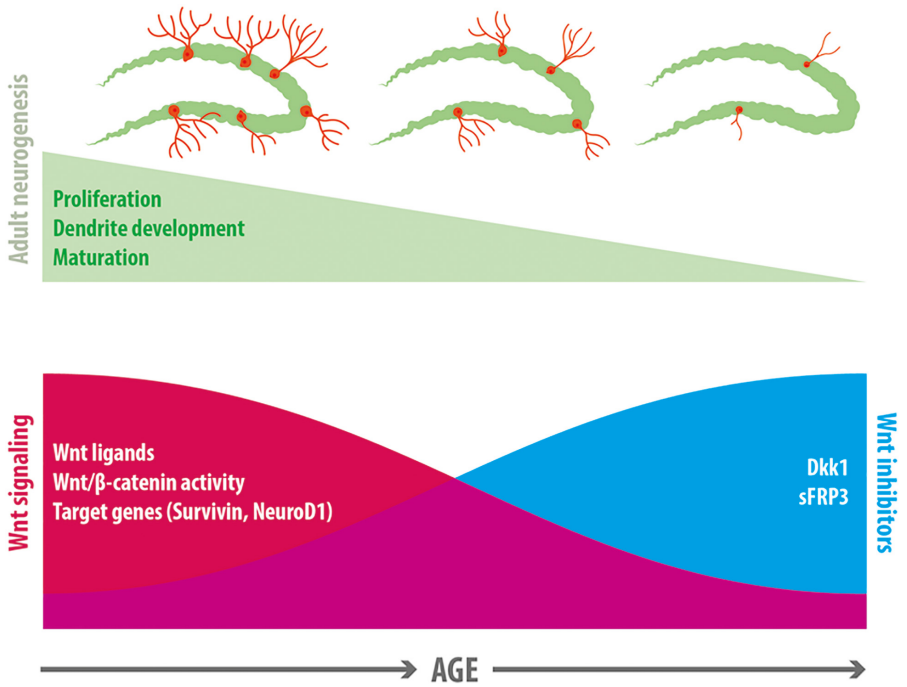

FIGURE 2 | Wnt signaling in the age-related decline in neurogenesis. A reduction in neurogenesis is observed in the dentate gyrus with age, which is accompanied by a decline in proliferation of neural precursor cells, a decreased dendritic development and delayed maturation of adult-born neurons. Evidence exists indicating that a decline in Wnt signaling is associated with this reduction of neurogenesis. In normal aging there is a decrease in the expression of most Wnt ligands in hippocampal astrocytes, a decrease in canonical Wnt signaling activity in the dentate gyrus, and a reduction in the expression of Wnt target genes that control neurogenesis (including Survivin and NeuroD1). Concomitantly, there is an increase in the expression of the Wnt inhibitors sFRP3 and Dkk1 in the hippocampus with age.

decreased Survivin promoter activity and NPC proliferation compared to control medium. Survivin is a Wnt target gene (Tapia et al., 2006), and lentivirus-mediated expression of Survivin in the dentate gyrus of aged mice (13-month-old), increased proliferation (Miranda et al., 2012). This study also determined that Wnts released by astrocytes promote NPC proliferation by inducing Survivin expression, and that most Wnt ligands are downregulated in aged astrocytes. Interestingly, wheel running, a well characterized inducer of neurogenesis in young and aged hippocampus (van Praag et al., 1999, 2005), induced an increase in the number of Wnt3 expressing cells concomitantly with an increase in the density of immature neurons in the dentate gyrus (Okamoto et al., 2011), suggesting that Wnt3 could mediate the stimulation of neurogenesis in the adult hippocampus.

In addition to the downregulation of Wnt signals, in aging there is an increase in endogenous Wnt inhibitors. Increased levels of Dkk1 were observed in the hippocampus of aged mice (Seib et al., 2013; Kase et al., 2019). Interestingly, loss of Dkk1 restored neurogenesis in old mice (2-year-old) and increased the dendritic complexity of newborn neurons. Moreover, loss of Dkk1 restored spatial working memory and memory consolidation, and improved affective behavior in aged mice (Seib et al., 2013). sFRP3 was also increased in the aging hippocampus (Kase et al., 2019). Interestingly, genetic inhibition of sFRP3 in a mouse model of accelerated aging, rescued neural progenitor proliferation in the hippocampal dentate gyrus (Cho et al., 2019).

Wnt SIGNALING IN THE IMPAIRMENT OF NEUROGENESIS IN ALZHEIMER'S DISEASE: THERAPEUTIC IMPLICATIONS

Impaired neurogenesis is observed in several neuropsychiatric and neurodegenerative diseases such as mood disorders, epilepsy, Parkinson's disease and Alzheimer's disease (AD) (Lucassen et al., 2010; Winner and Winkler, 2015; Galan et al., 2017; Toda et al., 2019). AD is the most common type of dementia, it is estimated that 30 million people suffer form AD worldwide. AD is characterized by a progressive memory loss, impaired cognitive functions, neuronal loss and synaptic dysfunction. Histopathological hallmarks of AD are the extracellular deposition of amyloid β peptide (Aβ) forming amyloid plaques, and the presence of intracellular neurofibrillary tangles mainly composed by hyperphosphorylated tau proteins [reviewed in Selkoe and Hardy (2016)]. Aβ is generated from sequential proteolysis of amyloid precursor protein (APP) by β- and γ-secretase enzymes (O'Brien and Wong, 2011). In addition to neuronal loss, reduced neurogenesis was evidenced in the dentate gyrus of patients with AD pathology (Li et al., 2008; Crews et al., 2010; Ekonomou et al., 2015; Moreno-Jimenez et al.,

2019; Tobin et al., 2019). Post-mortem brain analysis from AD patients revealed a progressive decline in the number of newborn neurons, and in the maturation of these cells as the disease advanced (Moreno-Jimenez et al., 2019). Reduced neurogenesis has also been evidenced in different mouse models of AD, which show impairments in NPCs proliferation, differentiation and maturation of newborn neurons (Donovan et al., 2006; Rodriguez et al., 2008; Demars et al., 2010; Fiorentini et al., 2010; Hamilton et al., 2010; Abbott et al., 2013; Zeng et al., 2016; Choi et al., 2018). Interestingly, in AD mice deficits in neurogenesis precede Aβ plaque and NFT formation, suggesting that impairment in neurogenesis may mediate early cognitive decline (Demars et al., 2010; Fiorentini et al., 2010; Hamilton et al., 2010; Zeng et al., 2016). Recently, reduced number of neuroblasts in early stages of cognitive decline was determined in humans, suggesting that reduced neurogenesis may promote cognitive deficits in AD, or exacerbate them (Tobin et al., 2019). Because increased neurogenesis in the dentate gyrus is associated with improved cognitive capacities (Toda et al., 2019), there has been great interest in the potential of neurogenesis as a therapeutic target for conditions affecting cognition. In this regard, genetic manipulation of neurogenesis by inducing the expression of the proneural gene NeuroD1 in hippocampal progenitors restored spatial memory in a mouse model of AD (Richetin et al., 2015). This evidence supports the potential of neurogenesis as a therapeutic target to prevent or improve cognitive deficits in normal aging and pathological conditions.

Interestingly, we and others have determined that hippocampal neurogenesis is stimulated in AD mouse models through physiological (Hu et al., 2010; Rodriguez et al., 2011; Varela-Nallar et al., 2014; Tapia-Rojas et al., 2016; Choi et al., 2018), and pharmacological stimulation (Fiorentini et al., 2010; Abbott et al., 2013; Varela-Nallar et al., 2015; Choi et al., 2018; Zeng et al., 2019). These evidences demonstrate that NSCs in the hippocampus retains the ability to generate new neurons. In this context, the decrease in neurogenesis in AD could be due to a deterioration of the neurogenic niche. Wnt signaling is likely affected in the SGZ niche since compelling evidence indicate a downregulation of this signaling pathway is associated to the pathophysiology of AD [reviewed in De Ferrari and Inestrosa (2000); De Ferrari et al. (2014); Inestrosa and Varela-Nallar (2014); Oliva et al. (2018)]. Among the several components of the Wnt pathway that are altered in AD, increased levels of Dkk1 were found in post-mortem brains of AD patients (Caricasole et al., 2004), and in the hippocampus of the TgCRND8 mouse model of AD (Rosi et al., 2010), expressing a double mutant form of the human APP. Also, increased levels of active GSK-3β was observed in the dentate gyrus of TgCRND8 mice, suggesting a downregulation of Wnt signaling activity in this area (Rosi et al., 2010). Moreover, in AD patients altered gene expression was found for the soluble Wnt inhibitor WIF-1 in the temporal lobe (Humphries et al., 2015), Wnt7b and intracellular components of canonical Wnt signaling in the entorhinal cortex and hippocampus (Riise et al., 2015), and FZD3 in prefrontal cortex (Folke et al., 2019). In addition, a genetic variant of the Wnt co-receptor LRP6, showing reduced activation of the canonical Wnt signaling has been associated to late-onset AD (De Ferrari et al., 2007; Alarcon et al., 2013).

Considering the crucial role of the Wnt signaling in the regulation of neurogenesis, it might be possible that the dysregulation of this signaling pathway may contribute to neurogenesis deficits observed in AD. Of note, overexpression of Wnt3 restored neurogenesis in the hippocampus of the 5xFAD mouse model of AD (Choi et al., 2018), that express human APP and PSEN1 with a total of five AD-linked mutations. As well, overexpression of Wnt3a was also able to restore neurogenesis levels in the dentate gyrus of 3xTgAD mice, bearing human APP, tau and PSEN1 with AD-linked mutations (Shruster and Offen, 2014). These evidences indicate that in AD brain, neurogenesis is able to respond to exogenous Wnt stimulation, and suggest that Wnt manipulation is an attractive therapeutic target to promote neurogenesis in this pathological condition (**Figure 3**).

Supporting the association between Wnt signaling impairment and reduced neurogenesis, several drugs able to enhance neurogenesis in AD models have shown to modulate components of the Wnt signaling pathway (**Figure 3**). Pharmacological inhibition of the key component of the Wnt signaling pathway GSK-3β, enhances neurogenesis in the hippocampus of AD mice (Fiorentini et al., 2010; Varela-Nallar et al., 2015; Zeng et al., 2019). Lithium, a widely used mood stabilizer that inhibits GSK-3α/β by competing with the cofactor magnesium, induced the proliferation and survival rate of NPCs in the SGZ of TgCRND8 mice (Fiorentini et al., 2010). Lithium treatment induced an increase in the number of immature neurons expressing nuclear β-catenin, supporting the activation of Wnt/β-catenin signaling in newborn neurons. Importantly, therapeutic concentrations of lithium induced proliferation of cultured AHPs, which was prevented by β-catenin knockdown (Wexler et al., 2008), indicating that lithium induced neurogenesis trough activation of the Wnt/β-catenin signaling pathway. Additionally, Andrographolide (ANDRO) one of the main constituents of the medicinal plant *Andrographis paniculata* (Panossian et al., 2000; Cheung et al., 2001), that inhibits GSK-3β through a substrate-competitive mode of action (Tapia-Rojas et al., 2015), promoted hippocampal neurogenesis in the APPswe/PSEN1ΔE9 mouse model of AD (Varela-Nallar et al., 2015). ANDRO treatment induced proliferation and increased the density of immature neurons in the dentate gyrus of AD mice, concomitantly with an increase in hippocampal levels of β-catenin and NeuroD1 in the hippocampus (Varela-Nallar et al., 2015). Importantly, ANDRO was shown to improve cognitive performance in APPswe/PSEN1ΔE9 mice (Serrano et al., 2014), and in J20 mice expressing human APP with two mutations linked to familial AD (Cisternas et al., 2019). More recently, Valproic acid (VPA), another selective inhibitor of GSK-3β used as an antiepileptic and mood-stabilizing drug, was shown to promote proliferation, increase the density of immature neurons, and improved learning and memory in the dentate gyrus of triple transgenic APPswe/PSEN1ΔE9/Nestin-GFP mice (Zeng et al., 2019). VPA treatment increased β-catenin levels, and induced the expression of NeuroD1, suggesting the activation of the Wnt signaling pathway in the hippocampus of AD mice.

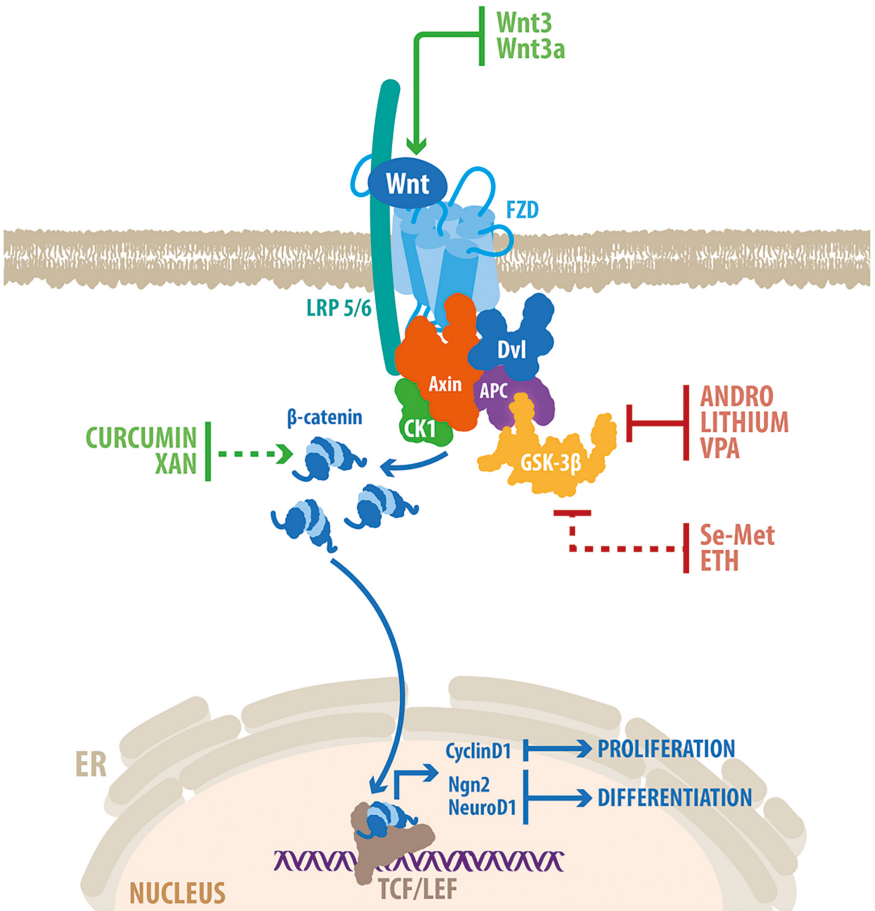

FIGURE 3 | Genetic and pharmacological activation of Wnt/β-catenin promotes neurogenesis in the hippocampus of AD models. Schematic representation of the Wnt/β-catenin signaling pathway. Wnt ligand binds to FZD and LRP5/6, which trigger the recruitment of a multiprotein complex composed also of Axin, APC, CK1 and GSK-3β. This prevents the phosphorylation and degradation of β-catenin that translocates into the nucleus where it binds to members of the TCF/LEF families of transcription factors, to modulate the transcription of target genes. The Wnt/β-catenin signaling components that are target of genetic activation (Wnt3 and Wnt3a) and drugs able to stimulate neurogenesis in the hippocampus of animal models of AD are indicated. Red lines indicate inhibition; green lines indicate activation. Dotted red line indicates GSK-3β inactivation through the PI3K/Akt pathway; dotted green line indicates that the precise mechanism of activation of the Wnt/ β-catenin signaling remains elusive. Some of the drugs (see text for details) have shown to induce the expression of target genes involved in Wnt-mediated induction of proliferation (Cyclin D1) and differentiation (Ngn2 and NeuroD1) in adult hippocampal neurogenesis. VPA, valproic acid; Se-Met, Selenomethionine; ETH, Ethosuximide; XAN, Xanthoceraside.

In addition, the biological trace element Selenomethionine (Se-Met) and Ethosuximide (ETH), which inactivate GSK-3β through the PI3K/Akt pathway, also promoted neurogenesis in AD models (Tiwari et al., 2015; Zheng et al., 2017). Together with the inactivation of GSK-3β, Se-Met increased β-catenin levels, induced the expression of Cyclin D1, and increased cell proliferation and neurogenesis in the hippocampus of a 3xTg AD mice (Zheng et al., 2017). On the other hand, treatment with the antiepileptic drug ETH, reversed cognitive dysfunction, and increased proliferation and neuronal differentiation in the dentate gyrus of a rat model of AD induced by the injection of Aβ (1-42) into the hippocampus (Tiwari et al., 2015). ETH prevented the Aβ-induced reduction in the expression of neurogenesis-related genes (including Ngn2 and NeuroD1), and Wnt signaling components, suggesting that the effects of ETH may be mediated by β-catenin signaling (Tiwari et al., 2015).

Curcumin, a natural polyphenol compound derived from turmeric (*Curcuma longa*), was also suggested to induced neurogenesis through the activation of Wnt/β-catenin signaling pathway. Curcumin encapsulated in PLGA nanoparticles induced NSC proliferation and neuronal differentiation in the hippocampus of an Aβ-induced rat model of AD, and reduced the cognitive deficits (Tiwari et al., 2014). Curcumin enhanced nuclear translocation of β-catenin, decreased GSK-3β levels, and increased promoter activity of Cyclin D1. In the hippocampus, curcumin enhanced the expression of Wnt3a, Dvl, FZD1 and LRP5/6, and the Wnt target genes Ngn2 and NeuroD1, and reduced the expression of the negative regulators of Wnt signaling WIF-1 and Dkk1. Interestingly, pharmacological and genetic inhibition of the Wnt pathway blocked the stimulation of neurogenesis mediated by curcumin, indicating that the effects of curcumin are mediated by activation of Wnt/β-catenin signaling.

Another natural product, Xanthoceraside (XAN), a triterpenoid saponin monomer extracted from the husks of *Xanthoceras sorbifolia Bunge,* ameliorated the cognitive impairment and concomitantly increased NSCs proliferation and neuronal differentiation in APPswe/PS1ΔE9 mice (Zhu et al., 2018). Interestingly, XAN treatment enhanced the expression of Wnt3a, increased the levels of inactive GSK-3β and induced nuclear translocation of β-catenin in the hippocampus of APP/PS1 mice, suggesting that XAN may promote neurogenesis by enhancing the Wnt/β-catenin signaling pathway (Zhu et al., 2018). Moreover, Dkk1 inhibited the effects of XAN in cultured NSC.

CONCLUDING REMARKS

The reviewed studies indicate that the Wnt signaling plays multiple roles in adult hippocampal neurogenesis including NPCs proliferation, fate-commitment, development and maturation of newborn neurons. Evidences suggest a stage-specific expression of particular receptors that might activate different Wnt signaling cascades to control the progression of neurogenesis. Although the role of the canonical Wnt co-receptor LRP6 support this notion, the role of other co-receptors that control the activation of non-canonical Wnt signaling remains to be elucidated. The identification of Wnt co-receptors involved in adult neurogenesis is a critical issue that should be addressed to gain a more comprehensive understanding of how canonical and non-canonical Wnt signaling are regulated during adult neurogenesis. In addition, it will be interesting to further study the downstream signaling components and effectors involved in the regulation of adult hippocampal neurogenesis by non-canonical Wnt signaling.

Several studies indicate that Wnt proteins released by hippocampal astrocytes and progenitor cells are crucial components of the SGZ niche. In addition, endogenous Wnt inhibitors are also components of the neurogenic microenvironment that dynamically regulate Wnt-mediated neurogenesis under physiological conditions. Considering the increasing number of Wnt regulators identified to date, it will be interesting to further investigate the contribution of these molecules to the dynamic control of neurogenesis.

In agreement with the critical roles of Wnt signaling in adult neurogenesis, evidence indicates that Wnt signaling is associated with the age-dependent decline in neurogenesis. Concomitantly with the decrease in the generation of new neurons, in normal aging there is a reduction in the expression of Wnt proteins, an increase in the expression of Wnt inhibitors, and a decrease in canonical Wnt signaling activity in the dentate gyrus. Wnt dysfunction might also underlie the impairment of neurogenesis observed in AD. Interestingly, genetic and pharmacological activation of Wnt signaling was shown to restore adult hippocampal neurogenesis, and also to improve cognitive performance in animal models of AD. Although it is not yet known how neurogenesis contribute to hippocampal function in humans, compelling evidence in animal models suggest that adult-born neurons are important for learning and memory, cognitive flexibility and mood regulation. In addition, recent findings support that neurogenesis impairment contributes to cognitive decline in aging and AD. Therefore, a better understanding on the molecular mechanisms involved in the regulation of neurogenesis may have important therapeutic implications. The reviewed evidence suggests that stimulation of Wnt signaling emerges as an attractive strategy to enhance endogenous neurogenesis and improve hippocampal-dependent cognitive function.

AUTHOR CONTRIBUTIONS

SBA, DV-B, and MDM wrote and revised the manuscript. LV-N, wrote, drafted, and edited the manuscript. All authors approved the final version as submitted.

FUNDING

This work was supported by FONDECYT N°1190461 to LV-N and CONICYT N° 21151115 to SBA.

ACKNOWLEDGMENTS

Graphic work was carried out by Felipe G. Serrano (www.illustrative-science.com).

REFERENCES

Abbott, A. C., Calderon Toledo, C., Aranguiz, F. C., Inestrosa, N. C., and Varela-Nallar, L. (2013). Tetrahydrohyperforin increases adult hippocampal neurogenesis in wild-type and APPswe/PS1DeltaE9 mice. *J. Alzheimers Dis.* 34, 873–885. doi: 10.3233/jad-121714

Aberle, H., Bauer, A., Stappert, J., Kispert, A., and Kemler, R. (1997). beta-catenin is a target for the ubiquitin-proteasome pathway. *EMBO J.* 16, 3797–3804. doi: 10.1093/emboj/16.13.3797

Aimone, J. B., Deng, W., and Gage, F. H. (2011). Resolving new memories: a critical look at the dentate gyrus, adult neurogenesis, and pattern separation. *Neuron* 70, 589–596. doi: 10.1016/j.neuron.2011.05.010

Alarcon, M. A., Medina, M. A., Hu, Q., Avila, M. E., Bustos, B. I., Perez-Palma, E., et al. (2013). A novel functional low-density lipoprotein receptor-related protein 6 gene alternative splice variant is associated with Alzheimer's disease. *Neurobiol. Aging* 34, e1709–e1718.

Anacker, C., and Hen, R. (2017). Adult hippocampal neurogenesis and cognitive flexibility - linking memory and mood. *Nat. Rev. Neurosci.* 18, 335–346. doi: 10.1038/nrn.2017.45

Arredondo, S. B., Guerrero, F. G., Herrera-Soto, A., Jensen-Flores, J., Bustamante, D. B., Onate-Ponce, A., et al. (2020). Wnt5a promotes differentiation and development of adult-born neurons in the hippocampus by noncanonical Wnt signaling. *Stem Cells* 38, 422–436. doi: 10.1002/stem.3121

Artegiani, B., and Calegari, F. (2012). Age-related cognitive decline: Can neural stem cells help us? *Aging* 4, 176–186. doi: 10.18632/aging.100446

Bafico, A., Liu, G., Yaniv, A., Gazit, A., and Aaronson, S. A. (2001). Novel mechanism of Wnt signalling inhibition mediated by Dickkopf-1 interaction with LRP6/Arrow. *Nat. Cell Biol.* 3, 683–686. doi: 10.1038/35083081

Bakker, A., Kirwan, C. B., Miller, M., and Stark, C. E. (2008). Pattern separation in the human hippocampal CA3 and dentate gyrus. *Science* 319, 1640–1642. doi: 10.1126/science.1152882

Ben Abdallah, N. M., Slomianka, L., Vyssotski, A. L., and Lipp, H. P. (2010). Early age-related changes in adult hippocampal neurogenesis in C57 mice. *Neurobiol. Aging* 31, 151–161. doi: 10.1016/j.neurobiolaging.2008.03.002

Bengoa-Vergniory, N., and Kypta, R. M. (2015). Canonical and noncanonical Wnt signaling in neural stem/progenitor cells. *Cell. Mol. Life Sci.* 72, 4157–4172. doi: 10.1007/s00018-015-2028-6

Bielen, H., and Houart, C. (2014). The Wnt cries many: Wnt regulation of neurogenesis through tissue patterning, proliferation, and asymmetric cell division. *Dev. Neurobiol.* 74, 772–780. doi: 10.1002/dneu.22168

Bilic, J., Huang, Y. L., Davidson, G., Zimmermann, T., Cruciat, C. M., Bienz, M., et al. (2007). Wnt induces LRP6 signalosomes and promotes dishevelled-dependent LRP6 phosphorylation. *Science* 316, 1619–1622. doi: 10.1126/science.1137065

Boldrini, M., Fulmore, C. A., Tartt, A. N., Simeon, L. R., Pavlova, I., Poposka, V., et al. (2018). Human hippocampal neurogenesis persists throughout aging. *Cell Stem Cell* 22, 589–599.e5. doi: 10.1016/j.stem.2018.03.015

Bonaguidi, M. A., Wheeler, M. A., Shapiro, J. S., Stadel, R. P., Sun, G. J., Ming, G. L., et al. (2011). *In vivo* clonal analysis reveals self-renewing and multipotent adult neural stem cell characteristics. *Cell* 145, 1142–1155. doi: 10.1016/j.cell.2011.05.024

Bovolenta, P., Rodriguez, J., and Esteve, P. (2006). Frizzled/RYK mediated signalling in axon guidance. *Development* 133, 4399–4408. doi: 10.1242/dev.02592

Brown, J. P., Couillard-Despres, S., Cooper-Kuhn, C. M., Winkler, J., Aigner, L., and Kuhn, H. G. (2003). Transient expression of doublecortin during adult neurogenesis. *J. Comp. Neurol.* 467, 1–10. doi: 10.1002/cne.10874

Buechling, T., Bartscherer, K., Ohkawara, B., Chaudhary, V., Spirohn, K., Niehrs, C., et al. (2010). Wnt/Frizzled signaling requires dPRR, the Drosophila homolog of the prorenin receptor. *Curr. Biol.* 20, 1263–1268. doi: 10.1016/j.cub.2010.05.028

Butler, M. T., and Wallingford, J. B. (2017). Planar cell polarity in development and disease. *Nat. Rev. Mol. Cell Biol.* 18, 375–388. doi: 10.1038/nrm.2017.11

Caricasole, A., Copani, A., Caraci, F., Aronica, E., Rozemuller, A. J., Caruso, A., et al. (2004). Induction of Dickkopf-1, a negative modulator of the Wnt pathway, is associated with neuronal degeneration in Alzheimer's brain. *J. Neurosci.* 24, 6021–6027. doi: 10.1523/jneurosci.1381-04.2004

Cheung, H. Y., Cheung, C. S., and Kong, C. K. (2001). Determination of bioactive diterpenoids from Andrographis paniculata by micellar electrokinetic chromatography. *J. Chromatogr. A* 930, 171–176. doi: 10.1016/s0021-9673(01)01160-8

Cho, C. H., Yoo, K. H., Oliveros, A., Paulson, S., Hussaini, S. M. Q., van Deursen, J. M., et al. (2019). sFRP3 inhibition improves age-related cellular changes in BubR1 progeroid mice. *Aging Cell* 18:e12899. doi: 10.1111/acel.12899

Choi, S. H., Bylykbashi, E., Chatila, Z. K., Lee, S. W., Pulli, B., Clemenson, G. D., et al. (2018). Combined adult neurogenesis and BDNF mimic exercise effects on cognition in an Alzheimer's mouse model. *Science* 361:eaan8821. doi: 10.1126/science.aan8821

Choi, S. H., and Tanzi, R. E. (2019). Is Alzheimer's disease a neurogenesis disorder? *Cell Stem Cell* 25, 7–8. doi: 10.1016/j.stem.2019.06.001

Cisternas, P., Oliva, C. A., Torres, V. I., Barrera, D. P., and Inestrosa, N. C. (2019). Presymptomatic treatment with andrographolide improves brain metabolic markers and cognitive behavior in a model of early-onset Alzheimer's disease. *Front. Cell. Neurosci.* 13:295. doi: 10.3389/fncel.2019.00295

Clevers, H., and Nusse, R. (2012). Wnt/beta-catenin signaling and disease. *Cell* 149, 1192–1205. doi: 10.1016/j.cell.2012.05.012

Cong, F., Schweizer, L., and Varmus, H. (2004). Wnt signals across the plasma membrane to activate the beta-catenin pathway by forming oligomers containing its receptors, Frizzled and LRP. *Development* 131, 5103–5115. doi: 10.1242/dev.01318

Coras, R., Siebzehnrubl, F. A., Pauli, E., Huttner, H. B., Njunting, M., Kobow, K., et al. (2010). Low proliferation and differentiation capacities of adult hippocampal stem cells correlate with memory dysfunction in humans. *Brain* 133, 3359–3372. doi: 10.1093/brain/awq215

Crews, L., Adame, A., Patrick, C., Delaney, A., Pham, E., Rockenstein, E., et al. (2010). Increased BMP6 levels in the brains of Alzheimer's disease patients and APP transgenic mice are accompanied by impaired neurogenesis. *J. Neurosci.* 30, 12252–12262. doi: 10.1523/jneurosci.1305-10.2010

Cruciat, C. M., and Niehrs, C. (2013). Secreted and transmembrane wnt inhibitors and activators. *Cold Spring Harb. Perspect. Biol.* 5:a015081. doi: 10.1101/cshperspect.a015081

Cui, X. P., Xing, Y., Chen, J. M., Dong, S. W., Ying, D. J., and Yew, D. T. (2011). Wnt/beta-catenin is involved in the proliferation of hippocampal neural stem cells induced by hypoxia. *Ir. J. Med. Sci.* 180, 387–393. doi: 10.1007/s11845-010-0566-3

Danielson, N. B., Kaifosh, P., Zaremba, J. D., Lovett-Barron, M., Tsai, J., Denny, C. A., et al. (2016). Distinct contribution of adult-born hippocampal granule cells to context encoding. *Neuron* 90, 101–112. doi: 10.1016/j.neuron.2016.02.019

De, A. (2011). Wnt/Ca2+ signaling pathway: a brief overview. *Acta Biochim. Biophys. Sin.* 43, 745–756. doi: 10.1093/abbs/gmr079

De Ferrari, G. V., Avila, M. E., Medina, M. A., Perez-Palma, E., Bustos, B. I., and Alarcon, M. A. (2014). Wnt/beta-catenin signaling in Alzheimer's disease. *CNS Neurol. Disord. Drug Targets* 13, 745–754. doi: 10.2174/1871527312666131223113900

De Ferrari, G. V., and Inestrosa, N. C. (2000). Wnt signaling function in Alzheimer's disease. *Brain Res. Brain Res. Rev.* 33, 1–12. doi: 10.1097/00002093-199501002-00001

De Ferrari, G. V., Papassotiropoulos, A., Biechele, T., Wavrant De-Vrieze, F., Avila, M. E., Major, M. B., et al. (2007). Common genetic variation within the low-density lipoprotein receptor-related protein 6 and late-onset Alzheimer's disease. *Proc. Natl. Acad. Sci. U.S.A.* 104, 9434–9439. doi: 10.1073/pnas.0603523104

Demars, M., Hu, Y. S., Gadadhar, A., and Lazarov, O. (2010). Impaired neurogenesis is an early event in the etiology of familial Alzheimer's disease in transgenic mice. *J. Neurosci. Res.* 88, 2103–2117. doi: 10.1002/jnr.22387

Deng, W., Aimone, J. B., and Gage, F. H. (2010). New neurons and new memories: How does adult hippocampal neurogenesis affect learning and memory? *Nat. Rev. Neurosci.* 11, 339–350. doi: 10.1038/nrn2822

Dennis, C. V., Suh, L. S., Rodriguez, M. L., Kril, J. J., and Sutherland, G. T. (2016). Human adult neurogenesis across the ages: an immunohistochemical study. *Neuropathol. Appl. Neurobiol.* 42, 621–638. doi: 10.1111/nan.12337

Denny, C. A., Burghardt, N. S., Schachter, D. M., Hen, R., and Drew, M. R. (2012). 4- to 6-week-old adult-born hippocampal neurons influence novelty-evoked exploration and contextual fear conditioning. *Hippocampus* 22, 1188–1201. doi: 10.1002/hipo.20964

Devenport, D. (2014). The cell biology of planar cell polarity. *J. Cell Biol.* 207, 171–179. doi: 10.1083/jcb.201408039

Donovan, M. H., Yazdani, U., Norris, R. D., Games, D., German, D. C., and Eisch, A. J. (2006). Decreased adult hippocampal neurogenesis in the PDAPP mouse model of Alzheimer's disease. *J. Comp. Neurol.* 495, 70–83. doi: 10.1002/cne.20840

Drew, L. J., Kheirbek, M. A., Luna, V. M., Denny, C. A., Cloidt, M. A., Wu, M. V., et al. (2016). Activation of local inhibitory circuits in the dentate gyrus by adult-born neurons. *Hippocampus* 26, 763–778. doi: 10.1002/hipo.22557

Ekonomou, A., Savva, G. M., Brayne, C., Forster, G., Francis, P. T., Johnson, M., et al. (2015). Stage-specific changes in neurogenic and glial markers in Alzheimer's disease. *Biol. Psychiatry* 77, 711–719. doi: 10.1016/j.biopsych.2014.05.021

Encinas, J. M., Michurina, T. V., Peunova, N., Park, J. H., Tordo, J., Peterson, D. A., et al. (2011). Division-coupled astrocytic differentiation and age-related depletion of neural stem cells in the adult hippocampus. *Cell Stem Cell* 8, 566–579. doi: 10.1016/j.stem.2011.03.010

Eriksson, P. S., Perfilieva, E., Bjork-Eriksson, T., Alborn, A. M., Nordborg, C., Peterson, D. A., et al. (1998). Neurogenesis in the adult human hippocampus. *Nat. Med.* 4, 1313–1317.

Faigle, R., and Song, H. (2013). Signaling mechanisms regulating adult neural stem cells and neurogenesis. *Biochim. Biophys. Acta* 1830, 2435–2448. doi: 10.1016/j.bbagen.2012.09.002

Fiorentini, A., Rosi, M. C., Grossi, C., Luccarini, I., and Casamenti, F. (2010). Lithium improves hippocampal neurogenesis, neuropathology and cognitive functions in APP mutant mice. *PLoS One* 5:e14382. doi: 10.1371/journal.pone.0014382

Folke, J., Pakkenberg, B., and Brudek, T. (2019). Impaired Wnt signaling in the prefrontal cortex of Alzheimer's disease. *Mol. Neurobiol.* 56, 873–891. doi: 10.1007/s12035-018-1103-z

Freese, J. L., Pino, D., and Pleasure, S. J. (2010). Wnt signaling in development and disease. *Neurobiol. Dis.* 38, 148–153.

Galan, L., Gomez-Pinedo, U., Guerrero, A., Garcia-Verdugo, J. M., and Matias-Guiu, J. (2017). Amyotrophic lateral sclerosis modifies progenitor neural proliferation in adult classic neurogenic brain niches. *BMC Neurol.* 17:173. doi: 10.1186/s12883-017-0956-5

Gao, B., Song, H., Bishop, K., Elliot, G., Garrett, L., English, M. A., et al. (2011). Wnt signaling gradients establish planar cell polarity by inducing Vangl2 phosphorylation through Ror2. *Dev. Cell* 20, 163–176. doi: 10.1016/j.devcel.2011.01.001

Gao, Z., Ure, K., Ables, J. L., Lagace, D. C., Nave, K. A., Goebbels, S., et al. (2009). Neurod1 is essential for the survival and maturation of adult-born neurons. *Nat. Neurosci.* 12, 1090–1092. doi: 10.1038/nn.2385

Garbe, D. S., and Ring, R. H. (2012). Investigating tonic Wnt signaling throughout the adult CNS and in the hippocampal neurogenic niche of BatGal and insTopGal mice. *Cell. Mol. Neurobiol.* 32, 1159–1174. doi: 10.1007/s10571-012-9841-3

Ge, S., Goh, E. L., Sailor, K. A., Kitabatake, Y., Ming, G. L., and Song, H. (2006). GABA regulates synaptic integration of newly generated neurons in the adult brain. *Nature* 439, 589–593. doi: 10.1038/nature04404

Goncalves, J. T., Bloyd, C. W., Shtrahman, M., Johnston, S. T., Schafer, S. T., Parylak, S. L., et al. (2016). *In vivo* imaging of dendritic pruning in dentate granule cells. *Nat. Neurosci.* 19, 788–791. doi: 10.1038/nn.4301

Gordon, M. D., and Nusse, R. (2006). Wnt signaling: multiple pathways, multiple receptors, and multiple transcription factors. *J. Biol. Chem.* 281, 22429–22433. doi: 10.1074/jbc.r600015200

Gould, E., Reeves, A. J., Fallah, M., Tanapat, P., Gross, C. G., and Fuchs, E. (1999). Hippocampal neurogenesis in adult Old World primates. *Proc. Natl. Acad. Sci. U.S.A.* 96, 5263–5267. doi: 10.1073/pnas.96.9.5263

Green, J., Nusse, R., and van Amerongen, R. (2014). The role of Ryk and Ror receptor tyrosine kinases in Wnt signal transduction. *Cold Spring Harb. Perspect. Biol.* 6:a009175. doi: 10.1101/cshperspect.a009175

Grumolato, L., Liu, G., Mong, P., Mudbhary, R., Biswas, R., Arroyave, R., et al. (2010). Canonical and noncanonical Wnts use a common mechanism to activate completely unrelated coreceptors. *Genes Dev.* 24, 2517–2530. doi: 10.1101/gad.1957710

Gu, Y., Arruda-Carvalho, M., Wang, J., Janoschka, S. R., Josselyn, S. A., Frankland, P. W., et al. (2012). Optical controlling reveals time-dependent roles for adult-born dentate granule cells. *Nat. Neurosci.* 15, 1700–1706. doi: 10.1038/nn.3260

Hamilton, L. K., Aumont, A., Julien, C., Vadnais, A., Calon, F., and Fernandes, K. J. (2010). Widespread deficits in adult neurogenesis precede plaque and tangle formation in the 3xTg mouse model of Alzheimer's disease. *Eur. J. Neurosci.* 32, 905–920. doi: 10.1111/j.1460-9568.2010.07379.x

Hattiangady, B., and Shetty, A. K. (2008). Aging does not alter the number or phenotype of putative stem/progenitor cells in the neurogenic region of the hippocampus. *Neurobiol. Aging* 29, 129–147. doi: 10.1016/j.neurobiolaging.2006.09.015

Heppt, J., Wittmann, M.-T., Zhang, J., Vogt-Weisenhorn, D., Prakash, N., Wurst, W., et al. (2020). Canonical Wnt-signaling modulates the tempo of dendritic growth of adult-born hippocampal neurons. *bioRxiv* [Preprint]. doi: 10.1101/2020.01.14.905919

Hermle, T., Guida, M. C., Beck, S., Helmstadter, S., and Simons, M. (2013). Drosophila ATP6AP2/VhaPRR functions both as a novel planar cell polarity core protein and a regulator of endosomal trafficking. *EMBO J.* 32, 245–259. doi: 10.1038/emboj.2012.323

Hollands, C., Bartolotti, N., and Lazarov, O. (2016). Alzheimer's disease and hippocampal adult neurogenesis; exploring shared mechanisms. *Front. Neurosci.* 10:178. doi: 10.3389/fnins.2016.00178

Hsieh, J., Nakashima, K., Kuwabara, T., Mejia, E., and Gage, F. H. (2004). Histone deacetylase inhibition-mediated neuronal differentiation of multipotent adult neural progenitor cells. *Proc. Natl. Acad. Sci. U.S.A.* 101, 16659–16664. doi: 10.1073/pnas.0407643101

Hsieh, J. C., Kodjabachian, L., Rebbert, M. L., Rattner, A., Smallwood, P. M., Samos, C. H., et al. (1999). A new secreted protein that binds to Wnt proteins and inhibits their activities. *Nature* 398, 431–436. doi: 10.1038/18899

Hu, Y. S., Xu, P., Pigino, G., Brady, S. T., Larson, J., and Lazarov, O. (2010). Complex environment experience rescues impaired neurogenesis, enhances synaptic plasticity, and attenuates neuropathology in familial Alzheimer's disease-linked APPswe/PS1DeltaE9 mice. *FASEB J.* 24, 1667–1681. doi: 10.1096/fj.09-136945

Huang, H. C., and Klein, P. S. (2004). The Frizzled family: receptors for multiple signal transduction pathways. *Genome Biol.* 5:234. doi: 10.1186/gb-2004-5-7-234

Humphries, C. E., Kohli, M. A., Nathanson, L., Whitehead, P., Beecham, G., Martin, E., et al. (2015). Integrated whole transcriptome and DNA methylation analysis identifies gene networks specific to late-onset Alzheimer's disease. *J. Alzheimers Dis.* 44, 977–987. doi: 10.3233/JAD-141989

Inestrosa, N. C., and Varela-Nallar, L. (2014). Wnt signaling in the nervous system and in Alzheimer's disease. *J. Mol. Cell Biol.* 6, 64–74. doi: 10.1093/jmcb/mjt051

Inestrosa, N. C., and Varela-Nallar, L. (2015). Wnt signalling in neuronal differentiation and development. *Cell Tissue Res.* 359, 215–223. doi: 10.1007/s00441-014-1996-4

Ishitani, T., Kishida, S., Hyodo-Miura, J., Ueno, N., Yasuda, J., Waterman, M., et al. (2003). The TAK1-NLK mitogen-activated protein kinase cascade functions in the Wnt-5a/Ca(2+) pathway to antagonize Wnt/beta-catenin signaling. *Mol. Cell. Biol.* 23, 131–139. doi: 10.1128/mcb.23.1.131-139.2003

Israsena, N., Hu, M., Fu, W., Kan, L., and Kessler, J. A. (2004). The presence of FGF2 signaling determines whether beta-catenin exerts effects on proliferation or neuronal differentiation of neural stem cells. *Dev. Biol.* 268, 220–231. doi: 10.1016/j.ydbio.2003.12.024

Jackstadt, R., Hodder, M. C., and Sansom, O. J. (2020). WNT and β-catenin in cancer: genes and therapy. *Annu. Rev. Cancer Biol.* 4, 177–196.

Jang, M. H., Bonaguidi, M. A., Kitabatake, Y., Sun, J., Song, J., Kang, E., et al. (2013). Secreted frizzled-related protein 3 regulates activity-dependent adult hippocampal neurogenesis. *Cell Stem Cell* 12, 215–223. doi: 10.1016/j.stem.2012.11.021

Jones, C., and Chen, P. (2007). Planar cell polarity signaling in vertebrates. *Bioessays* 29, 120–132. doi: 10.1002/bies.20526

Kalamakis, G., Brune, D., Ravichandran, S., Bolz, J., Fan, W., Ziebell, F., et al. (2019). Quiescence modulates stem cell maintenance and regenerative capacity in the aging brain. *Cell* 176, 1407–1419.e14. doi: 10.1016/j.cell.2019.01.040

Karalay, O., Doberauer, K., Vadodaria, K. C., Knobloch, M., Berti, L., Miquelajauregui, A., et al. (2011). Prospero-related homeobox 1 gene (Prox1) is regulated by canonical Wnt signaling and has a stage-specific role in adult hippocampal neurogenesis. *Proc. Natl. Acad. Sci. U.S.A.* 108, 5807–5812. doi: 10.1073/pnas.1013456108

Kase, Y., Otsu, K., Shimazaki, T., and Okano, H. (2019). Involvement of p38 in age-related decline in adult neurogenesis via modulation of Wnt signaling. *Stem Cell Rep.* 12, 1313–1328. doi: 10.1016/j.stemcr.2019.04.010

Kempermann, G., Jessberger, S., Steiner, B., and Kronenberg, G. (2004). Milestones of neuronal development in the adult hippocampus. *Trends Neurosci.* 27, 447–452. doi: 10.1016/j.tins.2004.05.013

Knoth, R., Singec, I., Ditter, M., Pantazis, G., Capetian, P., Meyer, R. P., et al. (2010). Murine features of neurogenesis in the human hippocampus across the lifespan from 0 to 100 years. *PLoS One* 5:e8809. doi: 10.1371/journal.pone.0008809

Kohler, S. J., Williams, N. I., Stanton, G. B., Cameron, J. L., and Greenough, W. T. (2011). Maturation time of new granule cells in the dentate gyrus of adult macaque monkeys exceeds six months. *Proc. Natl. Acad. Sci. U.S.A.* 108, 10326–10331. doi: 10.1073/pnas.1017099108

Kohn, A. D., and Moon, R. T. (2005). Wnt and calcium signaling: beta-catenin-independent pathways. *Cell Calcium* 38, 439–446. doi: 10.1016/j.ceca.2005.06.022

Koval, A., and Katanaev, V. L. (2011). Wnt3a stimulation elicits G-protein-coupled receptor properties of mammalian Frizzled proteins. *Biochem. J.* 433, 435–440. doi: 10.1042/BJ20101878

Kronenberg, G., Reuter, K., Steiner, B., Brandt, M. D., Jessberger, S., Yamaguchi, M., et al. (2003). Subpopulations of proliferating cells of the adult hippocampus respond differently to physiologic neurogenic stimuli. *J. Comp. Neurol.* 467, 455–463. doi: 10.1002/cne.10945

Kuhl, M., Sheldahl, L. C., Malbon, C. C., and Moon, R. T. (2000a). Ca(2+)/calmodulin-dependent protein kinase II is stimulated by Wnt and Frizzled homologs and promotes ventral cell fates in Xenopus. *J. Biol. Chem.* 275, 12701–12711. doi: 10.1074/jbc.275.17.12701

Kuhl, M., Sheldahl, L. C., Park, M., Miller, J. R., and Moon, R. T. (2000b). The Wnt/Ca2+ pathway: a new vertebrate Wnt signaling pathway takes shape. *Trends Genet.* 16, 279–283. doi: 10.1016/s0168-9525(00)02028-x

Kuhn, H. G., Dickinson-Anson, H., and Gage, F. H. (1996). Neurogenesis in the dentate gyrus of the adult rat: age-related decrease of neuronal progenitor proliferation. *J. Neurosci.* 16, 2027–2033. doi: 10.1523/JNEUROSCI.16-06-02027.1996

Kuwabara, T., Hsieh, J., Muotri, A., Yeo, G., Warashina, M., Lie, D. C., et al. (2009). Wnt-mediated activation of NeuroD1 and retro-elements during adult neurogenesis. *Nat. Neurosci.* 12, 1097–1105. doi: 10.1038/nn.2360

Lacefield, C. O., Itskov, V., Reardon, T., Hen, R., and Gordon, J. A. (2012). Effects of adult-generated granule cells on coordinated network activity in the dentate gyrus. *Hippocampus* 22, 106–116. doi: 10.1002/hipo.20860

Lavado, A., Lagutin, O. V., Chow, L. M., Baker, S. J., and Oliver, G. (2010). Prox1 is required for granule cell maturation and intermediate progenitor maintenance during brain neurogenesis. *PLoS Biol.* 8:e1000460. doi: 10.1371/journal.pbio.1000460

Lazarov, O., and Hollands, C. (2016). Hippocampal neurogenesis: Learning to remember. *Prog. Neurobiol.* 138-140, 1–18. doi: 10.1016/j.pneurobio.2015.12.006

Leuner, B., Kozorovitskiy, Y., Gross, C. G., and Gould, E. (2007). Diminished adult neurogenesis in the marmoset brain precedes old age. *Proc. Natl. Acad. Sci. U.S.A.* 104, 17169–17173. doi: 10.1073/pnas.0708228104

Li, B., Yamamori, H., Tatebayashi, Y., Shafit-Zagardo, B., Tanimukai, H., Chen, S., et al. (2008). Failure of neuronal maturation in Alzheimer disease dentate gyrus. *J. Neuropathol. Exp. Neurol.* 67, 78–84. doi: 10.1097/nen.0b013e318160c5db

Lie, D. C., Colamarino, S. A., Song, H. J., Desire, L., Mira, H., Consiglio, A., et al. (2005). Wnt signalling regulates adult hippocampal neurogenesis. *Nature* 437, 1370–1375. doi: 10.1038/nature04108

Logan, C. Y., and Nusse, R. (2004). The Wnt signaling pathway in development and disease. *Annu. Rev. Cell Dev. Biol.* 20, 781–810. doi: 10.1146/annurev.cellbio.20.010403.113126

Lucassen, P. J., Stumpel, M. W., Wang, Q., and Aronica, E. (2010). Decreased numbers of progenitor cells but no response to antidepressant drugs in the hippocampus of elderly depressed patients. *Neuropharmacology* 58, 940–949. doi: 10.1016/j.neuropharm.2010.01.012

MacDonald, B. T., Tamai, K., and He, X. (2009). Wnt/beta-catenin signaling: components, mechanisms, and diseases. *Dev. Cell* 17, 9–26. doi: /10.1016/j.devcel.2009.06.016

Mardones, M. D., Andaur, G. A., Varas-Godoy, M., Henriquez, J. F., Salech, F., Behrens, M. I., et al. (2016). Frizzled-1 receptor regulates adult hippocampal neurogenesis. *Mol. Brain* 9:29. doi: 10.1186/s13041-016-0209-3

Marin-Burgin, A., Mongiat, L. A., Pardi, M. B., and Schinder, A. F. (2012). Unique processing during a period of high excitation/inhibition balance in adult-born neurons. *Science* 335, 1238–1242. doi: 10.1126/science.1214956

Mathews, K. J., Allen, K. M., Boerrigter, D., Ball, H., Shannon Weickert, C., and Double, K. L. (2017). Evidence for reduced neurogenesis in the aging human hippocampus despite stable stem cell markers. *Aging Cell* 16, 1195–1199. doi: 10.1111/acel.12641

Mentink, R. A., Rella, L., Radaszkiewicz, T. W., Gybel, T., Betist, M. C., Bryja, V., et al. (2018). The planar cell polarity protein VANG-1/Vangl negatively regulates Wnt/beta-catenin signaling through a Dvl dependent mechanism. *PLoS Genet.* 14:e1007840. doi: 10.1371/journal.pgen.1007840

Mikels, A. J., and Nusse, R. (2006). Purified Wnt5a protein activates or inhibits beta-catenin-TCF signaling depending on receptor context. *PLoS Biol.* 4:e115. doi: 10.1371/journal.pbio.0040115

Miranda, C. J., Braun, L., Jiang, Y., Hester, M. E., Zhang, L., Riolo, M., et al. (2012). Aging brain microenvironment decreases hippocampal neurogenesis through Wnt-mediated survivin signaling. *Aging Cell* 11, 542–552. doi: 10.1111/j.1474-9726.2012.00816.x

Moreno-Jimenez, E. P., Flor-Garcia, M., Terreros-Roncal, J., Rabano, A., Cafini, F., Pallas-Bazarra, N., et al. (2019). Adult hippocampal neurogenesis is abundant in neurologically healthy subjects and drops sharply in patients with Alzheimer's disease. *Nat. Med.* 25, 554–560. doi: 10.1038/s41591-019-0375-9

Nusse, R., and Varmus, H. E. (1982). Many tumors induced by the mouse mammary tumor virus contain a provirus integrated in the same region of the host genome. *Cell* 31, 99–109. doi: 10.1016/0092-8674(82)90409-3

O'Brien, R. J., and Wong, P. C. (2011). Amyloid precursor protein processing and Alzheimer's disease. *Annu. Rev. Neurosci.* 34, 185–204. doi: 10.1146/annurev-neuro-061010-113613

Okamoto, M., Inoue, K., Iwamura, H., Terashima, K., Soya, H., Asashima, M., et al. (2011). Reduction in paracrine Wnt3 factors during aging causes impaired adult neurogenesis. *FASEB J.* 25, 3570–3582. doi: 10.1096/fj.11-184697

Olariu, A., Cleaver, K. M., and Cameron, H. A. (2007). Decreased neurogenesis in aged rats results from loss of granule cell precursors without lengthening of the cell cycle. *J. Comp. Neurol.* 501, 659–667. doi: 10.1002/cne.21268

Oliva, C. A., Montecinos-Oliva, C., and Inestrosa, N. C. (2018). Wnt signaling in the central nervous system: new insights in health and disease. *Prog. Mol. Biol. Transl. Sci.* 153, 81–130. doi: 10.1016/bs.pmbts.2017.11.018

Ortiz-Matamoros, A., and Arias, C. (2019). Differential changes in the number and morphology of the new neurons after chronic infusion of Wnt7a, Wnt5a, and Dkk-1 in the adult hippocampus *in vivo*. *Anat. Rec.* 302, 1647–1657. doi: 10.1002/ar.24069

Panossian, A., Hovhannisyan, A., Mamikonyan, G., Abrahamian, H., Hambardzumyan, E., Gabrielian, E., et al. (2000). Pharmacokinetic and oral bioavailability of andrographolide from Andrographis paniculata fixed combination Kan Jang in rats and human. *Phytomedicine* 7, 351–364. doi: 10.1016/S0944-7113(00)80054-9

Qu, Q., Sun, G., Murai, K., Ye, P., Li, W., Asuelime, G., et al. (2013). Wnt7a regulates multiple steps of neurogenesis. *Mol. Cell. Biol.* 33, 2551–2559. doi: 10.1128/MCB.00325-13

Rattner, A., Hsieh, J. C., Smallwood, P. M., Gilbert, D. J., Copeland, N. G., Jenkins, N. A., et al. (1997). A family of secreted proteins contains homology to the cysteine-rich ligand-binding domain of frizzled receptors. *Proc. Natl. Acad. Sci. U.S.A.* 94, 2859–2863. doi: 10.1073/pnas.94.7.2859

Richetin, K., Leclerc, C., Toni, N., Gallopin, T., Pech, S., Roybon, L., et al. (2015). Genetic manipulation of adult-born hippocampal neurons rescues memory in a mouse model of Alzheimer's disease. *Brain* 138, 440–455. doi: 10.1093/brain/awu354

Riise, J., Plath, N., Pakkenberg, B., and Parachikova, A. (2015). Aberrant Wnt signaling pathway in medial temporal lobe structures of Alzheimer's disease. *J. Neural Transm.* 122, 1303–1318. doi: 10.1007/s00702-015-1375-7

Rios-Esteves, J., Haugen, B., and Resh, M. D. (2014). Identification of key residues and regions important for porcupine-mediated Wnt acylation. *J. Biol. Chem.* 289, 17009–17019. doi: 10.1074/jbc.M114.561209

Rios-Esteves, J., and Resh, M. D. (2013). Stearoyl CoA desaturase is required to produce active, lipid-modified Wnt proteins. *Cell Rep.* 4, 1072–1081. doi: 10.1016/j.celrep.2013.08.027

Rodriguez, J. J., Jones, V. C., Tabuchi, M., Allan, S. M., Knight, E. M., LaFerla, F. M., et al. (2008). Impaired adult neurogenesis in the dentate gyrus of a triple transgenic mouse model of Alzheimer's disease. *PLoS One* 3:e2935. doi: 10.1371/journal.pone.0002935

Rodriguez, J. J., Noristani, H. N., Olabarria, M., Fletcher, J., Somerville, T. D., Yeh, C. Y., et al. (2011). Voluntary running and environmental enrichment restores impaired hippocampal neurogenesis in a triple transgenic mouse model of Alzheimer's disease. *Curr. Alzheimer Res.* 8, 707–717. doi: 10.2174/156720511797633214

Rosi, M. C., Luccarini, I., Grossi, C., Fiorentini, A., Spillantini, M. G., Prisco, A., et al. (2010). Increased Dickkopf-1 expression in transgenic mouse models of neurodegenerative disease. *J. Neurochem.* 112, 1539–1551. doi: 10.1111/j.1471-4159.2009.06566.x

Roy, N. S., Wang, S., Jiang, L., Kang, J., Benraiss, A., Harrison-Restelli, C., et al. (2000). In vitro neurogenesis by progenitor cells isolated from the adult human hippocampus. *Nat. Med.* 6, 271–277. doi: 10.1038/73119

Saneyoshi, T., Kume, S., Amasaki, Y., and Mikoshiba, K. (2002). The Wnt/calcium pathway activates NF-AT and promotes ventral cell fate in Xenopus embryos. *Nature* 417, 295–299. doi: 10.1038/417295a

Sato, A., Yamamoto, H., Sakane, H., Koyama, H., and Kikuchi, A. (2010). Wnt5a regulates distinct signalling pathways by binding to Frizzled2. *EMBO J.* 29, 41–54. doi: 10.1038/emboj.2009.322

Schafer, S. T., Han, J., Pena, M., von Bohlen Und Halbach, O., Peters, J., and Gage, F. H. (2015). The Wnt Adaptor Protein ATP6AP2 regulates multiple

stages of adult hippocampal neurogenesis. *J. Neurosci.* 35, 4983–4998. doi: 10.1523/JNEUROSCI.4130-14.2015

Schulte, G. (2010). International Union of Basic and Clinical Pharmacology. LXXX. The class Frizzled receptors. *Pharmacol. Rev.* 62, 632–667. doi: 10.1124/pr.110.002931

Schwarz, T. J., Ebert, B., and Lie, D. C. (2012). Stem cell maintenance in the adult mammalian hippocampus: a matter of signal integration? *Dev. Neurobiol.* 72, 1006–1015. doi: 10.1002/dneu.22026

Seib, D. R., Corsini, N. S., Ellwanger, K., Plaas, C., Mateos, A., Pitzer, C., et al. (2013). Loss of Dickkopf-1 restores neurogenesis in old age and counteracts cognitive decline. *Cell Stem Cell.* 12, 204–214. doi: 10.1016/j.stem.2012.11.010

Seib, D. R., and Martin-Villalba, A. (2015). Neurogenesis in the normal ageing hippocampus: a mini-review. *Gerontology* 61, 327–335. doi: 10.1159/000368575

Selkoe, D. J., and Hardy, J. (2016). The amyloid hypothesis of Alzheimer's disease at 25 years. *EMBO Mol. Med.* 8, 595–608. doi: 10.15252/emmm.201606210

Semenov, M., Tamai, K., and He, X. (2005). SOST is a ligand for LRP5/LRP6 and a Wnt signaling inhibitor. *J. Biol. Chem.* 280, 26770–26775. doi: 10.1074/jbc.M504308200

Serafino, A., Giovannini, D., Rossi, S., and Cozzolino, M. (2020). Targeting the Wnt/beta-catenin pathway in neurodegenerative diseases: recent approaches and current challenges. *Expert Opin. Drug Discov.* 15, 803–822. doi: 10.1080/17460441.2020.1746266

Serrano, F. G., Tapia-Rojas, C., Carvajal, F. J., Hancke, J., Cerpa, W., and Inestrosa, N. C. (2014). Andrographolide reduces cognitive impairment in young and mature AbetaPPswe/PS-1 mice. *Mol. Neurodegener.* 9:61. doi: 10.1186/1750-1326-9-61

Sheldahl, L. C., Park, M., Malbon, C. C., and Moon, R. T. (1999). Protein kinase C is differentially stimulated by Wnt and Frizzled homologs in a G-protein-dependent manner. *Curr. Biol.* 9, 695–698. doi: 10.1016/S0960-9822(99)80310-8

Shruster, A., and Offen, D. (2014). Targeting neurogenesis ameliorates danger assessment in a mouse model of Alzheimer's disease. *Behav. Brain Res.* 261, 193–201. doi: 10.1016/j.bbr.2013.12.028

Shtutman, M., Zhurinsky, J., Simcha, I., Albanese, C., D'Amico, M., Pestell, R., et al. (1999). The cyclin D1 gene is a target of the beta-catenin/LEF-1 pathway. *Proc. Natl. Acad. Sci. U.S.A.* 96, 5522–5527. doi: 10.1073/pnas.96.10.5522

Snyder, J. S., Kee, N., and Wojtowicz, J. M. (2001). Effects of adult neurogenesis on synaptic plasticity in the rat dentate gyrus. *J. Neurophysiol.* 85, 2423–2431. doi: 10.1152/jn.2001.85.6.2423

Sorrells, S. F., Paredes, M. F., Cebrian-Silla, A., Sandoval, K., Qi, D., Kelley, K. W., et al. (2018). Human hippocampal neurogenesis drops sharply in children to undetectable levels in adults. *Nature* 555, 377–381. doi: 10.1038/nature25975

Spalding, K. L., Bergmann, O., Alkass, K., Bernard, S., Salehpour, M., Huttner, H. B., et al. (2013). Dynamics of hippocampal neurogenesis in adult humans. *Cell* 153, 1219–1227. doi: 10.1016/j.cell.2013.05.002

Suh, H., Deng, W., and Gage, F. H. (2009). Signaling in adult neurogenesis. *Annu. Rev. Cell Dev. Biol.* 25, 253–275. doi: 10.1146/annurev.cellbio.042308.113256

Sun, J., Bonaguidi, M. A., Jun, H., Guo, J. U., Sun, G. J., Will, B., et al. (2015). A septo-temporal molecular gradient of sfrp3 in the dentate gyrus differentially regulates quiescent adult hippocampal neural stem cell activation. *Mol. Brain* 8:52. doi: 10.1186/s13041-015-0143-9

Tapia, J. C., Torres, V. A., Rodriguez, D. A., Leyton, L., and Quest, A. F. (2006). Casein kinase 2 (CK2) increases survivin expression via enhanced beta-catenin-T cell factor/lymphoid enhancer binding factor-dependent transcription. *Proc. Natl. Acad. Sci. U.S.A.* 103, 15079–15084. doi: 10.1073/pnas.0606845103

Tapia-Rojas, C., Aranguiz, F., Varela-Nallar, L., and Inestrosa, N. C. (2016). Voluntary running attenuates memory loss, decreases neuropathological changes and induces neurogenesis in a mouse model of Alzheimer's disease. *Brain Pathol.* 26, 62–74. doi: 10.1111/bpa.12255

Tapia-Rojas, C., Schuller, A., Lindsay, C. B., Ureta, R. C., Mejias-Reyes, C., Hancke, J., et al. (2015). Andrographolide activates the canonical Wnt signalling pathway by a mechanism that implicates the non-ATP competitive inhibition of GSK-3beta: autoregulation of GSK-3beta *in vivo*. *Biochem. J.* 466, 415–430. doi: 10.1042/BJ20140207

Tetsu, O., and McCormick, F. (1999). Beta-catenin regulates expression of cyclin D1 in colon carcinoma cells. *Nature* 398, 422–426. doi: 10.1038/18884

Tiwari, S. K., Agarwal, S., Seth, B., Yadav, A., Nair, S., Bhatnagar, P., et al. (2014). Curcumin-loaded nanoparticles potently induce adult neurogenesis and reverse cognitive deficits in Alzheimer's disease model via canonical Wnt/beta-catenin pathway. *ACS Nano* 8, 76–103. doi: 10.1021/nn405077y

Tiwari, S. K., Seth, B., Agarwal, S., Yadav, A., Karmakar, M., Gupta, S. K., et al. (2015). Ethosuximide Induces Hippocampal Neurogenesis and Reverses Cognitive Deficits in an Amyloid-beta Toxin-induced Alzheimer Rat Model via the Phosphatidylinositol 3-Kinase (PI3K)/Akt/Wnt/beta-Catenin Pathway. *J. Biol. Chem.* 290, 28540–28558. doi: 10.1074/jbc.M115.652586

Tobin, M. K., Musaraca, K., Disouky, A., Shetti, A., Bheri, A., Honer, W. G., et al. (2019). Human hippocampal neurogenesis persists in aged adults and Alzheimer's disease patients. *Cell Stem Cell.* 24, 974–982.e3. doi: 10.1016/j.stem.2019.05.003

Toda, T., and Gage, F. H. (2018). Review: adult neurogenesis contributes to hippocampal plasticity. *Cell Tissue Res.* 373, 693–709. doi: 10.1007/s00441-017-2735-4

Toda, T., Parylak, S. L., Linker, S. B., and Gage, F. H. (2019). The role of adult hippocampal neurogenesis in brain health and disease. *Mol. Psychiatry* 24, 67–87. doi: 10.1038/s41380-018-0036-2

Toni, N., and Schinder, A. F. (2015). Maturation and functional integration of new granule cells into the adult hippocampus. *Cold Spring Harb. Perspect. Biol.* 8:a018903. doi: 10.1101/cshperspect.a018903

Topol, L., Jiang, X., Choi, H., Garrett-Beal, L., Carolan, P. J., and Yang, Y. (2003). Wnt-5a inhibits the canonical Wnt pathway by promoting GSK-3-independent beta-catenin degradation. *J. Cell Biol.* 162, 899–908. doi: 10.1083/jcb.200303158

van Amerongen, R., Mikels, A., and Nusse, R. (2008). Alternative wnt signaling is initiated by distinct receptors. *Sci. Signal.* 1:re9. doi: 10.1126/scisignal.135re9

van Praag, H., Kempermann, G., and Gage, F. H. (1999). Running increases cell proliferation and neurogenesis in the adult mouse dentate gyrus. *Nat. Neurosci.* 2, 266–270. doi: 10.1038/6368

van Praag, H., Schinder, A. F., Christie, B. R., Toni, N., Palmer, T. D., and Gage, F. H. (2002). Functional neurogenesis in the adult hippocampus. *Nature* 415, 1030–1034. doi: 10.1038/4151030a

van Praag, H., Shubert, T., Zhao, C., and Gage, F. H. (2005). Exercise enhances learning and hippocampal neurogenesis in aged mice. *J. Neurosci.* 25, 8680–8685. doi: 10.1523/JNEUROSCI.1731-05.2005

Varela-Nallar, L., Arredondo, S. B., Tapia-Rojas, C., Hancke, J., and Inestrosa, N. C. (2015). Andrographolide stimulates neurogenesis in the adult hippocampus. *Neural Plast.* 2015:935403. doi: 10.1155/2015/935403

Varela-Nallar, L., and Inestrosa, N. C. (2013). Wnt signaling in the regulation of adult hippocampal neurogenesis. *Front. Cell. Neurosci.* 7:100. doi: 10.3389/fncel.2013.00100

Varela-Nallar, L., Rojas-Abalos, M., Abbott, A. C., Moya, E. A., Iturriaga, R., and Inestrosa, N. C. (2014). Chronic hypoxia induces the activation of the Wnt/beta-catenin signaling pathway and stimulates hippocampal neurogenesis in wild-type and APPswe-PS1DeltaE9 transgenic mice *in vivo*. *Front. Cell. Neurosci.* 8:17. doi: 10.3389/fncel.2014.00017

Wexler, E. M., Geschwind, D. H., and Palmer, T. D. (2008). Lithium regulates adult hippocampal progenitor development through canonical Wnt pathway activation. *Mol. Psychiatry* 13, 285–292. doi: 10.1038/sj.mp.4002093

Wexler, E. M., Paucer, A., Kornblum, H. I., Palmer, T. D., and Geschwind, D. H. (2009). Endogenous Wnt signaling maintains neural progenitor cell potency. *Stem Cells* 27, 1130–1141. doi: 10.1002/stem.36

Winner, B., and Winkler, J. (2015). Adult neurogenesis in neurodegenerative diseases. *Cold Spring Harb. Perspect. Biol.* 7:a021287. doi: 10.1101/cshperspect.a021287

Yang, Y., and Mlodzik, M. (2015). Wnt-Frizzled/planar cell polarity signaling: cellular orientation by facing the wind (Wnt). *Annu. Rev. Cell Dev. Biol.* 31, 623–646. doi: 10.1146/annurev-cellbio-100814-125315

Zeng, Q., Long, Z., Feng, M., Zhao, Y., Luo, S., Wang, K., et al. (2019). Valproic acid stimulates hippocampal neurogenesis via activating the Wnt/beta-catenin signaling pathway in the APP/PS1/Nestin-GFP triple transgenic mouse model of Alzheimer's disease. *Front. Aging Neurosci.* 11:62. doi: 10.3389/fnagi.2019.00062

Zeng, Q., Zheng, M., Zhang, T., and He, G. (2016). Hippocampal neurogenesis in the APP/PS1/nestin-GFP triple transgenic mouse model of Alzheimer's disease. *Neuroscience* 314, 64–74. doi: 10.1016/j.neuroscience.2015.11.054

Zeng, X., Tamai, K., Doble, B., Li, S., Huang, H., Habas, R., et al. (2005). A dual-kinase mechanism for Wnt co-receptor phosphorylation and activation. *Nature* 438, 873–877. doi: 10.1038/nature04185

Zhao, C., Teng, E. M., Summers, R. G. Jr., Ming, G. L., and Gage, F. H. (2006). Distinct morphological stages of dentate granule neuron maturation in the adult mouse hippocampus. *J. Neurosci.* 26, 3–11. doi: 10.1523/JNEUROSCI.3648-05.2006

Zheng, R., Zhang, Z. H., Chen, C., Chen, Y., Jia, S. Z., Liu, Q., et al. (2017). Selenomethionine promoted hippocampal neurogenesis via the PI3K-Akt-GSK3β-Wnt pathway in a mouse model of Alzheimer's disease. *Biochem. Biophys. Res. Commun.* 485, 6–15. doi: 10.1016/j.bbrc.2017.01.069

Zhu, L., Chi, T., Zhao, X., Yang, L., Song, S., Lu, Q., et al. (2018). Xanthoceraside modulates neurogenesis to ameliorate cognitive impairment in APP/PS1 transgenic mice. *J. Physiol. Sci.* 68, 555–565. doi: 10.1007/s12576-017-0561-9

Conflict of Interest: The authors declare that the research was conducted in the absence of any commercial or financial relationships that could be construed as a potential conflict of interest.

frontiers in Cell and Developmental Biology

ORIGINAL RESEARCH
published: 29 September 2020
doi: 10.3389/fcell.2020.561179

Celecoxib Exerts Neuroprotective Effects in β-Amyloid-Treated SH-SY5Y Cells Through the Regulation of Heme Oxygenase-1: Novel Insights for an Old Drug

*Emanuela Mhillaj[1], Massimiliano Papi[2,3], Fabiola Paciello[2,3], Andrea Silvestrini[2,4], Rolando Rolesi[2,5], Valentina Palmieri[2,3], Giordano Perini[2,3], Anna Rita Fetoni[2,5], Luigia Trabace[6] and Cesare Mancuso[1,2]**

[1] Department of Healthcare Surveillance and Bioethics, Section of Pharmacology, Università Cattolica del Sacro Cuore, Rome, Italy, [2] Fondazione Policlinico Universitario Agostino Gemelli IRCCS, Rome, Italy, [3] Department of Neuroscience, Università Cattolica del Sacro Cuore, Rome, Italy, [4] Department of Basic Biotechnological Sciences, Intensivological and Perioperative Clinics, Università Cattolica del Sacro Cuore, Rome, Italy, [5] Department of Head and Neck Surgery, Università Cattolica del Sacro Cuore, Rome, Italy, [6] Department of Clinical and Experimental Medicine, University of Foggia, Foggia, Italy

OPEN ACCESS

Edited by:
Efthimios M. C. Skoulakis, Alexander Fleming Biomedical Sciences Research Center, Greece

Reviewed by:
Juni Sarkar, University of Southern California, Los Angeles, United States
Vijay Rangachari, The University of Southern Mississippi, United States

***Correspondence:**
Cesare Mancuso
cesare.mancuso@unicatt.it

Specialty section:
This article was submitted to Molecular Medicine, a section of the journal Frontiers in Cell and Developmental Biology

Received: 11 May 2020
Accepted: 31 August 2020
Published: 29 September 2020

Citation:
Mhillaj E, Papi M, Paciello F, Silvestrini A, Rolesi R, Palmieri V, Perini G, Fetoni AR, Trabace L and Mancuso C (2020) Celecoxib Exerts Neuroprotective Effects in β-Amyloid-Treated SH-SY5Y Cells Through the Regulation of Heme Oxygenase-1: Novel Insights for an Old Drug. Front. Cell Dev. Biol. 8:561179. doi: 10.3389/fcell.2020.561179

The formation and aggregation of amyloid-β-peptide (Aβ) into soluble and insoluble species represent the pathological hallmarks of Alzheimer's disease (AD). Over the last few years, however, soluble Aβ (sAβ) prevailed over fibrillar Aβ (fAβ) as determinant of neurotoxicity. One of the main therapeutic strategies for challenging neurodegeneration is to fight against neuroinflammation and prevent free radical-induced damage: in this light, the heme oxygenase/biliverdin reductase (HO/BVR) system is considered a promising drug target. The aim of this work was to investigate whether or not celecoxib (CXB), a selective inhibitor of the pro-inflammatory cyclooxygenase-2, modulates the HO/BVR system and prevents lipid peroxidation in SH-SY5Y neuroblastoma cells. Both sAβ (6.25–50 nM) and fAβ (1.25–50 nM) dose-dependently over-expressed inducible HO (HO-1) after 24 h of incubation, reaching statistical significance at 25 and 6.25 nM, respectively. Interestingly, CXB (1–10 μM, for 1 h) further enhanced Aβ-induced HO-1 expression through the nuclear translocation of the transcriptional factor Nrf2. Furthermore, 10 μM CXB counteracted the Aβ-induced ROS production with a mechanism fully dependent on HO-1 up-regulation; nevertheless, 10 μM CXB significantly counteracted only 25 nM sAβ-induced lipid peroxidation damage in SH-SY5Y neurons by modulating HO-1. Both carbon monoxide (CORM-2, 50 nM) and bilirubin (50 nM) significantly prevented ROS production in Aβ-treated neurons and favored both the slowdown of the growth rate of Aβ oligomers and the decrease in oligomer/fibril final size. In conclusion, these results suggest a novel mechanism through which CXB is neuroprotective in subjects with early AD or mild cognitive impairment.

Keywords: Alzheimer's disease, amyloid-β-peptide, bilirubin, carbon monoxide, cyclooxygenase, heme oxygenase, reactive oxygen species

INTRODUCTION

Alzheimer's disease (AD) is a neurodegenerative disorder characterized by progressive cognitive impairment, memory loss, inability to perform daily activities, and is the leading cause of dementia. The deposition of both senile plaques and neurofibrillary tangles, formed by the aggregation of fibrillar amyloid-β-peptide (fAβ) and hyperphosphorylated tau protein, respectively, are considered the pathological hallmarks of AD (Hardy and Selkoe, 2002). However, due to recent preclinical and clinical discoveries, such as the lack of correlation between senile plaque deposition and cognitive impairment or the therapeutic failure of drugs whose mechanism of action was aimed to reduce Aβ deposition or to increase its clearance, the involvement of fAβ in brain damage has been heavily questioned (Graham et al., 2017). Thus, significant research in the last decade has advanced a novel hypothesis that highlights the role of soluble forms of Aβ (sAβ), including the soluble oligomers produced during Aβ aggregation, as determinants of neurotoxicity (Selkoe and Hardy, 2016; Mhillaj et al., 2017). In this regard, a strong association has been shown between abnormal cerebral levels of sAβ forms and loss of synaptic plasticity (Wilcox et al., 2011; Park et al., 2013), inhibition of long-term potentiation (LTP) (Walsh et al., 2002), alteration of glutamatergic synapses (Green and LaFerla, 2008; Canas et al., 2014) and cognitive impairment (Tucci et al., 2014; Balducci et al., 2016; Mhillaj et al., 2018b). As far as the molecular mechanisms involved in AD, the strong and long-lasting neuroinflammatory response, together with the abnormal formation of reactive oxygen species and reactive nitrogen species (ROS and RNS, respectively), has been reported to be responsible for the increasing neuronal death, mainly in brain cognitive areas (e.g., hippocampus and frontal cortex) (reviewed in Agostinho et al., 2010). Incidentally, cyclooxygenase-2 (COX-2), by producing both free radicals and neuroinflammatory prostaglandins, plays a main role in AD pathogenesis and the administration of non-steroidal antinflammatory drugs (NSAIDs), including COX-2 inhibitors, has been considered a prophylactic approach to reduce the risk to develop AD (Hoozemans and O'Banion, 2005; Minghetti, 2007).

Heme oxygenase (HO) is a microsomal enzyme exerting important physiological functions through the biological activities of its metabolites. HO transforms hemoprotein's heme moieties into ferrous iron, carbon monoxide (CO) and biliverdin (BV), this latter being further reduced into bilirubin (BR) by the cytosolic biliverdin reductase (BVR) (Maines, 1997). Two isoforms of HO have been identified, the first inducible (HO-1) under pro-oxidant conditions and the second constitutive (HO-2) involved in the physiologic turnover of heme (Maines, 1997). Over the last 25 years, several papers have been published demonstrating a marked induction of HO-1 in neurons and glial cells from AD brain and this phenomenon has been explained as an attempt of the neural tissue to react against oxidant/inflammatory damage by increasing the production of neuroprotectants, such as CO and BR (Schipper et al., 2006; Hettiarachchi et al., 2017; Nitti et al., 2018). Intriguingly, the over-expression of HO-1 has been also detected in lymphocytes and plasma from AD subjects, thus putting forth the hypothesis that HO-1 is a peripheral biomarker of AD (Calabrese et al., 2006; Di Domenico et al., 2012). Since HO-1 and BVR may undergo post-translational modifications in AD hippocampi which impair their enzymatic activities (Barone et al., 2011a,b, 2012b), a common strategy to preserve neuroprotection is to up-regulate HO-1 through the administration of some drugs (e.g., atorvastatin) or herb-derived antioxidants (e.g., ferulic acid, curcumin, rosmarinic acid, etc.) (Barone et al., 2012a; Butterfield et al., 2012; Catino et al., 2015; Fetoni et al., 2015; Mhillaj et al., 2018a, 2019). Although this huge amount of data, the vast majority of which obtained by analyzing *postmortem* brain specimens, only few papers have addressed the role played by sAβ or fAβ in the regulation of HO-1 and BVR with results not always comparable. Indeed, earliest studies did not focus on the differential effects of Aβ aggregation status, maybe because this issue was not considered interesting at that time.

On these premises, the first aim of this work is to fully characterize, by using a pharmacological approach, the differential regulation of the HO/BVR system by both sAβ and fAβ in the human neuroblastoma SH-SY5Y cells, a reliable experimental system widely used to study neurodegeneration and AD (Marrazzo et al., 2019; Wang et al., 2019; Celik et al., 2020). Furthermore, since *in vivo* data have shown that the COX-2 inhibitor celecoxib (CXB) reduces neuroinflammation and prevents cognitive impairment and behavioral abnormalities in sAβ-treated rats, the second aim of this work is to investigate whether or not CXB modulates the HO/BVR system in SH-SY5Y cells, thus widening the *spectrum* of its therapeutic activity.

MATERIALS AND METHODS

Chemicals

Celecoxib was purchased from Tocris (BioTechne, Milan, Italy) and 1 mM stock solutions were prepared in DMSO. Bilirubin and Zinc-protoporphyrin-IX (ZnPP-IX, Frontier Scientific, Logan, UT, United States) were dissolved in alkaline aqueous solution. Tricarbonyldichlororuthenium (II) (CORM-2, Sigma-Aldrich, Milan, Italy) was dissolved in DMSO at the stock solution of 10 mM.

Aβ Preparation and Aggregation Analysis

The $A\beta_{1-42}$ peptide (hereafter referred to as Aβ) was purchased from Tocris (BioTechne, Milan, Italy). The soluble form of Aβ (sAβ) was obtained by dissolving the peptide in sterile distilled water at the concentration of 4 μM. For the fibrillary form (fAβ), the peptide was firstly dissolved in 100% hexafluoroisopropanol (HFIP) at the concentration of 4 μM and the solution evaporated to obtain the peptide film, as previously described (Stine et al., 2011). Then, the Aβ film was resuspended in DMSO, sonicated, diluted in 10 mM HCl and incubated at 37°C for 24 h.

For aggregation analysis, Aβ solutions were freshly prepared before each experiment by diluting either sAβ or fAβ in cell culture medium (see below) at the final concentrations of 25 nM and 6.25 nM, respectively; in selected experiments, both sAβ and fAβ were exposed to either 10 μM CXB or 50 nM BR or 50 nM CORM-2. Each sample was incubated at 37°C for 24 h under

quiescent conditions and no significant changes in the pH of the solutions were detected over time. Residual DMSO from CXB or CORM-2 stock solutions did not interfere with Aβ aggregation.

Aβ aggregation status was structurally characterized by dynamic light scattering (DLS) using Zetasizer Nano ZS (Malvern, Herrenberg, Germany), as previously described (Palmieri et al., 2014). Solvent-resistant micro-cuvettes have been used for experiments using a fixed position (4.65 mm) with an automatic attenuator and at a controlled temperature (37°C). For each sample, 3 measurements were averaged.

Sample imaging was performed by atomic force microscopy (AFM), as previously described (Palmieri et al., 2017). Briefly, Aβ samples at fixed time points, were drop casted of fresh cleaved Mica disks and air dried. After sample preparation, measurements were immediately performed with a NanoWizard II AFM (JPK Instruments AG, Berlin, Germany) using silicon cantilevers with high aspect-ratio conical silicon tips (CSC36 Mikro-Masch, Tallinn, Estonia).

Cell Culture

SH-SY5Y neuroblastoma cells were provided through the courtesy of Prof. Randall N. Pittman (Department of Pharmacology, University of Pennsylvania, Philadelphia, PA, United States) and cultured in Minimum Eagle's Medium (MEM, Euroclone, Pero, Italy):F12 (Gibco, Life Tecnologies, Monza, Italy) supplemented with 1X non-essential aminoacids (Euroclone), 1 mM sodium pyruvate (Gibco), 1.5 g/L sodium bicarbonate, 1% penicillin/streptomycin (Euroclone) and 10% fetal calf serum (FCS, Euroclone), in a humidified incubator at 37°C and 5% CO_2.

The day before the experiment, 1.2×10^6 SH-SY5Y cells (10^{th}–14^{th} passage) were seeded in 6-multiwell plates at a density of 120,000 cells/cm^2. After overnight incubation, cells were treated with either sAβ (6.25–50 nM) or fAβ (1.56–50 nM) for 24 h. In another experimental setting, SH-SY5Y cells were treated with CXB (0.5–20 μM) for 1 h and then exposed to either cell culture medium or 25 nM sAβ or 6.25 nM fAβ for 24 h. To evaluate the effects of HO blockade, SH-SY5Y cells were treated with CXB plus sAβ or fAβ as above in the presence of ZnPP-IX (2.5 μM). Finally, in selected experiments, cells were incubated with either BR (50 nM) or CORM-2 (50 nM) for 6 h and then replaced with media containing sAβ (25 nM) or fAβ (6.25 nM) plus BR or CORM-2, for further 24 h. Drug dilutions were prepared in fresh culture medium immediately before performing the experiments. All the pharmacological manipulations were performed in triplicate. No significant changes in the pH of cell culture medium were detected after each treatment.

Western Blot

Both HO-1 and HO-2 and BVR and β-actin levels in SH-SY5Y cells were detected by Western Blot as previously described (Catino et al., 2015). An anti-HO-2 antibody (1:1000, Stressgen, Enzo Life Sciences, DBA Italia, Segrate, Milan, Italy) was used. An anti-β-actin rabbit monoclonal antibody (1:1000; Stressgen) was used to detect β-actin. Nitrocellulose membranes were stripped and then re-probed with the anti-β-actin antibody to confirm equal protein loading. The HO-1 or HO-2 or BVR/β-actin ratios were calculated and expressed as a percentage compared to the control group.

Immunofluorescence Analysis

Immunofluorescence for 4-hydroxynonenals (4-HNE) and nuclear factor erythroid 2-related factor 2 (Nrf2) have been performed as previously described (Catino et al., 2015). Briefly, 100,000 cells, seeded in glass coverslips (10 mm diameter), were fixed with 4% paraformaldehyde for 15 min at room temperature, permeated with 0.1% Triton-X for 15 min before being blocked in 0.3% BSA for 20 min. Samples were then incubated for 3 h with primary rabbit anti-4-HNE (Cat#HNE11-S, Alpha Diagnostic, Int., San Antonio, TX, United States) or mouse anti-Nrf2 (Abcam, Cambridge, MA, United States) antibody diluted 1:100 in 0.3% BSA in phosphate buffered saline (PBS). At the end of incubation, all samples were washed twice in PBS and incubated at room temperature for 90 min, light-protected, with secondary antibodies diluted 1:1000 in PBS. Goat anti-rabbit 488 (Alexa Fluor) was used for 4-HNE, whereas donkey anti-mouse 546 (Alexa Fluor) was used to detect Nrf2 labeling. Moreover, cell nuclei were counterstained with DAPI (1:1000 in PBS) for 10 min at room temperature, in a light-protected environment. Subsequently, the samples were coverslipped with an antifade medium (ProLong Gold; Invitrogen). Images (40×) were obtained with a confocal laser scanning system (Nikon Ti-E, Confocal Head A1 MP, Tokyo, Japan). A semi-quantitative analysis of fluorescence signals was quantified with ImageJ (version 1.51s); each evaluation was conducted on at least 15 fields randomly selected for each of the experimental conditions. Control experiments were performed by omitting the primary antibody during processing of tissue randomly selected across experimental groups (not shown).

ROS Detection

The intracellular ROS were detected by fluorescence using the 2,7-dichlorofluorescein diacetate (DCFDA) Cellular ROS Assay kit (Abcam, Cambridge, MA, United States), according to the manufacturer's instructions. Briefly, SH-SY5Y cells were seeded into 96-well plates at a cell density of 2.5×10^4 cells/well and allowed to attach overnight. The day of the experiment, cells were washed and incubated with a freshly prepared solution of DCFDA (25 μM) at 37°C for 45 min in the dark. Immediately after, cells were washed and then incubated in 8-replicates for each of the established experimental protocols described above. Fluorescence signal was measured, with a reading time of 1 s, in a microplate reader (Victor3, Perkin Elmer, United States) with precision at 485 nm $<$ 0.5% and temperature control at 37°C, set at an excitation wavelength of 485 nm and an emission wavelength of 535 nm. Data were expressed as percentage of control after background subtraction.

Statistical Analysis

Analysis of the data were obtained by Graph Pad® 6.0 software. Results are presented as mean ± standard error of the mean (SEM) of N replicates per group. Data sets have been analyzed by One-way ANOVA followed by a

Tukey's multiple comparison test. Differences were considered statistically significant at $P < 0.05$.

RESULTS

Effects of Aβ on the HO/BVR System in SH-SY5Y Human Neuroblastoma Cells

As shown in **Figures 1A,B**, sAβ (6.25–50 nM for 24 h) increased HO-1 expression and 25 nM was the lowest concentration reaching statistical significance (**Figure 1B**, One-way ANOVA followed by Tukey's test, $^{***}P < 0.001$ vs. C). Similarly, in a first set of experiments, the effect of fAβ on HO-1 expression was tested by using the same concentration-range and time of incubation used for sAβ (**Figures 1C,D**); however, by analyzing these data, a significant induction of HO-1 as low as 6.25 nM fAβ was detected (**Figure 1D**, One-way ANOVA followed by Tukey's test, $^{**}P < 0.01$ vs. C). This last result focused the attention on the possible effects of fAβ on HO-1 induction at concentrations lower than 6.25 nM and suggested widening the dose-range including lowest fAβ concentrations. Indeed, a dose-dependent increase in HO-1 expression as low as 1.56 nM fAβ was detected (**Figures 1E,F**), and this set of experiments confirmed 6.25 nM fAβ as the lowest concentration able to increase significantly HO-1 protein level (**Figure 1F**, One-way ANOVA followed by Tukey's test, $^{***}P < 0.001$ vs. C). With regard to HO-2 and BVR (**Figures 2A–H**), neither sAβ nor fAβ significantly modulated HO-2 expression, whereas only fAβ up-regulated BVR, reaching statistical significance at 12.5 nM (**Figure 2H**, One-way ANOVA followed by Tukey's test, $^{**}P < 0.01$ vs. C). The lowest effective concentrations of sAβ or fAβ for 24 h were used for further studies. It is noteworthy to mention that at time points shorter than 24 h of incubation, neither sAβ nor fAβ had any significant effect on HO-1, HO-2 and BVR protein expression (data not shown).

Effects of CXB on Aβ-Mediated HO/BVR System in SH-SY5Y Human Neuroblastoma Cells

As shown in **Figures 3A,B**, CXB (0.5–20 μM for 1 h) dose-dependently over-expressed HO-1 in SH-SY5Y neurons, reaching statistical significance at 10 μM (**Figure 3B**, One-way ANOVA followed by Tukey's test, $^{*}P < 0.05$ vs. C). As far as the effect of CXB on Aβ-induced HO-1, **Figures 3C–F**, show as CXB (0.5–10 μM) potentiated 25 nM sAβ- and 6.25 nM fAβ- induced HO-1 up-regulation, respectively, reaching statistical significance at 10 μM (**Figure 3D**, One-way ANOVA followed by Tukey's test, $^{**}P < 0.01$ vs. C, $^{\#}P < 0.05$ vs. sAβ; **Figure 3F**, One-way ANOVA followed by Tukey's test, $^{***}P < 0.001$ vs. C, $^{\#}P < 0.001$ vs. fAβ). As shown in **Figures 4A–D**, no significant modulation of HO-2 and BVR protein levels by CXB have been detected (**Figure 4B**, One-way ANOVA followed by Tukey's test $P = 0.095$; **Figure 4D**, One-way ANOVA followed by Tukey's test $P = 0.151$).

A common mechanism through which HO-1 exerts neuroprotective effects in several cell types, including SH-SY5Y neurons, is the nuclear translocation of the transcriptional inducer Nrf2 (Johnson and Johnson, 2015). Therefore, the next step was to study whether CXB favors the Nrf2 cytosol-to-nucleus translocation in SH-SY5Y neurons. As shown in **Figure 5**, in neurons exposed to sAβ or fAβ, a faint-to-moderate Nrf2 translocation into the nucleus was detected, although some signal was confined into the cytoplasm (panels B-b2 and D-d2). Moreover, CXB induced a strong Nrf2 translocation

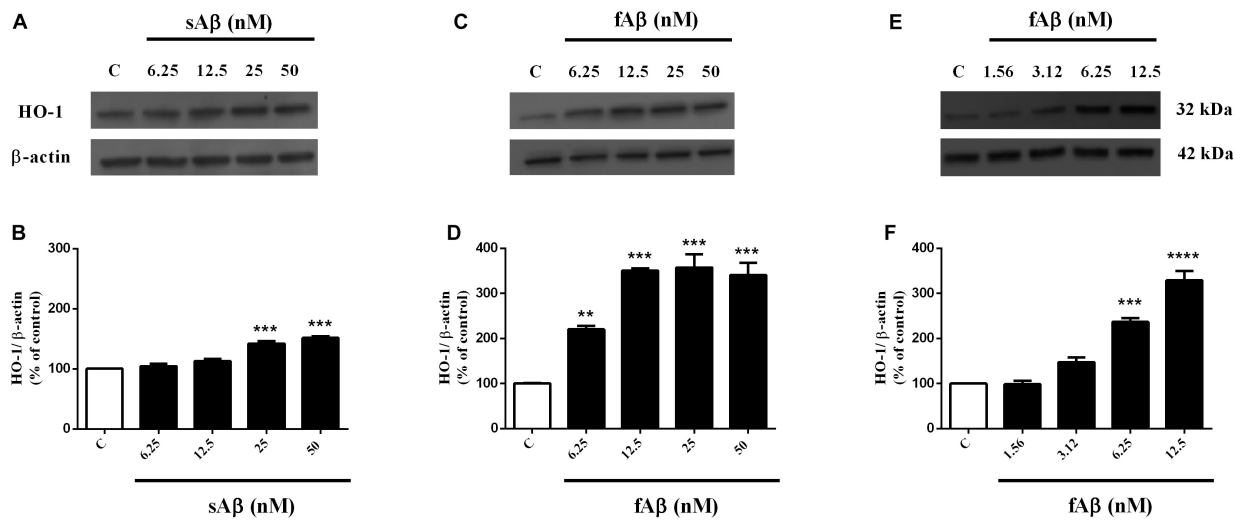

FIGURE 1 | Soluble and fibrillar Aβ (sAβ and fAβ, respectively) increase heme oxygenase-1 (HO-1) expression in SH-SY5Y neurons. SH-SY5Y cells were treated with sAβ (6.25–50 nM) and fAβ (1.56–50 nM) for 24 h and Western Blot was performed as described in Section "Materials and Methods." **(A,C,E)** Show representative gels regarding HO-1 protein expression following sAβ and fAβ treatment, as above. Bar graphs represent the quantification of HO-1 protein levels normalized for β-actin expression. Data are expressed as mean ± SEM of 3/4 replicates per group and analyzed by One-way ANOVA followed by Tukey's test: $^{***}P < 0.001$ vs. C **(B)**; $^{**}P < 0.01$ vs. C and $^{***}P < 0.001$ vs. C **(D)**; $^{***}P < 0.001$ vs. C and $^{****}P < 0.0001$ vs. C **(F)**. C, control.

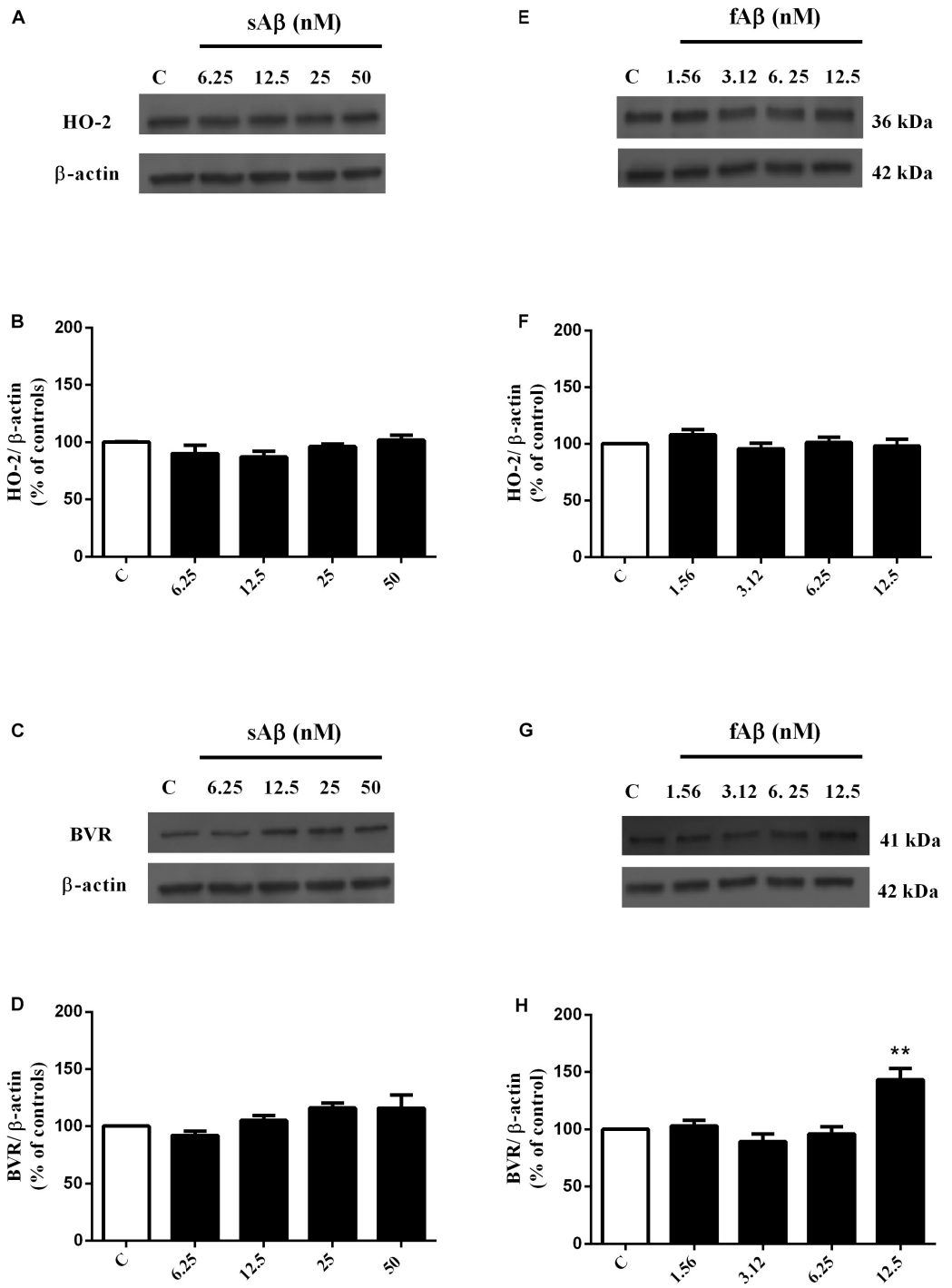

FIGURE 2 | Effects of soluble and fibrillar Aβ (sAβ and fAβ, respectively) on heme oxygenase-2 (HO-2) and biliverdin reductase (BVR) expression in SH-SY5Y neurons. SH-SY5Y cells were treated with sAβ (6.25–50 nM) and fAβ (6.25–50 nM) for 24 h and Western Blot was performed as described in Section "Materials and Methods." **(A,C,E,G)** Show representative gels regarding HO-2 and BVR protein expression following sAβ and fAβ treatment, as above. Bar graphs represent the quantification of HO-2 and BVR protein levels normalized for β-actin expression. Data are expressed as mean ± SEM of 4/5 replicates per group and analyzed by One-way ANOVA followed by Tukey's test: $^{**}P < 0.01$ vs. C **(H)**. C, control.

into the nucleus, as reported by the fluorescence signal (panels C-c2 and E-e2). Notably, quantitative analysis of the Nrf2 nucleus/cytoplasm *ratio* revealed that 10 μM CXB increased Nrf2 nuclear translocation in both 25 nM sAβ- and 6.25 nM fAβ- treated cells (**Figure 5F**, One-way ANOVA followed by Tukey's test, $^{***}P < 0.001$ vs. C, $^{*}P < 0.05$ vs. C, $^{\#}P < 0.001$

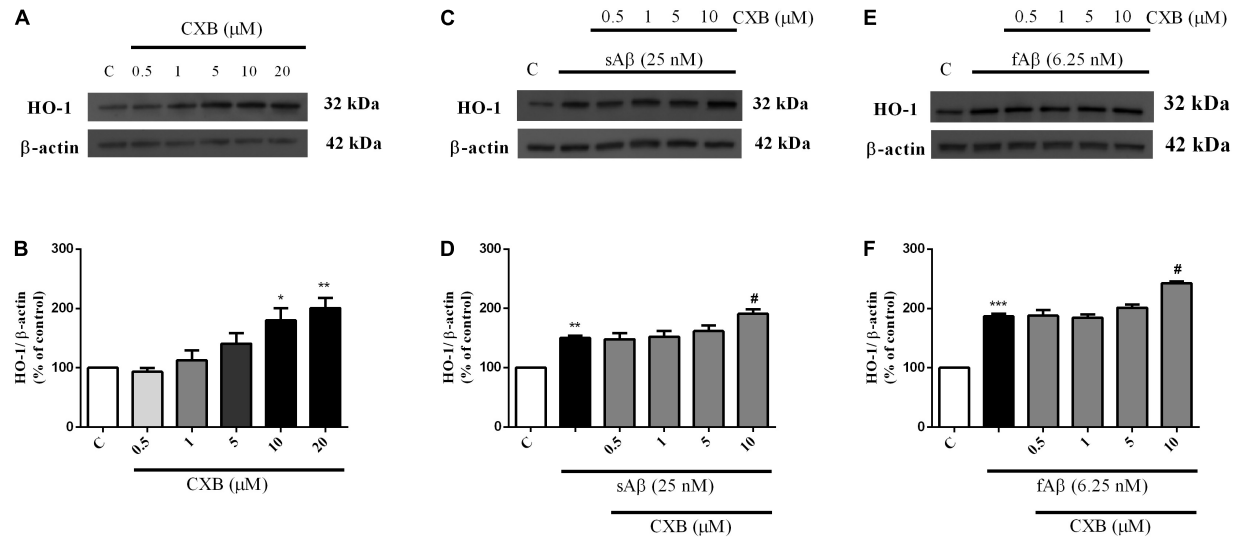

FIGURE 3 | Celecoxib (CXB) effects on basal and Aβ-induced heme oxygenase-1 (HO-1) expression in SH-SY5Y neurons. SH-SY5Y cells were treated with CXB (0.5–10 μM) for 1 h and then incubated with cell culture medium for 24 h **(A)**; in another set of experiments, SH-SY5Y cells were treated with CXB (0.5–10 μM) for 1 h and then incubated with 25 nM sAβ or 6.25 nM fAβ for 24 h (**C,E**, respectively). Following incubation, cells were harvested and Western Blot was performed as described in Section "Materials and Methods." **(A,C,E)** Show representative gels evaluating HO-1 protein expression. Bar graphs represent the quantification of HO-1 protein levels normalized for β-actin expression. Data are expressed as mean ± SEM of 4/5 replicates per group and analyzed by One-way ANOVA followed by Tukey's test: $^{*}P < 0.05$ and $^{**}P < 0.01$ vs. C **(B)**; $^{**}P < 0.01$ vs. C and $^{\#}P < 0.05$ vs. sAβ **(D)**; $^{***}P < 0.001$ vs. C and $^{\#}P < 0.001$ vs. fAβ **(F)**. C, control.

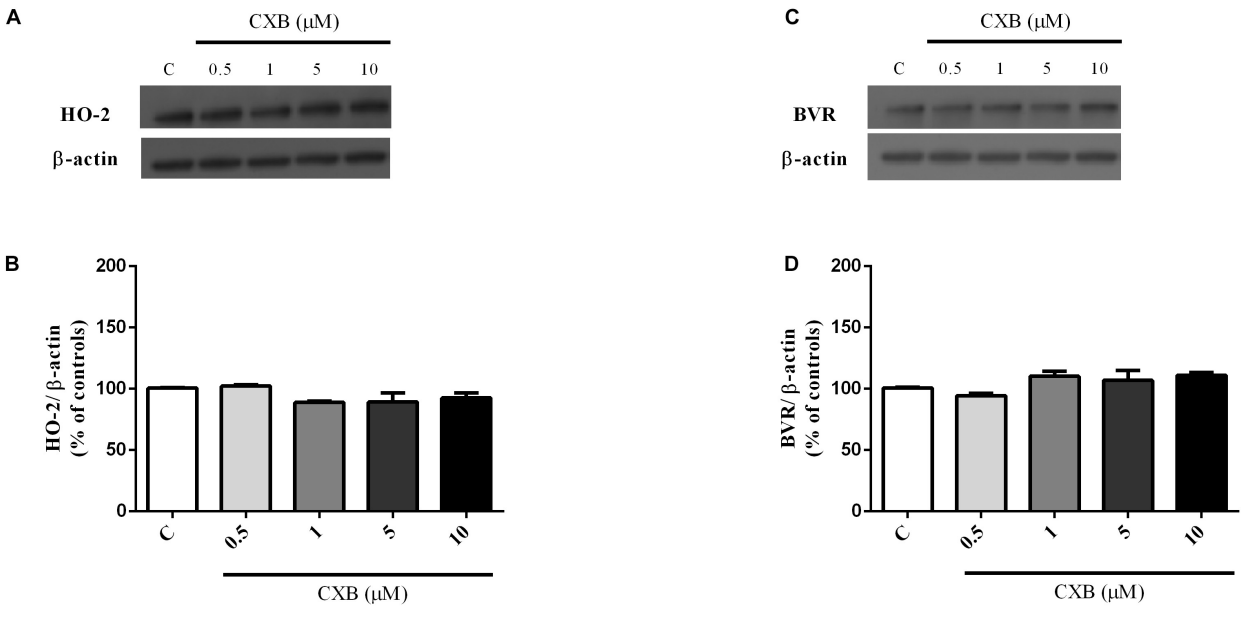

FIGURE 4 | Celecoxib (FA) effects on basal heme oxygenase-2 (HO-2) and biliverdin reductase (BVR) expression in SH-SY5Y neurons. SH-SY5Y cells were treated with CXB (0.5–10 μM) for 1 h and then incubated with cell culture medium for 24 h. Following incubation, cells were harvested and Western Blot was performed as described in Section "Materials and Methods." **(A,C)** Show representative gels evaluating HO-2 and BVR protein expression. Bar graphs represent the quantification of HO-2 and BVR protein levels normalized for β-actin expression. Data are expressed as mean ± SEM of 4/5 replicates per group and analyzed by one-way ANOVA followed by Tukey's test: $P > 0.05$.

vs. sAβ, $^{\circ}P < 0.01$ vs. fAβ), but CXB-induced Nrf2 nuclear translocation was greater in fAβ-exposed neurons (median fold change of sAβ+CXB/sAβ = 1.78 vs. fAβ+CXB/fAβ = 2.74), thus confirming the HO-1 induction detected in **Figures 3C–F**. Furthermore, these findings confirm that the exposure of SH-SY5Y cells to CXB is long enough to induce Nrf2 at the nuclear level and, presumably, to favor HO-1 over-expression during the 24 h incubation with either cell culture medium or sAβ

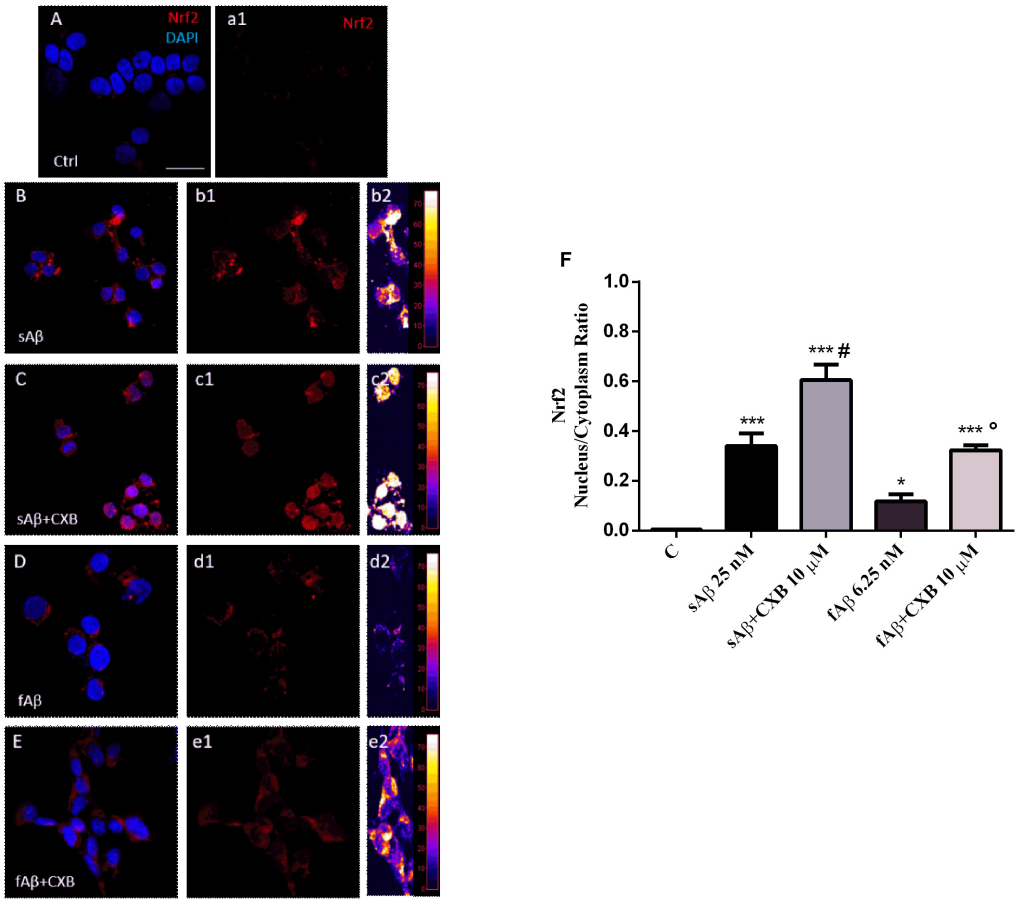

FIGURE 5 | Nrf2 activation and translocation into the nucleus in SH-SY5Y neurons. **(A–E)** Representative images from three independent immunofluorescence experiments in which double-labeling with DAPI and anti-Nrf2 antibody **(a1–e1)** was performed in 25 nM sAβ- or 6.25 nM fAβ- treated SH-SY5Y neurons without or with 10 μM CXB, as described in Section "Materials and Methods." Merged images are shown in **(A–E)**. **(b2–e2)** Images show the distribution of fluorescence intensity signal in a pseudo-color rainbow scale. Scale bar: 20 μm. **(F)** Represents the quantification of the Nrf2 nucleus/cytoplasm *ratio* in treated cells. Data are expressed as mean ± SEM of 11/13 replicates per group and analyzed by One-way ANOVA followed by Tukey's test: ***$P < 0.001$ vs. C, *$P < 0.05$ vs. C, #$P < 0.001$ vs. sAβ, °$P < 0.01$ vs. fAβ **(F)**. A.U., arbitrary units; C, Control.

or fAβ. Finally, these results mirror other findings in vascular endothelial cells and in macrophages, thus confirming how Nrf2-related transcription of cytoprotective genes in response to CXB is a conserved antioxidant mechanism (Wang et al., 2011; Al-Rashed et al., 2018). Incidentally, residual DMSO from CXB stock solution did not have any significant effect on protein levels and Nrf2 translocation.

Characterization of Aβ Aggregation Forms

Since both the rate of Aβ aggregation and size of oligomers/fibrils have been shown to vary depending on the concentration of the peptide and the buffer in which aggregation takes place (Nag et al., 2011; Nichols et al., 2015), these experiments have been carried out by using sAβ and fAβ at the lowest concentrations found effective to up-regulate HO-1, diluted in the cell culture medium and incubated at 37°C for 24 h under quiescent conditions. As shown in **Figure 6A**, 25 nM sAβ oligomerization starts after a lag-phase of ∼ 2 h, during which the peptide is prevalently in the monomeric form [hydrodynamic radius (RH)∼ 1 nm], sharply increases within 6 h and reaches a plateau at ∼ 8 h. As early as 3 h, small oligomers with RH ∼20 nm prevail (**Figure 6B**), whereas at the plateau the oligomer size reaches RH ∼ 110 nm (**Figure 6C**). These results have been confirmed by AFM experiments showing the presence of a few monomers together with oligomers throughout the whole oligomerization process (**Figures 6D,E**).

With regard to 6.25 nM fAβ, the lag-phase before fibril elongation is ∼10 h: over this time, a few fibrils with RH ∼44 nm and 1–2 μm in length have been detected (**Figures 6F,G,I**). Conversely, after 10 h, the formation of longer fibrils takes place and reaches a plateau at ∼20 h: at this last time-point, longer fibrils with RH ∼267 nm and ∼10–15 μm in length have been detected (**Figures 6H,J**). Over the whole fibrillation period, Aβ oligomers, with maximal RH ∼150 nm have been also detected, implying a mixed population of Aβ soluble and insoluble species in these samples (**Figures 6I,J**).

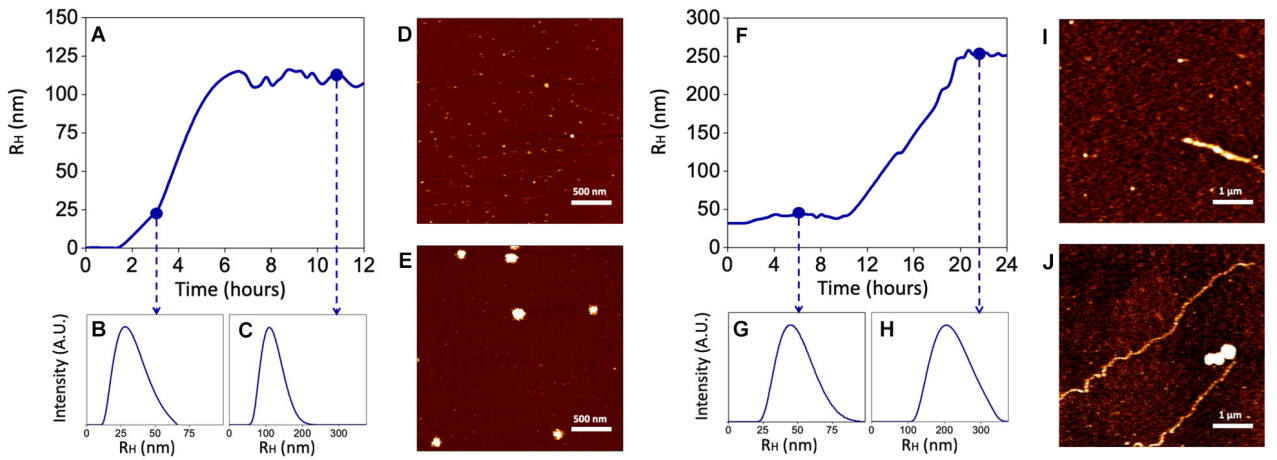

FIGURE 6 | Kinetics of Aβ aggregation and oligomer/fibril formation by Dynamic Light Scattering (DLS) and Atomic Force Microscopy (AFM). 25 nM sAβ or 6.25 nM fAβ were incubated in cell culture medium at 37°C for 24 h under quiescent conditions. At fixed time points, Aβ samples were drop casted of fresh cleaved Mica disks and air dried. **(A–C)** Show a representative monomers aggregation kinetics of 25 nM sAβ, measured by DLS. **(D,E)** Representative AFM micrographs of early oligomers **(D)** and oligomers after 12 h of aggregation **(E)** are reported. **(F–H)** 6.25 nM fAβ aggregation kinetics, assessed by DLS, are reported. Representative AFM images of fibrils before **(I)** and after **(J)** aggregation are reported with monomers and oligomers coexisting with fibrils in the final phase.

Effects of CXB on ROS Generation and Lipid Peroxidation in SH-SY5Y Cells

As mentioned in Section "Introduction," a common mechanism shared by sAβ and fAβ to induce neurodegeneration is the production of ROS, which in turn, up-regulate HO-1. Regarding the effect of CXB on Aβ-induced ROS production, data summarized in **Figures 7A,B**, demonstrate a significant antioxidant activity of 10 μM CXB against 25 nM sAβ and 6.25 nM fAβ, respectively, in SH-SY5Y neurons (**Figure 7A**, One-way ANOVA followed by Tukey's test, $^{***}P < 0.001$ vs. C, $^{\#}P < 0.01$ vs. sAβ; **Figure 7B**, One-way ANOVA followed by Tukey's test, $^{***}P < 0.0001$ vs. C, $^{\#}P < 0.001$ vs. fAβ). In this experimental system, 10 μM CXB alone weakly increased basal ROS production (**Figures 7A,B**, One-way ANOVA followed by Tukey's test, $^{*}P < 0.05$ vs. C).

To exclude a potential effect of CXB on Aβ aggregation as an adjuvant antioxidant mechanism, its effect on sAβ and fAβ aggregation has been studied. The results confirm the lack of any effect of 10 μM CXB on the aggregation of 25 nM sAβ and 6.25 nM fAβ over 24 h (data not shown).

Finally, in order to link the antioxidant effect of CXB with HO-1 over-expression, experiments with the HO-inhibitor ZnPP-IX have been performed according to current literature (Catino et al., 2015; Wang et al., 2016; Hui et al., 2018). As shown in **Figures 7C,D**, 2.5 μM ZnPP-IX fully counteracted 10 μM CXB-related ROS generation in SH-SY5Y cells treated with 25 nM sAβ, whereas the inhibitor only partially reverted ROS generation in 6.25 nM fAβ-exposed SH-SY5Y cells (**Figure 7C**, One-way ANOVA followed by Tukey's test, $^{\circ}P < 0.001$ vs. sAβ+CXB; **Figure 7D**, One-way ANOVA followed by Tukey's test, $^{\circ}P < 0.05$ vs. fAβ+CXB). Importantly, ZnPP-IX alone increased basal ROS production thus confirming the tonic antioxidant effect of HO-1 on SH-SY5Y cells (**Figures 7C,D**, One-way ANOVA followed by Tukey's test, $^{*}P < 0.05$ vs. C).

The differential effects of sAβ and fAβ on ROS production have been reflected on cell damage. As a biomarker of lipid peroxidation, 4-HNE have been assayed. As shown in **Figure 8**, 4-HNE labeling was faint in control cells (panel A), but increased markedly in cells treated with both sAβ (panels B-b3) and fAβ (panels C-c3), as also confirmed by fluorescence quantification (**Figures 8H,I**, One-way ANOVA followed by Tukey's test, $^{***}P < 0.001$ vs. C). Moreover, 10 μM CXB markedly reduced neuronal damage only in sAβ-treated cells (panels D-d3 and **Figure 8H**, One-way ANOVA followed by Tukey's test, $^{\#}P < 0.001$ vs. sAβ), whereas only a weak reduction in 4-HNE has been detected in neurons exposed to fAβ (panels E-e3 and **Figure 8I**, One-way ANOVA followed by Tukey's test, $^{\#}P < 0.01$ vs. fAβ). Finally, 2.5 μM ZnPP-IX significantly reverted CXB-related 4-HNE inhibition only in SH-SY5Y cells treated with sAβ (panel F-f3 and **Figure 8H**, One-way ANOVA followed by Tukey's $^{\circ}P < 0.001$ vs. sAβ+CXB). Residual DMSO from CXB stock solution did not have any significant effect on the results described above.

A possible mechanism through which CXB counteracts Aβ-induced ROS production and neurotoxicity is related to the ability of this drug to further increase Aβ induced-HO-1 up-regulation (**Figures 3C–F**), resembling a well-known mechanism involved in the neuroprotective effects of several agents under redox imbalance (Calabrese et al., 2008; Butterfield et al., 2012; Catino et al., 2015). In this frame, the inhibition of HO activity by ZnPP-IX confirms the main role played by HO-1 in CXB-related neuroprotection.

HO By-products With Neuroprotective Properties

The experiments described above demonstrated the main involvement of HO activity on CXB-mediated antioxidant effects. The next step was to identify which, among the HO by-products,

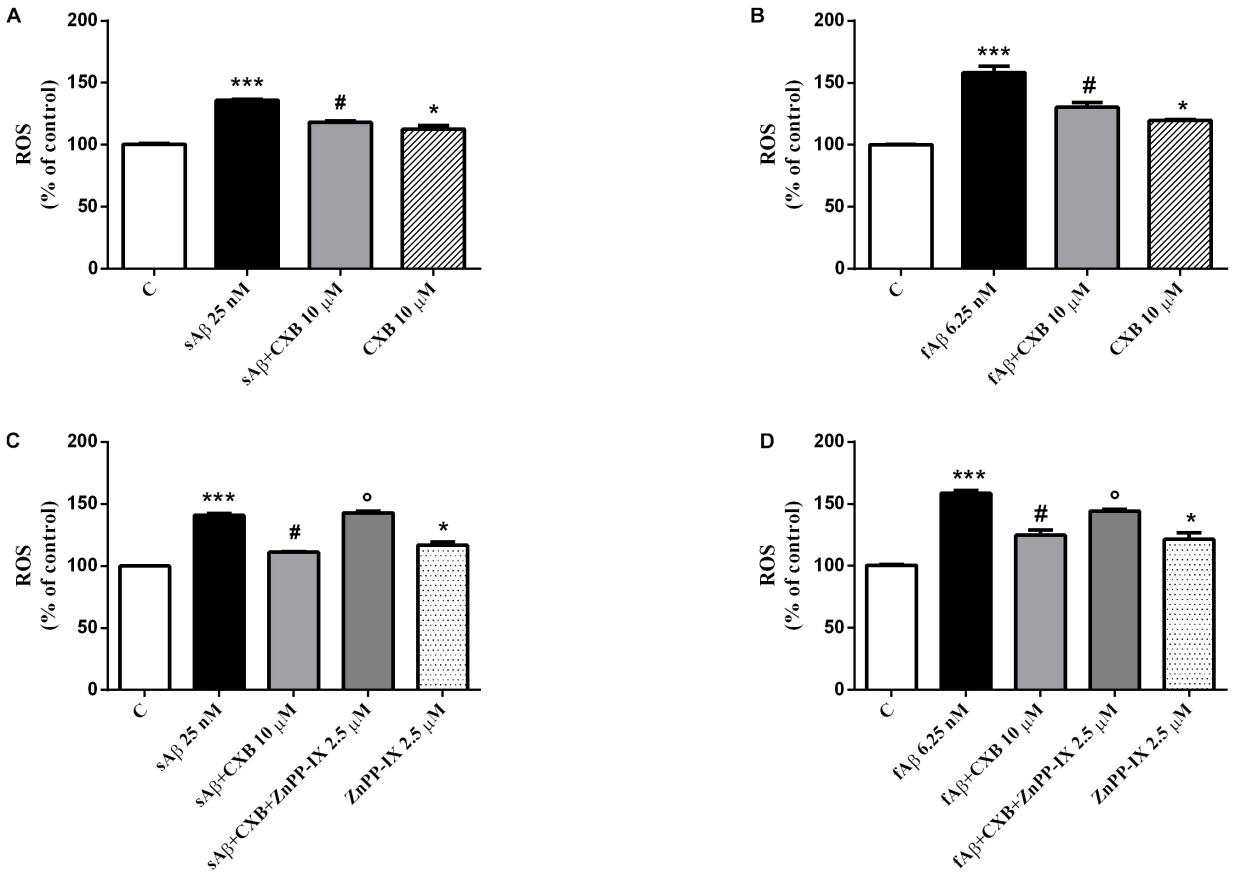

FIGURE 7 | Celecoxib (CXB) contrasts Aβ-induced reactive oxygen species (ROS) formation through the HO activity in SH-SY5Y neurons. SH-SY5Y cells were treated with 10 μM CXB for 1 h and then incubated with either cell culture medium or 25 nM sAβ **(A)** or 6.25 nM fAβ **(B)** for 24 h. Following incubation, intracellular ROS cells were measured by fluorimetric detection as described in Section "Materials and Methods." In selected experiments, SH-SY5Y neurons were incubated as above in the presence of 2.5 μM ZnPP-IX **(C,D)**. Data are expressed as a mean ± SEM of 12/14 replicates per group and analyzed by One-way ANOVA followed by Tukey's test: $^{***}P < 0.001$ vs. C, $^{\#}P < 0.01$ vs. sAβ, $^{*}P < 0.05$ vs. C **(A,C)**; $^{***}P < 0.0001$ vs. C, $^{\#}P < 0.001$ vs. fAβ, $^{*}P < 0.05$ vs. C **(B,D)**; $^{\circ}P < 0.001$ vs. sAβ+CXB **(C)**; $^{\circ}P < 0.05$ vs. fAβ+CXB **(D)**. C, control.

is involved in the antioxidant effects previously described. The major concern we had to face with, while designing these experiments, was the choice of both BR and CORM-2 (a CO donor) concentrations so that they could not result toxic when co- administered with either sAβ or fAβ. In order to solve this issue, BR and CORM-2 were both used at 50 nM, a concentration found safe for SH-SY5Y neurons (Dal-Cim et al., 2012; Catino et al., 2015). As shown in **Figures 9A,B**, 50 nM CORM-2 significantly reduced ROS production stimulated by both 25 nM sAβ and 6.25 nM fAβ, respectively (**Figure 9A**, One-way ANOVA followed by Tukey's test, $^{***}P < 0.001$ vs. C, $^{\#}P < 0.01$ vs. sAβ; **Figure 9B**, One-way ANOVA followed by Tukey's test, $^{**}P < 0.01$ vs. C, $^{\#}P < 0.01$ vs. fAβ), whereas 50 nM BV did not have any effect (data not shown). On the contrary, 50 nM BR significantly inhibited only 6.25 nM fAβ-induced ROS production (**Figure 9C**, One-way ANOVA followed by Tukey's test, $^{***}P < 0.001$ vs. C, **Figure 9D**, One-way ANOVA followed by Tukey's test, $^{***}P < 0.001$ vs. C, $^{\#}P < 0.01$ vs. fAβ).

In search for alternate mechanisms involved in CO and BR neuroprotective effects, specific experiments to assess their interaction with Aβ were performed. As shown in **Figure 10** and **Table 1**, both 50 nM CORM-2 and 50 nM BR prolonged the lag-phase of 25 nM sAβ oligomerization from 2 to 3 h and slowed the rate of oligomer formation, whereas only 50 nM BR reduced the oligomer size at plateau (RH ∼ 75 vs. 110 nm) (**Figure 10A** and **Table 1**, One-way ANOVA followed by Tukey's test, $^{**}P < 0.01$ vs. sAβ). With regard to 6.25 nM fAβ, neither 50 nM CORM nor 50 nM BR affected the rate of fibril elongation, whereas this latter reduced fibril RH at plateau (RH ∼ 209 vs. 267 nm) (**Figure 10B** and **Table 1**, One-way ANOVA followed by Tukey's test, $^{\#}P < 0.01$ vs. fAβ). Selected experiments have excluded any significant effect of ruthenium, contained in CORM-2, and residual DMSO on ROS generation as well as Aβ oligomer formation and fibril elongation (data not shown).

These last results show an unprecedented direct effect of both CO and BR on Aβ aggregation independent of the modulation of intracellular signaling pathways acting downstream. The gaseous nature of CO and the high liposolubility of BR may have a role in their direct interaction with Aβ over the transition through the structural states.

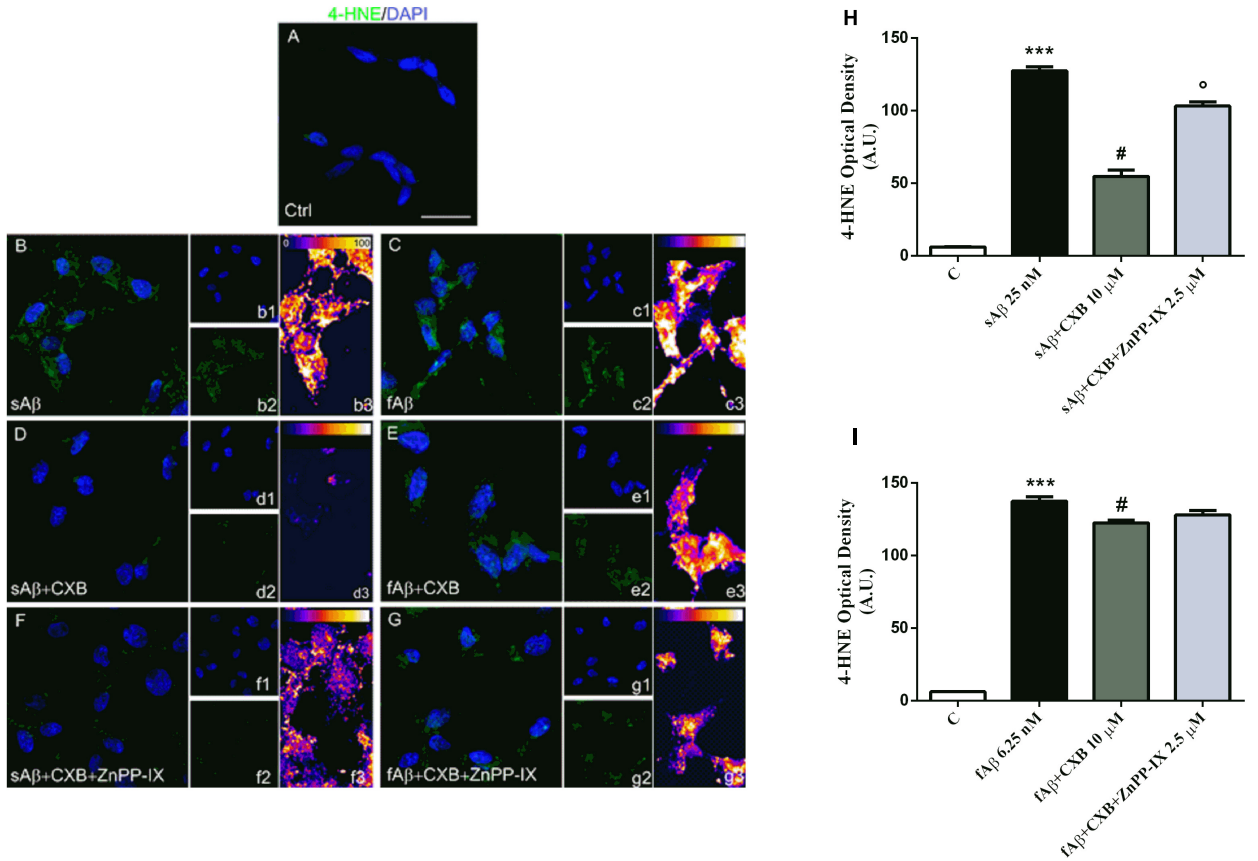

FIGURE 8 | Celecoxib (CXB) counteracts Aβ-induced lipid peroxidation through the HO activity in SH-SY5Y neurons. **(A–G)** Representative images from three independent immunofluorescence experiments in which double-labeling with DAPI **(b1–g1)** and anti-4-HNE antibody **(b2–g2)** was carried out in SH-SY5Y neurons treated as described in the legend of **Figure 5**. Merged images are shown in **(A–G)**. **(b3–g3)** Images showing the distribution of fluorescence intensity signal in a pseudo-color rainbow scale. Scale bar: 20 μm. **(H,I)** Represent the quantification of 4-HNE fluorescence. Data are expressed as mean ± SEM of 15 replicates per group and analyzed by One-way ANOVA followed by Tukey's test: $^{***}P < 0.001$ vs. C, $^{\#}P < 0.001$ vs. sAβ, $^{\circ}P < 0.001$ vs. sAβ+CXB **(H)**; $^{***}P < 0.001$ vs. C, $^{\#}P < 0.01$ vs. fAβ **(I)**. A.U., arbitrary units; C, Control.

DISCUSSION

The role of HO-1 in the pathogenesis of AD and its druggability are no longer matter of debate. Over the years, several research groups described a marked induction of HO-1 in *postmortem* brain tissues as well as in plasma and lymphocytes from patients with AD or mild cognitive impairment (MCI), this latter being the transitional phase from healthy aging to AD (Calabrese et al., 2006; Di Domenico et al., 2012). The rationale to explain HO-1 induction in AD is related to the neuroprotective features of this early gene/protein whose ability to prevent heme toxicity, enhanced during excessive free radical generation, and to release the antinflammatory gaseous molecule CO (Nitti et al., 2018), make this enzyme a pivotal player in the cell stress response (Mancuso et al., 2013; Motterlini and Foresti, 2017). However, a large slice of literature focused on the potential neurotoxic effects of a sustained HO-1 induction due to the accumulation of its by-products, but these two hypotheses were recently reconciled by keeping in mind the "dual" nature of HO-1. In this light, the potentiation of HO-1 up-regulation by drugs (e.g., atorvastatin) and nutritional herb-based agents (e.g., ferulic acid, rosmarinic acid) detected in several *in vitro* and *in vivo* preclinical models of free radical-induced diseases, is currently considered an effective neuroprotective response (Calabrese et al., 2008; Butterfield et al., 2012; Catino et al., 2015; Fetoni et al., 2015).

Another important issue to be focused is the range of concentrations of sAβ and fAβ used to up-regulate HO-1. In many papers, to achieve a marked increase in HO-1 level were necessary high concentrations of Aβ, in the range 10—20 μM, whereas in our study a significant HO-1 over-expression was detected as low as 25 nM sAβ and 6.25 nM fAβ, these concentrations being close to those detected in AD brain which are well below 1 μM (Nag et al., 2011 and references therein). These findings favor the translational application of our results and support the hypothesis of an early induction of HO-1, even in the absence of an excessive deposition of Aβ as occurs in the later phases of AD. On the other hand, CXB (10 μM) has been shown to exert protective effects through the activation of HO-1 in human arterial and venous endothelial cells (Al-Rashed et al., 2018). The dose of CXB was chosen taking

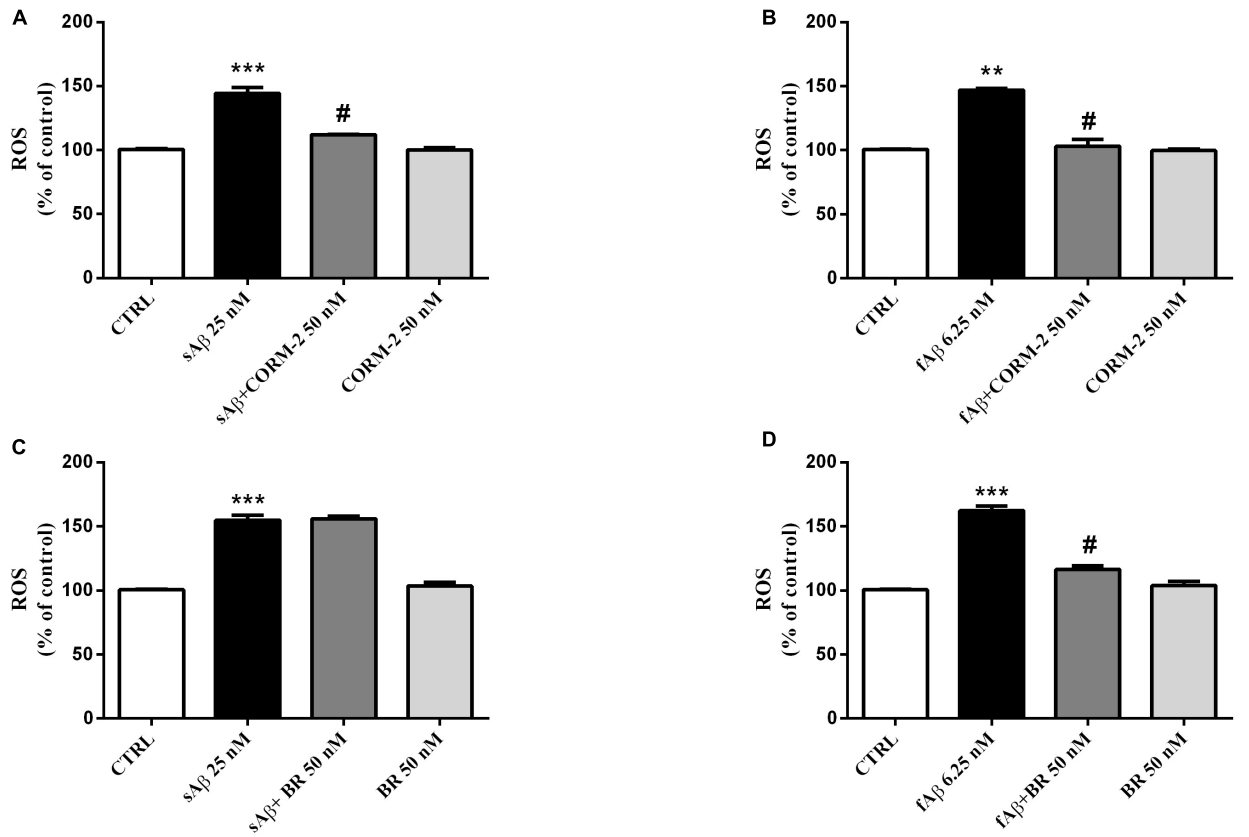

FIGURE 9 | Antioxidant effect of the carbon monoxide donor CORM-2 and bilirubin (BR) in SH-SY5Y neurons exposed to Aβ. SH-SY5Y neurons were treated with 50 nM CORM-2 or 50 nM BR alone or in the presence of either 25 nM sAβ or fAβ for 24 h. At the end of incubation, intracellular ROS cells were measured by fluorimetric detection as described in Section "Materials and Methods." Data are expressed as a mean ± SEM of 12/13 replicates per group and analyzed by One-way ANOVA followed by Tukey's test: $^{***}P < 0.001$ vs. C, $^{\#}P < 0.01$ vs. sAβ **(A)**; $^{**}P < 0.01$ vs. C, $^{\#}P < 0.01$ vs. fAβ **(B)**; $^{***}P < 0.001$ vs. C **(C)**; $^{***}P < 0.001$ vs. C, $^{\#}P < 0.01$ vs. fAβ **(D)**. C, control.

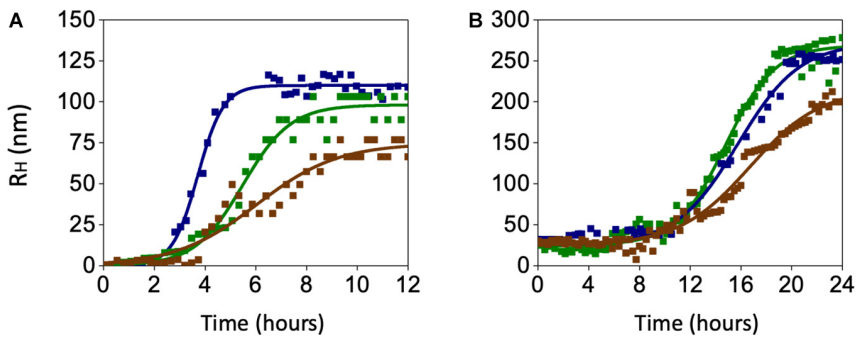

FIGURE 10 | Effects of carbon monoxide donor CORM-2 and bilirubin (BR) on the kinetics of Aβ aggregation. **(A)** A representative aggregation kinetics, measured by DLS, of 25 nM sAβ (blu squares) in the presence of 50 nM CORM-2 (green squares) or 50 nM BR (red squares) is reported. **(B)** A representative aggregation kinetics, measured by DLS, of 6.25 nM fAβ (blu squares) in the presence of 50 nM CORM-2 (green squares) or 50 nM BR (red squares) is reported (see section "Materials and Methods" for further details).

into account not only the drug-protein binding properties, but also based on the maximum plasma concentration, which has been reported to range approximately 2–8 μM in selected dosing regimens established in preclinical and clinical studies (Davies et al., 2000; Paulson et al., 2000, 2001).

Most of the research carried out with the purpose to study the involvement of HO-1 in AD, produced descriptive studies without addressing either the molecular mechanism(s) through which sAβ or fAβ regulate HO-1 expression or whether HO-1 modulation mitigates Aβ-induced brain injury. Our study

TABLE 1 | Effects of carbon monoxide donor CORM-2 and bilirubin (BR) on β-amyloid (Aβ) aggregation.

Treatment	Maximal R_H (nm)	p (hours^{-1})
sAβ (25 nM)	110 ± 5	0.861 ± 0.128
+ CORM-2 (50 nM)	98 ± 4	0.460 ± 0.040**
+ BR (50 nM)	75 ± 4**	0.273 ± 0.035**
fAβ (6.25 nM)	267 ± 4	0.202 ± 0.013
+ CORM-2 (50 nM)	266 ± 4	0.244 ± 0.013
+ BR (50 nM)	209 ± 6#	0.180 ± 0.012

*fAβ, fibrillar Aβ; nm, nanometers; RH, hydrodynamic radius; sAβ, soluble Aβ. Data are expressed as mean ± SEM (n = 3) and analyzed by One-way ANOVA followed by Tukey's post hoc test: **P < 0.01 vs. sAβ and #P < 0.01 vs. fAβ.*

supports the hypothesis that sAβ has a minor role in HO-1 regulation, whereas a marked induction of HO-1 has been detected as early as 24 h, a time-point long enough to allow the formation of Aβ oligomers. These last findings agree with previous studies on HO-1 induction by the Butterfield's group who incubated sAβ for 24 h in PBS before treating gerbil synaptosomes and rat cortical neurons (Sultana et al., 2005; Perluigi et al., 2006). Our data are also in good agreement with those by Cui et al. (2019) who detected a significant HO-1 over-expression in BV-2 microglial cells by using a purified preparation of Aβ oligomers. As far as the contribution of fAβ to HO-1 regulation, our results in SH-SY5Y cells corroborate a significant induction of HO-1 and agree with the few studies carried out in *postmortem* brain senile plaques and neurofibrillary tangles (Smith et al., 1994; Schipper et al., 1995). Although the transition from monomers to oligomers and fibrils has to be considered a *continuum*, since the three Aβ aggregating forms coexist in the brain over the natural history of AD, this set of experiments confirms that a different degree of HO-1 induction occurs over the transition from soluble to insoluble forms of Aβ. Intriguingly, the ability of CXB to further enhance HO-1 protein in SH-SY5Y is maintained regardless of the Aβ soluble or insoluble species (**Figure 3**). This evidence suggested interpreting the potential neuroprotective effect of CXB by evaluating not only the degree of HO-1 over-expression, but mainly the antioxidant outcomes. Definitely, HO-1 blockade fully reverted both CXB-related inhibition of ROS generation and lipid peroxidation damage in SH-SY5Y cells treated with sAβ, whereas in those exposed to fAβ the inhibition of HO-1 only partially counteracted CXB-related antioxidant effect and did not affect lipid peroxidation damage (**Figures 7**, **8**). These results strongly support the evidence of a major neuroprotective effect of CXB, through HO-1 induction, in sAβ-exposed SH-SY5Y cells.

The HO-1-dependent neuroprotective effect of CXB sheds new light on a drug whose efficacy in AD has long been debated. As early as 1997, many epidemiological studies revealed as NSAID treatment was associated with decreased risk to develop AD by reducing COX-dependent neuroinflammation. Among the determinants of this therapeutic effect, were both the type of NSAIDs used and the age of patients: the neuroprotective effect was greater with non-aspirin drugs (e.g., ibuprofen, sulindac, diclofenac) and in younger subjects (Imbimbo et al., 2010). However, these promising results were not confirmed by *ad hoc* designed clinical trials; a systematic review and meta-analysis by Miguel-Alvarez et al. (2015) has confirmed the lack of efficacy of NSAIDs, including the COX-2 inhibitor CXB, to improve cognitive skills and reduce disease severity in AD subjects. With regard to CXB, the randomized clinical trials studying its efficacy in AD enrolled either people older than 70 years with a family history of AD or patients with mild-to-moderate AD aged $\geq$ 50 years (Soininen et al., 2007; Group et al., 2008, 2009). That said, although not confirmed by published results, it is possible to argue that both aged subjects and AD patients recruited in these studies had already developed brain injury, due to Aβ aggregation/fibrillation, earlier than or during the clinical trials and this could be responsible, at least in part, for the lack of efficacy of CXB. Accordingly, Breitner et al. (2011) followed-up the ADAPT protocol for two additional years and found a significant reduction in AD incidence among the asymptomatic enrollees treated with NSAIDs and concluded that the efficacy of NSAID treatment depends on the stage of AD development being more effective during the earliest stage of the disease.

As far as the effectors downstream of HO-1 activation, the neuroprotective effects of CO and BR, through the down-regulation of pro-oxidant systems or direct free radical scavenging, respectively, have been extensively addressed (Piantadosi, 2008; Jansen and Daiber, 2012). Our results confirmed the ability of CO and BR to inhibit both sAβ- and fAβ- induced ROS formation and provided novel evidence for a direct effect of CO and BR in AD through the slowdown of the growth rate of Aβ oligomers and decrease in the oligomer/fibril final size. These results, *vis-à-vis* with those by Kim et al. (2019), who described the inhibitory effect of CO on the NF-κB-mediated BACE1 transcription, and by Barone et al. (2012a), who showed a strong relationship between BVR activation and BACE1 inhibition, confirm the neuroprotective role of a mild up-regulation of the HO-1/BVR system through both CO and BR. However, due to their chemical features, CO being a gas and BR a lipophilic molecule (Mancuso, 2017; Motterlini and Foresti, 2017), their potential effects on extracellular Aβ cannot be excluded.

The preclinical results described in this study parallel the clinical evidence mentioned above and put forth the adjuvant neuroprotective effect of CXB in patients with mild AD or in MCI subjects.

DATA AVAILABILITY STATEMENT

The original contributions presented in the study are included in the article, further inquiries can be directed to the corresponding author.

AUTHOR CONTRIBUTIONS

EM, MP, LT, and CM: conception and design of the work. EM, FP, AS, RR, VP, GP, and AF: study conduct and acquisition and of

the data. EM, AS, RR, VP, GP, LT, and CM: statistical analysis and interpretation of the data. EM, MP, and CM: drafting manuscript. All authors: revising manuscript content and approving final version of the manuscript.

FUNDING

This manuscript was supported by Catholic University's grants "Fondi Ateneo" to CM.

REFERENCES

Agostinho, P., Cunha, R. A., and Oliveira, C. (2010). Neuroinflammation, oxidative stress and the pathogenesis of Alzheimer's disease. *Curr. Pharm. Des.* 16, 2766–2778.

Al-Rashed, F., Calay, D., Lang, M., Thornton, C. C., Bauer, A., Kiprianos, A., et al. (2018). Celecoxib exerts protective effects in the vascular endothelium via COX-2-independent activation of AMPK-CREB-Nrf2 signalling. *Sci. Rep.* 8:6271. doi: 10.1038/s41598-018-24548-z

Balducci, C., Frasca, A., Zotti, M., Mhillaj, E., Grigoli, E., Iacobellis, M., et al. (2016). Toll-like receptor 4-dependent glial cell activation mediates the impairment in memory establishment induced by beta-amyloid oligomers in an acute mouse model of Alzheimer's disease. *Brain Behav. Immun.* 60, 188–197. doi: 10.1016/j.bbi.2016.10.012

Barone, E., Cenini, G., Sultana, R., Cini, C., Preziosi, P., Perluigi, M., et al. (2011a). Biliverdin reductase–a protein levels and activity in the brains of subjects with Alzheimer disease and mild cognitive impairment. *Biochim. Biophys. Acta* 1812, 480–487. doi: 10.1016/j.bbadis.2011.01.005

Barone, E., Cenini, G., Sultana, R., Coccia, R., Preziosi, P., Perluigi, M., et al. (2011b). Oxidative and nitrosative modifications of biliverdin reductase-A in the brain of subjects with Alzheimer's disease and amnestic mild cognitive impairment. *J. Alzheimers Dis.* 25, 623–633. doi: 10.3233/JAD-2011-110092

Barone, E., Mancuso, C., Sultana, R., Murphy, M. P., Head, E., and Butterfield, D. A. (2012a). Biliverdin reductase-A: a novel drug target for atorvastatin in a dog pre-clinical model of Alzheimer disease. *J. Neurochem.* 120, 135–146. doi: 10.1111/j.1471-4159.2011.07538.x

Barone, E., Sultana, R., Coccia, R., Mancuso, C., Perluigi, M., and Butterfield, D. A. (2012b). Heme oxygenase-1 posttranslational modifications in the brain of subjects with Alzheimer disease and mild cognitive impairment. *Free Radical Biol. Med.* 52, 2292–2301. doi: 10.1016/j.freeradbiomed.2012.03.020

Breitner, J. C., Baker, L. D., Montine, T. J., Meinert, C. L., Lyketsos, C. G., Ashe, K. H., et al. (2011). Extended results of the Alzheimer's disease anti-inflammatory prevention trial. *Alzheimers Dement* 7, 402–411. doi: 10.1016/j.jalz.2010.12.014

Butterfield, D. A., Barone, E., Cenini, G., Sultana, R., Murphy, M. P., Mancuso, C., et al. (2012). Atorvastatin treatment in a dog preclinical model of Alzheimer's disease leads to up-regulation of haem oxygenase-1 and is associated with reduced oxidative stress in brain. *Int. J. Neuropsychopharmacol.* 15, 981–987. doi: 10.1017/S1461145711001118

Calabrese, V., Calafato, S., Puleo, E., Cornelius, C., Sapienza, M., Morganti, P., et al. (2008). Redox regulation of cellular stress response by ferulic acid ethyl ester in human dermal fibroblasts: role of vitagenes. *Clin. Dermatol.* 26, 358–363. doi: 10.1016/j.clindermatol.2008.01.005

Calabrese, V., Sultana, R., Scapagnini, G., Guagliano, E., Sapienza, M., Bella, R., et al. (2006). Nitrosative stress, cellular stress response, and thiol homeostasis in patients with Alzheimer's disease. *Antioxid Redox Signal.* 8, 1975–1986. doi: 10.1089/ars.2006.8.1975

Canas, P. M., Simoes, A. P., Rodrigues, R. J., and Cunha, R. A. (2014). Predominant loss of glutamatergic terminal markers in a beta-amyloid peptide model of Alzheimer's disease. *Neuropharmacology* 76(Pt A), 51–56. doi: 10.1016/j.neuropharm.2013.08.026

Catino, S., Paciello, F., Miceli, F., Rolesi, R., Troiani, D., Calabrese, V., et al. (2015). Ferulic Acid Regulates the Nrf2/Heme Oxygenase-1 System and Counteracts Trimethyltin-Induced Neuronal Damage in the Human Neuroblastoma Cell Line SH-SY5Y. *Front. Pharmacol.* 6:305. doi: 10.3389/fphar.2015.00305

Celik, H., Karahan, H., and Kelicen-Ugur, P. (2020). Effect of atorvastatin on Abeta1-42 -induced alteration of SESN2, SIRT1, LC3II and TPP1 protein expressions in neuronal cell cultures. *J. Pharm. Pharmacol.* 72, 424–436. doi: 10.1111/jphp.13208

Cui, B., Zhang, S., Wang, Y., and Guo, Y. (2019). Farrerol attenuates beta-amyloid-induced oxidative stress and inflammation through Nrf2/Keap1 pathway in a microglia cell line. *Biomed. Pharmacother.* 109, 112–119. doi: 10.1016/j.biopha.2018.10.053

Dal-Cim, T., Molz, S., Egea, J., Parada, E., Romero, A., and Budni, J. (2012). Guanosine protects human neuroblastoma SH-SY5Y cells against mitochondrial oxidative stress by inducing heme oxigenase-1 via PI3K/Akt/GSK-3beta pathway. *Neurochem. Int.* 61, 397–404. doi: 10.1016/j.neuint.2012.05.021

Davies, N. M., McLachlan, A. J., Day, R. O., and Williams, K. M. (2000). Clinical pharmacokinetics and pharmacodynamics of celecoxib: a selective cyclo-oxygenase-2 inhibitor. *Clin. Pharmacokinet.* 38, 225–242. doi: 10.2165/00003088-200038030-00003

Di Domenico, F., Barone, E., Mancuso, C., Perluigi, M., Cocciolo, A., Mecocci, P., et al. (2012). HO-1/BVR-a system analysis in plasma from probable Alzheimer's disease and mild cognitive impairment subjects: a potential biochemical marker for the prediction of the disease. *J. Alzheimers Dis.* 32, 277–289. doi: 10.3233/JAD-2012-121045

Fetoni, A. R., Paciello, F., Rolesi, R., Eramo, S. L., Mancuso, C., Troiani, D., et al. (2015). Rosmarinic acid up-regulates the noise-activated Nrf2/HO-1 pathway and protects against noise-induced injury in rat cochlea. *Free Radic. Biol. Med.* 85, 269–281. doi: 10.1016/j.freeradbiomed.2015.04.021

Graham, W. V., Bonito-Oliva, A., and Sakmar, T. P. (2017). Update on Alzheimer's disease therapy and prevention strategies. *Annu. Rev. Med.* 68, 413–430. doi: 10.1146/annurev-med-042915-103753

Green, K. N., and LaFerla, F. M. (2008). Linking calcium to Abeta and Alzheimer's disease. *Neuron* 59, 190–194. doi: 10.1016/j.neuron.2008.07.013

Group, A. R., Martin, B. K., Szekely, C., Brandt, J., Piantadosi, S., Breitner, J. C., et al. (2008). Cognitive function over time in the Alzheimer's Disease Anti-inflammatory Prevention Trial (ADAPT): results of a randomized, controlled trial of naproxen and celecoxib. *Arch. Neurol.* 65, 896–905. doi: 10.1001/archneur.2008.65.7.nct70006

Group, A. R., Meinert, C. L., McCaffrey, L. D., and Breitner, J. C. (2009). Alzheimer's disease anti-inflammatory prevention trial: design, methods, and baseline results. *Alzheimers Dement* 5, 93–104. doi: 10.1016/j.jalz.2008.09.004

Hardy, J., and Selkoe, D. J. (2002). The amyloid hypothesis of Alzheimer's disease: progress and problems on the road to therapeutics. *Science* 297, 353–356. doi: 10.1126/science.1072994

Hettiarachchi, N. T., Boyle, J. P., Dallas, M. L., Al-Owais, M. M., Scragg, J. L., and Peers, C. (2017). Heme oxygenase-1 derived carbon monoxide suppresses Abeta1-42 toxicity in astrocytes. *Cell Death Dis.* 8:e2884. doi: 10.1038/cddis.2017.276

Hoozemans, J. J., and O'Banion, M. K. (2005). The role of COX-1 and COX-2 in Alzheimer's disease pathology and the therapeutic potentials of non-steroidal anti-inflammatory drugs. *Curr. Drug Targets CNS Neurol. Disord.* 4, 307–315.

Hui, Y., Chengyong, T., Cheng, L., Haixia, H., Yuanda, Z., and Weihua, Y. (2018). Resveratrol Attenuates the Cytotoxicity Induced by Amyloid-beta1-42 in PC12 Cells by Upregulating Heme Oxygenase-1 via the PI3K/Akt/Nrf2 Pathway. *Neurochem. Res.* 43, 297–305. doi: 10.1007/s11064-017-2421-7

Imbimbo, B. P., Solfrizzi, V., and Panza, F. (2010). Are NSAIDs useful to treat Alzheimer's disease or mild cognitive impairment? *Front. Aging Neurosci.* 2:19. doi: 10.3389/fnagi.2010.00019

Jansen, T., and Daiber, A. (2012). Direct antioxidant properties of Bilirubin and Biliverdin. Is there a role for Biliverdin Reductase?. *Front. Pharmacol.* 3:30. doi: 10.3389/fphar.2012.00030

Johnson, D. A., and Johnson, J. A. (2015). Nrf2–a therapeutic target for the treatment of neurodegenerative diseases. *Free Radic. Biol. Med.* 88(Pt. B), 253–267. doi: 10.1016/j.freeradbiomed.2015.07.147

Kim, H. J., Joe, Y., Chen, Y., Park, G. H., Kim, U. H., and Chung, H. T. (2019). Carbon monoxide attenuates amyloidogenesis via down-regulation of NF-kappaB-mediated BACE1 gene expression. *Aging Cell* 18:e12864. doi: 10.1111/acel.12864

Maines, M. D. (1997). The heme oxygenase system: a regulator of second messenger gases. *Annu. Rev. Pharmacol. Toxicol.* 37, 517–554. doi: 10.1146/annurev.pharmtox.37.1.517

Mancuso, C. (2017). Bilirubin and brain: a pharmacological approach. *Neuropharmacology* 118, 113–123. doi: 10.1016/j.neuropharm.2017.03.013

Mancuso, C., Santangelo, R., and Calabrese, V. (2013). The heme oxygenase/biliverdin reductase system: a potential drug target in Alzheimers disease. *J. Biol. Regul. Homeost Agents 27* 2(Suppl.), 75–87.

Marrazzo, P., Angeloni, C., and Hrelia, S. (2019). Combined treatment with three natural antioxidants enhances neuroprotection in a SH-SY5Y 3D culture model. *Antioxidants* 8:420. doi: 10.3390/antiox8100420

Mhillaj, E., Catino, S., Miceli, F. M., Santangelo, R., Trabace, L., Cuomo, V., et al. (2018a). Ferulic acid improves cognitive skills through the activation of the heme oxygenase system in the rat. *Mol. Neurobiol.* 55, 905–916. doi: 10.1007/s12035-017-0381-1

Mhillaj, E., Cuomo, V., and Mancuso, C. (2017). The contribution of transgenic and nontransgenic animal models in Alzheimer's disease drug research and development. *Behav. Pharmacol.* 28, 95–111. doi: 10.1097/FBP.0000000000000296

Mhillaj, E., Morgese, M. G., Tucci, P., Furiano, A., Luongo, L., Bove, M., et al. (2018b). Celecoxib prevents cognitive impairment and neuroinflammation in soluble amyloid beta-treated rats. *Neuroscience* 372, 58–73. doi: 10.1016/j.neuroscience.2017.12.046

Mhillaj, E., Tarozzi, A., Pruccoli, L., Cuomo, V., Trabace, L., and Mancuso, C. (2019). Curcumin and heme oxygenase: neuroprotection and beyond. *Int. J. Mol. Sci.* 20:2419. doi: 10.3390/ijms20102419

Miguel-Alvarez, M., Santos-Lozano, A., Sanchis-Gomar, F., Fiuza-Luces, C., Pareja-Galeano, H., Garatachea, N., et al. (2015). Non-steroidal anti-inflammatory drugs as a treatment for Alzheimer's disease: a systematic review and meta-analysis of treatment effect. *Drugs Aging* 32, 139–147. doi: 10.1007/s40266-015-0239-z

Minghetti, L. (2007). Role of COX-2 in inflammatory and degenerative brain diseases. *Subcell Biochem.* 42, 127–141.

Motterlini, R., and Foresti, R. (2017). Biological signaling by carbon monoxide and carbon monoxide-releasing molecules. *Am. J. Physiol. Cell Physiol.* 312, C302–C313. doi: 10.1152/ajpcell.00360.2016

Nag, S., Sarkar, B., Bandyopadhyay, A., Sahoo, B., Sreenivasan, V. K., Kombrabail, M., et al. (2011). Nature of the amyloid-beta monomer and the monomer-oligomer equilibrium. *J. Biol. Chem.* 286, 13827–13833. doi: 10.1074/jbc.M110.199885

Nichols, M. R., Colvin, B. A., Hood, E. A., Paranjape, G. S., Osborn, D. C., and Terrill-Usery, S. E. (2015). Biophysical comparison of soluble amyloid-beta(1-42) protofibrils, oligomers, and protofilaments. *Biochemistry* 54, 2193–2204. doi: 10.1021/bi500957g

Nitti, M., Piras, S., Brondolo, L., Marinari, U. M., Pronzato, M. A., and Furfaro, A. L. (2018). Heme Oxygenase 1 in the nervous system: does it favor neuronal cell survival or induce neurodegeneration? *Int. J. Mol. Sci.* 19, 2260. doi: 10.3390/ijms19082260

Palmieri, V., Bugli, F., Lauriola, M. C., Cacaci, M., Torelli, R., Ciasca, G., et al. (2017). Bacteria meet graphene: modulation of graphene oxide nanosheet interaction with human pathogens for effective antimicrobial therapy. *ACS Biomater. Sci. Eng.* 3, 619–627. doi: 10.1021/acsbiomaterials.6b00812

Palmieri, V., Lucchetti, D., Gatto, I., Maiorana, A., Marcantoni, M., Maulucci, G., et al. (2014). Dynamic light scattering for the characterization and counting of extracellular vesicles: a powerful noninvasive tool. *Res. Paper* 16:2583.

Park, J., Jang, M., and Chang, S. (2013). Deleterious effects of soluble amyloid-beta oligomers on multiple steps of synaptic vesicle trafficking. *Neurobiol. Dis.* 55, 129–139. doi: 10.1016/j.nbd.2013.03.004

Paulson, S. K., Hribar, J. D., Liu, N. W., Hajdu, E., Bible, R. H., Jr, Piergies, A., et al. (2000). Metabolism and excretion of [(14)C]celecoxib in healthy male volunteers. *Drug Metab. Dispos.* 28, 308–314.

Paulson, S. K., Vaughn, M. B., Jessen, S. M., Lawal, Y., Gresk, C. J., Yan, B., et al. (2001). Pharmacokinetics of celecoxib after oral administration in dogs and humans: effect of food and site of absorption. *J. Pharmacol. Exp. Ther.* 297, 638–645.

Perluigi, M., Joshi, G., Sultana, R., Calabrese, V., Coccia, R., Cini, C., et al. (2006). In vivo protective effects of ferulic acid ethyl ester against amyloid-beta peptide 1-42-induced oxidative stress. *J. Neurosci. Res.* 84, 418–426. doi: 10.1002/jnr.20879

Piantadosi, C. A. (2008). Carbon monoxide, reactive oxygen signaling, and oxidative stress. *Free Radic. Biol. Med.* 45, 562–569. doi: 10.1016/j.freeradbiomed.2008.05.013

Schipper, H. M., Bennett, D. A., Liberman, A., Bienias, J. L., Schneider, J. A., Kelly, J., et al. (2006). Glial heme oxygenase-1 expression in Alzheimer disease and mild cognitive impairment. *Neurobiol. Aging* 27, 252–261. doi: 10.1016/j.neurobiolaging.2005.01.016

Schipper, H. M., Cisse, S., and Stopa, E. G. (1995). Expression of heme oxygenase-1 in the senescent and Alzheimer-diseased brain. *Ann. Neurol.* 37, 758–768. doi: 10.1002/ana.410370609

Selkoe, D. J., and Hardy, J. (2016). The amyloid hypothesis of Alzheimer's disease at 25 years. *EMBO Mol. Med.* 8, 595–608. doi: 10.15252/emmm.201606210

Smith, M. A., Kutty, R. K., Richey, P. L., Yan, S. D., Stern, D., Chader, G. J., et al. (1994). Heme oxygenase-1 is associated with the neurofibrillary pathology of Alzheimer's disease. *Am. J. Pathol.* 145, 42–47.

Soininen, H., West, C., Robbins, J., and Niculescu, L. (2007). Long-term efficacy and safety of celecoxib in Alzheimer's disease. *Dement Geriatr. Cogn. Disord.* 23, 8–21. doi: 10.1159/000096588

Stine, W. B., Jungbauer, L., Yu, C., and LaDu, M. J. (2011). Preparing synthetic Abeta in different aggregation states. *Methods Mol. Biol.* 670, 13–32. doi: 10.1007/978-1-60761-744-0_2

Sultana, R., Ravagna, A., Mohmmad-Abdul, H., Calabrese, V., and Butterfield, D. A. (2005). Ferulic acid ethyl ester protects neurons against amyloid beta- peptide(1-42)-induced oxidative stress and neurotoxicity: relationship to antioxidant activity. *J. Neurochem.* 92, 749–758. doi: 10.1111/j.1471-4159.2004.02899.x

Tucci, P., Mhillaj, E., Morgese, M. G., Colaianna, M., Zotti, M., Schiavone, S., et al. (2014). Memantine prevents memory consolidation failure induced by soluble beta amyloid in rats. *Front. Behav. Neurosci.* 8:332. doi: 10.3389/fnbeh.2014.00332

Walsh, D. M., Klyubin, I., Fadeeva, J. V., Cullen, W. K., Anwyl, R., Wolfe, M. S., et al. (2002). Naturally secreted oligomers of amyloid beta protein potently inhibit hippocampal long-term potentiation in vivo. *Nature* 416, 535–539. doi: 10.1038/416535a

Wang, J. S., Ho, F. M., Kang, H. C., Lin, W. W., and Huang, K. C. (2011). Celecoxib induces heme oxygenase-1 expression in macrophages and vascular smooth muscle cells via ROS-dependent signaling pathway. *Naunyn Schmiedebergs Arch. Pharmacol.* 383, 159–168. doi: 10.1007/s00210-010-0586-6

Wang, X., Zhang, M., and Liu, H. (2019). LncRNA17A regulates autophagy and apoptosis of SH-SY5Y cell line as an in vitro model for Alzheimer's disease. *Biosci. Biotechnol. Biochem.* 83, 609–621. doi: 10.1080/09168451.2018.1562874

Wang, Y., Miao, Y., Mir, A. Z., Cheng, L., Wang, L., Zhao, L., et al. (2016). Inhibition of beta-amyloid-induced neurotoxicity by pinocembrin through Nrf2/HO-1 pathway in SH-SY5Y cells. *J. Neurol. Sci.* 368, 223–230. doi: 10.1016/j.jns.2016.07.010

Wilcox, K. C., Lacor, P. N., Pitt, J., and Klein, W. L. (2011). Abeta oligomer-induced synapse degeneration in Alzheimer's disease. *Cell. Mol. Neurobiol.* 31, 939–948. doi: 10.1007/s10571-011-9691-4

Conflict of Interest: The authors declare that the research was conducted in the absence of any commercial or financial relationships that could be construed as a potential conflict of interest.

frontiers in Cell and Developmental Biology

ORIGINAL RESEARCH
published: 13 May 2021
doi: 10.3389/fcell.2021.601600

Neural Stem Cell-Derived Exosomes Regulate Neural Stem Cell Differentiation Through miR-9-Hes1 Axis

Ping Yuan[1,2], Lu Ding[1], Huili Chen[1], Yi Wang[1], Chunhong Li[1], Shu Zhao[1], Xiaoyu Yang[1], Yizhao Ma[1], Jie Zhu[1], Xinrui Qi[1], Yanyan Zhang[1], Xiaohuan Xia[1,3] and Jialin C. Zheng[1,3,4]**

[1] Center for Translational Neurodegeneration and Regenerative Therapy, Tenth People's Hospital of Tongji University, Shanghai, China, [2] Department of Cardio-Pulmonary Circulation, School of Medicine, Shanghai Pulmonary Hospital, Tongji University, Shanghai, China, [3] Translational Research Institute of Brain and Brain-Like Intelligence, Shanghai Fourth People's Hospital affiliated to Tongji University School of Medicine, Shanghai, China, [4] Collaborative Innovation Center for Brain Science, Tongji University, Shanghai, China

Exosomes, a key element of the central nervous system microenvironment, mediate intercellular communication via horizontally transferring bioactive molecules. Emerging evidence has implicated exosomes in the regulation of neurogenesis. Recently, we compared the neurogenic potential of exosomes released from primary mouse embryonic neural stem cells (NSCs) and astrocyte-reprogrammed NSCs, and observed diverse neurogenic potential of those two exosome populations *in vitro*. However, the roles of NSC-derived exosomes on NSC differentiation and the underlying mechanisms remain largely unknown. In this study, we firstly demonstrated that NSC-derived exosomes facilitate the differentiation of NSCs and the maturation of both neuronal and glial cells in defined conditions. We then identified miR-9, a pro-neural miRNA, as the most abundantly expressed miRNA in NSC-derived exosomes. The silencing of miR-9 in exosomes abrogates the positive effects of NSC-derived exosomes on the differentiation of NSCs. We further identified *Hes1* as miR-9 downstream target, as the transfection of Hes1 siRNA restored the differentiation promoting potential of NSC-derived exosomes after knocking down exosomal miR-9. Thus, our data indicate that NSC-derived exosomes facilitate the differentiation of NSCs via transferring miR-9, which sheds light on the development of cell-free therapeutic strategies for treating neurodegeneration.

Keywords: exosome, miRNA, miR-9, Hes1, differentiation, maturation, neural stem cells

OPEN ACCESS

Edited by:
Stylianos Kosmidis, Columbia University, United States

Reviewed by:
Zheng Gang Zhang, Henry Ford Hospital, United States
Bei Shi, Affiliated Hospital of Zunyi Medical College, China
Hua Han, Fourth Military Medical University, China
Hua Teng, Henry Ford Hospital, United States, in collaboration with reviewer ZZ

****Correspondence:***
Jialin C. Zheng
jialinzheng@tongji.edu.cn
Xiaohuan Xia
xiaohuan_xia1@163.com

Specialty section:
This article was submitted to Molecular Medicine, a section of the journal Frontiers in Cell and Developmental Biology

Received: *01 September 2020*
Accepted: *16 April 2021*
Published: *13 May 2021*

Citation:
Yuan P, Ding L, Chen H, Wang Y, Li C, Zhao S, Yang X, Ma Y, Zhu J, Qi X, Zhang Y, Xia X and Zheng JC (2021) Neural Stem Cell-Derived Exosomes Regulate Neural Stem Cell Differentiation Through miR-9-Hes1 Axis. Front. Cell Dev. Biol. 9:601600. doi: 10.3389/fcell.2021.601600

Abbreviations: AD, Alzheimer's disease; CNS, central nervous system; E13.5, embryonic day 13.5; EXOs, neural stem cell-derived exosomes; HD, Huntington's disease; HUEVs, human umbilical vein endothelial cells; miRNA, microRNA; MSC, mesenchymal stromal cell; NanoFCM, nano-flow cytometry; NSC, neural stem cell; NTA, nanoparticle tracking analysis; PD, Parkinson's disease; RT, room temperature; RT-qPCR, quantitative reverse transcription-polymerase chain reaction; SDS-PAGE, sodium dodecyl sulfate polyacrylamide gel electrophoresis; TBI, traumatic brain injury; TEM, transmission electron microscopy; TPM, transcript per million.

INTRODUCTION

Neurodegenerative diseases, including Alzheimer's disease (AD), Parkinson's disease (PD), and Huntington's disease (HD), are a heterogeneous group of disorders that display the progressive neurodegeneration in specific regions of the central nervous system (CNS), leading to the function abnormalities and disabilities. Among neurodegenerative diseases, especially age-related ones, the impairment of neurogenesis is one key pathological feature (Steiner et al., 2006; Zhang et al., 2007). Due to the failure of clinical trial of drugs for eliminating key risk factors (e.g., Aβ) of neurodegenerative disorders, to maintain and expand the neural stem cell (NSC) pool and to facilitate the regenerative potential of NSCs have been considered as a promising therapeutic strategy for treating these diseases (Steiner et al., 2006; Abdipranoto et al., 2008). The stemness and differentiation potential of NSCs are regulated by cell extrinsic factors in the NSC niche (Yang, 2004; Kageyama et al., 2019; Ahmad et al., 2020). For example, during early CNS development, Notch signaling keeps NSCs uncommitted via activating its intercellular effectors, HES and HEY transcriptional repressor families (Tomita et al., 1996; Engler et al., 2018). Notch signaling also work in concert with SHH and Wnt pathways to facilitate NSCs proliferation (Engler et al., 2018; Ahmad et al., 2020). Thus, the temporal patterning of aforementioned pathways in the NSC niche controls NSC maintenance, differentiation, and cell lineage commitment (Noelanders and Vleminckx, 2017; Engler et al., 2018). Emerging evidence has implicated exosomes as a key part of the NSC niche (Zhang et al., 2017; Ma et al., 2019). Exosomes, a key mediator of intercellular communication, are small bilipid layer-enclosed extracellular vesicles (30–150 nm) that regulate various physiological and pathological processes through horizontally transferring bioactive cargos among cells (Valadi et al., 2007; Ramachandran and Palanisamy, 2012; Xia et al., 2019b). Zhang et al. reported that hypothalamic NSC-derived exosomes significantly slowdown aging-mediated hypothalamic NSC loss through transferring exosomal miRNAs (Zhang et al., 2017). Due to the potential effects of exosomes in the regulation of NSCs, the application/administration of stem cell-derived exosomes as a novel approach to stimulate endogenous neurogenesis (Oh et al., 2017; Yang et al., 2017). For instance, systemic administration of multipotent mesenchymal stromal cell (MSC)-derived exosomes effectively improves functional recovery by promoting endogenous angiogenesis and neurogenesis in rats after traumatic brain injury (TBI) (Xin et al., 2013; Zhang et al., 2015). MSC-derived exosomes, loaded with microRNAs (miRNAs), such as miR-124 or miR-17∼92, improve neurological function via enhancing the neuronal identity of cortical NSCs in TBI and ischemia animal models (Xin et al., 2017; Yang et al., 2017, 2019). Exosomes derived from human umbilical vein endothelial cells (HUVEs) also promote the proliferation and stemness maintenance of NSCs, displaying a potential to expand NSC pool during brain regeneration (Zhang et al., 2018).

Although great progress has been made to demonstrate the roles of exosomes in neurogenesis and neuroregeneration, multiple knowledge gaps remain there to be filled. For example, we are still in lack of information including but not limited to the effects and underlying mechanisms of embryonic NSC-derived exosomes (EXOs) on the regulation of NSCs and the potential interplay between EXOs and diverse signaling pathways in the NSC niche. To address those questions, we for the first time reported the involvement of the EXOs in the regulation of embryonic NSCs in defined conditions (Ma Y. et al., 2018; Ma et al., 2019). Interestingly, although EXOs have no significant effects on the proliferation of NSCs, those exosomes promote the generation of neurons from NSCs (Ma Y. et al., 2018; Ma et al., 2019). Our findings unveil the neurogenic potential of EXOs, however, the exact roles of EXOs in NSC differentiation and the underlying mechanisms remain largely unknown. To investigate the effects of EXOs on NSCs, in the current study, we co-cultured mouse embryonic NSCs with EXOs, and observed positive effects of EXOs on the fate commitment of NSCs and maturation of differentiated cells. We then examined the abundance of miRNAs in EXOs through microarray- and RT-qPCR-based approaches, and identified miR-9 as the most highly enriched one. We further demonstrated the essential roles of miR-9 in NSC differentiation by either directly manipulating the expression of miR-9 in NSCs or silencing exosomal miR-9 in the EXO-NSC co-culture system. Lastly, we identified the key downstream target of exosomal miR-9, *Hes1*, since silencing *Hes1* restored the differentiation promoting potential of miR-9-deleted EXOs. Our study demonstrated an important role of EXOs in the regulation of NSCs and dissected the underlying molecular mechanisms, which, provides the theories foundation for the amplification of EXOs in treating neurodegenerative diseases.

MATERIALS AND METHODS

Isolation and Enrichment of Mouse NSCs

NSCs were isolated from mouse fetal brain tissue as previously described (Ma K. et al., 2018). Briefly, cortical tissues were isolated from embryonic day 13.5 (E13.5) C57BL/6J mice and triturate physically 15–20 times. Dissociated tissues were filtered through 40 μm filter. Single cells were cultured in substrate-free tissue culture flasks for the formation of neurospheres in NSC proliferation medium, containing NeuroCult® NSC Basal Medium (Stem Cell Technologies), NeuroCult® NSC Proliferation Supplements (Stem Cell Technologies), 20 ng/mL FGF2 (BioWalkersville), 20 ng/mL EGF (BioWalkersville), and 2 μg/mL heparin (Sigma), N2 supplement (Gibco), 2 mM L-glutamine (ThermoFisher), 100 IU/mL penicillin (ThermoFisher), and 100 μg/mL streptomycin (ThermoFisher). Primary neurospheres were collected, centrifuge at low speed to remove flowing cells, dissociated into single cells by accutase (Sigma) for 5 min at 37°C, and re-plated for a second round of neurosphere formation. Enriched NSCs were harvested after three rounds of neurosphere formation.

Differentiation of NSCs

The differentiation of NSCs was carried out as previously described (Ma et al., 2019). Briefly, 5×10^3 NSCs were planted

on Matrigel-coated coverslips in 24-well plate with DMEM/F12 (Gibco) supplemented with 1 × N2 supplement (Gibco), 1 × B27 supplement (Gibco), 1.0 mM GlutaMAX (ThermoFisher), 10 ng/mL brain-derived neurotrophic factor (BDNF) (Peprotech), 10 ng/mL glial cell line-derived neurotrophic factor (GDNF) (Peprotech), and 2% Knockout Serum Replacement (Gibco). The medium was changed every 2 days.

Collection of Exosomes

Exosomes were isolated from the culture medium of NSCs as previously described (Ma Y. et al., 2018). Briefly, 6×10^6 NSCs were plated in poly-L-Ornithine/laminin-coated 10 cm dish and cultured in NSC proliferation medium for 12 h. The supernatants were collected and exosomes were collected by gradient centrifugation: supernatants were first centrifuged at 300 g for 10 min to remove flowing cells, at 3,000 g for 20 min to remove cellular debris, at 10,000 g for 30 min to remove intracellular organelles and then at 100,000 g for 2 h to precipitate exosomes. All steps of centrifugation were handled at 4°C. Exosomal protein concentrations were determined with a BCA Protein Assay Kit (Pierce). For PKH67 labeling, every 100 μg exosomes were incubated with 2 nmol PKH67 for 10 min at room temperature (RT). Exosomes were re-collected through ultra-speed centrifugation.

Agonist/Antagonist/siRNA and Transfection

The agomiR control, agomiR-9, antagomiR control, antagomiR-9, siRNA scrambled control, and Hes1 siRNA were purchased from GenePharma (GenePharma). Transfection of 20 nM agomiR-9/antagomiR-9/Hes1 siRNA or their corresponding controls was performed using the Lipofectamine 2000 reagent (Invitrogen) according to the manufacturer's instruction.

Transmission Electron Microscopy

Negative staining of exosome suspensions followed by imaging in a transmission electron microscope was used to determine vesicle shape and size distribution. Aliquots of exosome suspensions were dispensed onto sheets of Parafilm in a humidified petri dish and the vesicles were deposited on carbon-coated grid (300-mesh) for 3 min. Subsequently, the grid was negatively stained with 1% uranyl acetate for 3 min and excess stain was blotted off. The droplets of exosomes were removed with filter paper and air-dried at RT. Images were taken by transmission electron microscopy (JEM-1230, JEOL).

Nanoparticle Tracking Analysis

The size and number of exosomes were carried out as previously described (Ma Y. et al., 2018). Briefly, isolated EVs were resuspended in 150 μL PBS and diluted at 1:100 in PBS. 1 mL solution was used for NTA that was assessed on NanoSight NS300 system (Malvern Instruments) with a sCMOS camera. The conditions of the measurements were set at 25°C, 1 cP viscosity, 25 s per capture frame and 60 s measurement time. Three individual measurements were applied for determining the size and concentration of exosomes.

Nano-Flow Cytometry

The size and number of exosomes were identified by NanoFCM. NanoFCM is applicable when the refractive index of input samples are the same or similar to that of silica particles. The standard working curve of scattering light intensity is established using silica standard sphere. EVs isolated from 50 mL conditioned medium were resuspended in 100 μL PBS for NanoFCM. The particle size distribution of exosome samples is measured based on the scattering intensity.

Immunocytochemistry

Differentiated NSCs were fixed in 4% formaldehyde for 20 min at RT and then washed with PBS for three times. The fixed cells were permeabilized with 0.2% Triton X-100 in PBS for 10 min, blocked with 2% BSA in PBS for 1 h at RT, and then incubated overnight at 4°C with primary antibodies including Map2 (rabbit, Sigma, 1:200), βIII-Tubulin (Tuj1) (mouse, Millipore, 1:200), Glast (rabbit, Abcam, 1:100), and GFAP (chick, CST, 1:200). Coverslips were washed with PBS for three times and incubated for 1 h at RT with secondary antibodies including anti-rabbit IgG (coupled with Alexa Fluor 568, Life Technologies), anti-rabbit IgG (coupled with Alexa Fluor 488, Life Technologies), anti-chicken IgG (coupled with Alexa Fluor 488, Life Technologies), and anti-mouse IgG (coupled with Alexa Fluor 488, Life Technologies). Coverslips were mounted using VectaShield (Vector Laboratories) and images were taken by a Zeiss AX10 fluorescence microscope accompanied with ZEN 2.3 (blue edition) software. For quantification of the percentage of specific cell types in each experiment, cell type-specific antigen positive cells were counted from 15 random fields per group in three coverslips (five fields each).

Quantitative Reverse Transcription-Polymerase Chain Reaction

The mRNA and miRNA were isolated from cell samples using RNeasy mini kit (Qiagen) according to the manufacturer's instructions. Genomic DNA was removed and cDNA was synthesized using DNase I digestion kit (Qiagen) and miScript II reverse transcription kit (Qiagen), respectively. Transcripts were amplified using gene-specific primer (**Supplemental Table 1**) and SYBR green PCR kit (Qiagen) with the ABI7500 (Applied Biosystems). All RT-qPCR results measured each sample in triplicate and no-template blanks were used for negative controls. Amplification curves and gene expression were normalized to the house-keeping gene *Gapdh* (for mRNA) and *U6* snRNA (for miRNA).

Western Blotting

Western blotting was performed as previously described (Gao et al., 2019). Exosomes were lysed in RIPA lysis and extraction buffer (ThermoFisher) containing a protease inhibitor cocktail (Sigma). Protein concentrations were determined with a BCA Protein Assay Kit (Pierce). Proteins (20–30 mg) were separated by sodium dodecyl sulfate polyacrylamide gel electrophoresis (SDS-PAGE) and electrophoretic transferred

to polyvinylidene fluoride membranes (Millipore and Bio-Rad). Membranes were incubated with primary antibodies for CD9 (rabbit, Abcam, 1:2,000), Flottlin1 (mouse, BD Biosciences; 1:5,000), TSG (rabbit, Abcam, 1:1,000), APOA1 (rabbit, Affinity Biosciences; 1:500), APOA2 (rabbit, Affinity Biosciences; 1:500), Hes1 (rabbit, Affinity Biosciences; 1:500), and β-actin (mouse, CST; 1:1,000) overnight at 4°C followed by a secondary anti-rabbit or anti-mouse antibody (Cell Signaling Technologies, 1:10,000) incubation. Antigen-antibody complexes were visualized by Pierce ECL Western Blotting Substrate (ThermoFisher). For data quantification, films were scanned with a CanonScan 9950F scanner; the acquired images were analyzed using ImageJ program.

MicroRNAs Microarray

Total RNA was extracted from EXOs and 3 μg total RNA per sample was used as input material for the small RNA library. Sequencing libraries were generated using NEBNext® Multiplex Small RNA Library Prep Set for Illumina® (NEB). The clustering of the index-coded samples was performed on a cBot Cluster Generation System using TruSeq SR Cluster Kit v3-cBot-HS (Illumia). After cluster generation, the library preparations were sequenced on an Illumina Hiseq 2,500/2,000 platform and 50 bp single-end reads were generated. Raw data (raw reads) of fastq format were firstly processed through custom perl and python scripts for quality control. The small RNA tags were mapped to reference sequence by Bowtie without mismatch to analyze their expression and distribution on the reference. Mapped small RNA tags were used to looking for known miRNA. miRBase 20.0 was used as reference for known miRNA, miRDeep2, and sRNA-tools-cli were used to obtain novel miRNAs and draw the secondary structures, respectively. miRNA expression levels were estimated by transcript per million (TPM).

Statistical Analyses

All results are the means of at least three independent experiments ± SE. The statistical difference between two independent groups was analyzed with the unpaired Student's *t*-test, and that among more than two groups was assessed with the parametric one-way ANOVA with *post hoc* Bonferroni test. Significance was considered when $p < 0.05$.

RESULTS

EXOs Promote the Differentiation of NSCs

To test the effects of EXOs on the differentiation of NSCs, we isolated and characterized ultracentrifugation-enriched EXOs. TEM visualized the cup-shaped appearance of exosomes with sizes less than 200 nm (**Figure 1A**). Western blotting analysis detected strong expression of three positive protein markers of exosomes including TSG101, CD9, and Flotillin-1, in the collected exosome samples (**Figure 1B**). Additionally, negative protein markers APOA1 and APOA2 were expressed in NSC lysate but not in the exosome samples, confirming the purity of exosomes (**Figure 1C**). Both NTA and NanoFCM analyses further confirmed the typical size distribution of ultracentrifugation-enriched EXOs (30–150 nm), confirming the purification of EXOs (**Figures 1D,E**).

The internalization of exosomes by NSCs was validated by incubating PKH67-labeled exosomes with primary NSCs for 12 h (**Supplementary Figure 1**). We then co-cultured NSCs with 15 μg/mL EXOs in differentiation conditions for 6 days. The immunofluorescence analysis suggested that EXOs enhanced NSC differentiation, ascertained by higher proportions of $Tuj1^+$ neuronal and $GFAP^+$ glial cells in exosome-treated groups versus PBS controls (**Figure 2A**). Next, we examined the effects of EXOs on neuronal and glial maturation. The immunofluorescence analysis indicated that more matured neurons ($Map2^+$ cells) and astrocytes ($Glast^+$ cells) were presented in EXO-treated groups, compared to PBS controls (**Figure 2B**). RT-qPCR analysis also revealed an increase in the levels of transcripts corresponding to pre-mature neuronal markers (β*III-tubulin*), pre-mature astroglial markers (*GFAP*), matured neuronal markers (*Map2*) and matured astroglial markers (*GS*) in EXO-treated group, compared to PBS controls, confirming the immunostaining results (**Figure 2C**). The effects of EXOs on NSC differentiation were further confirmed by co-culturing EXOs with NSCs in differentiation conditions for 3 and 9 days (**Supplementary Figures 2**, **3**). Thus, our observations suggested that EXOs facilitate the differentiation of NSCs and the maturation of both neuronal and glial cells.

miR-9 Is Abundantly Expressed in EXOs

To dissect the mechanisms underlying the positive effects of EXOs on differentiation and maturation, we examined the exosomal miRNA profile through miRNA microarray. 565 mouse miRNAs have been identified by microarray. Among all detected miRNAs, miR-9 displayed the highest abundance (**Figure 3A**) and readcount (TPM) (**Figure 3B**). This result was validated by RT-qPCR that, of the top 10 miRNAs with the highest readcounts, miR-9 exhibited lowest Ct value (**Figure 3C**). Both results indicate the highest abundance of miR-9 in EXOs.

miR-9 Positively Regulates NSC Differentiation

Interestingly, multiple reports have implied the neurogenic roles of *miR-9* (Coolen et al., 2012, 2013). To confirm it, we examined the effects of miR-9 on NSC differentiation by perturbation-of-function approaches using specific antagonist and agonist, antagomiR-9 and agomiR-9, respectively. NSCs were firstly transfected with either miR-9 antagonist (antagomiR-9) or its corresponding control (antagomiR-C) and cultured in differentiation conditions for 6 days. The knockdown efficiency was validated by RT-qPCR, where significant down-regulation of miR-9 expression levels was observed in antagomiR-9 group, compared to antagomiR-C group (**Figure 4A**). Immunofluorescence analysis demonstrated a significant decrease in the proportions of both $Tuj1^+$ and $GFAP^+$ cells once we inhibited miR-9 expression during the differentiation of NSCs (**Figure 4B**). Furthermore, we also observed a significant

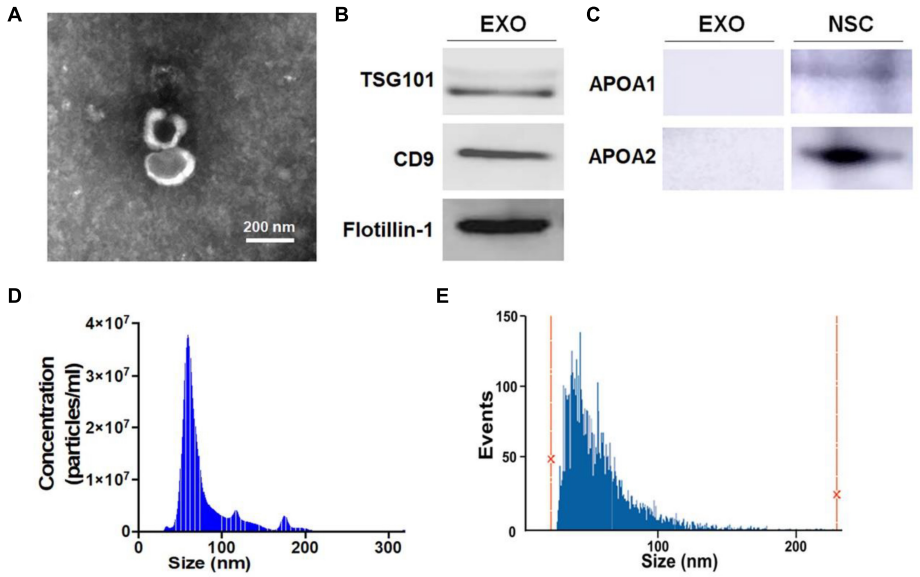

FIGURE 1 | Characterization of exosomes (EXOs). **(A)** Purified exosomes were observed under transmission electron microscopy (TEM) using negative staining. **(B)** The levels of positive exosomal markers TSG101, CD9, and Flotillin-1 in protein lysates of neural stem cells (NSC)-derived exosome pellets were determined by western blotting. **(C)** The levels of negative exosomal markers APOA1 and APOA2 in protein lysates of NSC-derived exosome pellets and NSCs were determined by western blotting. **(D,E)** Particle-size distribution of exosomes was determined by NanoSight analysis (NTA) in panel **(D)** and NanoFCM in panel **(E)** technologies. Scale bar 200 nm in panel **(A)**.

decrease in the proportions of both Map2$^+$ and Glast$^+$ cells in antagomiR-9 group versus controls (**Figure 4C**). Our findings were corroborated by RT-qPCR analysis that revealed a significant decrease in the expression levels of transcripts corresponding to pre-mature cell markers (β*III-tubulin* and *GFAP*) and matured cell markers (*Map2* and *GS*), in antagomiR-9 group versus controls (**Figure 4D**). Thus, our results indicate that the lack of miR-9 blocks or delays the cell fate commitment of NSCs and the maturation of differentiated cells.

Next, we transfected NSCs with either miR-9 agonist (agomiR-9) or control agonist (agomiR-C). Transfected cells were then cultured in differentiation conditions for 6 days. AgomiR-9 transfection significantly increased the expression levels of miR-9 in NSCs (**Figure 5A**). The proportions of both Tuj1$^+$/Map2$^+$ neurons and GFAP$^+$/Glast$^+$ astrocytes also increased significantly in agomiR-9 group, compared with agomiR-C group (**Figures 5B,C**). Additionally, the transcript levels of pre-mature cell markers (β*III-tubulin* and *GFAP*) and matured cell markers (*Map2* and *GS*) were similarly increased in agomiR-9 group versus controls, validated by RT-qPCR analysis (**Figure 5D**). Taken together, our results demonstrated *that miR-9 functions* as an important regulator in enhancing the differentiation of NSCs and the maturation of both neurons and glia.

Exosomes Regulate NSC Differentiation via miR-9

To determine whether the positive effects of EXOs on NSC differentiation is mediated by miR-9, we transfected NSCs with either antagomiR-9 or antagomiR-C using the approach described above and collected exosomes in the culture medium 48 h post transfection. RT-qPCR analysis revealed that the expression levels of miR-9 was significantly reduced in exosomes derived from antagomiR-9 transfected NSCs (EXO-antagomiR-9), compared to EXOs and antagomiR-C-transfected NSCs (EXO-antagomiR-C) (**Figure 6A**). NSCs were then co-cultured with either EXO-antagomiR-9 or EXO-antagomiR-C under differentiation conditions for 6 days. RT-qPCR analysis revealed that the expression levels of miR-9 were significantly increased in NSCs co-cultured with EXO-antagomiR-C, compared with PBS controls (**Figure 6B**). Moreover, no difference in miR-9 expression was observed between EXO-antagomiR-9-treated and PBS control groups. The immunofluorescence analysis demonstrated that the positive influence of EXO-antagomiR-C on NSC differentiation was abrogated by depleting exosomal miR-9, determined by the quantification of Tuj1$^+$ neurons and GFAP$^+$ astrocytes (**Figure 6C**). In addition, the positive effects of EXO-antagomiR-C on cell maturation was compromised by knocking down exosomal miR-9, ascertained by the significant decrease in the proportions of Map2$^+$ neurons and Glast$^+$ astrocytes in EXO-antagomiR-9 group versus EXO-antagomiR-C group (**Figure 6D**). The expression levels of transcripts corresponding to pre-mature cell markers (β*III-tubulin* and *GFAP*) and matured cell markers (*Map2* and *GS*) were also significantly reduced in EXO-antagomiR-9 group, compared to EXO-antagomiR-C group (**Figure 6E**). Together, our results suggested that miR-9 is the key cargo in mediating the effects of EXOs on the differentiation of NSCs and the maturation of both neurons and glia.

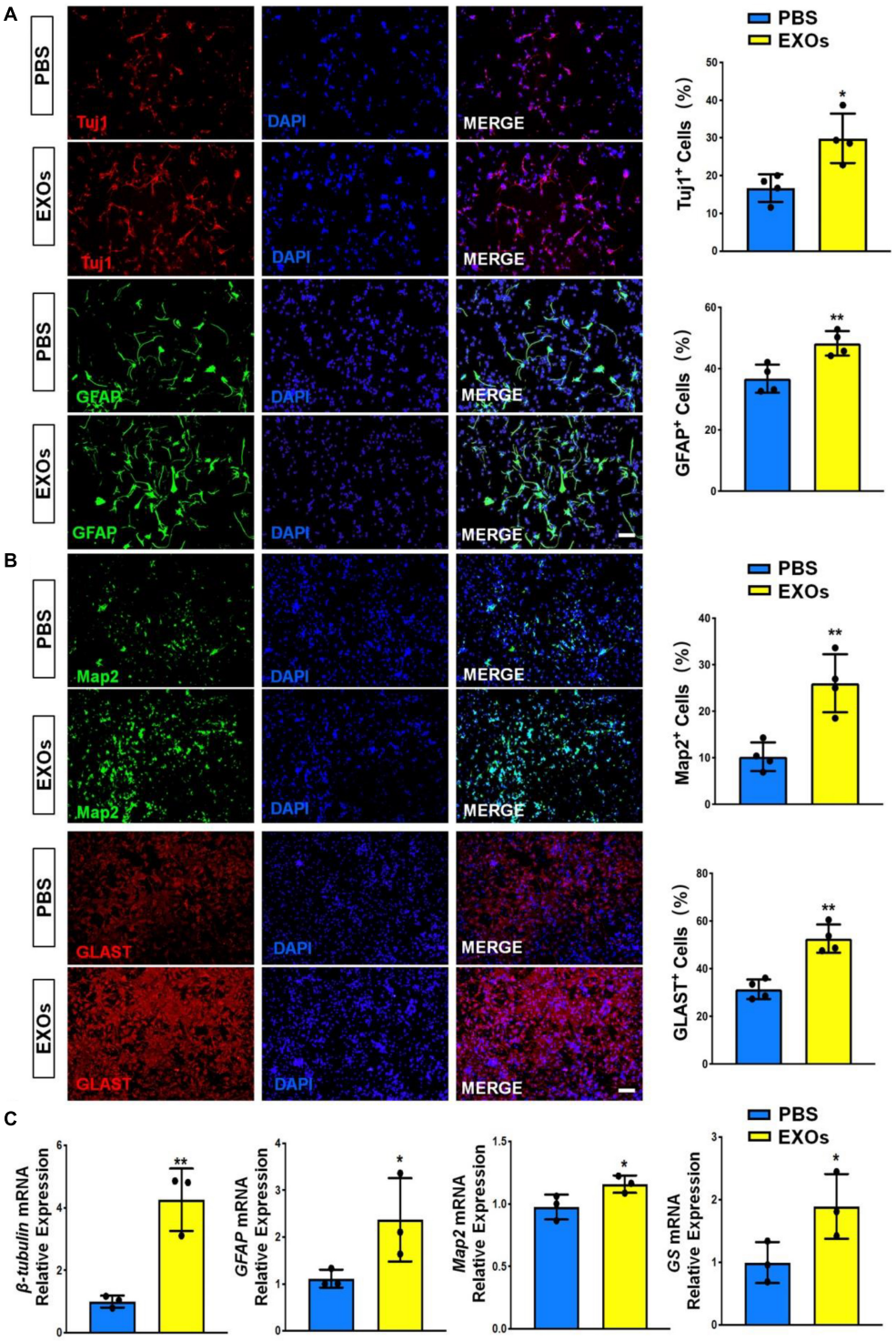

FIGURE 2 | Exosomes promote NSC differentiation. **(A)** NSCs were co-cultured with exosomes for 6 days in differentiation conditions. Representative images of pre-mature neuronal (Tuj1) and glial (GFAP) markers staining were shown. Proportions of cells expressing pre-mature cell-specific immunoreactivities were determined (in the right panel). **(B)** Representative images of matured neuronal (Map2) and glial (Glast) staining were shown. Proportions of cells expressing matured cell-specific immunoreactivities were determined (in the right panel). **(C)** The transcript expression of pre-mature cell markers (β*III-tubulin* and *GFAP*) and matured cell markers (*Map2* and *GS*) was determined by RT-qPCR analysis. Data were represented as mean ± SE from three independent experiments. * and ** denote $p < 0.05$ and $p < 0.01$, respectively. Scale bar 100 μm in panel **(A,B)**.

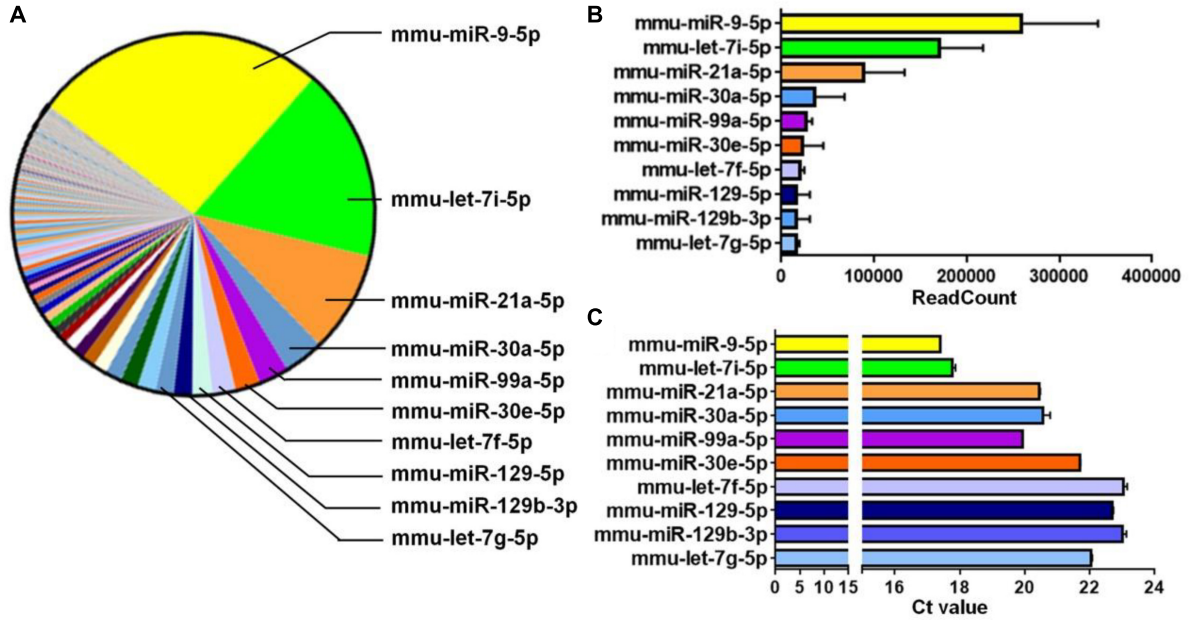

FIGURE 3 | miR-9 is predominantly expressed in EXOs. **(A)** The microRNAs (miRNAs) profiles of NSC-derived exosomes were determined by miRNA microarray and a parts of whole table for the readcounts of all detected miRNAs was generated. The 10 miRNAs with the most readcounts were marked on the right. **(B)** The readcounts of the top 10 most abundantly expressed miRNAs. Data were represented as mean ± SD from three independent biological samples. **(C)** The Ct value of RT-qPCR analysis for the top 10 most abundantly expressed miRNAs, identified by miRNA microarray, in NSC-derived exosomes. Data were represented as mean ± SE from three independent experiments.

Exosomes Regulate NSC Differentiation via miR-9-Hes1 Axis

To gain insight into the mechanism underlying exosomal miR-9 influence on NSC differentiation, we examined the expression patterns of known miR-9 target genes including *Foxg1*, *Foxp2*, *Hes1*, *Map1b*, *Msi1*, *Pax6*, *REST*, *Tlx*, and *Zic5* (Clovis et al., 2012; Coolen et al., 2013; Radhakrishnan and Anand, 2016). RT-qPCR results demonstrated that the expression levels of *Hes1*, *Map1b*, *REST*, and *Foxp2* transcripts were up-regulated significantly in antagomiR-9-transfected NSCs, compared to both PBS and antagomiR-C controls (**Figure 7A**). RT-qPCR analysis also found that the knockdown of miR-9 in EXOs reversed the negative effects of EXOs on the expression levels of *Hes1*, *Map1b*, and *REST* transcripts, but not that of *Foxp2* transcripts in NSCs (**Figure 7B**). Furthermore, *Hes1* transcript levels displayed the largest fold changes among aforementioned three genes, therefore, we chose *Hes1* as exosomal miR-9 target candidate for following studies. We then carried out western blotting to confirm the inverse correlation between *Hes1* and miR-9 expression. Down-regulation of Hes1 protein levels was observed in agomiR-9-transfected NSCs versus controls (**Figure 7C**). The direct interaction between miR-9 and *Hes1* 3′ untranslated region (UTR) was validated by dual luciferase assay. Co-transfection of agomiR-9 and Dual-Luciferase reporter constructs containing the wild-type *Hes1* 3′UTR, but not that containing miR-9 target site mutated *Hes1* 3′UTR, significantly decreased the firefly activity in HEK293A cells, normalized by the Rellina activity, indicating miR-9 directly targets *Hes1* (**Figure 7D**).

We carried out loss-of-function study to address the effects of Hes1 on NSC differentiation. NSCs were transfected with either Hes1 siRNA or scrambled control (control siRNA) and cultured in differentiation conditions for 6 days. The knockdown efficiency was validated by RT-qPCR, where significant reduction of *Hes1* expression levels was observed in Hes1 siRNA group, compared to control siRNA group (**Figure 8A**). Immunofluorescence analysis demonstrated a significant increase in the proportions of both Tuj1$^+$ and GFAP$^+$ cells once Hes1 expression was inhibited during NSC differentiation (**Figure 8B**). Furthermore, higher proportions of both Map2$^+$ and Glast$^+$ cells were observed in Hes1 siRNA group versus control siRNA group (**Figure 8C**). Our findings were confirmed by RT-qPCR analysis which revealed a significant elevation in the expression levels of transcripts corresponding to pre-mature cell markers (β*III-tubulin* and *GFAP*) and matured cell markers (*Map2* and *GS*) in Hes1 siRNA group versus control siRNA group (**Figure 8D**). Both immunofluorescence and RT-qPCR analyses revealed Hes1 as an important repressor of NSC differentiation.

At last, we investigated whether or not Hes1 acts as the downstream target of exosomal miR-9 during NSC differentiation. NSCs were co-cultured with either EXO-antagomiR-9 or EXO-antagomiR-C. A subgroup in EXO-antagomiR-9 group was co-transfected with Hes1 siRNA to inhibit Hes1 expression. NSCs treated with PBS of the same volume as exosome suspension and then transfected with scrambled siRNA were utilized as control group. NSCs in all

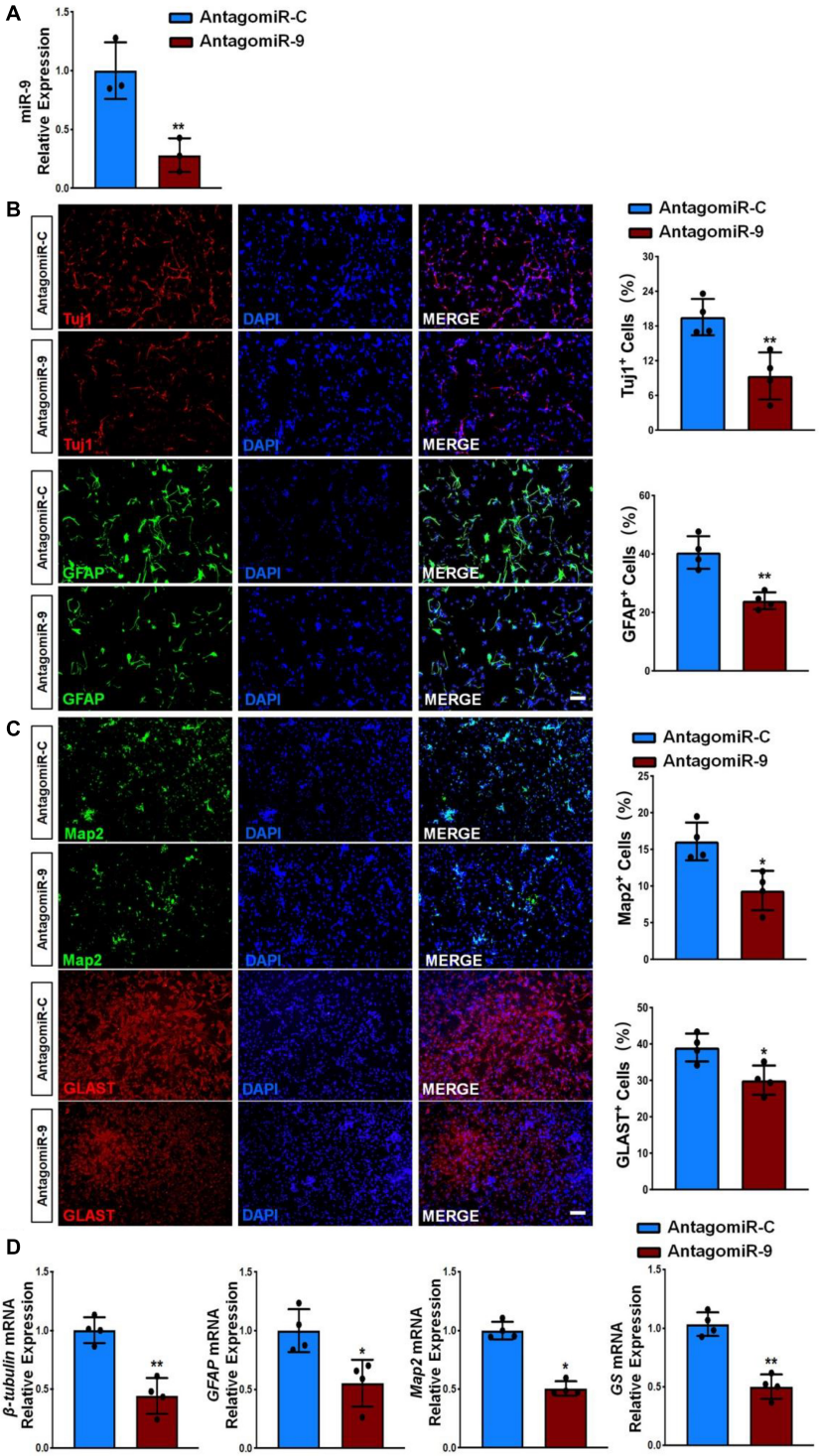

FIGURE 4 | miR-9 loss-of-function inhibits NSC differentiation. **(A)** NSCs transfected with either antogomiR-C or antogomiR-9 were cultured for 6 days in differentiation conditions. The transfection efficiency was determined by quantifying the intracellular miR-9 expression levels via RT-qPCR analysis. **(B)** Representative images of pre-mature cell markers (Tuj1 and GFAP) staining were shown. Proportions of cells exhibiting immunoreactivities of pre-mature cell markers ($Tuj1^+$ and $GFAP^+$) were determined (in the right panel). **(C)** Representative images of matured cell markers (Map2 and Glast) staining were shown. Proportions of cells exhibiting immunoreactivities of pre-mature cell markers ($Map2^+$ and $Glast^+$) were determined (in the right panel). **(D)** The expression levels of transcripts corresponding to pre-mature cell markers (*βIII-tubulin* and *GFAP*) and matured cell markers (*Map2* and *GS*) was determined by RT-qPCR analysis. Data were represented as mean ± SE from three independent experiments. * and ** denote $p < 0.05$ and $p < 0.01$, respectively. Scale bar 100 μm in panel **(B,C)**.

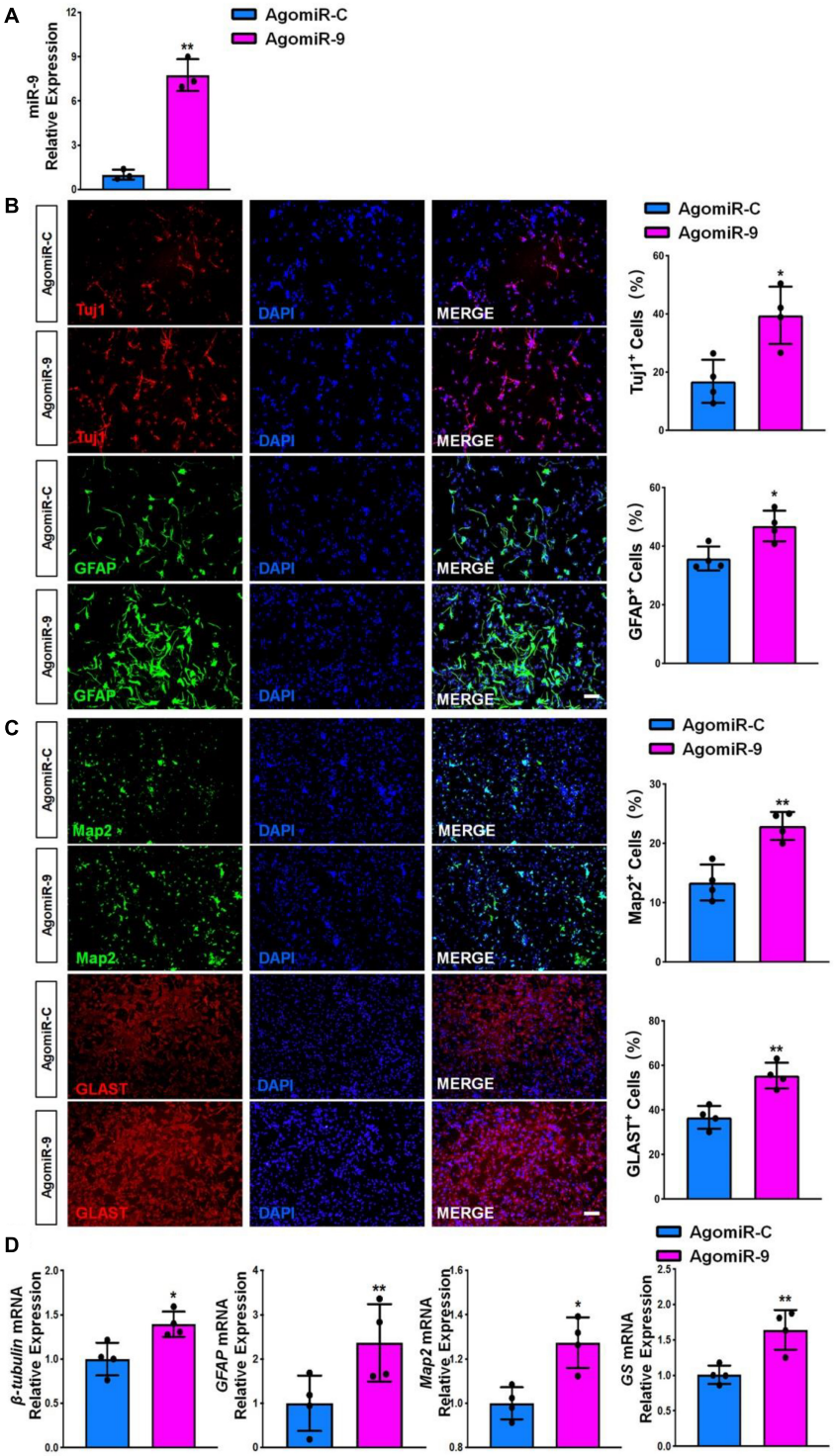

FIGURE 5 | miR-9 gain-of-function promotes NSC differentiation. **(A)** NSCs transfected with either agomiR-C or agomiR-9 were cultured for 6 days in differentiation conditions. The transfection efficiency was determined by quantifying the intracellular miR-9 expression levels via RT-qPCR analysis. **(B)** Representative images of pre-mature cell markers (Tuj1 and GFAP) staining were shown. Proportions of cells exhibiting immunoreactivities of pre-mature cell markers (Tuj1$^+$ and GFAP$^+$) were determined (in the right panel). **(C)** Representative images of matured cell markers (Map2 and Glast) staining were shown. Proportions of cells exhibiting immunoreactivities of pre-mature cell markers (Map2$^+$ and Glast$^+$) were determined (in the right panel). **(D)** The expression levels of transcripts corresponding to pre-mature cell markers (β*III-tubulin* and *GFAP*) and matured cell markers (*Map2* and *GS*) was determined by RT-qPCR analysis. Data were represented as mean ± SE from three independent experiments. * and ** denote $p < 0.05$ and $p < 0.01$, respectively. Scale bar 100 μm in panel **(B,C)**.

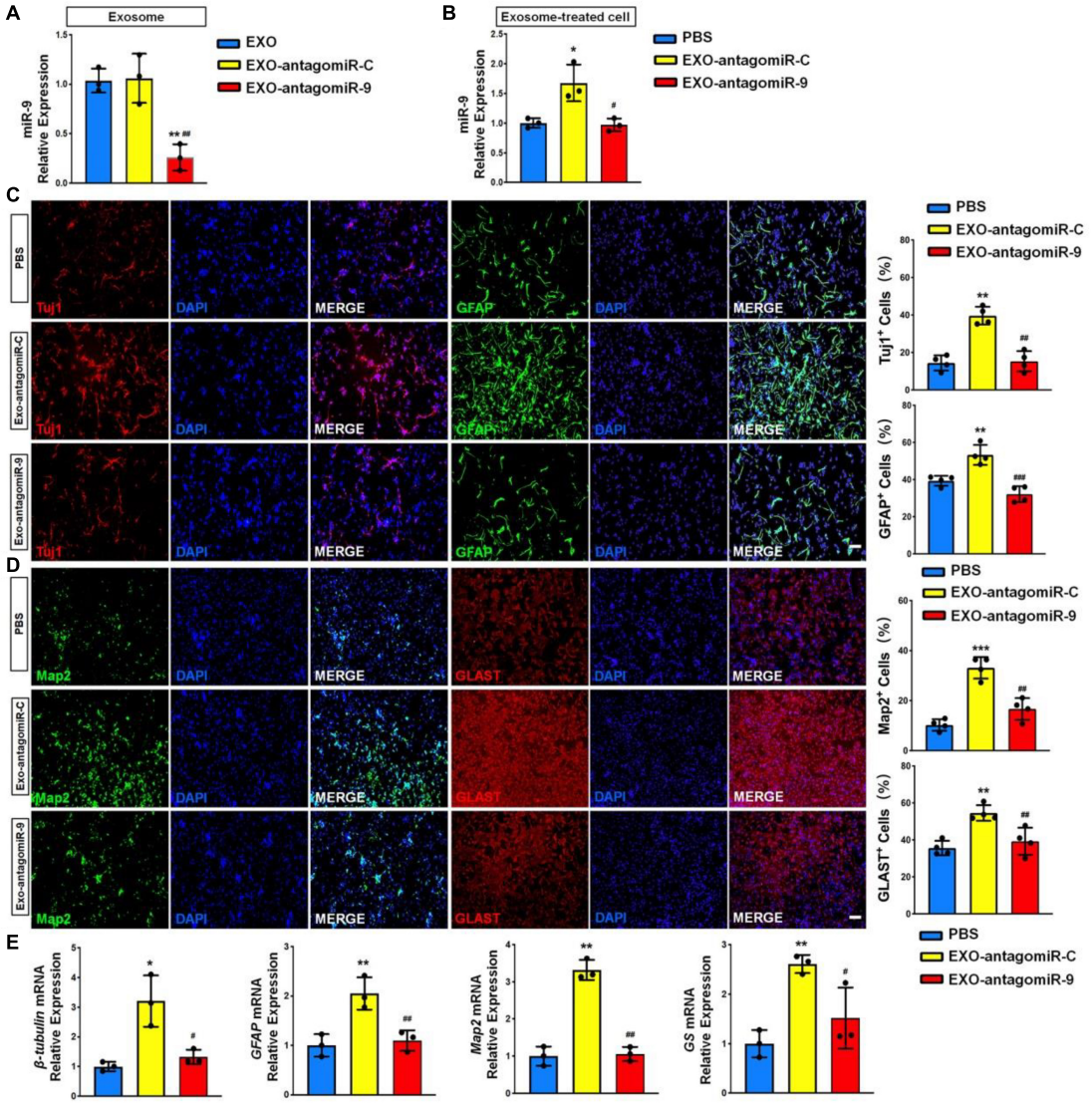

FIGURE 6 | miR-9 mediates the effects of EXOs on NSC differentiation. **(A)** NSCs were transfected with either antogomiR-C or antogomiR-9. The knockdown of miR-9 expression levels in exosomes derived from antogomiR-9-transfected NSCs were validated by RT-qPCR. **(B)** NSCs treated with PBS, EXO-antagomiR-9, or EXO-antagomiR-C were cultured for 6 days in differentiation conditions. The expression levels of miR-9 in NSCs treated with PBS or exosomes were determined by RT-qPCR analysis. **(C)** Representative images of pre-mature cell markers (Tuj1 and GFAP) staining were shown. Proportions of cells exhibiting immunoreactivities of pre-mature cell markers ($Tuj1^+$ and $GFAP^+$) were determined (in the right panel). **(D)** Representative images of matured cell markers (Map2 and Glast) staining were shown. Proportions of cells exhibiting immunoreactivities of pre-mature cell markers ($Map2^+$ and $Glast^+$) were determined (in the right panel). **(E)** The expression levels of transcripts corresponding to pre-mature cell markers (β*III-tubulin* and *GFAP*) and matured cell markers (*Map2* and *GS*) were determined by RT-qPCR analysis. Data were represented as mean ± SE from three independent experiments. * and ** denote $p < 0.05$ and $p < 0.01$ in comparison to control, respectively. # and ## denote $p < 0.05$ and $p < 0.01$ in comparison to EXO-antagomiR-C group, respectively. Scale bar 100 μm in panel **(C,D)**. $^{***}p < 0.001$, $^{\#\#\#}p < 0.001$.

groups were cultured in differentiation conditions for 6 days. RT-qPCR analysis demonstrated that the reduction of *Hes1* transcript expression in EXO-antagomiR-C groups was abrogated by knocking down miR-9 in EXOs (**Figure 9A**). The upregulation of *Hes1* transcript expression in EXO-antagomiR-9 groups was further eliminated by Hes1 siRNA treatment, validating the transfection efficiency of Hes1 siRNA. Quantification of cell type-specific markers revealed that the silencing of Hes1 significantly restored the proportions of pre-mature $Tuj1^+$ neurons and $GFAP^+$ astrocytes (**Figure 9B**). Besides, the proportions of matured cells ($Map2^+$ neurons and $Glast^+$ astrocytes) were similarly restored after down-regulating Hes1 expression in EXO-antagomiR-9 group (**Figure 9C**). RT-qPCR results also demonstrated similar patterns that the Hes1 repression by siRNA significantly enhance the expression levels of transcripts corresponding to pre-mature cell markers (β*III-tubulin* and *GFAP*) and matured cell markers (*Map2* and *GS*) in EXO-antagomiR-9 group (**Figure 9D**). Taken together, these results

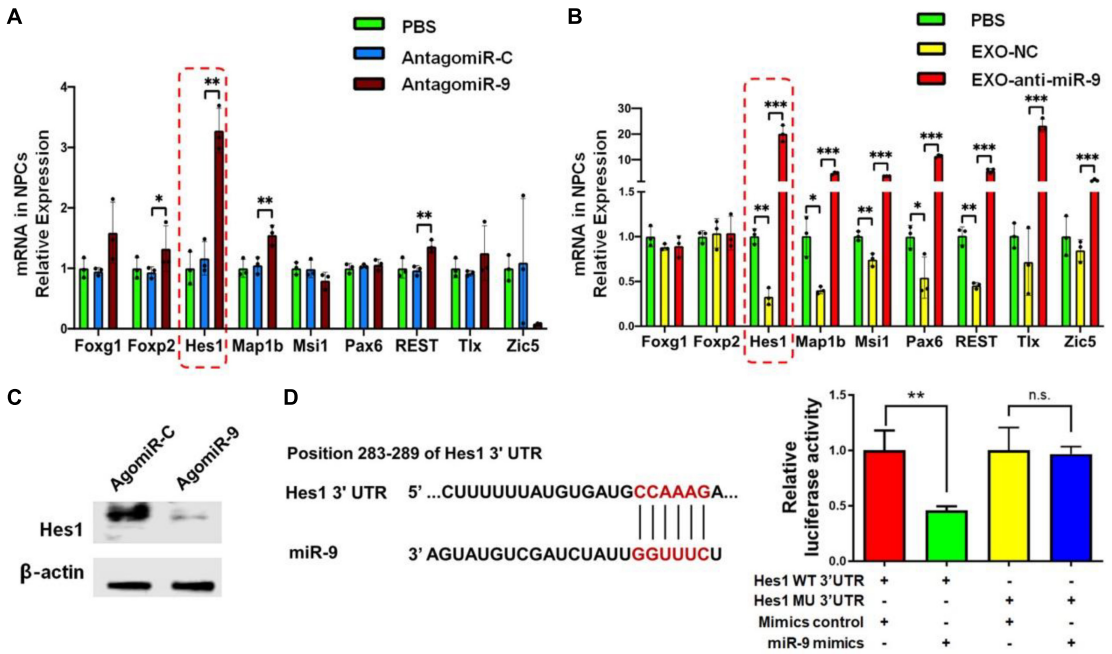

FIGURE 7 | *Hes1* expression is negatively regulated by miR-9 in NSCs. **(A)** The expression levels of transcripts corresponding to known targets of miR-9 in NSCs transfected with either antagomiR-9 or antagomiR-C were determined by RT-qPCR analysis. **(B)** The expression levels of transcripts corresponding to known targets of miR-9 in NSCs co-cultured with either EXO-antagomiR-9 or EXO-antagomiR-C were determined by RT-qPCR analysis. **(C)** Representative western blotting results showing the expression of Hes1 and β-actin proteins in either agomiR-C- or agomiR-9-transfected NSCs. **(D)** The predicted consequential pairing of *Hes1* 3′UTR (top) and miR-9 (bottom) on the TargetScan website (left). Repression of luciferase activities by the *Hes1* 3′UTR were dependent on miR-9 (right). Firefly luciferase activities were normalized to the internal control, Renilla luciferase activities. Data were represented as mean ± SE from three independent experiments. *, **, and *** denote $p < 0.05$, $p < 0.01$, and $p < 0.001$, respectively. ns, non-significance in comparison to control.

suggested that *Hes1* transcripts were targeted by exosomal miR-9-mediated repression for facilitating the differentiation of NSCs and the maturation of both neurons and glia.

DISCUSSION

Neurodegeneration is the progressive neuronal atrophy and loss-of-function, which is present in various neurodegenerative diseases. The transplantation of stem cells with regenerative capacity has shown great promise for treating these diseases (Wang et al., 2007; Kim et al., 2015). Previous studies from us and other groups show that only a small proportion of transplanted cells survive and differentiate into neurons (Li et al., 2001; Tian et al., 2015). Recent evidence has suggested that stem cells participate in brain remodeling and functional recovery by paracrine effect rather than cell replacement, since stem cell-secreted exosomes elicit similar biological activity to the stem cells themselves (Camussi and Quesenberry, 2013; Zhang et al., 2015). Post administration, these exosomes achieve their regenerative function majorly through promoting endogenous neurogenesis and angiogenesis (Zhang et al., 2015, 2018). Currently, multiple types of stem cells including MSCs, HUVEs, embryonic stem cells have been utilized to study the feasibility of exosome-based cell free therapeutic strategy, and among them, MSCs are the most commonly investigated one (Zhang et al., 2015). Unlike the aforementioned types of stem cells, NSCs are the cell sources that directly generate neurons and neuroglia in the brain, implying EXOs may exhibit strong neurogenic potential. Recent studies showed that EXOs alleviate mitochondrial damage and synaptic dysfunction in cortical neurons of AD mouse (Li et al., 2020). However, the effects of EXOs on neurogenesis during CNS development remain vague. We previously reported the important roles of EXOs in regulating embryonic NSC proliferation and differentiation (Ma Y. et al., 2018; Ma et al., 2019). In this study, we followed our previous work and demonstrated that EXOs enhance the differentiation of NSCs and the maturation of both neuronal and glial cells in defined conditions. miRNA microarray and RT-qPCR analyses identified miR-9 as the most abundantly expressed miRNAs in EXOs. The perturbation-of-function approaches further confirmed the important role of miR-9 in the regulation of NSCs. And last, we showed that the positive effects of EXOs on NSC differentiation could be abrogated by depleting exosomal miR-9. Thus, our study unveils a possible mechanism for the EXO-mediated NSC differentiation.

Brain development follows a precise temporal and spatial patterning, which requires complicated regulatory network for the proper regulation of NSC in both embryonic and post-natal stages. In our study, we collected NSCs from the cortical tissue of mouse embryos at E13.5, when robust neurogenesis takes place *in vivo* (Semple et al., 2013). Since the majority of neurons

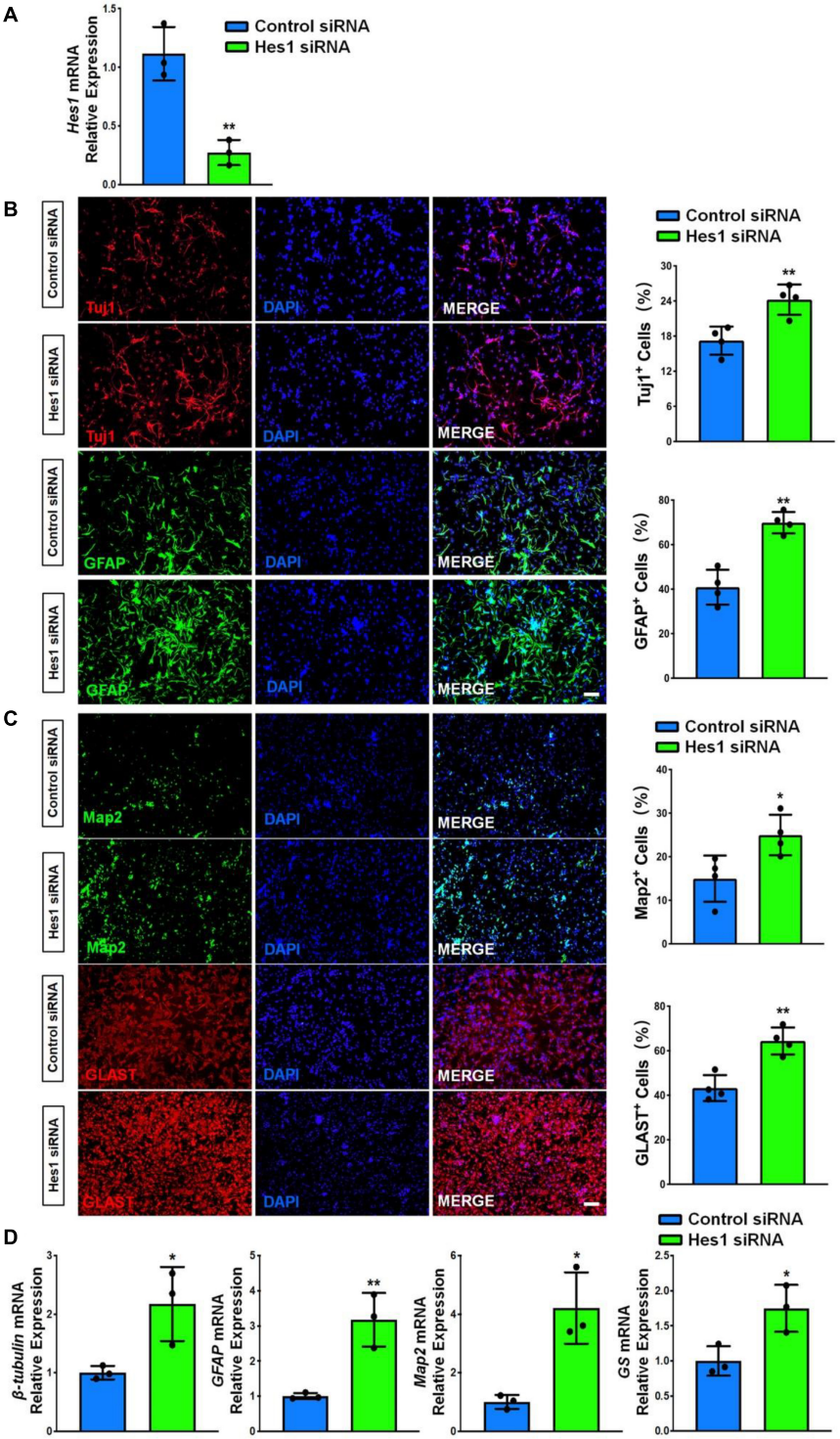

FIGURE 8 | *Hes1* loss-of-function enhances NSC differentiation. **(A)** NSCs transfected with either Hes1 siRNA or scrambled control were cultured for 6 days in differentiation conditions. The transfection efficiency was determined by quantifying the intracellular *Hes1* expression levels via RT-qPCR analysis. **(B)** Representative images of pre-mature cell markers (Tuj1 and GFAP) staining were shown. Proportions of cells exhibiting immunoreactivities of pre-mature cell markers ($Tuj1^+$ and $GFAP^+$) were determined (in the right panel). **(C)** Representative images of matured cell markers (Map2 and Glast) staining were shown. Proportions of cells exhibiting immunoreactivities of pre-mature cell markers ($Map2^+$ and $Glast^+$) were determined (in the right panel). **(D)** The expression levels of transcripts corresponding to pre-mature cell markers (β*III-tubulin* and *GFAP*) and matured cell markers (*Map2* and *GS*) was determined by RT-qPCR analysis. Data were represented as mean ± SE from three independent experiments. * and ** denote $p < 0.05$ and $p < 0.01$, respectively. Scale bar 100 μm in panel **(B,C)**.

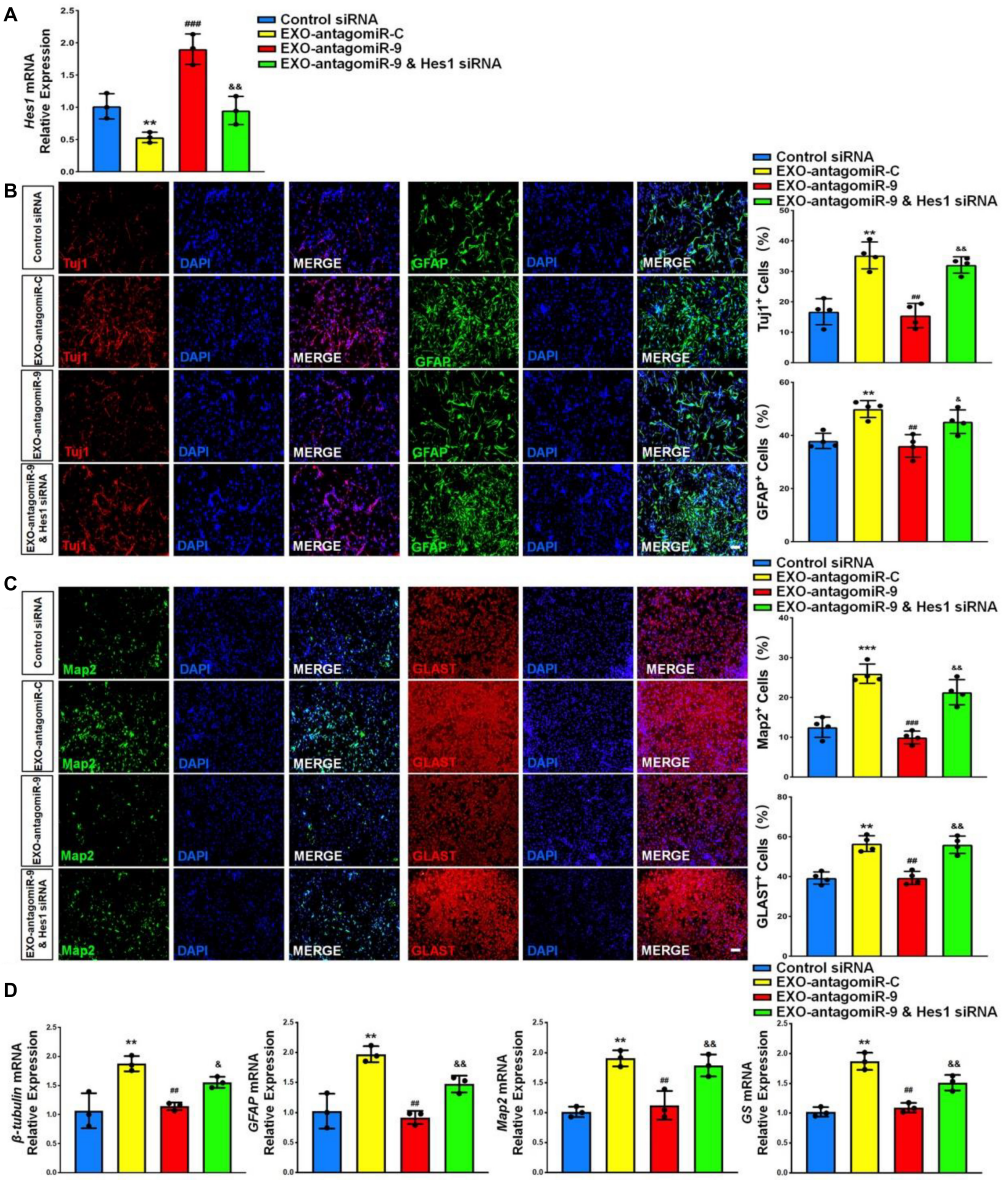

FIGURE 9 | Exosomal miR-9 regulates NSC differentiation via repressing *Hes1*. **(A)** NSCs were divided into four groups for scrambled siRNA transfection, EXO-antogomiR-C co-culture, EXO-antogomiR-9 co-culture, or EXO-antogomiR-9 co-culture with Hes1 siRNA transfection. NSCs were then cultured in differentiation conditions for 6 days. The expression levels of *Hes1* in each group were determined by RT-qPCR. **(B)** Representative images of pre-mature cell markers (Tuj1 and GFAP) staining were shown. Proportions of cells exhibiting immunoreactivities of pre-mature cell markers (Tuj1$^+$ and GFAP$^+$) were determined (in the right panel). **(C)** Representative images of matured cell markers (Map2 and Glast) staining were shown. Proportions of cells exhibiting immunoreactivities of pre-mature cell markers (Map2$^+$ and Glast$^+$) were determined (in the right panel). **(D)** The expression levels of transcripts corresponding to pre-mature cell markers (β*III-tubulin* and *GFAP*) and matured cell markers (*Map2* and *GS*) were determined by RT-qPCR analysis. Data were represented as mean ± SE from three independent experiments. *, **, and *** denote $p < 0.05$, $p < 0.01$, and $p < 0.001$ in comparison to control, respectively. #, ##, and ### denote $p < 0.05$, $p < 0.01$, and $p < 0.001$ in comparison to EXO-antagomiR-C group, respectively. & and && denote $p < 0.05$ and $p < 0.01$ in comparison to EXO-antagomiR-9 group, respectively. Scale bar 100 μm in panel **(C,D)**.

and glia have not been differentiated and matured during early CNS development, the self-regulation is an important aspect for NSC regulation (Semple et al., 2013). Besides classic signaling pathways, our study indicates EXOs as an important element of NSC niche. Through secreting exosomes, NSCs enhance their commitment, facilitating the proper generation of neurons and glia during brain development. It is worth-noting that multiple single cell RNA-seq data have reveals NSCs are heterogeneous during embryonic neurogenesis (Zhong et al., 2018). NSCs can divide symmetrically and asymmetrically to generate NSCs and differentiated cells at the same time (Gotz and Huttner, 2005). It raises an interesting question that whether all NSCs secrete

EXOs to promote the differentiation of entire NSC population or only a sub-population of NSCs secrete EXOs to promote the differentiation of another NSC sub-population. The answer of this question can further explain extend our understanding of the roles of EXOs in the regulation of NSCs, which is currently under investigation.

miR-9, the most abundant expressed EXO miRNA, is a key regulator of proper timing of neurogenesis (Radhakrishnan and Anand, 2016). During development, miR-9 is one of the most highly expressed miRNAs in the early and adult vertebrate brain (Kapsimali et al., 2007; Bonev et al., 2011, 2012; Radhakrishnan and Anand, 2016). Shibata et al. further demonstrated that miR-9 is enriched in proliferative zone in telencephalon, which is widely involved in regulating proliferation, maturation, and differentiation of neurons (Bonev et al., 2011, 2012; Shibata et al., 2011). Our observations further corroborate the importance of miR-9 in regulating NSC differentiation through perturbation-of-function approaches. Several studies have suggested that the exosomal miRNA expression signatures are cell type-dependent (Baumgart et al., 2017; Ma et al., 2019). For instance, high-throughput screening and ectopic expression approaches showed that the intracellular levels of free miRNAs significantly influence the exosomal miRNA profile (Squadrito et al., 2014; Ma et al., 2019). Embryonic NSCs express high levels of miR-9 (data not shown), as miR-9 is required to maintain their neurogenic competence. It explains, partially at least, the high expression levels of cellular and exosomal miR-9. It is also worth-noting that multiple active mechanisms for sorting miRNAs into exosomes were discovered recently. In these active sorting processes, RNA-binding proteins including nSMase2 (Kosaka et al., 2013), hnRNPA2B1 (Villarroya-Beltri et al., 2013), and AGO2 (McKenzie et al., 2016) were recruit to transport miRNAs with specific motifs into exosomes. However, there is no evidence that implies the specific binding of miR-9 with these proteins, leaving the protein-based sorting of exosomal miR-9 as an open question for future investigation.

Currently, miR-9 has been proved to target multiple genes during brain development and NSC differentiation including *Hes1*, *REST*, *Zic5*, *Foxg1*, *Foxp2*, *Pax6*, *Msi1*, *Tlx*, and *Map1b* (Clovis et al., 2012; Coolen et al., 2013; Radhakrishnan and Anand, 2016). In our system, *Hes1* is the gene that demonstrates the largest fold change after co-culturing NSCs with EXOs. Hes1 is a basic helix-loop-helix transcriptional repressor that promotes the maintenance of NSCs and gliogenesis by inhibiting pro-neural gene expression (Tan et al., 2012). Being activated by Notch signaling pathway, Hes1 down-regulates *Ascl1*, *Ngn2*, and other pro-neural genes to block neurogenesis, maintaining the proper timing of neural tube development (Hatakeyama et al., 2004). Surprisingly, our observations suggest that, in a defined condition, miR-9-Hes1 axis may equally modulate neurogenesis and gliogenesis at the same time, instead of regulating the cell fate commitment toward different lineages. Our results are supported by others' studies that investigate the effects of Hes1 on human NSC differentiation (Yang et al., 2020). Thus, our finding, together with others' observations (Kobayashi and Kageyama, 2010; Mendez-Maldonado et al., 2018; Yang et al., 2020), indicates that the involvement of Notch signaling and

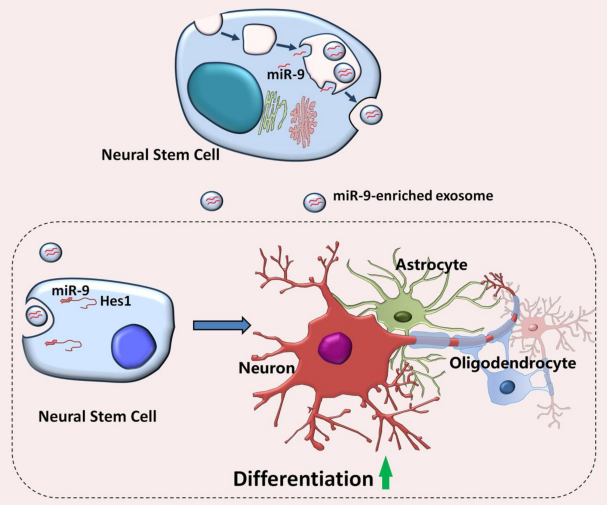

FIGURE 10 | Proposed model of EXO-mediated regulation of NSCs. Embryonic NSCs secrete exosomes enriched with miR-9. After internalizing by neighboring NSCs, exosomes release miR-9 into the recipient cells, leading to the repression of differentiation repressor gene, Hes1. The inhibition of Hes1 then facilitates the differentiation of NSCs and the maturation of both neuronal and glial cells.

Hes1 in NSC regulation is highly time- and condition-dependent. During CNS development, Hes1 acts as a key neural fate determinant in early stage and then functions as an anti-neural regulator in post-natal stage (Kobayashi and Kageyama, 2010; Mendez-Maldonado et al., 2018). Furthermore, Hes1 has been reported to negatively regulate Notch signaling in a feedback manner during CNS development (Kobayashi and Kageyama, 2010; Boareto et al., 2017). In our study, we have observed the significant up-regulation of key Notch signaling components *Dll1*, *Notch1*, and *Notch2* expression in Hes1 down-regulated NSCs (**Supplementary Figure 4**). Our results imply that the Hes1 loss-of-function may induce a compensation of Notch activity that overcomes the influence of Hes1 knockdown on gliogenesis in our model. Besides, we found that exosomal miR-9 also negatively regulated the expression levels of *REST*, and *Map1b*. REST is a neuronal repressor that facilitates the generation of glial cells from NSCs (Xia et al., 2019a). Map1b is a key protein in enhancing axonal growth and branching by stabilizing axonal microtubules (Bouquet et al., 2004). Our results suggest EXOs and exosomal miR-9 may serve as a general promoter of differentiation, instead of regulating the cell fate commitment toward certain lineage. Thus, although we cannot exclude the involvement of REST and Map1b in the exosomal miR-9-mediated neurogenesis, it is highly likely that both REST and Map1b are not the main downstream effectors of exosomal miR-9. Thus, our results identify exosome-mediated miR-9 transferring as a powerful and effective approach, other than direct surface contact (e.g., Notch signaling pathway) and soluble factor diffusion (e.g., Wnt and Shh signaling pathway), in intercellular communication that regulates neurogenesis.

Besides, mounting evidence implicates exosomes as a perfect natural drug delivery system for treating CNS disorders (Alvarez-Erviti et al., 2011; Haney et al., 2015). Except for regular small molecule drugs, miRNAs that may possess therapeutic potential by targeting multiple risk genes were recruited in these pioneer studies, and miR-124, a well-known pro-neural miRNA, is the most widely used one (Xia et al., 2019b). For example, miR-124a-loaded exosomes that were secreted by MSCs or HEK293 cells significantly enhance adult neurogenesis post ischemia and TBI (Yang et al., 2017), repress *REST* expression in Huntington's disease mouse model (Lee et al., 2017), promote the polarization of microglia into anti-inflammatory phenotype under neuroinflammatory conditions (Yang et al., 2019), and reduce in viability or clonogenicity of glioma cells (Lang et al., 2017). Although miR-124 and miR-9 have different seed sequences, they are considered as two central miRNAs in controlling neuron fate and synaptic morphology (Stappert et al., 2015; Xue et al., 2016). The important neurogenic functions of miR-9 make it a promising candidate for exosome-based delivery in treating neurodegeneration and enhancing neuroregeneration, especially in accelerating adult neurogenesis *in vivo*, which will be examined in our future works.

In summary, our study demonstrated the abundant expression of miR-9, a key regulator of proliferation and neuronal differentiation, in EXOs (**Figure 10**). We further showed that the positive effects of EXOs on NSC differentiation are mediated by miR-9 and its downstream gene *Hes1*. Thus, our study, combining with our previous reports, provides a possible mechanism for the exogenous NSC-mediated modification of microenvironment in favor to differentiation and neurogenesis, shedding light on the development of exosome-based cell free therapeutic strategies to activate adult neurogenesis *in vivo*.

DATA AVAILABILITY STATEMENT

The raw data supporting the conclusions of this article will be made available by the authors, without undue reservation.

ETHICS STATEMENT

The animal study was reviewed and approved by The Institutional Animal Care and Use Committee of Tongji University School of Medicine.

AUTHOR CONTRIBUTIONS

JZhe and XX designed the experiments. PY, LD, HC, CL, SZ, XY, and YM performed the experiments. PY, XX, YW, CL, JZhu, XQ, and YZ analyzed the data. XX, PY, YW, and JZhe prepared the manuscript. All authors read and approved the final manuscript.

FUNDING

This work was supported in part by research grants from the National Natural Science Foundation of China (Nos. 91949204 and 81830037 to JZhe, 81971145 and 81901333 to XX, and 81870042 to PY), Shanghai Sailing Program (No. 19YF1451700 to XX), Shanghai Blue Cross Brain Hospital Co., Ltd., and Shanghai Tongji University Education Development Foundation (No. 000000381/2018108 to JZhe).

ACKNOWLEDGMENTS

The author is grateful to Yuju Li for excellent technical help.

SUPPLEMENTARY MATERIAL

The Supplementary Material for this article can be found online at: https://www.frontiersin.org/articles/10.3389/fcell.2021.601600/full#supplementary-material

REFERENCES

Abdipranoto, A., Wu, S., Stayte, S., and Vissel, B. (2008). The role of neurogenesis in neurodegenerative diseases and its implications for therapeutic development. *CNS Neurol. Disord. Drug Targets* 7, 187–210. doi: 10.2174/187152708784083858

Ahmad, I., Teotia, P., Erickson, H., and Xia, X. (2020). Recapitulating developmental mechanisms for retinal regeneration. *Prog. Retin Eye Res.* 76:100824. doi: 10.1016/j.preteyeres.2019.100824

Alvarez-Erviti, L., Seow, Y., Yin, H., Betts, C., Lakhal, S., and Wood, M. J. (2011). Delivery of siRNA to the mouse brain by systemic injection of targeted exosomes. *Nat. Biotechnol.* 29, 341–345. doi: 10.1038/nbt.1807

Baumgart, S., Hölters, S., Ohlmann, C. H., Bohle, R., Stöckle, M., Ostenfeld, M. S., et al. (2017). Exosomes of invasive urothelial carcinoma cells are characterized by a specific miRNA expression signature. *Oncotarget* 8, 58278–58291. doi: 10.18632/oncotarget.17619

Boareto, M., Iber, D., and Taylor, V. (2017). Differential interactions between Notch and ID factors control neurogenesis by modulating Hes factor autoregulation. *Development* 144, 3465–3474. doi: 10.1242/dev.152520

Bonev, B., Pisco, A., and Papalopulu, N. (2011). MicroRNA-9 reveals regional diversity of neural progenitors along the anterior-posterior axis. *Dev. Cell* 20, 19–32. doi: 10.1016/j.devcel.2010.11.018

Bonev, B., Stanley, P., and Papalopulu, N. (2012). MicroRNA-9 Modulates Hes1 ultradian oscillations by forming a double-negative feedback loop. *Cell Rep.* 2, 10–18. doi: 10.1016/j.celrep.2012.05.017

Bouquet, C., Soares, S., von Boxberg, Y., Ravaille-Veron, M., Propst, F., and Nothias, F. (2004). Microtubule-associated protein 1B controls directionality of growth cone migration and axonal branching in regeneration of adult dorsal root ganglia neurons. *J. Neurosci.* 24, 7204–7213. doi: 10.1523/jneurosci.2254-04.2004

Camussi, G., and Quesenberry, P. J. (2013). Perspectives on the potential therapeutic uses of vesicles. *Exosomes Microvesicles* 1:10.5772/57393.

Clovis, Y. M., Enard, W., Marinaro, F., Huttner, W. B., and De Pietri Tonelli, D. (2012). Convergent repression of Foxp2 3′UTR by miR-9 and miR-132 in embryonic mouse neocortex: implications for radial migration of neurons. *Development* 139, 3332–3342. doi: 10.1242/dev.078063

Coolen, M., Katz, S., and Bally-Cuif, L. (2013). miR-9: a versatile regulator of neurogenesis. *Front. Cell. Neurosci.* 7:220.

Coolen, M., Thieffry, D., Drivenes, Ø, Becker, T. S., and Bally-Cuif, L. (2012). miR-9 controls the timing of neurogenesis through the direct inhibition of antagonistic factors. *Dev. Cell* 22, 1052–1064. doi: 10.1016/j.devcel.2012.03.003

Engler, A., Zhang, R., and Taylor, V. (2018). Notch and neurogenesis. *Adv. Exp. Med. Biol.* 1066, 223–234. doi: 10.1007/978-3-319-89512-3_11

Gao, G., Zhao, S., Xia, X., Li, C., Li, C., Ji, C., et al. (2019). Regulates microglial activation and pro-inflammatory exosome release: relevance to the pathogenesis of Alzheimer's disease. *Front. Cell. Neurosci.* 13:264.

Gotz, M., and Huttner, W. B. (2005). The cell biology of neurogenesis. *Nat. Rev. Mol. Cell Biol.* 6, 777–788.

Haney, M. J., Klyachko, N. L., Zhao, Y., Gupta, R., Plotnikova, E. G., He, Z., et al. (2015). Exosomes as drug delivery vehicles for Parkinson's disease therapy. *J. Control Release* 207, 18–30.

Hatakeyama, J., Bessho, Y., Katoh, K., Ookawara, S., Fujioka, M., Guillemot, F., et al. (2004). Hes genes regulate size, shape and histogenesis of the nervous system by control of the timing of neural stem cell differentiation. *Development* 131, 5539–5550. doi: 10.1242/dev.01436

Kageyama, R., Shimojo, H., and Ohtsuka, T. (2019). Dynamic control of neural stem cells by bHLH factors. *Neurosci. Res.* 138, 12–18. doi: 10.1016/j.neures.2018.09.005

Kapsimali, M., Kloosterman, W. P., de Bruijn, E., Rosa, F., Plasterk, R. H., and Wilson, S. W. (2007). MicroRNAs show a wide diversity of expression profiles in the developing and mature central nervous system. *Genome Biol.* 8:R173.

Kim, J. A., Ha, S., Shin, K. Y., Kim, S., Lee, K. J., Chong, Y. H., et al. (2015). Neural stem cell transplantation at critical period improves learning and memory through restoring synaptic impairment in Alzheimer's disease mouse model. *Cell Death Dis.* 6:e1789. doi: 10.1038/cddis.2015.138

Kobayashi, T., and Kageyama, R. (2010). Hes1 regulates embryonic stem cell differentiation by suppressing Notch signaling. *Genes Cells* 15, 689–698. doi: 10.1111/j.1365-2443.2010.01413.x

Kosaka, N., Iguchi, H., Hagiwara, K., Yoshioka, Y., Takeshita, F., and Ochiya, T. (2013). Neutral sphingomyelinase 2 (nSMase2)-dependent exosomal transfer of angiogenic microRNAs regulate cancer cell metastasis. *J. Biol. Chem.* 288, 10849–10859. doi: 10.1074/jbc.m112.446831

Lang, F. M., Hossain, A., Gumin, J., Momin, E. N., Shimizu, Y., Ledbetter, D., et al. (2017). Mesenchymal stem cells as natural bio-factories for exosomes carrying miR-124a in the treatment of gliomas. *Neuro Oncol.* 20, 380–390. doi: 10.1093/neuonc/nox152

Lee, S. T., Im, W., Ban, J. J., Lee, M., Jung, K. H., Lee, S. K., et al. (2017). Exosome-based delivery of miR-124 in a Huntington's disease model. *J. Mov. Disord.* 10, 45–52. doi: 10.14802/jmd.16054

Li, B., Liu, J., Gu, G., Han, X., Zhang, Q., and Zhang, W. (2020). Impact of neural stem cell-derived extracellular vesicles on mitochondrial dysfunction, sirtuin 1 level, and synaptic deficits in Alzheimer's disease. *J. Neurochem.* 154, 502–518. doi: 10.1111/jnc.15001

Li, Y., Chen, J., Wang, L., Lu, M., and Chopp, M. (2001). Treatment of stroke in rat with intracarotid administration of marrow stromal cells. *Neurology* 56, 1666–1672. doi: 10.1212/wnl.56.12.1666

Ma, K., Deng, X., Xia, X., Fan, Z., Qi, X., Wang, Y., et al. (2018). Direct conversion of mouse astrocytes into neural progenitor cells and specific lineages of neurons. *Transl. Neurodegener.* 7:29.

Ma, Y., Li, C., Huang, Y., Wang, Y., Xia, X., and Zheng, J. C. (2019). Exosomes released from neural progenitor cells and induced neural progenitor cells regulate neurogenesis through miR-21a. *Cell Commun. Signal.* 17:96.

Ma, Y., Wang, K., Pan, J., Fan, Z., Tian, C., Deng, X., et al. (2018). Induced neural progenitor cells abundantly secrete extracellular vesicles and promote the proliferation of neural progenitors via extracellular signal-regulated kinase pathways. *Neurobiol. Dis.* 124, 322–334. doi: 10.1016/j.nbd.2018.12.003

McKenzie, A. J., Hoshino, D., Hong, N. H., Cha, D. J., Franklin, J. L., Coffey, R. J., et al. (2016). KRAS-MEK signaling controls Ago2 sorting into exosomes. *Cell Rep.* 15, 978–987. doi: 10.1016/j.celrep.2016.03.085

Mendez-Maldonado, K., Vega-López, G., Caballero-Chacón, S., Aybar, M. J., and Velasco, I. (2018). Activation of Hes1 and Msx1 in transgenic mouse embryonic stem cells increases differentiation into neural crest derivatives. *Int. J. Mol. Sci.* 19:4025. doi: 10.3390/ijms19124025

Noelanders, R., and Vleminckx, K. (2017). How Wnt signaling builds the brain: bridging development and disease. *Neuroscientist* 23, 314–329. doi: 10.1177/1073858416667270

Oh, H. J., Shin, Y., Chung, S., Hwang, D. W., and Lee, D. S. (2017). Convective exosome-tracing microfluidics for analysis of cell-non-autonomous neurogenesis. *Biomaterials* 112, 82–94. doi: 10.1016/j.biomaterials.2016.10.006

Radhakrishnan, B., and Anand, A. A. P. (2016). Role of miRNA-9 in brain development. *J. Exp. Neurosci.* 10, 101–120.

Ramachandran, S., and Palanisamy, V. (2012). Horizontal transfer of RNAs: exosomes as mediators of intercellular communication. *Wiley Interdiscip. Rev. RNA* 3, 286–293. doi: 10.1002/wrna.115

Semple, B. D., Blomgren, K., Gimlin, K., Ferriero, D. M., and Noble-Haeusslein, L. J. (2013). Brain development in rodents and humans: identifying benchmarks of maturation and vulnerability to injury across species. *Prog. Neurobiol.* 10, 1–16. doi: 10.1016/j.pneurobio.2013.04.001

Shibata, M., Nakao, H., Kiyonari, H., Abe, T., and Aizawa, S. (2011). MicroRNA-9 regulates neurogenesis in mouse telencephalon by targeting multiple transcription factors. *J. Neurosci.* 31, 3407–3422. doi: 10.1523/jneurosci.5085-10.2011

Squadrito, M. L., Baer, C., Burdet, F., Maderna, C., Gilfillan, G. D., Lyle, R., et al. (2014). Endogenous RNAs modulate microRNA sorting to exosomes and transfer to acceptor cells. *Cell Rep.* 8, 1432–1446. doi: 10.1016/j.celrep.2014.07.035

Stappert, L., Roese-Koerner, B., and Brustle, O. (2015). The role of microRNAs in human neural stem cells, neuronal differentiation and subtype specification. *Cell Tissue Res.* 359, 47–64. doi: 10.1007/s00441-014-1981-y

Steiner, B., Wolf, S., and Kempermann, G. (2006). Adult neurogenesis and neurodegenerative disease. *Regen. Med.* 1, 15–28. doi: 10.2217/17460751.1.1.15

Tan, S. L., Ohtsuka, T., González, A., and Kageyama, R. (2012). MicroRNA9 regulates neural stem cell differentiation by controlling Hes1 expression dynamics in the developing brain. *Genes Cells* 17, 952–961. doi: 10.1111/gtc.12009

Tian, C., Li, Y., Huang, Y., Wang, Y., Chen, D., Liu, J., et al. (2015). Selective generation of dopaminergic precursors from mouse fibroblasts by direct lineage conversion. *Sci. Rep.* 5:12622.

Tomita, K., Ishibashi, M., Nakahara, K., Ang, S. L., Nakanishi, S., Guillemot, F., et al. (1996). Mammalian hairy and enhancer of split homolog 1 regulates differentiation of retinal neurons and is essential for eye morphogenesis. *Neuron* 16, 723–734. doi: 10.1016/s0896-6273(00)80093-8

Valadi, H., Ekström, K., Bossios, A., Sjöstrand, M., Lee, J. J., and Lötvall, J. O. (2007). Exosome-mediated transfer of mRNAs and microRNAs is a novel mechanism of genetic exchange between cells. *Nat. Cell Biol.* 9, 654–659. doi: 10.1038/ncb1596

Villarroya-Beltri, C., Gutiérrez-Vázquez, C., Sánchez-Cabo, F., Pérez-Hernández, D., Vázquez, J., Martin-Cofreces, N., et al. (2013). Sumoylated hnRNPA2B1 controls the sorting of miRNAs into exosomes through binding to specific motifs. *Nat. Commun.* 4:2980.

Wang, Y., Chen, S., Yang, D., and Le, W. D. (2007). Stem cell transplantation: a promising therapy for Parkinson's disease. *J. Neuroimmune Pharmacol.* 2, 243–250.

Xia, X., Teotia, P., and Ahmad, I. (2019a). miR-29c regulates neurogliogenesis in the mammalian retina through REST. *Dev. Biol.* 450, 90–100. doi: 10.1016/j.ydbio.2019.03.013

Xia, X., Wang, Y., Huang, Y., Zhang, H., Lu, H., and Zheng, J. C. (2019b). Exosomal miRNAs in central nervous system diseases: biomarkers, pathological mediators, protective factors and therapeutic agents. *Prog. Neurobiol.* 183:101694. doi: 10.1016/j.pneurobio.2019.101694

Xin, H., Katakowski, M., Wang, F., Qian, J. Y., Liu, X. S., Ali, M. M., et al. (2017). MicroRNA cluster miR-17-92 cluster in exosomes enhance neuroplasticity and functional recovery after stroke in rats. *Stroke* 48, 747–753. doi: 10.1161/strokeaha.116.015204

Xin, H., Li, Y., Cui, Y., Yang, J. J., Zhang, Z. G., and Chopp, M. (2013). Systemic administration of exosomes released from mesenchymal stromal cells promote functional recovery and neurovascular plasticity after stroke in rats. *J. Cereb. Blood Flow Metab.* 33, 1711–1715. doi: 10.1038/jcbfm.2013.152

Xue, Q., Yu, C., Wang, Y., Liu, L., Zhang, K., Fang, C., et al. (2016). miR-9 and miR-124 synergistically affect regulation of dendritic branching via the AKT/GSK3beta pathway by targeting Rap2a. *Sci. Rep.* 6:26781.

Yang, B., Xu, Z., He, Z., Li, X., Wu, Z., Xu, J., et al. (2020). High expression of miR-374a-5p inhibits the proliferation and promotes differentiation of Rencell

VM cells by targeting Hes1. *Neurosci. Res.* 2020:S0168-0102(20)30439-9. doi: 10.1016/j.neures.2020.09.002

Yang, J., Zhang, X., Chen, X., Wang, L., and Yang, G. (2017). Exosome mediated delivery of miR-124 promotes neurogenesis after ischemia. *Mol. Ther. Nucleic Acids* 7, 278–287. doi: 10.1016/j.omtn.2017.04.010

Yang, X. J. (2004). Roles of cell-extrinsic growth factors in vertebrate eye pattern formation and retinogenesis. *Semin. Cell Dev. Biol.* 15, 91–103. doi: 10.1016/j.semcdb.2003.09.004

Yang, Y., Ye, Y., Kong, C., Su, X., Zhang, X., Bai, W., et al. (2019). MiR-124 enriched exosomes promoted the M2 polarization of microglia and enhanced hippocampus neurogenesis after traumatic brain injury by inhibiting TLR4 pathway. *Neurochem. Res.* 44, 811–828. doi: 10.1007/s11064-018-02714-z

Zhang, C., McNeil, E., Dressler, L., and Siman, R. (2007). Long-lasting impairment in hippocampal neurogenesis associated with amyloid deposition in a knock-in mouse model of familial Alzheimer's disease. *Exp. Neurol.* 204, 77–87. doi: 10.1016/j.expneurol.2006.09.018

Zhang, Y., Chopp, M., Meng, Y., Katakowski, M., Xin, H., Mahmood, A., et al. (2015). Effect of exosomes derived from multipluripotent mesenchymal stromal cells on functional recovery and neurovascular plasticity in rats after traumatic brain injury. *J. Neurosurg.* 122, 856–867. doi: 10.3171/2014.11.jns14770

Zhang, Y., Kim, M. S., Jia, B., Yan, J., Zuniga-Hertz, J. P., Han, C., et al. (2017). Hypothalamic stem cells control ageing speed partly through exosomal miRNAs. *Nature* 548, 52–57. doi: 10.1038/nature23282

Zhang, Y. Z., Liu, F., Song, C. G., Cao, X. L., Zhang, Y. F., Wu, H. N., et al. (2018). Exosomes derived from human umbilical vein endothelial cells promote neural stem cell expansion while maintain their stemness in culture. *Biochem. Biophys. Res. Commun.* 495, 892–898. doi: 10.1016/j.bbrc.2017.11.092

Zhong, S., Zhang, S., Fan, X., Wu, Q., Yan, L., Dong, G., et al. (2018). A single-cell RNA-seq survey of the developmental landscape of the human prefrontal cortex. *Nature* 555, 524–528. doi: 10.1038/nature25980

Conflict of Interest: The authors declare that the research was conducted in the absence of any commercial or financial relationships that could be construed as a potential conflict of interest.

frontiers in Cell and Developmental Biology

ORIGINAL RESEARCH
published: 07 July 2021
doi: 10.3389/fcell.2021.684516

TRPV1 Antagonist Prevents Neonatal Sevoflurane-Induced Synaptic Abnormality and Cognitive Impairment in Mice Through Regulating the Src/Cofilin Signaling Pathway

*Yuqiang Liu[1], Han Yang[1], Yifei Fu[1], Zhenglong Pan[1], Fang Qiu[1], Yanwen Xu[2], Xinping Yang[1], Qian Chen[3], Daqing Ma[3] and Zhiheng Liu[1]**

[1] Department of Anesthesiology, Shenzhen Second People's Hospital, The First Affiliated Hospital of Shenzhen University, Shenzhen, China, [2] Shenzhen Key Laboratory of Neurosurgery, Shenzhen Second People's Hospital, The First Affiliated Hospital of Shenzhen University Health Science Center, Shenzhen, China, [3] Division of Anaesthetics, Pain Medicine and Intensive Care, Department of Surgery and Cancer, Faculty of Medicine, Imperial College London, Chelsea and Westminster Hospital, London, United Kingdom

OPEN ACCESS

Edited by:
Alex Dranovsky,
Columbia University, United States

Reviewed by:
Sheik Pran Babu Sardar Pasha,
University of California, Davis, United States
Ling Zhao,
Sun Yat-sen University, China

***Correspondence:**
Zhiheng Liu
zhiheng_liu_tongji@163.com

Specialty section:
This article was submitted to Molecular Medicine, a section of the journal Frontiers in Cell and Developmental Biology

Received: 23 March 2021
Accepted: 14 June 2021
Published: 07 July 2021

Citation:
Liu Y, Yang H, Fu Y, Pan Z, Qiu F, Xu Y, Yang X, Chen Q, Ma D and Liu Z (2021) TRPV1 Antagonist Prevents Neonatal Sevoflurane-Induced Synaptic Abnormality and Cognitive Impairment in Mice Through Regulating the Src/Cofilin Signaling Pathway. Front. Cell Dev. Biol. 9:684516. doi: 10.3389/fcell.2021.684516

Long-term neurodevelopmental disorders following neonatal anesthesia have been reported both in young animals and in children. The activation of transient receptor potential vanilloid 1 (TRPV1) channels in hippocampus adversely affects neurodevelopment. The current study explored the underlying mechanism of TRPV1 channels on long-lasting cognitive dysfunction induced by anesthetic exposure to the developing brain. we demonstrated that TRPV1 expression was increased after sevoflurane exposure both *in vitro* and *in vivo*. Sevoflurane exposure to hippocampal neurons decreased the synaptic density and the surface GluA1 expression, as well as increased co-localization of internalized AMPAR in early and recycling endosomes. Sevoflurane exposure to newborn mice impaired learning and memory in adulthood, and reduced AMPAR subunit GluA1, 2 and 3 expressions in the crude synaptosomal fractions from mouse hippocampus. The inhibition of TRPV1 reversed the phenotypic changes induced by sevoflurane. Moreover, sevoflurane exposure increased Src phosphorylation at tyrosine 416 site thereby reducing cofilin phosphorylation. TRPV1 blockade reversed these suppressive effects of sevoflurane. Our data suggested that TRPV1 antagonist may protect against synaptic damage and cognitive dysfunction induced by sevoflurane exposure during the brain developing stage.

Keywords: TRPV1, sevoflurane, synapse, learning and memory, Src, cofilin

Abbreviations: AMPARs, α-amino-3-hydroxy-5-methyl-4-isoxazolepropionate receptors; BDNF, brain-derived neurotrophic factor; CNS, central nervous system; Ctrl, control; DIV, day *in vitro*; DRG, dorsal root ganglia; EEA1, early endosome antigen 1; FC, fear conditioning; GABA, γ-aminobutyrate; GAPDH, glyceraldehyde-3-phosphate dehydrogenase; HDAC2, histone deacetylase 2; LAMP1, lysosomal-associated membrane protein 1; NMDA, N-methyl-D-aspartic acid; NORT, novel object recognition test; P, postnatal day; PNS, peripheral nervous system; Sev, sevoflurane; TRPV1, Transient receptor potential vanilloid 1.

INTRODUCTION

General anesthetic agents are essential to be used to provide a safe and comfortable condition so that complex surgical procedures can be performed. However, there has been an increasing concern that prolonged or repetitious anesthetic exposure may cause long-lasting neurotoxicity and cognitive dysfunction, especially in the young animal and in children (Sanders et al., 2013; Wu et al., 2019). Preclinical studies have shown that exposure early developing brain to commonly used anesthetics may cause certain neurofunctional impairments, such as learning and memory deficits, anxiety-like behaviors and emotional reactivities (Vutskits and Xie, 2016; Colon et al., 2017). However, the underlying molecular and cellular mechanisms are still unclear. Recent childhood cohort studies have shown that a single short exposure to general anesthesia for less than 1 h did not alter neurocognitive functions and behavior (Davidson et al., 2016; Sun et al., 2016; Warner et al., 2018; McCann et al., 2019); However, processing speed and fine motor abilities were decreased after repeated anesthetics exposure (Warner et al., 2018). Thus, the underlying mechanisms of neuronal injury and neurologic dysfunction induced by repeated and prolonged anesthetic exposure deserve further study in the young.

Transient receptor potential vanilloid 1 (TRPV1) is a ligand-gated non-specific cation channel prominently expressed in the dorsal root ganglia (DRG) sensory neurons. This receptor is gated by capsaicin, heat, protons and several exogenous molecules (Alter and Gereau, 2008). TRPV1 has been extensively characterized and is known to play a role in the pain and inflammation processing in the sensory neurons (Palazzo et al., 2010, 2012; Wang Y. et al., 2018). TRPV1 also contributes to neurological diseases, including epilepsy, anxiety, depression and learning and memory disorders (Marsch et al., 2007; Edwards, 2014). In the peripheral nervous system (PNS), certain general and local anesthetics activated and sensitized the TRPV1 channel (Cornett et al., 2008; Leffler et al., 2008), suggesting that this channel may contribute to pain modulation and inflammation in the context of surgery. However, in the central nervous system (CNS), few studies have been conducted on the potential impact of TRPV1 in the developing brain under general anesthesia. Hence, we wonder whether TRPV1 affects the cognitive function in neonatal brain development after anesthetic exposure. In the present study, the effects of sevoflurane, a commonly used inhalational agent, on TRPV1-regulated synaptic density and memory changes together with the underlining molecular mechanisms including the Src/Cofilin signaling pathway were investigated in both cultured mouse hippocampal neuronal cells and C57BL/6 mouse neonates.

MATERIALS AND METHODS

Cell Culture and Treatment

Mouse hippocampal neuronal cell line (HT22 cells) was obtained from the Sun Yat-sen University and cultured as described previously (Liu et al., 2019). Briefly, the cells were maintained in DMEM medium, supplemented with 10% fetal bovine serum (GIBCO BRL, Rockville, MD, United States) and 1% antibiotics (penicillin/streptomycin, 100 U/ml, GIBCO, Waltham, MA, United States), in a humidified incubator containing 5% CO_2 balanced with air at 37°C. Primary cultures of hippocampal neurons were prepared from the dissociated hippocampus of neonatal mice (<24 h) using a previously described protocol (Liu et al., 2018). The neurons were plated on coverslips coated with Matrigel for at least for 14 days *in vitro* (DIV) before using. The cultures were maintained in a humidified 5% CO_2 atmosphere balanced with air at 37°C. Both HT22 cells or mouse hippocampal neurons were treated with 4% sevoflurane for 6 h as described by Liu et al. (2019). A selective TRPV1 antagonist, SB 366791 (TOCRIS, Bristol, United Kingdom), was administered to the cell culture medium 1 h with its final concentration of 10 μM before the sevoflurane treatment.

Experimental Mice

All experimental procedures on mice were approved by the Animal Research Ethics Committee of the Shenzhen Second People's Hospital and Sun Yat-sen Memorial Hospital. The experiments were performed in these two institutions. C57BL/6 postnatal day seven litter mice with their mothers were obtained from the Guangdong Provincial Laboratory Animal Centre (Guangzhou, China). A single mother and her litters were housed in a cage under a 12 h light-dark cycle at the room temperature of 23 ± 1°C) and 55% humidity. All mice had free access to food and water. Seven-day-old mice of both genders were used for the experiments.

Grouping and Sevoflurane Exposure

At postnatal day 7 (P7), the litters were randomly divided into four groups (n = 10–14/group): (1) Control group (Ctrl); (2) TRPV1 antagonist treatment (SB 366791) group; (3) sevoflurane exposure group (Sev); (4) SB 366791 combined with sevoflurane group (Sev + SB366791). SB 366791 (TOCRIS, Bristol, United Kingdom) was dissolved in DMSO and diluted with normal saline to the appropriate concentration for administration. SB 366791 (500 μg/kg) was injected intraperitoneally 1 h before sevoflurane treatment. Litters were placed in an acrylic chamber and exposed 60% oxygen (balanced with nitrogen) with or without (controls) 3% sevoflurane for 2 h daily for 3 consecutive days as described in previous studies (Lu et al., 2017). During exposure, all litters were kept warm on a pre-heated plate at 37°C. Mice were returned to the housing cages after the treatment. They were allowed to grow for behavioral tests at postnatal day 65 (P65). Another cohorts after treatments were allowed to grow the similar age of those for behavioral tests and then anesthetized using sodium pentobarbital (65 mg/kg, intraperitoneal injection) and sacrificed to harvest brain tissue for further measurements.

Open Field Test

Mice were placed in the center of a white poly-vinyl chloride apparatus (50 × 50 × 50 cm), and were allowed to continuously locomote for 10 min. The arena was videotaped and analyzed using SMART software (Panlab, Kent, United Kingdom).

Novel Object Recognition Test (NORT)

Mice were habituated in a square chamber (50 × 50 × 50 cm) with white walls and floor for 10 min on the first day and for 5 min on the second day. The box and objects were cleaned before and between the uses. 24 h after the last habituation, the mice were placed in the chamber with two objects and allowed to freely explore for 5 min "sample phase." Two hours after the initial exploration, the mice were placed back into the same arena with two objects for 5 min "acquisition phase," during which one of objects was replaced by a novel object. Exploration counts of each object during two phases were counted. The recognition index was calculated as the percentage of counts spent exploring the novel object over the total exploration counts during the acquisition phase.

Fear Conditioning Test

The task was performed using a freeze monitor system (San Diego Instruments; San Diego, CA, United States). Background noise level was 65 dB; overhead lighting was used, and 20% ethanol was used as an odor. Mice were placed into a training chamber and allowed to freely explore for 5 min followed by three tone presentations (CS: 5 kHz, 85 dB for 20 s); each tone, was followed by electrical foot-shocks (US: 0.45 mA for 1 s). The interval between three trials was 120 s. Twenty four hours after the training, the mice were placed in the same chamber for 5 min, and freezing behavior was assessed. Forty eight hours later, the mice were tested for freezing responses to the cue. For the cued test, the conditioning chamber was modified as follows: white-walled triangular chamber was replaced with a Plexiglas box, and 2% aloe vera detergent was used as an odor. A dim lamp was used instead of the overhead lighting. Mice were allowed to explore the new environment for 5 min followed by three tones (85 dB, 20 s).

Immunofluorescent Staining

Hippocampal neuronal cultures and HT22 cells were fixed with PBS containing 4% paraformaldehyde for 1 h at room temperature, washed with PBS, permeabilized with 0.1% Triton X-100 in PBS and blocked in freshly prepared blocking solution (3% donkey serum and 0.2% Triton X-100 in PBS) for 1.5 h at room temperature. The samples were incubated at 4°C overnight with primary antibodies diluted in the blocking solution. After washing with PBS-T (0.2% Triton X-100 in PBS), the samples were incubated with corresponding secondary antibodies for 1 h at room temperature. The following primary antibodies were used (dilution, source): TRPV1 (1:200, NB100-1617, Novus Biologicals, Littleton, CO, United States), MAP2 (1:200, ab5392, Abcam, Cambridge, United Kingdom), synaptophysin (1:500, MAB329, Millipore, Darmstadt, Germany), homer 1 (1:200, 160003, Synaptic Systems, Göttingen, Germany) and Src (1:200, 2110S, Cell Signaling, Beverly, United States).

To visualize surface GluA1, the neurons were fixed with 4% formaldehyde/4% sucrose in PBS. After washing and blocking, surface α-amino-3-hydroxy-5-methyl-4-isoxazolepropionate (AMPA) receptors (AMPARs) were labeled with mouse anti-GluA1 N-terminal antibody (1:200, MAB2263, Millipore, Darmstadt, Germany). Then, the neurons were permeabilized with 0.1% Triton X-100 for 15 min, blocked and incubated with a rabbit anti-GluA1 antibody (1:200, AB1504, Millipore, Darmstadt, Germany) against the intracellular C-terminal domain to stain total GluA1 (tGluA1) at 4°C overnight. After washing with PBS, the neurons were incubated with Alexa Flour-conjugated secondary antibodies. Immunofluorescence images were acquired on a confocal system (LSM 800, Carl Zeiss, Oberkochen, Germany). The images were processed for quantitative analysis using Image-Pro Plus.

To investigate the endosomal distribution of internalized AMPAR in neurons, internalized GluA2 (iGluA2) were labeled and their co-localization with early, recycling and late endosomes was systematically examined using known markers, including early endosome antigen 1 (EEA1), Stx13 and lysosomal-associated membrane protein 1 (LAMP1), respectively, in neurons. Surface GluA2 antibody (extracellular N-terminal domain, Millipore, Darmstadt, Germany) were used to label sGluA2 in the growth medium for 10 min; the cells were rinsed once, stimulated for 2 min with 100 μM AMPA plus 100 μM APV at 37°C. After rinsing, the neurons were returned to the original growth medium for 45 min to allow the internalized AMPAR to recycle back to the cell surface. After washing once with pre-cooled 3% BSA-containing ACSF, the neurons were incubated with non-conjugated mouse secondary antibody at 10°C for 30 min. Then, the neurons were fixed with parafix (4% formaldehyde/4% sucrose/1 × PBS), permeabilized, blocked and incubated with rabbit antibodies against various endosomal markers overnight. Internalized GluA2, endosomal markers and MAP2 were detected using the corresponding secondary antibodies conjugated with Alexa Flour 647, 555, and 488, respectively. Co-localization of internalized AMPAR with each marker was measured as described previously (Lee et al., 2004).

For immunostaining in hippocampal sections, mice were anesthetized with pentobarbital sodium and perfused transcardially with physiological saline, then with 4% formaldehyde. Brains were post-fixed with 4% formaldehyde for 24 h at 4°C, followed by dehydration in 30% sucrose solution for 48 h. Coronal sections from the hippocampus were cut at 10 μm on a cryostat (Leica, Germany), and mounted onto slides. Sections were washed with PBS, and blocked (3% donkey serum and 0.2% Triton X-100 in PBS) for 2 h. Sections were then incubated overnight with anti-synaptophysin (1:500, Millipore, Darmstadt, Germany), followed by secondary antibodies. Immunofluorescence images were acquired on a confocal system (LSM 800, Carl Zeiss, Oberkochen, Germany). The images were processed for quantitative analysis using Image-Pro Plus.

Synaptosomal Fraction Preparation

Hippocampal tissue samples were homogenized in buffer A (5 mM HEPES, pH 7.4, 1 mM $MgCl_2$, 0.5 mM $CaCl_2$, 1 mM DTT, and 0.32 M sucrose) containing protease inhibitor and phosphatase inhibitor cocktail (Roche, Mannheim, Germany). The homogenate was centrifuged at 1,400 g for 10 min at 4°C, and the supernatant was discarded. The pellet was resuspended in buffer A and centrifuged at 710 g for 10 min at 4°C to yield supernatant fraction (S1). The S1 was centrifuged again at 13,800 g for 20 min at 4°C. The pellet was resuspended in

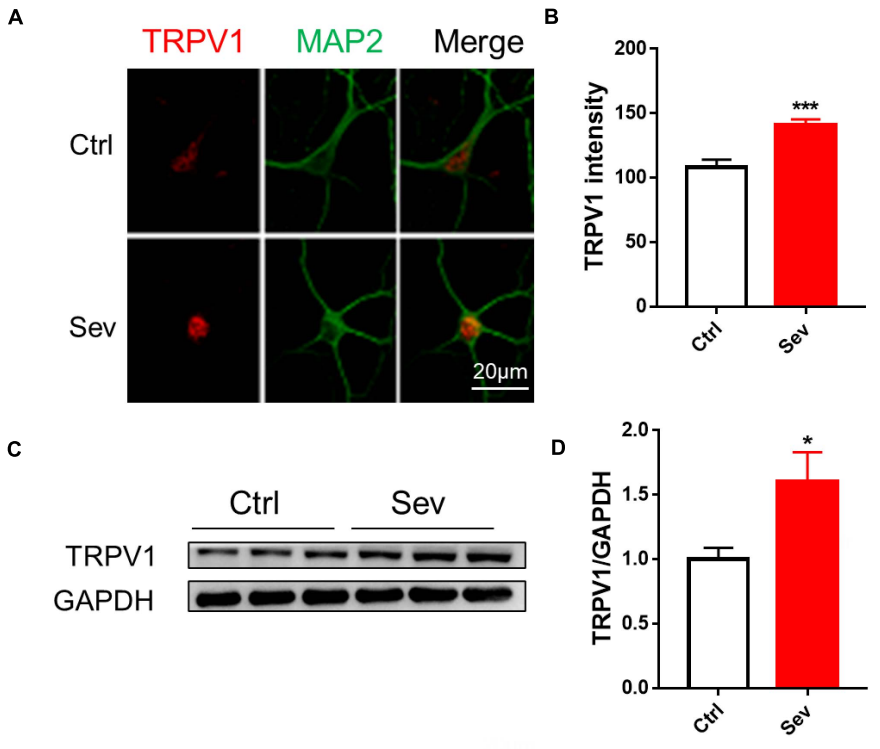

FIGURE 1 | Sevoflurane increased protein levels of TRPV1 channels *in vivo* and *in vitro*. **(A)** Fluorescent images of TRPV1 in hippocampal neurons **(B)** Quantitative analyzed the optical density of TRPV1 protein signal [3 cultures per group, unpaired *t*-test, $t_{(22)} = 4.6$, $p < 0.001$]. **(C)** Anesthesia with 3% sevoflurane 2 h daily for 3 days at P7 increased the expression of TRPV1 in the hippocampus of mice harvested at P9 **(D)** Quantification of the Western blot shows that sevoflurane anesthesia increased the protein levels of TRPV1 compared to that observed under the control conditions [$n = 6$, unpaired *t*-test, $t_{(10)} = 2.5$, $p = 0.0343$]. Data are presented as the mean ± SEM. $^{*}p < 0.05$; $^{***}p < 0.001$. Ctrl, control; Sev, sevoflurane.

buffer B (6 mM Tris, pH 8.1, 0.32 M sucrose, 1 mM EDTA, 1 mM EGTA, and 1 mM DTT) containing protease inhibitor and phosphatase inhibitor cocktail. The suspension was used as the crude synaptosomal preparation and analyzed by Western blot.

Western Blot

The brain tissues were homogenized in RIPA buffer (Beyotime, Shanghai, China) supplemented with protease and phosphatase inhibitors (Roche, Mannheim, Germany) on ice and stored at −80°C until use. Protein concentrations in the supernatant were determined using a BCA assay kit (Beyotime, Shanghai, China). The proteins were separated through the polyacrylamide SDS gels and transferred to 0.45 μm PVDF membrane (Millipore, Darmstadt, Germany). After blocking with 5% non-fat milk, the membranes were incubated with a primary antibody at 4°C overnight. The membranes were then incubated with appropriate HRP-conjugated secondary antibodies (anti-mouse: 1:5,000, 7076S, Cell Signaling; anti-rabbit: 1:5,000, 7074S, Cell Signaling) after washing with TBST (TBS containing 0.2% Tween-20). Then, immunoreactivity was detected by a chemiluminescent reagent (Amersham-GE, Pittsburgh, United States). The following primary antibodies were used (dilution, source): TRPV1 (1:1,000, NB100-1617, Novus Biologicals, Littleton, CO), GAPDH (1:3,000, 2118S, Cell Signaling), GluA1 (1:1,000, AB1504, Millipore), GluA2 (1:1,000, 13607S, Cell Signaling), GluA3 (1:500, MAB5416, Millipore), Src (1:1,000, 2110S, Cell Signaling), p-Src (Tyr416) (1:1,000, 2101S, Cell Signaling), p-Src (Tyr527) (1:1,000, 2105S, Cell Signaling), cofilin (1:1,000, 5175S, Cell Signaling), and p-cofilin (1:1,000, 3313S, Cell Signaling).

Co-immunoprecipitation

Total protein extracts were obtained from the hippocampal brain tissue of mice. The tissue samples were homogenized in NP-40 lysis buffer (Thermo Fisher Scientific, United States) containing protease and phosphatase inhibitors. The homogenate was incubated on ice for 30 min and then centrifuged at 10,000 g for 10 min at 4°C. The supernatants were immunoprecipitated using a Dynabeads Protein G IP kit (Thermo Fisher Scientific, United States) according to the manufacturer's instructions. Five micrograms of anti-Src (2110S, Cell Signaling) were used. Western blot was subsequently performed as described above.

Data Analysis

Data were expressed as the mean ± SEM and analyzed with unpaired student *t*-test and one-way ANOVA followed by *post hoc* Bonferroni test wherever appropriate using GraphPad Prism 7 software (GraphPad Software, La Jolla, California,

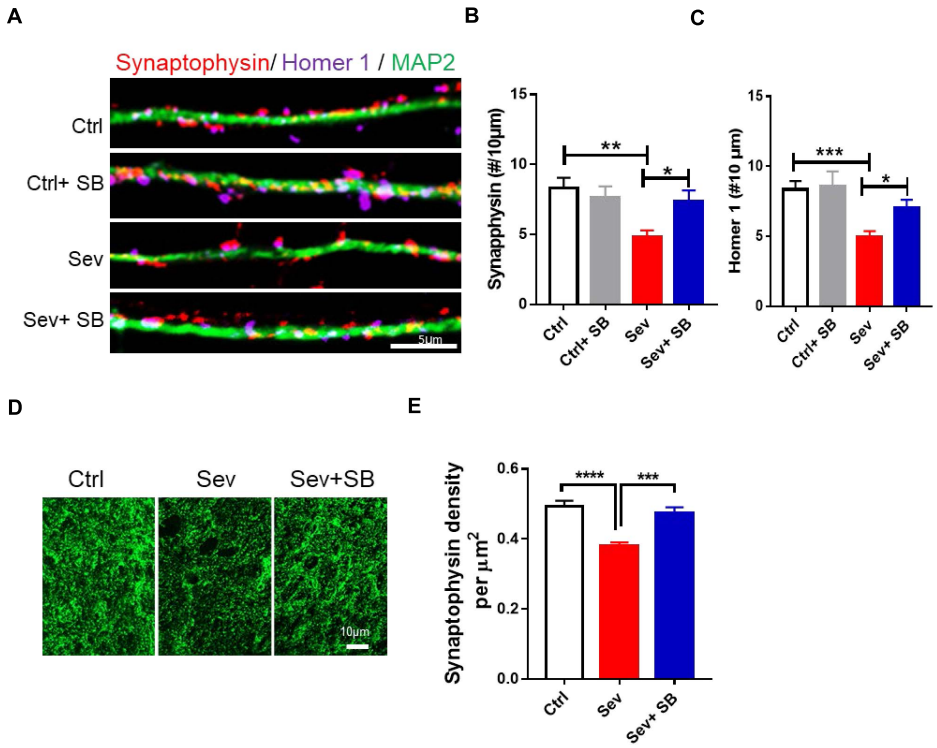

FIGURE 2 | Pretreatment with TRPV1 antagonist SB 366791 significantly suppressed synaptic density loss induced by sevoflurane exposure. **(A)** Fluorescent images of synaptophysin and homer 1 puncta density in hippocampal neurons in the Ctrl and Sev cultures treated with TRPV1 antagonist SB 366791 (10 μM). **(B,C)** Quantitative analysis of synaptophysin **(B)** and homer 1 **(C)** puncta density in the Ctrl and Sev cultures [3 cultures per group, one-way ANOVA, synaptophysin: $F_{(3,56)} = 5.0$, $p = 0.0041$, homer 1: $F_{(3,58)} = 6.9$, $p < 0.001$]. **(D,E)** Representative fluorescent images **(D)** and quantitative analysis **(E)** of synaptophysin puncta density in the CA1 area of the with or without SB 366791(500 μg/kg) treatment mice [7 mice per group, $F_{(2,\ 18)} = 18.2$, $p < 0.0001$]. Data are presented as the mean ± SEM. ANOVA followed by Bonferroni *post hoc* test. $^{*}p < 0.05$; $^{**}p < 0.01$; $^{***}p < 0.001$; $^{****}p < 0.0001$. Ctrl, control; Sev, sevoflurane; SB, SB 366791.

United States). A *p*-value less than 0.05 was considered to be a statistical significance.

RESULTS

Sevoflurane Exposure Reduced Synaptic Density *in vitro* and *in vivo*

Sevoflurane (4%) exposed to primary hippocampal neurons significantly increased TRPV1 expression (**Figures 1A,B**). The TRPV1 expressions were also increased in the hippocampus following sevoflurane treatment in mice (**Figures 1C,D**).

Then, the role of TRPV1 on synaptic density changes was examined after sevoflurane exposure. In the primary hippocampal neuronal cultures at DIV 16 before and after sevoflurane exposure with or without SB 366791, the changes of synaptic density indicated with synaptophysin and homer 1 puncta were significantly decreased by approximate 41 and 40%, respectively, in the sevoflurane-treated cultures compared with the control cultures (**Figures 2A–C**). Furthermore, pretreatment with SB 366791 for 1 h significantly ameliorated the toxic effects of 4% sevoflurane exposure on neuronal synaptic density (**Figures 2A–C**). Then, we quantified the synaptic density in the CA1 area in mice. The density of synaptophysin puncta in the Sevoflurane treated mice was significantly reduced by about 24% compared with that in the control mice (**Figures 2D,E**), whilst SB 366791 reversed this reduction (**Figures 2D,E**).

TRPV1 Inhibition Reversed Sevoflurane Exposure Induced Cognitive Function Impairment and AMPAR Delivery Deficiency

Considering that sevoflurane was shown to specifically affect the synaptic puncta by inducing the changes of TRPV1 expression, we determined the effect of TRPV1 on cognitive dysfunction in adulthood induced by sevoflurane exposure of the developing brain. Initially, we assessed the locomotor activity in mice in the open field test. In the mice pre-treated with SB 366791 (SB366791 group), the total distance was similar to that of the wild type mice (Ctrl group) at P65. Additionally, no behavioral deficits were detected in the Sevoflurane with or without SB 366791treated mice (**Figure 3A**). No differences were found in the center of the arena between any of the groups (data not shown). There were no significant differences in locomotor activity during the 3 training days. In the case of NORT, sevoflurane treated mice had significantly lower recognition index than that in the controls (**Figure 3B**). Pre-treatment with TRPV1 antagonists SB

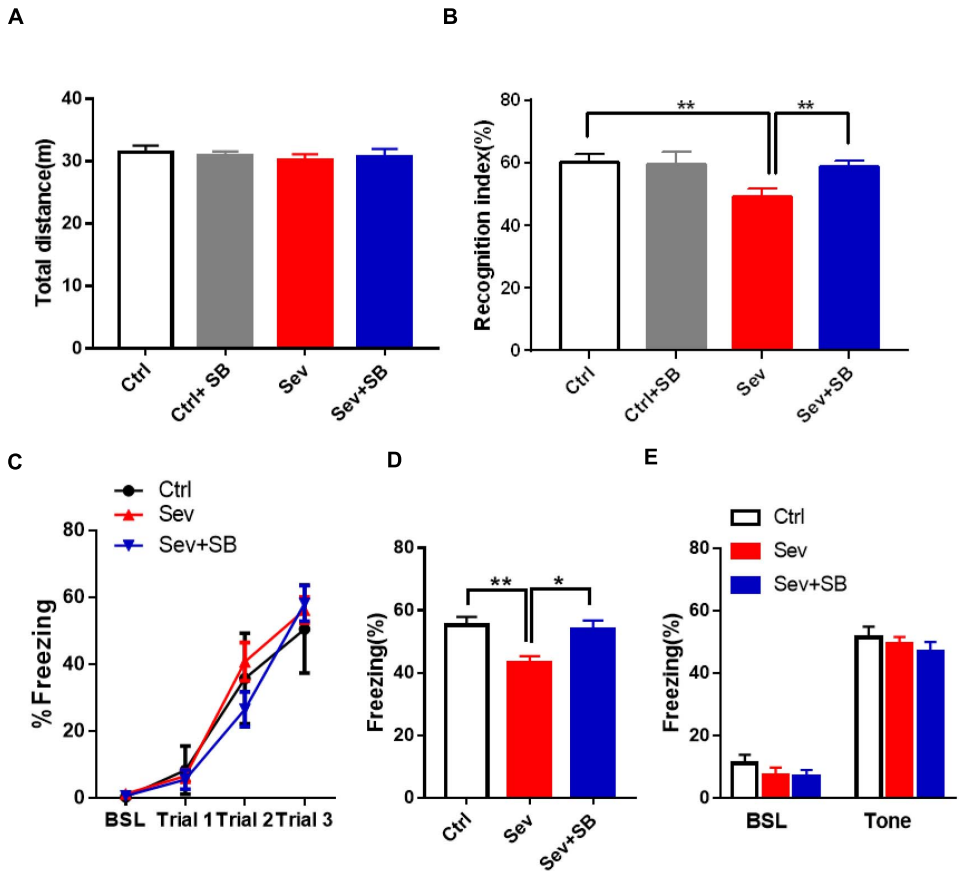

FIGURE 3 | SB 366791 mitigated sevoflurane-induced cognitive impairment in adult mice. **(A)** Total travel distance during 10 min locomotor activity test in the open field test of Ctrl (n = 12), Ctrl + 500 μg/kg SB 366791 (n = 10), Sev (n = 13), and Sev + 500 μg/kg SB 366791 (n = 14) mice. **(B)** Recognition index of Ctrl (n = 10), Ctrl + 500 μg/kg SB 366791 (n = 10), Sev (n = 13), and Sev + 500 μg/kg SB 366791 (n = 14) mice [one way ANOVA, $F_{(3,\ 43)} = 5.8$, $p = 0.0021$]. **(C)** Percentage of freezing in Ctrl (n = 12), Sev (n = 12), and Sev + 500 μg/kg SB 366791 (n = 10) mice during fear conditioning training. **(D)** Percentage of freezing in Ctrl (n = 12), Sev (n = 12) and Sev + 500 μg/kg SB 366791 (n = 10) mice during the contextual memory test [one way ANOVA, $F_{(2,\ 31)} = 6.9$, $p = 0.0034$]. **(E)** Percentage of freezing of Ctrl (n = 12), Sev (n = 12), and Sev + 500 μg/kg SB 366791 (n = 10) mice during the cued test. Data are presented as the mean ± SEM. ANOVA followed by Bonferroni *post hoc* test. $^*p < 0.05$; $^{**}p < 0.01$. Ctrl, control; Sev, sevoflurane; SB, SB 366791.

366791 abolished this effect of sevoflurane (**Figure 3B**). Then fear conditioning test, which assesses the hippocampal- dependent and hippocampus-independent memory, was performed. During the training period, all mice exhibited an increase in freezing elicited by the tone and there was no difference between groups (**Figure 3C**). In the case of the FC contextual test conducted 24 h after the training, sevoflurane treated mice had significantly lower freezing when the animals were place into the same context (**Figure 3D**), while, SB 366791 abrogated the decline induced by sevoflurane (**Figure 3D**). However, no significant differences were observed in the FC tone test among the groups (**Figure 3E**).

Synaptic AMPA receptor delivery contributes to learning and memory (Mitsushima et al., 2011; Knafo et al., 2012). To test whether TRPV1 is required for changing synaptic AMPAR delivery after sevoflurane exposure, crude synaptosomal fractions from mouse hippocampus were isolated, and both synaptosomal and total AMPAR subunits were detected. Sevoflurane exposure decreased the levels of synaptosomal GluA1, 2 and 3 AMPAR subunits compared to that in the control mice, and SB 366791 maintained the levels of these AMPAR subunits (**Figures 4A,B**). The levels of AMPAR in the post-nuclear supernatant fraction (total protein) remained similar in all groups of mice (**Figures 4A,C**). Meanwhile, the surface GluA1 AMPARs in neurons were assessed with immunofluorescence staining. Sevoflurane had a significantly lower surface GluA1 (sGluA1) expression, and pre-treatment with SB 366791 suppressed this reduction induced by sevoflurane exposure (**Figure 5**).

TRPV1 Inhibition Reversed Sevoflurane Exposure Induced AMAPR Accumulation in Early and Recycling Endosomes

To determine the cellular mechanism of AMPAR trafficking deficiency in neurons after sevoflurane treatment, internalized GluA2 (iGluA2) was stained to systematically examine its co-localization with early, recycling and late endosomes based on known markers, EEA1, Stx13, and LAMP1, respectively. After sevoflurane treatment, the remaining iGluA2 in neurons showed

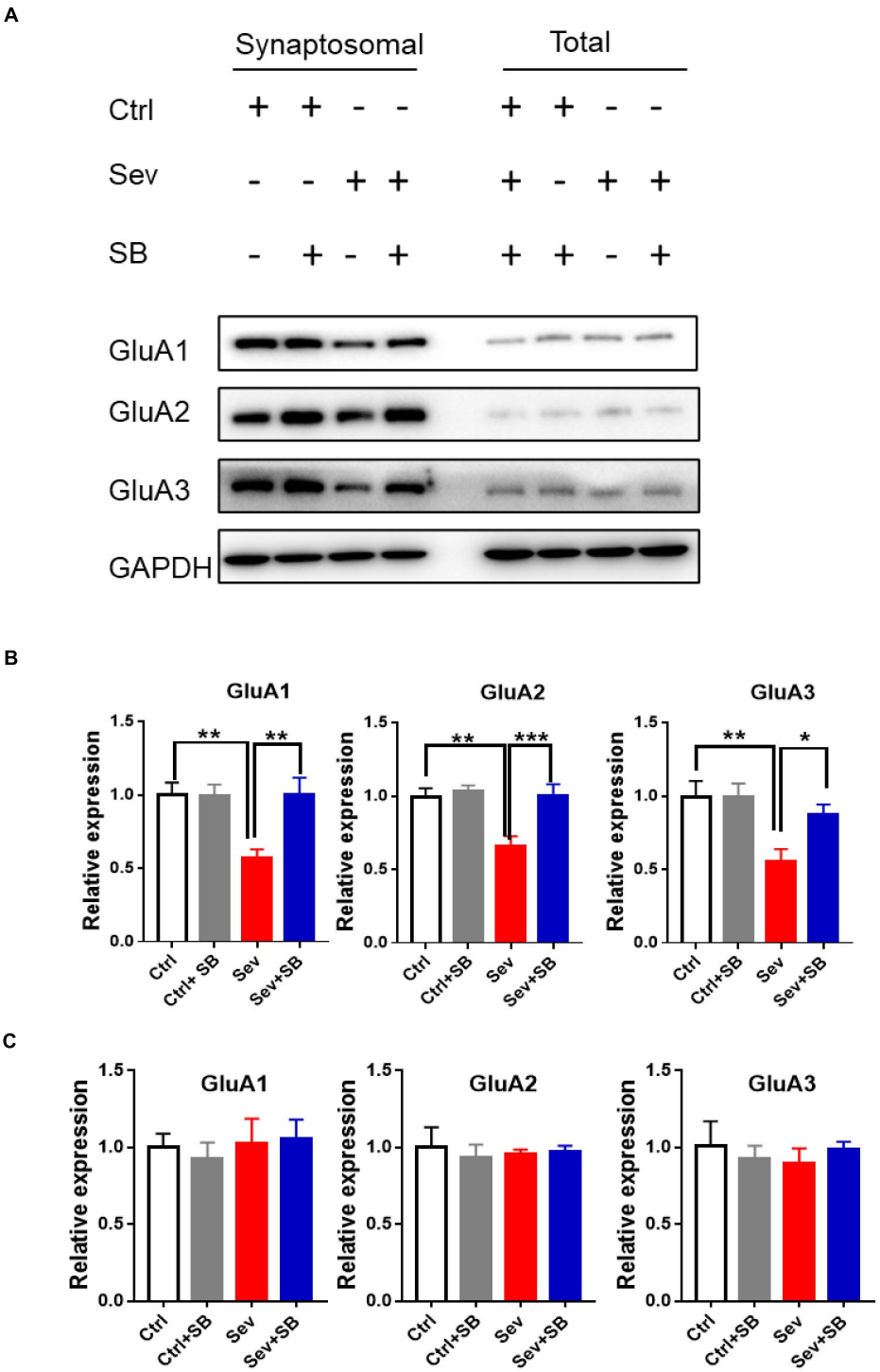

FIGURE 4 | Pre-treatment with TRPV1 antagonist SB 366791 reversed the decrease of the GluA1/2/3 AMPAR subunits caused by sevoflurane exposure. **(A)** Representative Western blots of GluA1/2/3 proteins in crude synaptosomal preparations and total cell lysate obtained from the hippocampal tissue of Ctrl, Ctrl + 500 μg/kg SB 366791, Sev and Sev + 500 μg/kg SB 366791 mice. **(B)** Quantitative analysis of the Western blots [crude synaptosomal, n = 8–10 mice per group, one way ANOVA, GluA1: $F_{(3,\ 32)} = 6.5$, $p = 0.0015$; GluA2: $F_{(3,\ 32)} = 7.6$, $p = 0.0006$; GluA3: $F_{(3,\ 32)} = 6.0$, $p = 0.0023$]. **(C)**: quantitative analysis of the Western blots (total protein, n = 8–10 mice per group). Data are presented as the mean ± SEM. ANOVA followed by Bonferroni *post hoc* test. $^{*}p < 0.05$; $^{**}p < 0.01$; $^{***}p < 0.001$. Ctrl, control; Sev, sevoflurane; SB, SB 366791.

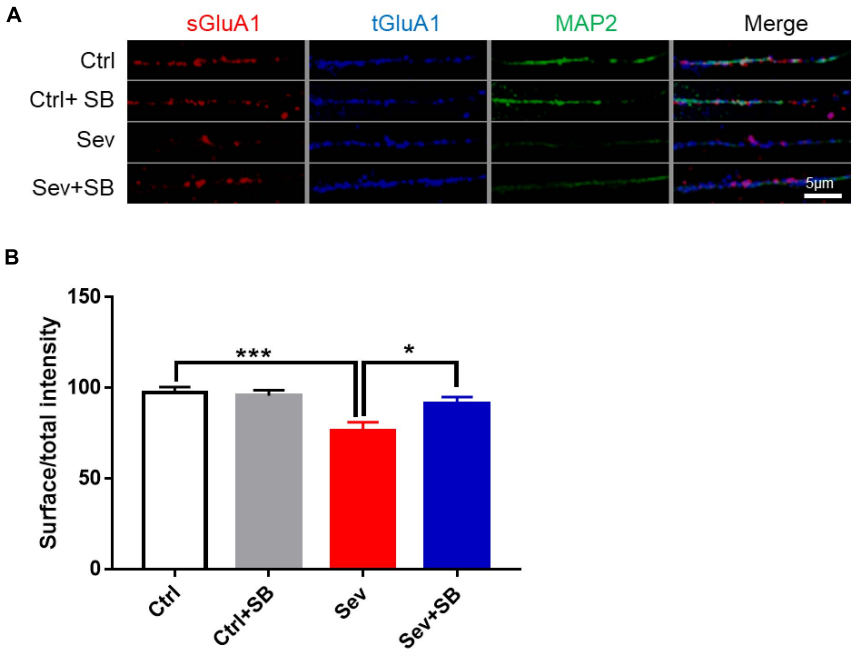

FIGURE 5 | SB 366791 attenuated sevoflurane-induced reduction of surface GluA1 in hippocampus neurons. **(A)** Fluorescent images of surface GluA1 (sGluA1) and total GluA1 (tGluA1) staining in hippocampus neurons from Ctrl and Sev cultures treated with TRPV1 antagonist SB 366791 (10 μM). **(B)** Quantitative analysis of **(A)** [3 cultures per group, one-way ANOVA, $F_{(3,\ 40)} = 7.0$, $p = 0.0007$]. Data are presented as the mean ± SEM. ANOVA followed by Bonferroni *post hoc* test. $^{*}p < 0.05$; $^{***}p < 0.001$. Ctrl, control; Sev, sevoflurane; SB, SB 366791.

a significantly higher co-localization with EEA1 and Stx13 than that in the control neurons. SB 366791 ameliorated the increased co-localization of iGluA2 with the EEA1 and Stx13 induced by sevoflurane treatment (**Figures 6A,B,D,E**). However, the co-localization of iGluA2 with LAMP1 was similar in all group of neurons (**Figures 6C,F**).

TRPV1 Interacted With Src and Decreased Cofilin Phosphorylation

Then, the impact of TRPV1 on endosome sorting was analyzed at the molecular level. A non-receptor tyrosine kinase Src is associated with the regulation of cell proliferation and differentiation (Ohnishi et al., 2011). Downregulation of Src can protect mouse brain from injury (Paul et al., 2001; Purcell and Carew, 2003; Liu et al., 2010; Ward et al., 2019). Therefore, we hypothesized that TRPV1 may retain learning and memory by targeting Src cellular signaling. Co-localization of TRPV1 with Src was detected in HT22 mouse hippocampal neuronal cell line (**Figure 7A**), and co-immunoprecipitation experiments were performed to examine possible interaction between TRPV1 and Src in hippocampal tissue after sevoflurane exposure. The data obtained using mouse hippocampal extract and anti-Src antibody showed that TRPV1 could interact with Src *in vivo* (**Figure 7B**). The expression of p-Src (Tyr 416) was significantly increased after sevoflurane treatment (**Figures 7C,D**), and pre-treatment with SB 366791 suppressed this increasement induced by sevoflurane exposure (**Figures 7C,D**).

Cofilin is an essential regulatory protein with crucial roles in learning and memory through modulating synaptic plasticity and AMPAR mobility (Rust et al., 2010). Previous study reported that cofilin was regulated by Src that triggered cofilin phosphorylation thereby affecting brain function (Wang et al., 2015). Therefore, we hypothesized that TRPV1 may maintain synaptic density and memory by targeting the Src-cofilin pathway. Our results showed that cofilin phosphorylation was significantly reduced in Sev group, while pretreatment with SB 366791 for 1 h before sevoflurane treatment significantly inhibited the reduction of cofilin phosphorylation (**Figures 7E,F**).

DISCUSSION

In the current study, we demonstrated that repetitious sevoflurane exposure on postnatal day 7 mice led to long-term learning and memory deficits. In neuronal cultures, sevoflurane exposure increased TRPV1 expression, decreased synaptic density, crude synaptosomal and neuronal surface AMPAR expression, as well as defected early and recycling endosomal trafficking in hippocampal neurons. The underlying molecular mechanism may be mediated through an increase in p-Src (Tyr 416) and a decrease in p-cofilin. However, pre-treatment with TRPV1 antagonist SB 366791 before sevoflurane exposure reversed the detrimental effects of sevoflurane both in mice and the hippocampal neurons (**Figure 8**).

Neurotransmitter receptors, γ-aminobutyrate (GABA) and N-methyl-D-aspartic acid (NMDA) receptors in particular, and

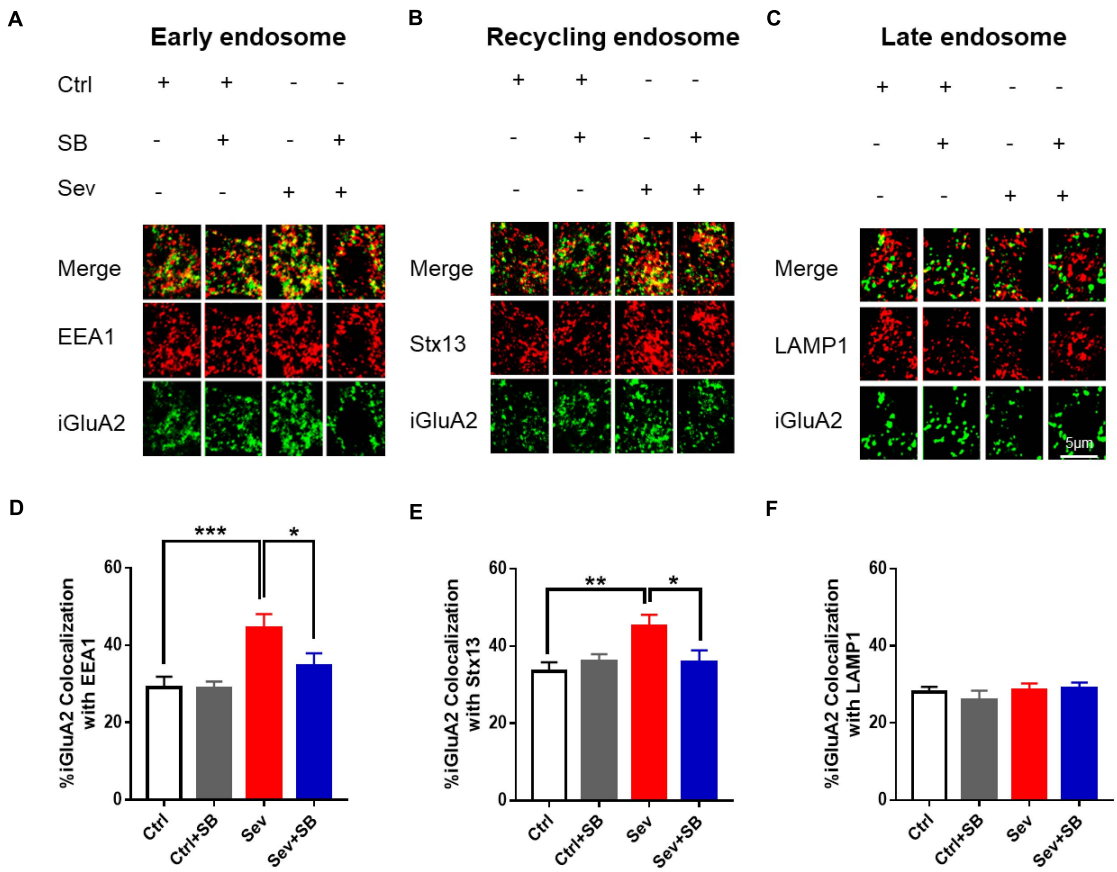

FIGURE 6 | Pretreatment with TRPV1 antagonist SB 366791 reversed the sevoflurane-induced accumulation of internalized AMPAR in endosomes. **(A)** Co-localization of internalized GluA2 (iGluA2, green) and EEA1 (red) in the cell bodies of hippocampal neurons from the Ctrl and Sev cultures treated with TRPV1 antagonist SB 366791 (10 μM). **(B)** Co-localization of iGluA2 and Stx13 (red). **(C)** Co-localization of iGluA2 and LAMP1 (red). **(D)** Quantification of **(A)**. [3 cultures per group, one-way ANOVA, $F_{(3,\ 82)} = 6.2$, $p = 0.0008$]. **(E)** Quantification of **(B)**. [3 cultures per group, one-way ANOVA, $F_{(3,\ 80)} = 3.8$, $p = 0.0129$]. **(F)** Quantification of **(C)** [3 cultures per group, one-way ANOVA, $F_{(3,\ 51)} = 0.5$, $p > 0.05$]. Data are presented as the mean ± SEM. ANOVA followed by Bonferroni *post hoc* test. $^*p < 0.05$; $^{**}p < 0.01$; $^{***}p < 0.001$. Ctrl, control; Sev, sevoflurane; SB, SB 366791.

other ion channels are molecular targets of general anesthetics (Hemmings et al., 2005), suggesting that multiple anesthetic effects may be associated with various molecular targets in various regions of the nervous system. TRPV1 is a ligand-gated non-specific cation channel responding to various noxious stimuli (Julius, 2013). Previous studies shown that TRPV1 is activated and sensitized by local anesthetics in rodent sensory neurons as well as in HEK293T cells expressing TRPV1 (Leffler et al., 2008). Sevoflurane can sensitize TRPV1 to capsaicin and protons and reduce the threshold for heat activation in nociceptive neurons (Cornett et al., 2008). Our recent data demonstrated that the level of TRPV1 channel was increased in HT22 cells after treated with sevoflurane (Liu et al., 2019). HT22 cells are of neuronal origin; however, these cells may not accurately reflect the mechanisms of the normal neurons; hence, we used primary mouse neurons to investigate the role of TRPV1 in sevoflurane-induced neurotoxicity. The both *in vivo* and *in vitro* data of the present study indicated that the TRPV1 expression in neurons was increased after sevoflurane treatment which in line with our previous study (Liu et al., 2019). Interestingly, another study showed that sevoflurane upregulated the expression of TRPV1 in the airways (Liu et al., 2020). Therefore, all these indicated that sevoflurane can activate this channel in both central nervous system (CNS) and peripheral tissue. However, the underlying mechanism of these effects remains unclear. For instance, sevoflurane may regulate TRPV1 via a ligand-gated mechanism similar to activation of TRP channels by other anesthetics (Matta et al., 2008); the exact mechanisms remain unknown and warrants further study.

Neurons communicate via synapse, and certain changes in synapses are related to a number of brain diseases. We and other (Xiao et al., 2016) reported that synaptic density was reduced after sevoflurane treatment both *in vivo* and *in vitro*. TRPV1 is involved in various functions, including synaptic plasticity in the CNS. Capsaicin, a TRPV1 agonist, upregulated histone deacetylase 2 (HDAC2) resulting in the reduction of synaptic molecules and loss of synaptic density (Wang S. E. et al., 2018). In the present study, TRPV1 antagonist SB 366791 was able to prevent synaptic density

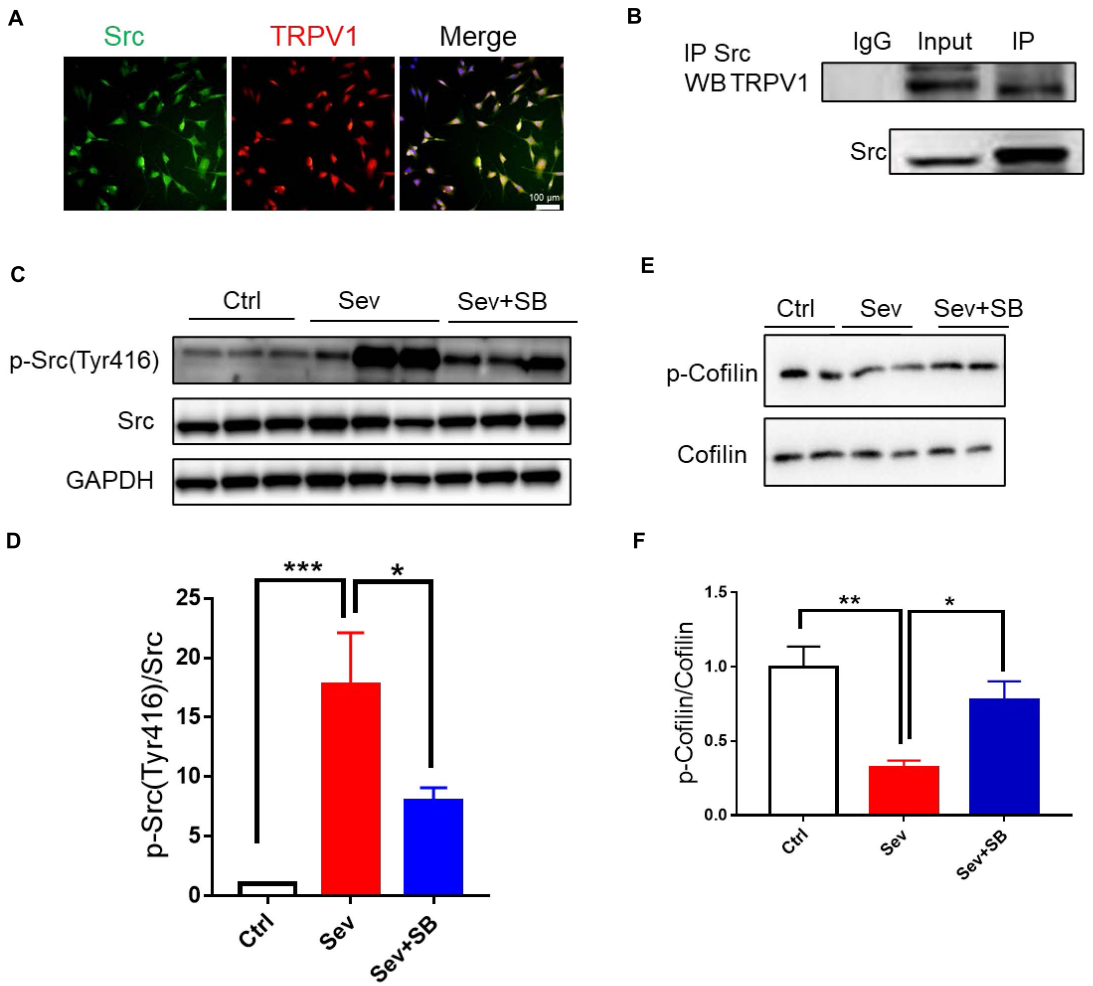

FIGURE 7 | TRPV1 binds to Src and suppresses inhibition of cofilin. **(A)** Representative image of TRPV1 (red) and Src (green) fluorescence in HT22 cell line. **(B)** Co-immunoprecipitation of Src and TRPV1 using anti-Src antibody in hippocampal protein extracts from control mice. **(C,D)** Representative image **(C)** and relative expression of **(D)** Src phosphorylation at tyrosine 416 (p-Src) after with or without SB 366791 (500 μg/kg) treatment [n = 6/group, one-way ANOVA, $F_{(2,\ 15)} = 10.4$, $p = 0.0015$]. **(E)** Representative Western blot bands. **(F)** Quantitative analysis of **(E)** [5 mice per group, one-way ANOVA, $F_{(2,\ 12)} = 9.3$, $p = 0.0036$]. Data are presented as the mean ± SEM. ANOVA followed by Bonferroni *post hoc* test. $^{*}p < 0.05$; $^{**}p < 0.01$; $^{***}p < 0.001$. Ctrl, control; Sev, sevoflurane; SB, SB 366791.

decline. Thus, the activation of TRPV1 by sevoflurane reduced synaptic density in hippocampus, and this morphological alteration may subsequently contribute to the impairment of learning and memory.

The causal link between exposure a developing brain to commonly used anesthetics and brain development has not been established and remains controversial despite extensive preclinical studies. Lengthy or repeated exposure of 6–7-day-old rodents to equivalent anesthetics (such as isoflurane, sevoflurane or desflurane) resulted in an impairment of learning and memory in adulthood (Satomoto et al., 2009; Kodama et al., 2011; Ramage et al., 2013; Tao et al., 2016). However, other studies reported that exposure of neonatal non-human primates and rodents to anesthetics did not affect learning and memory (Fredriksson et al., 2007; Zhou et al., 2016). In the present study, exposure of neonatal mice at postnatal day 7–3% sevoflurane 2 h daily for 3 consecutive days resulted in learning and memory dysfunction in the NORT and contextual fear conditioning in adulthood. However, sevoflurane exposure has no effect on tone fear learning. Because the contextual fear conditioning was the hippocampal dependent learning, and tone fear conditioning was hippocampal independent learning (Phillips and LeDoux, 1992; Medina et al., 2002). It is possible that the amygdala function was unlikely impaired and the expression of TRPV1 in the amygdala remained unchanged, thus sevoflurane did not induce memory impairment which was consistent with the previous studies (Ni et al., 2020; Wang et al., 2020).

Published literature suggested that anesthetic exposure to the young and aged animals caused learning and memory disabilities (Dai et al., 2020; Fei et al., 2020; Zheng et al., 2020). In general, adult age animals are resistant to anesthetics-induced neuronal injury although the mechanisms responsible for this difference are unknown. A previous study suggested that extra-synaptic NMDA receptors, which is enriched in the young than the adult

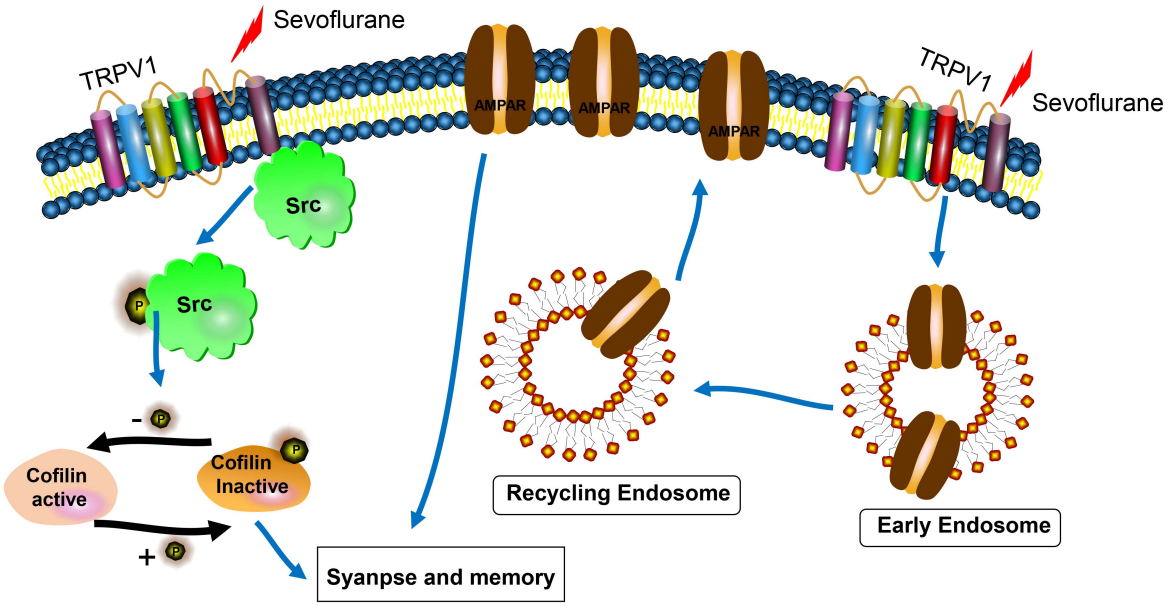

FIGURE 8 | Scheme for the proposed mechanisms of TRPV1 antagonist protection of synaptic loss and memory defects induced by sevoflurane exposure. The underlying mechanisms may be involved with the interactions of TRPV1 and Src, cofilin activation, and AMPAR trafficking deficiency.

age, contributed the sevoflurane induced neurotoxicity (Wang et al., 2016) and this may provide partial explanation. However, adult age animals are not free from neurotoxicity which was also documented previously (Jevtovic-Todorovic et al., 2000). Importantly, under both anesthesia and surgery, the neuronal injuries and hence cognitive impairment in adults were readily detected (Vizcaychipi et al., 2014).

The levels of AMPAR GluA1/2/3 subunits were significantly decreased in the hippocampal synapses of sevoflurane-exposed mice which is similar to the findings of a previous study that pentobarbital and chloral hydrate reduced the expression of cortical and striatal neuronal surface AMPAR (Carino et al., 2012). The various AMPAR GluA subunits were not altered under SB366791 treatment which is not cell toxic (Liu et al., 2019). Previous study has also shown that either upregulation or knockdown of TRPV1 did not affect the expression of GluA1 and GluA2 (Giordano et al., 2012; Du et al., 2020). Thus, SB 366791 itself did not affect the expression of AMPAR. Therefore, sevoflurane decreased the expression of the AMPAR GluA1 subunit in the cultured hippocampal neurons was due to its inherent pharmacological effects, and pre-treatment with TRPV1 antagonist preserved the AMPAR trafficking was likely related to its blocking effect of TRPV1 changes induced by sevoflurane. Considering the results of previous studies, the effect of anesthetics on AMPAR trafficking is unlikely to depend on drug type. A reduction in the number of the receptors in the cell surface pool was accompanied by an increase in the number of the receptors in the intracellular pool. In the current study, the total AMPAR levels were not changed after sevoflurane treatment; thus, changes in the internalization or surface pool would account for AMPAR redistribution. Endosome sorting is the source of AMPA receptor mobilization (Park et al., 2004). Thus, blocking endosome sorting will impact the AMPAR trafficking and subsequent memory impairment. The data of our immunostaining experiments *in vitro* indicated that sevoflurane induced iGluA2 accumulation in the early and recycling endosomes in neurons, and pre-treatment with a TRPV1 antagonist ameliorated this accumulation, suggesting that TRPV1 may be required for AMPAR trafficking. AMPAR trafficking is associated with multiple proteins, including Stx13, Rab11, SNAP47, Rab8, synaptobrevin 2, etc. (Brown et al., 2007; Esteban, 2008; Jurado et al., 2013; Gu et al., 2016). In the present study, inhibition of TRPV1 abolished iGluA2 accumulation in the endosomes, indicating that TRPV1 may interact with endosomal proteins in mice although it warrants further study.

The present study indicated that TRPV1 may interact with Src cellular signaling, and sevoflurane exposure increased the phosphorylation of Src at tyrosine 416. Src can regulate the activities of FAK and cofilin to control neuronal migration (Wang et al., 2015). In p140Cap-knockout mice, over-activation of Src downregulated the RhoA/ROCK/cofilin signaling pathway to impact synaptic plasticity as well as learning and memory (Repetto et al., 2014). Similar to the impairment of the RhoA/ROCK/cofilin pathway induced by Src activation, a decrease in phosphorylation of cofilin was observed in the present study, while SB 366791 reversed this reduction caused by sevoflurane exposure. Brain-derived neurotrophic factor (BDNF) can activate cofilin signaling (Tong et al., 2012); thus, we cannot rule out a possibility that sevoflurane exposure inhibits BDNF to induce the TRPV1-mediated changes in synaptic density and cognitive function. However, our results indicated that the TRPV1 channel and cofilin likely interact each other *per se*.

Our work is not without limitations. First, the both N and C terminals of TRPV1 all contains specific structural domains

with slightly different physiological functions; for example, the N-terminal is responsible for a thermal sensor of TRPV1 and channel activity (Yao et al., 2011; Du et al., 2019) whilst C-terminal domains of TRPV1 was reported to be involved in thermo-TRP channel activity, the regulation of voltage-gated channel opening and phosphorylation (Kwak et al., 2000; Goswami et al., 2007; Moiseenkova-Bell et al., 2008; Wang and Chuang, 2011). In our current study, only N-terminal antibodies were used and, therefore, the whole picture changes of TRPV1 are unknown. Second, neonatal mice were only used to study the neurotoxicity of sevoflurane in the current study. Thus, whether the current findings and underlying mechanisms were also evident in adult or even in older age is subjected for future study.

CONCLUSION

In conclusion, our results suggested the TRPV1/Src/cofilin signaling pathway likely mediated the abnormalities in synaptic density and neurocognitive function induced by sevoflurane exposure in mice at the brain development stage. These findings may provide a mechanistic foundation for identification of novel therapeutic targets of sevoflurane induced neurotoxicioty.

DATA AVAILABILITY STATEMENT

The original contributions presented in the study are included in the article/supplementary material, further inquiries can be directed to the corresponding author/s.

ETHICS STATEMENT

The animal study was reviewed and approved by the Committee on the Animal Research Ethics of the Shenzhen Second People's Hospital and Sun Yat-sen Memorial Hospital.

AUTHOR CONTRIBUTIONS

YL and ZL: intellectual ideas and experimental design and manuscript writing. YL, HY, YF, ZP, FQ, and YX: experimental procedures. YL, FQ, XY, and QC: statistical analysis. All authors manuscript editing and revisions.

FUNDING

This work was supported by the National Natural Science Foundation of China (82001138), China Postdoctoral Science Foundation (2019M653078), Science and technology planning Project of Shenzhen Municipality (JCYJ20190806164601647), and Projects of International Cooperation of Shenzhen (GJHZ20180926170402056).

ACKNOWLEDGMENTS

We would like to thank Department of Anesthesiology, Sun Yat-sen Memorial Hospital, for allowing us to use their research facilities.

REFERENCES

Alter, B. J., and Gereau, R. W. T. (2008). Hotheaded: TRPV1 as mediator of hippocampal synaptic plasticity. *Neuron* 57, 629–631. doi: 10.1016/j.neuron.2008.02.023

Brown, T. C., Correia, S. S., Petrok, C. N., and Esteban, J. A. (2007). Functional compartmentalization of endosomal trafficking for the synaptic delivery of AMPA receptors during long-term potentiation. *J. Neurosci.* 27, 13311–13315. doi: 10.1523/JNEUROSCI.4258-07.2007

Carino, C., Fibuch, E. E., Mao, L. M., and Wang, J. Q. (2012). Dynamic loss of surface-expressed AMPA receptors in mouse cortical and striatal neurons during anesthesia. *J. Neurosci. Res.* 90, 315–323. doi: 10.1002/jnr.22749

Colon, E., Bittner, E. A., Kussman, B., McCann, M. E., Soriano, S., and Borsook, D. (2017). Anesthesia, brain changes, and behavior: insights from neural systems biology. *Prog. Neurobiol.* 153, 121–160. doi: 10.1016/j.pneurobio.2017.01.005

Cornett, P. M., Matta, J. A., and Ahern, G. P. (2008). General anesthetics sensitize the capsaicin receptor transient receptor potential V1. *Mol. Pharmacol.* 74, 1261–1268. doi: 10.1124/mol.108.049684

Dai, C. L., Li, H., Hu, X., Zhang, J., Liu, F., Iqbal, K., et al. (2020). Neonatal exposure to anesthesia leads to cognitive deficits in old age: prevention with intranasal administration of insulin in mice. *Neurotox. Res.* 38, 299–311. doi: 10.1007/s12640-020-00223-y

Davidson, A. J., Disma, N., de Graaff, J. C., Withington, D. E., Dorris, L., Bell, G., et al. (2016). Neurodevelopmental outcome at 2 years of age after general anaesthesia and awake-regional anaesthesia in infancy (GAS): an international multicentre, randomised controlled trial. *Lancet* 387, 239–250. doi: 10.1016/S0140-6736(15)00608-X

Du, Q., Liao, Q., Chen, C., Yang, X., Xie, R., and Xu, J. (2019). The role of transient receptor potential vanilloid 1 in common diseases of the digestive tract and the cardiovascular and respiratory system. *Front. Physiol.* 10:1064. doi: 10.3389/fphys.2019.01064

Du, Y., Fu, M., Huang, Z., Tian, X., Li, J., Pang, Y., et al. (2020). TRPV1 activation alleviates cognitive and synaptic plasticity impairments through inhibiting AMPAR endocytosis in APP23/PS45 mouse model of Alzheimer's disease. *Aging Cell* 19:e13113. doi: 10.1111/acel.13113

Edwards, J. G. (2014). TRPV1 in the central nervous system: synaptic plasticity, function, and pharmacological implications. *Prog. Drug Res.* 68, 77–104. doi: 10.1007/978-3-0348-0828-6_3

Esteban, J. A. (2008). Intracellular machinery for the transport of AMPA receptors. *Br. J. Pharmacol.* 153(Suppl. 1), S35–S43. doi: 10.1038/sj.bjp.0707525

Fei, X., Wang, J. X., Wu, Y., Dong, N., and Sheng, Z. Y. (2020). Sevoflurane-induced cognitive decline in aged mice: involvement of toll-like receptors 4. *Brain Res. Bull.* 165, 23–29. doi: 10.1016/j.brainresbull.2020.08.030

Fredriksson, A., Ponten, E., Gordh, T., and Eriksson, P. (2007). Neonatal exposure to a combination of N-methyl-D-aspartate and gamma-aminobutyric acid type A receptor anesthetic agents potentiates apoptotic neurodegeneration and persistent behavioral deficits. *Anesthesiology* 107, 427–436. doi: 10.1097/01.anes.0000278892.62305.9c

Giordano, C., Cristino, L., Luongo, L., Siniscalco, D., Petrosino, S., Piscitelli, F., et al. (2012). TRPV1-dependent and -independent alterations in the limbic cortex of neuropathic mice: impact on glial caspases and pain perception. *Cereb. Cortex* 22, 2495–2518. doi: 10.1093/cercor/bhr328

Goswami, C., Hucho, T. B., and Hucho, F. (2007). Identification and characterisation of novel tubulin-binding motifs located within the C-terminus of TRPV1. *J. Neurochem.* 101, 250–262. doi: 10.1111/j.1471-4159.2006.04338.x

Gu, Y., Chiu, S. L., Liu, B., Wu, P. H., Delannoy, M., Lin, D. T., et al. (2016). Differential vesicular sorting of AMPA and GABAA receptors. *Proc. Natl. Acad. Sci. U.S.A.* 113, E922–E931. doi: 10.1073/pnas.1525726113

Hemmings, H. C. Jr., Akabas, M. H., Goldstein, P. A., Trudell, J. R., Orser, B. A., and Harrison, N. L. (2005). Emerging molecular mechanisms of general anesthetic action. *Trends Pharmacol. Sci.* 26, 503–510. doi: 10.1016/j.tips.2005.08.006

Jevtovic-Todorovic, V., Benshoff, N., and Olney, J. W. (2000). Ketamine potentiates cerebrocortical damage induced by the common anaesthetic agent nitrous oxide in adult rats. *Br. J. Pharmacol.* 130, 1692–1698. doi: 10.1038/sj.bjp.0703479

Julius, D. (2013). TRP channels and pain. *Annu. Rev. Cell Dev. Biol.* 29, 355–384. doi: 10.1146/annurev-cellbio-101011-155833

Jurado, S., Goswami, D., Zhang, Y., Molina, A. J., Sudhof, T. C., and Malenka, R. C. (2013). LTP requires a unique postsynaptic SNARE fusion machinery. *Neuron* 77, 542–558. doi: 10.1016/j.neuron.2012.11.029

Knafo, S., Venero, C., Sanchez-Puelles, C., Pereda-Perez, I., Franco, A., Sandi, C., et al. (2012). Facilitation of AMPA receptor synaptic delivery as a molecular mechanism for cognitive enhancement. *PLoS Biol.* 10:e1001262. doi: 10.1371/journal.pbio.1001262

Kodama, M., Satoh, Y., Otsubo, Y., Araki, Y., Yonamine, R., Masui, K., et al. (2011). Neonatal desflurane exposure induces more robust neuroapoptosis than do isoflurane and sevoflurane and impairs working memory. *Anesthesiology* 115, 979–991. doi: 10.1097/ALN.0b013e318234228b

Kwak, J., Wang, M. H., Hwang, S. W., Kim, T. Y., Lee, S. Y., and Oh, U. (2000). Intracellular ATP increases capsaicin-activated channel activity by interacting with nucleotide-binding domains. *J. Neurosci.* 20, 8298–8304. doi: 10.1523/jneurosci.20-22-08298.2000

Lee, S. H., Simonetta, A., and Sheng, M. (2004). Subunit rules governing the sorting of internalized AMPA receptors in hippocampal neurons. *Neuron* 43, 221–236. doi: 10.1016/j.neuron.2004.06.015

Leffler, A., Fischer, M. J., Rehner, D., Kienel, S., Kistner, K., Sauer, S. K., et al. (2008). The vanilloid receptor TRPV1 is activated and sensitized by local anesthetics in rodent sensory neurons. *J. Clin. Invest.* 118, 763–776. doi: 10.1172/JCI32751

Liu, D. Z., Ander, B. P., Xu, H., Shen, Y., Kaur, P., Deng, W., et al. (2010). Blood-brain barrier breakdown and repair by Src after thrombin-induced injury. *Ann. Neurol.* 67, 526–533. doi: 10.1002/ana.21924

Liu, D., Yuan, J., Fei, X., Zhu, Y., Zhou, Y., Zhang, C., et al. (2020). Effects of inhalation of sevoflurane at different concentrations on TRPV1 in airways of rats at different developmental stages. *Life Sci.* 249:117472. doi: 10.1016/j.lfs.2020.117472

Liu, Y., Chen, C., Liu, Y., Li, W., Wang, Z., Sun, Q., et al. (2018). TRPM7 is required for normal synapse density, learning, and memory at different developmental stages. *Cell Rep.* 23, 3480–3491. doi: 10.1016/j.celrep.2018.05.069

Liu, Y., Yang, H., Sun, C., Wang, Z., and Liu, Z. (2019). Protective effects of TRPV1 inhibition against sevoflurane-induced cell death. *Neurosci. Lett.* 707:134270. doi: 10.1016/j.neulet.2019.05.024

Lu, H., Liufu, N., Dong, Y., Xu, G., Zhang, Y., Shu, L., et al. (2017). Sevoflurane acts on ubiquitination-proteasome pathway to reduce postsynaptic density 95 protein levels in young mice. *Anesthesiology* 127, 961–975. doi: 10.1097/ALN.0000000000001889

Marsch, R., Foeller, E., Rammes, G., Bunck, M., Kossl, M., Holsboer, F., et al. (2007). Reduced anxiety, conditioned fear, and hippocampal long-term potentiation in transient receptor potential vanilloid type 1 receptor-deficient mice. *J. Neurosci.* 27, 832–839. doi: 10.1523/JNEUROSCI.3303-06.2007

Matta, J. A., Cornett, P. M., Miyares, R. L., Abe, K., Sahibzada, N., and Ahern, G. P. (2008). General anesthetics activate a nociceptive ion channel to enhance pain and inflammation. *Proc. Natl. Acad. Sci. U.S.A.* 105, 8784–8789. doi: 10.1073/pnas.0711038105

McCann, M. E., de Graaff, J. C., Dorris, L., Disma, N., Withington, D., Bell, G., et al. (2019). Neurodevelopmental outcome at 5 years of age after general anaesthesia or awake-regional anaesthesia in infancy (GAS): an international, multicentre, randomised, controlled equivalence trial. *Lancet* 393, 664–677. doi: 10.1016/S0140-6736(18)32485-1

Medina, J. F., Repa, J. C., Mauk, M. D., and LeDoux, J. E. (2002). Parallels between cerebellum- and amygdala-dependent conditioning. *Nat. Rev. Neurosci.* 3, 122–131. doi: 10.1038/nrn728

Mitsushima, D., Ishihara, K., Sano, A., Kessels, H. W., and Takahashi, T. (2011). Contextual learning requires synaptic AMPA receptor delivery in the hippocampus. *Proc. Natl. Acad. Sci. U.S.A.* 108, 12503–12508. doi: 10.1073/pnas.1104558108

Moiseenkova-Bell, V. Y., Stanciu, L. A., Serysheva, I. I., Tobe, B. J., and Wensel, T. G. (2008). Structure of TRPV1 channel revealed by electron cryomicroscopy. *Proc. Natl. Acad. Sci. U.S.A.* 105, 7451–7455. doi: 10.1073/pnas.0711835105

Ni, C., Qian, M., Geng, J., Qu, Y., Tian, Y., Yang, N., et al. (2020). DNA methylation manipulation of memory genes is involved in sevoflurane induced cognitive impairments in aged rats. *Front. Aging Neurosci.* 12:211. doi: 10.3389/fnagi.2020.00211

Ohnishi, H., Murata, Y., Okazawa, H., and Matozaki, T. (2011). Src family kinases: modulators of neurotransmitter receptor function and behavior. *Trends Neurosci.* 34, 629–637. doi: 10.1016/j.tins.2011.09.005

Palazzo, E., Luongo, L., de Novellis, V., Berrino, L., Rossi, F., and Maione, S. (2010). Moving towards supraspinal TRPV1 receptors for chronic pain relief. *Mol. Pain* 6:66. doi: 10.1186/1744-8069-6-66

Palazzo, E., Luongo, L., de Novellis, V., Rossi, F., Marabese, I., and Maione, S. (2012). Transient receptor potential vanilloid type 1 and pain development. *Curr. Opin. Pharmacol.* 12, 9–17. doi: 10.1016/j.coph.2011.10.022

Park, M., Penick, E. C., Edwards, J. G., Kauer, J. A., and Ehlers, M. D. (2004). Recycling endosomes supply AMPA receptors for LTP. *Science* 305, 1972–1975. doi: 10.1126/science.1102026

Paul, R., Zhang, Z. G., Eliceiri, B. P., Jiang, Q., Boccia, A. D., Zhang, R. L., et al. (2001). Src deficiency or blockade of Src activity in mice provides cerebral protection following stroke. *Nat. Med.* 7, 222–227. doi: 10.1038/84675

Phillips, R. G., and LeDoux, J. E. (1992). Differential contribution of amygdala and hippocampus to cued and contextual fear conditioning. *Behav. Neurosci.* 106, 274–285. doi: 10.1037//0735-7044.106.2.274

Purcell, A. L., and Carew, T. J. (2003). Tyrosine kinases, synaptic plasticity and memory: insights from vertebrates and invertebrates. *Trends Neurosci.* 26, 625–630. doi: 10.1016/j.tins.2003.09.005

Ramage, T. M., Chang, F. L., Shih, J., Alvi, R. S., Quitoriano, G. R., Rau, V., et al. (2013). Distinct long-term neurocognitive outcomes after equipotent sevoflurane or isoflurane anaesthesia in immature rats. *Br. J. Anaesth.* 110(Suppl. 1), i39–i46. doi: 10.1093/bja/aet103

Repetto, D., Camera, P., Melani, R., Morello, N., Russo, I., Calcagno, E., et al. (2014). p140Cap regulates memory and synaptic plasticity through Src-mediated and citron-N-mediated actin reorganization. *J. Neurosci.* 34, 1542–1553. doi: 10.1523/JNEUROSCI.2341-13.2014

Rust, M. B., Gurniak, C. B., Renner, M., Vara, H., Morando, L., Gorlich, A., et al. (2010). Learning, AMPA receptor mobility and synaptic plasticity depend on n-cofilin-mediated actin dynamics. *EMBO J.* 29, 1889–1902. doi: 10.1038/emboj.2010.72

Sanders, R. D., Hassell, J., Davidson, A. J., Robertson, N. J., and Ma, D. (2013). Impact of anaesthetics and surgery on neurodevelopment: an update. *Br. J. Anaesth.* 110(Suppl. 1), i53–i72. doi: 10.1093/bja/aet054

Satomoto, M., Satoh, Y., Terui, K., Miyao, H., Takishima, K., Ito, M., et al. (2009). Neonatal exposure to sevoflurane induces abnormal social behaviors and deficits in fear conditioning in mice. *Anesthesiology* 110, 628–637. doi: 10.1097/ALN.0b013e3181974fa2

Sun, L. S., Li, G., Miller, T. L., Salorio, C., Byrne, M. W., Bellinger, D. C., et al. (2016). Association between a single general anesthesia exposure before age 36 months and neurocognitive outcomes in later childhood. *JAMA* 315, 2312–2320. doi: 10.1001/jama.2016.6967

Tao, G., Xue, Q., Luo, Y., Li, G., Xia, Y., and Yu, B. (2016). Isoflurane is more deleterious to developing brain than desflurane: the role of the Akt/GSK3beta signaling pathway. *Biomed. Res. Int.* 2016:7919640. doi: 10.1155/2016/7919640

Tong, L., Prieto, G. A., Kramar, E. A., Smith, E. D., Cribbs, D. H., Lynch, G., et al. (2012). Brain-derived neurotrophic factor-dependent synaptic plasticity is suppressed by interleukin-1beta via p38 mitogen-activated protein kinase. *J. Neurosci.* 32, 17714–17724. doi: 10.1523/JNEUROSCI.1253-12.2012

Vizcaychipi, M. P., Watts, H. R., O'Dea, K. P., Lloyd, D. G., Penn, J. W., Wan, Y., et al. (2014). The therapeutic potential of atorvastatin in a mouse model of postoperative cognitive decline. *Ann. Surg.* 259, 1235–1244. doi: 10.1097/SLA.0000000000000257

Vutskits, L., and Xie, Z. (2016). Lasting impact of general anaesthesia on the brain: mechanisms and relevance. *Nat. Rev. Neurosci.* 17, 705–717. doi: 10.1038/nrn.2016.128

Wang, J. T., Song, L. Z., Li, L. L., Zhang, W., Chai, X. J., An, L., et al. (2015). Src controls neuronal migration by regulating the activity of FAK and cofilin. *Neuroscience* 292, 90–100. doi: 10.1016/j.neuroscience.2015.02.025

Wang, S. E., Ko, S. Y., Kim, Y. S., Jo, S., Lee, S. H., Jung, S. J., et al. (2018). Capsaicin upregulates HDAC2 via TRPV1 and impairs neuronal maturation in mice. *Exp. Mol. Med.* 50:e455. doi: 10.1038/emm.2017.289

Wang, S., and Chuang, H. H. (2011). C-terminal dimerization activates the nociceptive transduction channel transient receptor potential vanilloid 1. *J. Biol. Chem.* 286, 40601–40607. doi: 10.1074/jbc.M111.256669

Wang, W. Y., Jia, L. J., Luo, Y., Zhang, H. H., Cai, F., Mao, H., et al. (2016). Location- and subunit-specific NMDA receptors determine the developmental sevoflurane neurotoxicity through ERK1/2 signaling. *Mol. Neurobiol.* 53, 216–230. doi: 10.1007/s12035-014-9005-1

Wang, Y., Gao, Y., Tian, Q., Deng, Q., Wang, Y., Zhou, T., et al. (2018). TRPV1 SUMOylation regulates nociceptive signaling in models of inflammatory pain. *Nat. Commun.* 9:1529. doi: 10.1038/s41467-018-03974-7

Wang, Y., Qian, M., Qu, Y., Yang, N., Mu, B., Liu, K., et al. (2020). Genome-Wide screen of the hippocampus in aged rats identifies mitochondria, metabolism and aging processes implicated in sevoflurane anesthesia. *Front. Aging Neurosci.* 12:122. doi: 10.3389/fnagi.2020.00122

Ward, K. R., Featherstone, R. E., Naschek, M. J., Melnychenko, O., Banerjee, A., Yi, J., et al. (2019). Src deficient mice demonstrate behavioral and electrophysiological alterations relevant to psychiatric and developmental disease. *Prog. Neuropsychopharmacol. Biol. Psychiatry* 93, 84–92. doi: 10.1016/j.pnpbp.2019.02.017

Warner, D. O., Zaccariello, M. J., Katusic, S. K., Schroeder, D. R., Hanson, A. C., Schulte, P. J., et al. (2018). Neuropsychological and behavioral outcomes after exposure of young children to procedures requiring general anesthesia: the mayo anesthesia safety in kids (MASK) study. *Anesthesiology* 129, 89–105. doi: 10.1097/ALN.0000000000002232

Wu, L., Zhao, H., Weng, H., and Ma, D. (2019). Lasting effects of general anesthetics on the brain in the young and elderly: "mixed picture" of neurotoxicity, neuroprotection and cognitive impairment. *J. Anesth.* 33, 321–335. doi: 10.1007/s00540-019-02623-7

Xiao, H., Liu, B., Chen, Y., and Zhang, J. (2016). Learning, memory and synaptic plasticity in hippocampus in rats exposed to sevoflurane. *Int. J. Dev. Neurosci.* 48, 38–49. doi: 10.1016/j.ijdevneu.2015.11.001

Yao, J., Liu, B., and Qin, F. (2011). Modular thermal sensors in temperature-gated transient receptor potential (TRP) channels. *Proc. Natl. Acad. Sci. U.S.A.* 108, 11109–11114. doi: 10.1073/pnas.1105196108

Zheng, F., Fang, P., Chang, J., Chen, M., Zhong, Q., Chen, T., et al. (2020). Methylene blue protects against sevoflurane-induced cognitive dysfunction by suppressing Drp1 deSUMOylation in aged mice. *Neurochem. Res.* 45, 956–963. doi: 10.1007/s11064-020-02976-6

Zhou, Z. B., Yang, X. Y., Tang, Y., Zhou, X., Zhou, L. H., and Feng, X. (2016). Subclinical concentrations of sevoflurane reduce oxidative stress but do not prevent hippocampal apoptosis. *Mol. Med. Rep.* 14, 721–727. doi: 10.3892/mmr.2016.5336

Conflict of Interest: The authors declare that the research was conducted in the absence of any commercial or financial relationships that could be construed as a potential conflict of interest.

frontiers in Cell and Developmental Biology

ORIGINAL RESEARCH
published: 15 July 2021
doi: 10.3389/fcell.2021.678182

Requirements of Postnatal proBDNF in the Hippocampus for Spatial Memory Consolidation and Neural Function

*Wei Sun[1,2], Hong Cheng[1,3], Yang Yang[2], Dongxin Tang[1], Xiaolian Li[4] and Lei An[1,2,3,5]**

[1] Behavioral Neuroscience Laboratory, The First Affiliated Hospital of Guizhou University of Traditional Chinese Medicine, Guiyang, China, [2] Department of Pediatric, The First Affiliated Hospital, Guizhou University of Traditional Chinese Medicine, Guiyang, China, [3] Department of Neurology, Guizhou University of Traditional Chinese Medicine, Guiyang, China, [4] Department of Neurology, Jinan Geriatric Hospital, Jinan, China, [5] Department of Physiology, University of Saskatchewan, Saskatoon, SK, Canada

OPEN ACCESS

Edited by:
Efthimios M. C. Skoulakis, Alexander Fleming Biomedical Sciences Research Center, Greece

Reviewed by:
Denise Manahan-Vaughan, Ruhr University Bochum, Germany
Xiangyang Xie, Tianjin Medical University, China
Theodore Constantine Dumas, George Mason University, United States

***Correspondence:**
Lei An
al_totti@sina.com;
anlei776@gzy.edu.cn;
lei.an@gzucm.edu.cn

Specialty section:
This article was submitted to Molecular Medicine, a section of the journal Frontiers in Cell and Developmental Biology

Received: 09 March 2021
Accepted: 03 June 2021
Published: 15 July 2021

Citation:
Sun W, Cheng H, Yang Y, Tang D, Li X and An L (2021) Requirements of Postnatal proBDNF in the Hippocampus for Spatial Memory Consolidation and Neural Function. Front. Cell Dev. Biol. 9:678182. doi: 10.3389/fcell.2021.678182

Mature brain-derived neurotrophic factor (BDNF) and its downstream signaling pathways have been implicated in regulating postnatal development and functioning of rodent brain. However, the biological role of its precursor pro-brain-derived neurotrophic factor (proBDNF) in the postnatal brain remains unknown. The expression of hippocampal proBDNF was blocked in postnatal weeks, and multiple behavioral tests, Western blot and morphological techniques, and neural recordings were employed to investigate how proBDNF played a role in spatial cognition in adults. The peak expression and its crucial effects were found in the fourth but not in the second or eighth postnatal week. Blocking proBDNF expression disrupted spatial memory consolidation rather than learning or memory retrieval. Structurally, blocking proBDNF led to the reduction in spine density and proportion of mature spines. Although blocking proBDNF did not affect N-methyl-D-aspartate (NMDA) receptor (NMDAR) and α-amino-3-hydroxy-5-methyl-4-isoxazolepropionic acid receptor (AMPAR) subunits, the learning-induced phosphorylation of the GluN2B subunit level declined significantly. Functionally, paired-pulse facilitation, post-low-frequency stimulation (LFS) transiently enhanced depression, and GluN2B-dependent short-lasting long-term depression in the Schaffer collateral-CA1 pathway were weakened. The firing rate of pyramidal neurons was significantly suppressed around the target region during the memory test. Furthermore, the activation of GluN2B-mediated signaling could effectively facilitate neural function and mitigate memory impairment. The findings were consistent with the hypothesis that postnatal proBDNF played an essential role in synaptic and cognitive functions.

Keywords: hippocampus, long-term depression, memory consolidation, NMDA receptors, proBDNF

INTRODUCTION

Mature brain-derived neurotrophic factor (mBDNF) plays an important role in neural circuit formation (Fernandes et al., 2015; Li et al., 2019), which is a critical step in aiding in hippocampus (HPC)-dependent memory in adolescents and adults (Lu et al., 2014; Itoh et al., 2016). Like many other neurotrophins, mBDNF is initially produced as a longer precursor molecule,

pro-brain-derived neurotrophic factor (proBDNF), which elicits an opposing response to that of mBDNF (Lu et al., 2005; Deinhardt and Chao, 2014). For example, in contrast to the role of mBDNF in cell survival and memory formation, proBDNF can bind to $p75^{NTR}$, induce apoptosis (Je et al., 2012; Sun et al., 2012) and axonal retraction (Yang F. et al., 2009), and inhibit neuronal migration (Xu et al., 2011). Hence, the interest has grown in understanding the underlying mechanism and roles of neurotrophins in synaptic competition and elimination during neural circuit formation (Yang F. et al., 2009; Je et al., 2012; Yang et al., 2014). Although the structural and functional roles of perinatal mBDNF in cognitive processing are defined (Lu et al., 2014), the potential roles of proBDNF are still unclear.

Research studies have shown that N-methyl-D-aspartate (NMDA) receptors (NMDARs) play important roles in synaptic plasticity, brain development, and learning and memory (Bannerman et al., 2014) and are also involved in BDNF-dependent cognitive development (Lu et al., 2014; Nakai et al., 2014; Itoh et al., 2016). The downregulation of mBDNF reduces, and exogenous mBDNF enhances NMDAR-mediated neural responses (Itoh et al., 2016). The activation of the cAMP-dependent protein kinase (PKA)/cAMP response-element binding protein (CREB) pathway by glutamate *via* the stimulation of NMDARs is essential for the effects of mBDNF on dendritic development and the formation of neural circuits during postnatal development (Finsterwald et al., 2010) by the selective strengthening of necessary synapses in an activity-dependent manner (Lu et al., 2005; Choo et al., 2017). Treatment of rats with ketamine, an NMDA-channel antagonist, caused a significant increase in CREB and mBDNF protein levels in the HPC, as well as PKA phosphorylation levels (Reus et al., 2011). More importantly, experiments conducted in BDNF heterozygous animals demonstrated that the subunit composition of NMDARs in the HPC was altered (Klug et al., 2012). Different effects were observed in dorsal hippocampal regions involved in learning and memory and ventral regions involved in fear and anxiety-like behavior. Intriguingly, both mBDNF and proBDNF are secreted in adulthood, but the highest levels of proBDNF are observed perinatally (Yang J. et al., 2009). The prenatal proBDNF requirement is impacted by neuronal depolarization (Yang J. et al., 2009), which can control the BDNF-induced expression of NMDAR subunits at the transcriptional level (Suzuki et al., 2005). Moreover, proBDNF negatively regulates neural remodeling by selectively facilitating NMDAR-dependent neurotransmission (Yang et al., 2014) and neural activity (Sun et al., 2019). Therefore, NMDARs may be important mediators of proBDNF-induced defects in neurodevelopment and neurocognition.

To address the aforementioned issues, the variations in the expression of hippocampal proBDNF (at different periods from birth to adulthood) were tested, and then the effects of blocking proBDNF at its peak expression on spatial learning and memory of adult rats were assessed. Using a combination of morphological, Western blot and pharmacological methods, this study attempted to identify the role of proBDNF in spine development and the expression and phosphorylation of the subunits of glutamatergic receptors [including α-amino-3-hydroxy-5-methyl-4-isoxazolepropionic acid receptors (AMPARs) and NMDARs]. Meanwhile, the role of proBDNF in the synaptic function of the Schaffer collateral-CA1 pathway and the neural correlates of spatial behaviors were also assessed. To further confirm the findings, the pharmacological tools were employed to mitigate proBDNF-mediated deficits in cognitive and neural functions. These findings might help further understand the mechanisms by which proBDNF exerted its effects on synaptic and cognitive functions.

MATERIALS AND METHODS

Subjects

Wistar rats (Beijing Research Center for Experimental Animals, China) were maintained on a 12-h light/dark cycle (lights on at 7 a.m.) at constant temperature (21 ± 2°C) and humidity (45 ± 5%). All tests were conducted during the light period (between 2 p.m. and 5 p.m.). Animals had *ad libitum* access to food and water unless food was restricted prior to the training of lever press tests. During behavioral tasks, rats were maintained at ∼85% of free feeding weight, which was compared with a standard growth curve (Donaldson, 1924). All procedures were in accordance with the Care and Use of Animals Committee of Guizhou University of Traditional Chinese Medicine (SCXK-2013-0020).

The day of birth was designated as postnatal day (PD) 0, and pups were weaned on PD21. A total of 418 male offspring from an average of 84 litters were randomly assigned to one of six groups: (Fernandes et al., 2015) anti-proBDNF (second week), (Choo et al., 2017) anti-proBDNF (fourth week), and (Je et al., 2012) anti-proBDNF (eighth week) groups received bilateral infusion of rabbit polyclonal anti-proBDNF antibody (Lim et al., 2015; Luo et al., 2016) in the CA1 region of the HPC throughout the entire second postnatal week (PD2w, from PD8 to PD14), fourth postnatal week (PD4w, from PD22 to PD28), and eighth postnatal week (PD8w, from PD50 to PD56), respectively; (Li et al., 2019) control group was treated with the same volume of the vehicle (artificial cerebrospinal fluid, ACSF) throughout the whole PD2w (Con@2w), PD4w (Con@4w), and PD8w (Con@8w); (Itoh et al., 2016) Anti+TBOA group, which received infusion of anti-proBDNF antibody during the postnatal weeks, was bilaterally infused with DL-threo-β-benzyloxyaspartate (DL-TBOA) 0.5 or 2.5 h before spatial training [Anti+TBOA0.5(a) or Anti+TBOA2.5(a)], immediately following behavioral training [Anti+TBOA(b)] or 0.5 h before probe test [Anti+TBOA(c)]; and (Lu et al., 2014) control group, which received infusion of ACSF during the postnatal weeks, was bilaterally infused with DL-TBOA 0.5 h before spatial training [TBOA(a)], immediately following behavioral training [TBOA(b)] or 0.5 h before probe test [TBOA(c)]; (Lu et al., 2005) naive group was reared as the control group without the treatment. Eight-week-old (PD56) adult rats were used for this study unless specific evaluation was required. Anti-proBDNF antibody was purchased from Alomone Labs, Ltd. (Jerusalem, Israel; Cat. No. ANT-006). DL-TBOA was purchased from Tocris Cookson (Ellisville, MO, United States).

ACSF was purchased from Beijing Leagene Biotechnology, Ltd. (Beijing, China).

Here, DL-TBOA was used to block glutamate transporters and increase extracellular glutamate levels, which in turn could activate the extrasynaptic GluN2B-NMDA receptor (Massey et al., 2004; Yang et al., 2005). Given that sex differences in BDNF signaling have been reported extensively (Kellogg et al., 2000; Wu et al., 2013; Luoni et al., 2016) and some molecular mechanisms in memory formation are also known to be sex-specific (Mizuno and Giese, 2010; Sundermann et al., 2016), only male rats were selected for the current study. Additionally, to exclude the possibility of accumulative effects of the drugs, separated groups were assigned in each behavioral experiment.

Surgery and Microinjection

Rats were anesthetized with isoflurane and placed in a stereotaxic frame (SN-3; Narishige, Japan) for surgery. Guide cannulae (22 gauge; Plastics One Inc., Roanoke, VA, United States) were bilaterally inserted above the CA1 region of the HPC (for PD2w: AP: −3.3 mm, ML: ±2.1 mm, DV: 2.4–2.6 mm; for PD4w: AP: −3.3 mm, ML: ± 2.3 mm, DV: 2.6–2.8 mm; for PD8w: AP: −3.3 mm, ML: ± 2.3 mm, DV: 2.6–2.9 mm). A stainless-steel stylet (30 gauge, 10 mm; Plastics One Inc.) was inserted into guide cannula to avoid obstruction. Rats were given at least 1 week to recover.

Infusions were achieved by inserting 30-gauge needles (10 mm; Small Parts Inc., Logansport, IN, United States) connected through PE-50 tube into a microsyringe pump (Harvard Apparatus, Holliston, MA, United States), extended 1.0 mm beyond the end of the cannulae. Needles were inserted into both cannulae, and then anti-proBDNF antibody (10 μg/μl), DL-TBOA (2.0 ng/μl), Ro25-6981 (2.0 ng/μl), or ACSF (vehicle) was infused into the HPC area (0.5 μl/min/side for 2 min) 30 min before testing began. The dose and route of administration were selected based on the results of the previous studies, which indicate the efficacy of anti-proBDNF antibody (Bai et al., 2016; Sun et al., 2018a, 2019). To testify whether the TBOA infusion 0.5 h before the training could still affect memory consolidation, DL-TBOA infusion was conducted 2.5 h before the training. The needles were left for an additional 3–5 min to allow the diffusion. Specifically, anti-proBDNF antibody was applied twice a day in a 12-h interval (at 9 a.m. and 9 p.m.) for 1 week. Drug treatments were counterbalanced across litters.

Protein Preparations and Analysis

Rats were killed by overdose of urethane, and hippocampi were rapidly dissected and homogenized in ice-cold lysis buffer (pH 7.4) containing a cocktail of protein phosphatase and proteinase inhibitors (Sigma, MA, United States). The samples were centrifuged at 14,000 rpm for 15 min at 4°C, and the supernatant was collected. Protein concentrations were detected by the bicinchoninic acid (BCA) assay. Twenty micrograms (15 μl) of total protein per lane was resolved in 10–15% SDS-PAGE gels followed by electro-transferring to PVDF membranes (Pall, Pensacola, FL, United States). Non-specific binding of antibodies to membranes was probed with the primary antibody: mouse anti-proBDNF (1:500, Cat. No. sc-65514; Santa Cruz Biotechnology, Santa Cruz, CA, United States), mouse anti-mBDNF (1:500, Cat. No. mab248; R&D Systems, Minneapolis, MN, United States), rabbit anti-p75^{NTR} (1:1,000, Cat. No. AB1554; Chemicon, CA, United States), rabbit anti-GluA1 (1:1,000, Cat. No. AB1504; Chemicon, CA, United States), rabbit anti-phospho(serine-831)GluA1 (1:500, Cat. No. 04823; Upstate Biotechnology, MA, United States), rabbit anti-mGluA2/3 (1:1,000, Cat. No. AB1506; Chemicon, CA, United States), rabbit anti-phospho(serine-880)GluA2 (1:3,000, Cat. No. 07294; Upstate Biotechnology, MA, United States), rabbit anti-GluN2A (1:1,000, Cat. No. 07632; Millipore, MA, United States), rabbit anti-phospho(serine-1232)GluN2A (1:1,000, Cat. No. crb2005001e; Cambridge Research Biochemicals, Billingham, United Kingdom), mouse anti-GluN2B antibody (1:1,000, Cat. No. 06600; Millipore, MA, United States), rabbit anti-phospho(serine-1303)GluN2B (1:1,000, Cat. No. ab81271; Abcam, Cambridge, United Kingdom), and mouse anti-β-actin (1:20,000, Cat. No. A5316; Sigma, MA, United States) overnight at 4°C. Mouse anti-β-actin was used as an internal control. Each band was normalized to the corresponding β-actin band. After further incubation in horseradish-peroxidase (HRP)-conjugated secondary goat anti-mouse or anti-rabbit IgG (1:1,000) (Southern Biotechnology Associates, AL, United States) for 2 h at room temperature, immunoreactivity was detected by ECL Western Blotting Detection Kit (CWBIO, China). The intensity of each band was measured by densitometry using Quantity One software (Bio-Rad Laboratories, Hercules, CA, United States). The learning-induced expression level was normalized by the expression of the naive group.

Locomotion and Anxiety-Like Behavior in the Open Field Task

Locomotor activity was assessed in a 5-min open field, which consisted of a 91.5 × 91.5 × 61 cm Perspex box with dark walls, as described previously (Mueller et al., 2010; Peters et al., 2010). The field was divided into a peripheral region (within 15.25 cm of the walls) and central region (61 × 61 cm) of approximately equal area. The distance traveled and the time spent within the peripheral/central region were recorded using VersaMax Activity Monitoring System (AccuScan Instruments, Columbus, OH, United States).

Motivation Test

Rats were trained to lever press for food pellets in standard operant conditioning chambers located inside sound-attenuating boxes (Med Associates, St. Albans, VT, United States). The chambers contained two retractable levers located on either side of a central food trough. As in the previous studies (Paterson et al., 2005; Sun et al., 2020, 2021b), rats were trained daily in 30-min sessions with one of two levers extended randomly when the cue light above the lever was on. The training started with continuous reinforcement. Rats were initially trained on a fixed-ratio (FR)-1 schedule (one lever-press response) with both levers reinforced, followed by the sequence FR-15, FR-30, and finally FR-60 schedule sessions. Rats were tested in a 30-min session till they reached 10 presses per min on FR-60.

MWM Test

A 150-cm-diameter circular pool was filled with water opacified with nontoxic black ink and kept at 25 ± 1°C. The tank was divided into four equal quadrants that were denominated clockwise I, II, III, and IV. A clear 10-cm-diameter platform was positioned in the center of quadrant III with its surface 2 cm below the water surface. The pool was surrounded by blue curtains with clearly distinctive cues. Movements were monitored by a tracking system (Ethovision 2.0; Noldus, Wageningen, Netherlands).

The test was divided into the training phase on day 1 and the probe phase, which was performed 24 h or immediately after training. During the training phase, each rat was trained for eight trials (30 s intertrial interval) to find the platform. The order of starting points was set pseudorandomly (II, I, III, IV, III, I, IV, II) but was the same for all animals. Rats that failed to find the platform within 60 s were guided and remained on it for 20 s. The escape latency of each trial was collected and calculated. During the probe phase, the platform was taken out, and rats were released from a novel drop point (between starting points I and II) and swam for 60 s. From the tracked swimming traces, a path proximity score was calculated by measuring the distance (cm) between the rat's position and the platform location (Maei et al., 2009; Tomas Pereira and Burwell, 2015; Kapadia et al., 2016). A distance measure was made 10 times per second and averaged across the probe test.

The long-term memory process can be generally divided into distinct stages: learning (acquisition), consolidation, and retrieval (Wang et al., 2006). Extensive studies have confirmed that the newly formed memories were susceptible to a variety of post-learning (minutes to half hour) manipulations, such as electroconvulsive shock, protein synthesis inhibitor, or hypothermia treatment (McGaugh, 2000; Kandel, 2001). Moreover, the disruptive effects of these post-learning manipulations decrease as the time interval between the acquisition and the intervention increases (Dudai et al., 2015). Intensive research in the past several decades suggests that this type of memory consolidation, occurring within minutes to hours after initial learning, may reflect the ongoing changes in the intracellular signaling pathways and new protein synthesis and gene expression by which subsequent modifications in synaptic properties and structures are produced (Izquierdo et al., 2006; Nadel et al., 2012). Regarding the conversion of short-term memory into long-term memory, in the Morris water maze (MWM) task, the memory acquisition is during the training phase on the first day. After memory acquisition, the memory is consolidating and will be assessed on the probe test on the second day. This eight-trial training, which can quickly be learned by rodents in the previous studies (de Quervain et al., 1998; Wong et al., 2007; Dong et al., 2013), has the advantage of clearly delineating the acquisition and memory consolidation phases (Ge et al., 2010; An and Sun, 2018).

Single-Unit Recording

One week before behavioral test, electrode implantation was conducted using previously reported procedures (Sun et al., 2018b, 2021,a). Briefly, rats were anesthetized with isoflurane and prepared for surgery. Impedance-measured (200–600 kΩ) microelectrodes were arrayed into a 4 × 8 matrix using 25-μm-diameter tungsten wires (California Fine Wires, Grover Beach, CA, United States) in a 35-gauge silica tube (World Precision Instruments, Sarasota, FL, United States). A cannula was attached to a silica tube. The proximal open end of the cannula was parallel to electrode tips. They were chronically implanted, and the left or right hemisphere was implanted randomly but counterbalanced between rats. A stainless-steel wire was used as ground electrode, and the electrode was fastened to the cranium by dental acrylic with skull screws.

Data were acquired on a Digital Cheetah system (Cheetah software; Neuralynx Inc., Bozeman, MT, United States). Unit signals were recorded *via* an HS-36-unit gain headstage (Neuralynx Inc.) mounted on the animal's head by means of lightweight cabling that passed through a commutator (Neuralynx Inc.). Unit activity was amplified (1,000–10,000 times) and sampled at 32 kHz and 600–6,000 Hz band-pass filters. The firing rates during the probe test were collected. The rats' behavior was monitored by a digital ceiling camera (Neuralynx Inc.), and the CCD camera's signal was fed to a frame grabber (sampling rate, 1 MHz) with the experimental time superimposed for offline analysis.

Spike sorting was performed with offline Neuralynx's software (SpikeSort 3D), using a combination of KlustaKwik, followed by manual adjustment of the clusters (Klusters software package). Briefly, multiple parameters were used to determine the clusters with the most often used combination of spike height, trough, and energy, associated with the waveforms (Hernandez et al., 2013; An et al., 2018). As in the previous studies (Stark et al., 2014; Sun et al., 2018b), units were graded for quality and classified as pyramidal neurons and fast-spiking (FS) interneurons.

Synaptic Plasticity at the Schaffer Collateral-CA1 Pathway

In vivo field excitatory postsynaptic potentials (fEPSPs) in the pyramidal layer of the hippocampal CA1 region were recorded as previously explained in the Materials and methods section (An and Sun, 2017, 2018; An et al., 2019). Briefly, rats were anesthetized with isoflurane and placed in a stereotaxic frame for surgery (SN-3; Narishige, Japan). Core body temperature was monitored throughout the experiment, and a heating pad was used to maintain the temperature of the animals at 36.5 ± 0.5°C. The scalp was opened, and small holes were drilled in the skull using a trephine for the monopolar recording (insulated platinum iridium wire; AM Systems; AP: −3.3 mm, ML: ± 2.3 mm, DV: 2.6–2.8 mm) and tungsten bipolar stimulating electrodes (FHC; ME; hippocampal Schaffer collaterals region; AP: −4.0 mm, ML: ± 3.3 mm, DV: −2.2 to −3.0 mm). The head side of each rat was chosen randomly but counterbalance among groups. After the electrodes were lowered and located properly in desired positions, input/output (I/O) curves and paired-pulse facilitation (PPF) were assessed. The frequency of test pulse recording ranged from 30 to 60 s.

A baseline recording was re-established for approximately 5–10 min following the completion of each recording. Low-frequency stimulation (LFS) (900 pulses of 1 Hz) was delivered to induce long-term depression (LTD). The stimuli were delivered every minute at an intensity that evoked a response of 60–70% of the maximum response, which was obtained from the I/O recording. Since LTD should last for at least hours, the expression of LTD in the current study can only be defined as a short-lasting long-term depression (SL-LTD). Initial data measurement was performed in Clampfit 9.0 (Molecular Devices, Sunnyvale, CA, United States). The fEPSPs slope was used to measure synaptic efficacy. The average amplitudes during the baseline period were normalized to 100%, and the relative amplitudes at every point were normalized relative to the baseline period. The average amplitude between 41 and 60 min after the completion of the LFS was used to analyze.

Spine Density Analysis

Immediately following the probe test (24 h after the training stage), rats were anesthetized by an intraperitoneal injection of sodium pentobarbital (80 mg/kg). The brains were removed without perfusion, rinsed in phosphate-buffered saline (PBS), and stained using the Golgi–Cox method, in accordance with the manufacturer's instructions (Rapid GolgiStain; FD Neurotechnologies, United States). Briefly, brain tissues were immersed in the impregnation solution made by mixing equal volumes of solutions A and B and stored at room temperature for 10 days in the dark. The brains were then transferred into solution C and stored at 4°C in the dark for 5 days. Sections were cut on a vibratome and mounted on gelatin-coated slides with solution C for natural drying at room temperature for 2 days. Brain sections (50 μm) that could be clearly evaluated and containing 50–150 μm of secondary dendrites from each imaged soma were selected (Yang C. et al., 2015; Li et al., 2017). Three CA1 pyramidal neurons per section and three sections per animal were analyzed. Each rat was treated as an independent sample. For spine categorization, the following criteria were used (Li et al., 2017): (Fernandes et al., 2015) mushroom: spine head diameter was $\geq$1.5 × spine neck diameter; (Choo et al., 2017) stubby: spine head and spine neck were approximately of the same width, and spine length was not significantly longer than head diameter; and (Je et al., 2012) thin: spine head and spine neck were approximately of the same width, and spine length was 2.5 times longer than spine head width. Spine densities were calculated as the mean number of spines per micrometer dendrite.

Statistical Analysis

To confirm the infusion and recording sites, electrolytic lesions were created by applying direct current (10 mA, 10 s). The infusion sites (see **Figure 1A**) and electrode placements (see **Figure 1B**) were identified with the aid of The Rat Brain in Stereotaxic Coordinates (1997, third edition). Only data obtained from rats with correctly inserted needles and probes were included in statistical analysis (see **Figure 5I** – top and **Figure 5I** – bottom).

Data are expressed as mean ± SEM. All analyses were performed with Neuroexplorer, Matlab (MathWorks) and SPSS 17.0 software. The data of the training stage during the MWM task, bodyweight changes, I/O curve, and PPF were compared using repeated measures ANOVA. Student's *t*-tests examined the data of histological observation, the expression of proBDNF during the postnatal period (**Figure 2A**), and the comparison of proBDNF and mBDNF levels to the 100% baseline level (**Figure 2B**). The percentage of time spent in quadrants (**Figure 4D**) was examined by Chi-square test. The data of Western blot tests, open field test, and lever-press test; the proximity score in the probe test (**Figure 4C**); and the normalized fEPSPs (**Figures 5D,E**) were examined by one-way ANOVA. A two-way ANOVA was employed to examine the data of the proximity score (**Figure 2J**), spine density, learning-induced pGluB2B level (**Figure 3F**), and neural firing frequency (**Figures 5G,H**). When the ANOVA reveals a significant main effect or interaction between main factors, data were further analyzed by Tukey's *post hoc* test. For comparisons of the percentage of neurons, Pearson's analyses were used. A $p < 0.05$ level of confidence was used in the analyses.

RESULTS

Blocking the Expression of Hippocampal proBDNF During the Postnatal Period Impairs Spatial Memory but Not Learning Ability

Figure 2A shows the changes of proBDNF levels across development in the HPC of the un-manipulated rats. All data were normalized by the level at PD3. The expression rose significantly from PD3 to PD24 (one-way ANOVA, effect of time: $F_{(6,35)} = 32.68$, $p < 0.001$; *post hoc*, PD2w or PD4w vs. PD0w, both $p < 0.05$). The proBDNF levels peaked at PD24, which was significantly higher than that at PD10 ($p < 0.05$). To detect whether neutralizing proBDNF with its antibody would potentially interfere with the expression of endogenous protein and its proteolysis to mBDNF, we assessed the proBDNF and mBDNF levels following the antibody infusion (**Figure 2B**). Two-way ANOVA revealed significant time effect ($F_{(3,30)} = 96.76$, $p < 0.001$), significant treatment effect ($F_{(1,10)} = 8.81$, $p < 0.01$), and significant interaction effect between time and treatment ($F_{(3,30)} = 32.63$, $p < 0.001$). Tukey's test showed that proBDNF levels were markedly lower than mBDNF levels 3 ($p < 0.05$) and 6 h ($p < 0.05$) following antibody infusions. The marked decline of proBDNF lasted for at least 6 h after the injection (*t*-test, 3 or 6 h vs. 100%, both $p < 0.05$), whereas the mBDNF level was not affected. Therefore, the observations following infusion reflected merely the proBDNF rather than the mBDNF effect. To confirm if infusion of anti-proBDNF antibody affects the level of proBDNF or its receptor, $p75^{NTR}$, we assessed their levels at PD56. Hippocampal proBDNF was not disrupted by postnatal blockage at PD2w or PD4w (**Figure 2C**; one-way ANOVA, effect of treatment: $F_{(2,15)} = 0.22$, $p > 0.05$), neither did the $p75^{NTR}$ (**Figure 2D**; effect of treatment: $F_{(2,15)} = 0.29$, $p > 0.05$). We failed to find a statistical difference in bodyweight from PD2w

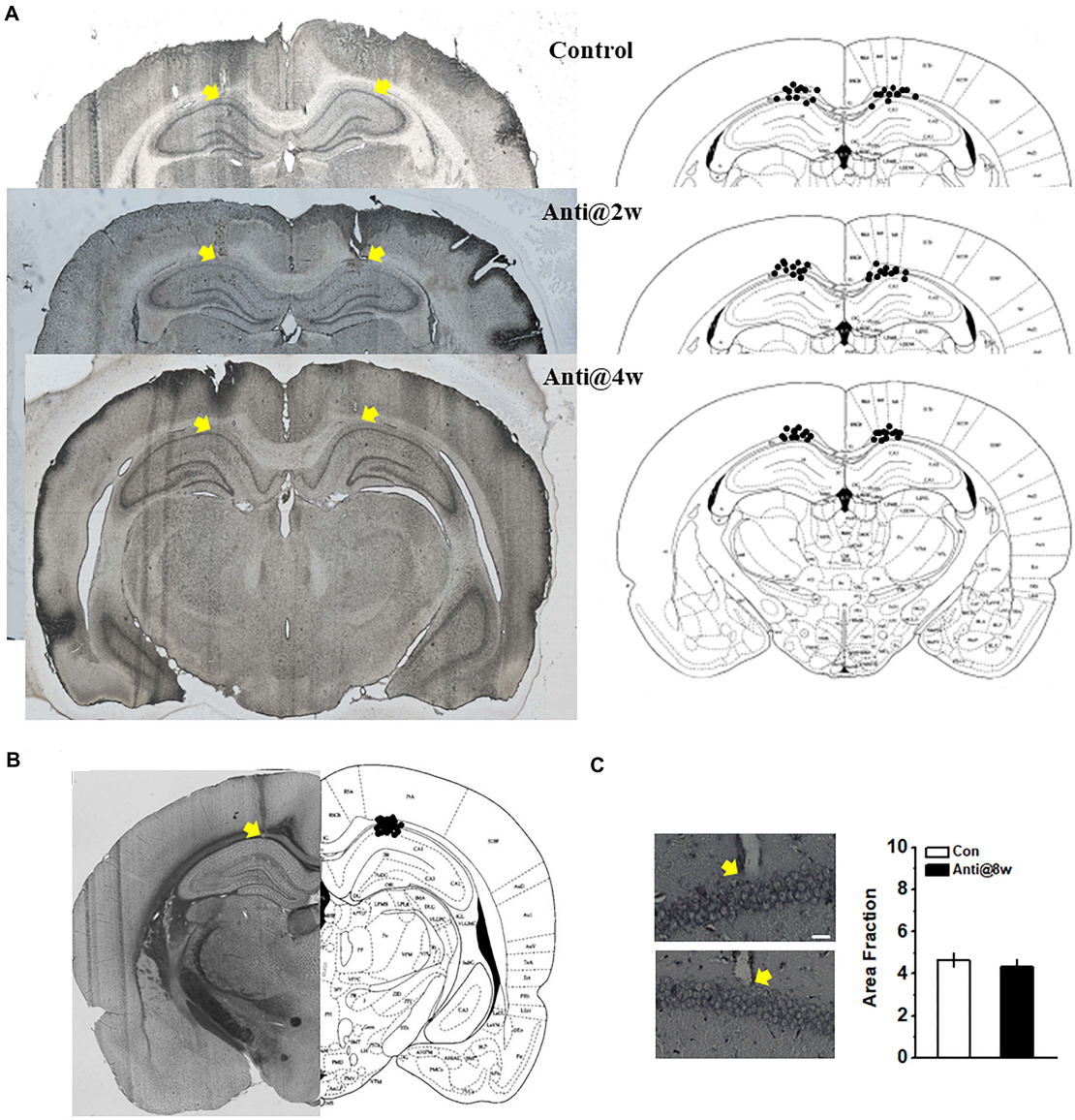

FIGURE 1 | Schematic representations of the cannulae and electrode placements and morphological alterations in the CA1 region. **(A)** Histological (left) and schematic (right) representations of the cannula placements. The control group infused with ACSF throughout the whole PD4w; the Anti@2w and Anti@4w groups were infused with anti-proBDNF antibody throughout the whole second and fourth postnatal weeks, respectively. The yellow arrows indicated the top of the cannulae. **(B)** Histological and schematic representations of electrode placements. **(C)** Following the open field test, infusion-induced neuronal damage was assessed by Silver staining (see **Supplementary Methods**). The white scale bar presented at the bottom of the photomicrograph indicated 25 μm. The yellow arrows indicated the electrode tips. There was no statistical difference in the quantification of neurodegeneration in CA1 neurons between the control (top) and anti-proBDNF (bottom) groups. The anti-proBDNF group was infused with anti-proBDNF antibody throughout the whole fourth postnatal week. The control group was treated with the same volume of the vehicle (ACSF) throughout the whole the fourth postnatal week. The treatment was conducted twice a day in a 12-h interval. $n = 6$ for each group.

to PD18w, either (**Figure 2E**; repeated-measures ANOVA, effect of time: $F_{(8,264)} = 0.51$, $p > 0.05$; interaction effect between time and treatment: $F_{(16,264)} = 0.27$, $p > 0.05$). Furthermore, the effects of infusion on locomotion, anxiety-like behavior, and motivation were tested, whereas no statistical difference was found in the total travel distance (**Figure 2F**, one-way ANOVA, effect of treatment: $F_{(2,15)} = 0.23$, $p > 0.05$) and the percentage of time spent in the center of the apparatus (**Figure 2G**, one-way ANOVA, effect of treatment: $F_{(2,15)} = 0.29$, $p > 0.05$) in the open field test, or the motivation behavior (**Figure 2H**, one-way ANOVA, effect of treatment: $F_{(2,15)} = 0.26$, $p > 0.05$). Blocking proBDNF at PD2w, PD4w, or PD8w did not disrupt spatial acquisition, as exhibited by a significantly decreased latency among groups in the training phase (**Figure 2I**,

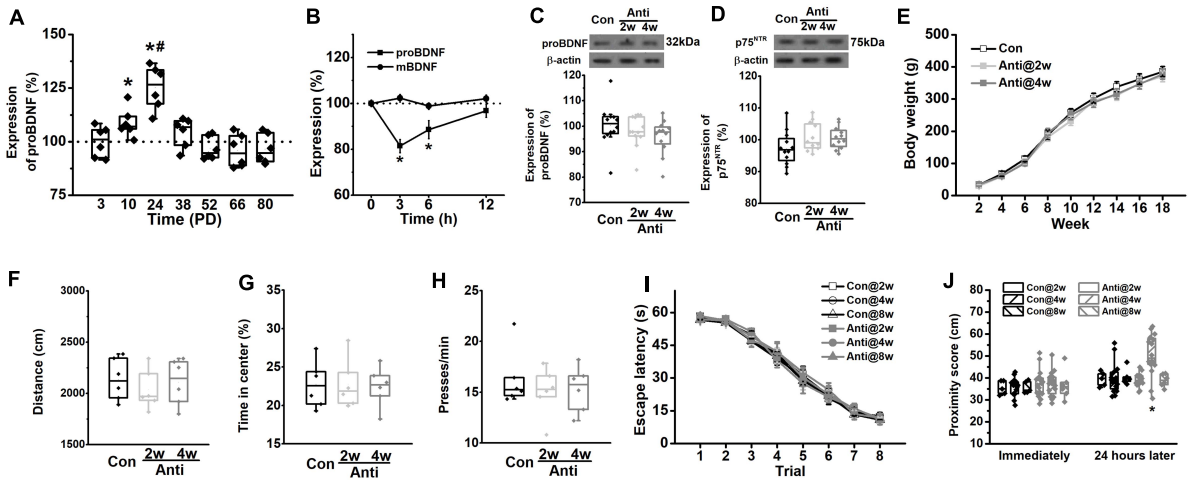

FIGURE 2 | Blockage of proBDNF expression during the postnatal period induces spatial learning impairments. **(A)** The level of proBDNF in the hippocampus. (*$p < 0.05$, vs. 100%; #$p < 0.05$, vs. PD10). $n = 6$ per time point. **(B)** The expression of proBDNF in the hippocampus immediately, 3, 6, and 12 h after anti-proBDNF antibody infusion. $n = 6$ per group. (*$p < 0.05$, vs. matched mBDNF). **(C)** The proBDNF level and **(D)** the p75NTR level at PD56 were detected in rats, which were infused with anti-proBDNF antibody throughout the second postnatal week (Anti2w) and the fourth postnatal week (Anti4w), respectively. $n = 12$ per group. **(E)** Bodyweight changes from PD14 to PD126. **(F)** Travel distance. **(G)** The percentage of time spent in the center of the apparatus in the open field test. $n = 6$ per group. **(H)** Press time per min in the motivation test. $n = 6$ per group. **(I)** Escape latency. **(J)** The swim proximity score during the MWM task. Note that rats in the Con@8w and Anti@8w groups were tested at PD12w, whereas rats in other groups were tested at PD8w. (*$p < 0.05$, vs. Anti@2w, Anti@8w, or Con). $n = 5$ for the Con@2w group, $n = 5$ for the Con@8w group, $n = 6$ for the Anti@8w group, and $n = 16$ for other each group.

repeated-measures ANOVA, effect of trial: $F_{(7,406)} = 76.29$, $p < 0.001$; effect of age: $F_{(2,61)} = 0.68$, $p > 0.05$; effect of treatment: $F_{(1,62)} = 1.05$, $p > 0.05$; interaction effect between age and treatment: $F_{(2,124)} = 0.21$, $p > 0.05$). Additionally, the mean time spent in thigmotaxis and floating during spatial training was comparable among groups (**Supplementary Figure 1**). However, infusion at PD4w, but not PD2w or PD8w, made rats away from target quadrant 1 day after acquisition training (**Figure 2J**, two-way ANOVA, effect of treatment: $F_{(1,62)} = 18.71$, $p < 0.001$, *post hoc*, Anti@4w vs. other groups, all $p < 0.05$; effect of age: $F_{(2,124)} = 1.03$, $p > 0.05$; effect of between treatment and age: $F_{(2,124)} = 0.34$, $p > 0.05$), but not immediately following training (effect of treatment: $F_{(1,62)} = 0.26$, $p > 0.05$). Additionally, our findings indicate that blocking proBDNF expression but not affecting $p75^{NTR}$ expression or function by the infusion of anti-proBDNF antibody induces behavioral deficits in adults (**Supplementary Figure 2**). There was no statistical difference in area fraction between the Con and Anti@4w groups (**Figure 1C**, *t*-test, $t_{10} = 0.0$, $p > 0.05$). Our findings also ruled out the possibility that repeated infusions induced neuroinflammatory or neurodegeneration has contributed to the behavioral and physiological changes. Furthermore, our previous study found that exogenous proBDNF exerts pivotal effects on the use of cognitive strategies to facilitate the spatial learning process (An et al., 2018). Therefore, it remains possible that the deficit in memory consolidation was driven by a less precise learning strategy. However, blocking proBDNF during the postnatal period did not induce the learning strategy preference (**Supplementary Figure 3**). Together, the above results demonstrate the essential role of hippocampal proBDNF at PD4w in spatial memory function in adulthood. Therefore, we chose to block proBDNF activity at PD4w in the following experiments.

Blocking Postnatal proBDNF Expression Decreases Spine Density and Learning-Induced Phosphorylated GluN2B-NMDA Receptor Subunit Level

At an early developmental stage, proBDNF is an important regulator of dendritic structure and synaptic plasticity. Crucially, endogenous proBDNF regulates learning-induced phosphorylation of glutamate receptors and spatial memory formation (Deinhardt and Chao, 2014; Yang et al., 2014; Shirayama et al., 2015; Sun et al., 2018a). Collectively, the spine density and the subunits of glutamate receptors were estimated during the memory formation period, which is generally believed to end within 0–3 h following the learning phase (Alonso et al., 2002; Slipczuk et al., 2009; Haynes et al., 2015). We failed to find learning-induced modifications in spine density (**Figure 3A** – middle, two-way ANOVA, $F_{(1,22)} = 0.16$, $p > 0.05$) or interaction effect between treatment and training ($F_{(1,22)} = 0.09$, $p > 0.05$), whereas two-way ANOVA revealed a significant anti-proBDNF antibody treatment effect ($F_{(1,22)} = 17.27$, $p < 0.001$). Furthermore, we classified spines into mushroom, stubby, and thin spines and found a significant anti-proBDNF antibody treatment effect (**Figure 3A** – bottom, two-way ANOVA, $F_{(1,22)} = 20.31$, $p < 0.05$) but no interaction effect between treatment and training ($F_{(1,22)} = 0.13$, $p > 0.05$) or training effect ($F_{(1,22)} = 0.18$, $p > 0.05$). Two-way ANOVA analysis indicated that a significant effect of training was found in GluA1 (**Figure 3B** – left, $F_{(1,38)} = 16.55$,

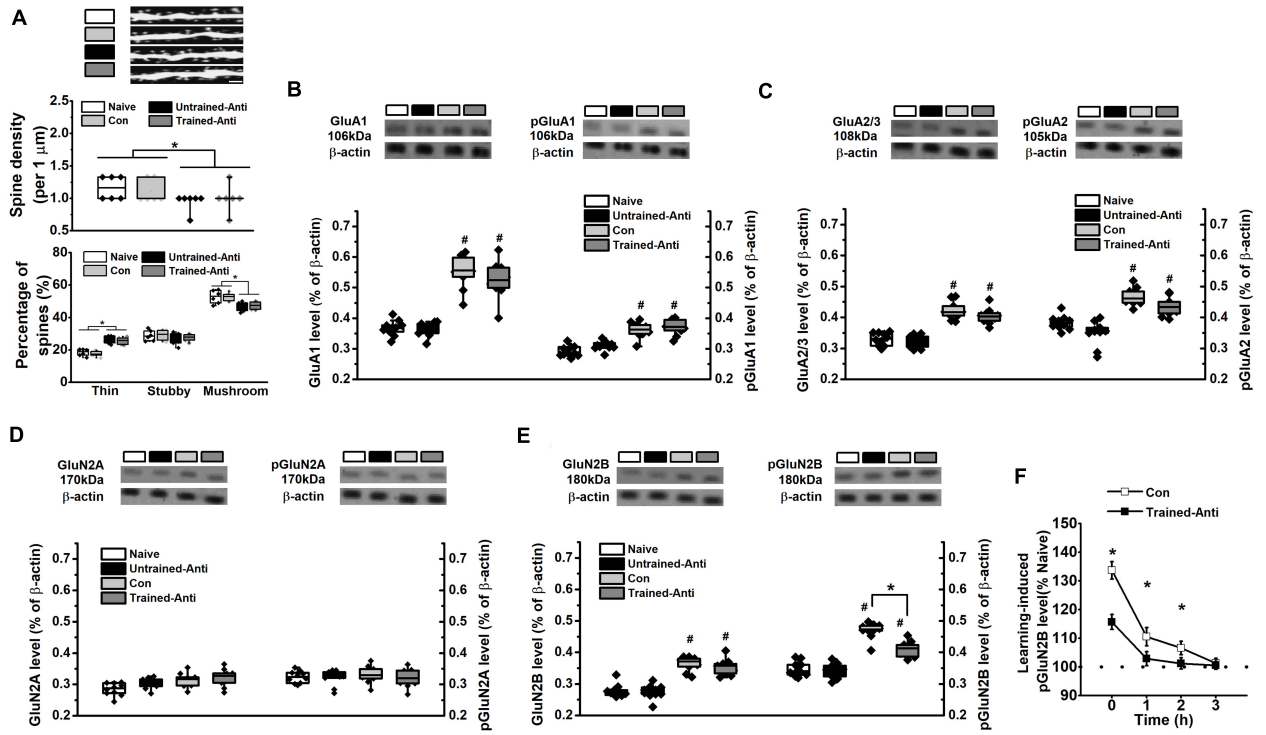

FIGURE 3 | Blocking proBDNF reduces spine number and learning-related GluN2B expression. The samples from rats that performed spatial training in the MWM task were collected immediately following the training phase and selected for detecting spine density and the expression of glutamatergic receptor subunits. **(A)** Spine alteration in naive, untrained-antiproBDNF, trained control, and trained-antiproBDNF rats (top). Quantification of spine density (middle) and the proportion of spine (bottom). Scale bars, 5 μm. $n = 6$ per group. Sample images were projected at minimal intensity and inverted, background was then subtracted, followed by brightness/contrast adjustment. The expression and phosphorylation of GluA1 **(B)** and the expression of GluG2/3 and the phosphorylation of GluA2 **(C)** of AMPAR subunits. $n = 10$ per group. The expression and phosphorylation of GluN2A **(D)** and GluN2B **(E)** of NMDAR subunits. (*$p < 0.05$, Con vs. Trained-Anti; #$p < 0.05$, vs. matched Naive and Untrained-Anti). $n = 10$ per group. Note that the data of dendritic spine and glutamatergic receptors tests were subjected to a two-way ANOVA in which training status (trained or not trained) and treatment (anti-proBDNF antibody, ACSF, or no treatment) were dependent variables. **(F)** The expression of pGluN2B immediately, 1, 2, and 3 h following spatial training. (*$p < 0.05$, Con vs. Trained-Anti). $n = 10$ per group.

$p < 0.01$), phosphorylated GluA1 (pGluA1, **Figure 3B** – right, $F_{(1,38)} = 10.29$, $p < 0.01$), GluA2/3 (**Figure 3C** – left, $F_{(1,38)} = 13.37$, $p < 0.01$), and phosphorylated GluA2 (pGluA2, **Figure 3C** – right, $F_{(1,38)} = 15.83$, $p < 0.01$), but not GluN2A (**Figure 3D** – left, $F_{(1,38)} = 0.54$, $p > 0.05$) or phosphorylated GluN2A (pGluN2A, **Figure 3D** – right, $F_{(1,38)} = 0.47$, $p > 0.05$). Meanwhile, statistical differences in pGluA1 expression were found between the Con and Naive groups ($p < 0.05$) and the Trained-Anti and Untrained-Anti groups ($p < 0.05$). There was no statistical effect of anti-proBDNF antibody infusion on GluA1 ($F_{(1,38)} = 0.36$, $p > 0.05$), pGluA1 ($F_{(1,38)} = 0.57$, $p > 0.05$), GluA2/3 ($F_{(1,38)} = 0.62$, $p > 0.05$), pGluA2 ($F_{(1,38)} = 0.65$, $p > 0.05$), GluN2A ($F_{(1,38)} = 0.68$ $p > 0.05$), or pGluN2A ($F_{(1,38)} = 0.44$, $p > 0.05$). No interaction effects between treatment and training were found on GluA1 ($F_{(1,38)} = 0.15$, $p > 0.05$), pGluA1 ($F_{(1,38)} = 0.59$, $p > 0.05$), GluA2/3 ($F_{(1,38)} = 0.37$, $p > 0.05$), pGluA2 ($F_{(1,38)} = 0.93$, $p > 0.05$), GluN2A ($F_{(1,38)} = 0.33$, $p > 0.05$), or p GluN2A ($F_{(1,38)} = 0.26$, $p > 0.05$).

Similarly, although no effect of anti-proBDNF antibody infusion (**Figure 3E** – left, two-way ANOVA, $F_{(1,38)} = 0.45$, $p > 0.05$) or interaction effect between training and treatment ($F_{(1,38)} = 0.29$, $p > 0.05$) was found, a significant effect of training ($F_{(1,38)} = 17.31$, $p < 0.01$) on the GluN2B level was observed. Importantly, a significant effect of infusion (**Figure 3E** – right, two-way ANOVA, $F_{(1,38)} = 6.26$, $p < 0.05$), training ($F_{(1,38)} = 19.93$, $p < 0.001$), and interaction effect between training and treatment ($F_{(1,38)} = 5.78$, $p < 0.05$) was found in phosphorylated GluN2B(pGluN2B). Furthermore, Tukey's test showed that the pGluN2B level of the Trained-Anti group was significantly lower than that of the Con group ($p < 0.05$). Meanwhile, there were statistical differences in pGluN2B expression between the Con and Naive groups ($p < 0.05$) and the Trained-Anti and Untrained-Anti groups ($p < 0.05$). The learning-induced pGluN2B expression was gradually weakened following MWM training (**Figure 3F**, two-way ANOVA, effect of time: $F_{(3,54)} = 87.28$, $p < 0.001$) and completely turned to basal level within 3 h, indicating that the upregulated activation of pGluN2B was learning-related. Furthermore, a significant downregulation by blocking proBDNF expression was detected at 1 and 2 h following the training phase (interaction effect between infusion and time: $F_{(3,54)} = 54.59$, $p < 0.001$; *post hoc*, $p < 0.05$).

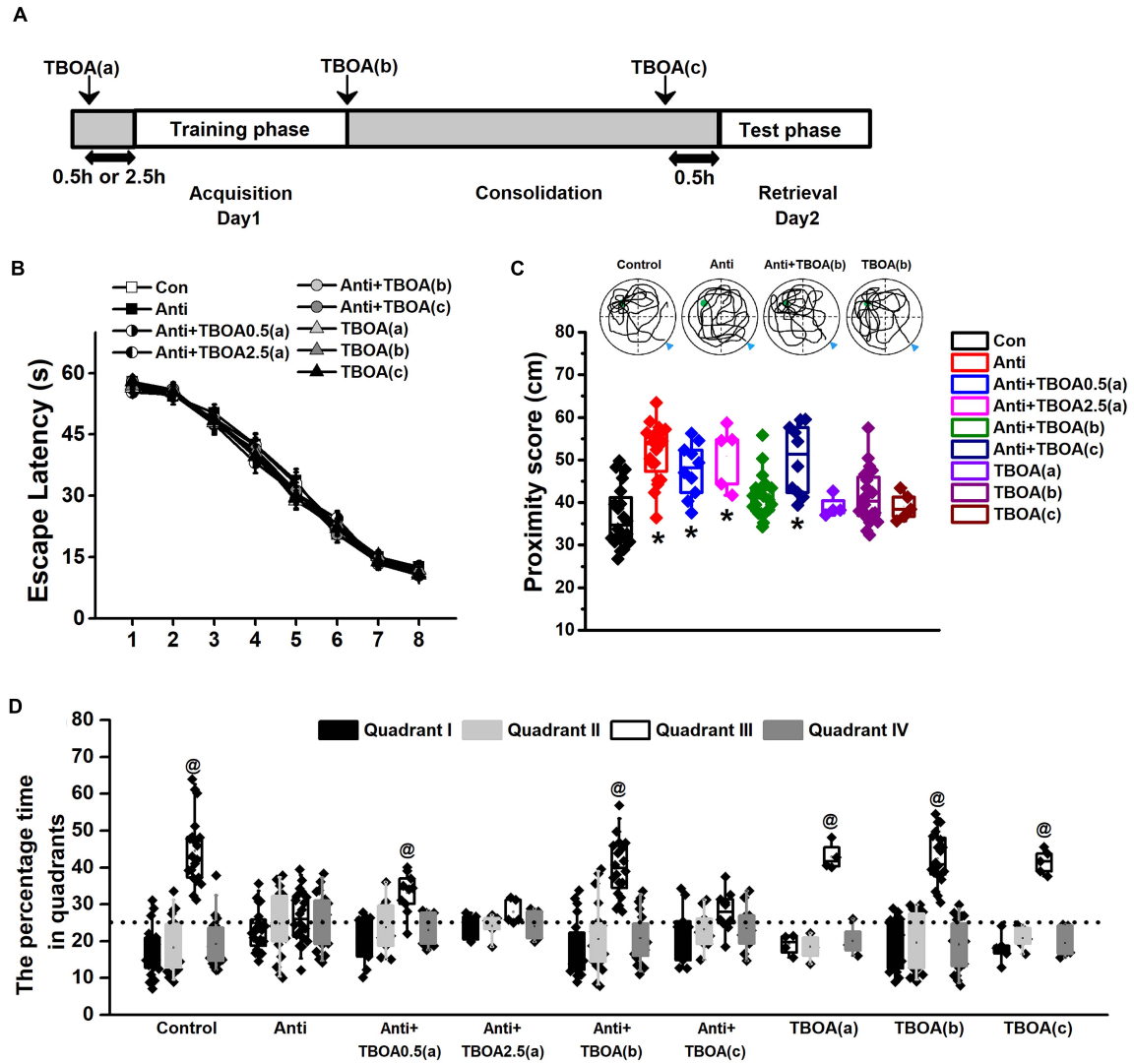

FIGURE 4 | Activation of GluN2B can rescue memory consolidation induced by blocking postnatal proBDNF. The infusion of TBOA was conducted 0.5 (Anti+TBOA0.5(a)) or 2.5 h (Anti+TBOA2.5(a)) before spatial training (acquisition), immediately following training (consolidation; Anti+TBOA(b)), and 30 min prior to probe memory test (retrieval; Anti+TBOA(c)), respectively. **(A)** Schematic description of the experimental timeline. **(B)** Escape latency in the training phase and **(C)** the swim proximity score during the probe trial. Note the sample swimming traces demonstrating the swimming trajectories of the control, Anti+TBOA(b), and TBOA(b) groups rather than the Anti group superimposed on target quadrant. The triangle indicated the start point during probe trial. (*$p < 0.05$, vs. control, Anti+TBOA(b), TBOA(a), TBOA(b), or TBOA(c)). **(D)** The percentage of time spent in each quadrant during the probe test. @ $p < 0.05$, vs. other quadrants. Note the data from rats (control, Anti, Anti+TBOA(b), and TBOA(b) groups) used in the single-unit recording were included. $n = 20$ for the control, Anti, Anti+TBOA(b), and TBOA(b) groups, $n = 10$ for the Anti+TBOA0.5(a) and Anti+TBOA(c) groups, $n = 5$ for the Anti+TBOA2.5(a) group, $n = 4$ for the TBOA(a) group, and $n = 5$ for the TBOA(c) group.

Additionally, since blocking of proBDNF affected synaptic structure, it would be necessary to compare if there was difference in actin protein among groups. However, we found that the levels of β-actin were comparable (**Supplementary Figure 4**), indicating that the above findings were not due to differences in loading or the overall levels.

Activation of GluN2B-Mediated Pathway Reverses Memory Consolidation Defect

To further confirm that postnatal blockage of proBDNF expression is involved in the GluN2B-mediated pathway and decipher the deteriorated effect on memory consolidation, but not the acquisition or retrieval stage, DL-TBOA, which could activate GluN2B-mediated signaling (Brancaccio et al., 2017; An and Sun, 2018), was infused into the HPC 0.5 or 2.5 h before the training phase (acquisition; Anti+TBOA0.5(a) or Anti+TBOA2.5(a)), immediately following training (consolidation; Anti+TBOA(b)), and 0.5 h before the test phase (retrieval; Anti+TBOA(c)), respectively (**Figure 4A**). Firstly, the escape latency of all groups, including groups that would be subgrouped to Anti+TBOA(b), Anti+TBOA(c), TBOA(a), TBOA(b), and TBOA(c) groups, did not change (**Figure 4B**,

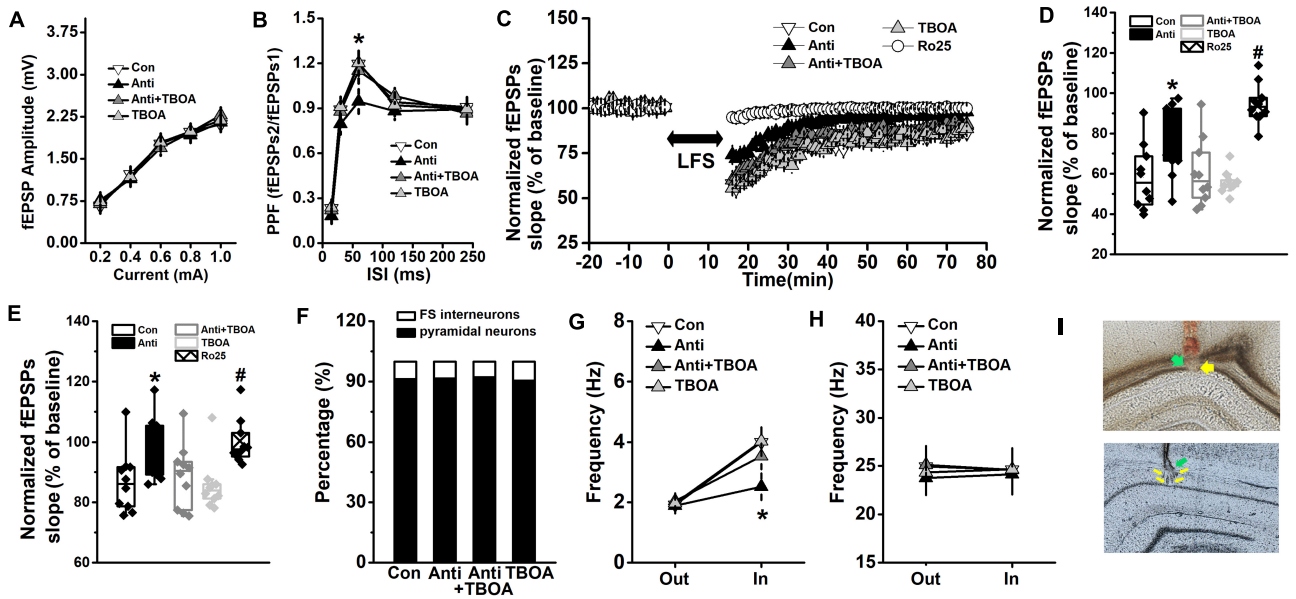

FIGURE 5 | GluN2B-dependent neural function is enhanced by TBOA. The Anti group was bilaterally infused with anti-proBDNF antibody into the CA1 region throughout the whole PD4w, whereas the Con group received the same volume of ACSF. Eight-week-old rats were selected for detecting hippocampal synaptic function in the Schaffer collateral-CA1 pathway immediately following TBOA (Anti+TBOA and TBOA groups), Ro25 (Ro25 group), or ACSF (Con and Anti groups) injection. **(A)** Input–output curves of fEPSP slopes. **(B)** PPF, a form of short-term plasticity, was measured and expressed as the ratio of fEPSPs2 to fEPSPs1. (*$p < 0.05$, Anti vs. other groups). **(C)** Characteristic time courses of fEPSP slope. Arrow represented application of LFS. **(D)** The effects on PTD, which was determined as response 1 min after LFS. (*$p < 0.05$, Anti vs. other groups; #$p < 0.05$, Ro25 vs. other groups) **(E)** Time coursing changes in fEPSPs slope. Magnitude of SL-LTD was determined as responses in the last 20 min (between 56 and 75 min). (*$p < 0.05$, Anti vs. other groups; #$p < 0.05$, Ro25 vs. other groups). $n = 10$ per group. When rats were tested in the probe trial that was conducted 24 h following the last training trial, neural activity around the target platform area was recorded. TBOA (Anti+TBOA and TBOA groups) or ACSF (Con and Anti groups) infusion was conducted 30 min prior to the behavioral test. **(F)** The proportion of pyramidal neuron and FS interneuron. **(G)** Firing rate of pyramidal neurons out of target area (Out) and around the targeted platform (In) during the probe test. **(H)** Firing rate of FS interneuron out of target area (Out) and around the targeted platform (In) during the probe test. (*$p < 0.05$, Anti vs. other groups). $n = 10$ per group. **(I)** The histological representations of the recording sites during the fEPSPs (top) and neuronal activity (bottom) experiments. The green and yellow arrows indicate infusion site and recording site, respectively.

repeated-measures ANOVA, effect of treatment: $F_{(8,105)} = 0.73$, $p > 0.05$). In the meantime, the injection of TBOA 0.5 or 2.5 h before spatial training did not affect anti-proBDNF-infused rat's learning ability. In the probe test, the proximity scores of the control (Con), Anti+TBOA(b), and vehicle [TBOA(a), TBOA(b), and TBOA(c)] groups were significantly shorter than that of the anti-proBDNF-infused (Anti) group (**Figure 4C**, one-way ANOVA: $F_{(8,115)} = 83.51$, $p < 0.001$; *post hoc*, Con, Anti+TBOA(b), TBOA(a), TBOA(b), or TBOA(c) vs. Anti, all $p < 0.05$). The TBOA treatment before memory retrieval did not disrupt animals' performance (*post hoc*, TBOA(c) vs. control, $p > 0.05$), indicating that the lack of a rescue effect in the Anti+TBOA(c) group was not attributed to acute effect from TBOA infusion. When the TBOA infusion was performed 2.5 h prior to the acquisition training, no statistical difference was found between the Anti+TBOA2.5(a) and Anti groups. The path proximity score of the Anti+TBOA0.5(a) group was significantly greater than those of the control, Anti+TBOA(b), TBOA(a), TBOA(b), and TBOA(c) groups (all $p < 0.05$). Meanwhile, the target quadrant (III) preference was found in the control (**Figure 4D**, Chi-square test, $\chi^2 = 11.79$, $p < 0.001$), Anti+TBOA(b) (Chi-square test, $\chi^2 = 10.18$, $p < 0.01$), TBOA(a) (Chi-square test, $\chi^2 = 14.03$, $p < 0.001$), TBOA(b) (Chi-square test, $\chi^2 = 11.92$, $p < 0.001$), and TBOA(c) (Chi-square test, $\chi^2 = 12.25$, $p < 0.001$) groups, but not the Anti (Chi-square test, $\chi^2 = 0.85$, $p > 0.05$), Anti+TBOA2.5(a) (Chi-square test, $\chi^2 = 0.71$, $p > 0.05$), and Anti+TBOA(c) (Chi-square test, $\chi^2 = 0.33$, $p > 0.05$) groups, indicating a reference memory disruption of the Anti, Anti+TBOA2.5(a), and Anti+TBOA(c) groups. Furthermore, although target quadrant bias was found in the Anti+TBOA0.5(a) group (Chi-square test, $\chi^2 = 5.62$, $p < 0.05$), no obvious difference in the time spent in the target quadrant was found between the Anti and Anti+TBOA0.5(a) groups. Therefore, the persistent effect from TBOA on the memory consolidation period could be the potential explanation of the slight memory recovery of the Anti+TBOA0.5(a) group, since the half-life of p-MeOazo-TBOA, an analog of TBOA, is longer than 3 h in 50 mm KPi buffer (pH 7.4) at 37°C (Hoorens et al., 2018). Additionally, we found that infusion of ACSF during the acquisition, consolidation, or retrieval period did not cause memory deficits (**Supplementary Figure 5**), and thus we could rule out an effect induced by cannula implantations. Therefore, our results indicated that the inhibition effect caused by blocking proBDNF on GluN2B-mediated pathway disrupted memory consolidation, but not acquisition ability or memory retrieval.

Activation of GluN2B-Mediated Pathway Rescues Presynaptic Neurotransmitter Release, GluN2B-Dependent SL-LTD, and Neural Activity

Memory formation during training acted to increase NMDAR responses, which were associated with synaptic transmission and neural plasticity (Yamazaki et al., 2015; Porter and Sepulveda-Orengo, 2019). Converging evidence supported that GluN2B-NMDAR-dependent LTD was necessary to mediate spatial memory consolidation (An and Sun, 2018; Sanchez-Rodriguez et al., 2019). Importantly, the correlation between behavior and neural activity was associated with memory capacity (Yang H. et al., 2015; Feng et al., 2019). To gain insight into the mechanisms of TBOA-ameliorated memory deficits, we assessed synaptic function and neural activity, which was recorded 10 cm around the platform during the probe test.

After the last trial of the training day, synaptic transmission, PPF, and synaptic plasticity were evaluated, and the traces of the fEPSPs are presented in **Supplementary Table 1**. No difference was found in synaptic transmission (**Figure 5A**, repeated-measures ANOVA, effect of treatment: $F_{(3,36)} = 1.17$, $p > 0.05$). Blockage of proBDNF by its antibody significantly declined the PPF (**Figure 5B**, repeated-measures ANOVA, effect of treatment × time: $F_{(12,144)} = 22.63$, $p < 0.001$; *post hoc*, Anti vs. Con, 60 ms: $p < 0.05$), whereas TBOA did rescue the attenuated PPF (Anti+TBOA vs. Anti, 60 ms: $p < 0.05$). The time course of fEPSPs slopes, which were normalized to the 20-min baseline period, was depressed and reached a stable level 15 min after LFS (**Figure 5C**, repeated-measures ANOVA, effect of treatment: $F_{(4,45)} = 45.77$, $p < 0.001$). Post-LFS transiently enhanced depression (PTD) was measured by comparing fEPSPs that were obtained during the first minute after LFS. The fEPSPs slope of PTD from the Anti-group was obviously higher than those from the Con, Anti-TBOA, or TBOA groups (**Figure 5D**, one-way ANOVA, effect of treatment: $F_{(4,46)} = 66.18$, $p < 0.001$; *post hoc*, Anti vs. Con or TBOA, both $p < 0.05$). At the last 20 min of the SL-LTD recording, the mean slope of the Anti-group was markedly higher than those of both the Con and TBOA groups (**Figure 5E**, one-way ANOVA, effect of treatment: $F_{(4,46)} = 37.39$, $p < 0.05$; *post hoc*, Anti vs. Con or TBOA, all $p < 0.05$). As expected, TBOA could mitigate the suppressive effects of anti-proBDNF antibody on PTD (Anti+TBOA vs. Anti, $p < 0.05$) and SL-LTD (Anti+TBOA vs. Anti, $p < 0.05$). Importantly, treatment with the GluN2B antagonist Ro25-6981 completely blocked PTD (Ro25 vs. Con, Anti, TBOA, or Anti-TBOA, all $p < 0.05$) and the expression of SL-LTD (Ro25 vs. Con, TBOA, or Anti-TBOA, all $p < 0.05$). Furthermore, in a separate group of rats, proBDNF expression was blocked in adulthood (at the eighth postnatal week), but synaptic function was comparable with the vehicle group when they were tested at 12 weeks old (**Supplementary Figure 6**). Additionally, long-term potentiation (LTP) was induced by high-frequency stimulation (HFS, 100 pulses of 100 Hz) as published methods (An and Sun, 2018; An et al., 2019). The fEPSPs slope of LTP was assessed, but no statistical difference was observed in the fEPSPs slope between the Con and Anti groups (one-way ANOVA, effect of treatment: $F_{(1,18)} = 0.73$, $p > 0.05$; Anti: 143.67 ± 4.98; Con: 140.89 ± 4.76).

Overall, 266 units were sorted by waveform characteristics and spiking patterns (pyramidal neurons: 62 from the control (CON) group, 65 from the anti-proBDNF (Anti) group, 59 from the Anti+TBOA group, and 57 from the TBOA group; FS interneurons: 6 from the CON group, 6 from the Anti-group, 5 from the Anti+TBOA group, and 6 from the TBOA group) (**Supplementary Figure 7A**). Application of anti-proBDNF antibody did not affect the percentage of population (**Figure 5F**, Pearson χ^2 test, $p > 0.05$). Blockage of proBDNF expression significantly decreased the firing frequency of pyramidal neurons around the targeted platform (**Figure 5G**, repeated-measures ANOVA, effect of treatment × time: $F_{(3,36)} = 12.73$, $p < 0.001$; *post hoc*, Anti vs. Con or TBOA, target: both $p < 0.05$), but not out of the target area. Furthermore, activation of GluN2B effectively enhanced the firing rate during memory test (Anti+TBOA vs. Anti, target: $p < 0.05$). No effect of treatment or time was found in FS interneurons (**Figure 5H**, effect of treatment: $F_{(3,36)} = 0.10$, $p > 0.05$). Additionally, there was no statistical difference in firing frequency of pyramidal neurons (**Supplementary Figure 7B**) of FS interneurons (**Supplementary Figure 7C**) during the baseline recording, which was conducted in rats' home-cage.

Overall, these findings further confirm that the impaired synaptic function and neural correlates of memory consolidation contribute to the cognitive deficits induced by blocking proBDNF expression. These observations also suggest that activation of the GluN2B-mediated pathway by TBOA can be one of the key measures for rescuing the memory disability.

DISCUSSION

Mature BDNF has been investigated for its positive roles in regulating synaptic development and function. Although it is established that proBDNF serves diverse biological functions (Guo et al., 2016), its role in the development of spatial cognition has been debated. In the present study, multiple lines of evidence demonstrated that the expression of hippocampal proBDNF in the fourth postnatal week played a vital role in spatial memory consolidation, but not in memory acquisition or retrieval. The study uncovered three striking features of postnatal proBDNF that were not previously recognized: first, the spine density and the proportion of mature spines declined in adults following the blocking of proBDNF in the fourth postnatal week. Second, blocking postnatal proBDNF attenuated synaptic function, including PPF, PTD, and SL-LTD, which were associated with the reduction in learning-induced pGluN2B expression. Third, the activation of the GluN2B pathway by TBOA immediately following acquisition training could effectively mitigate proBDNF-mediated memory deficits and synaptic responses and elevate the memory-related activity of pyramidal neurons in the HPC.

In support of the proBDNF levels that peaked at PD24, the mBDNF level was downregulated during a transient period of NMDAR-dependent inhibition/excitation imbalance around PD28 (Zhang et al., 2018). Moreover, Orefice et al. (2013)

found a similar critical period contributing to the distinct roles of somatically and dendritically synthesized mBDNF in spine shape and density. More specifically, the effect of proBDNF on spine density was not initiated at PD21 but between PD21 and PD28 during which spine pruning occurred (Orefice et al., 2016). Using mice expressing two alleles of bdnf with a HA tag to detect BDNF isoforms, Yang et al. (2014) found that the hippocampal proBDNF level was the highest at PD15, with a reduction at PD42 or later. This finding indicated that the effects of endogenous proBDNF protein would be the most robust in early postnatal development, consistent with the higher levels of $p75^{NTR}$ in the HPC at the early age (Woo et al., 2005; Yang J. et al., 2009), particularly in CA1 pyramidal cell apical dendrites, postsynaptic to the Schaffer collateral axon terminals (Woo et al., 2005). They also found that the potent effects of proBDNF played a role in the development of hippocampal circuitry, which might influence hippocampal-dependent functions later in life, as demonstrated in this study. Consistent with the crucial role of BDNF in spine outgrowth (Greenberg et al., 2009; Deinhardt and Chao, 2014), our findings indicated that proBDNF was required for spine development, and the blockage of proBDNF expression resulted in spine loss. A higher proportion of thin immature spines implied the role of postnatal proBDNF in spine pruning (Guo et al., 2016; Orefice et al., 2016). Actually, thin spines are thought to be highly motile and unstable structures characteristic of immature synapses, which can be transformed into more mature and stable phenotypes during early development (Dunaevsky et al., 1999). Therefore, the impairment of spatial memory consolidation may be attributed to the decline in the mushroom spine, which is strongly associated with memory formation (Bourne and Harris, 2007). Previous studies showed that proBDNF had an effect on learning strategy (An et al., 2018) and extinction of contextual fear memory but not on learning ability (Sun et al., 2018a). Importantly, blocking postnatal proBDNF did not result in an inefficient learning strategy, indicating that the deficit in memory consolidation was driven by a less precise learning strategy. Similar to previous findings (An et al., 2018; Sun et al., 2019), proBDNF-induced memory defects were not a result of impaired locomotion, anxiety-like behavior, or motivation. The specific mechanism of spine pruning remains unclear. The synaptic transmission and presynaptic calcium ion levels play significant roles (Segal et al., 2000). The notion is supported by the diminished PPF, which has been used as a measure of changes in presynaptic Ca^{2+} dynamics and neurotransmitter release probability (Burnashev and Rozov, 2005).

QQNMDAR activation stimulates both translation of dendritic BDNF mRNA and secretion of its translation products, mainly as proBDNF, which promotes spine maturation (Orefice et al., 2016). Depending on the age of the animals, the dynamic changes in the expression of GluN1, GluN2A, and GluN2B subunit mRNAs can lead to different mixtures of NMDA receptors in the developing HPC (Sans et al., 2000; Law et al., 2003). For example, higher GluN2B expression is found in postnatal brains, but GluN2A gradually becomes more prevalent in adulthood and advanced ages (Hestrin, 1992; Monyer et al., 1992, 1994). Considering the crucial role of proBDNF-$p75^{NTR}$ signaling in GluN2B-mediated spine maturation and synaptic function (Woo et al., 2005; Yang et al., 2014; Orefice et al., 2016), it is plausible that the increased expression of GluN2B subunit during postnatal weeks may be a critical mediator in proBDNF-mediated spine pruning and memory functions. The GluN2B mRNA levels peaked during the neonatal period, which was also observed in humans, with a decline to reach adult levels by 6–12 months (Law et al., 2003). BDNF mRNA levels increase approximately from 5-month infancy to adolescence and are maintained at a constant level throughout adulthood and aging (Webster et al., 2002). Interestingly, the significant increase in BDNF mRNA levels in the dorsolateral prefrontal cortex coincides with the time when the frontal cortex matures both structurally and functionally (Webb et al., 2001; Webster et al., 2002). Furthermore, the first postnatal month is characterized by an increase in the number of excitatory synapses (Steward and Falk, 1991). The activity-dependent activation of NMDA receptors can switch the effects of the proBDNF-$p75^{NTR}$ pathway on synaptic activity from potentiation to depression in the developing HPC (Langlois et al., 2013). The critical period of the increases in GABAergic inhibition, which is from the fourth toward the end of the fifth postnatal weeks, is overlapped with the time of peak proBDNF expression, suggesting a transitory period of synaptic balance during development (Zhang et al., 2018). Thus, the number and efficiency of inhibitory synapses may also be regulated during the postnatal days to adjust the strength of inhibition so as to counter the increased number of excitatory synapses. Given that NMDAR-mediated signaling is essential for the effects of BDNF on dendritic development (Finsterwald et al., 2010), blocking proBDNF during the early postnatal period may induce neurotransmission impairments, further leading to spine reduction. Future experiments are required to prove this hypothesis.

Memory formation during training acts to increase AMPAR and NMDAR phosphorylation (Mizuno et al., 2003; Barki-Harrington et al., 2009; Solomonia et al., 2013). Spatial learning induces the phosphorylation of hippocampal TrkB, Fyn, and GluN2B, which are associated with memory formation (Mizuno et al., 2003). The age-related declines in GluN2B expression in the frontal cortex are related to spatial reference learning deficits (Zamzow et al., 2016). Indeed, learning-induced tyrosine 1472 allows for the enhanced binding of GluN2B with PSD95, concentrating and holding NMDAR on synaptic membranes, and increasing synaptic function (Roche et al., 2001; Barki-Harrington et al., 2009; Xu, 2011). Moreover, the expression levels of GluA1, GluN2A, and GluN2B subunits of NMDAR are altered in the insular cortex after taste learning (Barki-Harrington et al., 2009). The differences in expression and phosphorylation of AMPAR and NMDAR subunits from different studies could be attributed to the differences in the fractionation protocol of learning tasks and specific brain areas (Adaikkan and Rosenblum, 2012).

Spines are the primary site for excitatory/inhibitory inputs to neurons, and a reduced spine number and changes in morphology contribute to synaptic dysfunction. Notably, proBDNF is known to facilitate synaptic depression at hippocampal synapses by mediating presynaptic glutamate

release and by regulating activation of postsynaptic glutamatergic receptors (Yang F. et al., 2009; Yang J. et al., 2009). Intriguingly, the downregulation of postnatal proBDNF levels does not affect the expression of glutamatergic receptors, but results in the suppression of learning-induced phosphorylation of the GluN2B-NMDA receptor, which has been associated with the induction of LTD (Ge et al., 2010; An and Sun, 2018). One underlying presynaptic mechanism of PTD is the rising Ca^{2+} concentration in terminal boutons (Burnashev and Rozov, 2005), disturbing the induction of long-term plasticity (Fioravante and Regehr, 2011). Furthermore, the phosphorylation of the GluN2B subunit is essential for activating a signaling cascade leading to the activation of memory-related plasticity (Zhou et al., 2007). It concurred with a previous finding that GluN2B-dependent LTD played pivotal roles in post-learning information sculpting (Dietz and Manahan-Vaughan, 2017). Other findings also indicated that memory consolidation rather than memory acquisition required the NMDAR-LTD mechanism to modify the hippocampal circuit to store fear memory (Liu et al., 2014). Previous evidence indicated that hippocampal GluN2B-dependent LTD could be induced following DL-TBOA infusions *in vitro* (Kratzer et al., 2012) and *in vivo* (Wong et al., 2007; An and Sun, 2018). In fact, DL-TBOA blocked the recycling of presynaptically released glutamate and caused accumulation of glutamate in the synaptic cleft, thus enhancing "spillover" and increasing the likelihood of extrasynaptic GluN2B-NMDA receptor activation (Massey et al., 2004; Yang et al., 2005). Additionally, the inhibitory effect of Ro25 on the induction of SL-LTD suggested that our findings were due to specific enhancement of GluN2B-dependent SL-LTD. Furthermore, a significant influence of postnatal proBDNF on HPC neuronal activity during memory formation and the involvement of GluN2B-mediated signaling in the memory consolidation process were found in the present study. Previous studies found that proBDNF-mediated $p75^{NTR}$ activation was responsible for controlling the performance in spatial memory tests and HPC excitability (Woo et al., 2005; Barrett et al., 2010). Our findings had some overlap with the evidence that mBDNF reduced action potential firing of FS cells in the hippocampal dentate gyrus, whereas proBDNF had no effect (Holm et al., 2009). Consistently, the training-induced increase in proBDNF expression promoted the firing rate of pyramidal neurons but not FS interneurons (An et al., 2018). Therefore, our findings extended the understanding of the effects of proBDNF on spatial memory function, which were mostly attributed to its actions on the learning-induced phosphorylation of GluN2B subunits and GluN2B-dependent neural function.

Through mediating C-terminal ubiquitination, TBOA can substantially enhance polyubiquitination of the GluA1 receptors (Jarzylo and Man, 2012). Presynaptically, an increase in glutamate concentrations in the early phase in the active synapse induced by low concentrations of DL-TBOA can be masked by AMPAR desensitization (Takayasu et al., 2004). Furthermore, the enhancement of the sodium ion current evoked by TBOA is attributed to its interaction with sodium ion carrier proteins, such as Na,K-ATPase (Bozzo and Chatton, 2010), which is co-localized with NMDA receptors and forms a function complex either by interacting directly or through some intermediate proteins (Akkuratov et al., 2015). Therefore, the rescuing effects of TBOA on GluN2B-NMDARs may be also involved in its effects on the activation of other glutamate receptors.

Spine maturation and pruning depend on neuronal activity and are required to refine neuronal connections in the developing brain (Segal et al., 2000; Bourne and Harris, 2007). Previous observations show that the long 3'UTR Bdnf mRNA, which is transported to dendrites for local translation (An et al., 2008), is essential for head enlargement and pruning of dendritic spines *in vivo* and *in vitro* (An et al., 2008; Kaneko et al., 2012; Orefice et al., 2013). For example, mice lacking long 3′UTR Bdnf mRNA display thinner and denser spines on the dendrites of CA1 pyramidal neurons in the HPC and L2/3 pyramidal neurons in the visual cortex (An et al., 2008; Kaneko et al., 2012). Furthermore, knocking down long 3′UTR Bdnf mRNA or blocking the transport of long 3′UTR Bdnf mRNA to dendrites inhibits spine maturation and pruning, whereas overexpressing long 3′UTR Bdnf mRNA enhances spine maturation and pruning in cultured hippocampal neurons (Orefice et al., 2013). Interestingly, the translation product of long 3′UTR Bdnf mRNA is mainly secreted as precursor BDNF. The overexpression of dendritic proBDNF alone or dendritic proBDNF plus 3'UTR Bdnf mRNA caused a significant increase in spine head width. More importantly, granule cells in $p75^{NTR}$ knockout mice had significantly smaller spine heads at both PD21 and PD28. These findings indicated that dendritically synthesized proBDNF from 3'UTR Bdnf mRNA promoted spine pruning and maturation *via* $p75^{NTR}$ (Orefice et al., 2016). The mechanisms by which proBDNF coincidently mediates the pruning and maturation of dendritic spines are unclear. However, the materials from eliminated spines may be recycled to activate spines, thus facilitating their growth. However, the hypotheses need further investigation.

The present results did not replicate the findings of a previous study, which showed increased spine density following spatial maze training and a correlation between spine density and behavioral performance (Mahmmoud et al., 2015; Dillingham et al., 2019). Actually, hippocampal dendritic spines are temporally dynamic structures, and as such, the time at which they are assessed may be a critical factor. A previous study found changes in CA1 spine clustering, but no change in density, 6 days after water-maze training (Rusakov et al., 1997). More detailed information on the time course of CA1 spine formation and turnover can be acquired from slice studies. For instance, initial plasticity, including spinogenesis along the dendritic shaft of CA1 neurons, following stimulation was designed to mimic long-term potentiation (Bourne and Harris, 2011). However, no overall change in spine density was observed 2 h after stimulation, suggesting a redistribution of spines and a balance between the loss and gain of spines (Bourne and Harris, 2011). Functional entorhinal cortex coupled with CA1 activity became more direct with additional training, thus producing a trisynaptic circuit bypass (Poirier et al., 2008), hence suggesting that the stage of learning was another critical factor in the eight-trial training-induced structural changes. One more possibility was that the typical light microscopy used in the current and previous studies did not have sufficient spatial resolution to properly resolve the

distinguishing features of spines (Harland et al., 2014; Wartman and Holahan, 2014). For example, Tonnesen et al. used super-resolution stimulated emission depletion imaging and found only few stubby spines (Tonnesen et al., 2014). Future studies, using a continuous spectrum, as suggested elsewhere (Yuste and Majewska, 2001; Arellano et al., 2007; Gipson and Olive, 2017), may provide more detailed information.

Some studies indicated an increase in proBDNF in the aged mouse HPC (Buhusi et al., 2017), whereas other studies showed that the aging-related accumulation of proBDNF did not occur (Michalski and Fahnestock, 2003; Silhol et al., 2007). The adverse effects of proBDNF accumulation over time in aged rodents would affect neuronal morphology and spine density, leading to synaptic and behavioral deficits (Perovic et al., 2013; Buhusi et al., 2017). Consistent with the NMDA-dependent switch of proBDNF actions on developing synapses (Langlois et al., 2013), our findings might extend these findings and indicate a bidirectional regulation of proBDNF in distinct developmental stages. Interestingly, spatial training increased proBDNF metabolism in both young and aged rats (Silhol et al., 2007). Studies performed on experimental/transgenic animals indicated that proBDNF tended to facilitate mature spines pruning. A recent study demonstrated that the effects of BDNF on the dendritic architecture of the hippocampal neurons were dependent on the neuron's maturation stage (Kellner et al., 2014). Furthermore, the interaction between compensatory mechanisms and gene environment may ultimately determine the lack of the effects of BDNF on the regulation of spine maturation and pruning (Orefice et al., 2016). Hence, it is important to note that blocking proBDNF expression by its antibody during the postnatal period, rather than gene mutations, should be an essential approach to provide direct evidence for its effects on brain function. Furthermore, the mechanism by which proBDNF exerts its effects, other than it being related to the GluN2B subunit, still needs further investigation, especially given that the effects were found after the developmental GluN2B to GluN2A shift. The estrogenic regulation of BDNF signaling is likely sex specific (Chan and Ye, 2017; Wei et al., 2017). Intriguingly, the inherent organization of the HPC in terms of hormonal responses is programmed early in life (Hill et al., 2012; Kight and McCarthy, 2017). In ovariectomized female rats, BDNF protein and mossy fiber synaptic function decreased, whereas orchidectomy led to what would seem to be the opposite effect in male rats (Scharfman and MacLusky, 2014). Presumably, the neonatal surge in hormone and BDNF levels, which accompany the sex differences in brain development, leads to a circuitry upon which adult BDNF levels exert a varying influence. Moreover, the sexual differences in neuronal signaling, especially those induced by BDNF, are observed in an early stage (Chan and Ye, 2017). Therefore, further experiments involving the sex-specific effects of proBDNF may provide more information.

In this study, we demonstrated that the blockage of proBDNF expression during the fourth postnatal week disrupted spatial memory consolidation by structurally reducing the ratio of mature spines and functionally suppressing synaptic function and neural activity. The learning-induced phosphorylation of GluN2B subunits is likely an important mechanism in inducing LTD and promoting neural correlate with the memory consolidation process. Taken together, our findings are important for obtaining a unifying concept of the biological roles of proBDNF in cognitive and neural functions.

DATA AVAILABILITY STATEMENT

The raw data supporting the conclusions of this article will be made available by the authors, without undue reservation.

ETHICS STATEMENT

The animal study was reviewed and approved by the Ethics Committee on the Care and Use of Animals Committee of Guizhou University of Traditional Chinese Medicine.

AUTHOR CONTRIBUTIONS

WS, YY, DT, and LA conceived and designed the experiments. WS, HC, and XL performed the experiments. WS, HC, XL, and LA analyzed the data. WS, YY, and LA wrote the manuscript. All authors contributed to the article and approved the submitted version.

FUNDING

This work was supported by Grants from the National Natural Science Foundation of China (31700929).

SUPPLEMENTARY MATERIAL

The Supplementary Material for this article can be found online at: https://www.frontiersin.org/articles/10.3389/fcell.2021.678182/full#supplementary-material

REFERENCES

Adaikkan, C., and Rosenblum, K. (2012). The role of protein phosphorylation in the gustatory cortex and amygdala during taste learning. *Exp. Neurobiol.* 21, 37–51. doi: 10.5607/en.2012.21.2.37

Akkuratov, E. E., Lopacheva, O. M., Kruusmagi, M., Lopachev, A. V., Shah, Z. A., Boldyrev, A. A., et al. (2015). Functional interaction between Na/K-ATPase and NMDA receptor in cerebellar neurons. *Mol. Neurobiol.* 52, 1726–1734. doi: 10.1007/s12035-014-8975-3

Alonso, M., Vianna, M. R., Depino, A. M., Mello e Souza, T., Pereira, P., Szapiro, G., et al. (2002). BDNF-triggered events in the rat hippocampus are required for both short- and long-term memory formation. *Hippocampus* 12, 551–560. doi: 10.1002/hipo.10035

An, J. J., Gharami, K., Liao, G. Y., Woo, N. H., Lau, A. G., Vanevski, F., et al. (2008). Distinct role of long 3' UTR BDNF mRNA in spine morphology and synaptic

plasticity in hippocampal neurons. *Cell* 134, 175–187. doi: 10.1016/j.cell.2008.05.045

An, L., and Sun, W. (2017). Prenatal melamine exposure impairs spatial cognition and hippocampal synaptic plasticity by presynaptic and postsynaptic inhibition of glutamatergic transmission in adolescent offspring. *Toxicol. Lett.* 269, 55–64. doi: 10.1016/j.toxlet.2017.02.005

An, L., and Sun, W. (2018). Acute melamine affects spatial memory consolidation via inhibiting hippocampal NMDAR-dependent LTD in rats. *Toxicol. Sci.* 163, 385–396. doi: 10.1093/toxsci/kfx039

An, L., Li, J., Luo, L., Huang, P., Liu, P., Tang, C., et al. (2019). Prenatal melamine exposure impairs cognitive flexibility and hippocampal synaptic plasticity in adolescent and adult female rats. *Pharmacol. Biochem. Behav.* 186:172791. doi: 10.1016/j.pbb.2019.172791

An, L., Li, X., Tang, C., Xu, N., and Sun, W. (2018). Hippocampal proBDNF facilitates place learning strategy associated with neural activity in rats. *Brain Struct. Funct.* 223, 4099–4113. doi: 10.1007/s00429-018-1742-x

Arellano, J. I., Benavides-Piccione, R., Defelipe, J., and Yuste, R. (2007). Ultrastructure of dendritic spines: correlation between synaptic and spine morphologies. *Front. Neurosci.* 1:131–143. doi: 10.3389/neuro.01.1.1.010.2007

Bai, Y. Y., Ruan, C. S., Yang, C. R., Li, J. Y., Kang, Z. L., Zhou, L., et al. (2016). ProBDNF signaling regulates depression-like behaviors in rodents under chronic stress. *Neuropsychopharmacology* 41, 2882–2892. doi: 10.1038/npp.2016.100

Bannerman, D. M., Sprengel, R., Sanderson, D. J., McHugh, S. B., Rawlins, J. N., Monyer, H., et al. (2014). Hippocampal synaptic plasticity, spatial memory and anxiety. *Nat. Rev. Neurosci.* 15, 181–192.

Barki-Harrington, L., Elkobi, A., Tzabary, T., and Rosenblum, K. (2009). Tyrosine phosphorylation of the 2B subunit of the NMDA receptor is necessary for taste memory formation. *J. Neurosci.* 29, 9219–9226. doi: 10.1523/jneurosci.5667-08.2009

Barrett, G. L., Reid, C. A., Tsafoulis, C., Zhu, W., Williams, D. A., Paolini, A. G., et al. (2010). Enhanced spatial memory and hippocampal long-term potentiation in p75 neurotrophin receptor knockout mice. *Hippocampus* 20, 145–152.

Bourne, J. N., and Harris, K. M. (2011). Coordination of size and number of excitatory and inhibitory synapses results in a balanced structural plasticity along mature hippocampal CA1 dendrites during LTP. *Hippocampus* 21, 354–373. doi: 10.1002/hipo.20768

Bourne, J., and Harris, K. M. (2007). Do thin spines learn to be mushroom spines that remember? *Curr. Opin. Neurobiol.* 17, 381–386. doi: 10.1016/j.conb.2007.04.009

Bozzo, L., and Chatton, J. Y. (2010). Inhibitory effects of (2S, 3S)-3-[3-[4-(trifluoromethyl)benzoylamino]benzyloxy]aspartate (TFB-TBOA) on the astrocytic sodium responses to glutamate. *Brain Res.* 1316, 27–34. doi: 10.1016/j.brainres.2009.12.028

Brancaccio, M., Patton, A. P., Chesham, J. E., Maywood, E. S., and Hastings, M. H. (2017). Astrocytes control circadian timekeeping in the suprachiasmatic nucleus via glutamatergic signaling. *Neuron* 93, 1420–1435.e5.

Buhusi, M., Etheredge, C., Granholm, A. C., and Buhusi, C. V. (2017). Increased hippocampal ProBDNF contributes to memory impairments in aged mice. *Front. Aging Neurosci.* 9:284. doi: 10.3389/fnagi.2017.00284

Burnashev, N., and Rozov, A. (2005). Presynaptic Ca2+ dynamics, Ca2+ buffers and synaptic efficacy. *Cell Calcium.* 37, 489–495. doi: 10.1016/j.ceca.2005.01.003

Chan, C. B., and Ye, K. (2017). Sex differences in brain-derived neurotrophic factor signaling and functions. *J. Neurosci. Res.* 95, 328–335. doi: 10.1002/jnr.23863

Choo, M., Miyazaki, T., Yamazaki, M., Kawamura, M., Nakazawa, T., Zhang, J., et al. (2017). Retrograde BDNF to TrkB signaling promotes synapse elimination in the developing cerebellum. *Nat. Commun.* 8:195.

de Quervain, D. J., Roozendaal, B., and McGaugh, J. L. (1998). Stress and glucocorticoids impair retrieval of long-term spatial memory. *Nature* 394, 787–790. doi: 10.1038/29542

Deinhardt, K., and Chao, M. V. (2014). Shaping neurons: long and short range effects of mature and proBDNF signalling upon neuronal structure. *Neuropharmacology* 76, 603–609. doi: 10.1016/j.neuropharm.2013.04.054

Dietz, B., and Manahan-Vaughan, D. (2017). Hippocampal long-term depression is facilitated by the acquisition and updating of memory of spatial auditory content and requires mGlu5 activation. *Neuropharmacology* 115, 30–41. doi: 10.1016/j.neuropharm.2016.02.026

Dillingham, C. M., Milczarek, M. M., Perry, J. C., Frost, B. E., Parker, G. D., Assaf, Y., et al. (2019). Mammillothalamic disconnection alters hippocampocortical oscillatory activity and microstructure: implications for diencephalic amnesia. *J. Neurosci.* 39, 6696–6713. doi: 10.1523/jneurosci.0827-19.2019

Donaldson, H. H. (1924). *The Rat; Data and Reference Tables for the Albino Rat (Mus Norvegius Albinus) and the Norway Rat (Musnorvegicus)*, 2 Edn. Philadelphia, PA: Philadelphia Press.

Dong, Z., Bai, Y., Wu, X., Li, H., Gong, B., Howland, J. G., et al. (2013). Hippocampal long-term depression mediates spatial reversal learning in the Morris water maze. *Neuropharmacology* 64, 65–73. doi: 10.1016/j.neuropharm.2012.06.027

Dudai, Y., Karni, A., and Born, J. (2015). The consolidation and transformation of memory. *Neuron* 88, 20–32. doi: 10.1016/j.neuron.2015.09.004

Dunaevsky, A., Tashiro, A., Majewska, A., Mason, C., and Yuste, R. (1999). Developmental regulation of spine motility in the mammalian central nervous system. *Proc. Natl. Acad. Sci. U.S.A.* 96, 13438–13443. doi: 10.1073/pnas.96.23.13438

Feng, K., Zhao, X., Liu, J., Cai, Y., Ye, Z., Chen, C., et al. (2019). Spaced learning enhances episodic memory by increasing neural pattern similarity across repetitions. *J. Neurosci.* 39, 5351–5360. doi: 10.1523/jneurosci.2741-18.2019

Fernandes, B. S., Steiner, J., Berk, M., Molendijk, M. L., Gonzalez-Pinto, A., Turck, C. W., et al. (2015). Peripheral brain-derived neurotrophic factor in schizophrenia and the role of antipsychotics: meta-analysis and implications. *Mol. Psychiatry* 20, 1108–1119. doi: 10.1038/mp.2014.117

Finsterwald, C., Fiumelli, H., Cardinaux, J. R., and Martin, J. L. (2010). Regulation of dendritic development by BDNF requires activation of CRTC1 by glutamate. *J. Biol. Chem.* 285, 28587–28595. doi: 10.1074/jbc.m110.125740

Fioravante, D., and Regehr, W. G. (2011). Short-term forms of presynaptic plasticity. *Curr. Opin. Neurobiol.* 21, 269–274. doi: 10.1016/j.conb.2011.02.003

Ge, Y., Dong, Z., Bagot, R. C., Howland, J. G., Phillips, A. G., Wong, T. P., et al. (2010). Hippocampal long-term depression is required for the consolidation of spatial memory. *Proc. Natl. Acad. Sci.* 107, 16697–16702. doi: 10.1073/pnas.1008200107

Gipson, C. D., and Olive, M. F. (2017). Structural and functional plasticity of dendritic spines-root or result of behavior? *Genes Brain Behav.* 16, 101–117. doi: 10.1111/gbb.12324

Greenberg, M. E., Xu, B., Lu, B., and Hempstead, B. L. (2009). New insights in the biology of BDNF synthesis and release: implications in CNS function. *J. Neurosci.* 29, 12764–12767. doi: 10.1523/jneurosci.3566-09.2009

Guo, J., Ji, Y., Ding, Y., Jiang, W., Sun, Y., Lu, B., et al. (2016). BDNF pro-peptide regulates dendritic spines via caspase-3. *Cell Death Dis.* 7:e2264. doi: 10.1038/cddis.2016.166

Harland, B. C., Collings, D. A., McNaughton, N., Abraham, W. C., and Dalrymple-Alford, J. C. (2014). Anterior thalamic lesions reduce spine density in both hippocampal CA1 and retrosplenial cortex, but enrichment rescues CA1 spines only. *Hippocampus* 24, 1232–1247. doi: 10.1002/hipo.22309

Haynes, P. R., Christmann, B. L., and Griffith, L. C. (2015). A single pair of neurons links sleep to memory consolidation in drosophila melanogaster. *Elife* 4:e03868.

Hernandez, L. F., Kubota, Y., Hu, D., Howe, M. W., Lemaire, N., and Graybiel, A. M. (2013). Selective effects of dopamine depletion and L-DOPA therapy on learning-related firing dynamics of striatal neurons. *J. Neurosci.* 33, 4782–4795. doi: 10.1523/jneurosci.3746-12.2013

Hestrin, S. (1992). Developmental regulation of NMDA receptor-mediated synaptic currents at a central synapse. *Nature* 357, 686–689. doi: 10.1038/357686a0

Hill, R. A., Wu, Y. W., Kwek, P., and van den Buuse, M. (2012). Modulatory effects of sex steroid hormones on brain-derived neurotrophic factor-tyrosine kinase B expression during adolescent development in C57Bl/6 mice. *J. Neuroendocrinol.* 24, 774–788. doi: 10.1111/j.1365-2826.2012.02277.x

Holm, M. M., Nieto-Gonzalez, J. L., Vardya, I., Vaegter, C. B., Nykjaer, A., and Jensen, K. (2009). Mature BDNF, but not proBDNF, reduces excitability of fast-spiking interneurons in mouse dentate gyrus. *J. Neurosci.* 29, 12412–12418. doi: 10.1523/jneurosci.2978-09.2009

Hoorens, M. W., Fu, H., Duurkens, R. H., Trinco, G., Arkhipova, V., Feringa, B. L., et al. (2018). Glutamate transporter inhibitors with photo-controlled activity. *Adv. Ther.* 1:1800028. doi: 10.1002/adtp.201800028

Itoh, N., Enomoto, A., Nagai, T., Takahashi, M., and Yamada, K. (2016). Molecular mechanism linking BDNF/TrkB signaling with the NMDA receptor in memory: the role of Girdin in the CNS. *Rev. Neurosci.* 27, 481–490. doi: 10.1515/revneuro-2015-0072

Izquierdo, I., Bevilaqua, L. R., Rossato, J. I., Bonini, J. S., Medina, J. H., and Cammarota, M. (2006). Different molecular cascades in different sites of the brain control memory consolidation. *Trends Neurosci.* 29, 496–505. doi: 10.1016/j.tins.2006.07.005

Jarzylo, L. A., and Man, H. Y. (2012). Parasynaptic NMDA receptor signaling couples neuronal glutamate transporter function to AMPA receptor synaptic distribution and stability. *J. Neurosci.* 32, 2552–2563. doi: 10.1523/jneurosci.3237-11.2012

Je, H. S., Yang, F., Ji, Y., Nagappan, G., Hempstead, B. L., and Lu, B. (2012). Role of pro-brain-derived neurotrophic factor (proBDNF) to mature BDNF conversion in activity-dependent competition at developing neuromuscular synapses. *Proc. Natl. Acad. Sci. U.S.A.* 109, 15924–15929. doi: 10.1073/pnas.1207767109

Kandel, E. R. (2001). The molecular biology of memory storage: a dialogue between genes and synapses. *Science* 294, 1030–1038. doi: 10.1126/science.1067020

Kaneko, M., Xie, Y., An, J. J., Stryker, M. P., and Xu, B. (2012). Dendritic BDNF synthesis is required for late-phase spine maturation and recovery of cortical responses following sensory deprivation. *J. Neurosci.* 32, 4790–4802. doi: 10.1523/jneurosci.4462-11.2012

Kapadia, M., Xu, J., and Sakic, B. (2016). The water maze paradigm in experimental studies of chronic cognitive disorders: theory, protocols, analysis, and inference. *Neurosci. Biobehav. Rev.* 68, 195–217. doi: 10.1016/j.neubiorev.2016.05.016

Kellner, Y., Godecke, N., Dierkes, T., Thieme, N., Zagrebelsky, M., and Korte, M. (2014). The BDNF effects on dendritic spines of mature hippocampal neurons depend on neuronal activity. *Front. Synaptic Neurosci.* 6:5. doi: 10.3389/fnsyn.2014.00005

Kellogg, C. K., Yao, J., and Pleger, G. L. (2000). Sex-specific effects of in utero manipulation of GABA(A) receptors on pre- and postnatal expression of BDNF in rats. *Brain Res. Dev. Brain Res.* 121, 157–167. doi: 10.1016/s0165-3806(00)00039-0

Kight, K. E., and McCarthy, M. M. (2017). Sex differences and estrogen regulation of BDNF gene expression, but not propeptide content, in the developing hippocampus. *J. Neurosci. Res.* 95, 345–354. doi: 10.1002/jnr.23920

Klug, M., Hill, R. A., Choy, K. H., Kyrios, M., Hannan, A. J., and van den Buuse, M. (2012). Long-term behavioral and NMDA receptor effects of young-adult corticosterone treatment in BDNF heterozygous mice. *Neurobiol. Dis.* 46, 722–731. doi: 10.1016/j.nbd.2012.03.015

Kratzer, S., Mattusch, C., Kochs, E., Eder, M., Haseneder, R., and Rammes, G. (2012). Xenon attenuates hippocampal long-term potentiation by diminishing synaptic and extrasynaptic N-methyl-D-aspartate receptor currents. *Anesthesiology* 116, 673–682. doi: 10.1097/aln.0b013e3182475d66

Langlois, A., Diabira, D., Ferrand, N., Porcher, C., and Gaiarsa, J. L. (2013). NMDA-dependent switch of proBDNF actions on developing GABAergic synapses. *Cereb Cortex* 23, 1085–1096. doi: 10.1093/cercor/bhs071

Law, A. J., Weickert, C. S., Webster, M. J., Herman, M. M., Kleinman, J. E., and Harrison, P. J. (2003). Expression of NMDA receptor NR1, NR2A and NR2B subunit mRNAs during development of the human hippocampal formation. *Eur. J. Neurosci.* 18, 1197–1205. doi: 10.1046/j.1460-9568.2003.02850.x

Li, A., Jing, D., Dellarco, D. V., Hall, B. S., Yang, R., Heilberg, R. T., et al. (2019). Role of BDNF in the development of an OFC-amygdala circuit regulating sociability in mouse and human. *Mol. Psychiatry* 26, 955–973. doi: 10.1038/s41380-019-0422-4

Li, M. Y., Miao, W. Y., Wu, Q. Z., He, S. J., Yan, G., Yang, Y., et al. (2017). A critical role of presynaptic cadherin/catenin/p140cap complexes in stabilizing spines and functional synapses in the neocortex. *Neuron* 94, 1155–1172.e8.

Lim, Y., Zhong, J. H., and Zhou, X. F. (2015). Development of mature BDNF-specific sandwich ELISA. *J. Neurochem.* 134, 75–85. doi: 10.1111/jnc.13108

Liu, X., Gu, Q. H., Duan, K., and Li, Z. (2014). NMDA receptor-dependent LTD is required for consolidation but not acquisition of fear memory. *J. Neurosci.* 34, 8741–8748. doi: 10.1523/jneurosci.2752-13.2014

Lu, B., Nagappan, G., and Lu, Y. (2014). BDNF and synaptic plasticity, cognitive function, and dysfunction. *Handb. Exp. Pharmacol.* 220, 223–250. doi: 10.1007/978-3-642-45106-5_9

Lu, B., Pang, P. T., and Woo, N. H. (2005). The yin and yang of neurotrophin action. *Nat. Rev. Neurosci.* 6, 603–614. doi: 10.1038/nrn1726

Luo, C., Zhong, X. L., Zhou, F. H., Li, J. Y., Zhou, P., Xu, J. M., et al. (2016). Peripheral brain derived neurotrophic factor precursor regulates pain as an inflammatory mediator. *Sci. Rep.* 6:27171.

Luoni, A., Berry, A., Raggi, C., Bellisario, V., Cirulli, F., and Riva, M. A. (2016). Sex-specific effects of prenatal stress on Bdnf Expression in response to an acute challenge in rats: a role for gadd45beta. *Mol. Neurobiol.* 53, 7037–7047. doi: 10.1007/s12035-015-9569-4

Maei, H. R., Zaslavsky, K., Teixeira, C. M., and Frankland, P. W. (2009). What is the most sensitive measure of water maze probe test performance? *Front. Integr. Neurosci.* 3:4. doi: 10.3389/neuro.07.004.2009

Mahmmoud, R. R., Sase, S., Aher, Y. D., Sase, A., Groger, M., Mokhtar, M., et al. (2015). Spatial and working memory is linked to spine density and mushroom spines. *PLoS One* 10:e0139739. doi: 10.1371/journal.pone.0139739

Massey, P. V., Johnson, B. E., Moult, P. R., Auberson, Y. P., Brown, M. W., Molnar, E., et al. (2004). Differential roles of NR2A and NR2B-containing NMDA receptors in cortical long-term potentiation and long-term depression. *J. Neurosci.* 24, 7821–7828. doi: 10.1523/jneurosci.1697-04.2004

McGaugh, J. L. (2000). Memory-a century of consolidation. *Science* 287, 248–251. doi: 10.1126/science.287.5451.248

Michalski, B., and Fahnestock, M. (2003). Pro-brain-derived neurotrophic factor is decreased in parietal cortex in Alzheimer's disease. *Brain Res. Mol. Brain Res.* 111, 148–154. doi: 10.1016/s0169-328x(03)00003-2

Mizuno, K., and Giese, K. P. (2010). Towards a molecular understanding of sex differences in memory formation. *Trends Neurosci.* 33, 285–291. doi: 10.1016/j.tins.2010.03.001

Mizuno, M., Yamada, K., He, J., Nakajima, A., and Nabeshima, T. (2003). Involvement of BDNF receptor TrkB in spatial memory formation. *Learn. Mem.* 10, 108–115. doi: 10.1101/lm.56003

Monyer, H., Burnashev, N., Laurie, D. J., Sakmann, B., and Seeburg, P. H. (1994). Developmental and regional expression in the rat brain and functional properties of four NMDA receptors. *Neuron* 12, 529–540. doi: 10.1016/0896-6273(94)90210-0

Monyer, H., Sprengel, R., Schoepfer, R., Herb, A., Higuchi, M., Lomeli, H., et al. (1992). Heteromeric NMDA receptors: molecular and functional distinction of subtypes. *Science* 256, 1217–1221. doi: 10.1126/science.256.5060.1217

Mueller, D., Bravo-Rivera, C., and Quirk, G. J. (2010). Infralimbic D2 receptors are necessary for fear extinction and extinction-related tone responses. *Biol. Psychiatry* 68, 1055–1060. doi: 10.1016/j.biopsych.2010.08.014

Nadel, L., Hupbach, A., Gomez, R., and Newman-Smith, K. (2012). Memory formation, consolidation and transformation. *Neurosci. Biobehav. Rev.* 36, 1640–1645. doi: 10.1016/j.neubiorev.2012.03.001

Nakai, T., Nagai, T., Tanaka, M., Itoh, N., Asai, N., Enomoto, A., et al. (2014). Girdin phosphorylation is crucial for synaptic plasticity and memory: a potential role in the interaction of BDNF/TrkB/Akt signaling with NMDA receptor. *J. Neurosci.* 34, 14995–15008. doi: 10.1523/jneurosci.2228-14.2014

Orefice, L. L., Shih, C. C., Xu, H., Waterhouse, E. G., and Xu, B. (2016). Control of spine maturation and pruning through proBDNF synthesized and released in dendrites. *Mol. Cell. Neurosci.* 71, 66–79. doi: 10.1016/j.mcn.2015.12.010

Orefice, L. L., Waterhouse, E. G., Partridge, J. G., Lalchandani, R. R., Vicini, S., and Xu, B. (2013). Distinct roles for somatically and dendritically synthesized brain-derived neurotrophic factor in morphogenesis of dendritic spines. *J. Neurosci.* 33, 11618–11632. doi: 10.1523/jneurosci.0012-13.2013

Paterson, N. E., Froestl, W., and Markou, A. (2005). Repeated administration of the GABAB receptor agonist CGP44532 decreased nicotine self-administration, and acute administration decreased cue-induced reinstatement of nicotine-seeking in rats. *Neuropsychopharmacology* 30, 119–128. doi: 10.1038/sj.npp.1300524

Perovic, M., Tesic, V., Mladenovic Djordjevic, A., Smiljanic, K., Loncarevic-Vasiljkovic, N., Ruzdijic, S., et al. (2013). BDNF transcripts, proBDNF and proNGF, in the cortex and hippocampus throughout the life span of the rat. *Age (Dordr)* 35, 2057–2070. doi: 10.1007/s11357-012-9495-6

Peters, J., Dieppa-Perea, L. M., Melendez, L. M., and Quirk, G. J. (2010). Induction of fear extinction with hippocampal-infralimbic BDNF. *Science* 328, 1288–1290. doi: 10.1126/science.1186909

Poirier, G. L., Amin, E., and Aggleton, J. P. (2008). Qualitatively different hippocampal subfield engagement emerges with mastery of a spatial memory task by rats. *J. Neurosci.* 28, 1034–1045. doi: 10.1523/jneurosci.4607-07.2008

Porter, J. T., and Sepulveda-Orengo, M. T. (2019). Learning-induced intrinsic and synaptic plasticity in the rodent medial prefrontal cortex. *Neurobiol. Learn. Mem.* 169:107117. doi: 10.1016/j.nlm.2019.107117

Reus, G. Z., Stringari, R. B., Ribeiro, K. F., Ferraro, A. K., Vitto, M. F., Cesconetto, P., et al. (2011). Ketamine plus imipramine treatment induces antidepressant-like behavior and increases CREB and BDNF protein levels and PKA and PKC phosphorylation in rat brain. *Behav. Brain Res.* 221, 166–171. doi: 10.1016/j.bbr.2011.02.024

Roche, K. W., Standley, S., McCallum, J., Dune Ly, C., Ehlers, M. D., and Wenthold, R. J. (2001). Molecular determinants of NMDA receptor internalization. *Nat. Neurosci.* 4, 794–802. doi: 10.1038/90498

Rusakov, D. A., Davies, H. A., Harrison, E., Diana, G., Richter-Levin, G., Bliss, T. V., et al. (1997). Ultrastructural synaptic correlates of spatial learning in rat hippocampus. *Neuroscience* 80, 69–77. doi: 10.1016/s0306-4522(97)00125-5

Sanchez-Rodriguez, I., Djebari, S., Temprano-Carazo, S., Vega-Avelaira, D., Jimenez-Herrera, R., Iborra-Lazaro, G., et al. (2019). Hippocampal long-term synaptic depression and memory deficits induced in early amyloidopathy are prevented by enhancing G-protein-gated inwardly-rectifying potassium channel activity. *J. Neurochem.* 153, 362–376. doi: 10.1111/jnc.14946

Sans, N., Petralia, R. S., Wang, Y. X., Blahos, J. II, Hell, J. W., and Wenthold, R. J. (2000). A developmental change in NMDA receptor-associated proteins at hippocampal synapses. *J. Neurosci.* 20, 1260–1271. doi: 10.1523/jneurosci.20-03-01260.2000

Scharfman, H. E., and MacLusky, N. J. (2014). Differential regulation of BDNF, synaptic plasticity and sprouting in the hippocampal mossy fiber pathway of male and female rats. *Neuropharmacology* 76, 696–708. doi: 10.1016/j.neuropharm.2013.04.029

Segal, I., Korkotian, I., and Murphy, D. D. (2000). Dendritic spine formation and pruning: common cellular mechanisms? *Trends Neurosci.* 23, 53–57. doi: 10.1016/s0166-2236(99)01499-x

Shirayama, Y., Yang, C., Zhang, J. C., Ren, Q., Yao, W., and Hashimoto, K. (2015). Alterations in brain-derived neurotrophic factor (BDNF) and its precursor proBDNF in the brain regions of a learned helplessness rat model and the antidepressant effects of a TrkB agonist and antagonist. *Eur. Neuropsychopharmacol.* 25, 2449–2458. doi: 10.1016/j.euroneuro.2015.09.002

Silhol, M., Arancibia, S., Maurice, T., and Tapia-Arancibia, L. (2007). Spatial memory training modifies the expression of brain-derived neurotrophic factor tyrosine kinase receptors in young and aged rats. *Neuroscience* 146, 962–973. doi: 10.1016/j.neuroscience.2007.02.013

Slipczuk, L., Bekinschtein, P., Katche, C., Cammarota, M., Izquierdo, I., and Medina, J. H. (2009). BDNF activates mTOR to regulate GluR1 expression required for memory formation. *PLoS One* 4:e6007. doi: 10.1371/journal.pone.0006007

Solomonia, R. O., Meparishvili, M., Mikautadze, E., Kunelauri, N., Apkhazava, D., and McCabe, B. J. (2013). AMPA receptor phosphorylation and recognition memory: learning-related, time-dependent changes in the chick brain following filial imprinting. *Exp. Brain Res.* 226, 297–308. doi: 10.1007/s00221-013-3435-2

Stark, E., Roux, L., Eichler, R., Senzai, Y., Royer, S., and Buzsaki, G. (2014). Pyramidal cell-interneuron interactions underlie hippocampal ripple oscillations. *Neuron* 83, 467–480. doi: 10.1016/j.neuron.2014.06.023

Steward, O., and Falk, P. M. (1991). Selective localization of polyribosomes beneath developing synapses: a quantitative analysis of the relationships between polyribosomes and developing synapses in the hippocampus and dentate gyrus. *J. Comput. Neurol.* 314, 545–557. doi: 10.1002/cne.903140311

Sun, W., Che, H., Li, J., Tang, D., Liu, X., Liu, W., et al. (2020). Dorsolateral striatal proBDNF improves reversal learning by enhancing coordination of neural activity in rats. *Mol. Neurobiol.* 57, 4642–4656. doi: 10.1007/s12035-020-02051-9

Sun, W., Li, J., Cui, S., Luo, L., Huang, P., Tang, C., et al. (2019). Sleep deprivation disrupts acquisition of contextual fear extinction by affecting circadian oscillation of hippocampal-infralimbic proBDNF. *eNeuro* 6:ENEURO.0165-19.2019.

Sun, W., Li, X., and An, L. (2018a). Distinct roles of prelimbic and infralimbic proBDNF in extinction of conditioned fear. *Neuropharmacology* 131, 11–19. doi: 10.1016/j.neuropharm.2017.12.018

Sun, W., Li, X., Tang, C., and An, L. (2018b). Acute low alcohol disrupts hippocampus-striatum neural correlate of learning strategy by inhibition of PKA/CREB pathway in rats. *Front. Pharmacol.* 9:1439. doi: 10.3389/fphar.2018.01439

Sun, W., Liu, P., Tang, C., and An, L. (2021). Melamine disrupts acetylcholine-mediated neural information flow in the hippocampal CA3-CA1 pathway. *Front. Behav. Neurosci.* 15:594907. doi: 10.3389/fnbeh.2021.594907

Sun, W., Wu, Y., Tang, D., Li, X., and An, L. (2021a). Melamine disrupts spatial reversal learning and learning strategy via inhibiting hippocampal BDNF-mediated neural activity. *PLoS One* 16:e0245326. doi: 10.1371/journal.pone.0245326

Sun, W., Yang, Y., Wu, Z., Chen, X., Li, W., and An, L. (2021b). Chronic cyanuric acid exposure depresses hippocampal LTP but does not disrupt spatial learning or memory in the morris water maze. *Neurotox Res.* [Epub ahead of print].

Sun, Y., Lim, Y., Li, F., Liu, S., Lu, J. J., Haberberger, R., et al. (2012). ProBDNF collapses neurite outgrowth of primary neurons by activating RhoA. *PLoS One* 7:e35883. doi: 10.1371/journal.pone.0035883

Sundermann, E. E., Maki, P. M., Rubin, L. H., Lipton, R. B., Landau, S., and Biegon, A. (2016). Female advantage in verbal memory: evidence of sex-specific cognitive reserve. *Neurology* 87, 1916–1924. doi: 10.1212/wnl.0000000000003288

Suzuki, K., Sato, M., Morishima, Y., and Nakanishi, S. (2005). Neuronal depolarization controls brain-derived neurotrophic factor-induced upregulation of NR2C NMDA receptor via calcineurin signaling. *J. Neurosci.* 25, 9535–9543. doi: 10.1523/jneurosci.2191-05.2005

Takayasu, Y., Iino, M., and Ozawa, S. (2004). Roles of glutamate transporters in shaping excitatory synaptic currents in cerebellar Purkinje cells. *Eur. J. Neurosci.* 19, 1285–1295. doi: 10.1111/j.1460-9568.2004.03224.x

Tomas Pereira, I., and Burwell, R. D. (2015). Using the spatial learning index to evaluate performance on the water maze. *Behav. Neurosci.* 129, 533–539. doi: 10.1037/bne0000078

Tonnesen, J., Katona, G., Rozsa, B., and Nagerl, U. V. (2014). Spine neck plasticity regulates compartmentalization of synapses. *Nat. Neurosci.* 17, 678–685. doi: 10.1038/nn.3682

Wang, H., Hu, Y., and Tsien, J. Z. (2006). Molecular and systems mechanisms of memory consolidation and storage. *Prog. Neurobiol.* 79, 123–135. doi: 10.1016/j.pneurobio.2006.06.004

Wartman, B. C., and Holahan, M. R. (2014). The impact of multiple memory formation on dendritic complexity in the hippocampus and anterior cingulate cortex assessed at recent and remote time points. *Front. Behav. Neurosci.* 8:128. doi: 10.3389/fnbeh.2014.00128

Webb, S. J., Monk, C. S., and Nelson, C. A. (2001). Mechanisms of postnatal neurobiological development: implications for human development. *Dev. Neuropsychol.* 19, 147–171. doi: 10.1207/s15326942dn1902_2

Webster, M. J., Weickert, C. S., Herman, M. M., and Kleinman, J. E. (2002). BDNF mRNA expression during postnatal development, maturation and aging of the human prefrontal cortex. *Brain Res. Dev. Brain Res.* 139, 139–150. doi: 10.1016/s0165-3806(02)00540-0

Wei, Y. C., Wang, S. R., and Xu, X. H. (2017). Sex differences in brain-derived neurotrophic factor signaling: functions and implications. *J. Neurosci. Res.* 95, 336–344. doi: 10.1002/jnr.23897

Wong, T. P., Howland, J. G., Robillard, J. M., Ge, Y., Yu, W., Titterness, A. K., et al. (2007). Hippocampal long-term depression mediates acute stress-induced spatial memory retrieval impairment. *Proc. Natl. Acad. Sci. U.S.A.* 104, 11471–11476. doi: 10.1073/pnas.0702308104

Woo, N. H., Teng, H. K., Siao, C. J., Chiaruttini, C., Pang, P. T., Milner, T. A., et al. (2005). Activation of p75NTR by proBDNF facilitates hippocampal long-term depression. *Nat. Neurosci.* 8, 1069–1077. doi: 10.1038/nn1510

Wu, Y. C., Hill, R. A., Gogos, A., and van den Buuse, M. (2013). Sex differences and the role of estrogen in animal models of schizophrenia: interaction with BDNF. *Neuroscience* 239, 67–83. doi: 10.1016/j.neuroscience.2012.10.024

Xu, W. (2011). PSD-95-like membrane associated guanylate kinases (PSD-MAGUKs) and synaptic plasticity. *Curr. Opin. Neurobiol.* 21, 306–312. doi: 10.1016/j.conb.2011.03.001

Xu, Z. Q., Sun, Y., Li, H. Y., Lim, Y., Zhong, J. H., and Zhou, X. F. (2011). Endogenous proBDNF is a negative regulator of migration of cerebellar granule cells in neonatal mice. *Eur. J. Neurosci.* 33, 1376–1384. doi: 10.1111/j.1460-9568.2011.07635.x

Yamazaki, T., Nagao, S., Lennon, W., and Tanaka, S. (2015). Modeling memory consolidation during posttraining periods in cerebellovestibular learning. *Proc. Natl. Acad. Sci. U.S.A.* 112, 3541–3546. doi: 10.1073/pnas.1413798112

Yang, C. H., Huang, C. C., and Hsu, K. S. (2005). Behavioral stress enhances hippocampal CA1 long-term depression through the blockade of the glutamate uptake. *J. Neurosci.* 25, 4288–4293. doi: 10.1523/jneurosci.0406-05.2005

Yang, C., Shirayama, Y., Zhang, J. C., Ren, Q., and Hashimoto, K. (2015). Regional differences in brain-derived neurotrophic factor levels and dendritic spine density confer resilience to inescapable stress. *Int. J. Neuropsychopharmacol.* 18:yu121.

Yang, F., Je, H. S., Ji, Y., Nagappan, G., Hempstead, B., and Lu, B. (2009). Pro-BDNF-induced synaptic depression and retraction at developing neuromuscular synapses. *J Cell Biol* 185, 727–741. doi: 10.1083/jcb.200811147

Yang, H., Cai, Y., Liu, Q., Zhao, X., Wang, Q., Chen, C., et al. (2015). Differential neural correlates underlie judgment of learning and subsequent memory performance. *Front. Psychol.* 6:1699. doi: 10.3389/fpsyg.2015.01699

Yang, J., Harte-Hargrove, L. C., Siao, C. J., Marinic, T., Clarke, R., Ma, Q., et al. (2014). proBDNF negatively regulates neuronal remodeling, synaptic transmission, and synaptic plasticity in hippocampus. *Cell Rep.* 7, 796–806. doi: 10.1016/j.celrep.2014.03.040

Yang, J., Siao, C. J., Nagappan, G., Marinic, T., Jing, D., McGrath, K., et al. (2009). Neuronal release of proBDNF. *Nat. Neurosci.* 12, 113–115. doi: 10.1038/nn.2244

Yuste, R., and Majewska, A. (2001). On the function of dendritic spines. *Neuroscientist* 7, 387–395.

Zamzow, D. R., Elias, V., Acosta, V. A., Escobedo, E., and Magnusson, K. R. (2016). Higher levels of phosphorylated Y1472 on GluN2B subunits in the frontal cortex of aged mice are associated with good spatial reference memory, but not cognitive flexibility. *Age (Dordr)* 38:50.

Zhang, H., Mu, L., Wang, D., Xia, D., Salmon, A., Liu, Q., et al. (2018). Uncovering a critical period of synaptic imbalance during postnatal development of the rat visual cortex: role of brain-derived neurotrophic factor. *J. Physiol.* 596, 4511–4536. doi: 10.1113/jp275814

Zhou, Y., Takahashi, E., Li, W., Halt, A., Wiltgen, B., Ehninger, D., et al. (2007). Interactions between the NR2B receptor and CaMKII modulate synaptic plasticity and spatial learning. *J. Neurosci.* 27, 13843–13853. doi: 10.1523/jneurosci.4486-07.2007

Conflict of Interest: The authors declare that the research was conducted in the absence of any commercial or financial relationships that could be construed as a potential conflict of interest.

Advantages of publishing in Frontiers

OPEN ACCESS
Articles are free to read for greatest visibility and readership

FAST PUBLICATION
Around 90 days from submission to decision

HIGH QUALITY PEER-REVIEW
Rigorous, collaborative, and constructive peer-review

TRANSPARENT PEER-REVIEW
Editors and reviewers acknowledged by name on published articles

Frontiers
Avenue du Tribunal-Fédéral 34
1005 Lausanne | Switzerland

Visit us: www.frontiersin.org
Contact us: frontiersin.org/about/contact

REPRODUCIBILITY OF RESEARCH
Support open data and methods to enhance research reproducibility

DIGITAL PUBLISHING
Articles designed for optimal readership across devices

FOLLOW US
@frontiersin

IMPACT METRICS
Advanced article metrics track visibility across digital media

EXTENSIVE PROMOTION
Marketing and promotion of impactful research

LOOP RESEARCH NETWORK
Our network increases your article's readership